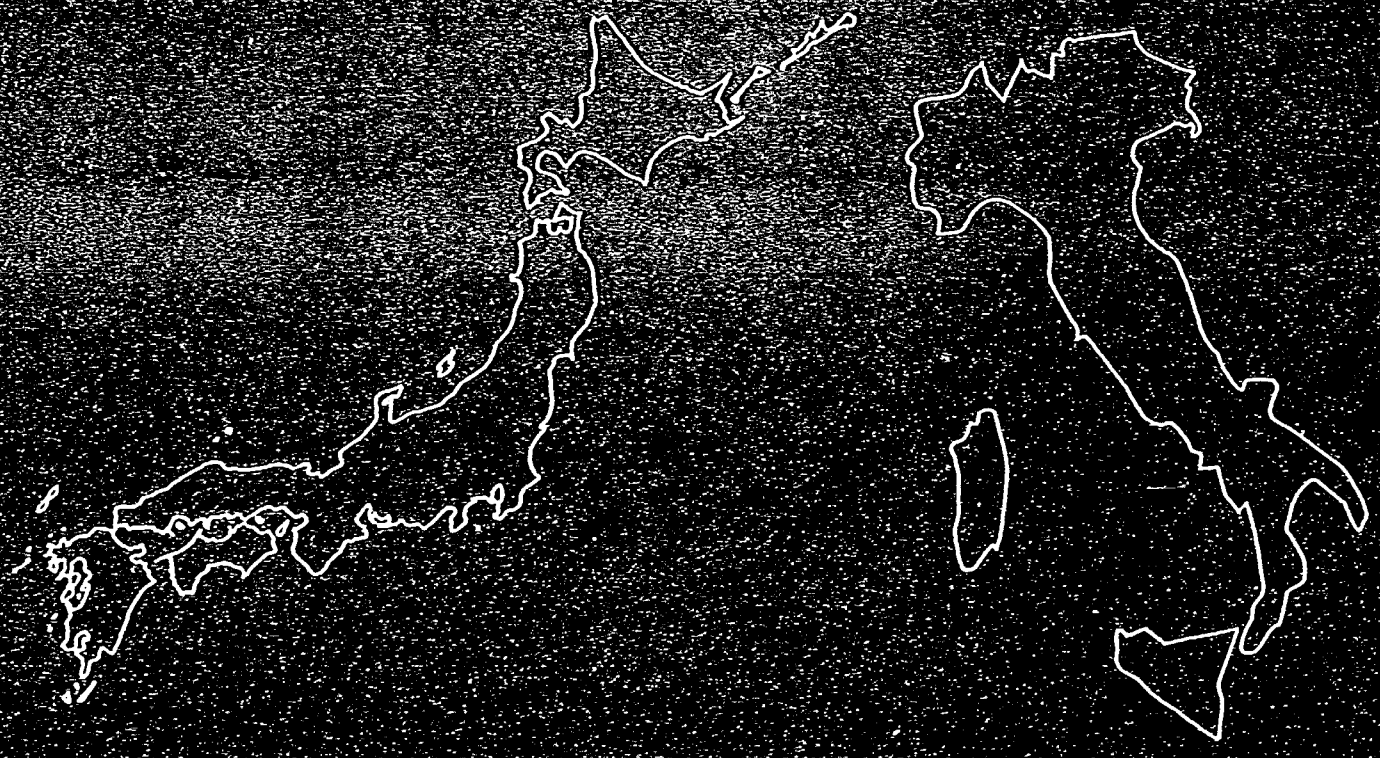
ISSN 0386-5878
Technical Memorandum
of PWRI No.3369

PROCEEDINGS OF THE FIRST JAPAN-ITALY WORKSHOP ON SEISMIC DESIGN OF BRIDGES



March 13 – 14, 1995
Tsukuba, Japan

Public Works Research Institute
Ministry of Construction

Copyright ©1995 by P.W.R.I.

All rights reserved. No part of this book may be reproduced by any means, nor translated into a machine language without the written permission of the Director General of P.W.R.I.

この報告書は，土木研究所長の承認を得て刊行したものである。したがって，本報告書の全部又は一部の転載，複製は，土木研究所長の文書による承認を得ずしてこれを行ってはならない。

ISSN0386-5878
Technical Memorandum
of PWRI No.3369

PROCEEDINGS OF THE FIRST JAPAN-ITALY WORKSHOP ON SEISMIC DESIGN OF BRIDGES

March 13 – 14, 1995
Tsukuba, Japan

Public Works Research Institute
Ministry of Construction

Synopsis:
This proceedings document the results of the First Japan-Italy Workshop on Seismic Design of Bridges. The Workshop was held at the Public Works Research Institute in Tsukuba Science City, Japan, on March 13 and 14, 1995.

Key words : Bridge, Seismic Desgin, Retrofitting, Design Code, Member Modeling

FOREWORD

The recent period has seen increasing exchanges between Japanese and European researchers in the field of the seismic design and retrofit of bridges. This favourable climate had led representatives of Japanese and Italian Institutions to decision of organizing a bi-lateral Italy-Japan Workshop on Seismic Design of Bridges, to be held in Rome, on February 15 and 16, 1995.

The disastrous event occurred in the Hanshin area on January 17, just a few weeks before the planned Workshop in Rome, made it impossible for the Japanase participants to leave their Country, many of them being directly involved in the post-earthquake emergency operations.

To reaffirm their will to cooperate and their belief that scientific progress is the most important resource to mitigate the effects of future natural disasters, the two parties agreed not to cancel the event, but simply to adjust its program to the new circumstances.

It was therefore decided to have it in Japan, in the premises of the PWRI in Tsukuba Science City, on March 13 and 14, 1995, to be called "First Japan-Italy Workshop on Seismic Design of Bridges", and also to combine it with a wider event with participants from the USA, this second event bearing the title of "International Workshop on Seismic Design of Bridges".

The first event saw the presentation of 8 papers from the Italian side (the participation has been extended to two Europeans specialists, from Greece and from Portugal) whose content spanned the field of Seismic Design Provisions, New Design Rules, Members Modeling, and Bridge Rehabilitation.

The USA followed by presenting 5 papers, dealing with the experience gained in their recent earthquakes and with the reflections of this experience on the research and on the design guidelines for new and existing bridges.

On the second day, the Japan side gave 6 fresh reports on various aspects of the last earthquake, with special emphasis on the damages to bridges, and to its impact on future design rules.

The content of this Volume of Proceedings includes the 14+13 papers that were originally foreseen for the meeting in Rome.

A study tour to the damaged area had been impeccably organized for all foreign participants on the two days of Wednesday and Thursday, March 15 and 16, 1995. The survey resulted to be of invaluable educational interest for all, showing once more what severe challange the earthquakes pose to the intelligence of men.

The two Workshops were supported by the Public Works Research Institute of the Ministry of Contruction, Japan. The University of Rome "La Sapienza" is to be thanked for the organization it had already finalized when the location had to be changed.

The coordinators for the Workshops were Dr. Kazuhiko Kawashima, Research Coordinator for Geospace Use at the Public Works Research Institute, presently Professor of Structural and Earthquake Engineering at the Tokyo Institute of Technology, and Dr. Paolo E. Pinto, Professor of Earthquake Engineering at the University of Rome "La Sapienza".

The technical staff of PWRI contributed with competence and dedication to the success of the Workshop and of the following study tour.

June 1995
Paolo E. Pinto
University of Rome "La Sapienza"

TABLE OF CONTENTS

ITALIAN (EUROPEAN) SIDE

I- 1) Shear, Normal Force, Bending Moment Interaction in Bridge Piers
(G. Fanti, G. Mancini) 1

I- 2) A Fiber Model for Elements under Cyclic Bending and Shear
(M. Petrangeli, P. E. Pinto) 20

I- 3) Displacement Based Seismic Design of Multi-Degree-of-Freedom Bridge Structures
(G. M. Calvi, G. R. Kingsley) 33

I- 4) Inelastic Response of Conventional and Isolated Bridges under Non-synchronous Seismic Input
(G. Monti, C. Nuti) 54

I- 5) Eurocode 8 Part.2 : Earthquake Resistant Design of Bridges
(P. E. Pinto) 72

I- 6) Irregular Bridges Designed According to Eurocode 8 : Numerical and Experimental Verifications
(G. M. Calvi, P.E. Pinto) 85

I- 7) Large-Scale Pseudodynamic Tests on Highly Irregular Bridges
(P. Negro, A. V. Pinto) 97

I- 8) The Use of Histeretic Dampers for the Seismic Protection of Bridges in Italy
(A. Marioni) 115

I- 9) The Seismic Retrofit of Marquam Bridge : A Case Study
(R. Medeot) 130

I-10) Seismic Design of the Fadalto Bridge
(G. Furlanetto, M. Bruni) 149

I-11) Programmed Maintenance of Motorway Bridges : Italian Experience in the Use of "Expert Systems"
(G. Camomilla, A. Dragotti, G. Nebbia, M. Romagnolo)
..... 156

I-12) Seismic Retrofitting of Two Large Span Bridges
(M. P. Petrangeli, M. Petrangeli) 169

I-13) Seismic Retrofit and Structural Rehabilitation of the Aglio Viaduct
(M. Romagnolo) 180

I-14) Design Criteria for Bridges of the Italian High Speed Railway System
(F. Braga, F. Brancaleoni, M. Colella, G. Traini)
..... 191

JAPAN SIDE

J- 1) Effect of Geological Irregularities on Ground Motion Characteristics
(Ryoji HAGIWARA, Riki HONDA) 207

J- 2) Consideration of Soil Liquefaction Potential in Seismic Design of Highway Bridge Foundation
(Yasuyuki KOGA, Yoshio NINOMIYA, Masuo KONDO)
..... 223

J- 3) A Stress-Strain Model for Confined Reinforced Concrete in Bridge Piers
(Jun-ichi HOSHIKUMA, Kazuhiko KAWASHIMA, Kazuhiro NAGAYA)
..... 246

J- 4) Residual Displacement Response Spectra and its Application
(Kazuhiko KAWASHIMA, Gregory A. MACRAE, Jun-ichi HOSHIKUMA, Kazuhiro NAGAYA) 268

J- 5) Strength and Ductility Characteristics of Steel Bridge Piers with Concrete Filler
(Kazuo YAMAZAKI, Shin-ichi EGAWA, Kiyokazu KUBOTA)
..... 290

J- 6) Nonlinear Response Evaluation of Shallow Foundations against Earthquake Ground Motions
(Hisanori OTSUKA, Shigeki UNJOH, Hidetoshi MUKAI)
..... 308

J- 7) A Study on the Deformation Characteristics of Precast Hollow Piers during Earthquakes
(Masanori NAKANO, Shigeru TAKAGI, Moriyuki OKOSHI)
..... 326

J- 8) Plannig of the New Tomei Expressway and Design/Construction of High-Rise Bridge Pier
(Kazuyuki MIZUGUCHI) 348

J- 9) Shaking Table Test for Large-Scale Seismic Isolated Structure using High Damping Rubber Bearings
(Yoji SUIZU, Chiaki SUDO, Shigenobu SUZUKI, Kengo GODA, Nobuyuki OGAWA, Yasuki OHTORI) 368

J-10) Elasto-Plastic Earthquake Response of Presstressed Concrete Cable-Stayed Bridges with Hysteretic-Type Bearing between Deck and Piers/Abutments
(Hisanori OTSUKA, Kazuyuki MIZUTORI, Yutaka YAMAHANA)
..... 380

J-11) Seismic Design for Making Continuous the Multiple Spans of A Viaduct on the Honshu-Shikoku Highway
(Shoichi SAEKI, Kazuo TADA, Kazuhiko YAMAGISHI) 403

J-12) Earthquake Response of Base-Isolated Multi-Span Continuous Bridge
(Yozo GOTO) 419

J-13) Seismic Characteristics and Vibration Control of PC Cable-Stayed Bridge under Construction
(Meguru TSUNOMOTO, Sunichi HIGUCHI, Yozo GOTO) 439

RESOLUTION

APPENDICES

1. Schedule of the Workshop
2. Opening Ceremony
3. Session Program of the Workshop
4. Closing Ceremony
5. Technical Study Tour
6. List of Participants

ITALIAN SIDE

SHEAR, NORMAL FORCE, BENDING MOMENT INTERACTION IN BRIDGE PIERS

G. Fanti G. Mancini

Department of Structural Engineering
Politecnico di Torino

ABSTRACT

In the piers of bridges and viaducts situated in seismic areas, the presence of combined compression and bending (M, N) and high shear (V) calls for the development of interaction models providing a realistic approximation of structural behaviour at the ultimate limit state. Using the ultimate resistant model proposed in the CEB-FIP Model Code 90, the effects of this interaction are analysed in terms of the reduction in the safety domains available in the M,N interaction diagrams for use in pier design. This analysis is applied to solid and boxed piers with non-dimensional shear span ratios between 0.5 and 1.25. Marked reductions in bearing capacity are observed for reduced shear span values and very high mechanical reinforcement ratios.

1. INTRODUCTION

Under design seismic actions, the piers of bridges and viaducts located in seismic zones are subjected to combined compression and bending (M, N) and high shear (V). In these conditions, the interaction between the forces involved must necessarily be taken into account in pier design, as they generally bring about a considerable reduction in strength, which is not observed in the presence of modest shear values.

The M,N,V interaction has been analysed from the experimental viewpoint by many Japanese, American and European authors [1] [2] [3] [4] [5] [6] who proposed checking procedures inspired by the ways in which the ULS is seen to be reached. Empirical and semi-empirical models have also been proposed [7] [8], to be used in pier design in the presence of high shear values.

A comparative analysis of the different test results obtained and the interpretation models proposed, as described in [9], however, shows that no physical model providing a close approximation of the M,N,V interaction at the ULS has yet been developed.

For the time being let us take into account only monotone actions so as to be able to use the M,N,V interaction model proposed in Model Code 90 [10] to work out a correct design approach for ULS dimensioning. The M,N,V interaction is therefore analysed below in terms of the reduction in the safety domains available in the interaction diagrams in the presence of combined compression and bending only (i.e., in conjunction with modest shear values).

Needless to say, in future, this procedure must be extended to cyclic action as well, through the definition of a suitable model and the relative strength deterioration and material deformability laws.

It should be noted, however, that since most bridge piers can be essentially conceived as multiple frames and individual piers, with either solid or boxed cross-sections, which may or may not involve the presence of first order eccentricity of the actions applied, it is necessary to investigate M,N,V interaction conditions corresponding to a non-dimensional shear span varying between 0.5 and 1.25. This makes it possible to identify the fundamental role played by this variable in determining the structural response.

2. MODELLING THE MATERIALS

In keeping with the foregoing considerations, concrete and steel are described on the basis of the monotone laws specified in Model Code 90; in particular, the relationship adopted for concrete is the parabola - rectangle law (fig. 1) expressed by:

$$\sigma_{cd} = 0.85\ f_{cd}\left[2\left(\frac{\varepsilon_c}{\varepsilon_{c1}}\right)-\left(\frac{\varepsilon_c}{\varepsilon_{c1}}\right)^2\right] \qquad \text{for } \varepsilon_c < \varepsilon_{c1}$$

$$\sigma_{cd} = 0.85\ f_{cd} = \nu_1 f_{cd} \qquad \text{for } \varepsilon_{c1} \le \varepsilon_c \le \varepsilon_{cu}$$

$$\sigma_{cd} = 0.00 \qquad \text{for } \varepsilon_c > \varepsilon_{cu}$$

where $\varepsilon_{c1} = 0.002$ and $\varepsilon_{cu} = 0.0035/0.002$, under compression and bending and axial compression, respectively. Such values apply if we assume $f_{ck} \le 50\text{MPa}$. When the strength exceeds 50 MPa, on the other hand, the limit values of ultimate strain must be modified through the application of a $50/f_{ck}$ ratio.

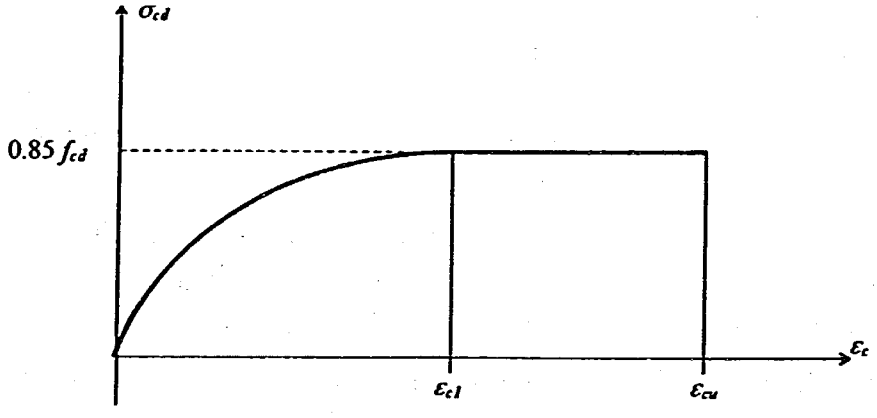


Fig. 1. *Parabola-rectangle stress-strain diagram for concrete.*

When dealing with concrete areas crossed by transverse reinforcement in tension, their behaviour in compression is described by taking the strength available in the concrete to be:

$$f_{cd2} = 0.6\left(1 - f_{ck}/250\right)f_{cd} = \nu_2 f_{cd}$$

Furthermore, characteristic tensile strength must be assumed to be:

$$f_{ctk\,min} = f_{ctk0,min}\left(f_{ck}/f_{ck0}\right)^{2/3} \qquad \text{with } f_{ctk0,min} = 0.95\text{MPa}$$

$$\text{and } f_{ctk0} = 10\text{MPa}$$

The behaviour of steel is described by a bilateral relationship with a perfectly plastic threshold symmetrical around the origin and characterised by strain at failure $\varepsilon_{su} = 0.01$ (fig. 2).

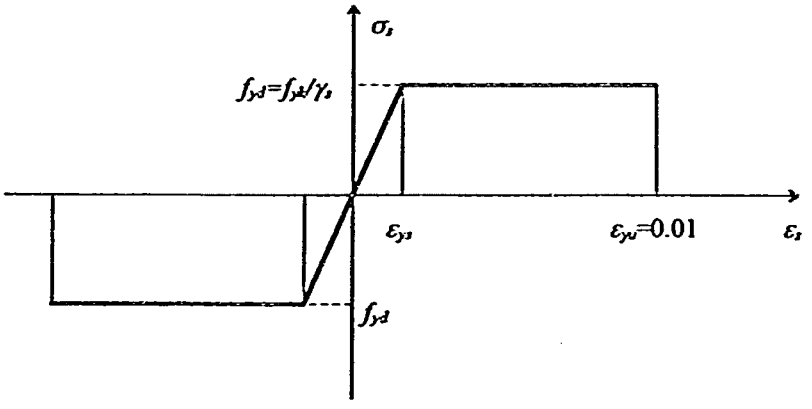


Fig. 2. *Design diagram for the reinforcement.*

3. ANALYSIS OF THE PHYSICAL MODEL OF BEHAVIOUR PROPOSED IN MODEL CODE 90

As is known, this approach disregards the presence of second order effects and essentially distinguishes between two possible resistant models, as summarised below:

- prevalence of compressive forces which do not require the presence of longitudinal reinforcement in the pier (model 1);
- prevalence of bending forces requiring the presence of longitudinal reinforcement in the pier (model 2).

In the first case (model 1), the ULS is reached through the opening of inclined cracks along the pier axis; consequently, it is necessary to make sure that the absolute values of the principal tensile stresses (σ_{c1}), in relation to the compressive stresses involved (σ_{c2}), do not exceed the following limits:

$$\text{for } \sigma_{c2} < f_{cd}/3 \quad : \quad \sigma_{c1} \le f_{ctk\,min}/1.5 \qquad (1)$$

$$\text{for } \sigma_{c2} \ge f_{cd}/3 \quad : \quad \sigma_{c1} \le f_{ctk\,min}\left(1 - \sigma_{c2}/f_{cd}\right) \qquad (2)$$

and that under no circumstance it turns out:

$$\sigma_{c2} > f_{cd1} \qquad (3)$$

The safety domain expressed by the foregoing conditions is illustrated in fig. 3. It is clear that the restrictions introduced in this manner will concern the range of normal force values associated with modest eccentricity levels.

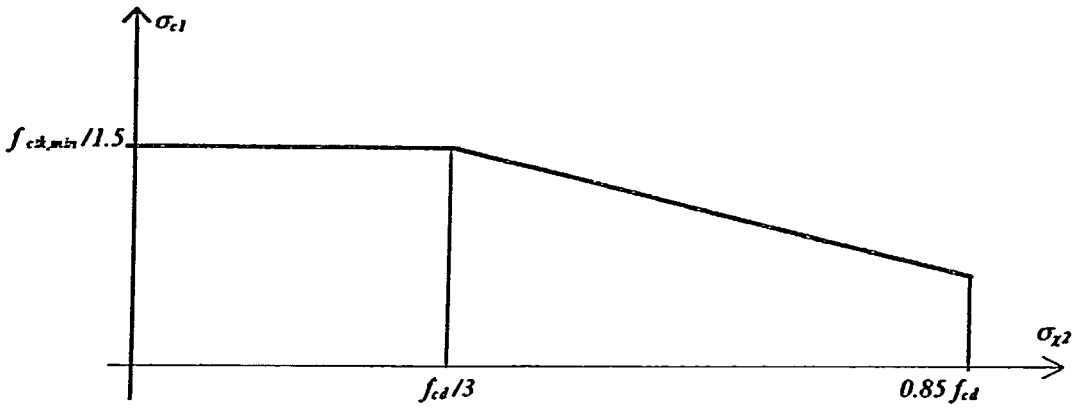


Fig. 3. *Stress limitations in the case of dominant compression.*

As for the second mechanism, since the limits specified for the principal tensile stresses in concrete are exceeded, inclined cracks will necessarily be present, and hence it becomes necessary to take into account two separate resistant models working in superposition. The first model envisages the formation of an inclined compression strut across the entire pier resulting from the composition, on the extreme faces of the section, of the resultants of the normal forces present in the concrete, N_c, as calculated when dimensioning the sections under compression and bending (for the sake of simplicity, we shall refer to the lower of the two compression resultants in concrete), and the percentage of acting shear necessary to affect the strut geometry so that its ends are located at the points of application of N_c. The second model consists of a truss made up of variable inclination compression struts and stirrups orthogonal to the pier axis, which is able to transfer the residual portion of the normal force (relative to the reinforcement) and acting shear (fig. 4).

The superposition of these two models, which is deemed theoretically acceptable [11], as the intervention of the second one does not conflict with the presence of the first, makes it possible to take into account both the unfavourable effect of inclined compression, due to the individual strut, upon the strength of the truss struts, and the favourable effect on stirrup dimensioning of the transverse component of the compressive force acting in the strut crossing the entire pier.

Consequently, in the second model, as a first approximation, ultimate checking can be performed simply by assessing the total level of compressive stresses in concrete.

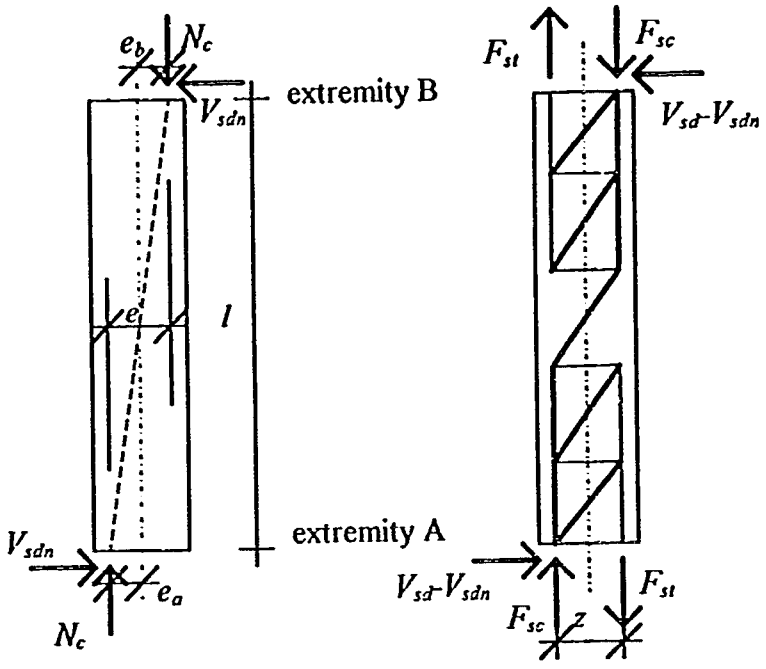


Fig. 4. *Model for columns with non dominant compression.*

The following symbols are adopted (with reference to the case of solid section):

- e_a, e_b: eccentricity of N_c at the ends A and B of the pier;
- $e = e_a + e_b$: distance of N_c resultants in the extreme sections;
- $\tan\gamma = e/l$: tangent of the compression strut inclination angle;
- $V_{sdn} = N_c \tan\gamma$: percentage of acting shear, V_{sdn}, transferred by the compression strut crossing the entire pier;
- ϑ: inclination angle of the compression struts in the second model;
- b_w and h: width and depth of the section, respectively;
- z: internal lever arm.

Thus, in the two models we get:

- model 1: $$\sigma_1 = \frac{N_c/\cos\gamma}{b_w h \cos\gamma}$$

- model 2: $$\sigma_2 = \frac{V_{sd} - V_{sdn}}{b_w z \sin\vartheta \cos\vartheta}$$

From the algebraic sum of the two stress levels, σ_1 and σ_2, which involves modest implications of a numerical nature, the checking relationship will be:

$$\sigma_1 + \sigma_2 \leq \sigma_{Rd} = f_{cd2}$$

In the stirrups, instead, it will be:

$$F_{st} = V_{sd} - V_{sdn} \leq \frac{A_{sw} f_{yd}}{s} z \operatorname{ctg}\vartheta$$

4. M,N,V INTERACTION IN SOLID PIERS

As already mentioned at point 1, the interaction between shear and normal force can be examined by identifying the limitations to the limit values of M,N imposed by the presence of shear.

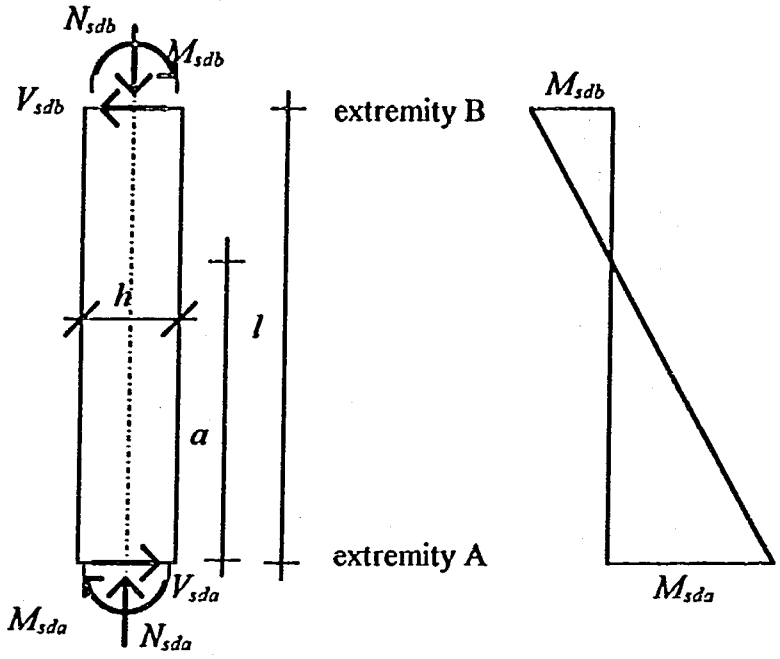


Fig. 5. *Acting action effects and moment diagram in a pier.*

With reference to fig. 5, let us consider, first of all, solid rectangular section piers loaded only at the ends and hence subjected to moments which vary linearly along the vertical axis of the pier. The following non-dimensional parameters are introduced:

- $\Psi = a/l$: non-dimensional shear span, referred to the end A of the pier;
- $\delta_h = l/h$: pier slenderness ratio;
- $\nu_{sd} = N_{sd} / b_w h f_{cd}$: non-dimensional acting normal force;
- $\nu_c = N_c / b_w h f_{cd}$: non-dimensional resultant of compressive stresses in concrete;
- $\mu_{sd} = M_{sd} / b_w h^2 f_{cd}$: non-dimensional acting bending moment;
- $\nu_{sd} = V_{sd} / b_w h f_{cd2}$: non-dimensional acting shear.

By imposing the conditions of equilibrium to pier rotation and translation, we get:

$$N_{sda} = N_{sdb}$$

$$V_{sda} = V_{sdb}$$

$$V_{sda} = \frac{M_{sda}}{a}; \qquad V_{sdb} = \frac{M_{sdb}}{l - a}$$

and therefore, by expressing the loading conditions at end B of the pier as a function of those present at end A, where the lower value of N_c has been assumed to be located, we find:

$$V_{sdb} = \frac{M_{sda}}{a}; \qquad M_{sdb} = M_{sda}\frac{1-a}{a}$$

Thus, in non-dimensional terms, loading conditions will be:

$$\nu_{sda} = \frac{M_{sda}}{ab_w h f_{cd2}} = \frac{\mu_{sda}}{\nu_2 \Psi \delta_h} \qquad (4)$$

$$\mu_{sdb} = \frac{M_{sdb}}{b_w h^2 f_{cd}} = \mu_{sda}\frac{1-\Psi}{\Psi}$$

At this point, the strength verification criteria set forth above must also be expressed in non-dimensional terms, always with reference to end A.

When compression prevails, it is possible, as a first approximation, to refer to the mean value of the compressive stress present in concrete and to assume a parabolic distribution of tangential stresses:

$$\sigma = \frac{N_c}{b_w h} = \nu_c f_{cd}$$

$$\tau_{max} = \frac{3}{2}\frac{V_{sd}}{b_w h} = \frac{3}{2}\nu_{sd}\nu_2 f_{cd}$$

Hence, the corresponding principal stresses turn out to be:

$$\sigma_{c1} = 0.5\ f_{cd}\left(\sqrt{9\nu_{sd}^2\nu_2^2 + \nu_c^2} - \nu_c\right)$$

$$\sigma_{c2} = 0.5\ f_{cd}\left(\sqrt{9\nu_{sd}^2\nu_2^2 + \nu_c^2} + \nu_c\right)$$

and it is easy to determine whether or not checking conditions (1) and (2), ensuring the desired safety level in the presence of prevalent compression (3), are satisfied.

If these conditions are not satisfied, the non prevalent compression model must be used instead. A new term, β_x, is introduced, i.e., the distance between the resultants of compressive forces in concrete and the section's most compressed edge, in order to determine the eccentricity of N_c:

$$e_a = \frac{h}{2} - \beta_a x_a; \qquad e_b = \frac{h}{2} - \beta_b x_b \qquad \text{hence}$$

$$\tan\gamma = \frac{e_a + e_b}{l} = \frac{\left(1 - \beta_a\frac{x_a}{h} - \beta_b\frac{x_b}{h}\right)}{\delta_h}\left(\psi < 1\right); \quad \tan\gamma = \frac{e_a + e_b}{l} = \frac{\left(\beta_b\frac{x_b}{h} - \beta_a\frac{x_a}{h}\right)}{\delta_h}\left(\psi \geq 1\right)$$

The checking condition for concrete relative to models 1 and 2 may then be expressed in non-dimensional terms:

- model 1 $$\sigma_1 = \frac{N_{cb}\left(1+\tan^2\gamma\right)}{b_w h} = \nu_{cb} f_{cd}\left(1+\tan^2\gamma\right)$$

- model 2 $$\sigma_2 = \frac{V_{sd} - N_{cb}\tan\gamma}{b_w z \sin\vartheta\cos\vartheta} = \frac{\left(\nu_{sd}\nu_2 - \nu_{cb}\tan\gamma\right) f_{cd}}{\sin\vartheta\cos\vartheta z/h}$$ and hence

$$\sigma_1 + \sigma_2 = f_{cd}\left[\nu_{cb}\left(1+\tan^2\gamma\right) + \frac{\nu_{sd}\nu_2 + \nu_{cb}\tan\gamma}{\sin\vartheta\cos\vartheta z/h}\right]$$

and by introducing expression (4):

$$\sigma_1 + \sigma_2 = f_{cd}\left[\nu_{cb}\left(1+\tan^2\gamma\right) + \frac{1}{\sin\vartheta\cos\vartheta z/h}\left(\frac{\mu_{sda}}{\Psi\delta_h} - \nu_{cb}\tan\gamma\right)\right] \qquad (5)$$

the pair of non-dimensional parameters, ν_{cb}, μ_{sda}, corresponding to the conditions in which the strength of the compression strut is highest, can be determined by setting $\sigma_1 + \sigma_2 = f_{cd2}$ and ϑ=45°, which amounts to satisfying the equation:

$$\nu_2 = \nu_{cb}\left(1+\tan^2\gamma\right) + \frac{2}{z/h}\left(\frac{\mu_{sda}}{\Psi\delta_h} - \nu_{cb}\tan\gamma\right) \qquad (6)$$

From eq. (6) it is possible to determine the limit value, $\mu_{sda\,lim}$, which μ_{sda} can reach for a given value of ν_{cb}:

$$\mu_{sda\,lim} = \left\{\left[\nu_2 - \nu_{cb}\left(1+\tan^2\gamma\right)\right]\frac{z/h}{2} + \nu_{cb}\tan\gamma\right\}\Psi\delta_h$$

It should be noted that this value, in addition to depending on the pier's geometric conditions (δ_h) and non-dimensional shear span (Ψ), is also a function of concrete class (ν_2); as a result, the M,N interaction diagrams turn out to be diversified not only for steel but for concrete as well.

At this point it is necessary to identify the possible limitations which the value $\mu_{sda\,lim}$ may impose, for a given value of ν_{sda}, on the corresponding interaction diagram with mechanical reinforcement ratios $\omega_1 = A_{s1} f_{yd} / b_w h f_{cd}$ and $\omega_2 = A_{s2} f_{yd} / b_w h f_{cd}$, as well as on a given type of steel (f_{yk}), concrete (f_{ck}) and cover value (d_1/h).

If we consider any point in the interaction diagram, as plotted in the presence of compression and bending only, corresponding to a pair of resisting actions μ_{rd}, ν_{rd}, the two following cases may occur:

- a) $\mu_{rd} \le \mu_{sda\,lim}$

which means that the presence of shear does not entail any further restrictions to the definition of the safety domain; transverse reinforcement can be optimised by setting:

$$\sigma_1 + \sigma_2 = f_{cd2}$$

and by determining ϑ accordingly; from eq. (5) we get:

$$\sin\vartheta\cos\vartheta = \frac{\frac{\mu_{sda}}{\psi\delta_h} - \nu_{cb}\tan\gamma}{\left[\nu_2 - \nu_{cb}\left(1+\tan^2\gamma\right)\right]\frac{z}{h}}$$

and therefore the corresponding transverse reinforcement must carry the acting force:

$$F_{stw} = V_{sd} - V_{sdn} = F_{rtw} = \frac{A_{sw}f_{yd}}{s} z\,\mathrm{ctg}\vartheta$$

Furthermore, to complete the resistant model, we must take into account the additional forces acting in the tension and compression chords:

$$F_{st,v} = \frac{1}{2}\left(V_{sd} - V_{sdn}\right)\mathrm{ctg}\vartheta = F_{rt,v} = A_{sl,v}f_{yd}$$

- b) $\mu_{rd} > \mu_{sda\,lim}$

in this case the pier is unable to satisfy the safety checks for the acting force values $\mu_{sd} = \mu_{rd}$ and $\nu_{sd} = \nu_{rd}$, since the simultaneous presence of shear gives rise to exceedingly high stresses in the concrete strut, and therefore the boundary of the safety domain must be modified accordingly. To this end, let us apply an iterative procedure to determine the pair of μ_{rd}, ν_{rd} values satisfying eq. (6) or at any rate the conditions specified for the case of prevalent compression (eqs. (1), (2) and (3)). This iterative procedure includes the following steps:

- b_1 : determining the relative position of the neutral axis (x/h) corresponding to the pair of reference values, μ_{rd}, ν_{rd};
- b_2: rotating around the neutral axis, assumed to be unchanged, the section's deformation configuration so as to reduce maximum strain;
- b_3: evaluating the new pair of values μ_{rd}, ν_{rd} corresponding to this reference configuration;
- b_4: verifying whether $\mu_{rd} \leq \mu_{sda\,lim}$, or whether it is an instance of prevalent compression;
- b_5: if the verification condition is not met, repeating the iterative cycle starting with step b_2, or, alternatively, introducing into the safety domain the new pair of $\bar{\mu}_{rd}$, $\bar{\nu}_{rd}$ values which satisfies the desired safety level .

By repeating this procedure for a sufficient number of points it proves possible to determine the new geometric configuration of the safety domain in the presence of M,N,V interaction.

5. EXAMPLES RELATING TO SOLID RECTANGULAR PIERS WITH NON-DIMENSIONAL SHEAR SPANS BETWEEN 0.5 AND 1.25

The procedure described above was used to plot the M,N,V interaction diagrams relating to solid rectangular sections characterised by the parameters expressed in the following table:

Ψ	ω	f_{ck} (MPa)
0.5	0.3	25
0.5	0.6	25
0.5	0.3	40
0.5	0.6	40
1	0.6	25
1.25	0.6	25

These diagrams are shown in figures 6 -11, with an additional variable, δ_h, taken into account in each.

From an analysis of these diagrams it is possible to make the following observations:

- the influence of shear is seen to be highest when Ψ is lowest;
- in heavily reinforced piers, where the stress level in concrete is higher, the influence of shear is particularly significant;
- concrete strength plays a minor role, despite the fact that higher strength values correspond to an increase in the influence of shear;
- the effects of shear are also seen to increase for low values of δ_h (short piers).

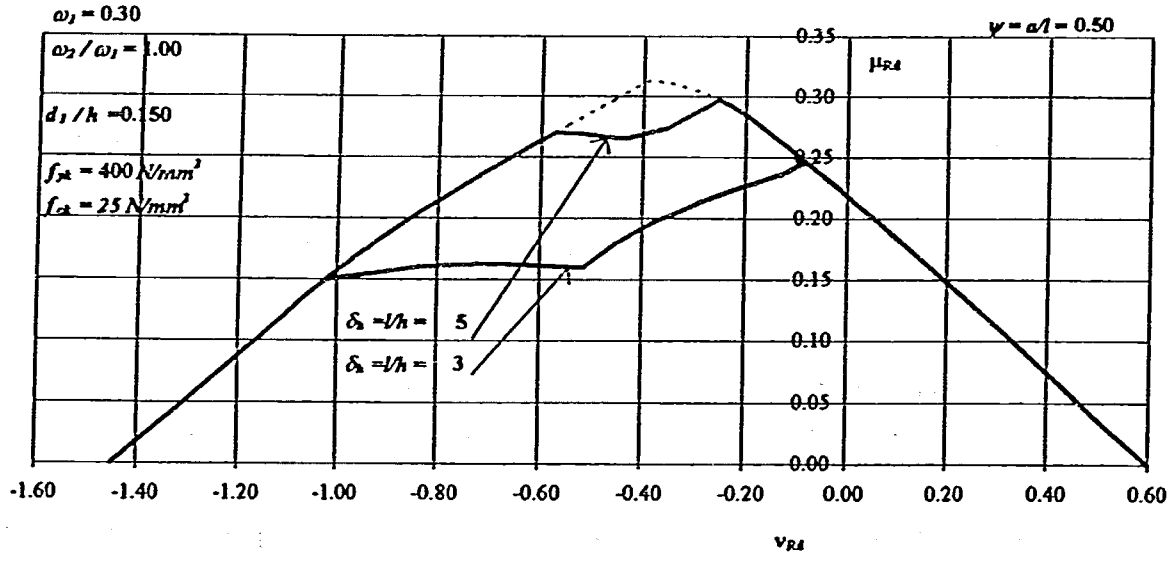


Fig. 6. M,N,V *interaction diagram for solid rectangular piers, plotted for* ω = 0.30, ψ = 0.50 *and* f_{ck} = 25 MPa.

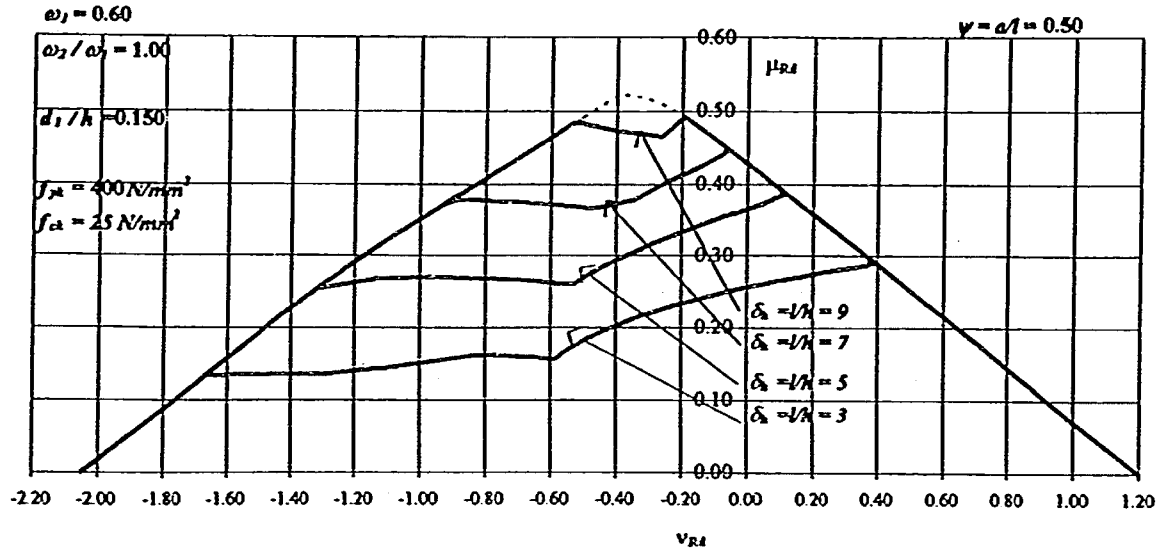


Fig. 7. M,N,V *interaction diagram for solid rectangular piers, plotted for* $\omega = 0.60$, $\psi = 0.50$ *and* $f_{ck} = 25$ MPa.

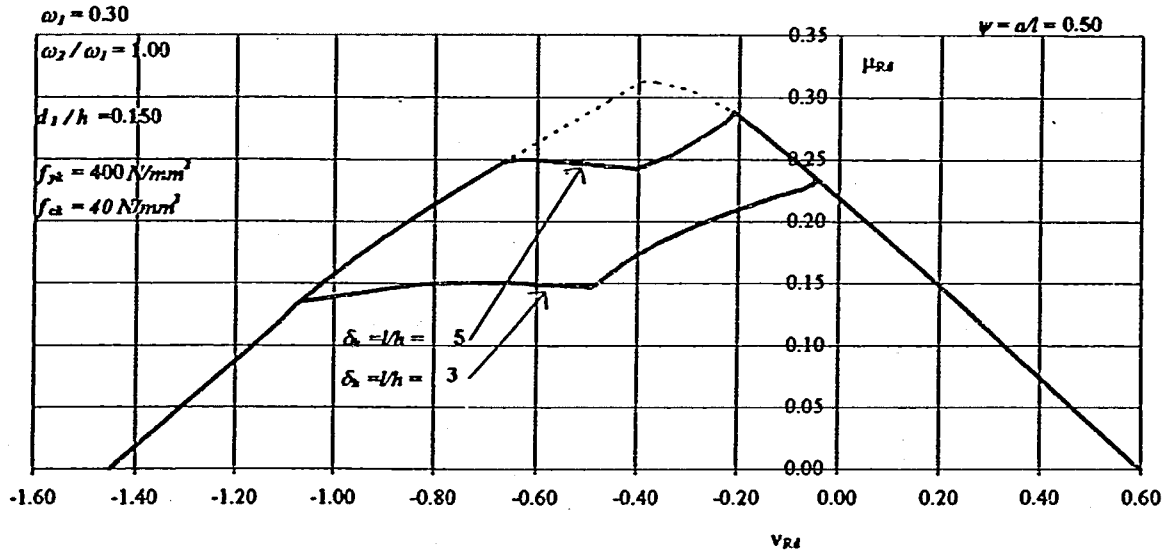


Fig. 8. M,N,V *interaction diagram for solid rectangular piers, plotted for* $\omega = 0.30$, $\psi = 0.50$ *and* $f_{ck} = 40$ Mpa.

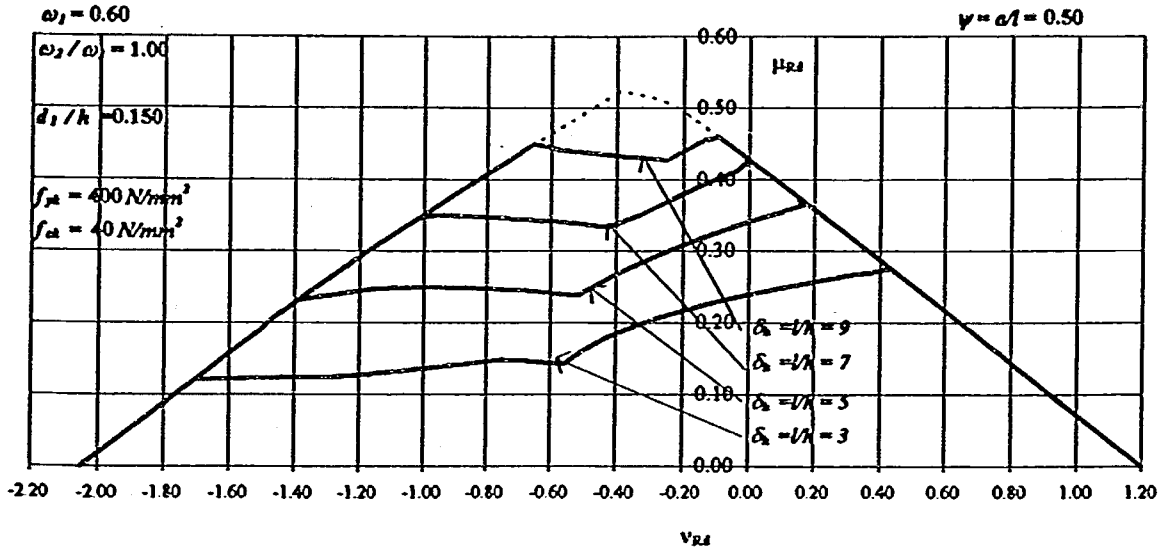


Fig. 9. M,N,V *interaction diagram for solid rectangular piers, plotted for* $\omega = 0.60$, $\psi = 0.50$ *and* $f_{ck} = 40$ MPa.

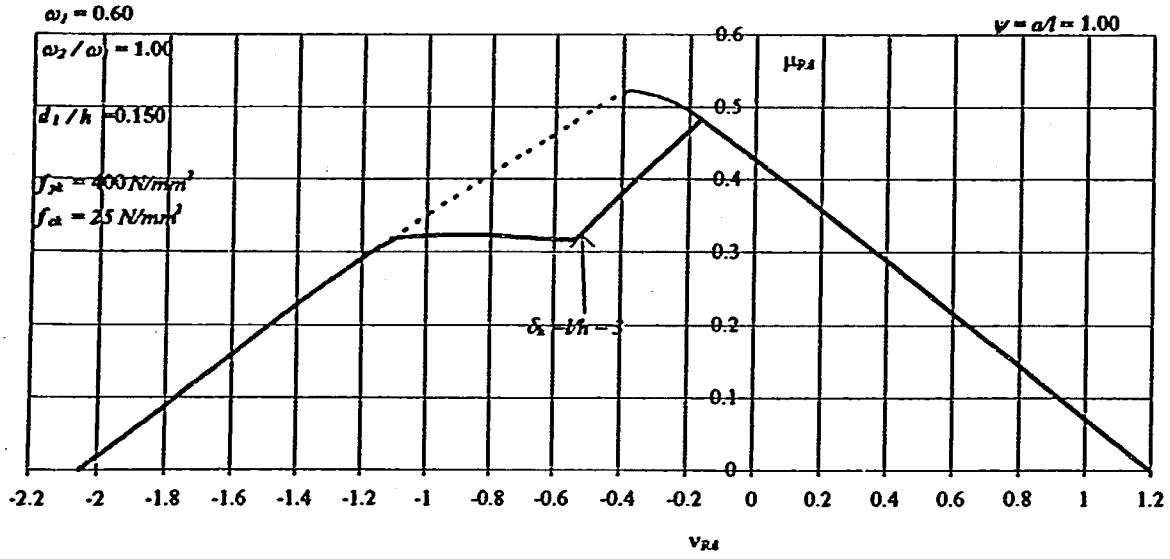


Fig.10. M,N,V *interaction diagram for solid rectangular piers, plotted for* $\omega = 0.60$, $\psi = 1.00$ *and* $f_{ck} = 25$ MPa.

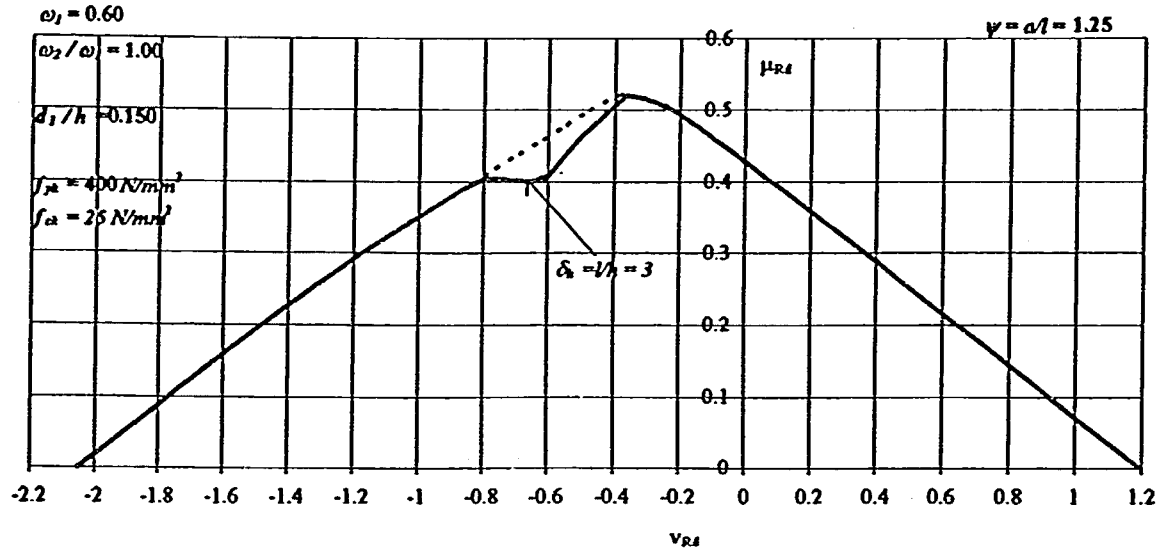


Fig.11. M,N,V *interaction diagram for solid rectangular piers, plotted for* $\omega = 0.60$, $\psi = 1.25$ *and* $f_{ck} = 25$MPa.

6. M,N,V INTERACTION IN BOXED RECTANGULAR PIERS

In this case it necessary to introduce the following additional variables:

- h_f: thickness of the rectangular pier walls parallel to the bending moment vector;
- b: total width of the section;
- b_w: total thickness of shear resistant walls;
- $\frac{A_c}{b_w h} = 2\frac{b}{b_w}\frac{h_f}{h} + 1 - 2\frac{h_f}{h}$: ratio between total area of the section and shear resistant area;

$$\nu_{sd} = \frac{N_{sd}}{A_c f_{cd}} \; ; \; \mu_{sd} = \frac{M_{sd}}{A_c h f_{cd}}$$

In non-dimensional terms, loading conditions will be:

$$\nu_{sd} = \frac{M_{sd}}{a b_w h \nu_2 f_{cd}} = \mu_{sda} \frac{Ac}{b_w h} \frac{1}{\Psi \delta_h \nu_2}$$

When compression is prevalent, the expressions of σ_{c1} and σ_{c2}, as given at point 4, are not modified.

When compression is not prevalent, instead, we get:

$$\sigma_1 = \nu_{cb} f_{cd}\left(1+\tan^2\gamma\right)\frac{Ac}{b_w h}$$

$$\sigma_2 = \frac{\left(\nu_{sd}\nu_2 - \nu_{cb}\tan\gamma A_c/b_w h\right)f_{cd}}{\sin\vartheta\cos\vartheta\ z/h} = \frac{\left(\mu_{sda}A_c/b_w h\Psi\delta_h - \nu_{cb}\tan\gamma A_c/b_w h\right)f_{cd}}{\sin\vartheta\cos\vartheta\ z/h}$$

By making the algebraic sum of the stresses, as in the previous case, we obtain:

$$\sigma_1+\sigma_2 = \frac{A_c}{b_w h} f_{cd}\left[\nu_{cb}\left(1+\tan^2\gamma\right)+\frac{\mu_{sda}/\Psi\delta_h - \nu_{cb}\tan\gamma}{\sin\vartheta\cos\vartheta z/h}\right]$$

and by imposing that the strength of the compression strut is reached for $\vartheta = 45°$, we find:

$$\nu_2 = \frac{A_c}{b_w h}\left[\nu_{cb}\left(1+\tan^2\gamma\right)+2\frac{\mu_{sda\,lim}/\Psi\delta_h - \nu_{cb}\tan\gamma}{z/h}\right]$$

from which we may determine the limit value of μ_{sdz}:

$$\mu_{sda\,lim} = \left(\frac{\nu_2}{A_c/b_w h} - \nu_{cb}\left(1+\tan^2\gamma\right)+\frac{2}{z/h}\nu_{cb}\tan\gamma\right)\Psi\delta_h z/2h$$

Now, by applying as above an iterative procedure, it is possible to identify the new boundary of the interaction domain, in the presence of M,N,V interaction.

7. EXAMPLES RELATING TO BOXED RECTANGULAR PIERS WITH NON-DIMENSIONAL SHEAR SPANS BETWEEN 1 AND 1.25

In this case again the M,N,V interaction diagrams are plotted, characterised by the following parameters:

Ψ	ω	f_{ck} (MPa)	h/h_f	b/b_w
1	0.3	25	10	10
1	0.6	25	10	10
1.25	0.3	25	10	10
1.25	0.6	25	10	10
1	0.3	25	10	5
1.25	0.3	25	10	5

Figs. 12 - 17 show these diagrams and the effects of the δ_h variable are also illustrated in each; the case with $\Psi = 0.5$ was not analysed, being deemed of little significance in relation to common pier types.

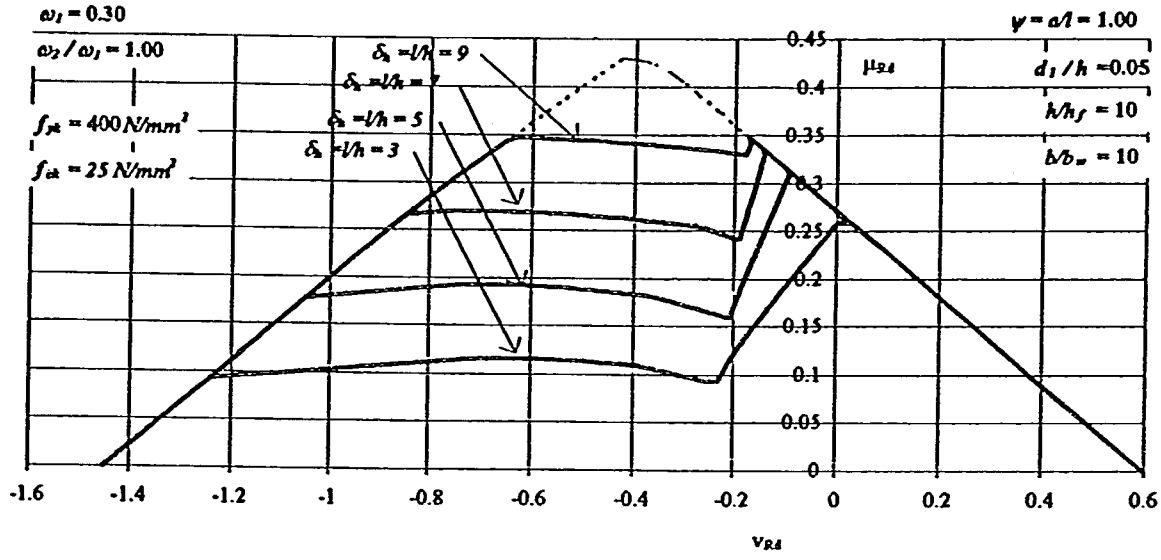


Fig. 12. M,N,V *interaction diagram for a boxed rectangular pier, plotted for* $\omega = 0.30$, $\psi = 1.00$ *and* $b / b_w = 10$.

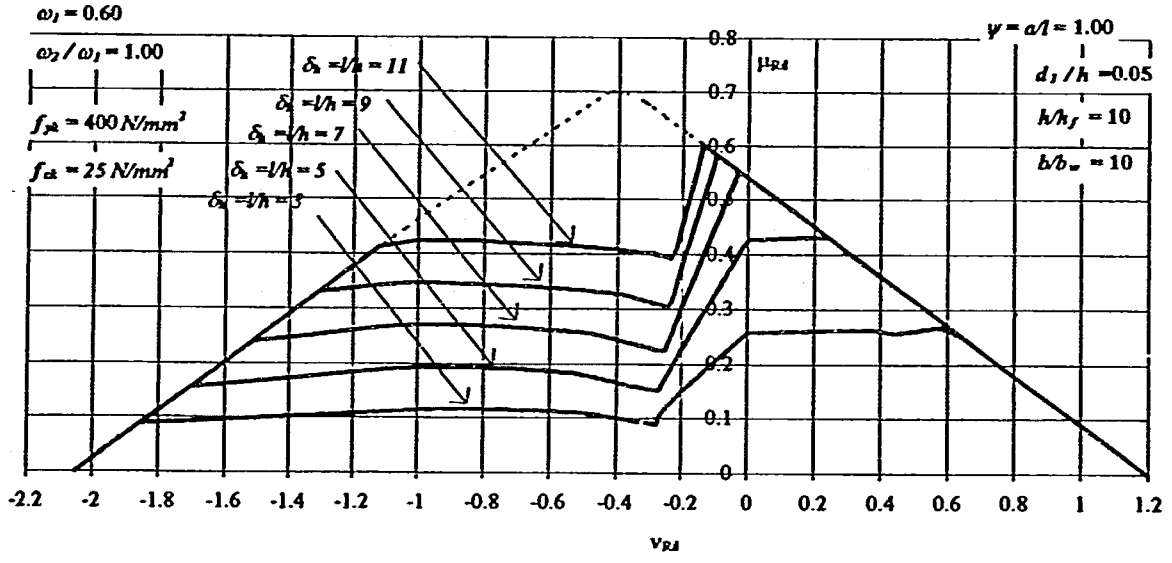


Fig.13. M,N,V *interaction diagram for a boxed rectangular pier, plotted for* $\omega = 0.60$, $\psi = 1.00$ *and* $b / b_w = 10$.

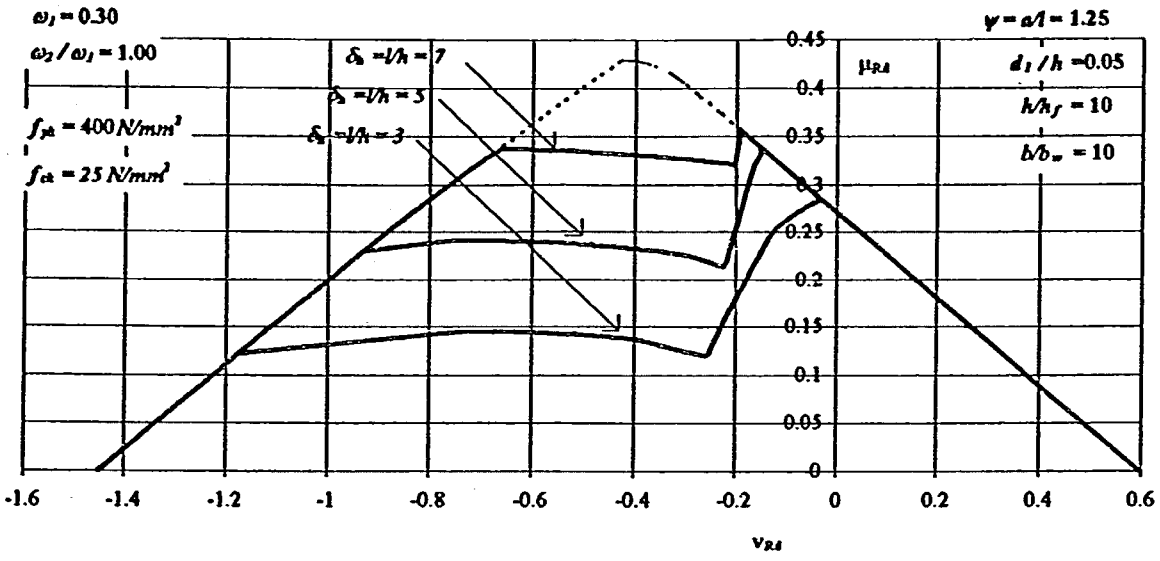


Fig.14. M,N,V *interaction diagram for a boxed rectangular pier, plotted for* $\omega = 0.30$, $\psi = 1.25$ and $b / b_w = 10$.

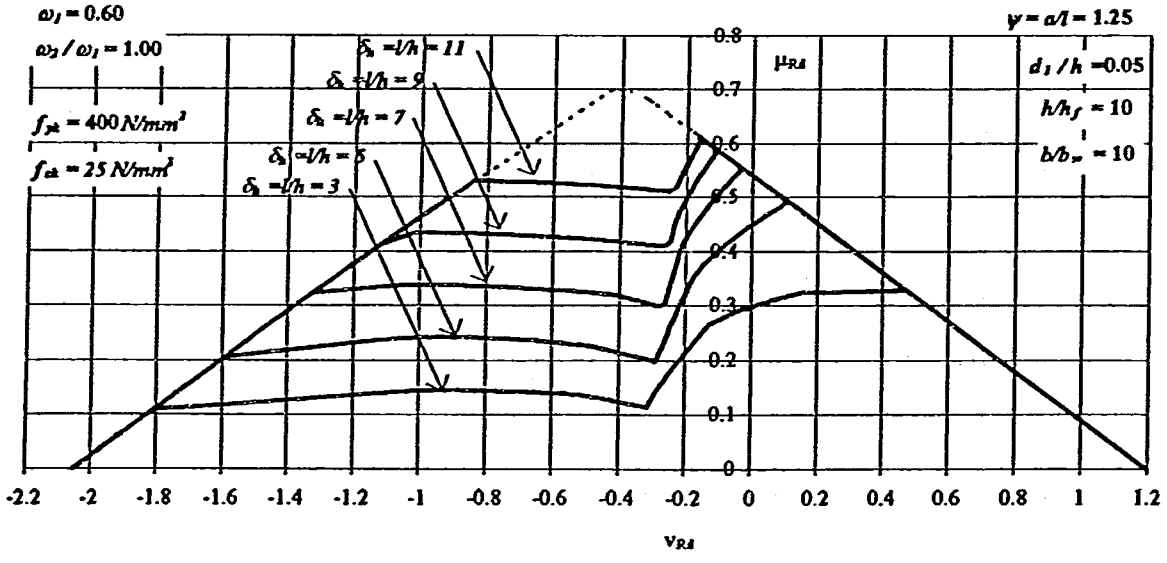


Fig. 15. M,N,V *interaction diagram for a boxed rectangular pier, plotted for* $\omega = 0.60$, $\psi = 1.25$ *and* $b / b_w = 10$.

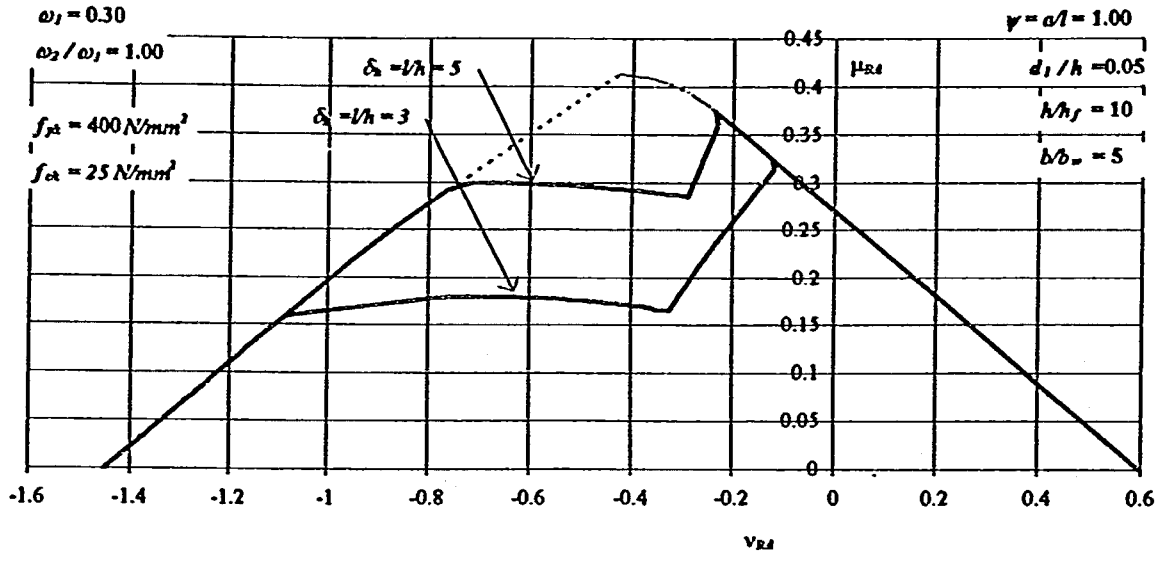


Fig. 16. M,N,V *interaction diagram for a boxed rectangular pier, plotted for* $\omega = 0.30$, $\psi = 1.00$ *and* $b / b_w = 5$.

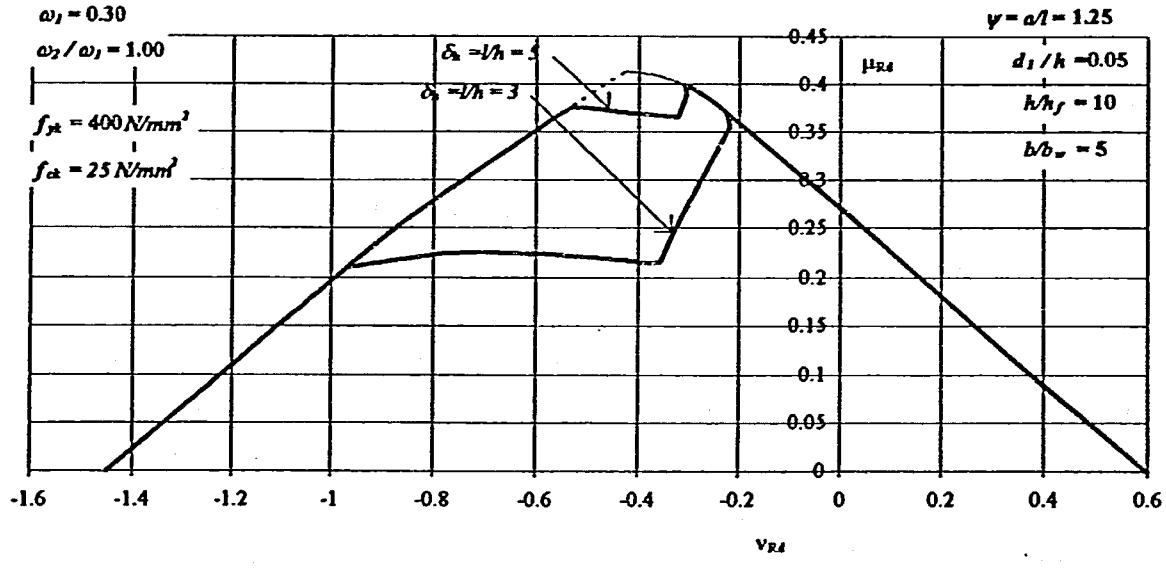


Fig. 17. M,N,V *interaction diagram for a boxed rectangular pier, plotted for* $\omega = 0.30$, $\psi = 1.25$ *and* $b / b_w = 5$.

From these figures it can be clearly seen that the effects of the M,N,V interaction is higher in boxed piers, compared to rectangular ones, due to need to concentrate in the webs the resultant of compressive forces in concrete coming from the outer zones of the section, of greater width. The influence of Ψ and ω parameters, as pointed out at point 5 above, is confirmed and it is easy to grasp the influence of the b/b_w variable: higher values of this parameter result in increased shear stresses and, obviously, entail a higher influence of shear on the M,N interaction diagram.

8. CONCLUSIONS

It is evident that high shear values, which certainly are present in combination with seismic actions, results in a marked reduction in the M,N interaction domains and hence makes independent design for normal and tangential forces unsafe. A correct design procedure must therefore take into account the M,N,V interaction between the three internal forces.

The basic parameters to be considered in order to define the magnitude of the interaction are: non-dimensional shear span (Ψ), mechanical rate of reinforcement (ω), pier slenderness δ_h, and, when dealing with boxed sections, the h/h_f and b/b_w parameters which define the section's geometry.

As mentioned above, the results obtained refer to the presence of monotone actions and therefore will have to be extended to the presence of cyclic action by introducing appropriate laws of material deterioration.

The results obtained confirm the indications given in [9] on the definition of the limit value of the M/Vh ratio for which the M,N,V interaction works.

REFERENCES

[1] Yamada, M. Furui, S.: "Shear Resistance and Explosive Cleavage Failure of Reinforced Concrete Members Subjected to Axial Load", Final Report, 8th Congress IABSE, New York, 1968, pp. 1091-1102.

[2] Yamada, M.: "Shear Strength Deformation and Explosion of Reinforced Concrete Short Columns", ACI SP42 "Shear in Reinforced Concrete", Detroit, V.2, 1974, pp. 617-638.

[3] Shohara, R., Kato, B.: "Ultimate Strength of Reinforced Concrete Members under Combined Loading", IABSE Colloquium "Advanced Mechanics in Reinforced Concrete", Delft, 1981, pp. 701-716.

[4] Minami, K., Wakabayashi, M.: "Rational Analysis of Shear in Reinforced Concrete Columns, IABSE Colloquium "Advanced Mechanics in Reinforced Concrete", Delft, 1981, pp. 603-614.

[5] Woodward, K. A., Jirsa, J. O., "Influence of Reinforcement on RC Short Column Resistance", Journal of Structural Engineering ASCE, V. 110, 1, 1984, pp. 90-104.

[6] König, G., Tang, S., Graham, C., "Untersuchung zum Nichtlinearen Verhalten von kurzen Stützen unter Erdbeben-Beanspruchung", Abschlussbericht, Institut für Bautechnik, Darmstadt, 1993.

[7] Kaneko, Y., Tanaka, Y., "Brittle Failure Criteria of Reinforced Concrete Short Columns Caused by Earthquake Loading", Proc. 7th World Conference on Earthquake Engineering, V. VII, Istanbul, 1980, pp. 565-568.

[8] Umehara, H., Jirsa, J. O., "Short Rectangular Reinforced Concrete Columns under Bidirectional Loading", Journal of Structural Engineering ASCE, V. 110, 3, 1984, pp. 605-618.

[9] CEB, Bulletin d'Information, No. 220, "Behaviour and Analysis of Reinforced Concrete Structures under Alternate Actions Inducing Inelastic Response", V. 2, May 1994, pp. 135-177.

[10] CEB-FIP, Model Code 1990, Bulletin d'Information No. 213/214, CEB, May 1993, pp. 165-167.

[11] Fanti. G., Mancini, G.: "Shear Prestressing Interaction in Ultimate Limit State Design", Developments in Short and Medium Span Bridge Engineering 94, Halifax, August 1994, pp. 617-628.

A FIBER MODEL FOR ELEMENTS UNDER CYCLIC BENDING AND SHEAR

M. Petrangeli P.E. Pinto

Department of Structural & Geotechnical Engineering
University of Rome "La Sapienza"

ABSTRACT

After a few years of successful application of the fiber beam element to the analysis of reinforced concrete structures, the introduction of the mechanisms of shear deformation and strength appears to be as the necessary further step towards a realistic description of the ultimate behaviour of shear sensitive structures.

The basic idea is to model the shear mechanism at each concrete fiber of a cross-section, assuming the strain field of the section as given by the superposition of the classical plane section hypothesis for the longitudinal strain field with a uniform distribution over the cross-section for the shear strain field. Transverse strains instead, are internal variables determined by imposing the equilibrium, separately at each fiber, between the concrete and the vertical steel reinforcement.
Since transverse strains components are not known in advance, and because of the non linear behaviour of the concrete and the steel, an iterative procedure is needed to find the equilibrium in the transverse direction.

In the paper the new approach to the shear modelling in nonlinear fiber beam elements is presented and the practical application to a 2D section is illustrated.

1. INTRODUCTION

When the shear span ratio is below 2, the behaviour of elements loaded monotonically to failure becomes brittle, due either to diagonal crushing of concrete in the web region and/or to the opening of wide inclined cracks.
Under cyclic loads, the mechanics of these short elements is such that they cannot be made acceptably ductile and dissipative by simply increasing the amount of lateral reinforcement, unless the longitudinal reinforcement and the axial force are also within proper, narrow, ranges.
The shear problem, however, tends to dominate the high cycle behaviour even for slender, essentially flexural, elements. One might not unreasonably state that ultimately all cyclic failures are shear failures, be that due to the disgregation of concrete within doubly diagonal cracks, or to the void between the two faces of large flexural cracks.

The reduction of shear capacity due to cyclic loading in the ductility range, as a function of the axial force, is now recognized, if in a crude manner, in the recent USA codes, the attention being called to the fact that the degraded shear strength must still be larger

than the flexural strength, if a premature shear failure has to be avoided.
The need for complete models, capable of describing the full range of behaviour of elements under axial force, bending and shear is particularly acute in earthquake engineering, where the design is purposely made for the limit state of collapse. Ideally, the analyses should be performed using realistically degrading and failing elements, so as to be able to monitor the response of the whole structure down to its final state. The lack of reliable elements of this type obscures our capability of judging whether a structure has failed or not, and it is among the major sources of error in the quantification of the design forces.

A state of the art on the available load deformation models for shear sensitive elements is included in a recent *CEB Bulletin* [1] where the following triple classification is proposed.

- *phenomenological models*, of the same type of those normally used for flexure, but with adjustable parameters so as to represent typical shear features.
- *composite models*, made up by superimposing independent models, both of empirical origin, for the shear and the flexural deformations
- *fundamental models*, attempting to capture, to varying degrees of accuracy, the mechanics of the phenomena. Only two models of this type are referenced in [1]. The one due to Bažant and Bhat [2] is the first to propose the introduction of diagonal cracking at each fiber of a fiber model, using a 3D constitutive law. The second one, due to Garstka et al. [3], superimposes a classical fiber model for the flexural deformations to a (hyperstatic, inelastic) truss model made up of longitudinal and transverse reinforcement and of a compression field in the concrete for the shear deformations.

The approach presented here moves along lines similar to those of Bažant and Bhat, with differences relating both to a few basic assumptions and to the algorithmic implementation.

1. BASIC ASSUMPTIONS OF THE MODEL

The proposed model has been developed bearing in mind its implementation in the existing fiber beam element as developed by the first writer in the last few years [4][5]. The section behaviour of this model is based on the plane section hypothesis without shear deformation. The triaxial stress state due to the confining effect of the stirrups can be taken into account in an approximate way via the calibration of the stress strain behaviour of each concrete fiber at the beginning of the analysis based on the amount of transverse reinforcement.
The model has proven its effectiveness in a number of applications to reinforced and prestressed concrete structures made up of essentially flexural elements [6]. The derivation of the element stiffness matrix is based on a flexibility approach where the forces along the element punctually satisfy the equilibrium and the sectional deformations are calculated from the corresponding forces via the section constitutive behaviour. The advantage of this approach over its alternatives lies in the capability of describing more accurately the highly non uniform distribution of the curvature occurring in the inelastic range, without the need for a refined meshing of the expected damage zones.
Although this element algorithm has proven to be very robust, its efficiency is certainly enhanced by the straightforward modelling adopted for the section behaviour, where the kinematics is predefined (i.e. plane section hypothesis). This philosophy has been retained when including the nonlinear shear modelling in the section behaviour, thus making

it possible a direct implementation of the new section subroutine and related material subroutines into the fiber beam element as it is.

In the extended model, the section strain field is based on the plane section hypothesis plus a uniform shear deformation over the section. The section strain and stress vectors are:

$$\epsilon = (\varepsilon_o \, \phi \, \varepsilon_{xy}) \tag{1}$$
$$\sigma = (N \, M \, T) \tag{2}$$

In the case of a two dimensional model, the strain field at each fiber as given by the section kinematic variables, Eq.(1), which in turn are the values of the element strain field at the Gauss's integration points, can be written:

$$\epsilon_x^i = \varepsilon_o - \phi y^i \tag{3}$$
$$\epsilon_{xy}^i = \varepsilon_{xy} \tag{4}$$

In ordinary beam theory, the strains in the transverse direction ϵ_y are neglected, since they are small and stresses-free. However, when inclined cracking due to the limited tensile strength of the concrete occurs, the unbalanced concrete stresses have to be balanced by the (transverse) steel reinforcement. The equilibrium condition allows the ϵ_y to be determined. This condition can be imposed according to two different criteria:
a) globally, referred to the whole height of the section, assuming ϵ_y as constant
b) locally, at all fibers into which the section is decomposed
The advantage of a) is self evident, although not substantial, since it simplifies, by using a single internal variable, the description of the vertical strain field. It is the criterion adopted in [2]. Physically, however, option a) makes little sense, since the combination of the longitudinal strains ϵ_x, which normally vary from compression to tension along the section height, with the shear strains ϵ_{xy} is such as to produce significant gradients of ϵ_y. Under this point of view, option b) seems more appropriate since the equilibrium in the transverse direction must be satisfied at each fiber according to the predominant deformations along the element axis (ϵ_x). This choice obviously implies the assumption of perfect bond between concrete and stirrups.
Incidentally, option b) is also better from a computational point of view since the iterations are carried out separately, at each fiber, according to the degree of non linearity of the fiber behaviour. Therefore the total number of fiber state determinations are reduced to a minimum avoiding to iterate on the whole section when highly non linear behaviour only takes place in few fibers. It must be pointed out that in this kind of models the bulk of the computational demand is in the fiber state determinations (i.e. constitutive behaviour monitoring) and that each equilibrium iteration using a section deformation variable, as in option a), automatically implies the state determination of all the fibers in the section.
According to option b), the proposed model must satisfy at each fiber the following equation:

$$\sigma_{y,c}^i A_{y,c}^i + \sigma_{y,s}^i A_{y,s}^i = 0 \tag{5}$$

where $\sigma_{y,c}^i = \sigma(\epsilon_x^i \, \epsilon_y^i \, \epsilon_{xy}^i)$ is the concrete stress in the transverse direction at fiber i, $\sigma_{y,s}^i = \sigma(\epsilon_y)$ is the stress in the stirrup at the same fiber and $A_{y,c}^i$, $A_{y,s}^i$ are their respective areas in the same direction.

In each equilibrium iteration, ϵ_x^i and ϵ_{xy}^i are constant since are defined based on the element strain field values at the given section while ϵ_y^i is the only unknown of the problem.
It can be noted that this approach gives the possibility of specifying a different 'effective' transverse steel area for each fiber depending upon the stirrup configuration. For example, the concrete cover can be modelled without confinement and also inside the core different confinements can be specified for different fibers.

3. CONSTITUTIVE BEHAVIOURS

Where the major difference with the purely flexural fiber beam element comes in is with the fiber constitutive behaviour for concrete. While the behaviour of the longitudinal and transverse steel is still uniaxial as it is the longitudinal steel in the previous fiber model, the concrete behaviour must now be of the 3-dimensional type.
And while the 1D modelling of concrete behaviour for general loading histories is well established, 3D models covering the entire range of the response, including tension, for general non proportional loading, are still basically research proposals, not ready for consistent practical implementation.

Another difference with the previous fiber element is that modelling of shear deformation requires a much more accurate description of the quasi-brittle tensile part of the concrete behaviour.
In the flexural fiber element, this contribution to the section stiffness, although important in principle, practically becomes negligible under large alternate bending with fully cracked section and can be accounted for via a simplified energy approach (i.e. tension stiffening) in the uncracked-cracked transition.
In this new model instead, where the shear stiffness and strength are given by the integral of the contribution of each concrete fiber, the importance of the tensile fracture mechanism is obviously of greater importance. This problem does not exist in the so called strut and tie or truss models where only the compressive concrete strut needs to be modelled [3] while the tensile part is carried by the steel tie.

For this initial implementation, a very simple concrete constitutive behaviour has been chosen, leaving open the possibility of installing other concrete models in the future.
The model adopted is of the incrementally linear (hypoelastic) type, known as equivalent uniaxial [7][8]. In this model the full matrix D, relating the stress increments along the principal axes to the corresponding strain increments, is replaced by a diagonal matrix (i.e. each $d\sigma_i$ depends on the corresponding $d\epsilon_i$ only) but with the strains $d\epsilon_i$ now being "equivalent" ones, in the sense that each one is a function of all the strain increments. The (tangent) modulus E_i relating $d\sigma_i$ with $d\epsilon_i$ is assumed to be given by a uniaxial (nonlinear) stress strain law, whose parameters are however functions of the current stress state. The expression adopted for E_i is given for example in [8] and need not to be repeated here.
The equivalent uniaxial strains depend on the Poisson ratio ν_i, for which appropriate dependency on the actual strain state must also be specified. The particular choice made in this study is discussed later.
Overall, the law adopted for the concrete is rather crude, since one cannot expect to be able to describe realistically all the complex phenomena occurring in a 3D continuum in the post elastic range by simply adjusting the values of the elastic parameters E_i and ν_i.
The use of relatively unsophisticated constitutive relationships, however, is justified both by the nature of the problem and by the way it is treated in the present approach. Regarding the nature, it is worth noting that the degree of interaction between the behaviours in the two orthogonal directions (the problem is essentially 2D) is either weak or altogether unexisting for the cases of tension-compression and tension-tension, respectively.

For compression-compression, the effect of the interaction is not essential since the problem is dominated by the longitudinal stresses; the behaviour in the other directions is basically a response to the applied longitudinal history according to the amount of transverse reinforcement steel. The second aspect relates to the kinematic constraint used at the section level, which apply to the ϵ_x and to the ϵ_{xy}, but not to the ϵ_y. In other words, the model does not impose continuity of the ϵ_y field across the fibers, and this limitation obviously reduces the interest for a very accurate constitutive law.

In the 2-dimensional case the equivalent strains at each fiber i are defined as follows:

$$\varepsilon^i_{1,eq} = \epsilon^i_1 + \nu^i_{12}\,\epsilon^i_2 \tag{6}$$

$$\varepsilon^i_{2,eq} = \epsilon^i_2 + \nu^i_{21}\,\epsilon^i_1 \tag{7}$$

The two Poisson's coefficients are a function of the stress-strain state and starting with the elastic value in the undamaged-uncracked region, change considerably when cracking or large compressive strains take place.
According to the previous remark on the interaction between the stresses on the principal (orthogonal) axes, also the Poisson's coefficients can be written with a good approximation as a function of the damage in one direction only. Therefore the following monotonic envelopes have been used where the Poisson's coefficients are a function of the corresponding equivalent strains:

$$\varepsilon^i_{j,eq} \geq 0 \qquad \nu^i_{ij} = \nu_{el}\, exp - (\varepsilon^i_{j,eq}/AA)^{E1} \tag{8}$$

$$\varepsilon^i_{j,eq} \leq 0 \qquad \nu^i_{ij} = \nu_{el} + (0.5 - \nu_{el}) exp - (\varepsilon^i_{j,eq}/BB)^{E2} \tag{9}$$

In the above equation, there are four parameters AA BB E1 and E2 plus the elastic Poisson's coefficient ν_{el}. A plot of these curves can be found in *Fig.1*. The curve shows the well known phenomena of large dilatancy at large compressive strains in the post peak behaviour of concrete, and the vanishing of any Poisson effect in the directions perpendicular to the crack plane (stress release).
Once the equivalent strains are known via Eq.(6)(7) and (8)(9) the stresses in the principal directions can be found using the uniaxial stress strain law.

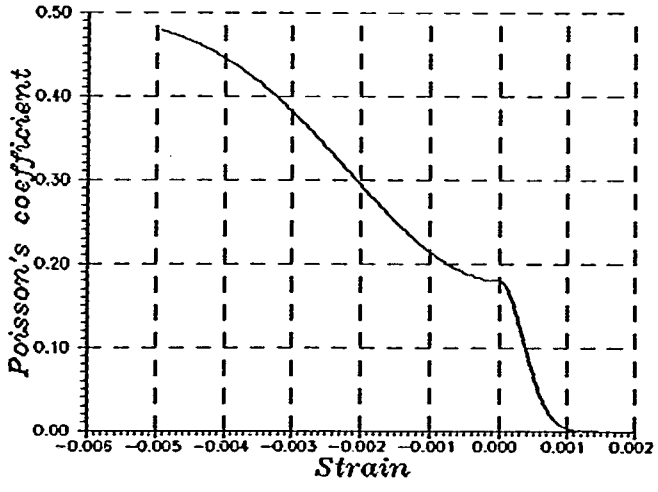


Fig.1 Poisson's coefficient in uniaxial loading

This law, together with the one used for the longitudinal and transverse steel, is plotted in *Fig.2* and *Fig.3*. Once the concrete stresses along the principal strain directions are known, the stresses in the longitudinal and transverse directions can be found via standard tensorial transformations. The same can be said for the material stiffness matrix which is written in the principal directions based on the tangent modulus of the uniaxial stress strain law and therefore reads:

$$\mathrm{D}^i = \begin{bmatrix} E_1^i & \nu_{12} E_2^i & 0 \\ (\nu_{21} E_1^i & E_2^i & 0 \\ 0 & 0 & \frac{E_1^i + E_2^i}{4}\left(1. - \frac{\nu_{12}^i + \nu_{21}^i}{2}\right) \end{bmatrix} \tag{10}$$

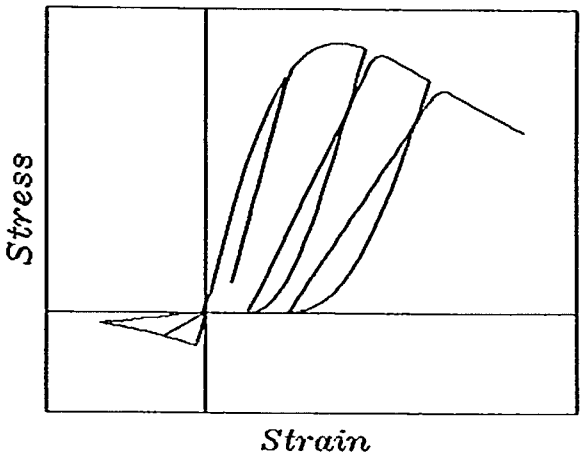


Fig.2 Concrete uniaxial behaviour

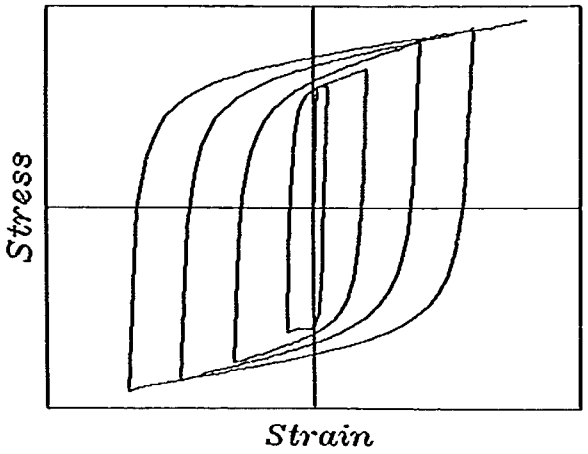


Fig.3 Steel stress strain law

Where E_1^i and E_2^i are the tangent Young's moduli along the principal directions at fiber i as found with the equivalent uniaxial stress strain law. It should be noted that the shear stiffness is not an outcome of the material behaviour but is defined as for an equivalent elastic material without dilatancy (i.e. coupling terms D_{13} and D_{23} are set to zero.)
Once matrix D^i has been transformed in the global reference system Eq.(5) can be linearized and satisfied via a standard iterative procedure as a nested loop inside each load increment:

$$\left(D_{21}^i \Delta\epsilon_x^i + D_{22}^i \Delta\epsilon_y^i + D_{23}^i \Delta\epsilon_{xy}^i\right) A_{y,c}^i + E_{y,s}^i \Delta\epsilon_y^i A_{y,s}^i = 0 \tag{11}$$

where the D_{rs}^i are the elements of the transformed D^i matrix.

4. SECTION FORCES AND STIFFNESS

Once the equilibrium in the transverse direction at each fiber is achieved, the section forces and stiffness can be found via the summation over the section of the concrete and longitudinal steel fiber contributions. For a given load step the resulting axial, bending and shear force increments can be found as follows:

$$\Delta N = \sum_{i=1}^{nc} \Delta\sigma_{x,c}^i A_{x,c}^i + \sum_{j=1}^{ns} \Delta\sigma_{x,s}^j A_{x,s}^j \tag{12}$$

$$\Delta M = \sum_{i=1}^{nc} \Delta\sigma_{x,c}^i A_{x,c}^i Y_c^i + \sum_{j=1}^{ns} \Delta\sigma_{x,s}^j A_{x,s}^j Y_s^j \tag{13}$$

$$\Delta T = \sum_{i=1}^{nc} \Delta\sigma_{xy,c}^i A_{x,c}^i \tag{14}$$

where $A^i_{x,c}$ and $A^j_{x,s}$ are the areas of the ith concrete fiber and j^{th} steel fiber in the longitudinal direction (parallel to the beam axis) and Y^i_c, Y^j_s are the distances of them from the centroid of the beam section.
It is noted that in this initial investigation the contribution of the longitudinal steel to the shear force and stiffness has been neglected although for large deformation the so called "dowel action" may not be negligible.

When assembling the section stiffness matrix, the concrete fiber stiffness must take into account the stiffening effect of the confining transverse steel. This is achieved via a static condensation of the internal degree of freedom in the transverse (Y) direction. Calling α^i the following transverse reinforcement ratio:

$$\alpha^i = \frac{A^i_{y,c}}{E^i_{y,s}A^i_{y,s} + D^i_{22}A^i_{y,c}} \tag{15}$$

the axial and shear stiffness of the fiber can be written as follows:

$$K^i_a = \left(D^i_{11} - D^i_{12}D^i_{21}\alpha^i\right) A^i_{x,c} \tag{16}$$

$$K^i_s = \left(D^i_{33} - D^i_{23}D^i_{32}\alpha^i\right) A^i_{x,c} \tag{17}$$

The section stiffness matrix is found by summation of each fiber contribution as for the section force:

$$\mathrm{K}_{11} = \sum_{1}^{nc} K^i_a + \sum_{j=1}^{ns} E^j_{x,s}A^j_{x,s} \tag{18}$$

$$\mathrm{K}_{12} = \sum_{i=1}^{nc} K^i_a Y^i_c + \sum_{j=1}^{ns} E^j_{x,s}A^j_{x,s}Y^j_s \tag{19}$$

$$\mathrm{K}_{22} = \sum_{i=1}^{nc} K^i_a Y^i_c Y^i_c + \sum_{j=1}^{ns} E^j_{x,s}A^j_{x,s}Y^j_s Y^j_s \tag{20}$$

$$\mathrm{K}_{33} = \sum_{i=1}^{nc} K^i_s \tag{21}$$

5. NUMERICAL IMPLEMENTATION AND EXAMPLES

The concepts discussed thus far have been implemented in a fiber section program with a structure very similar to the section subroutine used in the above mentioned 2D fiber beam element. Although a 3D fiber beam element is currently used, the implementation of this new shear modelling in this element may be computationally too demanding on standard PC based machines, and therefore this initial investigation has been limited to the 2D case. Preliminary tests have shown a factor of 5 to 10, depending on the complexity of the triaxial concrete constitutive behaviour adopted, in the computational demand between the old flexural model and the new one.

This section program takes as input, in addition to all the data needed to define the section geometry and the material behaviour, the axial force, the bending-shear ratio and the curvature history.
The analysis is then carried out checking the internal equilibrium at each fiber between the concrete and the steel in the transverse direction, and the global equilibrium for the axial force and the bending-shear ratio.

The numerical examples have been carried out on a typical reinforced concrete column $1m$ high with a square cross section of $0.25m^2$. Longitudinal reinforcement is made of $8\phi 24mm$ bars evenly distributed around the perimeter giving a reinforcement ratio of 1.45%. Two transverse reinforcement configurations have been used, $\phi 10mm$ stirrups at $67mm$ spacing for a total area per metre of $2360mm^2$ and $\phi 8mm$ stirrups at $67mm$ spacing for a total area per metre of $1508mm^2$.
The following values have been used for the concrete: cubic compressive strength $30MPa$, strain at peak 0.002, tensile strength $2.5MPa$, fracture energy $0.1kN/m$, Young's Modulus $30000MPa$, while for the longitudinal steel the characteristics are: yield stress $240MPa$, ultimate stress $380MPa$, strain at peak 0.12, strain at commencement of hardening 0.008, Young's modulus $200000MPa$.
The steel used for the stirrups has a simplified bilinear behaviour, with a hardening branch going from the yield point to the ultimate strength point. Unloading and reloading branches are elastic. Material properties are the same as for the longitudinal one.

Examples of the response of the element under imposed cyclic curvature history are shown in *Figs. 4, 5, 6* which refer to axial force ratios of 0, 0.1, 0.2 respectively.
In each of the Figures, *a)* shows the moment - curvature response, *b)* the shear force - shear strain response for the two different transverse reinforcement cofigurations, and *c)* the force - displacement relationship at the top of the column with and without shear deformation (dashed lines) for the $\phi 8mm$ stirrups arrangement. This force - displacement relationship is obtained by means of a simplified integration of the section deformations along the height. Ignoring the elastic deformation, and calling L the column length, and l_h the length of the plastic hinge, the displacement at the top is given by the expression: $V_c = (L - l_h/2)\phi l_h + l_h\varepsilon_{xy}$. In the curve without shear deformation only the first term on the right hand side has been considered. In the plots, $l_h = 0.5m$ has been assumed.
The moment - curvature curves in Figs. 4, 5 and 6 show the familiar traits of the cyclic flexural response under zero and increasing axial force. The influence of shear in these diagrams is negligible: for it to be discernible still shorter elements and higher axial forces would be required.
The T - ε_{xy} diagrams are much less familiar, since experimental results where the shear response is separated from the flexural one are rare (cfr. [9]). A number of features which can be anticipated on physical grounds with reference to simple mechanical idealizations do actually show up in the diagrams of Figs. *b)*.
One might start by noting the high stiffness in shear of the sections before the occurrence of cracking. Then, the enhancement of the shear strength with increasing axial force. One has in fact:

Axial Force (kN)	Shear Strength (kN)
0	240
750	370 (240 + 130)
1500	490 (240 + 250)

Where it can be noted how the increase in shear strength varies proportionally with N, and it is quite close to the figure $0.15N$ which is suggested in a number of codes, notably the Eurocode 2.

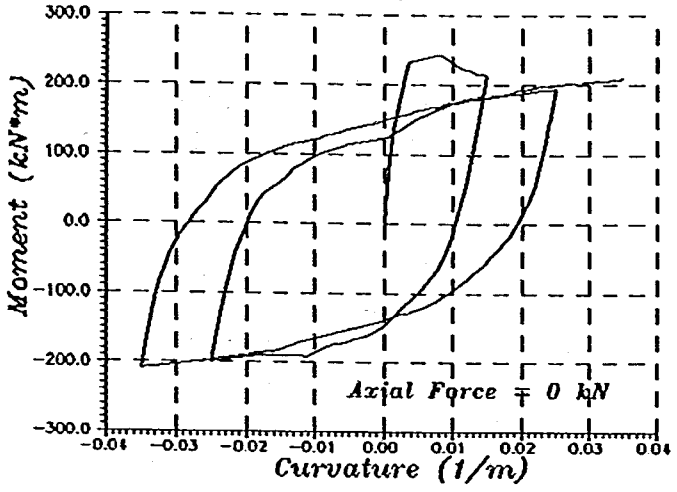


Fig.4a Moment curvature response. N = 0

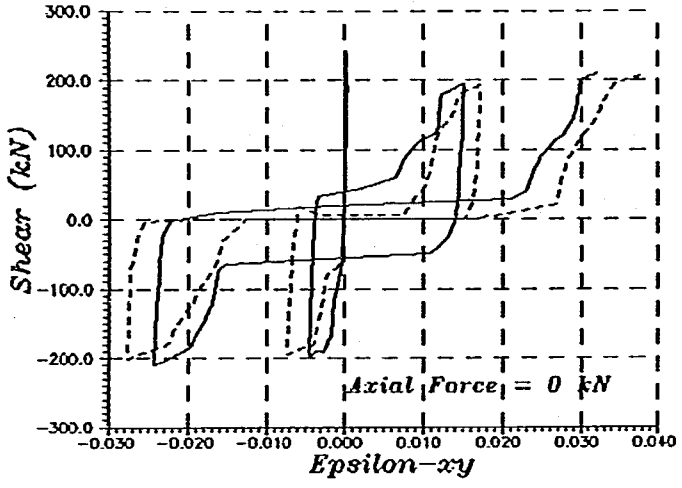


Fig.4b Shear Force - Shear Strain response. N = 0

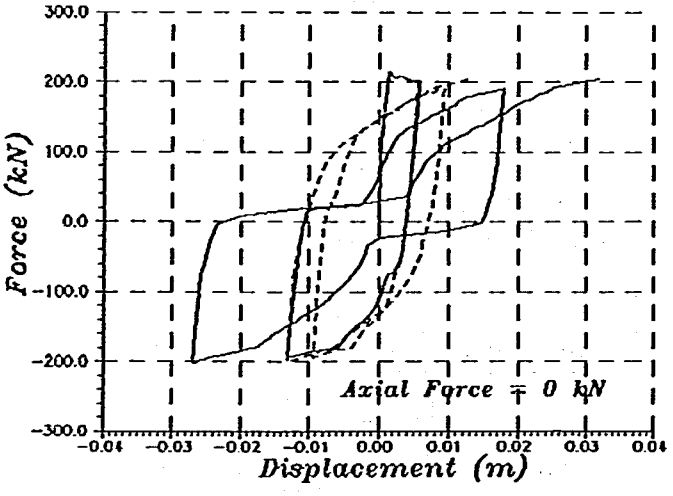


Fig.4c Force Displacement response. N = 0

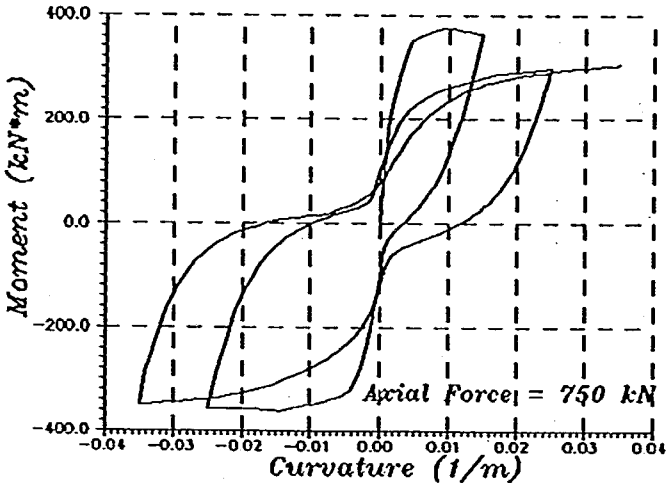


Fig.5a Moment curvature response. N = 750 kN

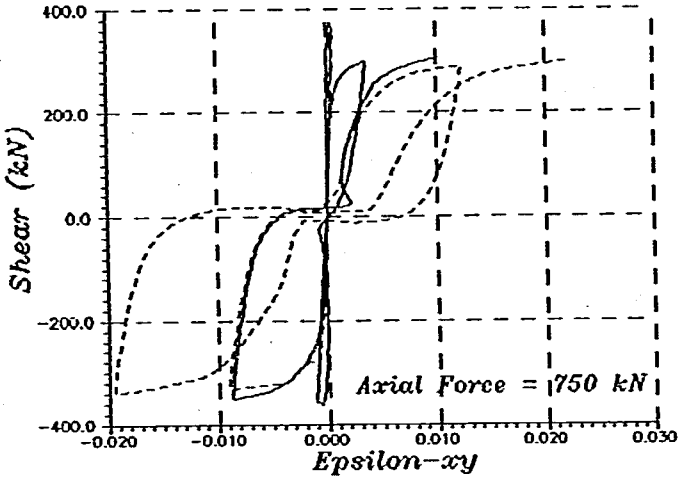


Fig.5b Shear Force - Shear Strain response. N = 750 kN

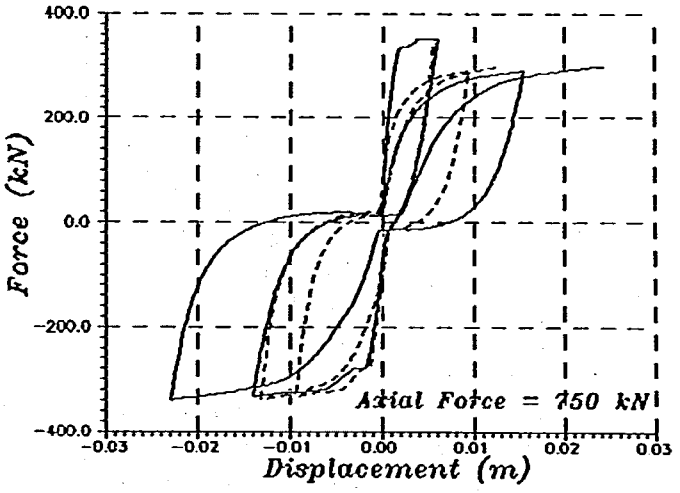


Fig.5c Force Displacement response. N = 750 kN

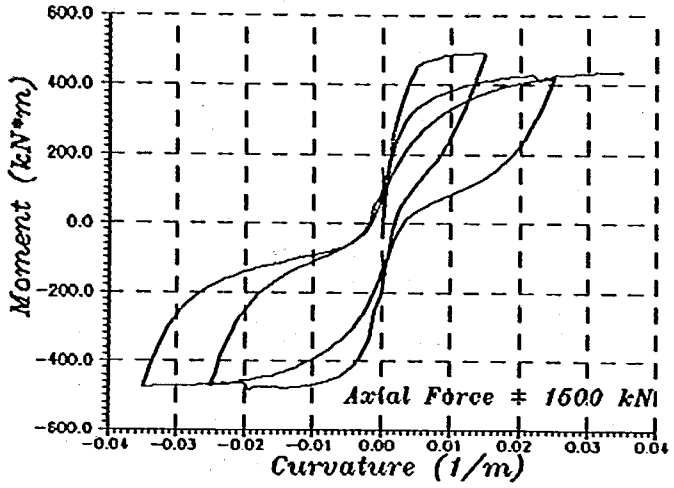


Fig.6a Moment curvature response. N = 1500 kN

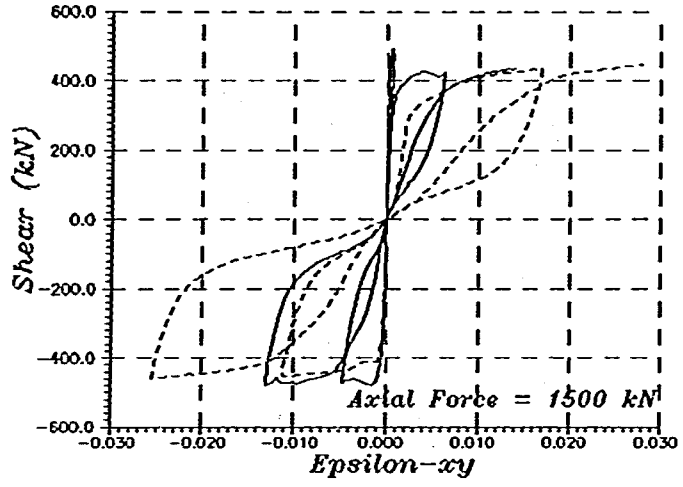


Fig.6b Shear Force - Shear Strain response. N = 1500 kN

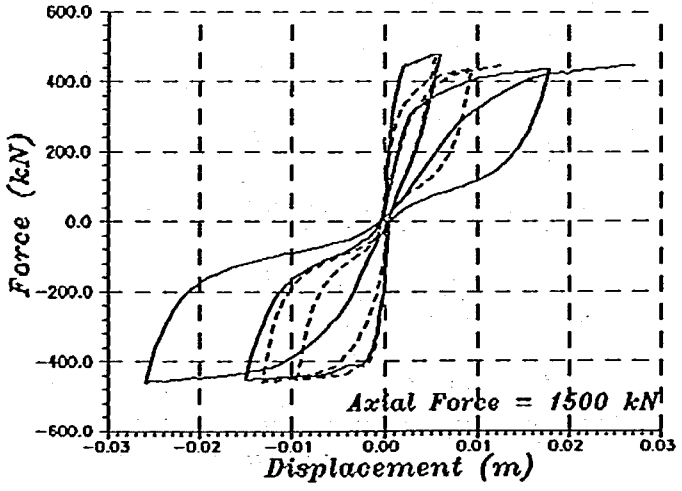


Fig.6c Force Displacement response. N = 1500 kN

Only after yielding in shear takes place the amount of transverse reinforcement starts influencing the response, in a way which depends on the magnitude of the axial force.

For $N = 0$, the response is dominated by the mechanism of diagonal crack opening and closing, with almost zero stiffness during load reversal and little influence of the amount of the stirrups. A similar behaviour could be obtained for an inelastic hysteretic truss made of two inclined concrete struts (acting alternately in tension and compression) and a steel tie, subjected to reversed shear. The zero stiffness portion is the interval between the unloading of the strut in compression and the loading (in compression) of the other strut cracked in tension. This loading takes place for a deformation larger than the one reached in the previous half cycle, due to the residual strains accumulated in the stirrups (i.e. the steel kinematic hardening). On this respect, it should be also pointed out that the present concrete model does not have a realistic hysteretic behaviour in tension (unloading and reloading branches are secant to the origin), especially for the transition branch at the origin (crack bridging).

With higher values of N, the phenomenon of loss of stiffness upon reversal is less pronounced, and it almost disappears for $N = 1500kN$. This type of behaviour also could be reproduced with the above mentioned truss system, since the presence of the normal force reduces the slack due to the residual (zero force) deformations.
There are two additional aspects to be noted as regards the effect of the axial force: the considerable increase in the overall stiffness and the sensitivity of the deformations to the amount of transverse reinforcement, once yielding in the steel has occurred. Both of these results are intuitively acceptable, although presently they cannot be supported with experimental observations.

The combined flexural - shear response is shown in the Figs.*c)* for the $\phi 8mm$ stirrups arrangement. For $N = 0$ the contribution of the shear deformation after yielding of steel is greater than the flexural one and it has a different mechanism therefore the shape of the diagrams is considerably affected. For $N = 750kN$ and $1500kN$ instead, although the contribution is still significant, the shape of the diagram is less affected since the section shear force deformation response is more similar to the flexural one.
It must be noted that the contribution of the shear deformations using the $\phi 10mm$ stirrups is much smaller, especially for the case of $N = 750kN$ and $1500kN$.

An interesting feature of the global response which is due to the shear behaviour is the degradation of the mechanical properties of the sections which the pure flexural model was not able to reproduce. Figs.*c)* show clearly how the shear contribution to the global deformation tends to increase with increasing cycles, which means that the shear behaviour is subjected to a stronger degradation than the flexural one, especially for high axial forces and inadequate confinement.

6. CONCLUSION

An attempt is made to account for shear-induced cracking and the action of transverse reinforcement to determine the contribution of shear to sectional deformability in a reinforced concrete element. The section deformation variables, ε_o , ϕ and ε_{xy} determined from the strain state along the beam longitudinal axis, are used to define the fiber strain state using the classical plane section hypothesis with the additional assumption of a uniform distribution of the shear strain ϵ_{xy} along the height of the section. No kinematic constraint is considered for the vertical deformations ϵ_y, which are found based on the equilibrium with the transverse reinforcement at each fiber, therefore no transmission of vertical stresses σ_y between adjacent fibers is considered.

A few preliminary applications of the model have been presented, for a section under a constant value of the axial force and cyclically varying M and T, for different amounts of transverse reinforcement. Although no comparison with experiments is available, the analyses yield results which are reasonable and consistent with the variation of the parameters.

Once the shear section model will have been introduced into the existing flexural element model, which is quite a straightforward task, it will be possible to perform analyses on sub-assemblages and on complete structures, so as to better calibrate the model and understand its limits Actually, although much more complicated than the classical fiber model without shear flexibility, the proposed approach still retains the basic limitation which are intrinsic to the beam theory. It is, however, believed to represent a step forward with respect to the current models based on truss and strut and tie analogies which, apart from their grossly idealized mechanics, cannot account on physical bases of the interaction between flexural and shear responses.

REFERENCES

[1] CEB (1994). *Behaviour and Analysis of Reinforced Concrete Structures under Alternate Actions Inducing Inelastic Response.* Vol.2: Frame Members(*). Bull. d'Inf. N. 220.
(*) *Chpt.2 Frame Members in Flexure and Axial Force with High Shear.*

[2] Z. Bažant and P.D. Bhat (1977). *Prediction of Hysteresis of Reinforced Concrete Members.* J. Struct. Div., ASCE, Vol.103, pp.153,166.

[3] B.Garstka, W.B. Krätzig and F.Stangenberg (1993). *Damage assessment in cyclically loaded reinforced concrete members.* Structural Dynamics, EURODYN' 93, Moan Ed., Balkema, Rotterdam. Vol.1, pp.121-128.

[4] M.Petrangeli (1991). *Un elemento finito di trave non lineare per strutture in cemento armato.* Tesi di laurea. University of Rome, Italy (in italian).

[5] Petrangeli M., Ciampi V., *A flexibility based 3-dimensional fiber beam element.* VIII Convegno Italiano di Meccanica Computazionale, Torino 15-17 Giugno 1994.

[6] M. Petrangeli and P.E. Pinto (1994) *Example A. Modern multispan bridge seismic response and assessment. Nonlinear and Linear models.* 2ND Int. Workshop on Seismic design of bridges, Queenstown, New Zealand.

[7] D. Darwin and D.A. Pecknold (1977). *Nonlinear Biaxial Stress Strain Law for Concret.* J. Eng. Mech., ASCE, Vol.103, pp.229-241.

[8] A.A. Elwi and D.W. Murray (1979). *A 3D Hypoelastic Concrete Constitutive Relationship.* J. Eng. Mech., ASCE, Vol.105, pp.623-641.

[9] J.B. Mander, S.M. Waheed, M.T.A. Chaudhary and S.S. Chen (1993). *Seismic Performance of Shear-Critical Reinforced Concrete Bridge Piers.* Technical Report NCEER-93-0010, Buffalo, New York 14260.

DISPLACEMENT BASED SEISMIC DESIGN OF MULTI-DEGREE-OF-FREEDOM BRIDGE STRUCTURES

G.M. Calvi, Associate Professor, Dipartimento di Meccanica Strutturale, Università degli Studi di Pavia, Via Abbiategrasso 211, 27100 Pavia, Italia

G.R. Kingsley, Senior Engineer, Atkinson-Noland and Associates, 2619 Spruce St., Boulder Colorado, 80302 USA.

ABSTRACT

The concept of displacement-based design is attractive for seismic design, primarily because it places the focus of design directly on displacement demand, and hence damage, rather than on force-reduction or behavior factors. A procedure is presented which extends the simple concept of displacement-based design to complex multi-degree-of-freedom (MDOF) bridge structures.

The procedure is based on the assumption of a displaced shape for the structure, and the subsequent reduction of the system to an equivalent single-degree-of-freedom (SDOF) system.

The process is shown to work well for the design of a symmetrical bridge, while suffering some shortcomings when applied to a highly irregular bridge. The topic of design-oriented displacement response spectra is also briefly addressed.

1. INTRODUCTION

There has been growing interest recently in the development of displacement based seismic design (DBD) procedures for RC structures [1,2]. This has stemmed partly from the recognition that, under seismic actions, displacements provide a more fundamental expression of structural response than forces, and that the structural design process should be oriented accordingly.

Since structural damage can be considered to be directly related to displacement demands, it can be controlled most efficiently through the imposition of displacement (or drift) limits rather than strength limits. In the force/strength-based design procedure, however, displacement limits are checked near the end of the design process for serviceability limits, or are considered in terms of ductility demands which are treated indirectly through the use of "behavior factors" or "response coefficients" that modify design forces. Placing design priority on the displacements first, with checks on strength at the end, allows for a much more consistent consideration of damage. Furthermore, displacement-based design offers the ability to explicitly control the displacement demand in each member rather than assigning a single, force-based behavior factor to the entire structure.

---

* Note: This paper is in course of publication by Earthquake Engineering and Structural Dynamics

The fundamental conceptual shift required in switching from a force-based to a displacement-based design approach has been presented in a companion paper by Kowalsky et al. [8] for the case of a single degree-of-freedom (SDOF) bridge pier structure. In summary, in a traditional force-based design the period of vibration of a structure is estimated (or calculated based on previous trial design), and a design acceleration response spectra is entered to determine, for a given level of damping, what the elastic force demand on the structure will be. Alternatively, the required displacement capacity for the structure can be specified, and the displacement response spectra consulted to determine the required period of vibration (stiffness) necessary to achieve it. In this manner, strength and stiffness become end-products of the design rather than primary design goals. For simple SDOF structures, the process outlined by Kowalsky et al. has been applied successfully to bridge piers over a range of possible desing parameters. However, application of the method to more complex MDOF structural systems is not necessarily straight forward, and requires some additional steps. In this paper, the DBD method described in the companion paper [8] is extended to the special case of MDOF bridge structures.

The first consideration, applicable to both SDOF and MDOF structures, is the establishment of appropriate design spectra for displacements, as discussed briefly below. The second requirement is the development of an equivalent SDOF representation of an MDOF structure which allows SDOF design spectra to be used. This is achieved by imposing a predefined displaced shape on the structure, and establishing the other properties of the equivalent SDOF structure accordingly. Following the development of these preliminary steps, the complete DBD process for MDOF structures is outlined, and example seismic designs of several bridges are presented, with comparisons to designs using traditional strength and ductility criteria. A fundamental problem which is not discussed in this paper is the definition of the target displacements (or better drifts) to be selected. This choice depends on the limit state, on the accepted level of damage and on the current design philosophy. For example from a comparison of the target drifts used in the two companion papers, which somehow reflect the American and the European practice, the European tendency to stiffer piers results clearly. A study of the correlation between characteristics of the piers, maximum displacement, ductility demand and level of damage will require extensive parametric simulations.

2. RESPONSE SPECTRA

Smoothed elastic response spectra recommended in a recent draft of Eurocode 8 [3] are shown in Figure 1 for a maximum ground acceleration of 0.35g on subsoil class B (as defined in the code).

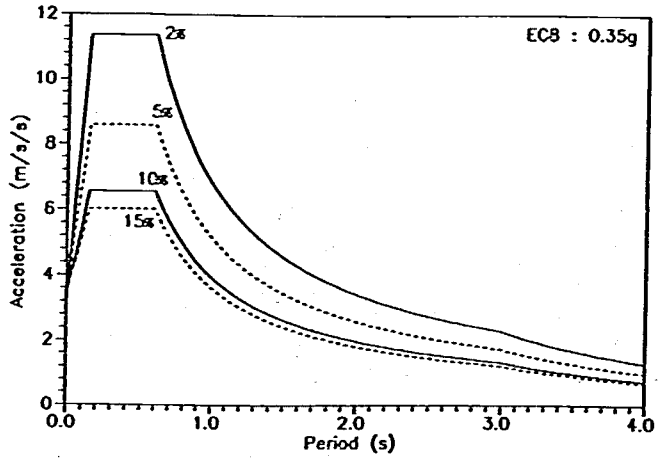


Figure 1 *Eurocode 8 Elastic Acceleration Response Spectra for Maximum Ground Acceleration of 0.35 g on Subsoil Class B.*

The corresponding displacement spectra, related to the spectral accelerations by a factor of $1/\omega^2$, are shown in Figure 2.

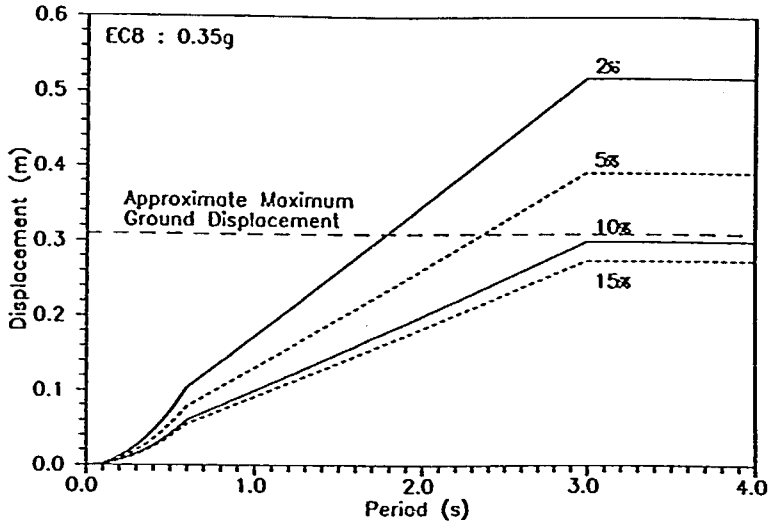


Figure 2 *Eurocode 8 Elastic Displacement Response Spectra for Maximum Ground Acceleration of 0.35 g on Subsoil Class B.*

Notice that for period longer than 3 s the moderate change in the slope of the acceleration spectrum results in a plateau in the displacement response spectra rather than linearly increasing displacement with increasing period. While the constant displacement zone represents an improvement over simpler design spectra, it creates a problem for displacement-based design, since the period becomes indeterminate for displacements greater than or equal to the plateau value. This may be significant for bridges which could enter the range of very long period structures. In actual displacement spectra, the displacements eventually decrease, with values for all damping levels converging towards the maximum ground displacement. An improved design displacement response spectra could be attained simply by replacing the constant displacement region with displacements decreasing to a single ground displacement at a large period. For example, EC8 [3] recommends, in the absence of more accurate determination, an approximate value for the maximum ground displacement:

$$\delta_g = 0.05 a_g S T_C T_D \qquad (1)$$

This displacement is shown in Figure 2. Since the forces and displacements of large period structures are relatively insensitive to small changes in period, such a simple approximation would probably be sufficient.

It is convenient, for either displacement-based or force-based design, to plot design spectra in terms of both accelerations and displacements, as shown in Figure 3.

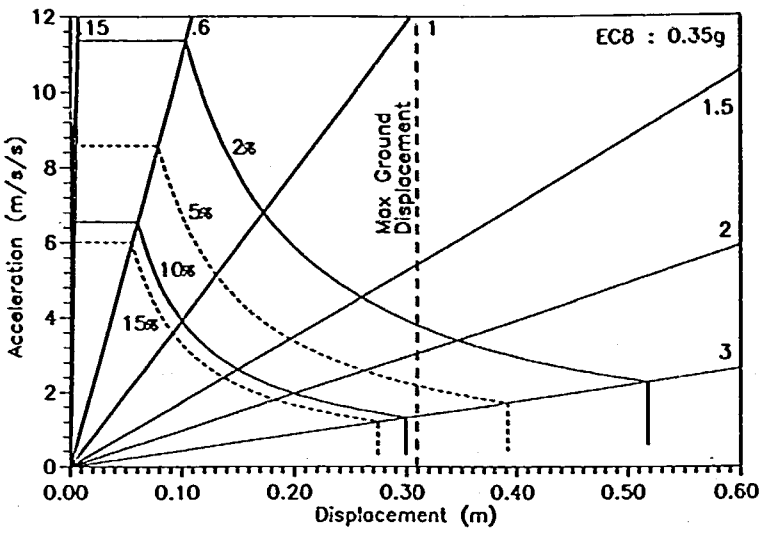


Figure 3 *Combined Acceleration and Displacement Response Spectra for Design*

Lines of constant period becomes a series of radial lines in this representation. With such a plot, the designer can maintain the primary focus on displacements without losing sight of the consequences of design decisions on the forces. Examples of spectra generated from earthquake records from the 1971 San Fernando earthquake and the 1979 Imperial Valley earthquake are plotted in terms of acceleration and displacements in Figure 4.

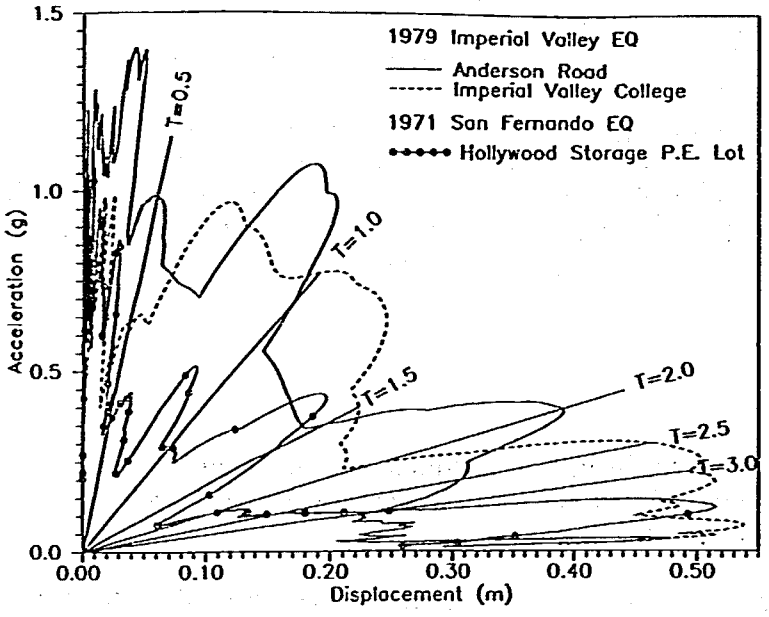


Figure 4 *Combined Acceleration and Displacement Response Spectra (2% damping) from the 1979 Imperial Valley and 1971 San Fernando earthquakes.*

With this representation, it is evident, for example, that a change in period from 1.5 to 2.0 seconds results in a significant drop in accelerations with nearly constant maximum displacement for the Imperial Valley College record; conversely, the same change in period for the Anderson road record results in a dramatic increase in displacements with nearly constant maximum acceleration.

3. DEFINITION OF THE EQUIVALENT SDOF STRUCTURE

With the assumption of a displaced shape, a MDOF structure may be completely described in terms of a single degree of freedom. Consider an n DOF structure, such as the one represented in Figure 5 by a simplified model of a three-pier bridge. It is desired to define an equivalent SDOF structure with mass m_e, stiffness K_e, damping ξ_e and with effective displacements and forces equal to δ_e and p_e respectively.

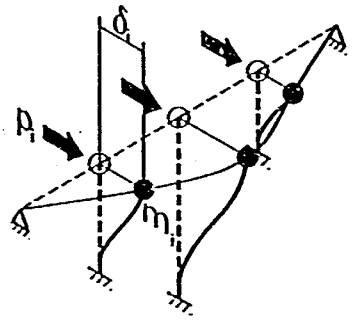


Figure 5 *Idealised MDOF Bridge Structure*

A constant displaced shape can be firstly defined in terms of n factors c_i such that

$$\delta_i = c_i \delta_e \tag{2}$$

It is also assumed that the acceleration at each DOF is proportional to the same displaced shape, thus

$$a_i = c_i a_e \tag{3}$$

It is required that the total applied force be equal for the MDOF and SDOF systems, thus

$$p_e = \sum_{i=1}^{n} p_i = \sum_{i=1}^{n} m_i a_i = a_e \sum_{i=1}^{n} m_i c_i \tag{4}$$

The effective mass of the equivalent SDOF structure can therefore be expressed as

$$m_e = \sum_{i=1}^{n} m_i c_i \tag{5}$$

The inertial forces at the individual DOF can be expressed in terms of the equivalent SDOF force

$$p_i = m_i a_i = m_i c_i a_e = p_e \frac{m_i c_i}{\sum_{k=1}^{n} m_k c_k} \tag{6}$$

Substituting c_i from equation (2) results in the more convenient expression:

$$p_i = p_e \frac{m_i \delta_i}{\sum_{k=1}^{n} m_k \delta_k} \tag{7}$$

The effective displacement is now defined such that the work done by the SDOF force is equivalent to the work done by the MDOF force system, i.e.:

$$p_e \delta_e = \sum_{i=1}^{n} p_i \delta_i \tag{8}$$

Solving (8) for δ_e and substituting for p_i from equation (7) yields the expression for the displacement of the equivalent SDOF structure:

$$\delta_e = \frac{\sum_{i=1}^{n} m_i \delta_i^2}{\sum_{i=1}^{n} m_i \delta_i} \tag{9}$$

The stiffness of the equivalent SDOF structure is simply

$$K_e = \frac{p_e}{\delta_e} \tag{10}$$

In order to use response spectra for design, the effective damping of the equivalent SDOF structure must also be defined. This may be approximated by first relating the expected damping in each member to the local displacement ductility demands, and then combining the results in a smeared damping factor for the structure. A number of authors have proposed relationships between hysteretic damping and ductility [4], with the form of the expression depending on the hysteretic model. For example, Shibata and Sozen [5] proposed

$$\xi_i = 0.2\left\{1 - \left[\frac{1}{(\mu_{\delta i})^{1/2}}\right]\right\} + 0.02 \qquad \text{i=1,2,...,m (number of members)} \tag{11}$$

where it should be noted that the indices now refer to members rather than degrees-of-freedom. This expression includes a constant equal to 0.02 to represent the viscous damping. The smeared damping factor may be evaluated using a technique such as the one suggested by Shibata and Sozen [5].

$$\xi_e = \sum_{i=1}^{m} \left(\frac{Q_i}{\sum_{k=1}^{m} Q_k} \right) \xi_i \tag{12}$$

where

$$Q_i = \frac{L}{6(EI)_i} \left(M_{ai}^2 + M_{bi}^2 - M_{ai} M_{bi} \right) \tag{13}$$

Note that this method requires an initial structural analysis to determine the expected member end moments.

4. THE DISPLACEMENT-BASED DESIGN PROCEDURE FOR MDOF STRUCTURES

The displacement-based design procedure for MDOF structures is outlined below, with the steps summarised in the flow chart of Figure 6.

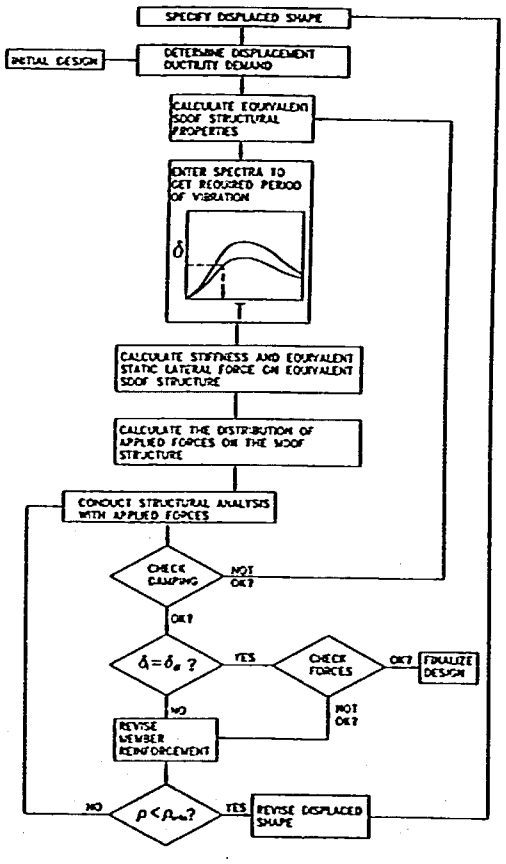


Figure 6 *Flow Chart for Displacement-based Design of MDOF Bridge Structures*

4.1 Displaced Shape

The first step is to define an initial displaced shape for the structure. To achieve uniform damage levels throughout the structure, the desired displaced shape may be reasonably based on the local drift limits for the piers.

$$\delta_{di} = drift * h_i \tag{14}$$

The notation δ_d is adopted to indicate the "desired displacement" which is imposed on the structure.

4.2 Damping

Using the desired displacement limit for each pier and the current member properties, the member ductility demands are defined, and hence the hysteretic damping of each member according to a relation such as the one given in equation (11). Damping properties of the structure play an important role in displacement based design. The stiffness (and strength) demand for the structure is largely a function of the damping, which is in turn a function of the member ductility. Explicit consideration of the damping coefficient in each member thus allows the designer to take into account many aspects of the expected hysteretic response of members rather than simply the ductility. Note, however, that there are no *specified* ductility demands; the values are calculated only as a convenience in the calculation of damping properties.

4.3 The Equivalent SDOF Structure

The displaced shape and member damping values are used to determine the displacement and damping of the equivalent SDOF structure according to equations (9) and (12). The displacement response spectra is then entered to determine the period of vibration of the equivalent SDOF structure, T_e. From the period, the effective stiffness and force in the equivalent SDOF structure can be calculated.

$$K_e = \frac{4\pi^2 m_e}{T_e^2} \tag{15}$$

$$p_e = K_e \delta_{de} \tag{16}$$

The effective force on the equivalent SDOF structure is then used to determine the lateral force distribution on the MDOF structure in accordance with equation (7).

4.4 Structural Analysis

The next step is to perform a structural analysis to determine the member forces and displacements under the applied force distribution. The displacement based design process requires explicit consideration of the strongly nonlinear response of RC structures in the structural analysis phase of the design. For this, a nonlinear "pushover" analysis under monotonically increasing loads would be the ideal tool. It is possible, and perhaps preferable in the initial stages of design, to make use of simple elastic analysis tools provided that the decreased stiffness characteristics of members displaced beyond the elastic limit are

appropriately considered. As discussed by Kowalsky et al. [8], the substitute structure method [5] is well suited to this process.
The fundamental criteria to be satisfied in the displacement based design is that the calculated structural displacements from the linear analysis are equal to the desired displacements, within a specified tolerance.

$$\delta_i \overset{?}{=} \delta_{di} \pm tol \tag{17}$$

4.5 Design Iterations

If the calculated displacements do not match the desired displacement distribution, then the stiffness of the piers must be appropriately modified by changing the reinforcement or the pier geometry. Once the desired displaced shape is achieved, the forces in the members must be checked against the member strength. The process is continued until the displaced shape matches the desired one, with sufficient capacity in all members to resist the applied force distribution. Kowalsky et al. [8] have presented a detailed consideration of this step of the design process in the companion paper.

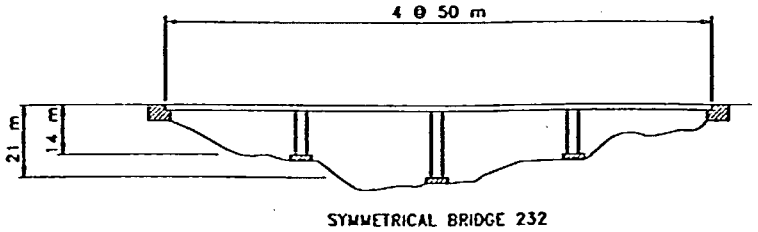
It will often happen in bridge structures that the reinforcement required to achieve the desired stiffness is less than the minimum reinforcement requirements specified by the code. This case has particular relevance to the MDOF design proceedure, since such a restriction makes it impossible to achieve the desired displaced shape; the displaced shape must therefore be revised. The new displacement may simply be assumed to be directly proportional to the ratio of the required reinforcement to the minimum reinforcement:

$$\begin{aligned} &\rho_{min} \leq \rho_{reqd} && \delta_d^{(new)} = \delta_d^{(last)} \\ &\rho_{min} > \rho_{reqd} && \delta_d^{(new)} = \left(\frac{\rho_{reqd}}{\rho_{min}}\right)\delta_d^{(last)} \geq \delta_{d\,\min} \end{aligned} \tag{18}$$

With a new displaced shape, the entire process must be started anew. It should be noted that this condition may, in some cases, be more appropriately treated by changing another design parameter such as the column section dimensions [8].

5. EXAMPLE BRIDGE DESIGNS

The proposed design procedure was evaluated by applying it to the several bridges designed previously using a force-based method as presented in reference [4]. All bridges had four 50 meter spans and identical pier sections, differing only in the heights of the three columns. The bridge deck was assumed to be pinned at the abutments, and the piers were assumed to be fully fixed at the base and pinned at the connection to the bridge deck. The designs of two bridges, shown in Figure 7, are presented in some detail. The first of these was symmetrical, with pier heights approximately in proportion to the expected displaced shape of the unconstrained bridge deck (2-3-2).



SYMMETRICAL BRIDGE 232

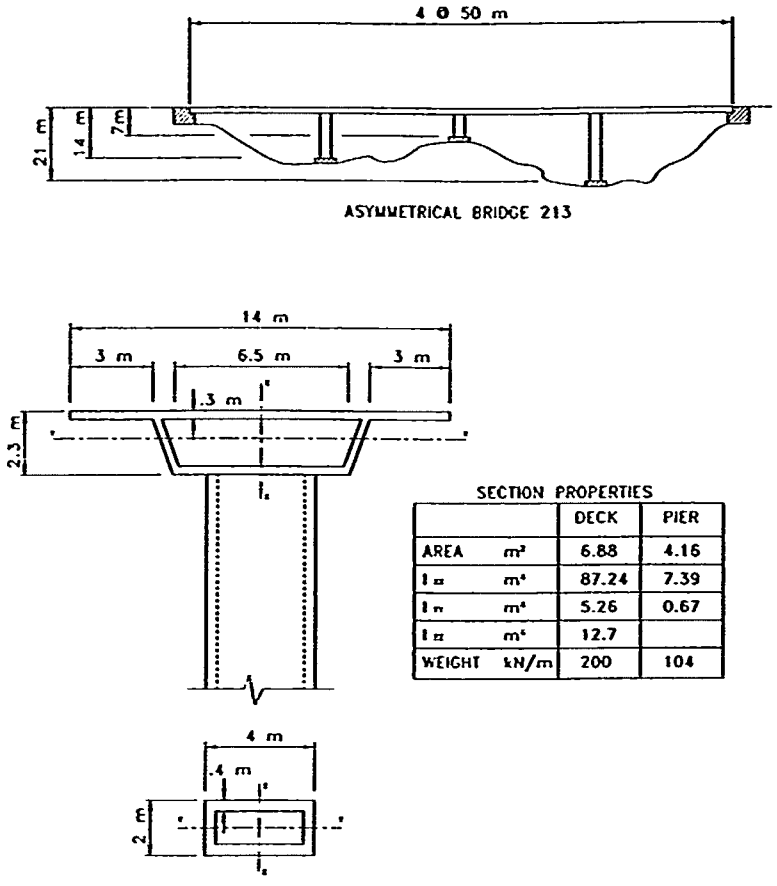


Figure 7 *Elevations and Section Properties of Symmetrical and Asymmetrical Bridges Used to Evaluate the Design Procedure*

The second was strongly asymmetrical, with pier heights in the proportion 2-1-3. The design of both bridges are described below.

5.1 Symmetrical Bridge Design

In the design of the symmetrical bridge, the initial target displaced shape was determined by specifying a desired drift of 1% in each of the piers, or displacements of .14m, .21m, and .14m respectively at the top the piers (see Table 1). Using the lumped masses and displaced shape specified in Table 1, the equivalent SDOF structure was defined as described in Section 3, resulting in a desired displacement of 0.17m. Entering the displacement spectrum defined in Section 2 with an assumed damping of 0.06 yielded a target period of vibration of 1.40 seconds, and the calculated force distribution shown in Table 1.

Table 1 Design of the Symmetrical Bridge

Pier	Lumped Mass (kNs^2/m)	Target Displacement (m)	First Force Distribution (kN)	Second Force Distribution (kN)	Geometrical Reinforcement Ratio	Displacement Ductility Demand	Calculated Max. Displ. ADAPTIC (m)
1	1056	0.140	2997	3330	0.75 %	2.2	0.140
2	1074	0.210	4572	5081	0.60 %	1.5	0.207
3	1056	0.140	2997	3330	0.75 %	2.2	0.140

As an initial design approximation, all piers were assumed to have minimum reinforcement (0.5%). Properties of the substitute structure were determined by assuming that each pier acted as a simple cantilever with a linear distribution of curvature up to yield, and constant curvature in the plastic hinge zone at the column base. The assumed plastic hinge length was given by [3]

$$l_p = 0.08h + 0.022d_b f_y \tag{19}$$

Linear analysis of the substitute structure resulted in displacements of .142m, .205m, and .142m respectively in the piers, and a calculated period of 1.39 seconds. Calculated moments were nearly equal to the pier moment capacities. In other words, the initial assumed design immediately satisfied the design criteria. However, evaluation of the damping according to equations (15)-(17) revealed that the initial assumption of the damping was incorrect, and that a damping value of 0.052 would be more appropriate. With the improved damping estimate, the target period for the structure became 1.32 seconds, and the subsequent increased design forces were those shown in Table 1. Under the new force distribution, two iterations on the pier reinforcement were necessary to satisfy the design requirements.

Several aspects of the design process are illustrated in Figures 8-10. In Figure 8, the target displaced shape is shown as three discreet points, and the calculated displaced shapes from four successive design iterations are shown as lines.

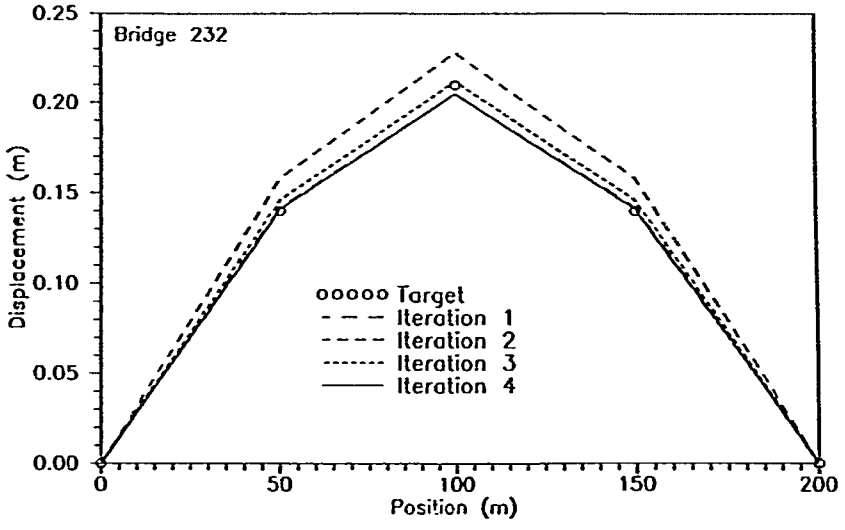


Figure 8 *Convergence of the Displaced Shape for the Symmetrical Bridge Design*

The first calculated displaced shape (iteration 1) was quite satisfactory, but with the updated damping and force distribution, the displacements of the same structure (iteration 2) exceeded the desired displacements at all degrees of freedom. Successive increases in the pier reinforcement (iterations 3 and 4) stiffened the structure, and reduced the displacements to near the target level. Figure 9 illustrates the convergence of the structure first mode period to the targets for the equivalent SDOF structure.

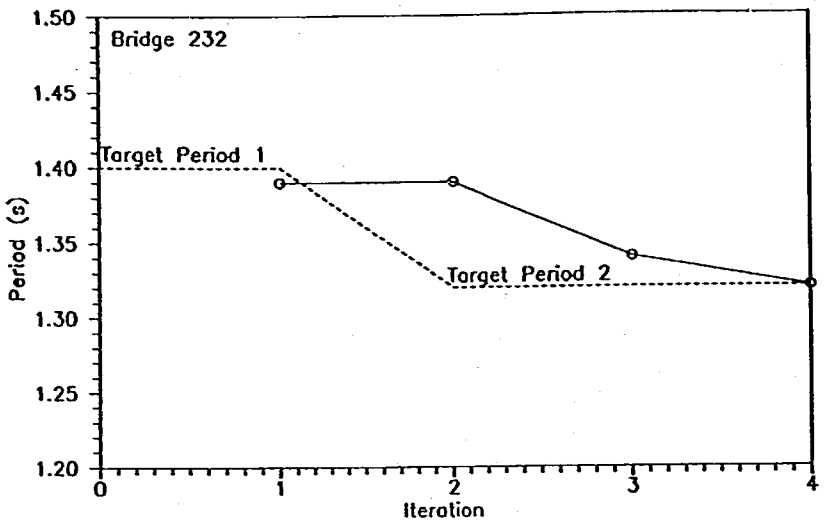


Figure 9 *Convergence of the Period of Vibration for the Symmetrical Bridge Design*

Finally, Figure 10 illustrates the error in the displacement and force distributions for each iteration.

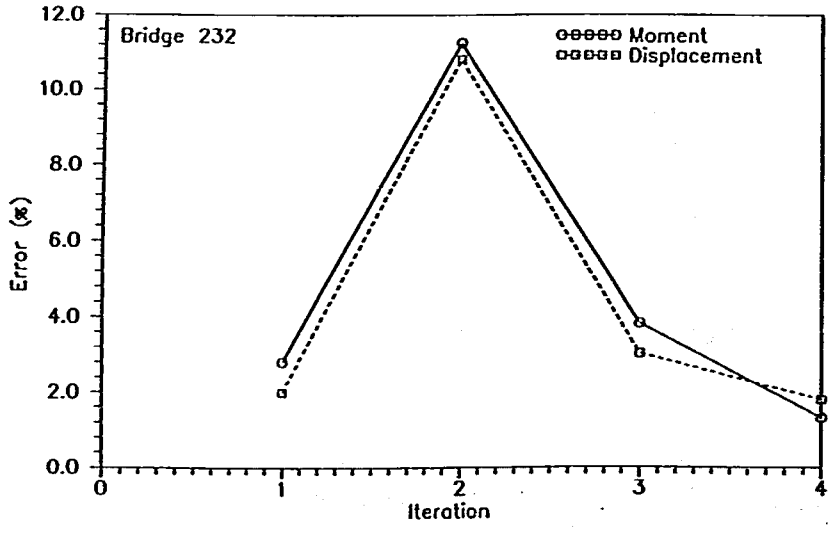


Figure 10 *Convergence of Displacement and Moment Capacity Errors for the Symmetrical Bridge Design*

The displacement error was calculated at each step by subtracting the calculated values from the target values, and dividing the RSS of the error by the RSS of the target displacements. Similarly, the error in moments was calculated as the difference between the calculated moment and the pier moment capacity. For the symmetrical bridge, the errors in displacements and moments were very similar.
Following the design, a nonlinear analysis of the bridge was conducted using the computer code ADAPTIC [7], subjecting the bridge to an artificially generated record developed to match the EC8 spectra. Similar analyses were presented in [4] for bridges designed using force-based methods. Hysteretic response of the individual bridge piers is shown in Figure 11.

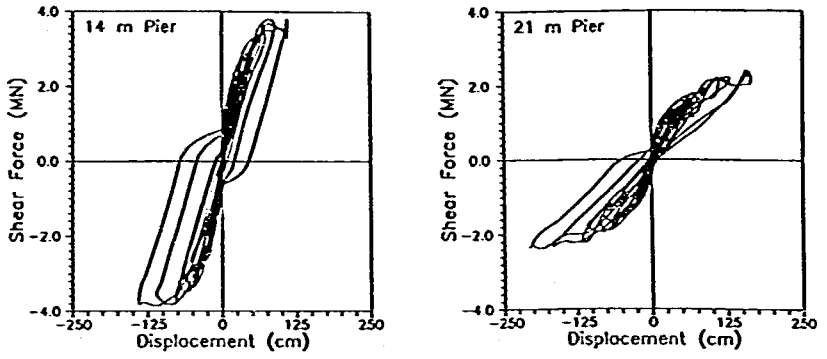


Figure 11 *Shear vs Dispalcement Response of (a) an Exterior Pier, and (b) the Interior Pier from the Nonlinear Analysis of the Symmetrical Bridge*

As shown in Table 1, the calculated maximum displacements from the nonlinear analysis agree very well with the desired design displacements. While such close agreement may not be expected from analysis with more realistic ground motion acceleration records, the results indicate that the basis of the design procedure is sound.

5.2 Asymmetrical Bridge Design

The asymmetrical bridge chosen to evaluate the design process poses several problems to the designer. As discussed by Calvi et al. [6], the relationship between the displaced shapes of the piers alone and of the bridge deck alone gives an indication of the irregularity of a bridge. When the displaced shape of the piers and the deck coincide, as in the symmetrical bridge discussed above, the dominant vibration mode is close to the mode assumed in the design, and the design forces and ductility demands in the piers can be reasonably well predicted. However, nonlinear time-history analyses of very irregular bridges tend to indicate ductility demands in short piers much greater than the behavior factor used in the design. Because of the difficulty of achieving uniform damage levels in the piers of such irregular bridges, the asymmetrical bridge discussed below was considered to provide an extreme challenge to the design process.
The initial assumed shape was based on uniform pier damage at a drift level of 0.6%. Because the natural mode shape of the bridge deck alone was significantly different than that desired for the piers, the deck was expected to constrain the two exterior piers, thus reducing the displacement and force demands to very low levels, and reducing required reinforcement to less than the minimum reinforcement level (0.5%). Conversely, the bridge deck would drive the center pier to displacements greater than the desired design displacements. Following the procedure outlined in Figure 6, it was expected that the design process would, after several iterations, result in a new displaced shape which reflected the interaction of the piers and the deck.

The actual progression of the target and calculated displaced shapes is shown for a few selected iterations in Figure 12.

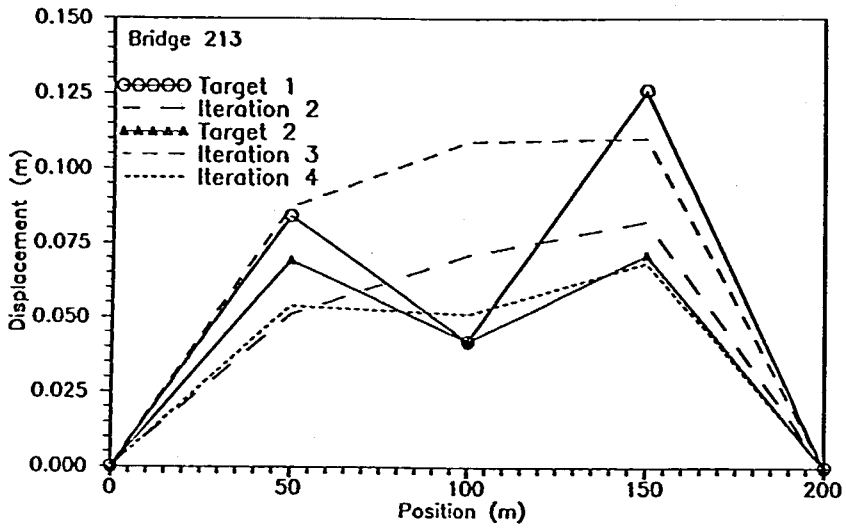


Figure 12 *Convergence of the Displaced Shape for the Asymmetrical Bridge Design*

The initial structural design assumed minimum reinforcement in all piers. At iteration 2, the calculated displaced shape indicated, as expected, that the target displacement was exceeded in the central pier, and not achieved in the exterior piers. Because the exterior piers were already at minimum reinforcement, the displaced shape was revised according to equation (18), with the result shown as target 2 in Figure 12. Because the applied forces were proportional to the displaced shape, the new shape resulted in decreased applied forces in the exterior piers, and increased force in the interior pier. Furthermore, the decrease in the desired displacements in the exterior piers decreased the effective displacement of the equivalent SDOF structure, thus reducing the target period of vibration, and increasing the total applied force on the structure. With the increase in total force, the displacements in all piers exceeded the targets in the next step (iteration 3), and the moment demand on the center pier increased dramatically. Increasing the reinforcement in the central pier improved the displaced shape, but, as shown in Figure 14, several iterations were required to stabilise the error in the moments, and after nine iterations, the error in the moments was still greater than 20%.

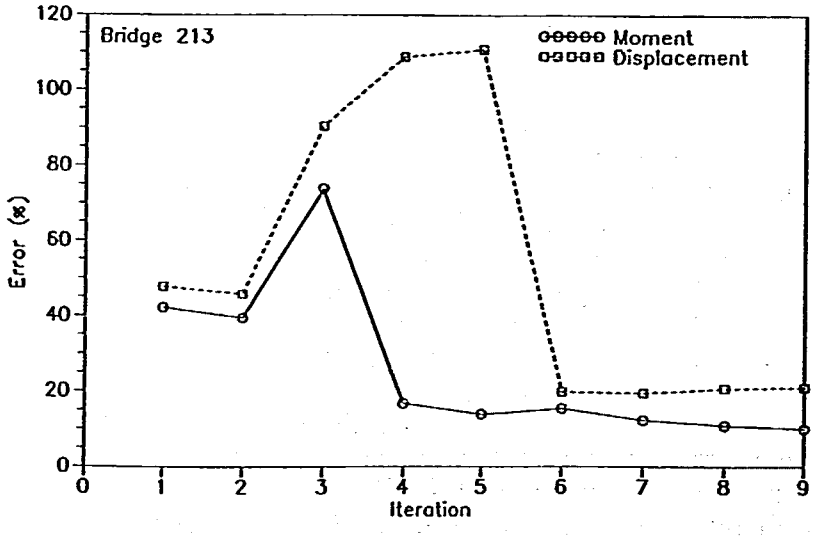


Figure 14 *Convergence of Displacement and Moment Capacity Errors for the Asymmetrical Bridge Design*

The end result was a continuous cycle of increasing strength demand in the interior pier, until the majority of the seismic force was resisted by the short center pier, i.e. the pier with the least capacity for ductile inelastic displacement.
The failure of the design process resulted from the attempted imposition of a single dominant mode shape on a structure whose natural modes of vibration were all significantly different from the chosen mode. Figure 15 shows the calculated mode shapes, periods, and participating mass for the three vibration modes of the bridge, assuming initial elastic stiffness of all piers with minimum reinforcement.

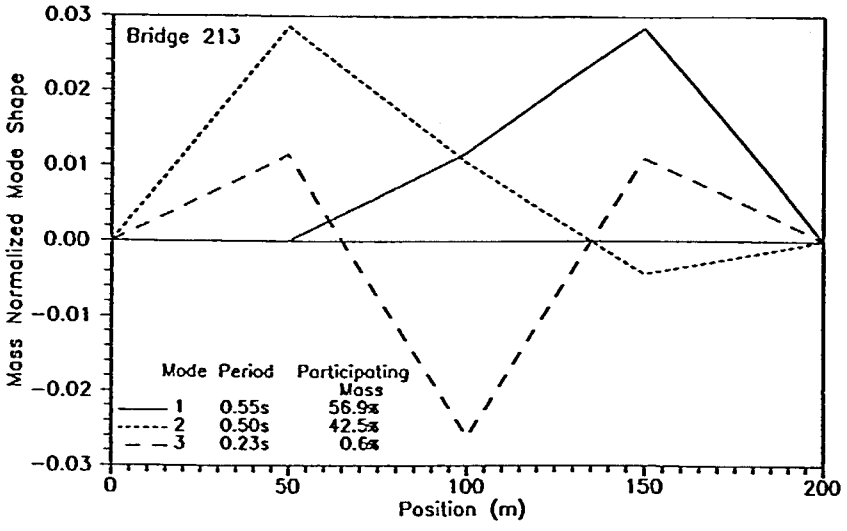


Figure 15 *Mode Shapes and Associated Periods of Vibration for the Asymmetrical Bridge (213) Assuming the Initial Elastic Stiffness for All Piers with Minimum Reinforcement*

Note that the first two modes have quite similar periods with large participating masses in both modes; no single mode can therefore be considered to be clearly dominant. For comparison, mode shapes and periods of the symmetrical bridge are given in Figure 16.

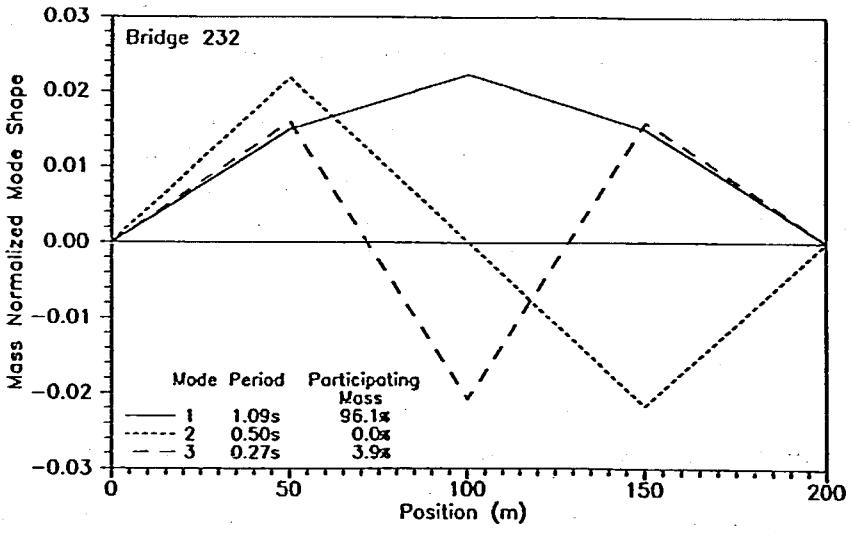


Figure 16 *Mode Shapes and Associated Periods of Vibration for the Symmetrical Bridge (232) Assuming the Initial Elastic Stiffness for All Piers with Minimum Reinforcement*

In this case, with 96.1% participating mass in the first mode and 0% in the second mode, the first mode completely dominated the behavior of the bridge, and the reduction of the MDOF structure to an SDOF structure with a constant displaced shape was well justified.
Nonlinear analysis of the asymmetrical bridge, with pier reinforcing ratios of 0.5%, 0.92%, and 0.5% for the 14 m, 7 m, and 21 m piers respectively [7], confirmed that the displaced shape for such bridges may be extremely erratic, with no single shape dominating the response. To illustrate the changing response over the duration of the ground motion, the equivalent SDOF displacement defined in Section 3 is used as a measure of the irregularity of the response by calculating it for the predicted displaced shape at each time step of the nonlinear analysis. Figure 17 shows the calculated equivalent SDOF displacement, normalised to the displacement of the interior pier, from analyses of both the symmetrical and asymmetrical bridges, also showing the values assumed in the first design steps, and values corresponding to the first and second modes shown in Figure 15. From Figure 17 it is clear that the assumed displaced shape for the symmetrical bridge was in close agreement with the nearly constant shape from the nonlinear analysis. On the other hand, no consistent shape emerged from the analysis of the asymmetrical bridge.

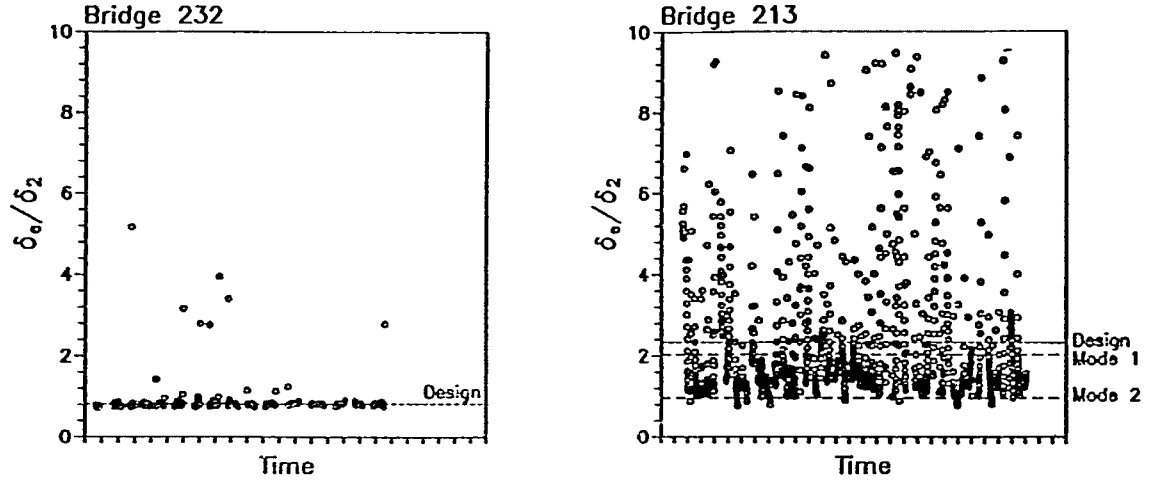


Figure 17 *Calculated Equivalent SDOF Displacement from the Nonlinear Analysis of (a) the Symmetrical Bridge, and (b) the Asymmetrical Bridge*

The exercise with the asymmetrical bridge showed that irregular structures require an explicit consideration of several modes of vibration, and that the assumption of a single dominant mode shape is unwarranted. The next logical step will be to extend the displacement based design method to the consideration of multiple modes, and to compare the effectiveness of such an approach to the analogous force-based modal analysis.

5.3 Relation between drift and ductility

It has been already mentioned that a key point of any displacement based design procedure is the definition of the accepted drift, which implies some evaluation of the relation between drift and damage, as presently implicitly accepted between ductility and damage. It is therefore interesting to observe that some approximate relation between ductility and drift can be easily derived. The yielding displacement (δ_y) can be approximately expressed as a function of curvature ductility (Φ_y) as:

$$\delta_y = \Phi_y \, h^2 / 3 \tag{20}$$

where h is the height of the pier. Writing then the ultimate displacement (δ_u) and the drift as follows:

$$\delta_u = \mu_\delta \, \delta_y \tag{21}$$

$$\text{drift} = \delta_u / h \tag{22}$$

The drift may then be expressed in terms of the yield curvature and the displacement ductility:

$$\text{drift} = \mu_\delta \, \Phi_y \, h / 3 \tag{23}$$

Assuming the yield deformation of steel to be $\varepsilon_{sy} = 2 \; 10^{-3}$, the curvature ductility can be approximately expressed as:

$$\Phi_y = \alpha \, \varepsilon_{sy} / H \tag{24}$$

where H is the section height and α depends on the depth of the compression zone at first yield, and must be between 1 and 2 for symmetrical sections. Assuming $\alpha = 1.5$, the drift in percent is obtained:

$$\text{drift}(\%) = \mu_\delta \; h / 10 \, H \tag{25}$$

From the above relationship, it can be seen that when the section depth is kept constant, as in the examples used in this paper, equal drifts should correspond to larger ductilities for shorter piers. It could then be proposed to select proportionally larger target drifts for taller piers, but it could be easily shown that this will typically result in minimum reinforcement for the tall piers, with a consequent reduction in ductility demand.

It could be also questioned whether displacement ductility should be accepted as a better damage index than drift; this topic is clearly beyond the scope of this paper.

5.4 Preliminary Comparison of Displacement and Force Designed Bridges

In order to show some preliminary comparisons of the results obtained by force and displacement based design methods, a few bridges have been designed with both methods and then analyzed with a simplified, yet reliable, nonlinear dynamic computer program [9]. The target drifts or the behaviour factors (q) have been varied in order to obtain similar results, therefore easier to compare, but remaining around values commonly accepted in Europe. All the piers were assumed to have cross sections similar to that shown in figure 7, with a depth of 6 m instead of 4, identical deck section and spans, while the pier heights were varied according to what is indicated in table 2.

Bridge	Design							Non Linear Analysis						Error		
	design meth.	target 1	target 2	target 3	ρ_1(%)	ρ_2(%)	ρ_3(%)	μ_{d1}	μ_{d2}	μ_{d3}	drift 1	drift 2	drift 3	err.1 %	err.2 %	err.3 %
102030	DBD	0.5%	0.5%	0.43%	0.40	3.00	0.25	2.87	1.33	1.32	0.39	0.54	0.48	+22	-8	-12
	DBD	0.6%	0.6%	0.45%	0.50	1.20	0.25	3.11	1.75	1.22	0.45	0.61	0.44	+25	-2	+2
	FBD	2	2	2	0.42	0.77	0.25	3.65	1.92	1.13	0.50	0.61	0.41	-83	+4	+44
	FBD	2.5	2.5	2.5	0.25	0.54	0.25	5.90	2.21	1.07	0.70	0.65	0.39	-136	+12	+57
	FBD	3	3	3	0.25	0.25	0.25	5.99	2.67	1.00	0.71	0.65	0.37	-140	+11	+67
203020	DBD	0.67%	0.67%	0.67%	0.65	0.40	0.65	1.95	1.45	1.95	0.60	0.60	0.60	+10	+10	+10
	DBD	0.75%	0.75%	0.75%	0.40	0.30	0.40	2.34	1.62	2.34	0.64	0.62	0.64	+15	+17	+15
	FBD	3	3	3	0.30	0.25	0.30	2.47	1.70	2.47	0.63	0.48	0.63	+18	+43	+18
203050	DBD	0.70%	0.70%	0.38%	0.90	1.40	0.25	1.93	1.36	1.00	0.64	0.73	0.37	+9	-4	+3
	FBD	3	3	3	0.33	0.25	0.25	3.00	2.16	1.00	0.77	0.78	0.35	0	+28	+67
202020	DBD	0.58%	0.80%	0.58%	0.25	1.20	0.25	2.04	1.96	2.04	0.50	0.68	0.50	+14	+15	+14
	FDB	3	3	3	0.25	0.49	0.25	2.02	2.50	2.02	0.49	0.41	0.49	+33	+17	+33
103010	DBD	0.50%	0.33%	0.50%	1.00	0.25	1.00	2.18	1.00	2.18	0.37	0.27	0.37	+26	+18	+26
	DBD	0.70%	0.38%	0.70%	0.60	0.25	0.60	2.71	1.00	2.71	0.41	0.25	0.41	+41	+34	+41
	FBD	2	2	2	0.74	0.25	0.74	2.69	1.00	2.69	0.42	0.27	0.42	-35	+50	-35
	FBD	3	3	3	0.36	0.25	0.36	3.69	1.00	3.69	0.49	0.27	0.49	-23	+67	-23
401050	DBD	0.18%	0.50%	0.14%	0.25	2.20	0.25	1.00	1.77	1.00	0.16	0.35	0.12	+11	+30	+14
	DBD	0.17%	0.71%	0.16%	0.25	1.80	0.25	1.00	2.63	1.00	0.15	0.50	0.12	+12	+30	+25
	FDB	2	2	2	0.25	1.47	0.25	1.00	3.14	1.00	0.15	0.56	0.12	+50	-57	+50
	FDB	3	3	3	0.25	0.93	0.25	1.00	3.80	1.00	0.14	0.62	0.11	+67	-27	+67
103050	DBD	0.60%	0.57%	0.33%	1.00	0.25	0.25	3.34	1.51	1.00	0.56	0.55	0.33	+8	+4	0
	FDB	3	3	3	0.26	0.25	0.25	6.57	1.34	1.00	0.80	0.49	0.25	-199	+55	+67

Table 2 **Bridges designed with force (the behaviour factor q is specified) and displacement (the inital and final target drifts d are shown) based methods. The numbers in the first column indicate the heights of the piers. The error reported in the last column is a measure of the difference between the appropriate design variable (q or d) and the corresponding maximum demand resulted from the analysis.**

process was shown to work well for the design of regular bridges and to be applicable even to highly irregular bridges.
The displacement-based design process offers several advantages over a force based process, among them the ability to explicitly consider the displacement demand (i.e. damage) in each member rather than assigning a single, force-based global behavior factor to the structure. The required force to be resisted becomes largely a function of the damping, and thus is related directly to the energy dissipation, hysteretic characteristics, and the acceptable damage on a local level.
Consideration of the complete design process and its application to two bridge examples highlighted both advantages and potential shortcomings of the method. Examination of simplified displacement response spectra showed that for large displacements the required period of vibration becomes indeterminate, since the displacement is constant over a range of periods. A careful review of displacement response spectra to determine appropriate smoothed spectra for design would be required before displacement-based design could be considered for any general class of structures. Secondly, the displacement-based method proposed shows difficulties in handling structures with several prominent modes of response rather than a single dominant mode, particularly when minimum reinforcement requirements restrict the ability of the designer to adjust member properties to the specific needs of the seismic design. Such problems are not insurmountable, but point to the need for more sophisticated analyses for highly irregular bridge structures.
Some simplified relationship between drift and ductility have been developed, as a function of geometry of the structure. This relationship has to be considered as a first, preliminary attempt towards extensive studies on the relations between design parameters and limit states on one side and damage state and probability of collapse on the other. This will require extensive parametric analyses, experimental tests and post earthquake observations. The results obtained from such studies will allow sounder comparison of different design methods, based on probabilistic evaluations of the expected damage and failure potential. Only after in-depth studies will it be possible to recommend appropriate target drifts to be used in the common practice.
Finally it is also important to underline that the selection of appropriate and realistic equivalent viscous damping, as a function of the hysteretic response, clearly plays a fundamental role in the design process. The uncertanties in the correlation of the two values (hysteretic and viscous damping) allows some freedom in the selection of the design value, that should therefore be appropriately calibrated on the base of parametric analyses and test results.

7. ACKNOWLEDGEMENTS

The authors would like to thank Alberto Pavese for his contributions to discussions of this work, and Paolo Moncecchi and Giovanna Carnevali for their help in conducting the analyses of the bridges.

8. REFERENCES

1. Moehle, J.P., "Displacement-Based Design of RC Structures Subjected to Earthquakes," Earthquake Spectra, Vol 8, No. 3, august 1992, pp. 403-428.

2. Priestley, M.J.N, "Myths and Fallacies in Earthquake Engineering - Conflicts Between Design and Reality", Proceedings of the Tom Paulay Symposium, "Recent Developments in Lateral Force Transfer in Buildings", La Jolla, California, September 20-22, 1993.

3. Eurocode 8: Earthquake Resistant Design of Structures, *Part 1-1: General Rules and Rules for Buildings- Seismic Actions and General Requirements for Structures* and *Part 2: Bridges*, Draft, April 1993.

The main results are reported in the same table, where reinforcement, ductility and drift are also shown for each pier. The last columns show a possible measure of the quality of the design method, in terms of the error between target drift, or ductility, and maximum dirft, or ductility, demand. The superiority of the displacement based method for the cases analyzed is evident: the difference between target and result is always less than 30 % in the case of displacement based designed bridges (DBD), and can go up to 200 % in the case of force based designed (FBD)bridges. It should be noticed that highly irregular bridges have been designed and analyzed, accepting a larger tolerance on the moment capacity errors. The displacement resulting from the nonlinear analysis of DBD bridges seems to be sistematically smaller than the target displacement, a simpe correction of the equivalent damping could therefore significantly improve the design method. A similar comment does not apply to FBD bridges.
Finally in figure 18 the displacement ductility demand for all the piers of the bridges considered is reported versus the maximum drift resulted from the analysis. The simplified relation (28) seems to be approximately confirmed, with an essentially linear relationship between ductility and drift, depending on the ratio of height to depth of the pier.

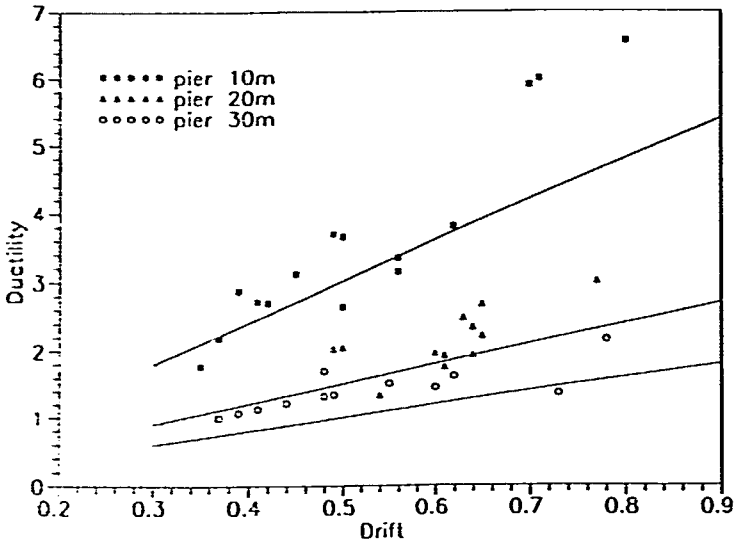


Figure 18 *Ductility demand versus drift as resulting from the nonlinear analysis of the bridges described in table 2. The lines resulting from the approximate relationship of eq. (25) are also shown*

SUMMARY AND CONCLUSIONS

A displacement-based seismic design procedure for MDOF structures has been presented, with example designs of regular and irregular bridges. The process, analogous to an equivalent static lateral load procedure, is based on the assumption of a displaced shape for the structure, and the subsequent reduction of the system to an equivalent SDOF system. With the determination of a desired displacement and damping in the equivalent SDOF structure, displacement response spectra are used to determine the required stiffness of the structure, and hence the applied force. Assuming that the applied forces in the MDOF structure are distributed in proportion to the displacements, the structure is analysed under the calculated force distribution, and the member reinforcement designed accordingly. The process is repeated until the stiffness and displaced shape of the structure converge to those specified in the design, with sufficient moment and displacement capacity in each member to satisfy the demand. The

4. Calvi, G.M., P. Moncecchi, e A. Pavese, "Progetto e Analisi Sismica di Ponti in CA", Dipartimento di Meccanica Strutturale, Università degli Studi di Pavia, Rapporto Scientifico n. 51, Giugno 1994.

5. Shibata, A., and Sozen, M.A., "Substitute-Structure Method for Seismic Design in R/C", ASCE Journal of the Structural Division, Vol. 102, No. ST1, January, 1976.

6. Calvi, G.M., Elnashai, S.A., and Pavese, A., "Influence of Regularity on the Response of RC Bridges", Proceedings of the Second International Workshop on Seismic Design and Retrofitting of Reinforced Concrete Bridges, Queenstown, New Zealand, August, 1994.

7. Izzuddin, B.A., and S.A. Elnashai, "ADAPTIC, A program for Adaptive Large Displacement Elastoplastic Dynamic Analysis of Steel, Concrete, and Composite Frames," Report No. ESEE 7/89, Engineering Seismology and Earthquake Engineering, Imperial College, London, 1989.

8. Kowalsky, M.J., M.J.N. Priestley, G.A. Macrae "Displacement-Based Design of RC Bridge Columns in Seismic Regions," (in course of publication by Earthquake Engineering and Structural Dynamics)

9. Giannini, R., G. Monti, C. Nuti and T. Pagnoni, "Aspidea - a program for nonlinear analysis of isolated bridges under nonsyncrhronous seismic action", Disat Report 5/92, Università dell'Aquila, 1992

INELASTIC RESPONSE OF CONVENTIONAL AND ISOLATED BRIDGES UNDER NON-SYNCHRONOUS SEISMIC INPUT

G. Monti[1] C. Nuti[2]

[1] Dipartimento di Ingegneria Strutturale e Geotecnica, Università "La Sapienza", Roma, Italy
[2] Dipartimento di Scienze, Storia dell'Architettura e Restauro, Università "G. D'Annunzio", Pescara, Italy

ABSTRACT

The results of an extensive numerical study on the nonlinear response of conventional and isolated bridges subjected to multi-support (M-S) seismic excitation are presented. The purpose of the study is to assess the effects of non-synchronous ground motion on the response of bridges designed under synchronous input, as in current engineering practice. Bridges of varying stiffness and with different force reduction factors (for the case of conventional bridges) and different protection levels (for the case of isolated bridges) have been designed for synchronous motion, and have subsequently been analysed in the non linear range under non-synchronous seismic input. For the case of isolated bridges, the design of piers and isolators has been made according to two strategies, *i.e.*, assigning the whole base shear to the piers and the abutments and assigning half of the base shear to the abutments and half to the piers. In the design of the piers the following actions were considered: isolators overstrength, dynamic effect of the pier mass, friction effects of sliding bearings and additional $P-\Delta$ effect due to the isolators displacement. For the case of conventional bridges, the result show that the bridges designed for synchronous input behave well also under M-S excitation and that the request of ductility in the piers is in good agreement with the selected design behaviour factors. For as regards the isolated bridges, the results show that the piers designed for synchronous input remain in the elastic range also in case of hardening isolators and that the first design strategy is preferable when the bridge is subjected to M-S excitation.

1. INTRODUCTION

While problems connected with the seismic performance of bridges have been faced for many years now, the effects of non-synchronous seismic motion on the behaviour of conventional and isolated bridges have received little attention. In recent seismic events these effects have dramatically revealed their importance, and the observed impressive unseatings of the decks have been attributed to the considerable relative displacements imposed at the pier bases due to the non-synchronism of the seismic motion.

The installation of strong motion arrays, though empirically, allowed to develop simple models of the ground motion incoherency, with second-moment fields fully characterized by the power spectral densities (PSD) at each station and by a coherence function, assumed to depend only on the relative distance between stations. Though simple in formulation, this approach provides the means to quantify the sensitivity of the structural response to the essential features of the phenomenon.

Studies on the response of extended-in-plan structures subjected to different motions at the supports have started some thirty years ago and continue until today (see for example [1,2,3]). Many of these studies focus on the algorithm to obtain the response, while others, see for example [4,5], are more design-oriented. Few studies [3,6] are known to the authors which deal with the inelastic behaviour of isolated bridges. However, these are only resticted to the simplest case of incoherence, that is, that related to the time-delay effect (wave transmission). Besides, it seems that modern seismic codes, while suggesting simplified analyses on linear systems with damping equivalent to the dissipation properties of the isolators, give guidelines that only implicitly account for the non-synchronous nature of seismic input, with semi-empirical provisions for extra seating lengths, adequate gaps in the joints, minimum imposed relative displacements between adjacent foundations, etc.

Numerical studies in this direction would be essential to verify whether the "behaviour factor" approach (conventional bridges) or the protection level assigned to the structure (isolated bridges) can be extended to the case of non-synchronous situations. In fact, the idea underlying the present study is to assess the relevance of non-rigid input motion on the peak inelastic response of bridge piers and isolators, and the extent of validity of the "behaviour factor" approach and of the protection level assigned by means of isolators.

The study consists of a parametric analysis on three bridge types: they all have 6 spans, of 50 m length each; the superstructure is the same in all cases, while the (uniform) heights of the piers take the values of 7.5, 10 and 15 m.

The soil motion is characterized by the same PSD at all pier bases, while the parameters controlling the loss of coherence have been made to vary between their respective extremes. In the case of isolated bridges, the design of piers and isolators has been made according to two strategies, *i.e.*, assigning the whole base shear to the piers and the abutments and assigning half of the base shear to the abutments and half to the piers. In the design the following actions have been considered: isolators overstrength, additional $P-\Delta$ effect due to the isolators displacement, dynamic effect of the pier mass and friction effects of sliding bearings.

2. SPATIAL MODEL FOR GROUND MOTION

The spatial variation of seismic ground motion can be thought of as the combination of three different phenomena: a) the *incoherence* effect, resulting from reflections and refractions of waves through the soil during their propagation (this effect is referred to as *geometric incoherence*), b) the so-called *wave-passage* effect, that is the difference in the arrival times of seismic waves at different stations, and c) the *local* effect, due to differences in local soil conditions under the various stations.

In this work spatial variability is described by means of the so-called *coherency function*. It is defined in terms of the cross-power spectral density (PSD) of ground accelerations $S_{ij}(\xi,\omega)$ between two stations i and j at a separation distance ξ

$$\gamma(\xi,\omega)=\frac{S_{ij}(\xi,\omega)}{\left[S_{ii}(\omega)\cdot S_{jj}(\omega)\right]^{1/2}} \qquad (1)$$

where ω is the circular frequency, and $S_{ii}(\omega)$ and $S_{jj}(\omega)$ are the PSD at the stations sites. In the special case, assumed in this study, where the same PSD is expected at each site ($S_{ii}(\omega) = S_{jj}(\omega) = S(\omega)$, that is, no local effect considered) the coherency function simplifies to

$$\gamma(\xi,\omega) = \frac{S_{ij}(\xi,\omega)}{S(\omega)} \tag{2}$$

Several expression for the coherency function have been proposed [4, 7, 8]. In this work the following model is adopted [9]

$$\gamma(\xi,\omega) = \exp\left[-\left(\frac{\alpha\,\omega\,\xi}{v_s}\right)^2\right]\exp\left[i\frac{\omega\,\xi^L}{v_{app}}\right] \tag{3}$$

The first term on the right-end side decays exponentially with the frequency ω, with the horizontal separation distance ξ between two stations i and j and, through the shear wave velocity v_s, with the inverse of the mechanical characteristics of the soil. The second term depends on the projected horizontal distance ξ^L along the wave propagation direction and on the wave circular frequency ω, and is a measure of the *wave-passage* delay due to the surface apparent velocity of waves v_{app}. In this study the coherency function is considered basically as a two-parameter function, having lumped the mechanical characteristic of the soil and the factor α into a single parameter expressed as the ratio v_s/α, and the second one being v_{app}. Note that when $v_s/\alpha \to \infty$ the first term tends to 1 and the incoherence effect results from the wave travelling only; if $v_{app} \to \infty$ the second term tends to 1 and the incoherence is due to the *geometric incoherence* only. It is seen that the adopted model for the coherency function does not contain parameters describing the *local* effect, which should be accounted for in the local spectra $S_{ii}(\omega)$.

The PSD function adopted in this work is the well-known Kanai-Tajimi spectrum modified by Clough-Penzien [10], expressed as

$$S(\omega) = S_0\,S_{CP}(\omega) = S_0\frac{\omega_f^4 + 4\zeta_f^2\omega_f^2\omega^2}{\left(\omega_f^2-\omega^2\right)^2 + 4\zeta_f^2\omega_f^2\omega^2}\,\frac{\omega^4}{\left(\omega_g^2-\omega^2\right)^2 + 4\zeta_g^2\omega_g^2\omega^2} \tag{4}$$

where S_0 is a scale factor, $S_{CP}(\omega)$ is the normalized Clough-Penzien spectrum, ω_f and ζ_f may be thought of as characteristic ground frequency and damping, and ω_g and ζ_g are the parameters of an additional filter, introduced to assure finite power for the PSD.

The scale factor S_0 depends on the peak ground acceleration (*PGA*) according to the following relation:

$$S_0 = \frac{PGA^2}{p^2\cdot \mathrm{Var}^*} \tag{5}$$

where p is the peak factor, given by [11]:

$$p = \sqrt{2\cdot\ln\frac{2.8\cdot\Omega\cdot t_{\max}}{2\pi}} \tag{6}$$

with

$$\Omega = \sqrt{\frac{\mathrm{E}[x^2]}{\mathrm{Var}[x]}} \tag{7}$$

where $E[x^2]$ is the mean square of the process and $\mathrm{Var}[x]$ the variance, that is the total power, of the process having PSD $S(\omega)$:

$$E[x^2] = \int_{-\infty}^{\infty} \omega^2 S(\omega) d\omega \tag{8}$$

$$\mathrm{Var}[x] = \int_{-\infty}^{\infty} S(\omega) d\omega \tag{9}$$

In Eq. (5) Var^* is:

$$\mathrm{Var}^*[x] = \int_{-\infty}^{\infty} S_{CP}(\omega) d\omega \tag{10}$$

The stochastic field is generated according to the *spectral representation method* [12], by which the space-time random field with zero mean, space-time covariance function $R(\xi,t)$, ξ being the separation distance, and frequency-wavenumber (F-K) spectrum $S(\kappa,\omega)$, where κ is the wavenumber, is simulated through

$$f(x,t) = \sqrt{2} \sum_{\eta=\pm 1} \sum_{j=0}^{J-1} \sum_{n=0}^{N-1} \left[S(\kappa_j,\omega_n) \Delta\kappa \, \Delta\omega \right]^{1/2} \cos\left(\eta \kappa_j x + \omega_n \left(t - \frac{x}{v_{app}} \right) + \phi_{jn}^{(\eta)} \right) \tag{11}$$

in which $\phi_{jn}^{(\eta)}$ are two sets of independent random phase angles uniformly distributed in $(0,2\pi]$.
In order to adopt the above equation, a discretization of the frequency-wavenumber spectrum is to be performed. The F-K spectrum is obtained as follows:

$$S(\kappa,\omega) = S(\omega) \cdot \Gamma(\kappa,\omega) \tag{12}$$

where

$$\Gamma(\kappa,\omega) = \frac{1}{2\pi} \int_{-\infty}^{\infty} |\gamma(\xi,\omega)| \, e^{-i\kappa\xi} d\xi = \frac{1}{2\sqrt{\pi}} \exp\left[-\left(\frac{v_s \kappa}{2\alpha\omega} \right)^2 \right] \frac{v_s}{\alpha|\omega|} \tag{13}$$

is the transform of the coherency function.
Note that the coherency function is employed by means of its modulus

$$|\gamma(\xi,\omega)| = \exp\left[-\left(\frac{\alpha\omega\xi}{v_s} \right)^2 \right] \tag{14}$$

that is, only the geometric incoherence term is preserved, since the wave-passage effect is included explicitly in the equation of the simulated field, by means of the time-shift x/v_{app}.
The discretization is performed within the limits of an upper cut-off wavenumber κ_u and an upper cut-off frequency ω_u, beyond which the contribution to the total power can be considered as negligible for practical purposes. Once the cut-offs are determined, the discrete wavenumber and frequency are given by

$$\begin{aligned} \kappa_j &= j\Delta\kappa \qquad j = 0,\ldots,M-1 \qquad \text{with } M \geq 2J \\ \omega_n &= n\Delta\omega \qquad n = 0,\ldots,L-1 \qquad \text{with } L \geq 2N \end{aligned} \tag{15}$$

where M and L are powers of 2, and J and N are also powers of 2, such that J is greater or equal than the number of points for the discretization in space of the field (number of sites where the field is wanted) and N is greater or equal than the number of points for the discretization in time of the field (number of points in the time histories). Note that $J\Delta\kappa = \kappa_u$ and $N\Delta\omega = \omega_u$.
Eq. (11) can be rewritten so to allow the utilization of the FFT method, as

$$f\left(x_r, t_s - \frac{x_r}{v_{app}}\right) = \sqrt{2}\,\mathrm{Re}\left[e^{-i\omega x_r / v_{app}}\left\{\sum_{\eta=\pm1}\sum_{j=0}^{J-1}\sum_{n=0}^{N-1}\left\{\left[S(\kappa_j,\omega_n)\Delta\kappa\,\Delta\omega\right]^{1/2} e^{i\phi_{jn}^{(\eta)}}\right\} e^{i\eta 2\pi rj/M} e^{i2\pi sn/L}\right\}\right] \quad (16)$$

in which:

$$\begin{aligned} x_r &= r\,\Delta x = r\frac{2\pi}{M\,\Delta\kappa} \qquad r = 0,\ldots,M-1 \\ t_s &= s\Delta t = s\frac{2\pi}{L\,\Delta\omega} \qquad s = 0,\ldots,L-1 \end{aligned} \quad (17)$$

The two-dimensional FFT is to be applied to the term in the braces in Eq. (16).
In order to account for the nonstationary nature of ground accelerations, the stationary time histories generated by means of Eq. (16) are modulated by means of an envelope function. The function chosen in this study is:

$$\begin{aligned} \zeta(t) &= \left(\frac{t}{t_1}\right)^2 && \text{for } 0 \le t \le t_1 \\ \zeta(t) &= 1 && \text{for } t_1 \le t \le t_2 \\ \zeta(t) &= \exp\left\{\frac{t-t_2}{t_3-t_2}\cdot\ln\alpha\right\} && \text{for } t_2 \le t \le t_{max} \end{aligned} \quad (18)$$

where t_1 and t_2 are the ramp duration and the decay starting time, respectively, t_{max} is the time history duration and α is the ratio of the amplitude envelope at t_{max} to that during the stationary phase $(t_1 \le t \le t_2)$. In this work: $t_1 = 2$ sec, $t_2 = 14$ sec, $t_{max} = 20$ sec and $\alpha = 0.25$.
The velocity and displacement histories, which are needed in a multi-support analysis, are obtained by integration of the acceleration histories according to a method suggested in [13], known as *baseline correction*, which minimizes the errors introduced in the numerical integration when passing from accelerations to velocities and displacements.

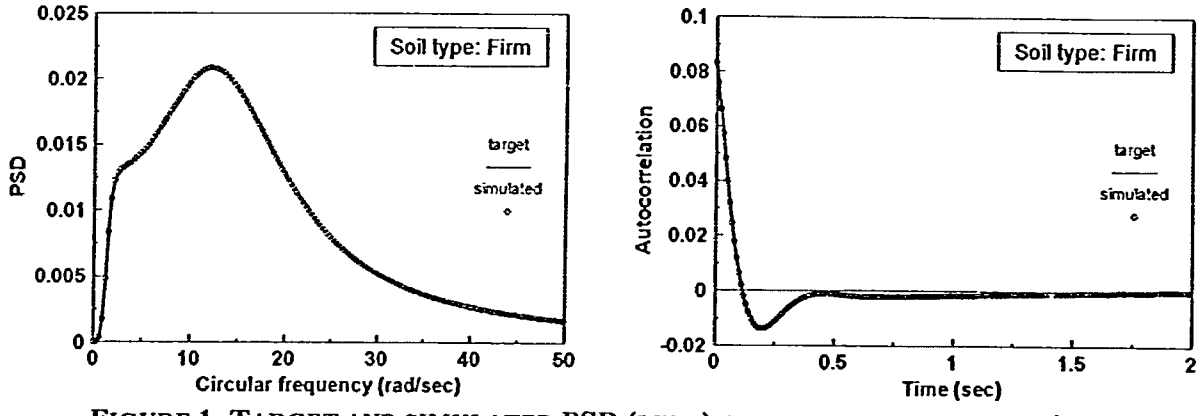


FIGURE 1. TARGET AND SIMULATED PSD (LEFT) AND AUTOCORRELATION (RIGHT).

Fig. 1 compares the auto-spectrum (left) and the autocorrelation function (right) of the simulations of Eq. (16) with the target spectrum in Eq. (4) and the target autocorrelation function. The number of simulations performed was 70. It is seen that both the generated PSD and the generated autocorrelation coincide with the target PSD and autocorrelation.
Fig. 2 compares the coherency functions of the simulations with the target coeherency functions at different stations and for two values of the parameter v_s/α= 300 and 600 m/s. Also in this case 70 simulations were performed. It should be noted that for both values of the parameter v_s/α the result is extremely satisfactory.

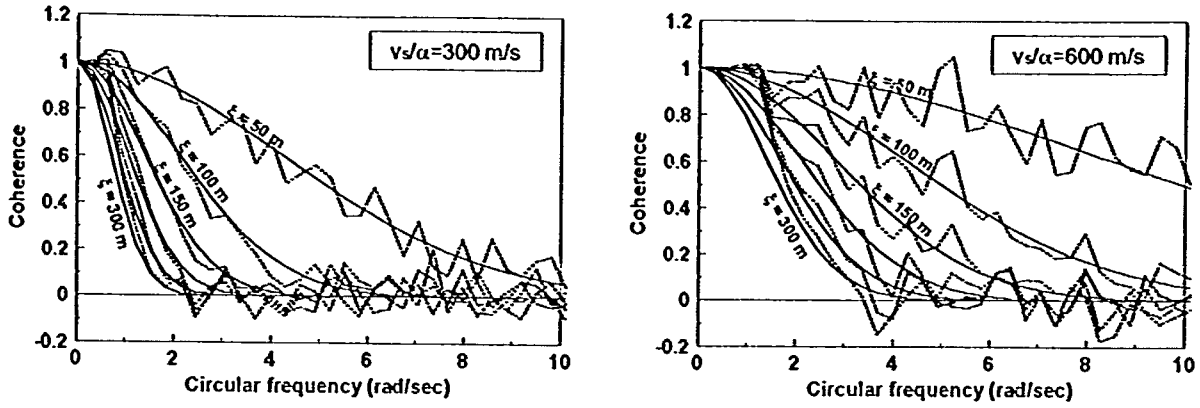


FIGURE 2. TARGET AND SIMULATED COHERENCY FUNCTIONS AT DIFFERENT STATIONS FOR v_s/α= 300 (LEFT) AND 600 M/S (RIGHT).

3. DESIGN OF BRIDGES

The bridge studied in this work is represented in Fig. 3. It is a 6-span continuous deck with 5 piers of the same height H and of 2.5 m diameter. The span length is 50.0 m. The deck has a dead load of 200 kN/m and it is transversally hinged to the piers and the abutments in the case of conventional bridges, whereas it is supported by isolators in the case of isolated bridges. Three different pier heights H have been studied: H= 7.50 m, 10.0 m and 15.0 m.

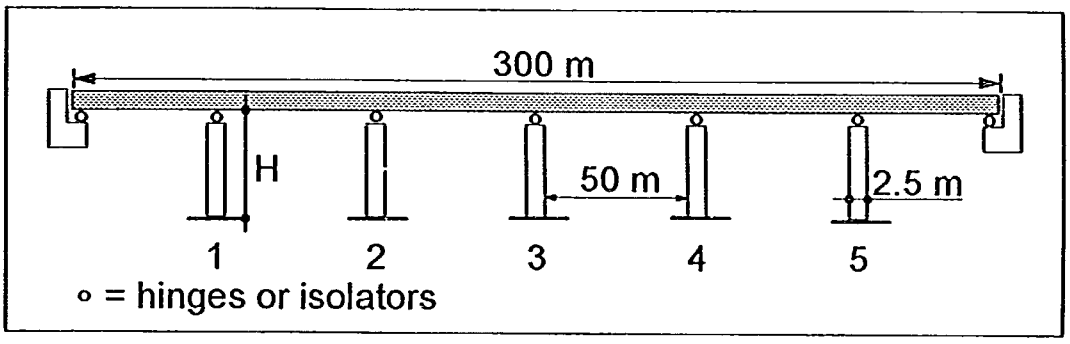


FIGURE 3. SCHEMATIC VIEW OF THE BRIDGE.

The three different pier heights are intended to produce three different degrees of bridge stiffness and have been chosen so as to obtain bridges with fundamental periods varying within rather large limits. The first three periods of vibration are listed in Table 1.

	H = 7.50 m	H = 10.00 m	H = 15.00 m
T_1 (sec)	0.43	0.60	1.20
T_2 (sec)	0.40	0.57	0.84
T_3 (sec)	0.33	0.41	0.48

TABLE 1. PERIODS OF VIBRATION OF THE BRIDGES EXAMINED.

The bridges, both conventional and isolated, have been designed elastically for the transverse direction only, under synchronous ground motion ($v_s/\alpha = \infty$ and $v_{app} = \infty$) which corresponds to the usual design assumption adopted in engineering practice. The soil has been assumed to be of type F (Firm) and M (Medium) for conventional bridges and of type F only for isolated bridges. The values adopted for the filter parameters in the PSD function in Eq. (4) are: for soil F, ω_f=15 (rad/sec), ζ_f=0.6, ω_g=1.5 (rad/sec), ζ_g=0.6, and for soil M, ω_f=10 (rad/sec),

ζ_f=0.4, ω_g=1.0 (rad/sec), ζ_g=0.6. In the elastic analyses performed to design the bridges, the cracked stiffness of the piers has been used, obtained from the uncracked stiffness (gross section) divided by a factor 2.5. The following material strengths have been used: for concrete $f_c = 35{,}000$ kPa, for steel $f_y = 440{,}000$ kPa, with ultimate strains equal to $\varepsilon_{cu} = 0.008$ and $\varepsilon_{su} = 0.10$, respectively. Material design factors were: 1.5 for concrete and 1.15 for steel.

3.1 Design of conventional bridges

The design has been made for the average of the maximum values of the response (bending moments M at the pier base) obtained using ten sets of accelerograms, generated according to Eq. (16) and scaled according to Eq. (5) to a PGA of 0.42 g, divided by the behaviour factor q. Three values of the behaviour factor were investigated: q= 2, 4, 6, which correspond to the design PGA= 0.21 g, 0.105 g, 0.07 g.
The piers, of height H, are designed to satisfy the following inequality:

$$M_u \geq M = F \cdot H + P \cdot \Delta \cdot 0.5(q+1) \tag{19}$$

where M_u is the resisting moment of the section at the pier base. The bending moment M at the pier base is obtained as the sum of the moment due to the shear force F plus that due to the $P-\Delta$ effect, where Δ is the pier top displacement obtained from the elastic analysis. Note that the correction factor $0.5(q+1)$ basically implies that only half of the $P-\Delta$ effect is considered. Table 2 lists the reinforcement ratios $\rho = A_s/A_g$ in the piers, where A_s is the reinforcing steel area and $A_g = 4.91$ m^2 is the area of the piers gross section, obtained for the three different behaviour factors. Note that no minimum reinforcement was considered.

Pier height	$\rho_{1,2,3}$ (q=2)	$\rho_{1,2,3}$ (q=4)	$\rho_{1,2,3}$ (q=6)
H = 7.50 m	1.38-2.64-3.46%	0.40-0.92-1.32%	0.06-0.40-0.64%
H = 10.0 m	1.21-2.30-2.88%	0.29-0.75-1.04%	0.05-0.35-0.52%
H = 15.0 m	0.63-1.44-1.84%	0.05-0.46-0.58%	0.05-0.10-0.23%

TABLE 2. REINFORCEMENT RATIO IN PIERS 1,2,3 FOR BEHAVIOUR FACTOR q= 2,4,6.

3.2 Design of isolated bridges

The design has been made for the average of the maximum values of the response (force at the pier top) obtained using ten sets of accelerograms scaled to a PGA of 0.42 g. Three values of the protection level were investigated: μ= 4.2, 5.3, 7.0, which correspond to the design PGA= 0.10 g, 0.08 g, 0.06 g. For the design phase, the deck was considered as rigid, hinged on the piers and supported by rollers on the abutments.
Two design criteria were followed:
A) the total shear force is equally shared among all the elements (piers and abutments), which basically imply that the same isolators are used on all the piers and abutments and that all the piers have the same strength, and
B) the two abutments resist 50% of the total shear force, while the remaining 50% is shared among the five piers, which implies that the isolators over the abutments are 2.5 times stronger than those on the piers.
The design of the isolators is performed according to:

$$F_{Y,iso} = \frac{F_{D,\max}}{\mu} \tag{20}$$

where $F_{Y,iso}$ is the isolator yield strength, $F_{D,max}$ is the maximum force (average on 10 analyses) transmitted from the deck to the pier below, and μ is the reduction factor of this force. The isolator stiffness is obtained as: $K_I = 150 \cdot F_Y$, which basically assures that the isolator yield displacement is always equal to 6 mm. Two values of the isolator hardening ratio b have been considered: b= 0.0 (no hardening) and $b = \bar{b}$ such that the hardening ratio of the pier-isolator system be equal to b_{tot}= 0.10. The value of $\bar{b}$ is easily obtained from

$$\bar{b} = b_{tot} \cdot \left(\frac{1}{K_P} + \frac{1}{K_I} \right)^{-1} \cdot \frac{1}{K_I} \tag{21}$$

where K_P is the stiffness of the pier considered as a cantilever. In the cases examined, the isolators hardening ratio turned out to be: $\bar{b} \approx$ 0.02-0.03.
The piers, of height H, are designed to satisfy the following inequality

$$M_u \geq H \cdot \left(F_{Y,iso} + F_{P,max} + c \cdot N_D + N_T \cdot \Delta_{max} \right) \cdot \gamma_o \tag{22}$$

where M_u is the resisting moment of the section at the pier base, $F_{P,max}$ is the base shear due to the mass of the pier itself and of the pier top (which are under the isolator), c is a friction coefficient, taken equal to 0.03 (teflon bearings assumed), N_D is the load applied on the isolator by the supported deck, N_T is the total load (deck+pier) considered lumped at the pier top, Δ_{max} is the maximum displacement (average on 10 analyses) at the pier top and γ_o = 1.2 is an overstrength factor recovering the uncertainties in the evaluation of $F_{Y,iso}$, c and Δ_{max}.

Pier height	μ	$F_{Y,iso}$ (kN)	$F_{P,max}$ (kN)	$c \cdot N_D$ (kN)	$N_T \cdot \Delta_{max}$ (kN)
H = 7.50 m	4.2	2910 (67%)	430 (10%)	257 (6%)	740 (17%)
	7.0	1745 (55%)	430 (14%)	257 (8%)	740 (23%)
H = 10.0 m	4.2	1973 (51%)	390 (10%)	257 (7%)	1226 (32%)
	7.0	1184 (39%)	390 (13%)	257 (8%)	1226 (40%)
H = 15.0 m	4.2	948 (26%)	280 (8%)	257 (7%)	2120 (59%)
	7.0	570 (18%)	280 (9%)	257 (8%)	2120 (65%)

TABLE 3. CONTRIBUTION OF TERMS IN EQ. (22) TO THE PIER DESIGN FORCE.

Pier height	Design	ρ (μ=4.2)	ρ (μ=5.3)	ρ (μ=7.0)
H = 7.50 m	A	1.55%	1.27%	0.98%
	B	1.04%	0.81%	0.58%
H = 10.0 m	A	2.07%	1.73%	1.44%
	B	1.21%	0.98%	0.81%
H = 15.0 m	A	3.22%	3.00%	2.76%
	B	2.53%	2.30%	2.07%

TABLE 4. REINFORCEMENT RATIO IN ALL THE PIERS FOR PROTECTION LEVELS μ = 4.2, 5.3, 7.0 WITH TWO DIFFERENT DESIGN STRATEGIES, A AND B.

The contributions to the pier design force of the different terms in Eq. (22) are evidenced in Table 3, where it can be seen that the base bending moment due to the $P-\Delta$ effect rules the design of the higher piers. Values of Δ_{max} determined from the elastic analyses are: 0.08 m for H = 7.50 m, 0.13 m for H = 10.0 m, and 0.23 m for H = 15.0 m.

Table 4 lists the pier reinforcement ratios obtained with the two design strategies A and B, for three different protection levels: $\mu = 4.2, 5.3, 7.0$. Also in this case no minimum reinforcement was considered. Note that the reinforcement ratios are higher than those obtained for the conventional bridges (compare for ex., $\rho_{1,2,3}$ (q=4) in Table 2 with ρ (μ=4.2) in Table 4 which have approximately the same design *PGA*). This is essentially due to γ_0 and to the additional forces considered in the design of isolated bridges: the whole $P-\Delta$ effect and friction.

4. NON LINEAR RESPONSE OF BRIDGES TO M-S EXCITATION

This section tries to provide an answer to the following question: what happens to bridges designed for a rigid input motion in case they are subjected to motions having the same frequency content but varying types and amounts of correlation between the support points?
In order to answer this question, the conventional and isolated bridges designed as described above, have been analysed under non-synchronous seismic motions having different coherence characteristics. The values considered in the parametric study are summarized in Table 5.

Pier height H (m)	7.50	10.00	15.00
v_s/α (m/s)	300	600	∞
v_{app} (m/s)	600	1200	∞
Conventional Bridges			
Soil type	F (Firm)		M (Medium)
Behaviour factor q	2	4	6
Isolated Bridges (on soil F only)			
Protection level μ	4.2	5.3	7.0
Hardening b_{tot}	0.0		0.1

TABLE 5. VALUES CONSIDERED IN THE PARAMETRIC STUDY.

The non linear analyses of conventional and isolated bridges have been carried out by means of the code ASPIDEA [14], under non-synchronous ground motion histories, with $PGA = 0.42g$. By combining all the parameters in Table 5, 162 cases for conventional bridges and 162 cases for isolated bridges resulted, for a total of 3240 nonlinear analyses.
Before describing the results, it is convenient to recall (see for example [10]) that the response of a structure under M-S excitation is obtained from the superposition of two contributions: a *dynamic* component induced by the inertia forces and a so-called *pseudo-static* component, due to the differences in support displacements. These latter can induce significant distortions in the structure thus modifying the response with respect to the case of synchronous input.
The results are presented through the envelopes of the maximum required displacement ductilities in the piers for the conventional bridges and of the maximum displacements of the isolators for the isolated bridges.
The results are organized in triplets of Figures with different values of the geometric incoherence term (v_s/α= 300, 600 and ∞ m/s). In each Figure for each value of the behavior factor q= 2,4,6 or of the protection level $\mu = 4.2, 5.3, 7.0$ adopted in the design, three curves obtained for v_{app}= 600, 1200 and ∞ m/s (the wave-passage effect) are represented.
When looking at the following triplets of Figures one should consider that the *geometric incoherence* (*i.e.* that ruled by the first term in Eq. 3) decreases from the top Figure with $v_s/\alpha = 300$ m/s to the bottom one with $v_s/\alpha = \infty$ m/s. In each Figure the *wave-passage* delay

(*i.e.* that ruled by the second term in Eq. 3) decreases as the apparent velocity v_{app} increases from 600 to ∞ m/s. The extreme cases are those with maximum incoherence $v_s/\alpha = 300$ m/s and $v_{app} = 600$ m/s (dash-dotted lines) and those with perfect coherence corresponding to the synchronous support motion cases (solid lines).

4.1 Conventional Bridges

The results of bridges with H=7.5 and 10.0 m only are presented, on soil types F and M. The requested ductility in the piers is evaluated as the mean obtained from analyses with ten different sets of ground motion histories.

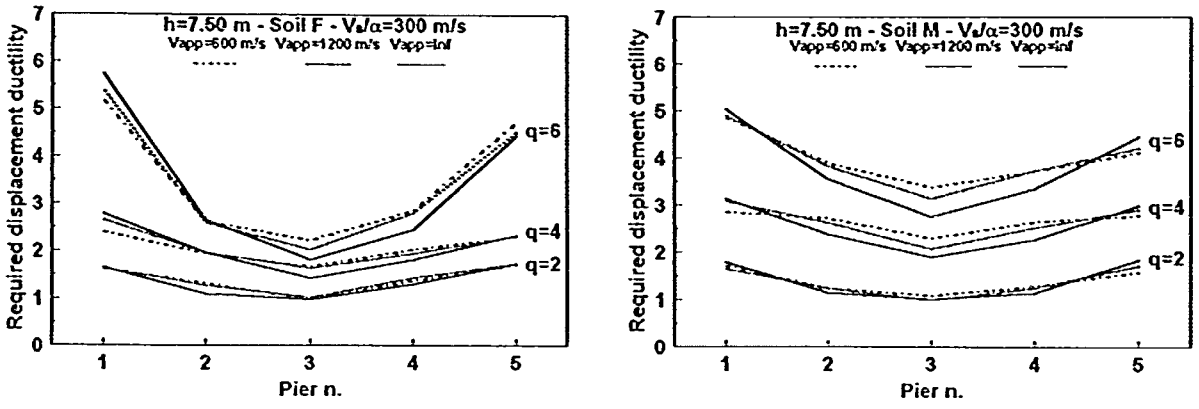


FIGURE 4. CONVENTIONAL BRIDGE H=7.5 M ON SOIL F AND M. REQUIRED DUCTILITY FOR $v_s/\alpha = 300$ M/S.

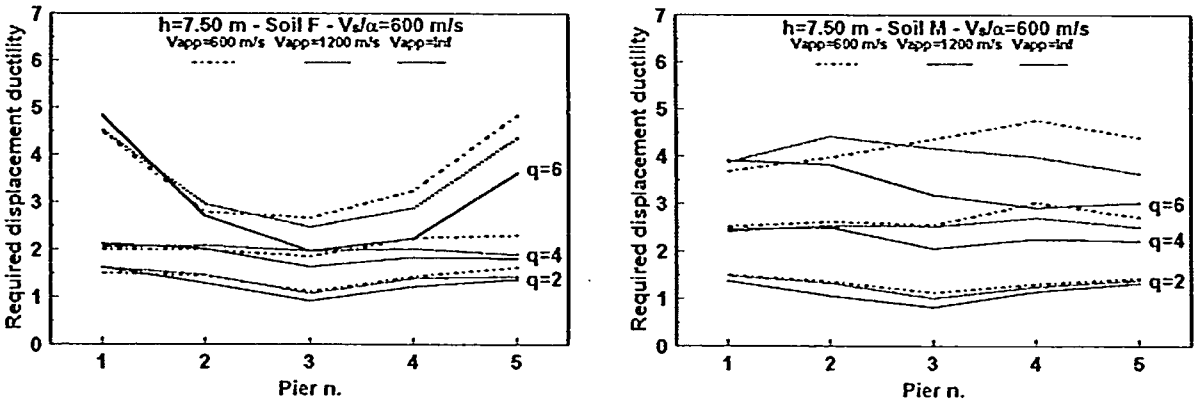


FIGURE 5. CONVENTIONAL BRIDGE H=7.5 M ON SOIL F AND M. REQUIRED DUCTILITY FOR $v_s/\alpha = 600$ M/S.

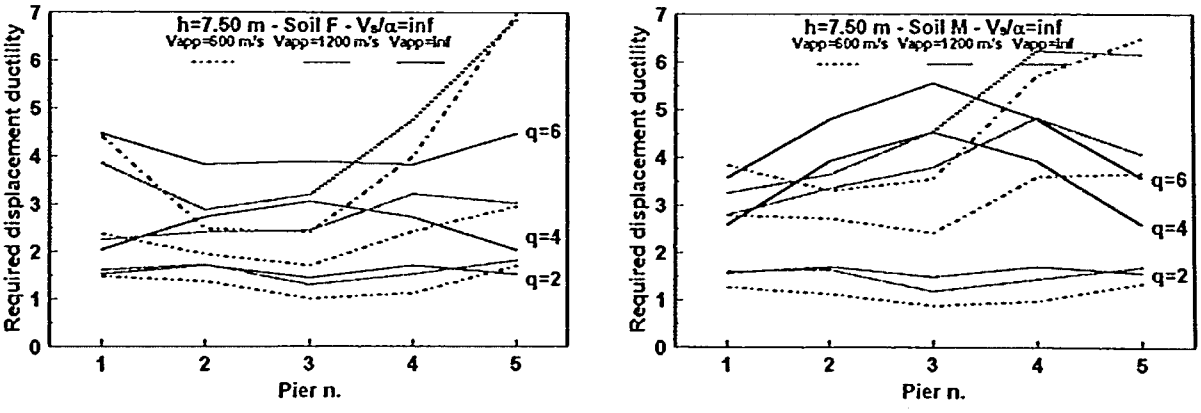


FIGURE 6. CONVENTIONAL BRIDGE H=7.5 M ON SOIL F AND M. REQUIRED DUCTILITY FOR $v_s/\alpha = \infty$ M/S.

We first comment on the Figs. 4 and 7, *i.e.*, the ones containing the cases of largest geometric uncorrelation. In these cases the response is due mainly, when not exclusively, to the imposed pseudo-static differential displacements at the piers bases. Wave propagation effects are irrelevant in this case. It is seen that the request of ductility distribution in the piers is practically the opposite of the first modal shape (this is more evident for q=6). This result comes to no surprise: in the rigid base design the lateral piers are subjected to lower forces than the central ones, and are consequently weaker. Since the soil displacements are such as to impose almost equal distortions to all piers, the weakest ones are called to greater ductility demands. This leads to the situation illustrated in Figs. 4 and 7, where the central piers have ductilities of about half of q, while for the lateral ones the values are closer to q.

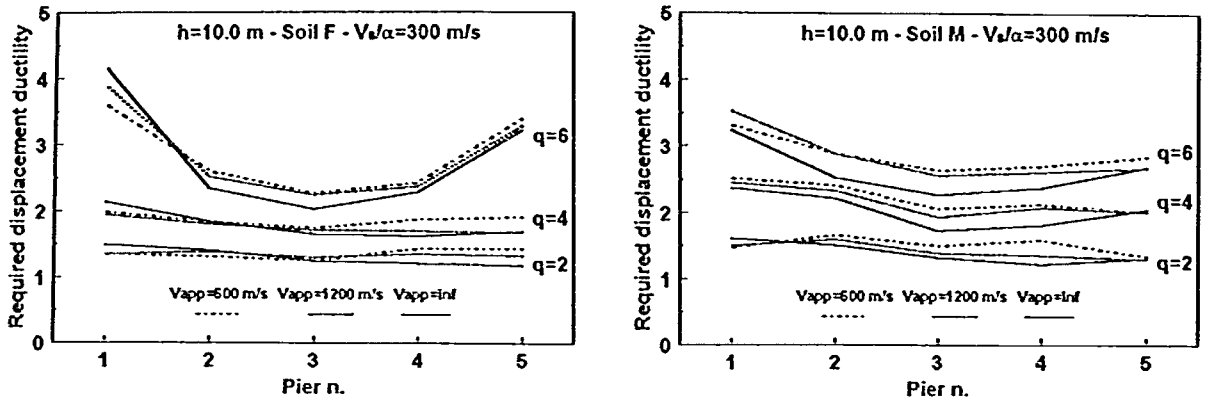


FIGURE 7. CONVENTIONAL BRIDGE H=10.0 M ON SOIL F AND M. REQUIRED DUCTILITY FOR v_s/α = 300 M/S.

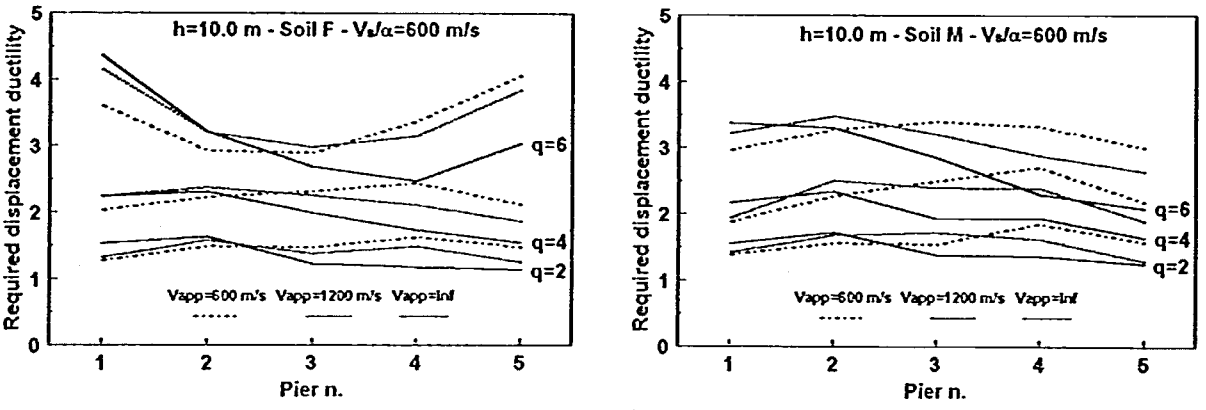


FIGURE 8. CONVENTIONAL BRIDGE H=10.0 M ON SOIL F AND M. REQUIRED DUCTILITY FOR v_s/α = 600 M/S.

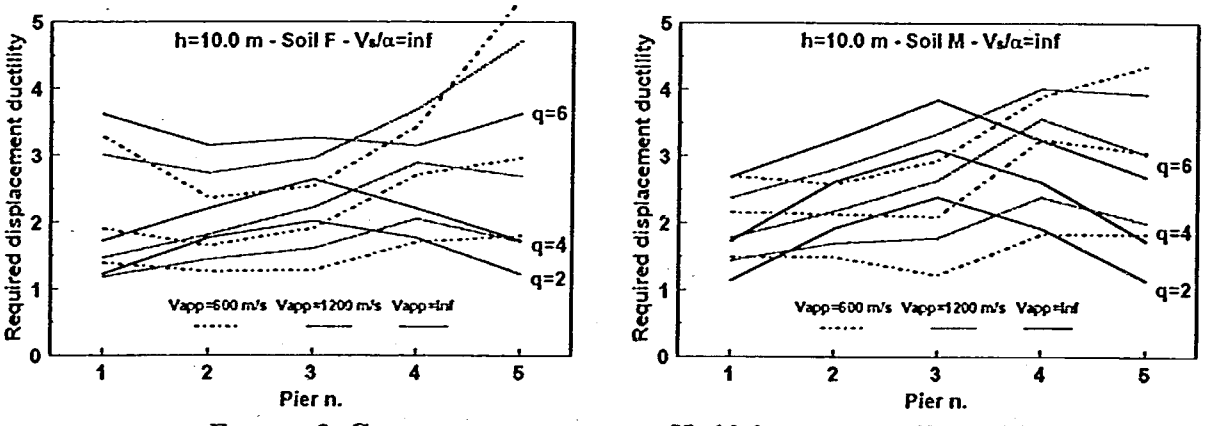


FIGURE 9. CONVENTIONAL BRIDGE H=10.0 M ON SOIL F AND M. REQUIRED DUCTILITY FOR $v_s/\alpha = \infty$ M/S.

The second extreme situation is when geometric incoherence is absent and the lack of correlation is only due to wave propagation (see Figs. 6 and 9). In this case we observe a significant sensitivity of the results to the parameter v_{app}, for a given value of q.

Overall, however, in almost all cases the presence of a certain amount of incoherence acts towards reducing the ductility demand in the central piers and increasing that in the lateral ones, with respect to the limit case of synchronous motion. This fact is significantly corroborated for the higher values of q. In any case, the values of the requested ductilities are still quite close to the selected values of q.

In concluding this section it appears that designing for a rigid motion provides the bridge with a higher global strength than for a non-synchronous motion. The request of ductility is not uniform among the various piers, but the values are well below the selected q-factors, with the only exception of a few sporadic cases. This amount of strength is enough to cope with the possibility of receiving a non-synchronous motion. The only exception has been observed for the lateral piers in the bridge with H=7.5 m, for which the rigid base assumption adopted in the design leads to a request of ductility close to the q-factor.

4.2 Isolated Bridges

The results are presented for the bridge with H= 10.0 m only, but they are representative also of the bridges with H= 7.5 m and 15.0 m which show similar behaviours. The results obtained for both values of hardening (0.0 and 0.1) are presented.

A first observation is that the design of the isolators resulted in a sufficient protection level for the piers to cope with a non-synchronous input, in the sense that in all cases they behaved elastically. As an example, the two worst cases relative to the design strategies A and B are reported in Fig. 10, where it is shown that all the piers remained in the elastic range. The cases presented are those with total hardening equal to 0.1 and friction coefficient equal to 0.03, which are the most unfavourable for the piers.

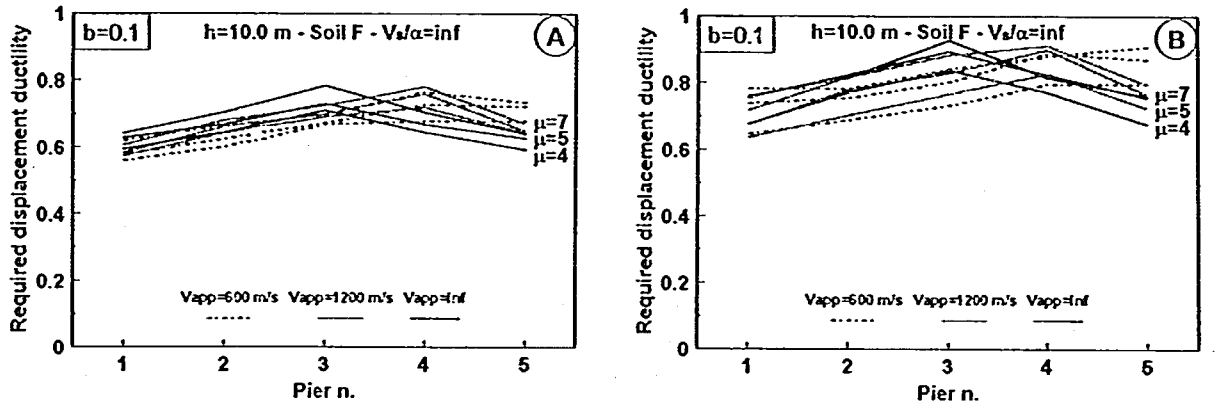
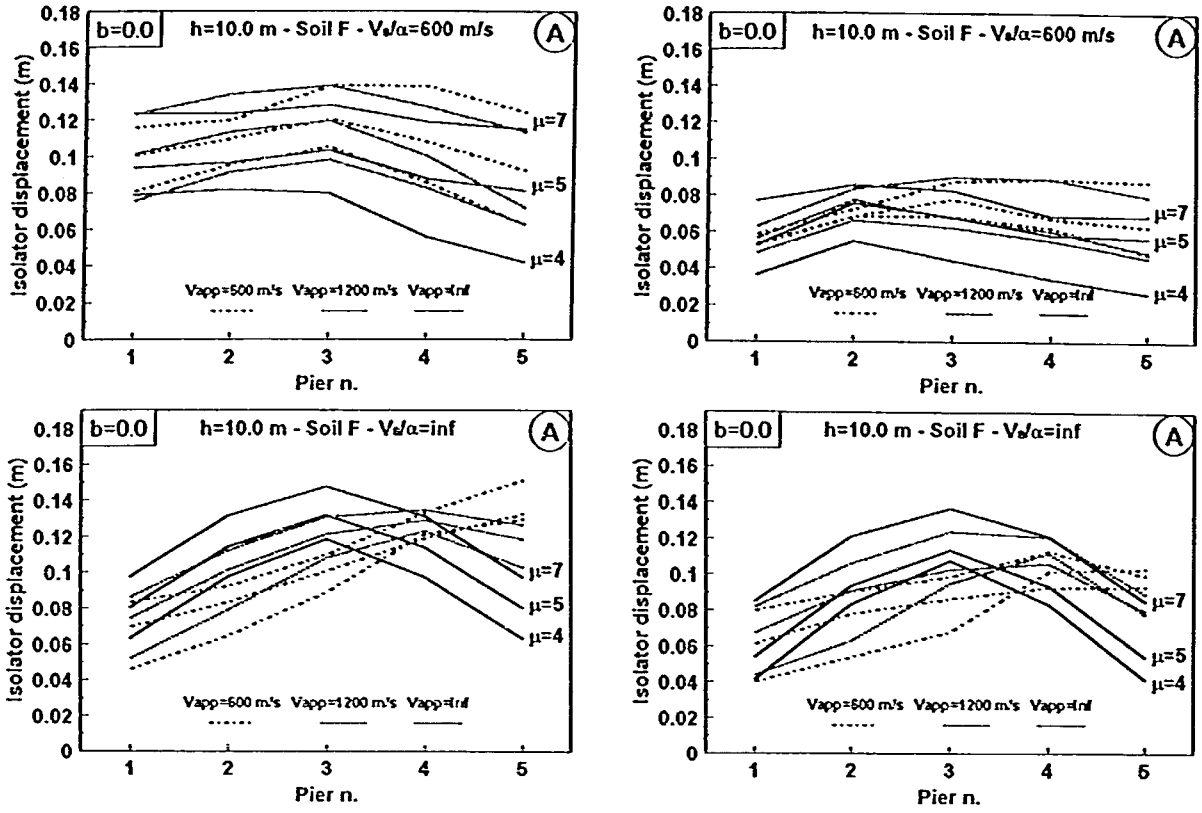


FIGURE 10. ISOLATED BRIDGE H=10.0 M. DESIGN A AND B. HARDENING 0.1. REQUIRED DUCTILITY FOR $v_s/\alpha = \infty$ M/S.

Having established the effectiveness of the assumed protection levels and of the two design criteria on the piers behaviour, it is all too natural to focus the attention on the isolators displacements, with the aim of identifying the effects of geometric and wave-passage incoherence on their response. In order to obtain an upper bound for the isolators displacements, in the nonlinear analyses the friction coefficient has been assumed equal to 0.003, that is, one tenth of that assumed for design.

As above for the ductilities, the isolator displacements are evaluated as the mean obtained from analyses with ten different sets of ground motion histories plus one standard deviation.



MEAN + 1 ST. DEV. ON 10 SIMULATIONS

MEAN ON 4 SIMULATIONS

FIGURE 11. COMPARISON OF CRITERIA FOR EVALUATING THE ISOLATORS DISPLACEMENTS FOR TWO DIFFERENT COHERENCE SITUATIONS.

In Fig. 11 the results obtained with this criterion are compared with a different one, currently proposed in Italy, which suggests to evaluate the isolator displacements as the mean obtained from analyses with four sets of ground motion histories. Comparing the results obtained with the two criteria, it is evident that the second criterion leads to unacceptable underestimates of the isolators displacements, with 100% error in some cases, when a certain degree of geometric incoherence is present (Fig. 11 top, with v_s/α = 600 m/s). On the other hand, this criterion yields almost correct estimates of the isolators displacements (with the exception of the isolator on pier 5) in the cases of synchronous input motion or when the incoherence is of deterministic nature with only wave passage effect (Fig. 11 bottom, with $v_s/\alpha = \infty$ m/s). Since it is beyond doubt that in many situations the geometric incoherence is a more credible source of uncorrelation than that due to deterministic wave-travelling, the adopted criterion seems to be more reliable.

The results regarding the isolators displacements are presented in Figs. 12-17.

In commenting the overall results of the analyses performed, a first general observation is that in all cases the isolators displacements on the piers of the bridges designed with strategy B are sistematically larger than those of case A. This was an expected behaviour, because the isolators on the piers of case B, having a lower global shear to resist, are more flexible than those of case A. However, it is to be noted that the maximum displacement observed (17.5 cm) is well below the admissible maximum displacement for the isolators considered in this study.

As expected, in the presence of hardening the isolators displacements are sensibly decreased (of the order of 10-25%, regardless of the design strategy). This favourable aspect has its counterpart in the increase of force transmitted to the piers below. However, as observed above, all the piers remained in the elastic range.

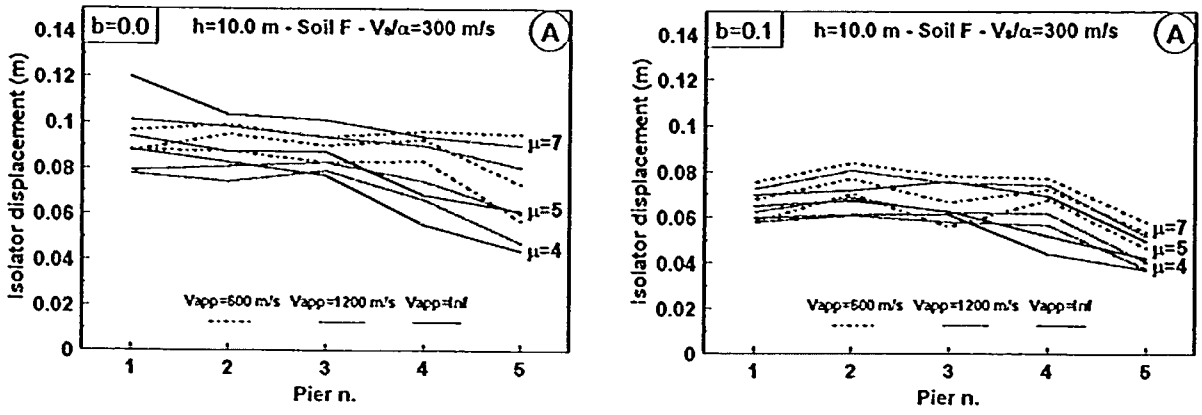


FIGURE 12. BRIDGE H=10.0 M. DESIGN A. TOTAL HARDENING = 0.0 AND 0.1. ISOLATORS DISPLACEMENT FOR v_s/α = 300 M/S.

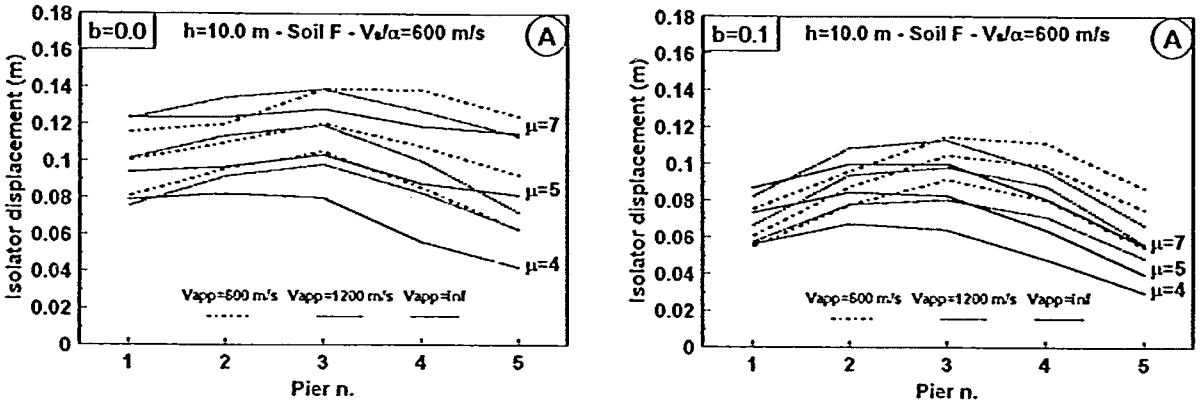


FIGURE 13. BRIDGE H=10.0 M. DESIGN A. TOTAL HARDENING = 0.0 AND 0.1. ISOLATORS DISPLACEMENT FOR v_s/α = 600 M/S.

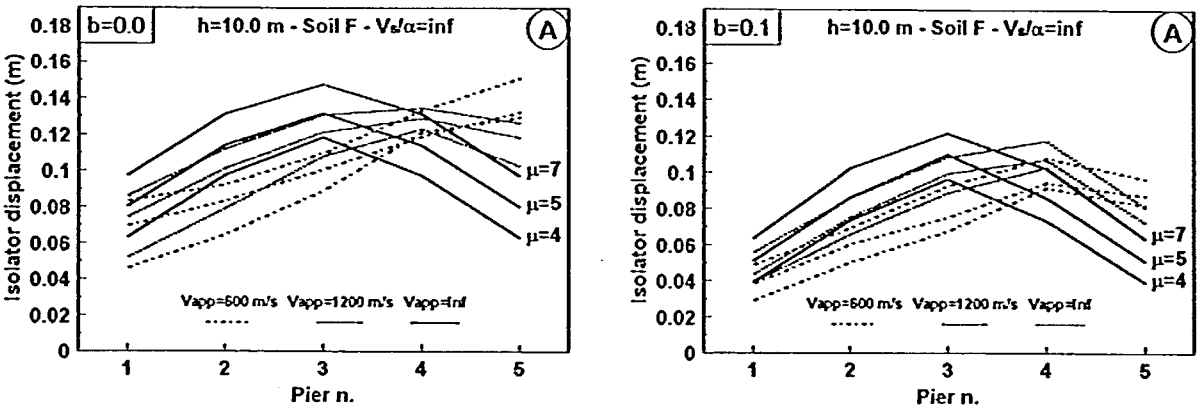


FIGURE 14. BRIDGE H=10.0 M. DESIGN A. TOTAL HARDENING = 0.0 AND 0.1. ISOLATORS DISPLACEMENT FOR $v_s/\alpha = \infty$ M/S.

In comparing the results relative to the synchronous case (solid lines in Figs. 14 and 17), it should be observed that for both bridges (A and B) the isolators on the central piers undergo larger displacements than those on the lateral ones. This suggest that the deck oscillates according to the first mode of vibration. This is even more evident for bridge B where the stiffer isolators on the abutments act as horizontal restraints thus forcing the deck on a simply supported beam configuration.

It is noted that the isolators displacements increase of the same quantity with increasing protection level, but the increase is not proportional to the increase of μ, therefore higher protection levels do not necessarily imply excessive isolators excursions.

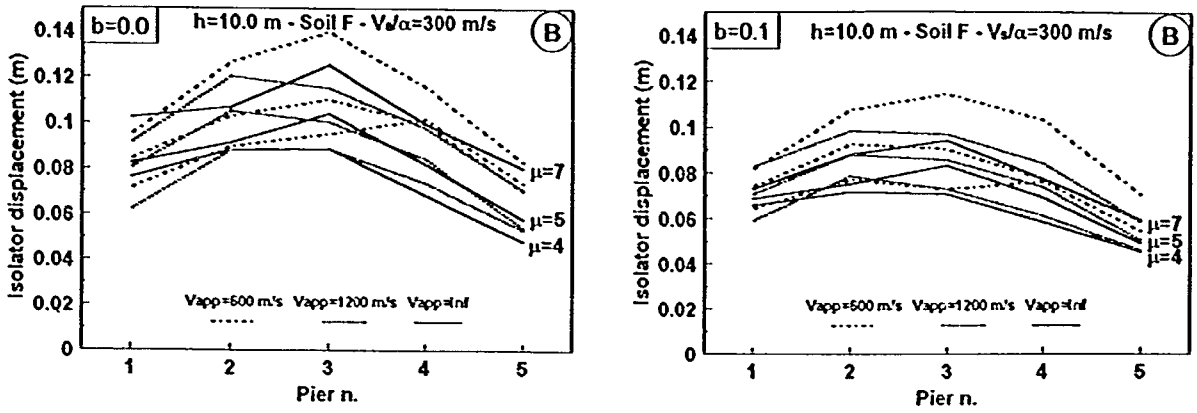


FIGURE 15. BRIDGE H=10.0 M. DESIGN B. TOTAL HARDENING = 0.0 AND 0.1. ISOLATORS DISPLACEMENT FOR v_s/α = 300 M/S.

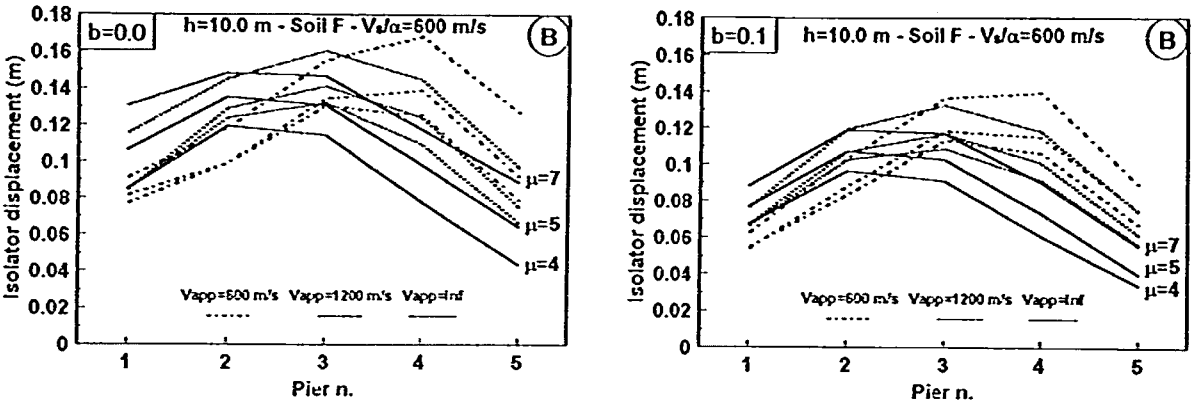


FIGURE 16. BRIDGE H=10.0 M. DESIGN B. TOTAL HARDENING = 0.0 AND 0.1. ISOLATORS DISPLACEMENT FOR v_s/α = 600 M/S.

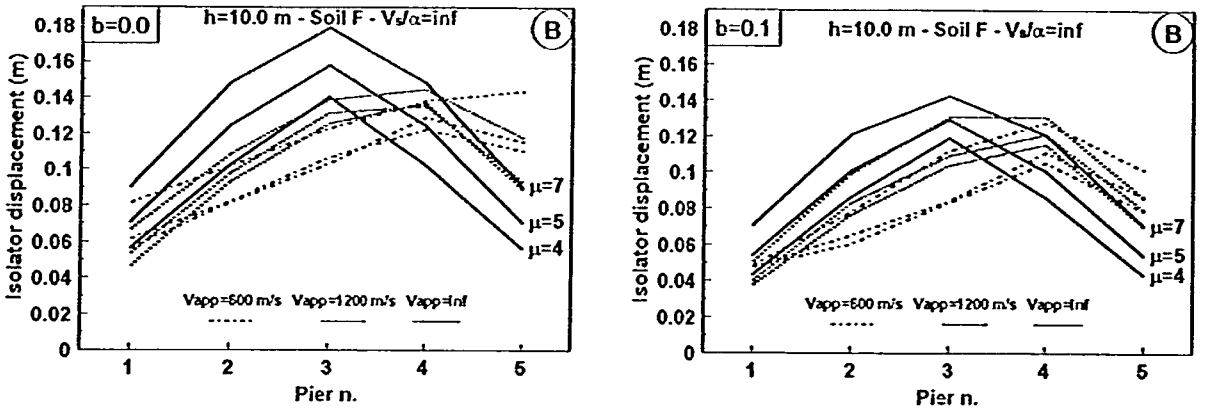


FIGURE 17. BRIDGE H=10.0 M. DESIGN B. TOTAL HARDENING = 0.0 AND 0.1. ISOLATORS DISPLACEMENT FOR $v_s/\alpha = \infty$ M/S.

As soon as the ground motion exhibits a certain degree of incoherence due to wave-travelling alone (dashed and dotted lines in Figs. 14 and 17), a clear directionality in the response is observed. This is due to the fact that the second term in Eq. (3) describing this phenomenon depends on the sign of the distance ξ between two stations. Since the first term describing the geometric incoherence effect is independent of the sign of ξ, when it increases the response distribution tends to be more symmetric. In this case a reduction of displacements for the isolators over the central pier is observed (almost 25% for zero hardening), whereas the directionality effect reduces the displacements of the isolators on the first encountered piers (1 and 2) and increases the displacements of the isolators on the last encounterd piers (4 and 5), with respect to the synchronous case (solid lines). This phenomenon is already triggered for

v_{app} = 1200 m/s, that is for trains of waves arriving at two consecutive piers with a time delay of only 4/100 seconds.
For increasing geometric incoherence (decreasing values of v_s/α) the displacements of the isolators are relatively uniform in the different piers, thus suggesting that the bridge deck does not move as the first modal shape because higher modes are excited under non-synchronous ground motion, as already observed in case of bridges with transverse rollers on the abutments [3]. This phenomenon is less evident in bridge B, where the isolators on the abutments are stiffer as mentioned above and prevent the deck from assuming straight configurations during its motion.
Another observation that goes with the one previously mentioned is that for increasing geometric incoherence the isolator displacements are smaller on the central piers and larger on the lateral ones, although to different degrees. This can be noted by comparing the cases of fully synchronous input (Figs. 14 and 17, solid lines) with all other cases in which some degree of uncorrelation of geometric nature is present (Figs. 12, 13 and 15, 16 all lines). This effect is positive in that it reduces the $P-\Delta$ effect due to the isolator displacement.
As a last remark, note that in bridge A the wave-passage effect is less evident when high geometric incoherence (low values of v_s/α) is present: for different values of v_{app} the differences in the displacement distributions in Fig. 12 are less evident than in the other cases.

5. CONCLUSIONS

The choice of the model for describing spatial variability of ground motion has been the first task of this study. The adopted model is very simple in formulation in that it depends on three parameters only (here lumped in two) which are easily identifiable on physical basis and therefore are easily assigned different values to model the recognized incoherence sources in a stochastic field. In this model, the coherency function is the product of two terms: the first uncorrelates the motions at different points exponentially, and the second simply represents the correlation between two generic points due to a time lag in the arrival of waves. Therefore, samples generated from the first term only are trains of waves travelling with the same speed and differing from one to another by random phase angles only, whereas the second term only would generate at each station identical processes, but shifted in time. While the second term has the nature of a deterministic model, the first one, on the contrary, is of purely stochastic nature: when it takes on large values the motions at two points become statistically uncorrelated (and, given the implicit assumption of gaussianity, also independent), so that at a given instant in time the two motions might hypothetically be the same but opposite in sign.
Following the recommendations contained in several modern bridge codes, to consider spatial variability of ground motions in the case of long bridges, three representative bridge models have been selected and designed for spatial variability, assuming a variety of combinations for the absolute and relative importance of the two terms of the coherency function. Other parameters have been included in the study, such as the soil type for conventional bridges and the isolators hardening for the isolated ones, thus resulting in a total of 324 cases. The designs have been made elastically, for three different values of the q-factor for conventional bridges and of the protection level μ for isolated bridges. Subsequently, the bridges have been analized in the nonlinear range under non-synchronous seismic action.
In few words, the problem has been posed in the following terms: what happens to bridges designed under synchronous input, *i.e.* according to consolidated practice, that are subjected to non-synchronous motion? The scope is to see if and how large inadequacies of under- or over-design this practice involves.

The results regarding the conventional bridges can be summarized as follows: designing for a rigid motion provides a global upper bound of the response and therefore a globally conservative design. There is difference, however, in how the the requests of ductility are distributed among the different piers, which even more evident for those case with a higher force reduction factor (q=6). For low uncorrelation, the requirements tend to be uniform, while for high incoherency, the distribution is essentially the opposite of the shape of the dominant mode. This result is not surprising: in the synchronous design, performed according to the first modal shape, the lateral piers are subjected to lower forces than the central ones, and are consequently weaker. Since the soil displacements impose almost equal distortions to all the piers, the weakest ones are called to greater ductility demands. This leads to requests of ductility in the central piers of about half of q, while in the lateral ones the values are close to q. It has also been observed that when the inputs to the supports are highly uncorrelated (*i.e.* the first term is dominant), the second term has negligible effects, regardless of its value. On the other hand, when incoherency is produced by wave travelling alone, the effect on the response consists essentially in an larger extraction of ductility from the last encountered piers, due to the directionality of the excitation.

As regards the isolated bridges, the piers have been designed accounting for the force transmitted by the isolator (including the overstrength), for the eventual presence of friction in the supports, for the force induced by the pier mass excited dynamically below the isolator and for the additional $P-\Delta$ effect induced by the displacement of the isolator. This method for designing the piers has revealed extremely reliable in the sense that, by accounting for all the above-mentioned phenomena, some of which are usually neglected in common practice, it prevented the piers from yielding in all of the cases examined.

For as regards the overall design approach, two design strategies have been followed: the first one prescribes to share the whole base shear among the seven isolators (five on the piers and two on the abutments), while the second one assigns 50% of the base shear to the isolators on the abutments and the remaining part to the isolators on the five piers. Thus, the first approach tends to distribute the stiffness equally among the points where the deck is supported, whereas the second strategy imposes stiffer supports on the abutments. With the first strategy, which yields stiffer isolators, systematically smaller isolators displacements are obtained. As regards the response of the whole bridge, it has to be noted the consequences of the already observed effect of "straightening" of the deck deformed shape for increasing incoherence on the behaviour of the bridges designed with the two different strategies. The first strategy, distributing uniformly the stiffnesses along the deck, does not prevent this behaviour from developing and therefore helps the displacements to distribute equally among the various isolators. The second strategy acts against the behaviour illustrated before, because the isolators on the abutments are stiffer than those on the piers and force the deck to deform closer to the first mode of vibration. It is to be noted that the first strategy, beyond being preferable for what just mentioned, is also more convenient from the constructive viewpoint because it allows to adopt the same type of isolator on all the supports, either pier or abutment.

As a last remark, it is to be underlined that the results obtained from this study are strictly dependent on the extreme regularity of the bridges examined and on the model that has been assumed for describing spatial variability. Additional studies are foreseen to investigate the behaviour of irregular bridges (with piers of different heights) and of different models of the coherency function.

REFERENCES

[1] Bodganoff, J.L., Goldberg, J.E. and Schiff, A.J. (1965). *Bull. of Seismological Society of America*, 55, 627-640.

[2] Perotti, F. (1990). 'Structural response to non-stationary multiple-support random excitation'. *Int. J. of Earthquake Engineering and Structural Dynamics*, Vol. 19, 513-527.

[3] Moerland, P., Nuti, C. and Pinto, P.E. (1993). 'Risposta dei ponti ad azioni nonsincrone'. Proc. 6° Conference "L' Ingegneria Sismica in Italia", Perugia 13-15 October, 1201-1212, (in Italian).

[4] Der Kiureghian, A. and Neuenhofer, A. (1992). 'Response spectrum method for multiple support seismic excitations'. *Int. J. of Earthquake Engineering and Structural Dynamics*, Vol. 21, 713-740.

[5] Heredia-Zavoni, E. and Vanmarcke, E.H. (1994). 'Seismic random-vibration analysis of multisupport-structural systems'. *J. of Engrg Mech. ASCE*, Vol. 120, No. 5, May, 1107-1128.

[6] Nuti, C. (1993). 'Il problema del nonsincronismo nella risposta dei ponti con dispositivi di dissipazione e con appoggi convenzionali'. *Atti delle Giornate AICAP*, Pisa, 253-260, (in Italian).

[7] Oliveira, C.S., Hao, H. and Penzien, J. (1991). 'Ground modelling for multiple input structural analysis'. *Structural Safety*, 79-93.

[8] Somerville, P., McLaren, J.P, Mrinal, K.S. and Helmberger, D.V. (1991). 'The influence of site conditions on the spatial incoherence of ground motions.' *Structural Safety*, 10, 1-13.

[9] Luco, J.E. and Wong, H.L. (1986). 'Response of rigid foundation to a spatially random ground motion'. *International Journal of Earthquake Engineering and Structural Dynamics*, Vol. 14, 891-908.

[10] Clough, R.W. and Penzien, J. (1975). *Dynamics of Structures*. McGraw-Hill, New York, N.Y.

[11] Vanmarcke, E.H. (1977). 'Structural response to earthquakes'. *Seismic Risk and Engineering Decision*. Lomnitz Ed., McGraw-Hill, New York, N.Y., 287-337.

[12] Shinozouka, M. (1972). 'Monte Carlo solution of structural dynamics'. *Comput. struct.* 2, 855-874.

[13] Jennings, P.C., Housner, G.W. and Tsai, N.C. (1969). 'Simulated earthquake ground motions for design purposes'. *Proceedings 4th WCEE*, Santiago, Chile, 145-160.

[14] Giannini, R., Monti, G., Nuti, C. and Pagnoni, T. (1992). 'ASPIDEA. A program for nonlinear analysis of isolated bridges under nonsynchronous seismic action'. *Pubbl. Dip. di Ingegneria delle Strutture delle Acque e del Terreno*, Università dell'Aquila, N. 5/92.

EUROCODE 8 PART 2: EARTHQUAKE RESISTANT DESIGN OF BRIDGES

P.E.Pinto

Department of Structural & Geotechnical Engineering
University of Rome "La Sapienza"

ABSTRACT

The paper describes the main features of the European Pre-Standard for the seismic design of bridges, which has been completed in 1994 and it is now applicable for experimental use. It is expected that the final Standard will come into force within three years.

1. INTRODUCTION

In June 1994 the European Committee for Standardization (CEN), in which 18 Countries are represented, has approved the document EC8 *Part 2: Earthquake Resistant Design of Bridges* as an European Prestandard (ENV). As such, the document has a planned lifetime of three years; after an enquiry among CEN member countries to be started on the third year of tentative use, the document will be either approved as a final Standard, or revised into a new Prestandard and left in use for an additional period of two years.

A draft of Part 2 started circulating by mid 1990: although the conceptual framework has remained unchanged, substancial modifications have been introduced, both in the general organization of the text and in several technical parts of it, as result of suggestions coming from the national review committees. The design of bridges using isolating devices has been developed ex novo.

The initial stages of life of a new code are inevitably painful, and a certain risk of rejection cannot be discounted, almost independently of the quality of the document: prudence advises not to venture into predictions about progress into life of this one.

Some assurance, however, comes from its inner logic, which may well not represent an absolute truth, but certainly reflects the present advanced state of thinking about codified structural design. And since the arch of this logic is made up of a reduced number of component parts, it should not be difficult in the future to locate possible deficiencies in one or another of these parts, and to introduce the appropriate refinements without touching the nature of the document.

What are the main component parts of the ENV EC8 Part 2, and the way they are linked together, constitutes the object of this presentation.

2. SCOPE AND STRUCTURE OF THE CODE

The code is essentially devoted to the design of road/railway bridges of the most common types and geometry: fully or partially continuous beam-like superstructures, with negligible curvatures in the horizontal and vertical planes, supported by vertical pier systems of various

types, e.g., simple or multiple bents, trusses, walls, etc. The material can be reinforced or prestressed concrete, steel, or composite.

The code can be used as reference for other bridge types, like arches, cable-stayed, suspension, etc, and also for bridges of "irregular" geometry such as highly skewed or curved bridges, but in all of these cases the provisions of the code are declared to be incomplete, and need to be supplemented by specific criteria and application rules.

The content of the code is subdivided into five logically arranged chapters, plus one devoted to seismic isolation, and includes nine Appendices, four of which have an informative and five a normative character.

The headings of the five main chapters, on which this presentation will essentially focus, are: *Basic Requirements and Compliance Criteria - Seismic Action - Analysis - Strength Verification - Specific Detailing Rules,* while the five normative Annexes are titled: *Accelerograms for Structural Analysis - Added Mass of Entrained Water for Immersed Piers - Calculation of Capacity Design Effects - Ductility of Special Bridges - Prototype Tests of Seismic Isolation Systems.*

3. BASIC REQUIREMENTS AND COMPLIANCE CRITERIA

The starting point is conceptually identical to that of all the other Eurocodes: I) statement of the objectives that the design is meant to achieve, II) definition of the fulfilment of these objectives in terms of target probabilities of exceedance during the lifetime of the structure, III) explanation of the specific means (criteria) used within the code in order to meet the objectives.

Since this chapter contains basic ideas but few, if any, practical provisions, it is of little appeal to those who from a code expect nothing more and nothing less than what is strictly needed to make it usable. From an opposite point of view, one that might be taken for ex by a knowledgeable professional whose only need is to know where to direct his capabilities, this chapter might well represent the really interesting one of the whole code.

The most general statement of EC8 Part 2 with regard to the design of bridges is that "*..communications shall be maintained, with appropriate reliability, after the design seismic event*", followed by a classification of bridges into three categories of decreasing importance, for which the design seismic event is progressively less severe. In the Appendix, it is indicated that a probability of exceedance of 10% in 50 years for the design action could be assumed for bridges of average importance.

Next, two limit states (LS) are identified, to serve as the basis for the design: the Ultimate: ULS, and the Serviceability: SLS.

The definition of the "Ultimate" is worth to be noted. It is a state still relatively far from the actual collapse of the bridge, in which considerable damage may have occurred to the parts expected to contribute to energy dissipation, but without much degradation, so as to allow for easy repair, and such as to preserve the capability of the bridge of carrying emergency traffic.

The code anticipates from now that in order to comply with the above requirements the deck should remain essentially elastic, while the dissipation of energy should take place in well defined regions of the piers.

The SLS is more commonly defined as a state of light damage, restricted to those structural parts which are meant to dissipate energy only, and such as not require reduction of traffic or immediate repairs.

4. CRITERIA FOR SATISFYING THE ULS

The designer is offered two fundamentally different choices to satisfy the ULS, i.e., to use or not to use the ductility. This choice is a free one for structures which are naturally ductile, like for ex. bridges with frame-like piers. It becomes a necessity when the morphology of the structure, notwithstanding the fact that the material itself may be intrinsically ductile, is such as to give rise to a global force-displacement diagram with essentially no horizontal portion.

Depending on the adopted choice, different paths are subsequently followed in the structural design process.

The steps where the differences are more significant are:

- assurance of a global ductile behaviour
  this step is obviously non existant for low-ductile structures.
  For ductile ones:
  I) as far as possible, plastic hinges should form simultaneously and in all the piers;
  II) in terms of global force-displacement, the structure should be able to sustain five full cycles at the ultimate displacement: d_u, defined as the one for which no failure occurs to the confining reinforcement in tension, and to the longitudinal reinforcement in buckling in all elements of the structure, and also no reduction of the *global* strength capacity of more than 20%.
  The ratio of d_u to the yield displacement d_y is by definition the design value of available displacement ductility.

- capacity design
  capacity design procedures must be applied when providing for the shear resistance in the plastic hinge zones and for the design of all the elements which have to remain elastic in order to ensure a stable dissipative mechanism.
  The full list of these elements, and the appropriate procedures are given in the following chapters of the code.

Other steps, anticipated as being necessary in order to comply with the ULS, for both ductile and non ductile bridges, are related to the control of the absolute and relative displacements of the various parts.

The control is necessary:
I) to exclude unseating of the superstructure. This is achieved by providing adequate seating lengths, and/or appropriate bearings or links such as shear keys, buffers, restraining cables, etc.
II) to avoid shocks between structural elements, which produce damages and make the response behaviour poorly or not predictable at all.

Detailed rules for the evaluation of the expected maximum displacements and for the dimensioning of the seating lengths, links, etc. are given in the last chapter: *Specific Detailing Rules*.

5. SEISMIC ACTION

Characterization of the motion at a point

For the generic translational component the definitions given in EC8 Part 1 apply. For the sake of selfsufficiency of this presentation, it is recalled that the basic description of the soil motion is in terms of an *elastic response spectrum*. The shape of this spectrum comprises four

portions, (i.e.: increasing acceleration, followed by constant acceleration, velocity and displacement, respectively) separated by the values of three periods.
The spectral shapes are assumed not to depend on the magnitude of the scaling factor, which is the peak ground acceleration (PGA).
The elastic response spectrum is to be considered as a uniform risk functional, whose ordinates have a probability of exceedance (given the value of the PGA) of 50%.

Three types of soil profiles are defined: A, B, C, ordered with decreasing overall stiffness; from profile A to C there is a shift of the corner periods towards higher values, while the maximum amplification is essentially unaffected, with only a 10% reduction foreseen for subsoil class C.

As in EC8 Part 1, representations of the seismic motion equivalent to the *elastic response spectrum* are allowed, in the form of a stationary gaussian random process characterized by a power density spectrum, or in the form of a number of artificially generated, spectrum-compatible, time histories.

The full characterization of the motion at a point includes the three orthogonal rotational components, i.e., the spatial derivatives of the translational motions. Simplified models are given in the Appendix (informative), based on the assumption that the entire motion is in the form of S waves, and both rotational response spectra and power density spectra are derived. For example, the rotational response spectrum about the axis i has the form:

$$S^{\theta}_{ci} = \omega/c \cdot S_c(T)$$

where $S_c(T)$ is the site-dependent response spectrum for the horizontal components, and c is the S-wave velocity.
In the text of the code it is said that rotational component are seldom important, and can normally be neglected. The Appendix adds that their contribution is only relevant in the case of structures that are both high and stiff, and when the structure is sensitive to torsional excitation. In most cases the total contribution to the response does not exceed 10%.

A fact which is peculiar to bridges, as distinct from buildings, is the possibility of having the foundations of the various piers resting on soil of different characteristics, with the implication that soil motion at these points is not only out-of-phase but likely also with a different frequency content. This fact would in principle rule out an analysis based on a response spectrum, a concept developed for a rigid-base motion of the entire structure.

Two approximate solutions for this problem are given in the code, both based on the use of a single spectrum for the whole structure. In the first case, the spectrum is a weighted average of the appropriate site-specific spectra at all piers, the weight being the shear force absorbed by each pier for a normalized displacement assigned to the bridge according to its dominant mode shape. The second option consists more simply in using as single spectrum the envelope of all the site-specific spectra appropriate for all the piers.

Characterization of the spatial variability

Consideration of the spatial variability is mandatory:
- for bridges whose length exceeds 600 m, even if the soil properties are uniform.
- when the soil beneath the bridge presents marked geological variations (ex. alluvial soil in one part and rock in another), or marked topographical features (ex. deep valleys).

Acceptable methods to account for spatial variability are described in the Appendix. Briefly, they may be classified into the following three types.

I) The motions at the various points are components of a random field, homogeneous in space (i.e. the differences in the motion depend from the relative distance between any two points only, not on their absolute positions), and stationary in time.
The random field is completely defined by the covariance matrix, whose diagonal terms contain the power spectral densities at the various stations, and the i,j terms the cross power spectral densities between stations i and j. This model is suited for linear random vibration analyses or, if correlated samples of the field are generated at every station by numerical simulation, for linear or non-linear step-by-step response analyses.

II) A simplified random field model, where independent, band-limited motions are generated and allocated to the nodes of square meshes, one square mesh of different size for each frequency band. The motion at a generic point is a weighted average of the motions defined at the four nodes of the squares.

III) A purely kinematic model, consisting on a set of static relative displacements, whose magnitude depends on the distance of the generic support point from a reference one. Calling ΔX this distance, the expression for the relative displacement is:

$$d = \Delta X \, vg/c_p \leq \sqrt{2}\, dg$$

where vg and dg are the peak ground velocity and displacement, and cp is the velocity of the compressive waves.

Once the effects of the statically applied relative displacement obtained (Ed), they have to be combined with the effects of the dynamic rigid-base motions (E_o), which can be made by using the expression:

$$E = \sqrt{E_o^2 + E_d^2}$$

6. ANALYSIS

Modelling of the structure and of the soil

In the case of straight bridges, it is permitted to use two separate models, for the analysis in the longitudinal and transverse direction, respectively.
When using linear methods of analysis, the actual stiffness of the various elements should be evaluated as realistically as possible. For this purpose: for non ductile bridges and for r.c. or prestressed components not undergoing yielding, the uncracked stiffness is to be used, while for ductile piers an effective moment of inertia, which takes into account of the distribution of the curvatures along the height, is suggested in the Appendix.

Soil deformability, and hence soil-structure interaction (SSI) may be disregarded where the contribution of soil flexibility to the total displacement (measured at the centre of mass of the deck), is less or equal to 30%. When SSI is considered, and the evaluation of soil properties is subject to uncertainty, upper and lower bounds have to be estimated, and the analysis repeated using the two sets of values.

Behaviour factors for linear analysis

The standard method envisaged by the code is a *linear analysis*, dynamic or static, coupled with the use of the design response spectrum. This latter is the same as defined in EC8 Part 1, with the proposed values of the behaviour factor q indicated in Table 1.

From Table 1 one may note that the maximum values of q is q = 3,5 for ductile bridges with concrete and steel piers. This value appears at first to be rather conservative, if compared with the values given by other codes, which for similar structures could be easily twice as high. This, however, has been a deliberate choice, based on the combination of two arguments.

Ductile Elements	Seismic behaviour	
	Limited Ductile	Ductile
Reinforced concrete piers		
Vertical piers in bending (a_s * ≥ 3.5)	1.5	3.5
Squat piers (a_s = 1.0)	1.0	1.0
Inclined struts in bending	1.2	2.0
Steel Piers		
Vertical piers in bending	1.5	3.5
Inclined struts in bending	1.2	2.0
Piers with normal bracing	1.5	2.5
Piers with eccentric bracing	-	3.5
Abutments	1.0	1.0
Arches	1.2	2.0
* a_S = H/L is the aspect ratio of the pier: For 1.0 < a_S < 3.5 the q-factors may be obtained by linear interpolation		

Table 1 - Maximum values of the behaviour factor q

The first one is the definition of the ULS which is, as discussed earlier, a state still distant from the exhaustion of the load-carrying capacity of the critical members.

The second one is that in a large number of cases bridges are to be considered as "irregular" structures, due to the inevitable concentration of ductility demand in a more or less reduced fraction of the piers. Presently, is not possible to derive general rules for detecting the situation just described and, especially, for determining the appropriate values of the forces to design those piers for.

Even q = 3,5 may be too high in certain situations. The code has a warning on this respect, stating that when it occurs that the design seismic force is predominantly absorbed by "one or two very stiff and strong elements (abutments or piers)", with the other more slender piers remaining elastic, q factors in excess of 1,2 must not be used without special justification.

Two further cases for possible reduction of the values of q have to be considered.
One is related to the amount of the design normalized axial force: $\eta_k = N/A_k f_{ck}$. When η_k exceeds 0,3 (it must not be > 0,6) q is linearly reduced to 1 for $\eta_k = 0,6$.
The second one depends on the intended locations of plastic hinges being accessible for inspection and repair or not. In the latter case the q-values are divided by a factor of 1,4.
For pile foundations, where accessibility is questionable at best, a q-value of 2,5 is given (1,5 for inclined piles), provided the piles are detailed for ductility.

Vertical component of the seismic motion

This component needs only to be considered "in the exceptional cases in which the piers are subjected to high bending stresses due to permanent actions of the deck", in all cases of prestressed concrete decks, and for the design of bearings and links.
The behaviour factor for the vertical direction is equal to 1.

Linear Dynamic Analysis

Modal analysis, with the total response obtained as a statistical combination of the modal maxima can be applied in all cases in which a linear analysis is allowed, a condition excluding bridges using isolating devices and "special" bridges as defined earlier, unless these latter are designed for a fully elastic behaviour.

For the combination of the modal maxima, both SRSS and the CQC rules are given, with their respective range of applicability.
Once the analysis is completed for each direction of the seismic action separately (and possibly with a different mechanical model and q-factor) the maximum action effects can be evaluated as:

$$E = \sqrt{E_x^2 + E_y^2 + E_z^2}$$

Alternatively, it is allowed to use as design seismic action A_{Ed} the most unfavourable of the following three combinations:

$$A_{Ex} \text{ "+" } 0{,}3\, A_{Ey} \text{ "+" } 0{,}30\, A_{Ez} \qquad x \rightarrow y \rightarrow z$$

where A_{Ex}, A_{Ey}, A_{Ez} are the design seismic actions in the directions z, y, z.

Linear static analysis

This is basically a first-mode method, in which the mode shape and the corresponding period are determined in an approximate way. Static forces are distributed according to the mode shape, and their intensity is obtained from the response spectrum.

The first-mode approximation can be considered as adequate in the following cases:
a) in the longitudinal direction for straight bridges and provided that the effective mass of the piers is not greater than 1/5 of the mass of the deck.
b) in the transverse direction for the case a), provided the bridge is approximately symmetric with respect to the centre of the deck (excentricity between centre of stiffness of the supporting elements and centre of mass of the deck less than 5% of the length of the bridge).
c) for bridges with simply supported spans with negligible interaction between adjacent piers, and provided the effective mass of the pier is not greater than 1/5 of the mass of the deck carried by the pier.

Depending on the characteristics of the bridge, different levels of approximation can be introduced in the model, so that one can have:
I) a rigid deck model;
II) a flexible deck model;
III) individual pier model.

Model I) is always applicable in the longitudinal direction of straight bridges, and in the transverse direction when the length (L) -width (B) ratio is not greater than 4 or, more generally, if the following condition is satisfied:

$$\Delta d/da \leq 0{,}20$$

where Δd is the maximum relative displacement and da is the average displacement of the pier tops in the transverse direction under a plausible distribution of (normalized) horizontal forces.

Model II) is the alternative to Model I). Fundamental period and mode shape are obtained by the Rayleigh method stopped, if so wished, at the first iteration.

In the transverse direction, in both cases of Model I) and II) an effective excentricity of the mass of the bridge has to be considered, given by the expression:

$$e = e_o + e_a + e_d$$

where e_o is the actual nominal excentricity between centres of mass and stiffness

$e_a = 0{,}03\ L$ is the accidental excentricity

$e_d = 0{,}03\ L\ \sqrt{1 + e_o/e_a}$ is an approximation of the dynamic amplification.

The moment about a vertical axis: $M_t = \pm F \cdot e$, where F is the total inertia force acting on the bridge, has to be resisted by the supporting elements (piers, abutments).

Non-linear dynamic analysis

In addition to isolated and to "special" bridges, ordinary bridges also can be analyzed by means of non-linear step-by-step methods, using as input time-histories which are compatible with the elasti spectrum (q = 1) appropriate for the site.
It is important to note, however, that this method can only be used *in addition* to the standard response spectrum analysis, to provide insight in the post-elastic response, and to compare required with available ductilities. In no case the results from the non-linear analysis can be used to relax requirements resulting from the response spectrum analysis.

7. STRENGTH VERIFICATION

This chapter provides information on:
a) evaluation of the design flexural and shear strengths;
b) the determination of the action effects on which to base the dimensioning of the elements intended to remain elastic (capacity design effects).

a) Design strength of the elements-mechanisms

The design value of the flexural strength: M_{Rd}, is calculated as for non seismic conditions, using the material safety factors: γ_M defined in the other Eurocodes: EC2 (concrete), EC3 (steel) and EC4 (composite). For reinforced concrete in particular, $\gamma_M = \gamma_c = 1{,}5$ for the concrete, and $\gamma_M = \gamma_S = 1{,}15$ for the reinforcing steel.
M_{Rd} is based on the actual geometry and amount of reinforcement of the section, and takes into account the axial force and the bending moment in the orthogonal direction.

For reinforced concrete, the design value of the shear strength depends on whether the zone under consideration is outside or inside a plastic hinge. In the former case, use is made of the same expressions valid for the non seismic conditions (given in EC2).

Within the plastic hinge one has instead:
- strength of the compressed diagonal:

$$V_{Rde} = 0{,}275\ \nu\ f_{ck}\ b_w\ d \qquad (\nu = 0{,}7 - f_{ck}/200)$$

where b_w and d are the thickness of the web and the depth of the section, respectively.

This formula gives about half of the strength one gets outside the plastic hinge, to account for the deterioration of the doubly diagonally cracked concrete.

- verification of shear reinforcement
the strength is the sum of the contribution of concrete and of that of the steel:

$$(V_{cd} + V_{wd})$$

with $V_{cd} = 2{,}5\ \tau_{Rd}\ b_w \cdot d \qquad (\tau_{Rd} = 0{,}035\ f_{ck}^{2/3})$
$V_{wd} = (A_{sw}/s)\ 0{,}9\ d\ f_{ywd}$

(A_{sw} and s are the area and the spacing of the stirrups, respectively, and f_{ywd} the design yield strength).
The contribution of the concrete is applicable only if $\eta_k > 0,1$.

The expression for V_{cd} is much simplified with respect to the one given for the zones outside the plastic hinges, where account is taken additively of the effect of the normal force, and of the geometric ratio of the longitudinal reinforcement. These two factors are believed to loose importance under cyclic shear and bending with considerable ductility demand (above ~ 3÷4).

b) capacity design effects

These effects depend, as it is well known, on the upper value that the flexural strength at the plastic hinges can attain due to a number of reasons. This moment overstrength is expressed as:

$$M_o = \gamma_o M_{Rd}$$

where γ_o, called overstrength factor, is given by:

$$\gamma_o = 0,7 + 0,2\ q$$

The dependence of γ_o on q is logical since one of the reasons for the overstrength is the amount of ductility which is used at a local and hence at a global level, which is reflected by q.
In the case of reinforced concrete sections, γ_o is also made dependent upon the amount of normal (compressive) force, which is a possible cause for the increase of the ultimate moment:

$$\gamma_o = [1 + 2\ (\eta_k - 0,1)^2] \cdot (0,7 + 0,2\ q)$$

A general procedure for evaluating the capacity design effects: F_C in any particular member is explained in an Annex of the code as follows: calling M_G the bending moment at a generic section due to dead load plus all other non seismic loads, and F_G the action effect (moment, shear, force, etc.) in some other element of interest, calculate the variation ΔF_C of the action effect F_G caused by the increase of the relevant bending moments from their values M_G to their overstrength values $\gamma_o M_{Rd}$: $\Delta M = \gamma_o M_{Rd} - M_G$.

The capacity design effect in the element of interest is: $F_C = F_G + \Delta F_C$.

Simplifications of the above approach are immediate when the bending moments are predominantly if not exclusively caused by the seismic action above.

Capacity design effects are to be used for the design of:
- the flexural and shear strength of the deck;
- the shear strength of the piers;
- the connections between deck and piers/abutments;
- the foundations of the piers/abutments.

8. SPECIFIC DETAILING RULES

The aspects of major relevance covered in this chapter are:
I) provisions for ensuring a ductile behaviour of the piers (and of the piles, when required). Since the deck must in general be designed for an elastic behaviour, it needs not to be detailed for ductility;
II) the design of bearings and links;
III) the design of the abutments.

I) Ductility of reinforced concrete piers

There are two conditions for exception from the need of detailing:
- $\eta_k \leq 0{,}08$
- for flanged cross-sections, if a curvature ductility $\mu_c = 13$ can be achieved with the maximum compressive strain not exceeding 0,35%.

The arrangement of the confining hoops and ties in the plastic hinge zones does not depart significantly from that required in EC8 Part 1 for the columns of buildings. Typical details are shown in Fig.1.
The minimum mechanical reinforcement ratio is given by the formulas:

- rectangular hoops $\omega_{wd,r} = 1.74 \frac{A_c}{A_{cc}} (0{,}009\ \mu_c + 0{,}17)\ \eta_k - 0{,}07 \geq \omega_{w\ min}$
- circular hoops $\omega_{wd,c} = 1{,}40\ \omega_{wd,r}$

where:
$\omega_{wd,r} = (A_{sw}/s{\cdot}b) \cdot f_{yd} / f_{cd}$
$\omega_{wd,c} = (4\ A_{sp} / D_{sp} \cdot s) \cdot f_{yd} / f_{cd}$

A_{sw} is the total area of hoops and ties in one direction
A_{sp}, A_{cc} are gross and confined concrete area, respectively, and the required curvature ductility μ_c and the minimum values of ω_w are given in Table 2.

Seismic behaviour	μ_c	$\omega_{w\ min}$
Ductile	13	0,12
Limited ductile	7	0,08

Table 2 - Minimum values of μ_c and $\omega_{w\ min}$

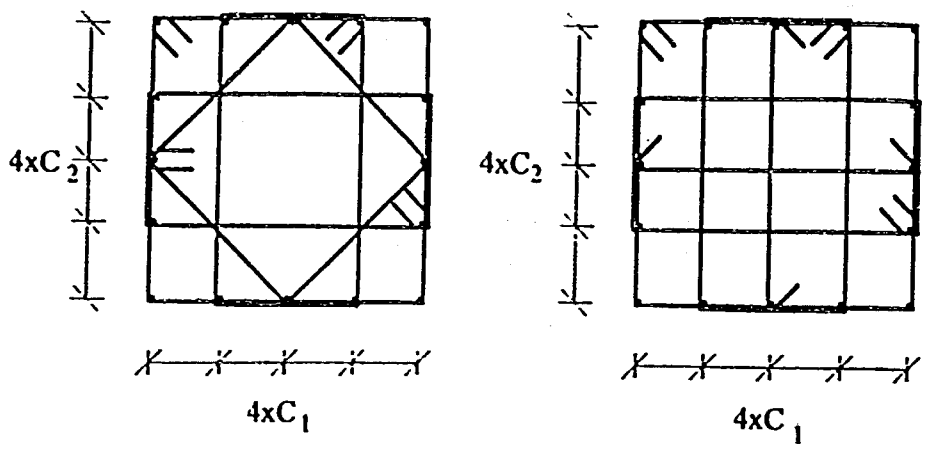
The amount of reinforcement required by the expressions above must be extended in full for a length L_h equal to the largest of the following:
- depth of the pier perpendicular to the axis of the hinge;
- distance from the section of maximum moment to the section where the moment is reduced to 80% of the max.

This length must be further increased by 50% if $\eta_k > 0{,}3$.
The reduction of the reinforcement along the height of the pier must be such that in the adjacent portion of length L_h at least 50% of the full amount is provided.

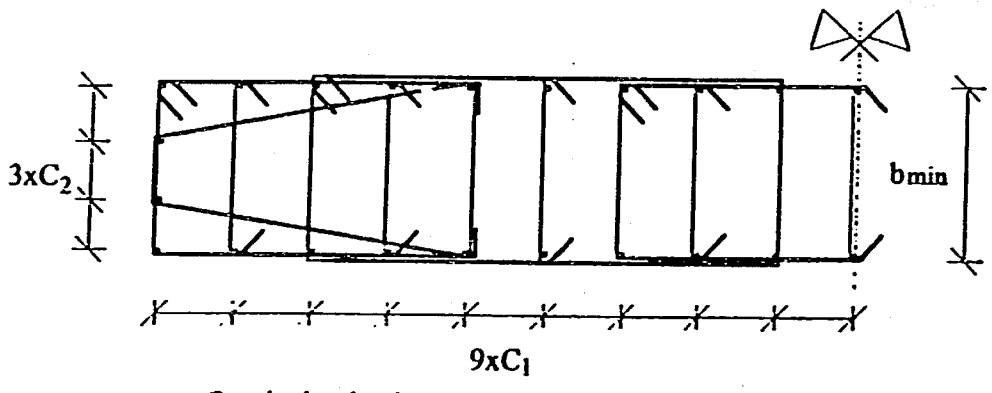
As mentioned earlier, the foundations are to be designed such as to remain elastic under the capacity design effects.
This is not always feasible in the case of pile foundations, where plastic zones may occur near the pile heads and at the interfaces of soil layers having markedly different shear deformability. In order to ensure integrity and ductile behaviour, piles need in these cases to be detailed in the same way and amount as indicated for the piers, for a minimum length of 5 pile diameters close to the foundation, and a length of 2 pile diameters on each side of the interface between layers.

II) Bearings and seismic links

The design of the connections between deck and piers/abutments is an important component of the design process aiming at satisfying the safety requirements of the ULS.
The criterion adopted is to require that:
- *fixed bearings* be either designed for capacity design effects or just for the effects coming from the design seismic condition, but in this case be combined with seismic links acting as a second line of defense.

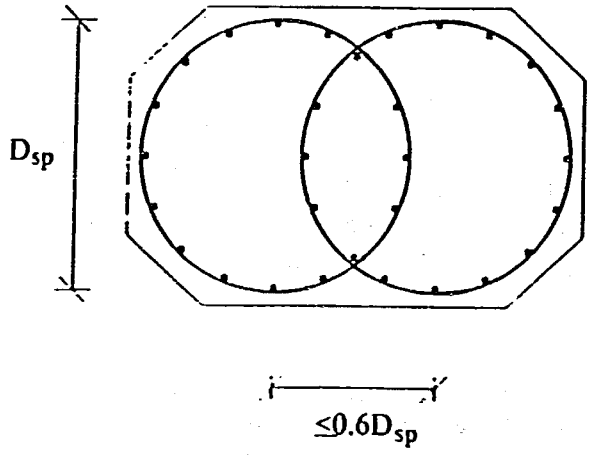


$C_1 \leq \min(b/3 , 350mm)$
C_2 need not be <200mm



Overlaping hooks + crossties (wall-type element)

Typical details using overlapping hooks and crossties



Typical detail using interlocking spirals

Figure 1 - Typical details of confining reinforcement

- *moveable bearings* be designed to accomodate without damage the total seismic displacement:

$$d_{Ed} = d_E + d_G + d_{Ts}$$

where:

d_E is the displacement due to the design seismic action, evaluated as: $d_E = q.d_{Ee}$, with d_{Ee} the value obtained from the linear analysis, dynamic or static

d_G is the long-term displacement due to permanent actions (ex. creep and shrinkage)

d_{Ts} is the displacement due to thermal effects to be combined with the seismic action, to be evaluated as: 0,4 d_T, with d_T the displacement due to design thermal effects.

In addition to the above, either adequate seating lengths or seismic links need to provided, as specified in the following:

- *elastomeric bearings*
  - when they are used without any other accompanying type of bearing or link to resist the seismic action, they are seen as isolating devices, and their design, as well as that of the whole bridge, is subject to the provisions of the relevant section of the code.
  - when they are used in combination with fixed bearings or seismic links which resist the design seismic action, they must be designed to accomodate without damage the maximum shear deformation

- *seismic links*

  In those cases where seismic links are required, they must be designed to resist:
  - capacity design effects, when the links are combined with elastomeric bearings
  - when links combine with moveable bearings, and the seating length is not adequate, in the absence of a rational analysis which accounts for the dynamic interaction between piers and desk, a force equal to: $\alpha \cdot Q$, where $\alpha = A_g/g$ with A_g the design ground acceleration, and Q the weight of the section of the deck which is linked or, when two deck sections are linked together, the least of the two weights.

  The links must be provided with a slack so as to remain inactive under the design seismic action

- *minimum overlap lengths*

  At supports where relative displacement between supported and supporting elements is intended to occur under seismic conditions, the integrity (ULS) of the bridge is guaranteed either by links (see above) or by an adequate overlap length.

  In the absence of a more accurate estimation, the minimum length: l_{ov} to be provided is given by:

$$l_{ov} = l_m + d_{eg} + d_{es}$$

  where:

  l_m is the minimum support length required for non-seismic situations ($\geq$ 40 cm)

  d_{eg} is the relative displacement of the two parts, due to the relative displacements of the soil

  d_{es} is the relative displacement due to the response of the structure under the design seismic action

In the case of a separation joint located within one span or over an intermediate pier, l_{ov} is estimated by taking the square roof of the sum of the squares of the values calculated for each of the two sides in the first case, or for the deck and the pier in the second.

III) <u>Reinforced concrete abutments</u>

Since the abutments are generally poor and difficult to control dissipative elements, the design criterion is to keep them elastic, under the design seismic action. This choice makes them subject to capacity design procedures.

A distinction is made between flexible or rigid types of connection with the deck.

In the case of *flexible connection* (moveable or elastomeric bearings) the capacity criterion requires the abutments to remain stable under the earth pressure including seismic effects, the inertia forces due to its own mass, and the actions from the bearings determined as capacity design effects, (30% increase of the friction coefficient, 30% increase of the stiffness of the elastomeric bearings, for the shear deformation due to the design seismic action).
If the earth pressure is determined on the basis of an acceptable displacement of the abutment, it has to be proved that this displacement does not in fact lead to the functional failure of the abutment.

In the case of *rigid connection*, the model adopted for the seismic analysis has to account, in an appropriate way, of the interaction between soil and abutment, using high and low estimates of the soil parameters. This analysis has to be made with q-factor equal to 1, and the resulting forces are used both for the design of the connection and the verification of the abutment.

9. CONCLUSIONS

The Eurocode 8 - Part 2, dealing with the seismic design of bridges, has been presented with sufficient detail to allow an opinion to be formed on both its general layout and the main operational procedures.
EC8 Part 2 contains also a section on the design of isolated bridges, which has been omitted here because of its specialized nature, which may be worth a separate presentation, and because it will be developed to include the adoption of dissipative devices.
Although the document draws from existing practice in the field, especially from U.S. and New Zealand, it has been planned and written from zero and with a fresh mind, a situation which normally favours a more rational outcome than by up-grading conceptually inadequate documents. The implication of a certain rationality does not obviously exclude the consciousness of the present limitations and the desire to improve both the concepts and the rules, whenever feasible. The three years experimental period is expected to give a tangible contribution towards these ends.

REFERENCES

Eurocode 8 - Earthquake Resistant Design of Structures - Part 2 - Bridges
European Prestandard ENV 1988-2. October 1994. CEN Brussels

IRREGULAR BRIDGES DESIGNED ACCORDING TO EUROCODE 8 NUMERICAL AND EXPERIMENTAL VERIFICATIONS

G.M. Calvi, Dipartimento di Meccanica Strutturale, Università degli Studi di Pavia

P.E. Pinto, Dipartimento di Ingegneria Strutturale e Geotecnica, Università di Roma "La Sapienza"

ABSTRACT

This paper describes the state of progress of an analytical and experimental research programme supported by the European Union (EU) in order to provide background and improvement to the design provisions contained in Eurocode 8, Part 2, Bridges. Pseudo-dynamic tests on unusually large scale models of bridges (1:2.5) and shaking table tests on models scaled to 1:8 are being performed. The specific purpose of these tests, as well as the criteria adopted to select and design the model bridges are illustrated. "Accurate" computer codes have been used to predict the response of all the tests: their real capabilities will be therefore experimentally verified to allow extensive and reliable parametric analyses in a second part of the project. A better calibration of EC8-Bridges will hopefully result.

1. INTRODUCTION

In June 1994 a document titled "Eurocode 8: Earthquake Resistant Design of Structures - Part 2, Bridges" [1] has been approved by the representatives of the eighteen members of CEN (Comité Europeén de Normalisation), which is the official body of the twelve EU countries and of the six EFTA countries entitled to release codes of standard.
This document is now being published as a European pre-standard, intended for experimental use and submission of comments, with an initially allotted life of three years. After this time period, CEN members will be invited to submit formal comments to be taken into account in the preparation of an official European Code of Standard.
In 1993 the Commission of the EU launched a programme of numerical and experimental research specifically aimed at providing a scientifically sound background to the provisions contained in EC8, particularly in the several areas where the supporting knowledge was felt to be inadequate. A sector of this program is devoted to bridges and five institutions from three European countries plus the Joint Research Centre (JRC) at Ispra (I) are involved in it.

The main objective is the improvement of the design procedures for "irregular" bridges, this being by definition the case when the application of a global force reduction factor (q-factor in EC8) produces unacceptable concentration of ductility demand in some pier. The solution is sought in two steps:

- the identification of one (or a set of) parameter(s) capable of detecting a situation of irregularity, and
- the formulation of a set of rules for assigning appropriate different q-factors to various parts of a bridge, or anyway the formulation of alternative design procedures.

To arrive to this result, large scale experimental tests and large numbers of numerical simulations will be run in parallel, with the objective of verifying the accuracy of the models and then to make use of them for extensive parametric simulations.

This paper describes the part of the ongoing activity which is in a more advanced state of progress, therefore allowing some discussion of preliminary results.

This part includes:

- pseudo dynamic tests (PDT) on models of four-spans bridges, with piers having hollow rectangular cross section, at a scale of 1:2.5;
- shaking table tests (STT) on bridge models scaled to 1:8, having three piers fixed to three different shaking tables;
- parametric analysis studies to verify the method proposed in EC8-2 and to classify bridges in regular and irregular classes, needing different design provisions;
- conceivement of alternative design methods for irregular bridges.

The selection of the models to be tested is the result of a vast preliminary analysis of several thousands of bridge configurations, in which three to five piers 10 to 50 m tall were arranged along the deck length in different combinations. Each hypothetical bridge was designed according to EC8, an inelastic time-history analysis was then performed to ascertain if some pier was showing a ductility demand not compatible with the design assumptions, in which case the bridge was defined irregular. Two base configurations, representative of rather extreme cases of regularity and irregularity, were then selected for PDT and STT tests. More refined numerical analyses were performed on these bridges to serve as pre-simulations of the actual tests.

2. OUTLINE OF THE EXPERIMENTAL PROGRAM

2.1 Pseudo-dynamic tests

The first experimental PSD tests will be performed on four bridges, whose unscaled geometry is shown in figure 1. The scale will be exactly 1:2.5, so that the models will have piers with heights of 2.8 (7.0), 5.6 (14.0) and 8.4 (21.0) meters, and cross sections of 0.80 x 1.60 (2.00 x 4.00) m, with wall thickness of 0.16 (0.40) m (in parenthesis the real dimensions are given).

The deck and the abutments are supposed to remain elastic and simulated numerically by means of sub-structuring techniques.

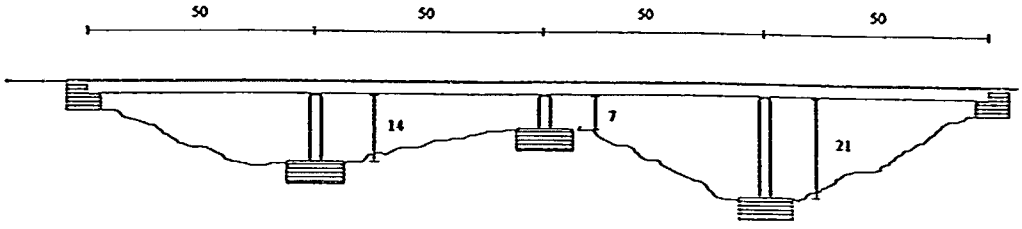
The superstructure is meant to be made of a deck running continuously over the piers, with pinned connections both with the piers top and the abutments.

The seismic action will be applied in the transverse direction.

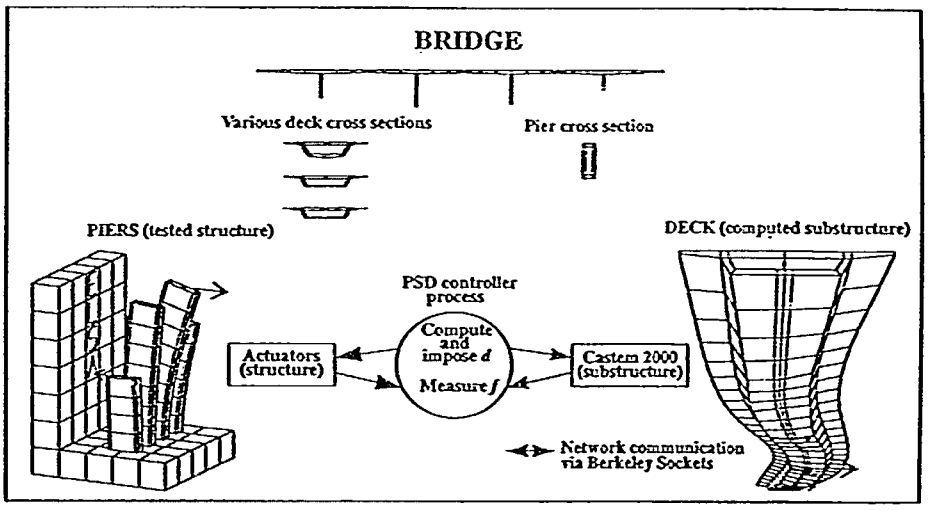
The bridges identified with 232 and 213A (the numbers reflect the sequencing of the three pier heights) have been designed according to EC8, for a PGA of 0.35 g.

Bridges 213B and 213C are variants of the EC8 design, corresponding to two different criteria, both starting from the evidence of the preliminary inelastic design, which showed that the

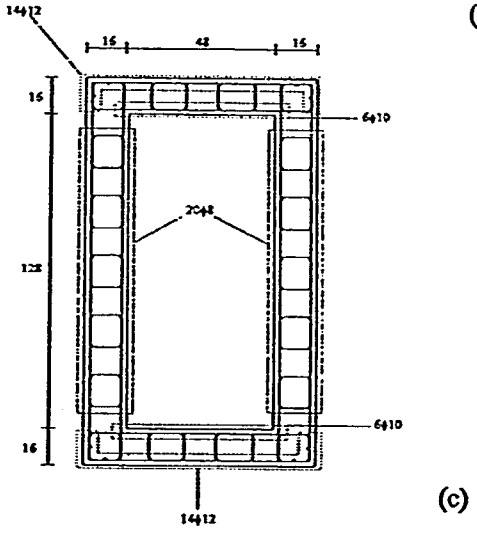
central pier is in a critical situation, with a ductility demand significantly higher than what assumed in the design phase. Bridge 213B attempts to improve the situation in a more obvious way, i.e. increasing the reinforcement of the central pier: the non-linear analysis shows in this case a reduced ductility demand. In bridge 213C the reinforcement of the central pier is kept constant, while it is increased in the two adjacent piers; in this case the design philosophy relies on more physical concepts, i.e. it tries to subtract forces from the central pier, and to increase its ductility capacity rather then reducing its ductility demand.



(a)



(b)



(c)

Fig. 1 PSD tests of bridges at the JRC, Ispra. Real bridge (a), testing apparatus (b), cross section of a model pier (c).

The reinforcement percentages finally adopted are shown in table 1.

BRIDGE	PIER1	PIER2	PIER3
232	1.15	0.64	1.15
213A	0.50	0.89	0.50
213B	0.50	1.59	0.50
213C	1.15	0.89	1.15

Table 1. Amount of longitudinal reinforcement (%) in the model piers
(0.50 % was assumed as minimum reinforcement percentage)

The horizontal loads will be applied against the concrete reaction wall of the ELSA laboratory at the JRC. Since the deck is supposed (and required by EC8) to remain elastic, its response will be simulated numerically, and the piers will be actually placed side-by-side assuming a total of three degrees of freedom corresponding to the translational components along the direction of the seismic input at the top of the piers. A sub-structuring technique will be therefore coupled with the PSD test method. The seismic input will be consistent with the spectrum given in the EC8 for medium soil (class B).

2.2 Shaking table tests

Two models are planned for the shaking table tests to be carried out at the ISMES laboratory in Bergamo (I). The arrangement of the tests is shown in figure 2: each one of the three piers is fixed to a different table. Both models correspond to bridge 213A, but are scaled to 1:8.
Also, it was technically impossible to build the two abutments providing a reasonable input motion to their base: two more shaking tables were not available, and it resulted impossible to fix them to the lateral shaking tables. The side spans were then ended at one third of their length and left free to oscillate. Therefore the response of this model tends to represent the central part of a longer bridge rather than a complete bridge. In this case the end sections could be viewed as corresponding to movement joints in the deck.
The horizontal accelerations are again applied in the transversal direction.
The piers have the solid I-shaped section shown in figure 2, with external dimensions 0.50 x 0.20 m, and are therefore approximately scaled to the ratio of 1:8 with respect to the already described assumed real dimensions. The heights of the model piers are 0.90-1.80-2.70 m, and also correspond with some approximation to the real heights of 7-14-21 m.
Due to the absence of the abutments, the deck cannot be simply pinned at the top of the piers: the rigid connection between deck and piers involves an exchange of torsional and bending moments between the two, so that the piers no longer act as pure cantilever. For a more detailed discussion of this aspect see [2].
These two models also have been designed according to EC8 for a PGA of 0.35 g. For the first one, the spectrum is the one, already used, for the intermediate soil type (class B of EC8), and during the tests it will be tried to keep three synchronous base acceleration.
The second model is intended to investigate the validity of the EC8 provisions for the case in which the piers rests on different soil types. To design, an average response spectrum is defined, valid for the entire bridge, where the different spectra appropriate for the various piers are weighted with the stiffness of the respective pier. During the test, each pier will be excited by sample non-synchronous accelerograms compatible with the spectrum appropriate to its soil conditions.

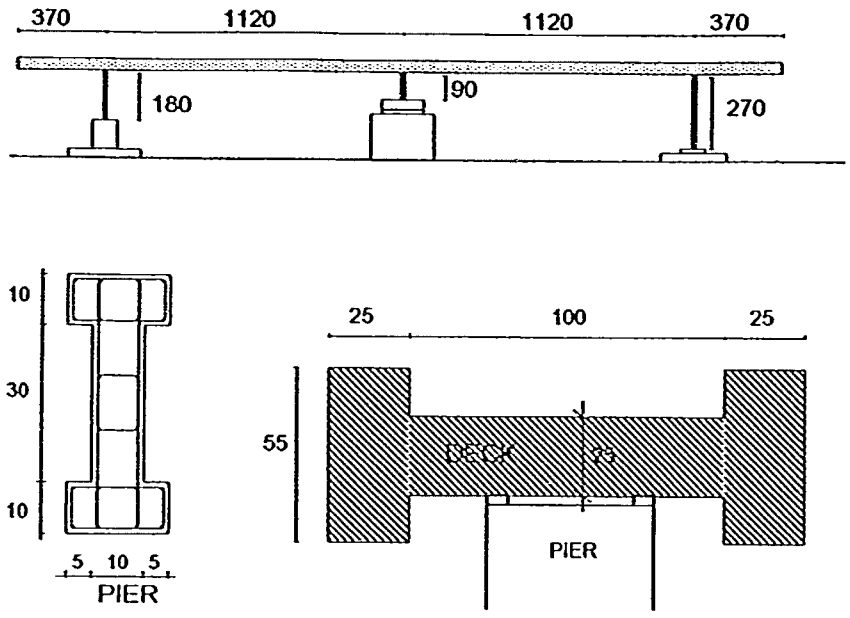


Fig. 2 Shaking table tests at ISMES. Elevation of the model, cross section of piers and deck. (measures given in cm)

3. NUMERICAL SIMULATIONS

3.1 Parametric analyses

Several thousands of bridges have been analyzed using several different computer programs, with a few main objectives:

- the verification of design procedures suggestes in ther present version of EC8-2;
- the definition of regular bridges, for which ordinary design rpocedures are acceorabke, and irregular bridges, for which more sophisticated methods need to be developed;
- the formulation of a "regularity index" to classify a priori a given bridge in the classes previously defined;
- the identification of fewer bridges to be analyzed in more detail and to be possibly tested.

Some of the results obtained are shown in figure 3, where the maximum required ductility is given as a function of a regularity index for a number of bridges. The effectiveness of the regularity index, defined in terms of a combinaiton of the whole bridge and of the deck alone [3], is clear from the figure.

On the base of these parametric analyses the bridges described in the previous and the following sections have been selected for more detailed studies.

3.2 Simulations of the pseudo-dynamic tests

Extensive comparative simulations of the four model tests have been carried out using either simplified (Takeda-like models) and relatively accurate (fibre models) analytical tools: see [4, 5, 6 and 7]. The level of agreement of the different analyses is in general acceptable. This is probably largely due to the simplicity of the structures considered. In order to illustrate the main characteristics of the response the main results presented in [8] will be briefly introduced and commented.

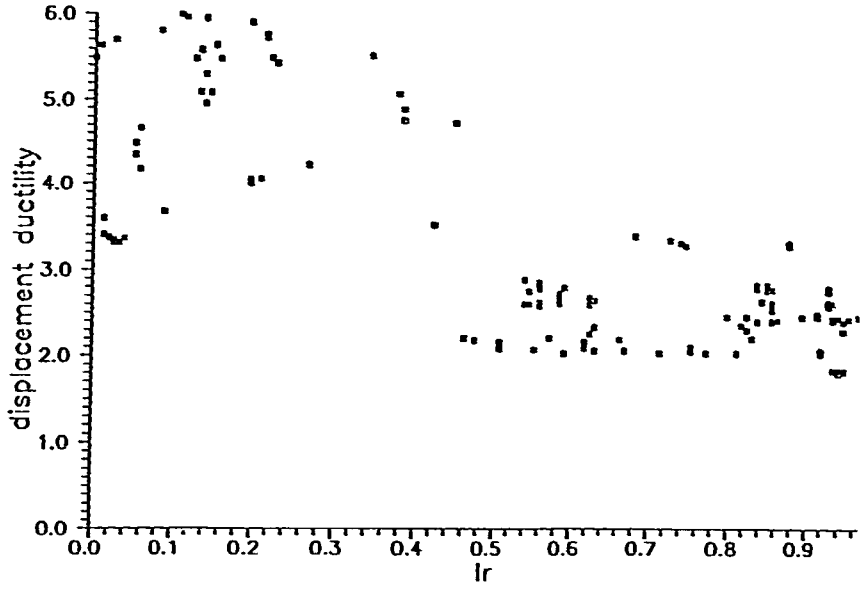


Fig. 3 Required ductility as a function of a regularity index

For example, the element presented in [4] makes use of beam-column elements with the non-linearity distributed and discretized along the element. A number of cross sections is monitored within each element during the analysis and at each time step the (tangent) element stiffness results from the integration of the sections properties, obtained in turn from the integration of filaments (fibres) properties described in terms of realistic stress-strain mono-axial laws of general nature.

The limitations in modelling are those common to most program of the same kind, being difficult or impossible to be taken into account:

- bond deterioration, and consequently any slip between concrete and steel and any yield penetration;
- contribution of non-linear shear behaviour to element deformability;
- shear flexure interaction for both strength and deformability.

The first limitation can have a significant influence on the yield displacement, while the second and third are believed to play a significant role in the case of the short central pier of bridges 213A\B\C.

The main results obtained for the four models are illustrated in table 2, where the maximum displacements, shear and required ductility are shown. The maximum values are the average values resulting from seven spectrum-compatible accelerograms.

Attention is called to bridge 213 and specifically to the consequences on the central pier of different design philosophies. From case B (central pier strengthened with respect to the EC8 design) to case C (central pier unvaried, outer piers strengthened) the displacement of the central (critical) pier results doubled (fig. 4). As expected, a strengthening of the central pier produces an attraction of larger shear forces (as shown in figure 5). The ratio of the shear forces in case B and C is also approximately two, depending essentially on the proportion of the flexural strengths.

The result for the case 213B, however, may not be fully reliable, since the analytical model neglects the shear deformability, which at this level of shear may be of the same order of magnitude as the flexural one. The stiffness of the pier may therefore be overestimated.

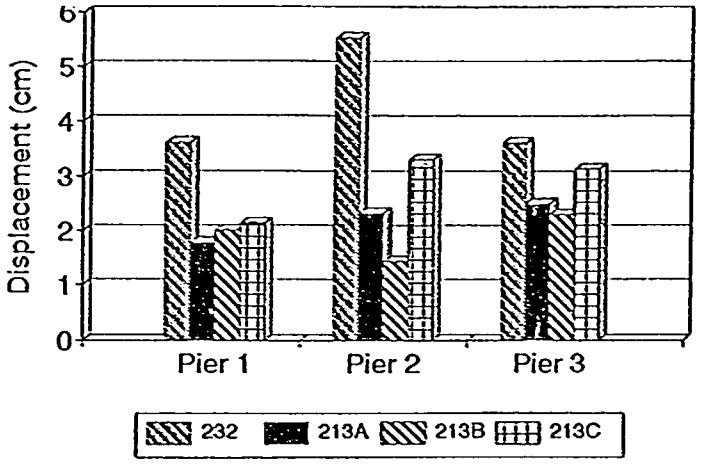


Fig. 4 Pseudodynamic tests models: maximum displacement at the top of the piers

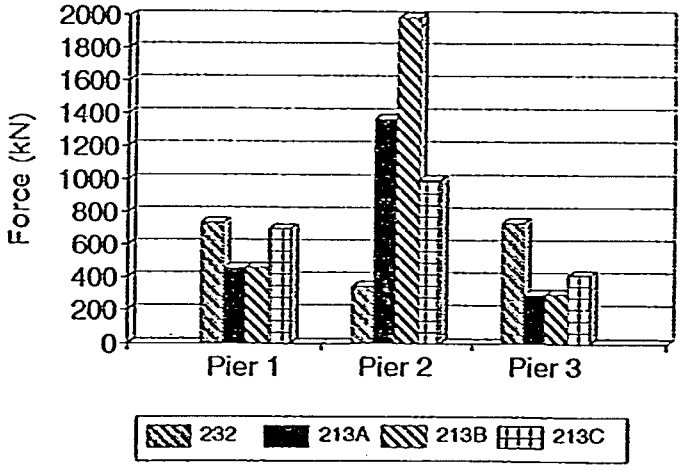


Fig. 5 Pseudodynamic tests models: maximum shear forces in the piers

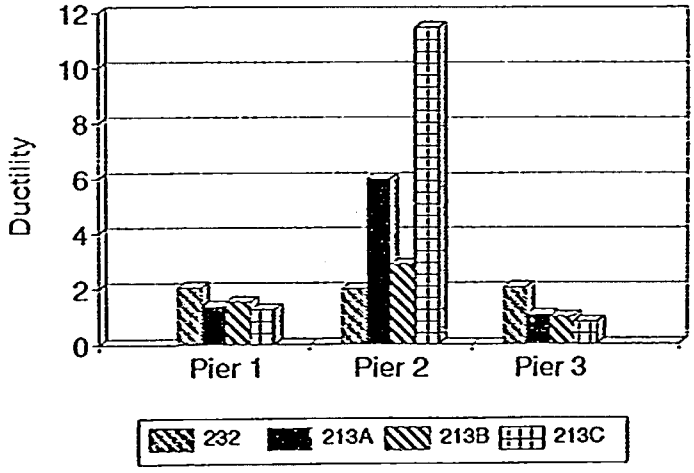


Fig. 6 Pseudodynamic tests models: maximum required displacement ductility of the pier

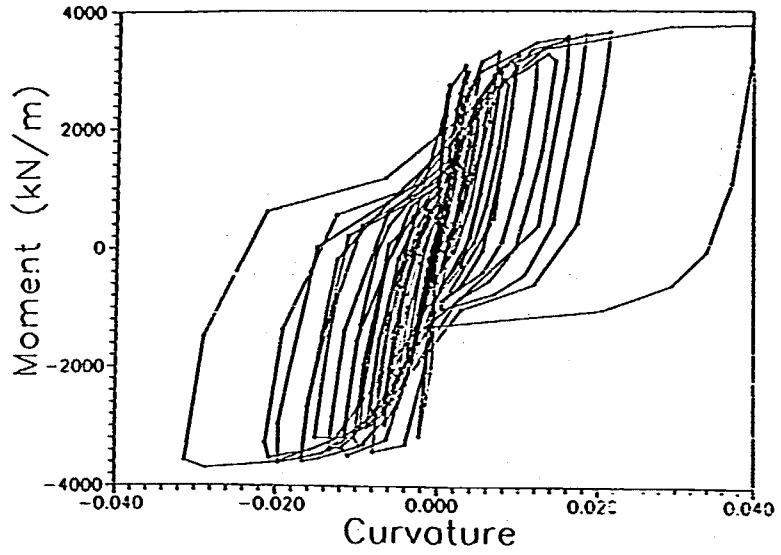


Fig. 7 PDT test, bridge 213A, central pier, base section, moment-curvature history

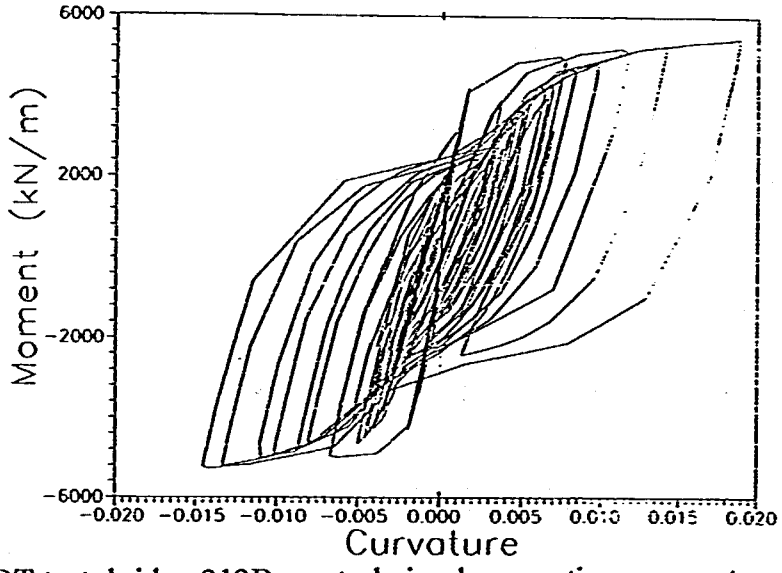


Fig. 8 PDT test, bridge 213B, central pier, base section, moment-curvature history

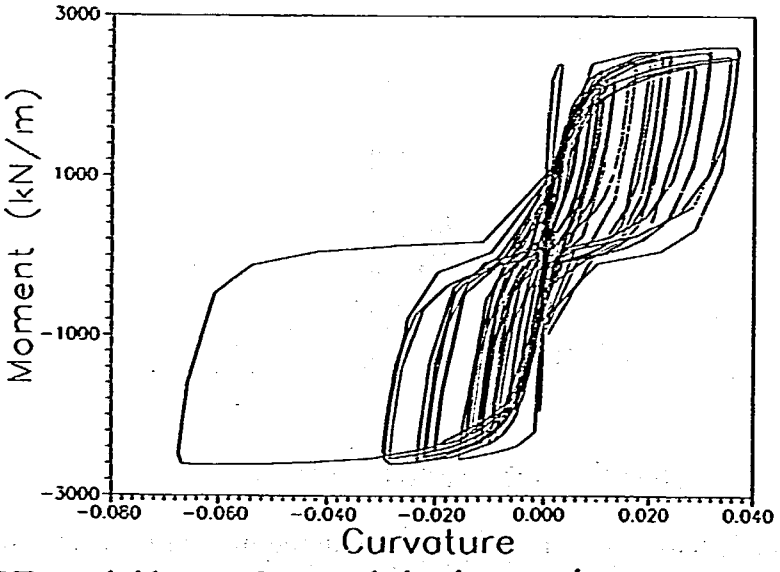


Fig. 9 PDT test, bridge 213C, central pier, base section, moment-curvature history

	PIER	BRIDGE TYPE			
		232	213A	213B	213C
Disp. (cm)	1	3.93	2.22	2.32	2.61
	2	6.09	3.01	1.60	3.93
	3	3.93	2.61	2.53	3.38
Shear (kN)	1	747	471	461	718
	2	350	1409	2007	1009
	3	747	301	300	429
Duct.	1	2.26	1.69	1.76	1.49
	2	2.20	7.72	3.20	13.55
	3	2.26	1.09	1.05	0.83

Table 2. Results from the analysis of the pseudodynamic tests models

Figure 6 Shows the maximum ductility demands, and it seems to prove that the design philosophy adopted in case C is not effective: while strengthening the central pier (case B) reduces the ductility demand, in case C the demand shots up to an unsustainable value.
The plots of the moment-curvature paths of the base section of the central pier during a response time history for the three cases A, B and C are shown in figures 7, 8 and 9. The assumed limit value of the curvature of the section is approximately 0.035 m^{-1}, value which is slightly exceeded only once in case A. In case B a large reduction of the demand (about one half) occurs, while in case C three cycles involve the attainment of the limit, and one cycle is very likely to induce the collapse of the section.

3.2 Shaking table tests

The pattern of the shaking table models is similar to that of the PDT models: a short central pier sided by one of twice its height on the right and one three times its height on the left. Cross sections of piers and deck are different, but have similar elastic stiffness, the abutments are not present and the scale is significantly reduced with respect to the PDT case.
The analytical simulations are presently available only for the case with similar soil conditions at the base of the three piers. The program described in [5] has been used for this simulation. The results shown in figures 10, 11 and 12 consist in the force-displacement histories at the top of the three piers during the response.
As expected, for the case of an irregular bridge like this one a standard design procedure such as the one proposed in the EC8 shows its inadequacy, being unable to produce acceptably uniform ductility demands using a single q-factor applied to the structure as a whole.
At the left pier the response is only moderately inelastic (fig. 10) at the central pier the displacement ductility demand far exceeds the design value (fig. 11), while the higher pier at the right shows an almost non-dissipative bi-linear behaviour essentially reflecting the opening and closing of the cracks (fig. 12).

4. PRELIMINARY DEVELOPMENT OF ALTERNATIVE DESIGN METHODS

The experimental and numerical studies briefly discussed have lead naturally to the development of new design methodologies which seek to improve the shortcomings of existing EC8 provisions. In [9] a method is outlined for the displacement-based design of multi-degree-of-freedom bridge structures. The procedures is based on the assumption of a displaced shape

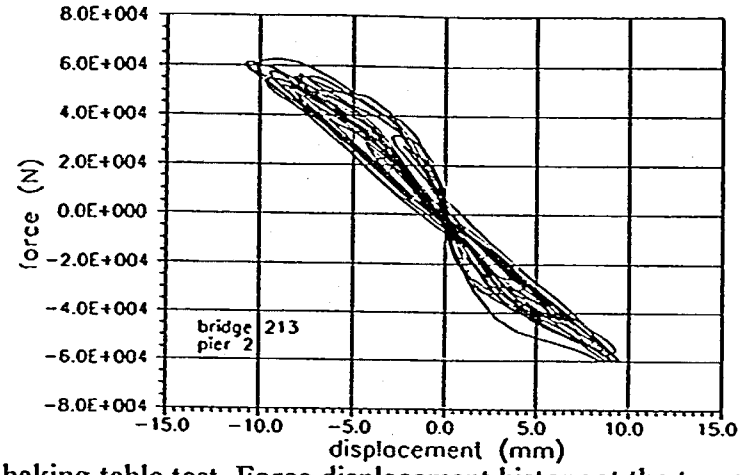


Fig. 10 Shaking table test. Force displacement history at the top of the pier 1.8 m high

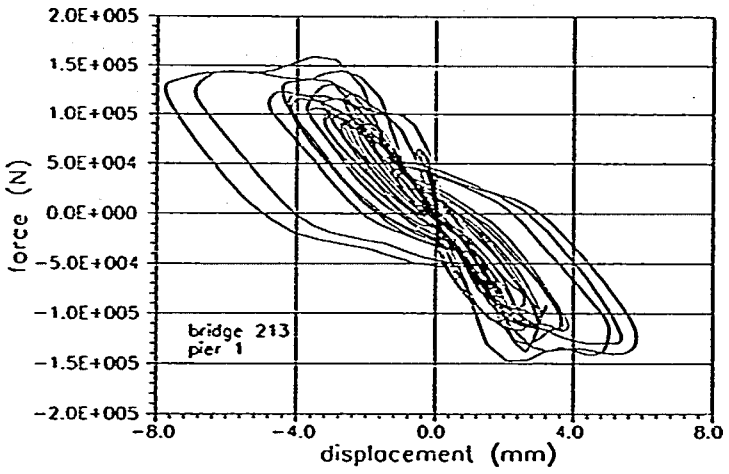


Fig. 11 Shaking table test. Force displacement history at the top of the pier 0.9 m high

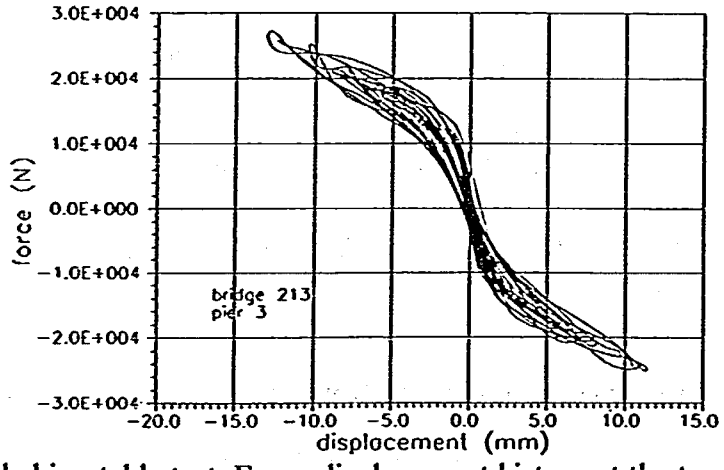


Fig. 12 Shaking table test. Force displacement history at the top of the pier 2.7 m high

for the structure, and the subsequent reduction of the system to an equivalent single-degree-of-freedom (SDOF) system. With the determination of a desired displacement and damping in the equivalent SDOF structure, displacement response spectra are used to determine the required stiffness of the structure, and hence the applied force. Assuming that the applied forces in the MDOF structure are distributed in proportion to the displacement, hte structure is analyzed under the calculated force distribution, and the member reinforcement designed accordingly. The process is repeated until the stiffness and displaced shape of the structure converge to those specified in the design. Such a displacement-based design process offers several advantages over a force-based process, among them the ability to explicitly consider the displacement demand (i.e. damage) in each member rather than assigning a single, force-based global behaviour factor to the structure. The required force to be resisted becomes largely a function of the damping, and thus is related directly to the energy dissipation, hysteretic characteristics, and the acceptable damage on a local level. The process was shown to work

better for the design of regular bridges than for highly irregular bridges with several prominent modes of vibration. In all cases, however, the results obtained with the displacement-based process were better than those obtained with a force-based process, i.e. the response predicted in the design phase was always more similar to the resposne obtained from a refined non-linear analysis.

4. CONCLUSIONS

Larger than proportional benefits can be expected from the integration of qualified research centres, each one having a specific area of expertise, into a common programme with well defined objectives.
Although joint research programmes are not a novelty, the programme presented in this paper combines, perhaps for the first time, large scale multi-degrees-of-freedom pseudo-dynamic tests with multiple shaking table tests and advanced numerical simulation.
The validation of the analytical models and, through them, the improvement of some unsatisfactory rules contained in the EC8, are among the benefits to be obtained.
It would not come unexpected if the tests would provide additional information related to behaviour, modelling and design (e.g. in relation to shear-flexure interaction, localised slip phenomena, effect of torsional rigidity of the deck on the inelastic response and capacity design procedures) which would contribute to important advances in the several still shadowy areas of earthquake engineering.

ACKNOWLEDGEMENTS

The authors wish to thank E. Alarcon, M. Casirati, J. Donea, A. Elnashai, G. Franchioni, J. Guedes, P. Moncecchi, P. Negro, A. Pavese, P. Pegon, A. Pinto, M. Petrangeli, G. Verzeletti, all participating in the research program at various titles. The Commission of the European Union is funding the research project through the HCM programme (Project N. ERB CHR XCT 920011).

REFERENCES

[1] *Eurocode 8, Structures in Seismic Regions - Design, Part 2, Bridges*, ENV 1998-2, CEN, Brussels, 1994

[2] Donea, J., G. Magonette, P. Negro, P. Pegon, A. Pinto, G. Verzeletti, *Pseudodynamic testing of large-scale models of civil engineering structures at the ELSA reaction wall*, Proc. of the 10 ECEE, Vienna, 1994

[3] Calvi, G. M., A. Elnashai and A. Pavese, *Influence of regularity on the response of R.C. bridges*, 2nd International Workshop on Seismic Design of Bridges, Queenstown 1994

[4] Petrangeli, M. and V. Ciampi, *A flexibility based 3-dimensional fiber beam element*, Proc. of the 8th Symposium of Computational Mechanics, Torino, 1994

[5] Izzuddin, B.A. and S.A. Elnashai, *Adaptic, A program for adaptive large displacement elastoplastic dynamic analysis steel concrete and composite frames*, report No. ESEE 7/89, Engineering Seismology and Earthquake Engineering, Imperial college, London, 1989

[6] Giannini, R., G. Monti, C. Nuti and T. Pagnoni, *Aspidea, a program for non-linear analysis of isolated bridges under non-synchronous seismic action*, Disat Report 5\92, Università dell'Aquila, 1992

[7] Guedes, J., P. Pegon and A. V. Pinto, *A Fiber Timoshenko beam element in CASTEM 2000*, SP of Applied Mechanics Unit, Safety Technology Institute, JRC, Ispra, 1994

[8] Petrangeli, M. and P. E. Pinto, *Non-linear dynamic analysis of the four model bridges to be tested at the JRC, Ispra*, PREC8 project, Preliminary Report, 1994

[9] Calvi, G. M., and G. R. Kingsley, *Displacement-based seismic design of multi-degree-of-freedom bridge structures*, Earthquake Engineering and Structural Dynamics, vol.24, 1995, 1247-1266.

LARGE-SCALE PSEUDODYNAMIC TESTS ON HIGHLY IRREGULAR BRIDGES

P. Negro A.V. Pinto

ELSA Laboratory, Safety Technology Institute
Joint Research Centre, European Commission
21020 Ispra (VA), Italy

ABSTRACT

Six large-scale (1:2.5) bridge specimens have been constructed and are being tested pseudodynamically at the European Laboratory for Structural Assessment (ELSA). The tests are being conducted in the framework of the activities of the integrated European programme of pre-normative research in support of Eurocode 8. The experimental programme is intended to assess the results of the numerical calculations, in view of a calibration and possible improvement of the design and analysis methods. The first part of the programme (testing of four bridges) has been devoted to exploring different design solutions aimed at obtaining a more homogeneous ductility demand in irregular bridges. A test to check the possibility to obtain a more homogenous ductility demand by means of the introduction of isolators is being prepared. A test in which asynchronous base-motion will be simulated at the base of the piers is also foreseen.

After a brief description of the activities of the pre-normative research programme, the series of pseudodynamic tests being conducted for the bridges are described. The preliminary results obtained for the first part of the programme (regular and irregular bridges with different reinforcement arrangements) are presented.

1. THE PRE-NORMATIVE RESEARCH PROGRAMME

The Eurocodes --the European provisional standards for constructions-- are being prepared by the European Committee for Standardization (CEN, Technical Committee No 250) under mandate of the European Commission. The Eurocodes are being released by the CEC as provisional norms (ENV). After a period of three years, during which comments are expected, the Eurocodes will be accepted as European norms (EV). The process of approval of each Eurocode has reached different stages. For the case of Eurocode 8 (EC8) [1], the code relevant to the design of structures in seismic areas, priority needs for supporting research have been identified.

A scientific network has been set up to accomplish a Pre-normative Research Programme in support of EuroCode 8 (PREC8), under the Human Capital and Mobility programme of the European Commission. The network groups 18 research organisations in the European Union. The identified priority topics are:

- *Reinforced concrete frames and walls*: The objective is to clarify the interrelation between a

number of design parameters used in EC8 which, in a combined form, influence the nonlinear behaviour of structures subjected to earthquake ground motion. The parameters under study include regularity classification, values of the behaviour factor, methods of analysis and effects of capacity design procedures. The project also addresses the clarification of the requirements specified in EC8 for reinforcing steel, in light of the new steel production technologies in Europe, and accounting for the ductility demands resulting from the design prescriptions included in EC8.

- *Infilled frames*: The main objective consists of contributing to the revision of all EC8 clauses which relate to the effect of infills on the seismic design and response of reinforced concrete frames and dual systems.
- *Bridges*: The main objectives for bridges are essentially related to regularity and behaviour factor procedures. Secondary objectives are related to capacity design procedures, second-order effects, asynchronous motion of piers and isolation/dissipation devices. Reference is made to EC8, Part 2 [2].
- *Foundations and retaining walls*: Of concern here are the seismic response and safety verification of direct foundations, deep foundations and retaining walls.

The role of ELSA in this programme [3] is to perform the necessary large-scale validation tests on various types of structures (frames and bridges). The same structures are tested at small-scale or component level or studied by numerical methods by the other partners in the PREC8 network.

2. ACTIVITIES OF THE BRIDGE GROUP

Having in view the objectives referred to above, the research programme of the Bridge Group includes the following main tasks [4]:

- *Definition of regularity*: Seismic design of bridges is ordinarily done, as for any civil engineering structure, by means of elastic methods of analysis. The equivalent elastic analysis is performed by reducing the values of the response spectrum by a force reduction factor, the q-factor in EC8. The value of the q-factor (and consequently the reduction in the elastic force and the expected ductility) is specified in the code as a function of many parameters, among which the regularity of the structure.
  The regularity issue is relevant in building design, as it is addressed by the group deling with reinforced concrete frames and walls. However, it is thought to be extremely important for bridges, so that the applicability of the q-factor approach to such structures is sometimes questioned. Bridges are very often quite irregular structures, with complex geometries both in plan and elevation. The irregularity leads to the concentration of forces and ductility demands in few stiffer elements, making the definition of a unique value of the q-factor very difficult.
  Simplified methods to classify the structure according to the regularity are sought.
- *Definition of design procedures for irregular bridges:* Different design procedures for highly irregular bridges are explored. The key issue is the concentration of ductility demand in stiffer elements. The high ductility demands in those elements may be reduced by designing them to be stronger, or by increasing the strength of the more flexible elements to reduce the forces attracted by the stiffer ones. Extensive numerical simulations are being performed to address this problem. The experimental programme is intended to confirm the results of the numerical analyses, as well as to check the adequacy of the acceptable level of damage assumed in the code.
- *Seismic isolation devices*: Seismic isolators and dissipators are being extensively used in bridge structures. This has important design implications, since the technology is relatively new and fast growing, and reliable data are not always available. The seismic isolation issue is being addressed in conjunction to the regularity issue only. The possibility of making more regular the behaviour of an irregular bridge by means of seismic isolators is explored. Results will be confirmed by a pseudodynamic test.

- *Asynchronous base motion*: The differences in the input motions at the base of the piers are usually neglected in design. In EC8, Part 2, however, the designer is warned about the importance of this effect in the case of geological discontinuities or large irregularities. The definition of the spatial distribution of the base motion is still an open problem, and so are its implications on design. Numerical analyses are being conducted to study the importance of the asynchronous base motion. A test will be conducted on a 1:8 scale specimen by using two shaking tables at ISMES. Another test will be conducted pseudodynamically on a larger scale specimen at ELSA.
- *Soil-structure interaction and second order effects*: These aspects are thought to affect the seismic design of bridges to a lesser degree. The soil-structure interaction is usually thought to play a beneficial role, however, the contribution of the deformability of the soil affects the design of the details. This problem is being addressed in the numerical simulations. Second order effects are being included in both the numerical and experimental activities.

The experimental part of the programme includes shaking table tests to be performed in Lisbon (LNEC) and Bergamo (ISMES) and pseudodynamic tests of six bridge models being performed in Ispra (JRC-ELSA).

3. THE LARGE-SCALE TESTING PROGRAM

The testing program at ELSA includes a preliminary cyclic test of one squat pier, and pseudodynamic tests on six complete bridges. The bridges have three piers with height ranging from 7 to 21 meters and identical cross sections (rectangular hollow section with 400 mm thickness) and a continuous deck (200m long). The scheme of the full-scale bridges is shown in Figure 1.

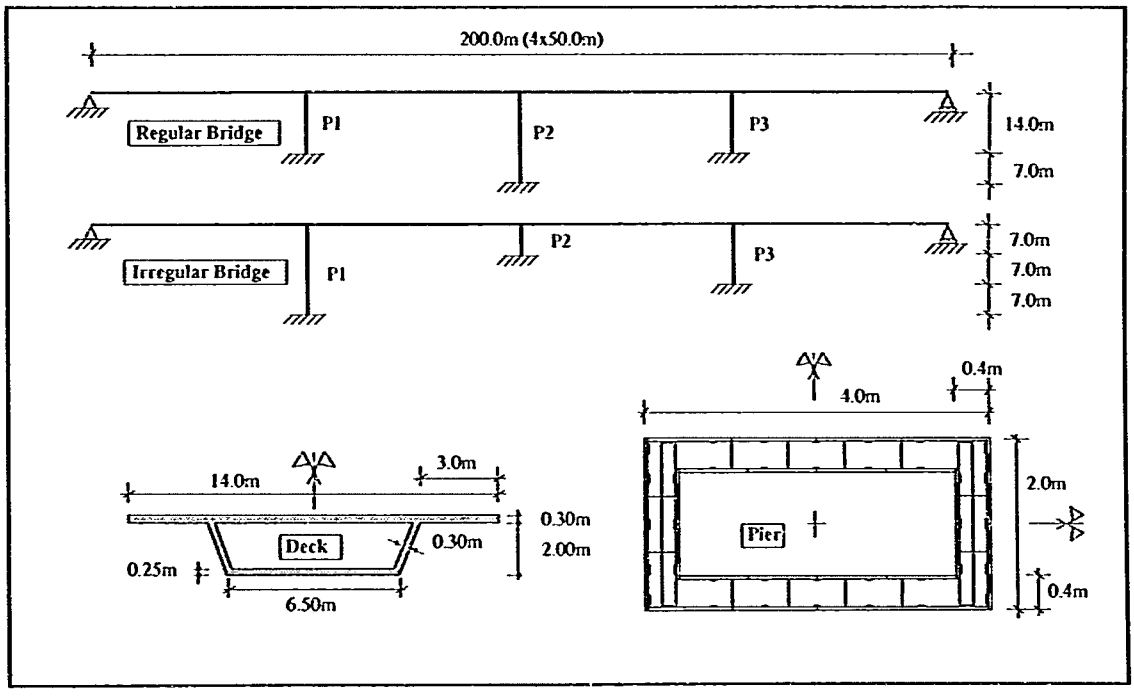


Figure 1. *Full-scale scheme of the bridges being tested pseudodynamically.*

Two different schemes were adopted, having in mind to test the structures in the direction orthogonal to the bridge axis. One represents a typical regular bridge. The regularity is intended in the sense that the fundamental deflected configuration of the structure is similar to the one of the deck alone. The other scheme -the one with the shortest pier in the middle-, is regarded as highly irregular, since the stiffness of the deck induces higher forces in the internal

stiffer pier.

In detail, the following six bridge specimens are being tested (see Table 1):

Table 1: Bridges selected to be tested pseudodynamically.

Bridge Identification Label	Pier 1		Pier 2		Pier 3	
	Full-size height [m]	Steel percentage	Full-size height [m]	Steel percentage	Full-size height [m]	Steel percentage
B232	14.0	1.15	21.0	0.62	14.0	1.15
B213A	14.0	0.50	7.0	0.92	21.0	0.50
B213B	14.0	0.50	7.0	1.69	21.0	0.50
B213C	14.0	1.15	7.0	0.50	21.0	1.15
B213A I/D	14.0	0.50	7.0	0.92	21.0	0.50
B213A N/S	14.0	0.50	7.0	0.92	21.0	0.50

The numbers which appear in the test identification labels represent the height modules in each of the three piers. The height module is 7 metres for the full-scale bridges, thus the bridge 232 has piers respectively 14, 21 and 14 metres high, and is the regular bridge. The other bridges - with 213 in the label- are irregular, with piers 14, 7 and 21 metres high.

The letters A, B and C in the label refer to the different design approaches. The label B213A stands for standard design according to EC8, part 2. The bridge B213B corresponds to the most straightforward design solution to the high ductility demands expected for the central pier, i.e. the central pier has been made stronger. In bridge B213C the taller piers have been made stronger instead, in an attempt to relieve the central pier from high forces.

The other two bridge specimens (B213A I/D and B213A N/S) are identical to the specimen B213A, but will be tested with seismic isolation devices and with asynchronous base motion respectively.

Presently, the first four specimens have been tested.

4. DESIGN AND CONSTRUCTION OF THE SPECIMENS

4.1. Design of the bridges

The bridges are representative of typical multi-span continuous-deck motorway bridges. The deck is a hollow-core prestressed concrete girder, with a full-scale width of 14 m. The deck ends at the abutments with shear-keys, to allow end rotations. The bridges have four identical spans of 50 m. The piers have constant rectangular hollow-core cross-section. As far as the height of the piers is concerned, two different profiles have been considered in the design, corresponding to different levels of structural regularity with reference to the behaviour of the structure in the transverse direction.

The regular configuration corresponds to a bridge for which the fundamental deflected shape of the deck alone is similar to that of the complete structure. This corresponds to the symmetric structure having the tallest pier in the centre (bridge B232).

The irregular bridge corresponds to the case for which the first mode of the structure is very different from the first-mode deflected shape of the deck alone.This configuration has been labelled as B213. The bridge is intended to be highly irregular. Beside the fact that the struc-

ture is not symmetric, the first-mode deflected shape of the deck induces much higher forces in the central, stiffer pier.

The design of the piers has first been carried out according to the current version of EC8, Part 2, Bridges [2]. As for the irregular structure, two different design approaches, non Eurocode 8-conforming, have been adopted, based on the findings of the preliminary nonlinear analyses. These may represent the two possible conceptual solutions to the irregularity issue. In one case (B213B), the reinforcement percentage of the shortest pier has been significantly increased (from 0.92% to 1.69%), with the aim to reduce the high ductility demand which was anticipated in the analysis. The other case (B213C), the strength of the taller piers has been increased (from 0.50% to 1.15%), so that the forces attracted by the shortest pier can, in principle, be reduced. A typical cross section layout is shown in Figure 2.

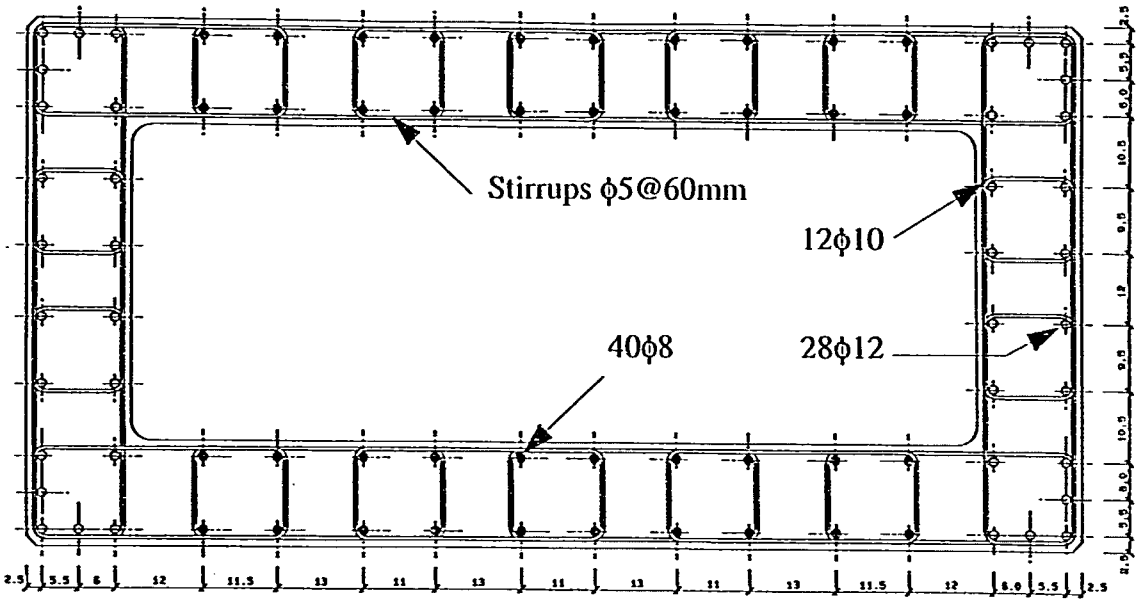


Figure 2. *Typical reinforcement lay-out (central pier of B213A).*

The bridge corresponding to the standard application of the design code will also be object of the tests with the view of including non-synchronous base-motions and seismic isolation devices. No special provisions have, however, been included in the design.

4.2. Scaling of the structures

As in any test, the choice of the scale factor is a compromise between costs, practical problems and apparatus capacity on one hand and realism of the tests and representativeness of the results on the other hand.

The deck was assumed to behave elastically, therefore it has been decided to take it into account through numerical modelling by means of the substructuring capabilities of the ELSA laboratory. The overall size of the specimen was thus not the limiting factor. Moreover, in pseudodynamic testing, the inertia forces are represented numerically in the computer controlling the test, thus the mass of the specimen was not the limiting factor either. The only practical limitation was given by the number of actuators to be placed on top of the piers to apply the necessary horizontal and vertical forces.

A scale factor of 2.5 was selected. This allows us to deform the stronger pier with three actua-

tors (2500 kN total force), without having to deal with excessively small specimen sizes.

The thickness of the hollow-core pier was chosen to be 160 mm, thus problems in the placement and curing of the concrete have been avoided. The minimum diameter of the rebars is 8 mm, and the diameter of the stirrups is 5 mm. Even if some differences in the bond mechanisms are expected, this is not supposed to limit the representativeness of the results. Pull-out tests are regularly being conducted in the plinths, and a set of prismatic elements to study the tension-stiffening characteristics of the confined concrete has been constructed.

4.3. Construction of the piers

Due to the high accuracy required in the execution, and to the reduced size of the elements, the construction of the piers was done in a precast concrete workshop.

The mix of the concrete was studied in detail before the construction. The formula which yielded the most accurate results, with acceptable workability was: normal strength Portland cement 350 kg/m^3, water 180 litres/m^3, aggregates 1790 kg/m^3. To obtain the necessary workability, special additives had to be put in the mix, to reach a slump value of 120 mm.

Only the prismatic part of the piers was done in the workshop. This was cast in special steel formwork, and full-length rebars were left for the connection with the plinth. Casting was done horizontally. A first casting operation was done for three sides of the hollow core section, the top side being cast the day after. No heat treatment was done for curing.

The prismatic parts were then transported to the working area of the ELSA laboratory. The plinth was cast in a separate phase, by keeping the prismatic part in position with the crane. Normal high-strength concrete was used for the plinths. The plinths were designed in such a way that the full strength of the pier could be reached without shear cracking of the plinth itself, which may have caused appreciable rotations of the end cross-section. To reduce the size of the plinths, and the weight of the complete piers, we decided to place a number of steel bars to prestress the plinth.

Considerable care has been put in the acceptance criteria: all the rebars to be used in the piers were taken from the same mill, and continuous testing of the concrete was carried out during the construction phase. The concrete turned out to be substantially homogeneous.

5. IMPLEMENTATION OF THE PSEUDODYNAMIC TEST METHOD

5.1. Pseudodynamic testing

A pseudodynamic test is one which, although carried out quasi-statically, uses on-line computer calculation and control together with experimental measurement of the actual properties of the structure to provide a realistic simulation of the dynamic response. The equations of motion for a discrete parameter model of the test structure are solved on-line using a step-by-step numerical time integration method. Inertial and viscous damping forces are modelled analytically - a relatively straightforward matter compared to the nonlinear structural restoring forces, which are measured experimentally because of the practical impossibility of modelling them accurately. The process automatically accounts for the hysteretic damping due to inelastic deformation and damage of the structural materials which is the major source of energy dissipation.

To simulate the earthquake response of a structure, a record of an actual or artificially generated earthquake ground acceleration history is given as input data to the computer running the pseudodynamic algorithm. The horizontal displacements of the controlled degrees of freedom

(where the mass of the structure can be considered to be concentrated) are calculated for a small time step using a suitable time integration algorithm. These displacements are then applied to the test structure by servo-controlled hydraulic actuators fixed to the reaction wall. Load cells on the actuators measure the forces necessary to achieve the required displacements and these structural restoring forces are returned to the computer for use in the next time-step calculation. Details of the capabilities of the ELSA Laboratory and of the pseudodynamic implementation are given elsewhere [3].

5.2. Substructuring technique

The pseudodynamic test method is a hybrid technique which combines the numerical integration of equations of motion of complex structures condensed on a reduced number of degrees-of-freedom (d.o.f.), with the experimental measurement of the reaction forces resulting from this motion. Despite the potential of the pseudodynamic technique, direct testing of very large civil engineering structures like bridges would require a number of controlled d.o.f. that could exceed the experimental capabilities. It is, however, possible to extend the field of application of the method, at least when the behaviour of a part of the structure is well known, by introducing a substructuring technique [5]. This technique takes advantage of the hybrid character of the pseudodynamic test method by combining the numerical simulation of the known part of the structure, the substructure, with the physical testing of the remaining structural part, the tested structure. The method is well suited for bridges since their largest part, the deck, can be assumed to be linear elastic and therefore modelled by any finite-element software: only the piers, whose dimensions remain reasonably small, and where damage is expected, are tested in the laboratory.

A further advantage, which is again well suited for bridges, is the possibility of dealing with situations where the seismic excitation is asynchronous or presents different amplitudes along the foundation.

The use of substructuring techniques in pseudodynamic testing implies, for the substructure, a model and the time integration of its spatially discrete equations of motion. This model may present a number of d.o.f. greater, by some orders of magnitude, than the number of nodes actually controlled by the pseudodynamic algorithm. Thus, if the substructure were handled by the PC program driving the pseudodynamic algorithm, the current capabilities of this controller program could easily be exceeded. To overcome this difficulty, the adopted strategy was to have two processes running in parallel: that one responsible for the pseudodynamic algorithm running in the PC (controller) and the other, responsible for the substructure, running in a remote workstation and communicating between them using standard network capabilities such as Berkeley sockets.

Consider the following system of semi-discrete differential equations

$$Ma + Cv + r(d) = f \tag{1}$$

which describes the motion of a structure with m degrees-of freedom, where a, v and d represent the acceleration, the velocity and the displacement vectors, r and f the structural internal force and the external force vectors M and C the mass and damping matrices.

To solve system (1), a numerical step-by-step integration method is adopted. The displacement and velocity vectors at step $(n + 1)$ can be written in terms of the acceleration vector and the previous step values which, when introduced in (1), lead to a discrete system of linear equations at time t_{n+1}:

$$\hat{M}a_{n+1} = \hat{f}_{n+1} \tag{2}$$

where $\hat{M}$ is a pseudo mass matrix and $\hat{f}_{n+1}$ a pseudo force vector.

Distinguishing between the quantities coming from the substructure (S) and the tested structure (T), system (2) may be rewritten as

$$\begin{bmatrix} {}^{S}\hat{M}_{ij} & {}^{S}\hat{M}_{i\beta} & 0 \\ {}^{S}\hat{M}_{\alpha j} & {}^{S}\hat{M}_{\alpha\beta} + {}^{T}\hat{M}_{\alpha\beta} & {}^{T}\hat{M}_{\alpha J} \\ 0 & {}^{T}\hat{M}_{I\beta} & {}^{T}\hat{M}_{IJ} \end{bmatrix} \cdot \begin{bmatrix} a^{j}_{n+1} \\ a^{\beta}_{n+1} \\ a^{J}_{n+1} \end{bmatrix} = \begin{bmatrix} {}^{S}\hat{f}^{i}_{n+1} \\ {}^{S}\hat{f}^{\alpha}_{n+1} + {}^{T}\hat{f}^{\alpha}_{n+1} \\ {}^{T}\hat{f}^{I}_{n+1} \end{bmatrix} \tag{3}$$

where i, j, refer to the internal d.o.f of the substructure, α, β to the common connection d.o.f. and I, J to the internal d.o.f. of the tested structure.

Condensing the unknowns a_j the controlling equation becomes

$$\begin{bmatrix} {}^{T}\hat{M}_{\alpha\beta} + \left({}^{S}\hat{M}_{\alpha\beta} - {}^{S}\hat{M}_{\alpha j}\, {}^{S}\hat{M}^{-1}_{ji}\, {}^{S}\hat{M}_{i\beta} \right) {}^{T}\hat{M}_{\alpha J} \\ {}^{T}\hat{M}_{I\beta} \qquad\qquad {}^{T}\hat{M}_{IJ} \end{bmatrix} \cdot \begin{bmatrix} a^{\beta}_{n+1} \\ a^{J}_{n+1} \end{bmatrix} = \begin{bmatrix} \left({}^{S}\hat{f}^{\alpha}_{n+1} - {}^{S}\hat{M}_{\alpha j}\, {}^{S}\hat{M}^{-1}_{ji}\, {}^{S}\hat{f}^{i}_{n+1} \right) + {}^{T}\hat{f}^{\alpha}_{n+1} \\ {}^{T}\hat{f}^{I}_{n+1} \end{bmatrix} \tag{4}$$

and the substructure is governed by

$${}^{S}\hat{M}_{ij} a^{j}_{n+1} = {}^{S}\hat{f}^{i}_{n+1} - {}^{S}\hat{M}_{i\beta} a^{\beta}_{n+1} \tag{5}$$

Equation (4) points out the differences between the conventional pseudodynamic test case and the one with substructuring. In the substructuring case, the pseudo mass matrix is modified by adding the term within parentheses supplied by the substructure process. In addition, at each time step, the pseudo force vector includes the terms from the substructure. The equation governing the substructure (5) requires the acceleration at the connection nodes.
Details of the ELSA implementation of pseudodynamic testing with substructuring are given in [6].

5.3. Test setup

The piers are aligned in front of the reaction wall, with the shorter one in the middle, as can be seen in Figure 3. The plinths of the piers are rigidly attached to the strong floor by means of steel bars passing through the floor itself. A stiff steel cap is connected with bolts and epoxy resin to the tip of the piers. The cap is used to apply the vertical load corresponding to the weight of the deck as well as to apply the horizontal loads which are required to impose the computed displacements.

The axial force (1700 kN) is applied by means of four actuators, placed inside the hollow core pier and connected to the cap and to instrumented steel bars embedded in the pier plinth. The vertical force is imposed at the beginning of the test. It remains practically constant, thanks to the hydraulic accumulators placed to compensate the effects of the horizontal displacement.

Two double-acting servo-hydraulic actuators (three for the central pier in the test B213B), capable of a load of 1.0 MN each are used to apply the horizontal displacements. They are connected by spherical joints to the steel cap at one side and to a steel plate attached to the reaction wall at the opposite side. The imposed displacements are measured with respect to two independent steel frames using digital optical transducers.

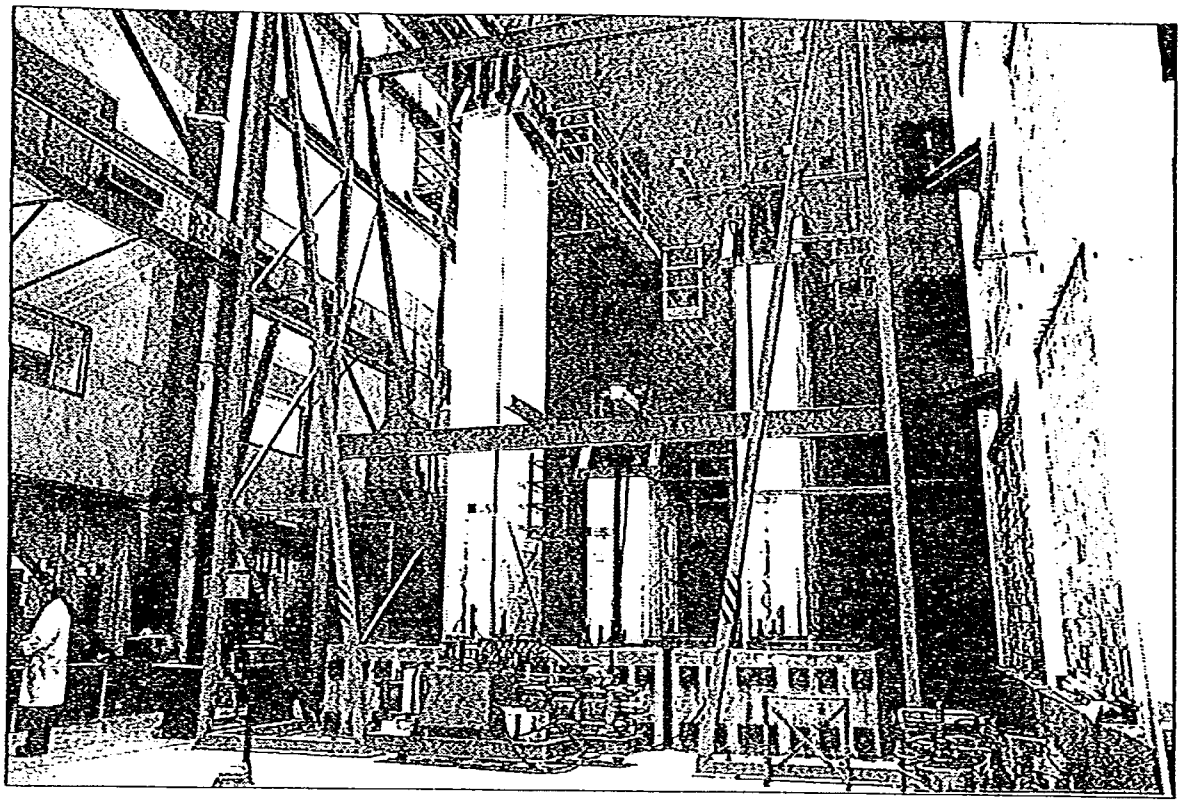


Figure 3. *Test set-up.*

5.4. Instrumentation

A schematic representation of the location of the displacement transducers is shown in Figure 4. Instrumentation includes both active measurements -those which are related to the pseudo-dynamic control algorithm-, and passive instruments. Passive instruments can be grouped in the following sets:

- *Rotations*: Pairs of displacement transducers (channels 1-18) have been placed at different levels on the two external opposite faces of the specimens to measure the local rotation. Additional pairs of transducers (19-26) were placed to monitor unexpected orthogonal rotations. Another set of transducers (27-28) is used to measure both the total rotation of the pier and its elongation.
- *Diagonal deformations:* The two diagonals were instrumented to measure the shear deformation (29-30).
- *Horizontal Displacements:* Another set of transducers (31-35) were placed at different levels between the side of the pier and a steel bar connected with swivel joints to the base and to the cap. This allows to monitor the deflected shape.
- *Section Warping: A* set of transducers (36-40) were placed on the same horizontal basis to follow the in-plane deformation of the cross-section.

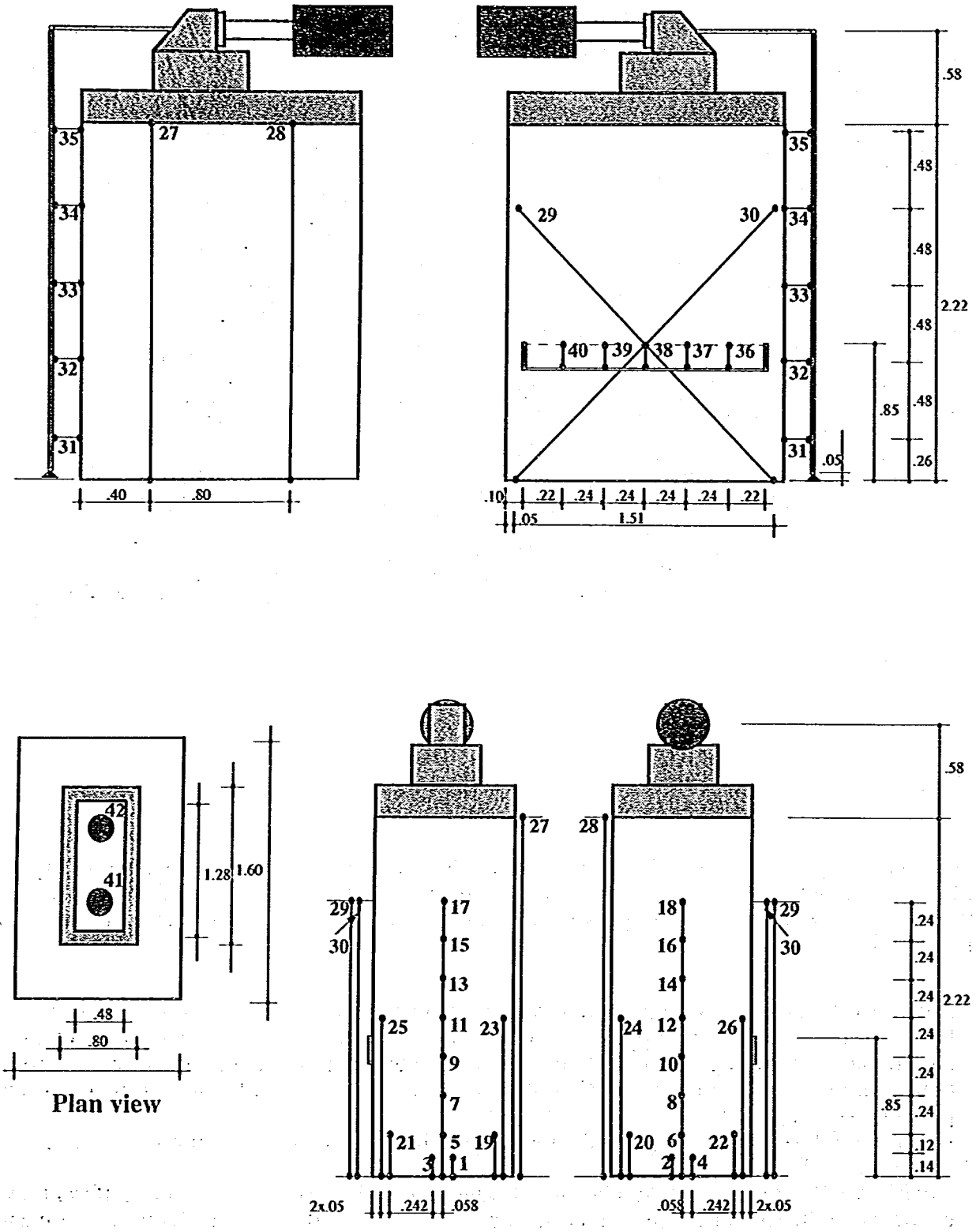


Figure 4: *Scheme of passive instrumentation.*

6. CYCLIC TEST

A preliminary cyclic test on one of the shorter piers (the one corresponding to the B213A bridge) was carried out. This test represented an opportunity to assess the adequacy of the instrumentation and of the loading apparatus. Moreover, it represented an opportunity to calibrate the computer models which had been used in predicting the results of the pseudodynamic tests. The cyclic test has been performed on one of the shorter piers, because it was thought that the models were not able to account for the large shear deformations which were expected for such short elements. Finally, the clear identification of the failure will assist in assessing the performances of the complete structure in the pseudodynamic tests.

The imposed displacement history included increasing amplitude cycles up to yielding, followed by three cycles for displacement ductility of 1.0, 3.0 and 6.0. A constant axial load of 1700 kN was applied. The measured global hysteresis loops are depicted in Figure 5.

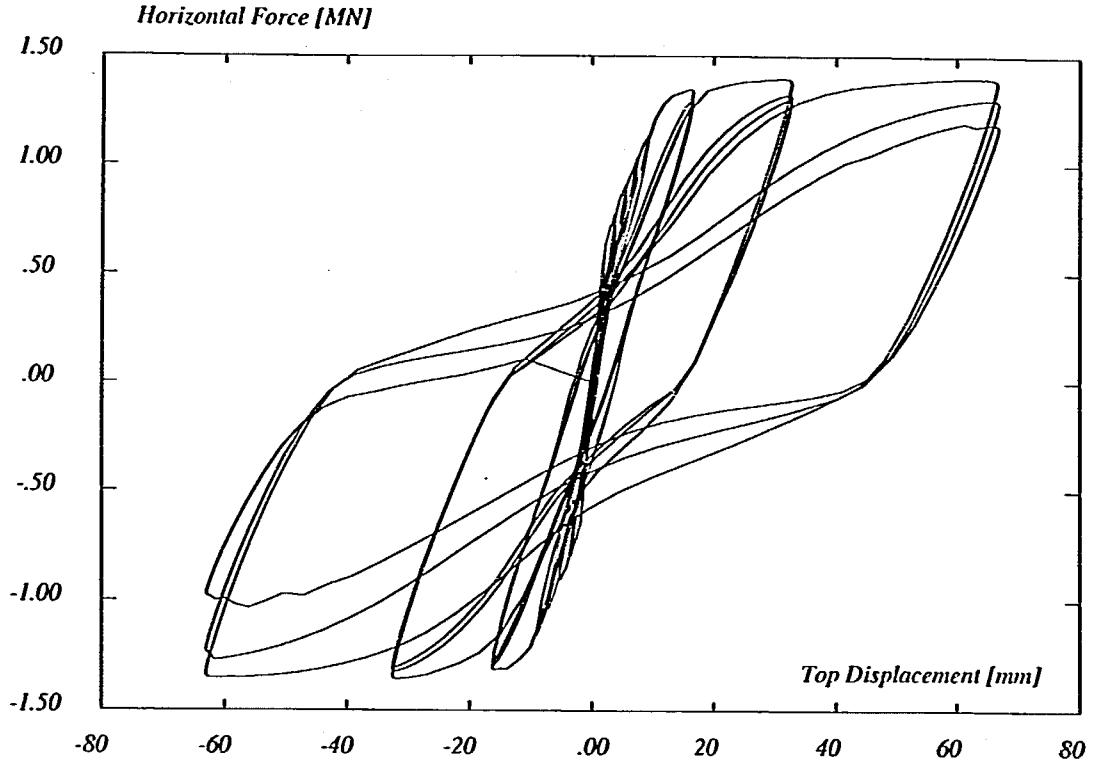


Figure 5. *Results of cyclic test.*

Flexural cracking of the pier started at a displacement of approximately 2 mm, followed by the opening of shear cracks. Yielding took place for a top displacement of about 12 mm. This value was considerably larger than the theoretical value, due to the contribution of the deformability of the plinth and the slippage of the bars in the foundation. For the ductility 3.0 cycles, increasing diagonal and flexural cracking was observed. Passing from ductility 3.0 to ductility 6.0, spalling of the concrete cover and buckling of rebars at the first reversal took place. The test was terminated after the rupture of the rebars, which followed the large deformations due to buckling in the previous half-cycle. Buckling was also observed at the main diagonal cracks.

The structure exhibited stable and dissipative cycles up to ductility 3.0. Damage was concentrated at the bottom of the pier, without noticeable spread of plasticity. The shear deformations

were found to be responsible for about 30% of the total top displacement. The energy dissipated by shear was, however, negligible. For higher ductility the damage increased, mainly due to buckling of rebars. Failure (reduction of 30% in the load capacity) took place during the third cycle at ductility 6.0. A comprehensive analysis of the results can be found in [7].

7. PSEUDODYNAMIC TESTS

Pseudodynamic tests have been performed, thus far, on bridges B232, B213A, B213B and B213C. The tests used one of the artificial accelerograms used in the analysis, with a nominal peak acceleration of 0.35 g. The accelerogram is depicted in Figure 6, together with the corresponding elastic response spectrum. The accelerogram was intended to fit the response spectrum specified in EC8 for peak ground acceleration 0.35 g and medium soil conditions.

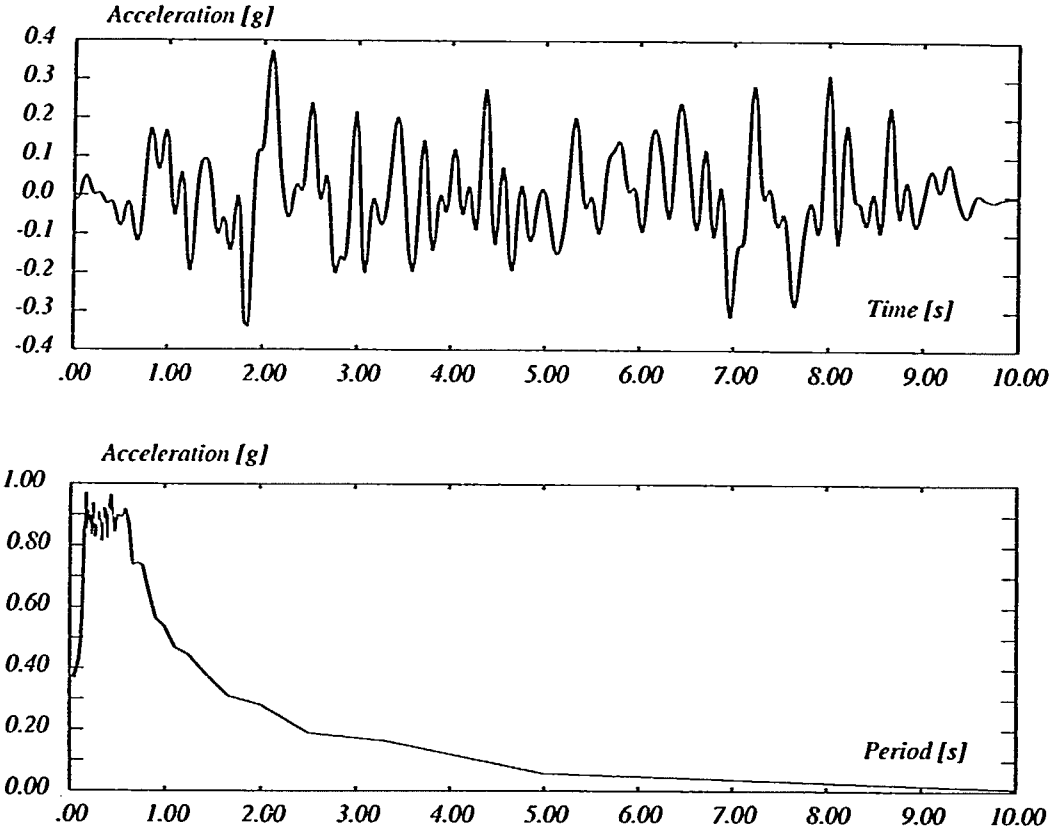


Figure 6. *Artificial accelerogram and response spectrum.*

The mass matrix to be used in the substructured part was scaled by λ^3, λ=2.5 being the geometrical scale factor, consequently the ordinates of the accelerogram were multiplied by λ, and the time scale was accordingly reduced. The original accelerogram of ten seconds became 4 seconds long. The axial load applied by the vertical actuators was independent from the mass values. A constant value of 1700 kN was applied, to keep the normalized axial load the same as in the real structure (ν=0.1).

The tests were performed on the four bridges for two intensity values. After the test with the design accelerogram, another test was performed by using the accelerogram multiplied by 1.2 for the bridges B213A, B213B and B213C and 2.0 for the bridge B232 -a smaller value would

not have caused major damage to the regular bridge-. The external piers in bridge B213A did not suffer significant damage during the test with the reference accelerogram at the nominal intensity, as expected. Therefore, they have been used again in the bridge B213B, and will also be used in the tests with seismic isolation and asynchronous base motion. The tests with the accelerogram multiplied by 1.2 have been physically performed on the short pier only, by providing a numerical model for the other piers. This has been done by using the substructuring capabilities of the pseudodynamic implementation. A nonlinear elastic model, calibrated with the results of the 1.0 test has been used.

The results of the tests are given in Figure 7 in terms of global hysteresis loops. Much work is needed for the interpretation of the experimental data, however, global quantities can be discussed. In Table 2 the extreme values of displacement and bending moment measured during the tests with the reference accelerogram are given:

Table 2: Measured global quantities for the tests with reference accelerogram.

Bridge	Pier 1		Pier 2		Pier 3	
	Top disp [mm]	Moment [MNm]	Top disp [mm]	Moment [MNm]	Top disp [mm]	Moment [MNm]
B232	43.9	4.079	62.1	2.954	43.9	4.079
B213A	21.6	2.395	24.2	3.766	27.9	2.267
B213B	24.5	2.416	22.5	5.216	27.6	2.167
B213C	17.1	2.795	20.3	2.617	25.9	2.514

The results of the test on bridge B232 comply with the regularity issue, as mentioned in EC8, part 2. Dissipation of energy takes place in all piers, and a ductile behaviour could have been assumed. The dissipative mechanism turned out to be stable and efficient, with demands roughly proportional to capacities, and an input signal 2 times larger than the design signal was applied without loss of capacity.

In the case of test B213A the dissipation of energy was limited to the short pier. This corresponds to the situation for which a warning is issued in EC8, part 2: Behaviour factors > 1.2 should not be used without special consideration, if the development of plastic hinges in the piers is not probable, because the piers do not reach yielding under the design seismic action. The ductility demand on the short pier is, however, reasonably small.

In the test B213B the short pier, which was stronger than in the previous bridge, attracted much larger forces, but experienced considerably lower ductility demands. Again, energy dissipation took place in the short pier only. The crack pattern was found to be much more spread than in the previous test.

In test B213C, the goal to obtain a more regular force distribution was achieved. The distribution of the maximum bending moment among the piers is, in fact, fairly constant. Ductility demands in the short pier are, however, much larger than in test B213A. The advantages of the corresponding design approach are, therefore, debatable.

8. CONCLUSIONS

A testing programme is being carried out as a part of the activities of the Bridge Group of the Network for Pre-normative Research in support of EC8. The scope of the tests is to study the implications of irregularity with the q-factor design approach. Up to now, four bridges have been tested pseudodynamically, including one regular bridge and one highly irregular, designed according to different design philosophies.

The tests were conducted taking full advantage of the substructuring capabilities of the ELSA Laboratory, and were repeated for two intensity levels. Much of the interpretation work is still on the way, while the tests with seismic-isolation and asynchronous base motion are being prepared.

ACKNOWLEDGEMENTS

The testing programme is a joint effort of the staff of the Applied Mechanics Unit. The experimental programme was directed by G. Verzeletti, Head of the ELSA Laboratory. The implementation of the substructuring technique is due to P. Buchet, G. Magonette, P. Pegon and P. Tognoli. E. Gutierrez designed the instrumentation scheme, D. Tirelli is dealing with the reduction of experimental data and J. Guedes with the preliminary interpretation of results. The enthusiasm of the laboratory staff has made possible the preparation and execution of the tests.

The collaboration with professor G.M Calvi, coordinator of PREC8 and of the Bridge Group, is acknowledged, and so are the constructive suggestions provided by professor P.E. Pinto, chairman of the technical committee for EC8.

REFERENCES

[1] Eurocode No 8, Structures in Seismic Regions - Design - Part 1 - General and Buildings - May 1988 edition, Report EUR 12266 EN, Commission of the European Communities, 1988.

[2] Eurocode No 8, Structures in Seismic Regions - Design - Part 2 - Bridges - Draft April 1993 - CEN, DOC. TC250/SC8/N76, 1993.

[3] Donea J., G. Magonette G., Negro P., Pegon P., Pinto A. and Verzeletti G. Pseudo-dynamic testing of large-scale models of civil engineering structures at the ELSA reaction wall. *Proc. of the 10th European Conference on Earthquake Engineering*, Vienna, 1994.

[4] Calvi G.M. and Pinto P.E. Seismic response of bridges: Design methods and behaviour factors. *Proc. of the 10th European Conference on Earthquake Engineering*, Vienna, 1994.

[5] Dermitzakis, S.N. and Mahin S.A. Development of substructuring techniques for on-line computer controlled seismic performance testing. *Report No. UCB/EERC-85/04.* Berkeley, California, 1985.

[6] Buchet, P. and Pegon P. PSD testing with substructuring - Implementation and use. *Special Publication* AMU, STI, EC, JRC, Ispra, Italy, 1994.

[7] Pinto A.V., Verzeletti G., Negro P. and Guedes J. Cyclic testing of a squat bridge-pier. *EUR Report* AMU, STI, EC, JRC, Ispra, Italy, (in preparation).

BRIDGE B232

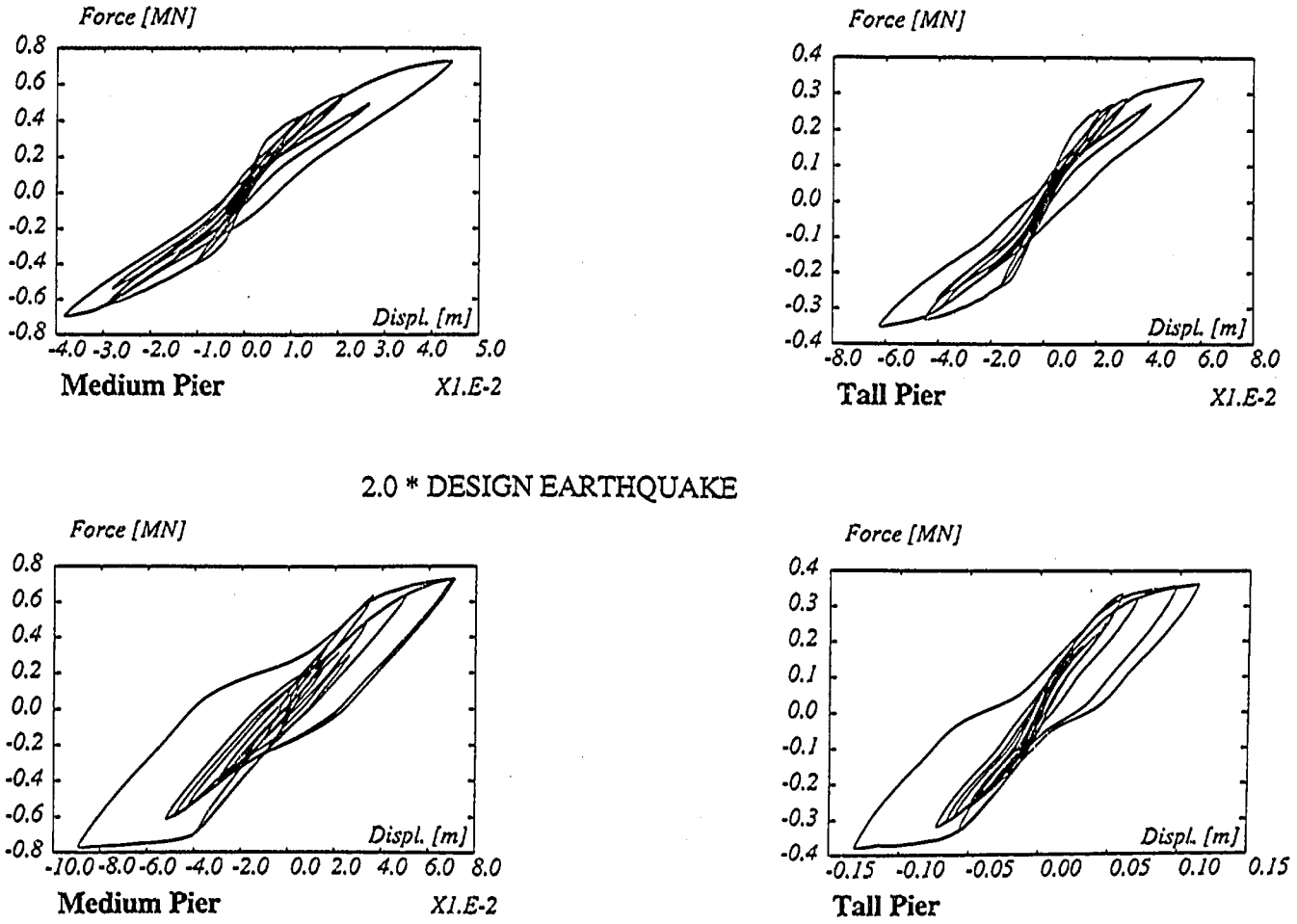
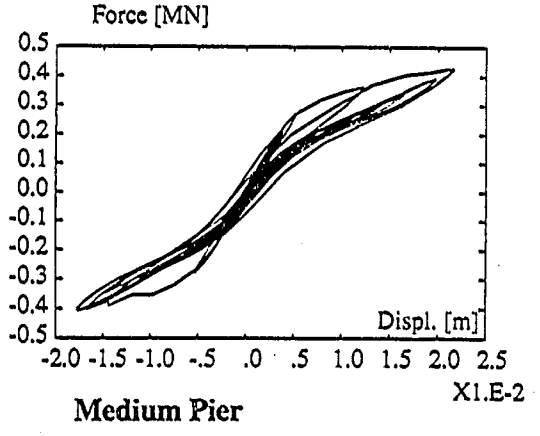
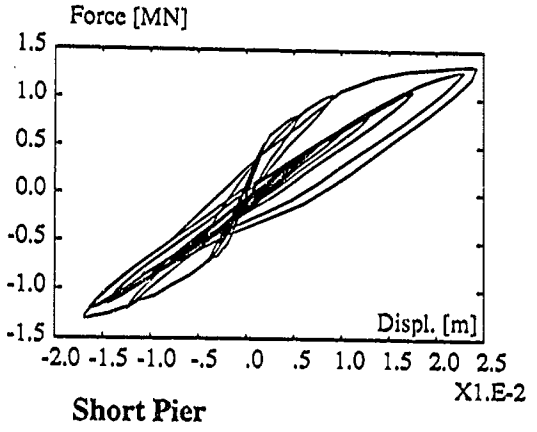


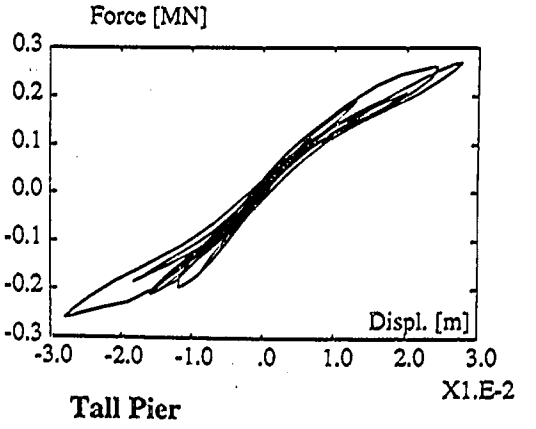
Figure 7: *Experimental hysteresis loops.*

BRIDGE B213A

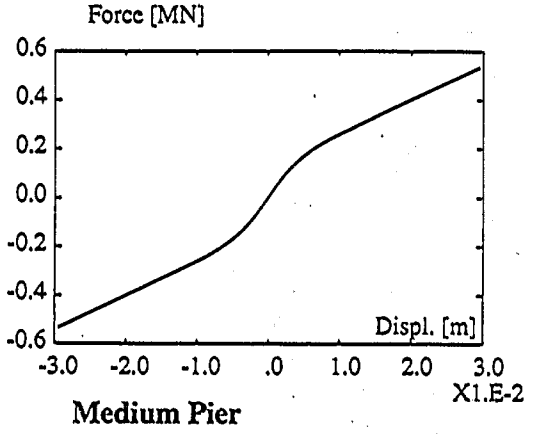
1.0 * DESIGN EARTHQUAKE

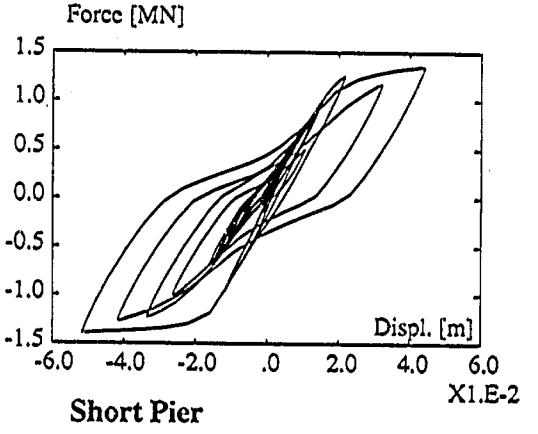






1.2 * DESIGN EARTHQUAKE





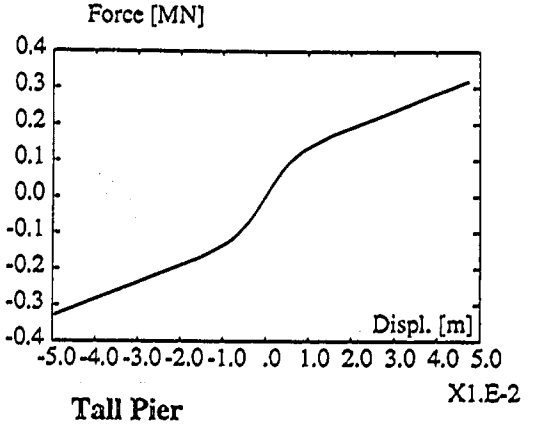
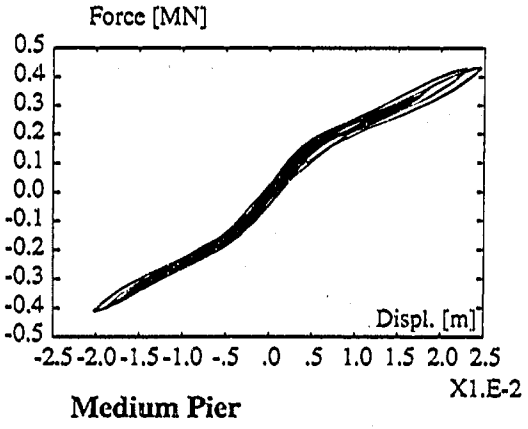


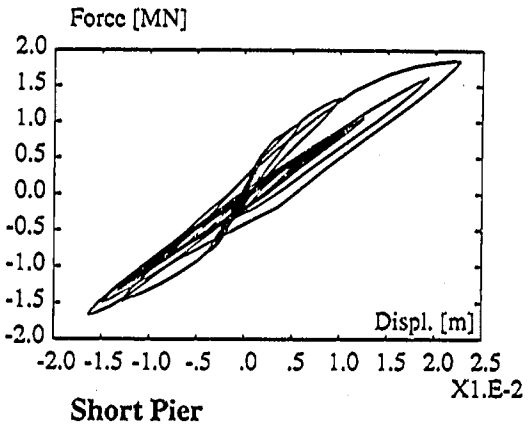
Figure 7 (cont'd): *Experimental hysteresis loops.*

BRIDGE B213B

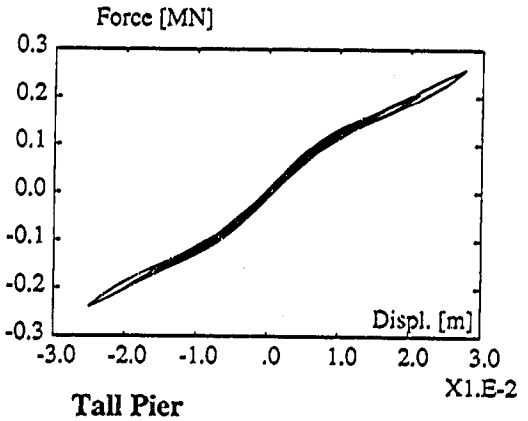
1.0 * DESIGN EARTHQUAKE



Medium Pier

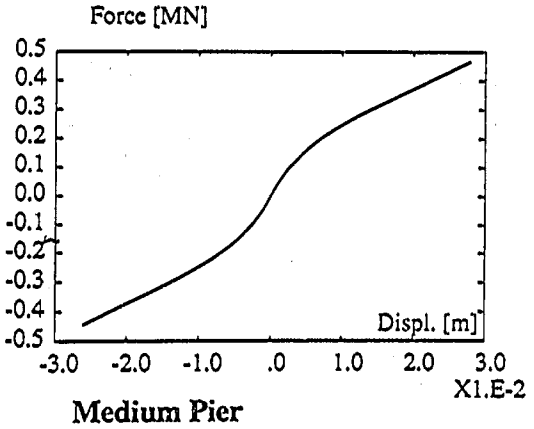


Short Pier

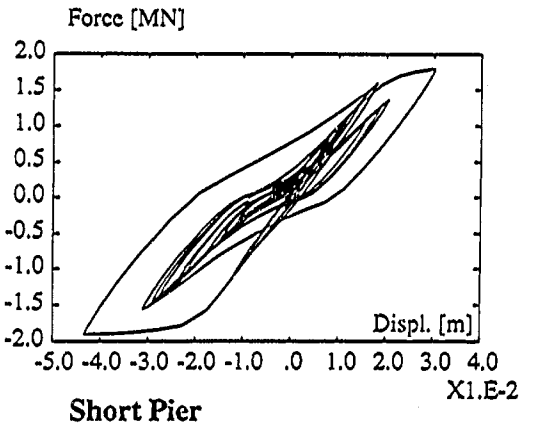


Tall Pier

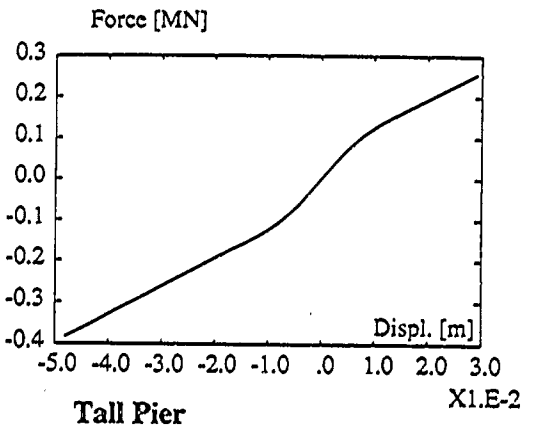
1.2 * DESIGN EARTHQUAKE



Medium Pier



Short Pier

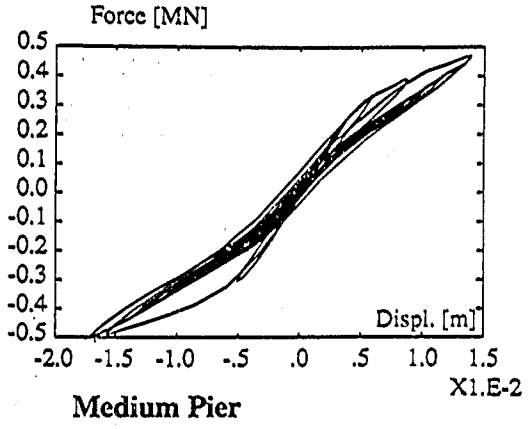


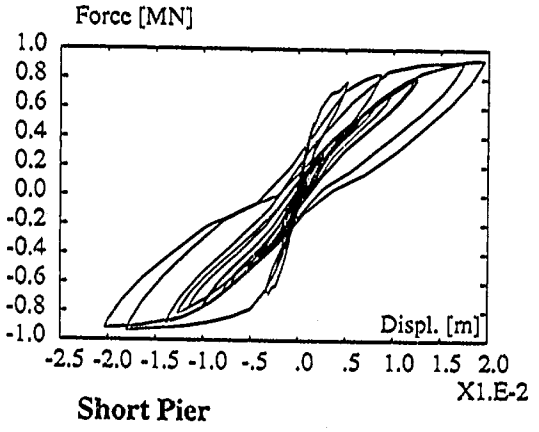
Tall Pier

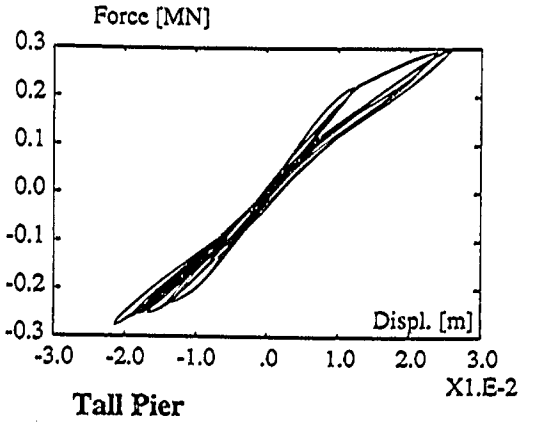
Figure 7 (cont'd): *Experimental hysteresis loops.*

BRIDGE B213C

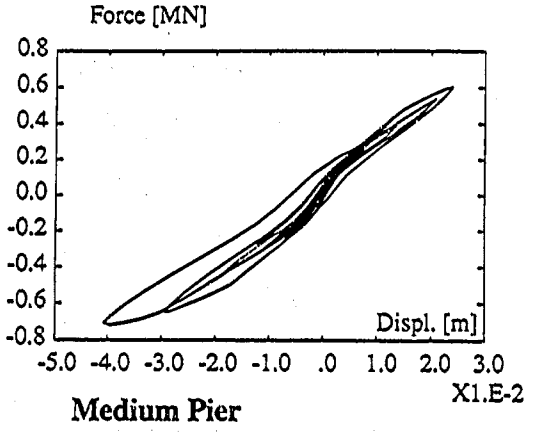
1.0 * DESIGN EARTHQUAKE

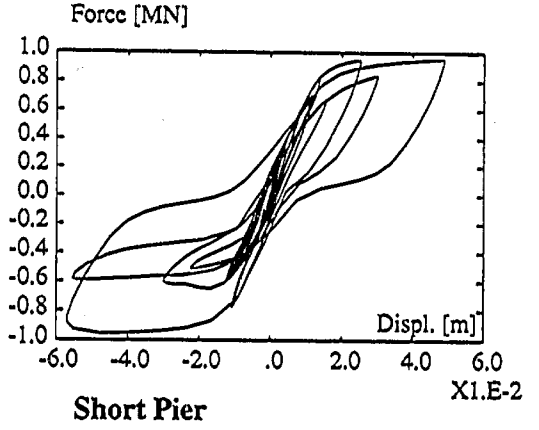






1.2 * DESIGN EARTHQUAKE





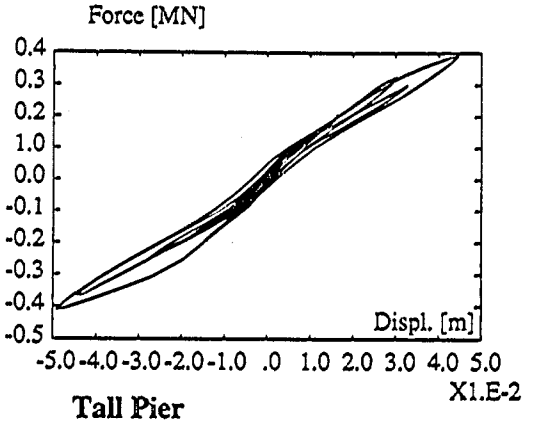


Figure 7 (cont'd): *Experimental hysteresis loops.*

THE USE HYSTERETIC DAMPERS FOR THE SEISMIC PROTECTION OF BRIDGES IN ITALY

A. Marioni

ALGA S.p.A. - Milano

ABSTRACT

Hysteretic dampers have been developped in Italy since 1980. The applications for the seismic protection of bridges until now are more then 150 for a total length of over 150 km of structures. The paper describes the opimization of the devices during 15 years of experience,and discuss some of the problems related to their utilization in the structure.

1. INTRODUCTION

Antiseismic devices have found large application in Italy for the seismic protection of bridges, both for new constructions and rehabilitation and upgrading of the exsisting ones. A large part of the devices utilized consist of hysteretic dampers based on the elastoplastic flexure of particular kinds of steel. In no other nation of the world the hysteretic dampers have found so large application as in Italy. The main reasons for this preference in respect to other devices may be summarized as follows.

Hysteretic dampers based on the elastoplastic flexure of steel are:

- reliable;
- not subject to particular maintenance requirements;
- not subject to ageing;
- not sensible to temperature variations.

Also the following considerations may have contributed to their large utilization.

In Italy continuous bridges are preferred to simply supported spans in order to minimize the number of the expansion joints that may generate problems for the maintenance and the driving comfort. Also in the case of seismic retrofitting of old bridges with simply supported spans normally the spans have been connected in order to avoid as far as possible the expansion joints.The longest continuous bridge without intermediate joints ever built in Italy and probably in the world is the Restello viaduct (100 km north of Venice) with a total length of 2.1 km.

Continuous bridges are subjected to very large forces due to earthquake and to very large movements due to thermal effects. Under these conditions the antiseismic devices becomes quite important and complicated machines because:

- either they are located in one position (for instance one abutment) in order to allowe free movement of the bridge; in that case they must be designed for very large forces;
- either they are distributed in many positions; in that case they must allowe the thermal movements of the bridge (normally by use of hydraulic shock transmission units).

So it is quite difficult to apply in these conditions other types of antiseismic devices like the base isolators.

2. OPTIMIZATION OF THE DEVICES

2.1 First devices

The first hysteretic devices have been utilized in Italy for the seismic protection of several bridges of the Udine - Tarvisio Motorway in the years 80's. These devices utilized so called Ω-shaped elastoplastic springs (see fig. 1)

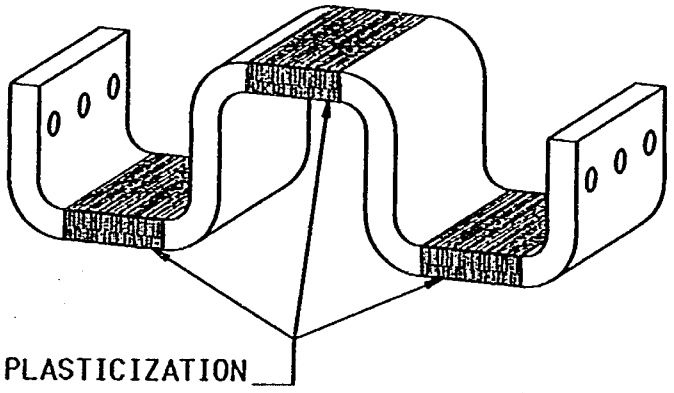


Fig. 1

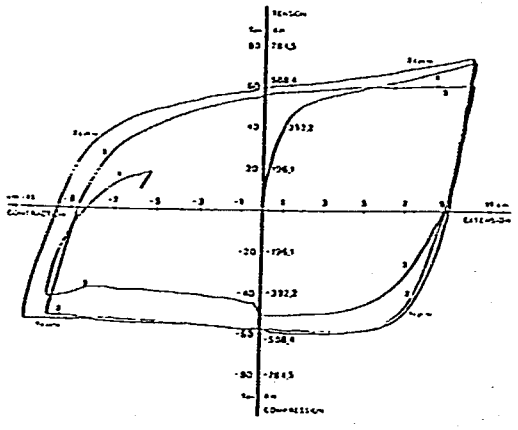


Fig. 2

The main concept on which the design of the Ω-shaped elements was based was to have uniform plasticization of large parts of the springs (the horizontal parts of the spring). However, due to the very large second order effects uniform plasticization was not perfecly reached; furthermore, due to the same effects, the springs showed a very evident non symmetric behaviour with hardening in tension and softening in tension (see fig. 2).

2.2 E-Shaped devices

From a structural point of view this device can be regarded as a symmetrical one-story, two-bays, portal frame, which is hinged at the base. Fig. 3 shows a typical prototype. The device is forced to deform antisymmetrically in the elasto-plastic range. The way this deformation occurs is shown in fig. 4; the central leg and the external legs are hinge-connected to different parts of the same structure which can undergo relative displacements. Fig. 4 shows also the diagrams of flexural moment and axial force in the device.
The main advantages of the scheme are the following:

1) The energy dissipation occurs only in the transverse beam of the portal frame, because the legs are designed to act essentially as lever arms; they do deform elastically but never go into the plastic range. The two parts of the beam are subjected to constant flexural moment. It is possible to realize a uniform plasticization with a very simple geometry, using a constant beam section.

2) The flexural moments have alternate sign in the two parts of the beam and the same occurs for the axial force. This allows the neutralization of the effects of geometry changes which would cause geometric hardening in tension and softening in compression.

3) The sign change of the axial force, in accordance with the sign variation of the flexural moment, permits to avoid the progressive accumulation of axial strain which is the main cause of deterioration, at increasing number of cycles, in devices in which, during alternate flexure, the axial force maintains a constant sign, (usually tension).

On the base of the simple scheme presented in fig. 4, it is easy to compute the relevant parameters of the response of the device, using very simple considerations based on small displacement theory of flexural beams in elasto-plastic flexure, and neglecting axial and shear deformation.
The device parameters which influence its behaviour are, (fig. 3) :

- s, thickness of the plate from which the device is cut;
- b, constant depth of the transverse beam;
- h, height of the lever arm;
- σ_y, yielding stress of the steel, considered as an elasto-perfectly plastic material.

The maximum force which can be applied at the bottom of the central leg, corresponding to complete plasticization is:

$$P_p = \frac{1}{2}\sigma_y \frac{s\,b^2}{h}$$

The displacement, σ_{max} , corresponding to an assigned maximum value of the surface strain, $\varepsilon = \varepsilon_{max}$ and disregarding the deformation of the legs is:

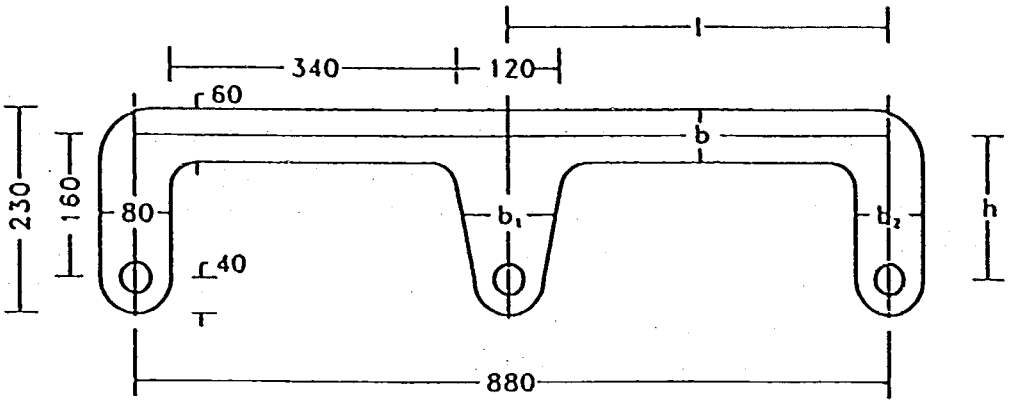
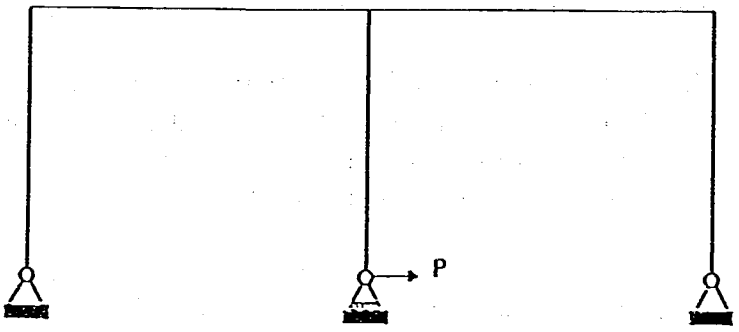
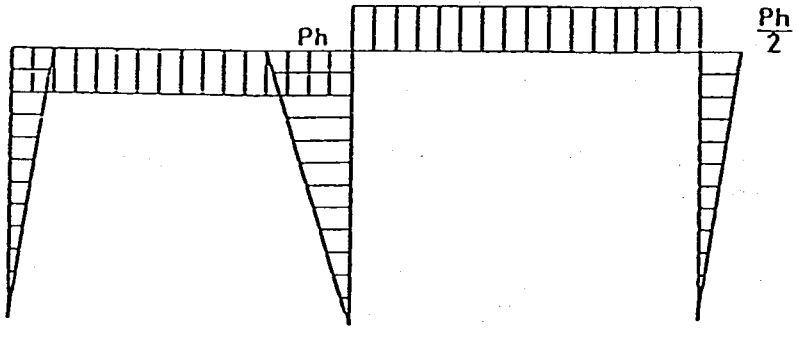
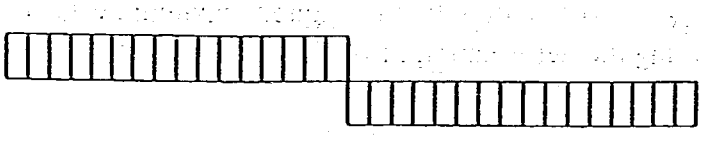


fig.3





FLEXURAL MOMENT



AXIAL FORCE

fig.4

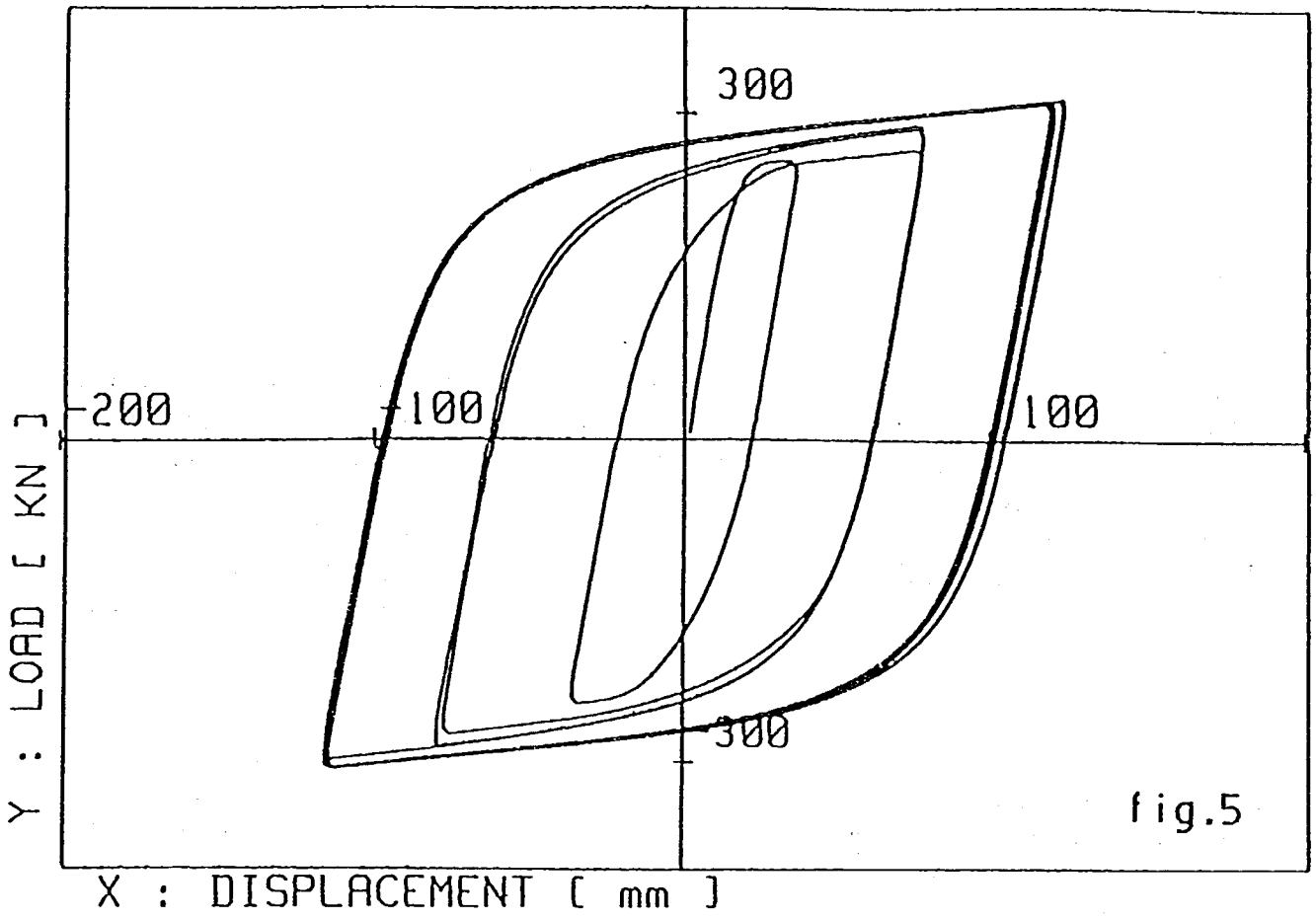

300
200
100
100
300
Y : LOAD [KN]
X : DISPLACEMENT [mm]

fig.5

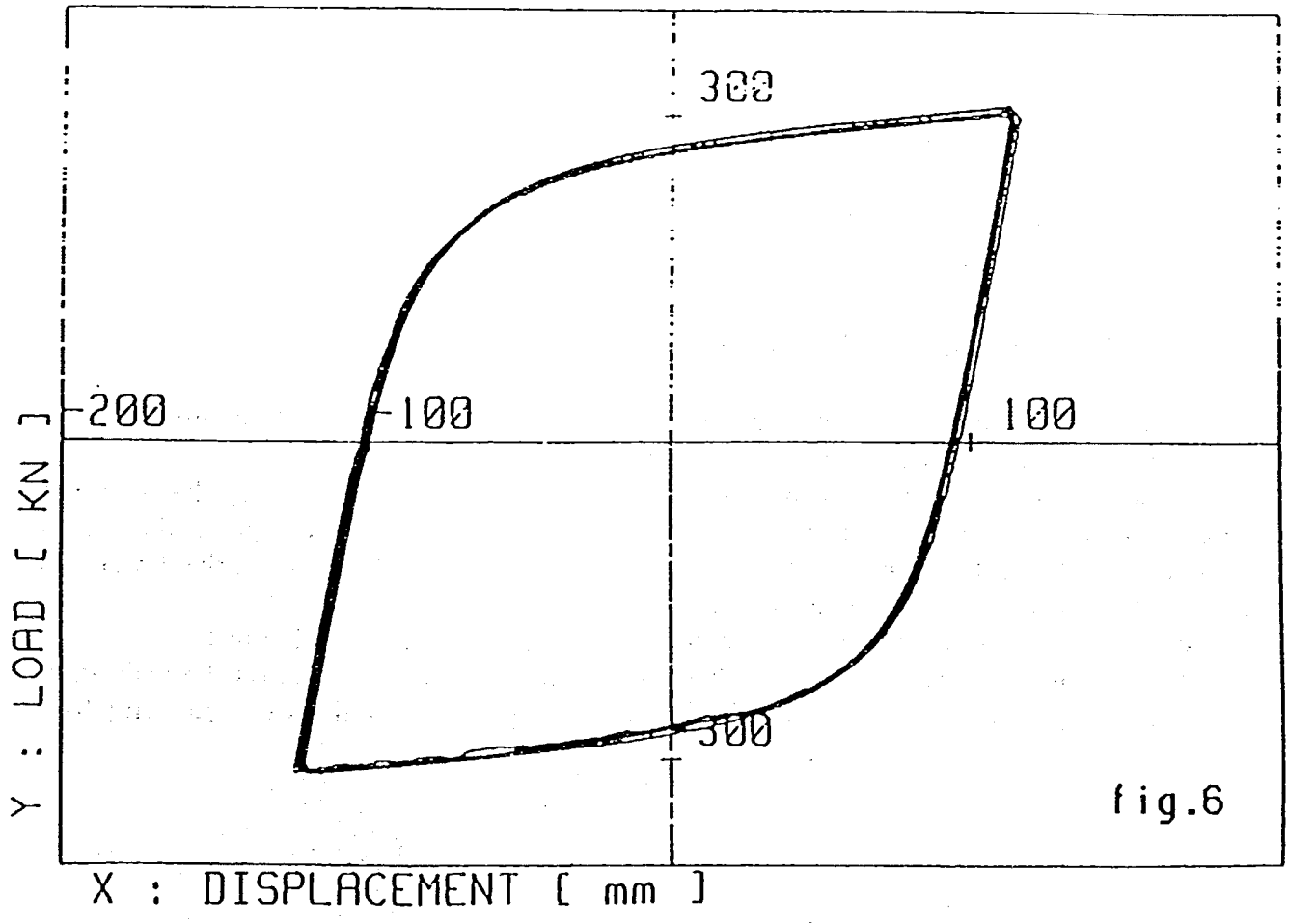

300
200
100
100
300
Y : LOAD [KN]
X : DISPLACEMENT [mm]

fig.6

$$\varepsilon_{max} = 2 \frac{h}{b} \varepsilon_{max} \frac{l}{}$$

For practical cases ε_{max} is normally assumed $\varepsilon_{max} = 3\%$.

This type of device has been developped in year 1988 by Prof V. Ciampi and patented. It has been applied in several projects including the Mortaiolo Viaduct that is over 9 km long. The laboratory tests performed confirmed the symmetrical behaviour in tension and compression and a very good low cycle fatigue life. This result was due not only to the geometry of the device that improved the efficiency but also to the selection of a very particular type of steel, suitable to perform many yield cycles before breaking.
The number of cycles that the devices can perform before breaking is a function of the selected ε_{max}. With $\varepsilon_{max} = 0.03$ the devices were able to perform more than 50 cycles (see fig. 5 and 6).

2.3 C-Shaped devices

A further improvement was reached in the histeretic devices utilizing a combination of C-shaped elementary energy dissipators. Each elementary dissipator consists of a circular arch. The depth of the section is variable in order to get uniform resistance and therefore uniform plasticization of all sections (see fig. 7)

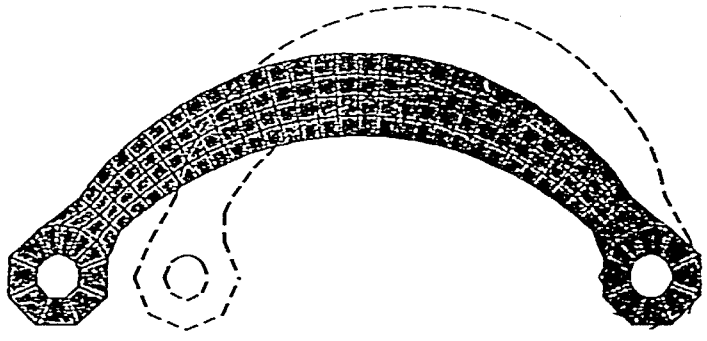


Figure 7 - Elementary C-shaped dissipator

The angular opening of the arches is normally near to π (semicircular arch) or greater when the displacement requirement is particularly high.

In a device the elementary dissipators are always connected in such a way that they are forced to deform antisimmetrically : it means for each compressed dissipator there is a tensioned one. In this way the effects of geometry changes are neutralized and the device can grant simmetrical behaviour in tension and compression.

The concepts of this device have been patented by V. Ciampi and the author in 1989.

The combination of many elementary dissipators with radial simmetry allows the realization of an antiseismic device with uniform behaviour for earthquake acting in any direction (fig. 8)

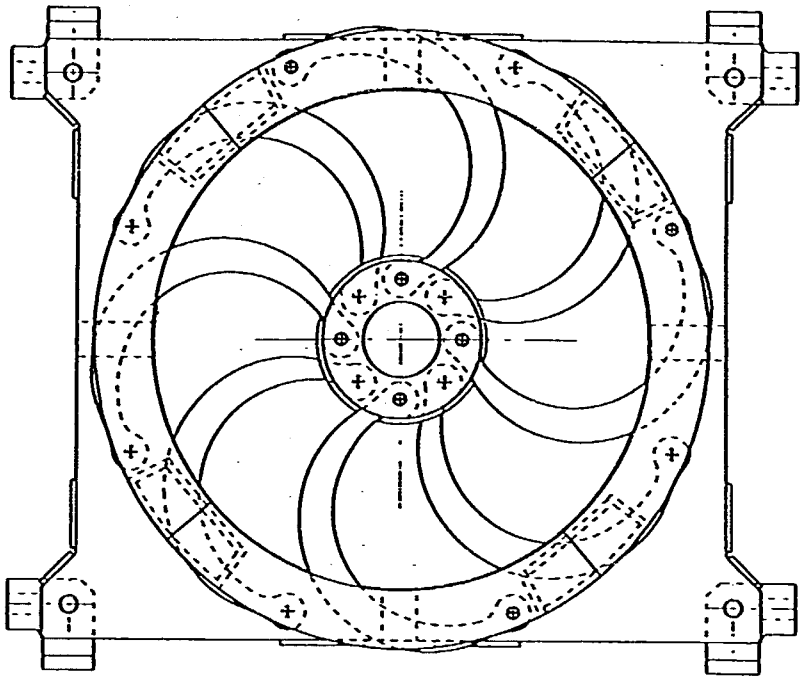


Figure 8 - Multidirectional energy dissipating device

Different design requirements like different responses in longitudinal and transverse directions or unidirectional devices can be easily met by a suitable arrangement of the elementary dissipators or by the combination of elementary dissipators with different stiffnesses. Fig. 9 shows a tipical arrangement for an unidirectional device. Fig: 10 shows the deformation of the dissipators at maximum displacement.

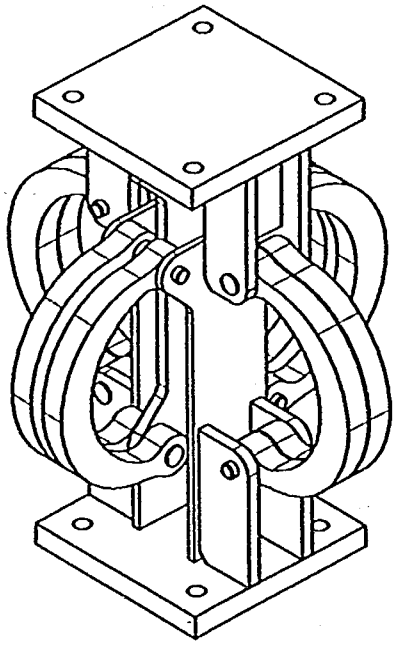


Figure 9 - Unidirectional energy dissipating device

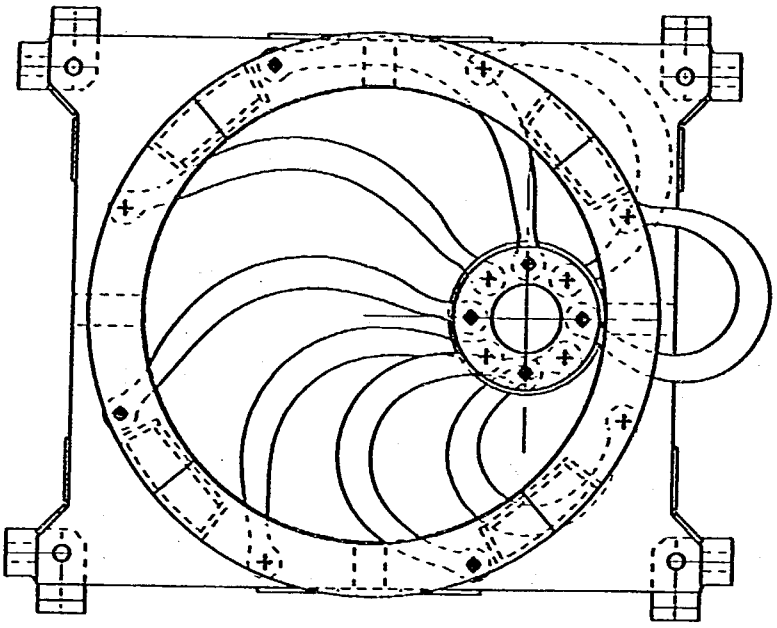


Figure 10 - Deformation of the device at maximum displacement

The simplified formulas for the design of the elementary dissipators are the following (see fig. 11).

Yielding force (complete plasticization)

$$Fy = \sigma_y \frac{sb^2_{max}}{6} \frac{1}{r(\cos a_0 + 1)}$$

Displacement

$$\delta = \frac{4r^2\varepsilon}{b_{max}} \sqrt{\cos\alpha_0 + 1} \left[\int_{\alpha_0}^{\pi} \sqrt{\cos\alpha_0 - \cos\alpha} d\alpha \right]$$

where

σ_y	=	yield stress of the steel
ε	=	assigned value of the strain, normally 3% at design displacement
S	=	thickness of the dissipator (constant)
b_{max}	=	maximum depth of the dissipator

The depth of the dissipator in the other sections is given by the formula:

$$b(\alpha) = b_{max} \sqrt{\frac{\cos\alpha_0 - \cos\alpha}{\cos\alpha_0 + 1}}$$

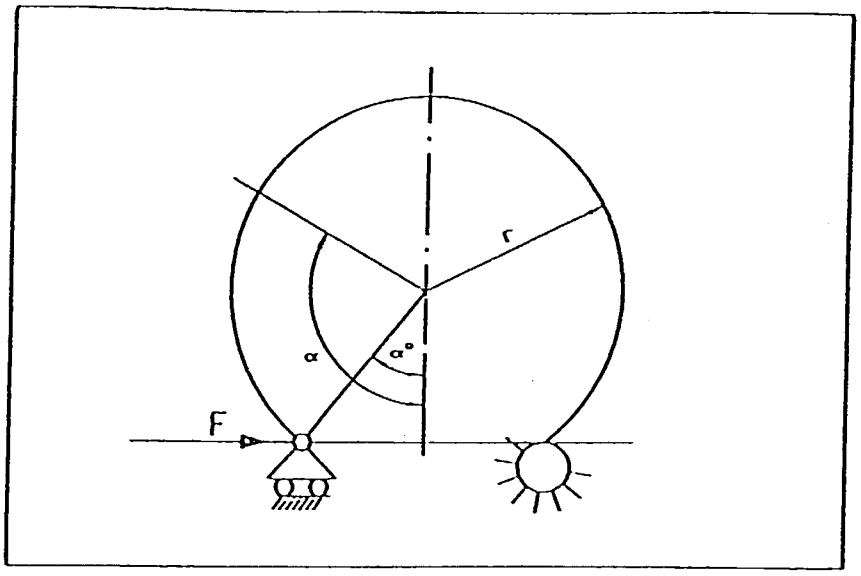


Figure 11 - Scheme of an elementary C-Shaped element

3. SCHEMES OF APPLICATION OF THE HYSTERETIC DAMPERS

As a first exemple we will consider a bridge consisting of a serie of simply supported spans. the simplest scheme is to consider each span connected to the pier through an hysteretic damper at one end and supported on a longitudinal sliding bearing at the other end. Selecting the yield force of the hysteretic damper also the maximum bending moment and shear force at the base of the piers are determined. Therefore the resistance of the pier can easily be designed in order to keep it within the elastic range(see fig. 12).

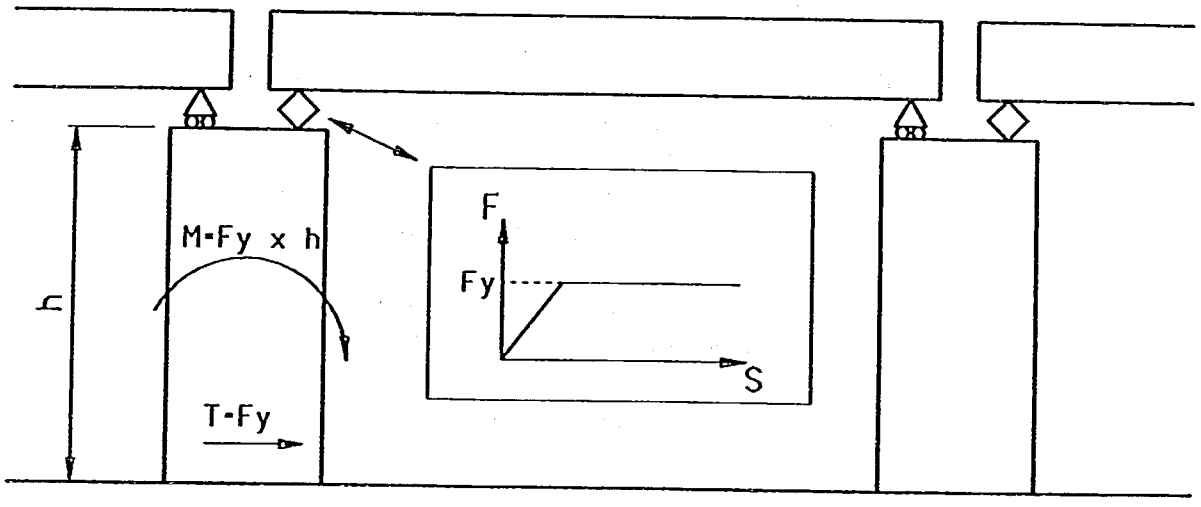


fig.12

In Italy all the bridges incorporating antiseismic devices are continuous. This kind of bridges is subject to important variations of length due to creep, shrinkage and temperature changes. These variations of length must be freely allowed.

The easiest solution in these cases is to connect the bridge to one abutment or to one strong pier and to provide sliding bearings on all the other supports. In that case all the longitudinal seismic actions are resisted by the hysteretic damper placed on the abutment or strong pier(see fig.13).

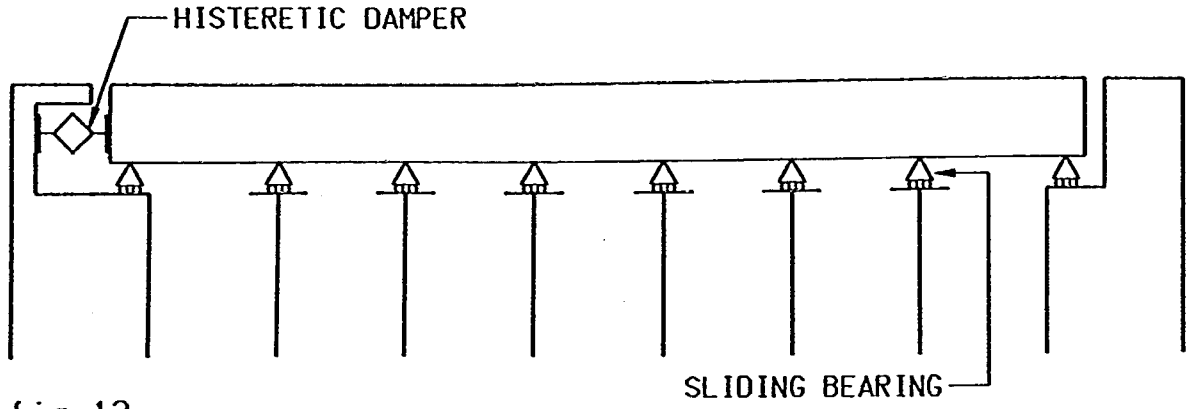


fig.13

This solution has been applied on the following viaducts:

NAME	LOCATION	YEAR	LENGTH (m)
Fella 1	Udine - Tarvisio	1981	2x840
Slizza	"	"	2x400
Coccau	"	1982	2x400
Val Freghizia	Milano - Napoli	1985	2x777
Aniene	"	1985	2x354
Acqua Marcia	"	1987	2x325
Savalano	Livorno-Civitavecchia	1991	2x1800

In many cases however it is not possible or not convenient to provide abutments or pier sufficientlly strong to resist the whole seismic action. In that cases it is convenient to shear the seismic action on as much as possible piers or columns.
In order to achieve this type of performance have been developped devices incorporating a shock transmission unit in serie with the hysteretic damper. This kind of device allows slow movements due to creep, shrinkage and temperature variations without significant reactions.
In case of rapid action such as earthquake the shock transmission unit acts as a rigid connection assuring the transmission of all the seismic forces through the associated hysteretic damper.
The scheme of a typical device with this type of performance and the functioning under slow movement and earthquake action is shown in the figures 14 - 15 - 16.

The most important applications of this solution are:

1 - Mortaiolo Viaduct
Livorno - Civitavecchia Motorway
total length 2 x 9643 m
built year 1990 - 92

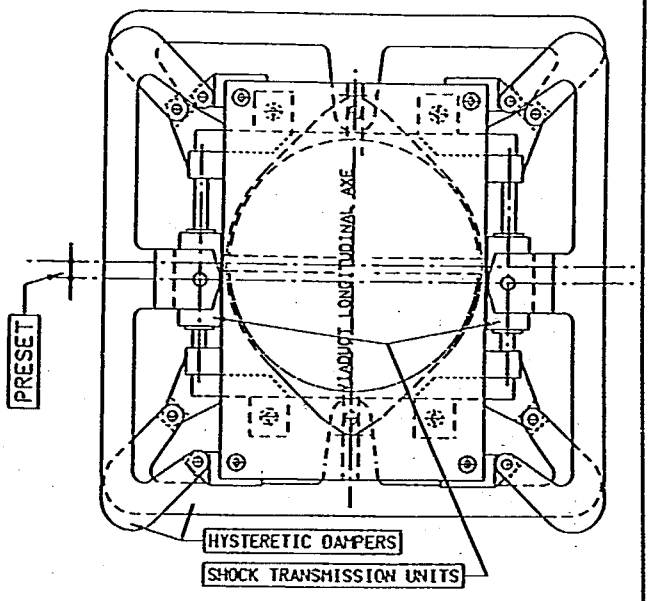


Fig.14 - Scheme of a multidirectional hysteretic bearings with longi_ tudinal shock transmission unit.

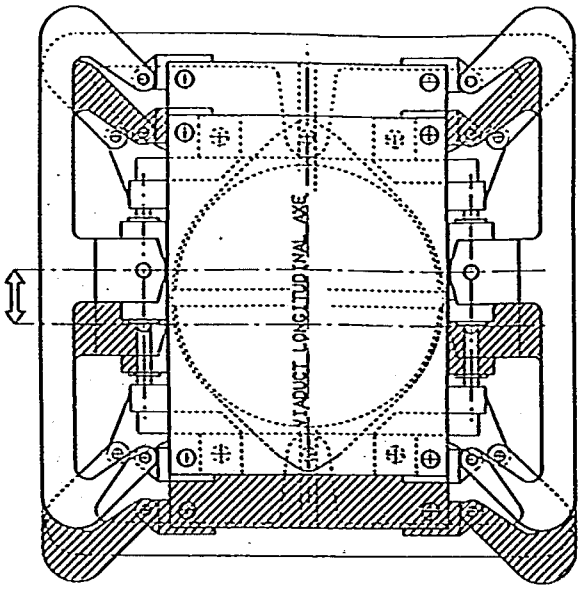


Fig.15 - Working scheme of a bearing device under slow longitudinal movement.

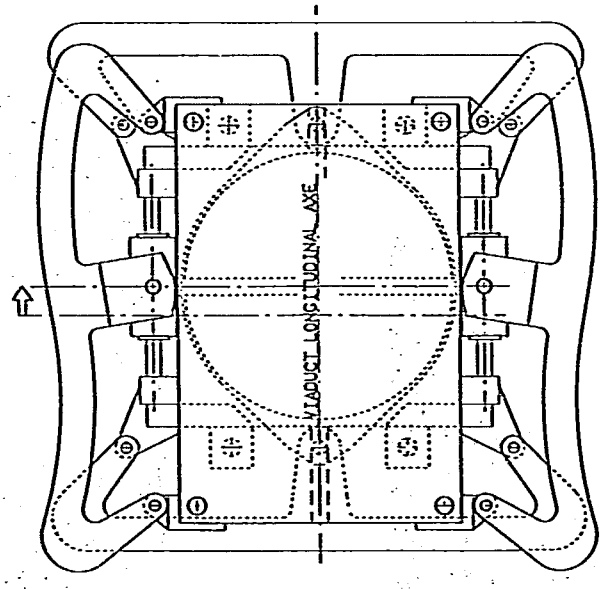


Fig.16 - Working of a bearing device under dynamic longitudinal movement.

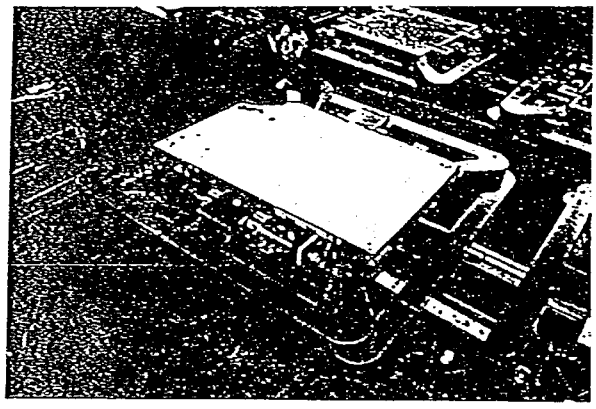


Fig.17 - Antiseismic bearing devices for the Mortaiolo Viaduct.

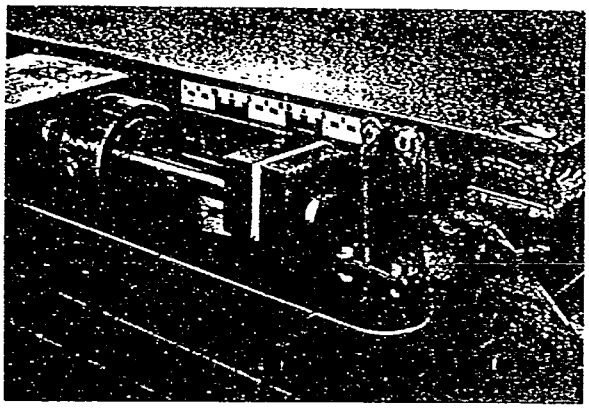


Fig.18 - Detail of the shock transmission unit and hysteretic damper with movement measurement scale.

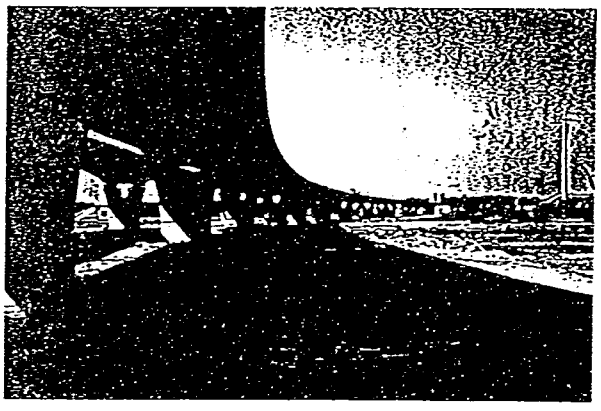


Fig.19 - View of the Mortaiolo Viaduct under construction.

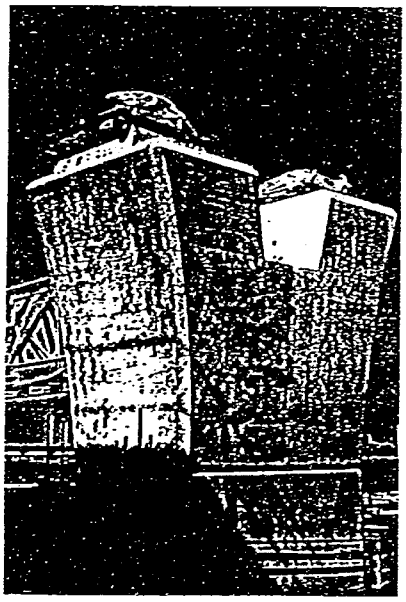


Fig.20 - Detail of a column of the mortaiolo Viaduct with the antiseismic bearings installed.

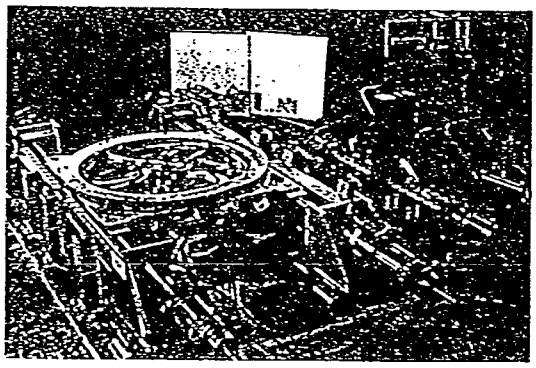


Fig.21 - Test on a full scale device of the Bolu Mountains Viaduct.

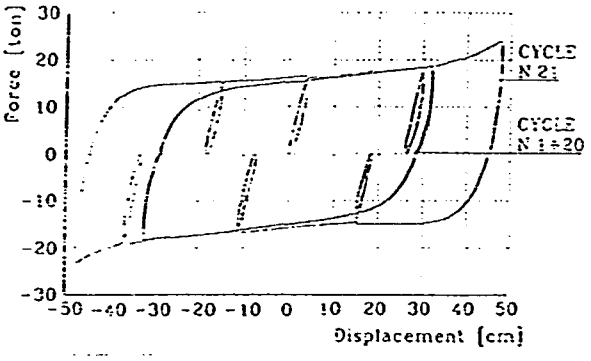


Fig.22 - Load deflection plot for the full scale device.

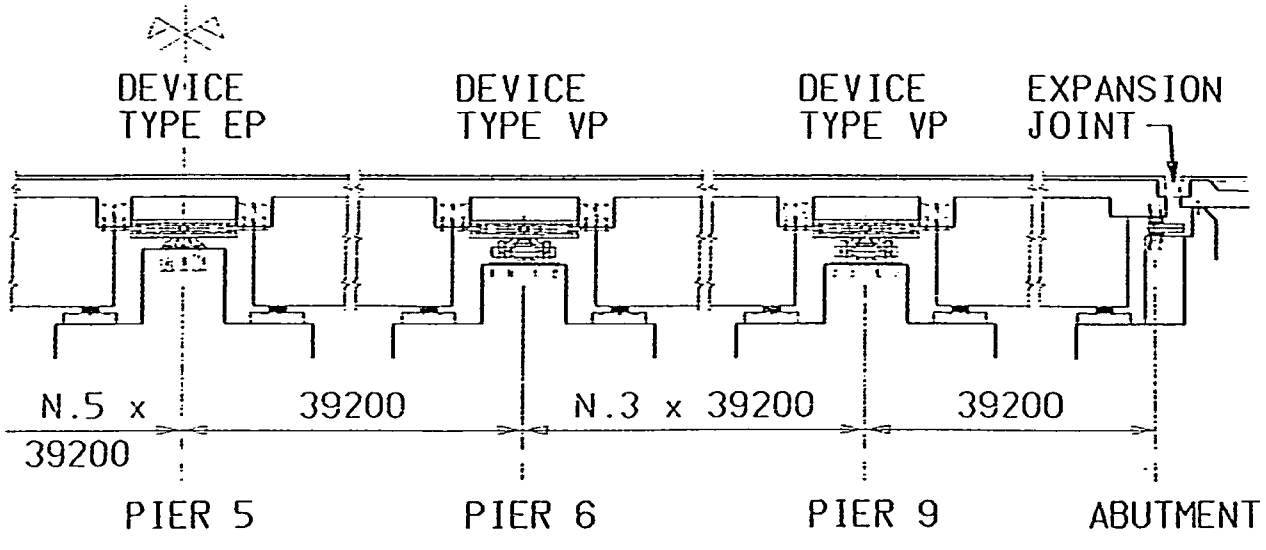


Fig.23 - Longitudinal section of Bolu Mountains Viaduct.

2 - Bolu Mountain Viaduct
Istanbul - Ankara Motorway (Turkey)
total length 4000 m
under construction

In the following figures are shown some details of the above mentioned projects and the utilized devices (see fig. 17 - 18 - 19 - 20 - 21 - 22 - 23).

For both the above mentioned projects there is an expansion joint every 10 spans (400 meter approximately).
For each bridge section of 10 spans, the device placed on the center pier is not provided with shock transmission units in order to provide fixity of the bridge under normal conditions. In these conditions the device on the center pier is subjected to the friction forces generated by the sliding bearings.
The friction forces normally assumed for sliding bearings with PTFE - stainless steel is normally assumed

$$f = 0.03$$

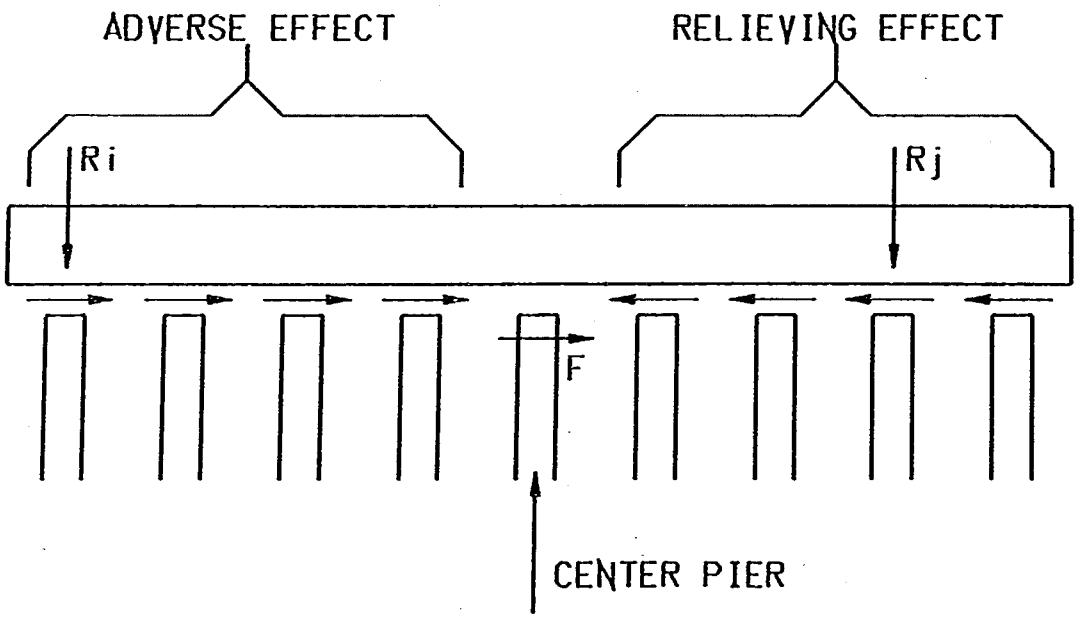


Fig. 24

To compute the resultant force on the center pier the friction effects at the two sides are not considered symmetrical but are affected by different coefficients.
In accordance with DIN 4141 Part 1 or prEN 1337 Part 1, when there are more than 10 bearings the following friction coefficient are assumed

adverse effect $f_a = 0.75\ f$

relieving effect $fr = 0.25\ f$

The resultant force on the center pier, taking into account the forces due to wind and braking Fb is:

$$F = fa \Sigma Ri + fr \Sigma Rj + Fb \leq \frac{Fy}{\gamma s}$$

and must not exceed the yield force Fy of the hysteretic dampers divided by a suitable safety factor (normally $\gamma_S = 1.35$)

4. CONCLUSIONS

The Italian experience in the use of hysteretic dampers for the seismic protection of bridges have been illustrated.
Antiseismic devices are objects that must function for about 30 seconds only in a structure during its lifespan of many decades.
The large utilization of hysteretic dampers in Italy reflects their high reliability in extreme ambiental conditions and also in case of lack of maintenance.

THE SEISMIC RETROFIT OF MARQUAM BRIDGE

A CASE STUDY

R. MEDEOT

FIP Industriale - Padua - Italy

ABSTRACT

The seismic retrofit project of Marquam Bridge - Portland, Oregon, USA is the first example of the application in the United States of high dissipative capacity isolators as well as shock transmitters developed and vastly applied in bridge seismic engineering in Italy during the last twenty years. The utilization of the above mentioned devices has permitted to ensure bridges complete anti-seismic protection as well as avoiding the need to strengthen pre-existing structural elements. The devices have undergone severe tests simulating actual normal service actions and seismic attack conditions. Said tests were passed with flying colors.

FOREWORD

As it is known, the design engineer facing a seismic retrofit must exercise certain preliminary choices that essentially depend on the type of pre-existent structure, the nature and seismicity of the site, norms currently in force, bridge owner specifications and requirements, etc.
In some cases, said choices are almost obligatory. In some others, there is the freedom of choice to opt for numerous solutions that have already been adopted with success.

Said solutions, notwithstanding their large variety, can be roughly grouped into two main types. To be more precise, into those that in the event of an earthquake tend to:

a. make structural members work together, thus creating temporary restraints that become automatically active during the earthquake itself;

b. limit the accelerations transmitted to the bridge deck and therefore reduce the inertial forces (in practice, the Base Seismic Isolation).

On the next page, Figure 1. schematically illustrates the possible seismic design strategies (the software) and their respective devices (the hardware).

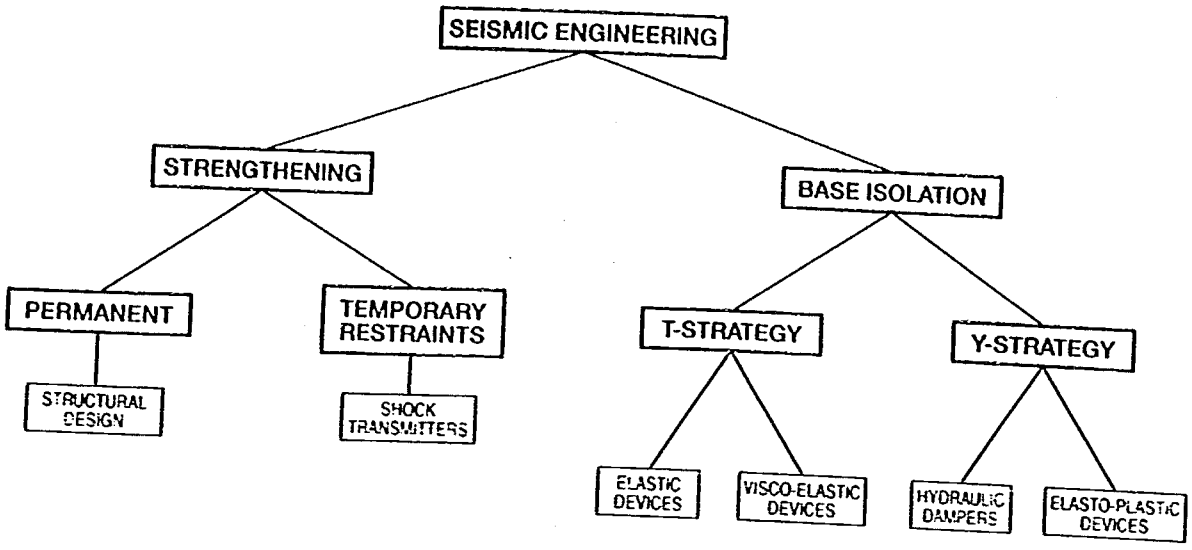


Figure 1. Seismic design approaches and their respective devices.

The so called T-strategy is based upon the reduction of the seismic response subsequent to the shift of the fundamental period of the structure.

The Y-strategy is based upon the limitation of the forces transmitted amongst various parts of the structure (in the case of bridges, between the deck and the piers or abutments) by means of devices capable of limiting the transmitted reactions to pre-established values.
This strategy is also characterized by a high level of dissipation that permits controlling and reducing relative displacements.

Naturally, it is possible to employ hybrid solutions, as in the case of the Marquam Bridge Retrofit Project, where both temporary restraints (shock-transmitters) as well as the Y-strategy (high dissipating isolators) have been adopted.

2. DESCRIPTION OF THE STRUCTURE

The Marquam Bridge over the Willamette River (see Fig. 2) comprises metal trusses carrying two superimposed roadways for a total length of 318 meters (*). The present static arrangement is of typical "Gerber girder" construction in which the two end-girders have a cantilever beam towards the center of the bridge, upon which the suspended central truss is supported (see Fig. 4).
The two end spans measure 92 meters, the central span has a total length of 134 meters - of which 79 meters comprise the central suspended truss. The values indicated for the spans represent the center to center distance between the piers. In plan view, the structure is characterized by a straight longitudinal axis.

(*) Note: The conversion of the measurement systems in force in the United States to ISO necessitated rounding off.

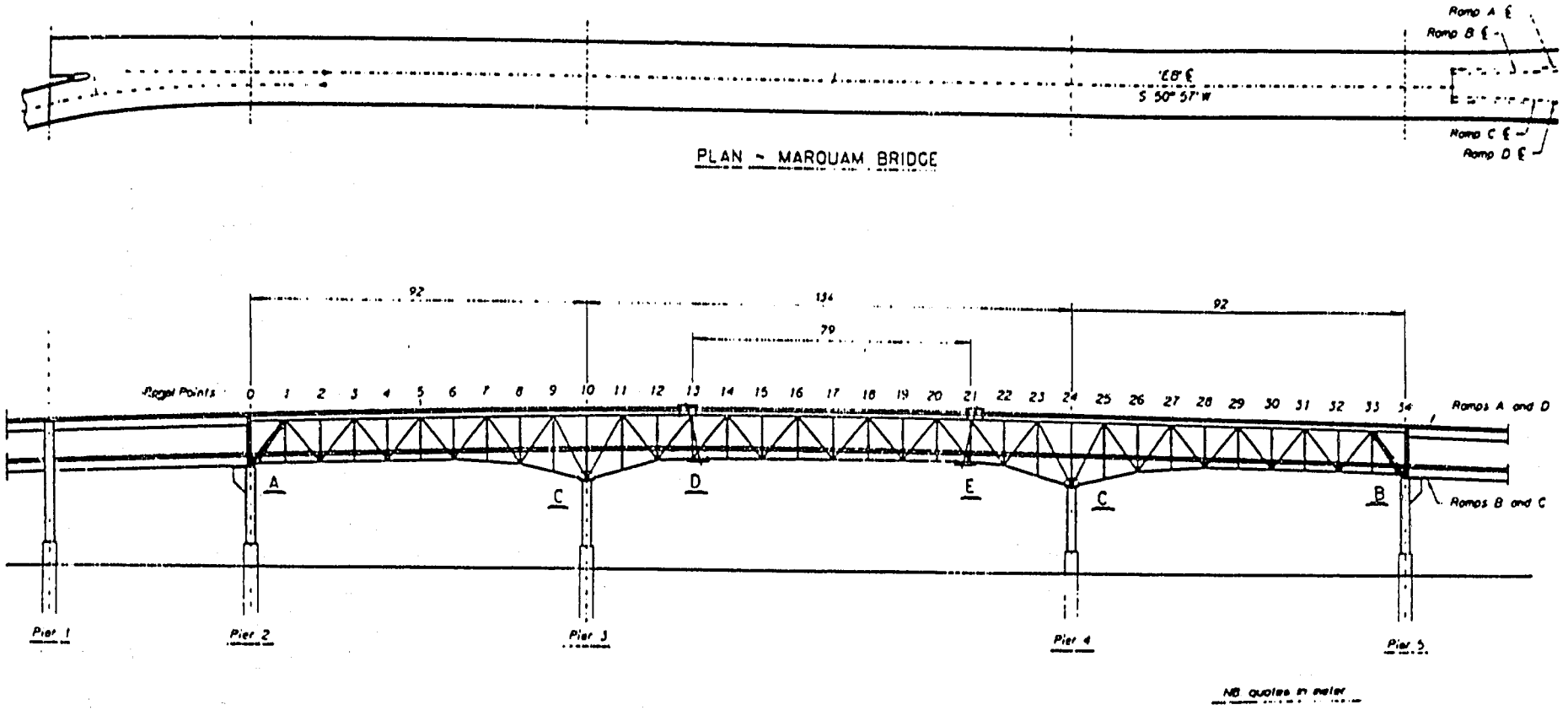


Figure 2. Plan and elevation of Marquam Bridge

The piers are reinforced concrete configured upon a two-uprights transverse framework connected by two beams (see Fig.3). The uprights have a center to center distance of 20 meters. Their upper section is circular with a diameter of 3,.7 meters while their lower section (below the high water mark) is elliptical (4,2 × 7,3 meters) with semi-circular ends. The main axis of the section forms a skewed angle of approximately 20 degrees with the longitudinal axis of the bridge. The uprights are connected by means of rectangular section struts placed, one each, at the top and where the section of the uprights changes from elliptical to circular.

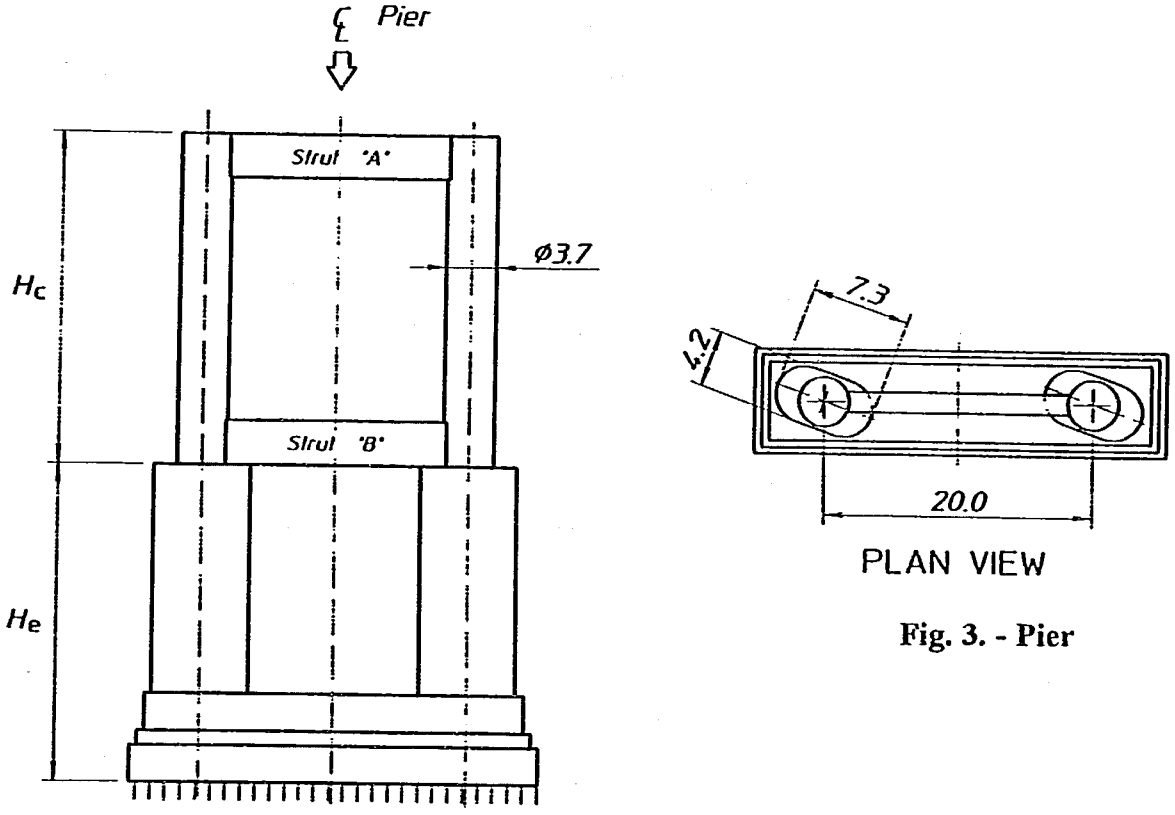


Fig. 3. - Pier

The height of the piers is listed in Table 1 below where H_c indicates the height of the upper circular section and H_e indicates the height of the lower, elliptical section.

Pier (#)	H_c (m.)	H_e (m.)
2	24,7	16,5
3	20,5	17,4
4	20,1	18,3
5	24,7	14,0

Table 3. - Height of Piers

3. SEISMIC REQUIREMENTS AND DESIGN APPROACH

A requirement for the following objectives was advanced in the Seismic Retrofit Project of the Marquam Bridge:

a. to attain the total seismic protection for the structure in the event of the Design Maximum Expected Earthquake in both the longitudinal and transverse directions.

b. to avoid the need for strengthening existing structural elements (i.e., piers, trusses, foundations, etc.).

c. to maintain the existing "bearing system" (i.e., "the static scheme on Fig. 4) for the service loads.

d. to limit the relative displacements to values compatible with the existing gaps (longitudinal deflection not to exceed $\pm$ 127 mm).

"Total seismic protection" signifies that the entire structure shall remain within the elastic limits during the most severe expected seismic attack, i.e., any structural damages shall be avoided.

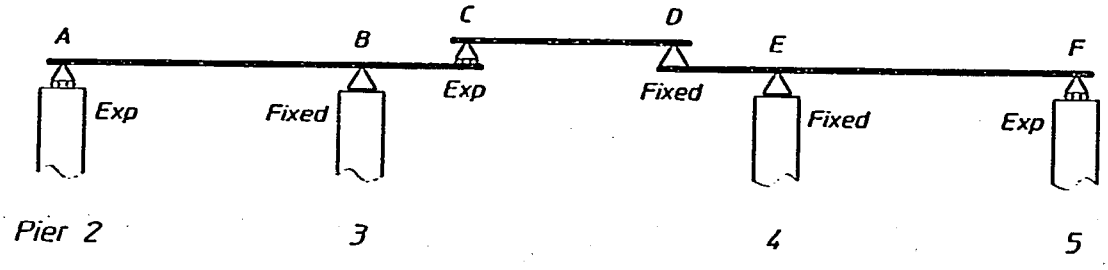


Fig. 4 The Bearing System of Marquam Bridge

The four objectives have been achieved through the replacement of the pre-existing vulnerable steel bearings by high dissipation isolators and the insertion of four shock transmitters at the expansion end of the suspended span.

The isolators are of the sliding type and essentially comprise:

- a free sliding pot-bearing that serves to transmit vertical loads and permits the lateral displacements in all directions
- a series of steel dissipating elements suitable to control the horizontal actions

The isolators installed at the expansion points (Piers 2 and 5) additionally comprise a shock transmitter which is active between superstructure and steel dissipating elements thus

accommodating thermal deformations without appreciable actions on said elements. It is worth mentioning that service loads (i.e., wind, braking actions, etc.) and moderate earthquakes do not stress the dissipating elements owing to the use of "sacrificial restrainers" (or shear keys). Said "sacrificial restraints" impede any displacement in the isolators of the "fixed" type (Piers 3 and 4) and the transverse movements on those of the "mobile" type (Piers 3 and 6). It thus follows that the objective c is attained.

In the event of the Design Maximum Expected Earthquake, the sacrificial restrainers fail and the shock-transmitters are activated (i.e., become rigid). As a consequence, the equivalent bearing system of the bridge becomes the following:

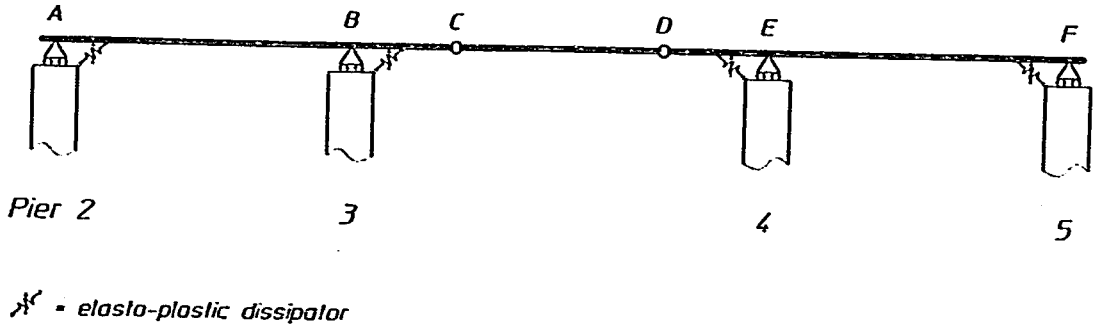


Fig. 5 Equivalent Bearing System during an earthquake attack.

The steel dissipating elements have elasto-plastic behaviour and therefore:

- permit control of the maximum lateral force transmitted to the piers
- ensure high dissipating capacity

Upon suitable choice of the dissipating elements' yield threshold, all piers remain within the elastic limits, even in the case of the most severe earthquake.
The high dissipating capacity of the dissipating elements permits maintaining relative displacements within the specified limits (see par. 4, Dynamic Analysis).

It must be then concluded that even objectives a, b and d are equally attained. In particular, objective b is reached beyond expectations as the appropriate choice of the yield threshold avoids having to reinforce the piers and foundations- with remarkable savings in costs and the execution timetable of the retrofit project.
In other words, the structure becomes hyperstatic, multi-span continuous girder type, which has proven to be the most effective when it comes to resisting seismic events.

4. SEISMIC ANALYSIS

During the preliminary stages of the project, a multi-modal linear analysis using a design spectrum in accordance with the AASHTO standards was conducted on the existing structure by way of orientation. The results demonstrated that the structure was absolutely incapable of resisting the Design Maximum Expected Earthquake.

Subsequently, and so as to verify the effect of introducing high dissipating isolators and shock transmitters in the structure, two mathematical models suitable to the conduct of a step-by-step non-linear analysis were set up (one for each main direction).
The numerical calculations were conducted using the DRAIN-2D program, developed at UC Berkeley, with the appropriate implements.

In the model, the trusses' distributed mass was concentrated at three intermediate points in both the end-spans and the suspended central truss. Analogously, the distributed masses of the piers were concentrated at three points in the elliptical uprights and at other three points in the circular uprights.

The seismic input was the following:

- Peak Bedrock Acceleration = 0,29 g (90% probability of non-exceedence in 50 years period)
- Soil Profile = Type II (S = 1,2)
- Synthetic (or artificial) time histories developed to match AASHTO response spectrum.

The configuration S_a (T) of the above mentioned unitary spectrum ($S_{max} = 1$) is therefore shown below:

$$S_a(T) = 0{,}4 + (1 - 0{,}4)\frac{T}{0{,}15} \quad \text{for} \quad 0 \le T \le 0{,}15\text{sec.}$$

$$S_a(T) = 1 \quad \text{for} \quad 0{,}15 \le T \le 0{,}575\text{sec.}$$

$$S_a(T) = \left(\frac{0{,}575}{T}\right)^r \quad \text{for} \quad 0{,}575\text{sec} \le T \le 8\text{sec.}$$

in accordance with the AASHTO Commentary, r = 2/3 was assumed for the multi-modal linear analysis and r = 1 for the generation of the accelerograms.

The four distinct accelerograms (time histories) used in the analysis of each of the two models of the structure (longitudinal + transversal) were generated using the SIMQKE program developed the University of California at Berkeley.

In the model, each one of the isolators was characterized by the following parameters:

F_y = yield threshold

s_y = displacement at yield point

K_p = stiffness beyond yield point

The elastic stiffness is defined as $K_e = F_y / s_y$.

For the type of dissipaters used in the Marquam Bridge Retrofit Project, the stiffness beyond yield point was $K_p = 0{,}02\,K_e$.

Tables 2 and 3 list the average of the 4 peak values obtained from the individual dynamic analyses performed using different accelerograms, in both the longitudinal and transverse directions respectively. The symbols have the following meaning:

s_b = deformation of the bearing (displacement of thrust minus displacement of the pier top)

F_b = force acting on each bearing

s_0 = displacement of the pier top

V_0 = total shear force upon the section under strut "A"

M_1 = total bending moment at pier mid-height

M_2 = total bending moment at pier bottom

Pier number	s_b (mm)	F_b (kN)	s_0 (mm)	V_0 (kN)	M_1 (MNm)	M_2 (MNm)
2	98,6	1 363	97,2	2 853	63,3	148,2
3	84,9	2 015	101,4	3 935	80,3	171,4
4	87,3	2 024	103,4	3 702	75,6	161,3
5	114,1	1 407	90,9	2 859	63,9	135,1

Table 2. - Longitudinal Dynamic Analysis Peak Values

Pier number	s_b (mm)	F_b (kN)	s_0 (mm)	V_0 (kN)	M_1 (MNm)	M_2 (MNm)
2	82,1	1 318	52,8	5 148	62,7	141,3
3	101,9	2 086	38,5	4 265	52,5	123,5
4	100,7	2 078	38,1	4 055	50,5	127,5
5	89,5	1 338	50,3	4 870	65,4	126,2

Table 3. - Transverse Dynamic Analysis Peak Values

5. TESTING

Each device type was tested at the FIP INDUSTRIALE laboratories and the tests were witnessed and certified by experts from the Earthquake Engineering Research Center (EERC) at the University of California at Berkeley.

5.1. Shock Transmitters

The rig used for testing the shock transmitters comprised bolted steel members, a double-action actuator and servo valve, a hydraulic power supply and a closed loop electronic control system.
A photograph of the test set-up is shown in Figure 6 and its relevant schematic view is presented in Figure 7.
The objectives of the test were to evaluate device force resistance at low (i.e., thermal) velocity as well as to verify their axial displacement capacity.

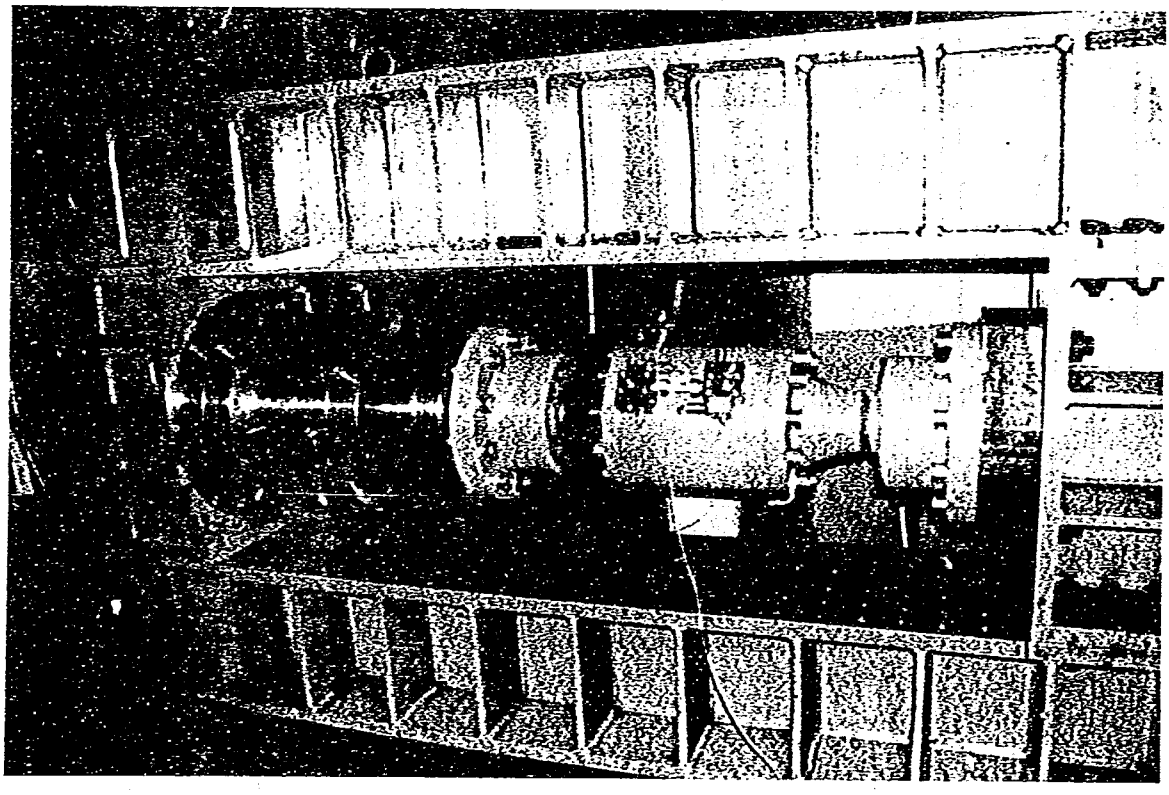


Figure 6. Test Set-up

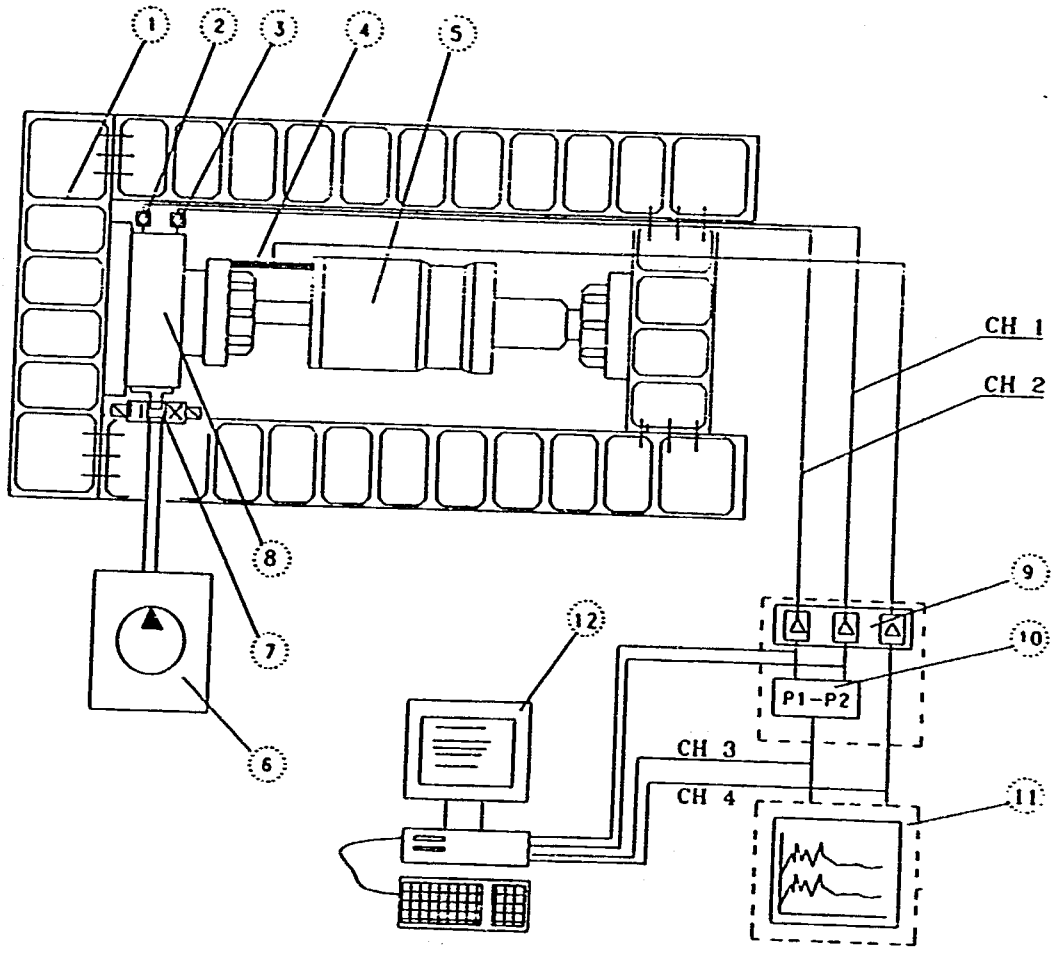


Figure 7. Test Set-up Schematic View

5.1.1 Impressed Deflection Test

Testing Procedure: The device shall have an impressed deflection ranging from 0 to 70 mm. to 0 to −70 mm to 0 within one hour. A continuous plot of the load and deflection shall be recorded to permit evaluation of the device.

Acceptance Criteria: During the impressed deflection cycle, the device shall develop no more force than 178 kN.

Results: The axial force *vs.* axial displacement response is presented in Figure 8.
The measured maximum response was 95 kN.

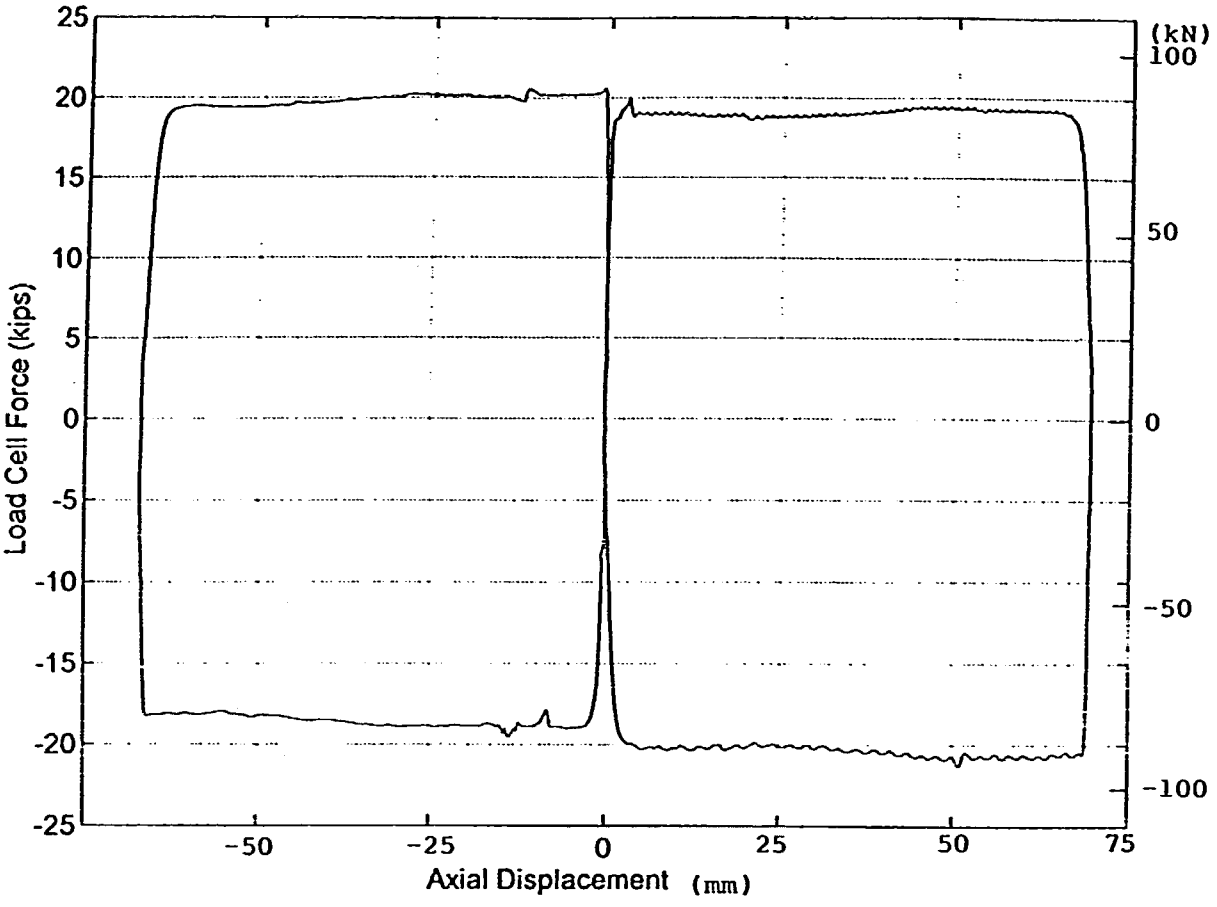


Figure 8. - Device OT 440/5.5"
Impressed Deflection Test. Axial Force vs. Impressed Displacement.

5.1.2 Simulated Dynamic Force Transfer Test

The test objective was to evaluate the stiffness of the device for impulse forces and constant forces.

Testing Procedure: The device shall have a force of 1958 kN applied in less than 0,5 seconds and the force sustained for 5 seconds. Then the force shall be inverted to −1958 kN for 0,5 seconds and sustained for 5 seconds.

Acceptance Criteria: The deflection during loading from 0 to 1958 kN and from 0 to −1958 kN shall be no greater than 6,6 mm. The deflection during the sustained portions shall not exceed 6,6 mm.

Results: The applied forces were in excess of the specified values (+ 2 029 - 2 051 respectively.) and the results are shown in Table 4 on the next page.

Type of Loading (kN)	Maximum Acceptance Displacement (mm)	Measured Displacement (mm)
0 - 2029	6,6	6,6
constant 2029	6,4	3,6
+ 2029 to –2051	–12,7	–10,2
constant –2051	–6,4	–3,3

Table 4. - Displacement Response of Device OT 440-5.5" in Simulated Dynamic Force Transfer Test.

The same tests were conducted on the ST shock transmitters unit installed in the "movable" type of bearings at the expansion points (Piers 2 and 5).
The results of the Impressed Deflection Test are shown in Figure 9. The maximum response force required by the specifications was 89 kN.

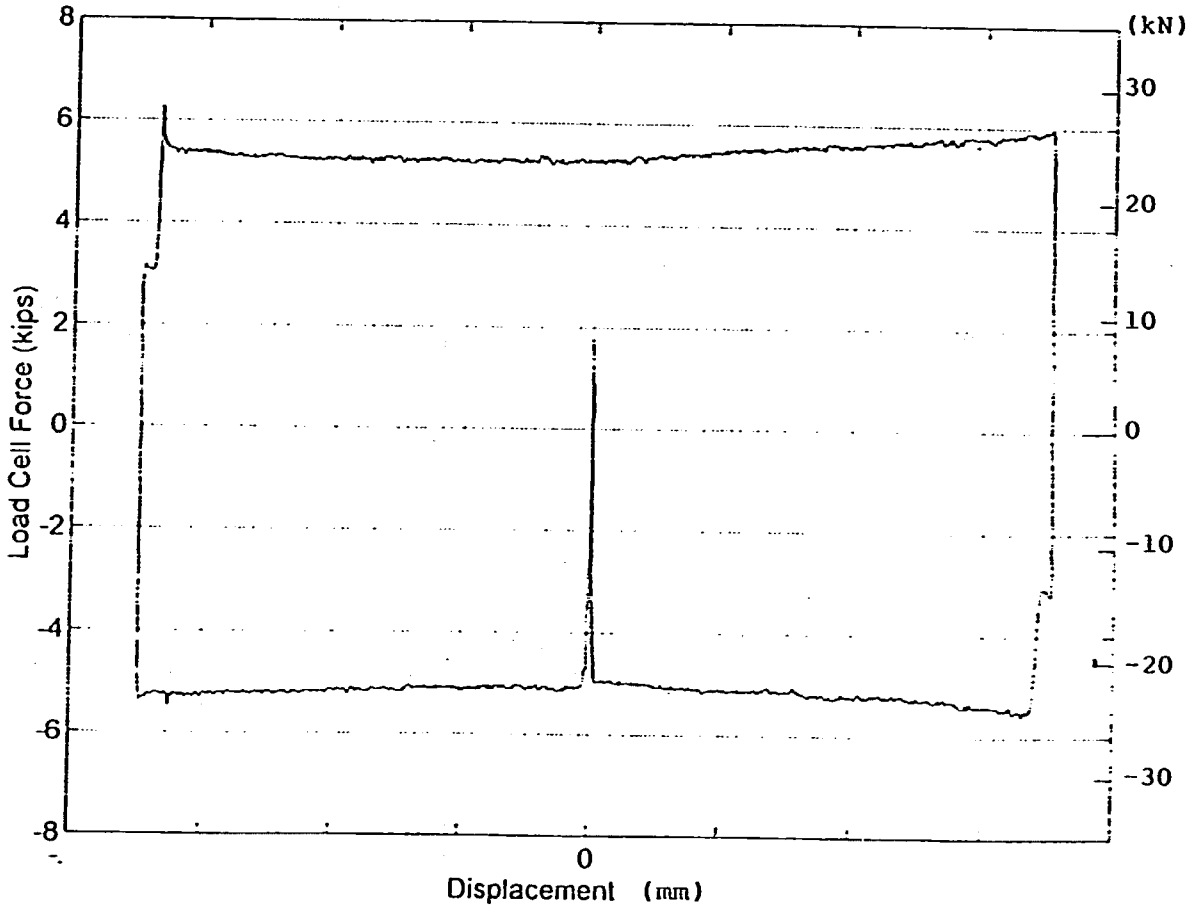


Figure 9. - Device ST-1 - Impressed Deflection Test

The measured maximum force was 28 kN.

The results of the Simulated Dynamic Force Transfer Test are given in Table 5. below.

Type of Loading (kN)	Maximum Acceptable Displacement (mm)	Measured Displacement (mm)
0 to +1709	7,6	5,8
constant +1709	7,6	6,1
+1709 to –1691	–14,2	–9,9
constant –1691	–7,6	–6,1

Table 5. - Displacement response of device ST-1 in Simulated Dynamic Force Transfer Test

5.2 Friction Test

The objective of the test was to provide a correction factor for the effect of velocity on the coefficient of friction in the Simulated Dynamic Load Test of sliding isolators.
The rig used to test the dimpled, lubricated PTFE discs (see Fig. 10) included one horizontal actuator (4) to impose the specified displacements and a hydraulic jack (13) to impose the required axial force on the disc.

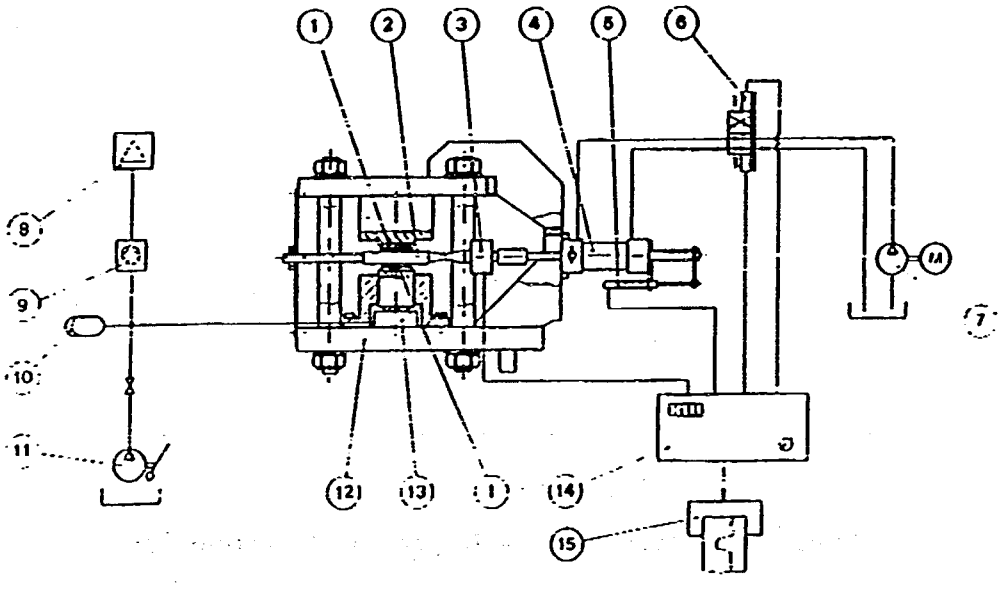


Figure 10. - Schematic view of the Test Set-up for PTFE samples.

Test Conditions:

—	Disc diameter	75 mm
—	Contact pressure	15,9 Mpa
—	Pre-load time	1 hour
—	Sliding distance	± 38 mm
—	Reference thermal speed	100 mm/min
—	Conventional seismic speed	12,5 mm/sec
—	Number of cycles (each test)	10

The results are listed in Table 6 below.

Specimen Set	μ_{static}	$\mu_{dynamic}$
1	0,003	0,010
2	0,003	0,009
μ_{mean}	0,003	~ 0,009

Table 6. - PTFE Static and Dynamic Coefficients of Friction

The ratio of the mean coefficient of friction listed in Table 6, equal to 3, was used to correct the hysteresis loops for the Simulated Dynamic Load Test of the seismic isolation bearings.

5.3 Seismic Isolators

The system used for testing the Seismic Isolators was composed of the FIP reaction block (rated at 9,000 ton.) with horizontal and vertical servo-controlled actuators, a hydraulic power supply, and a closed loop electronic control system.
On the next page, a schematic view of the testing arrangement is presented in Figure 11 and a photograph of the same is illustrated in Figure 12.

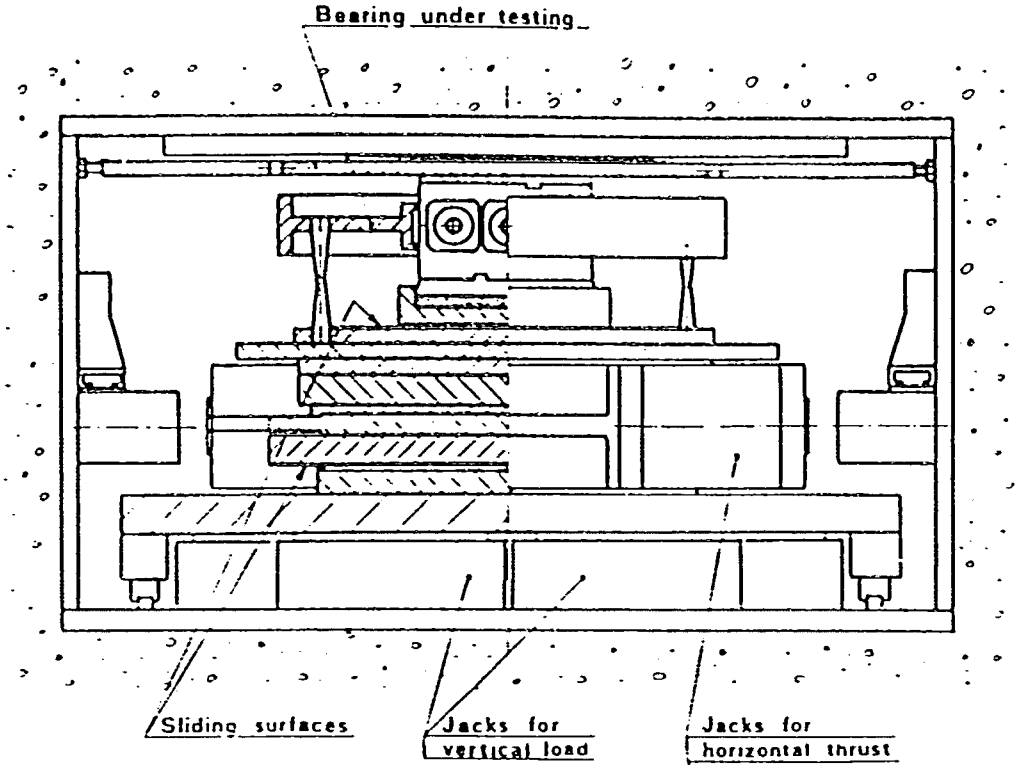


Figure 11. - Schematic view of Test Set-up for Seismic Isolators

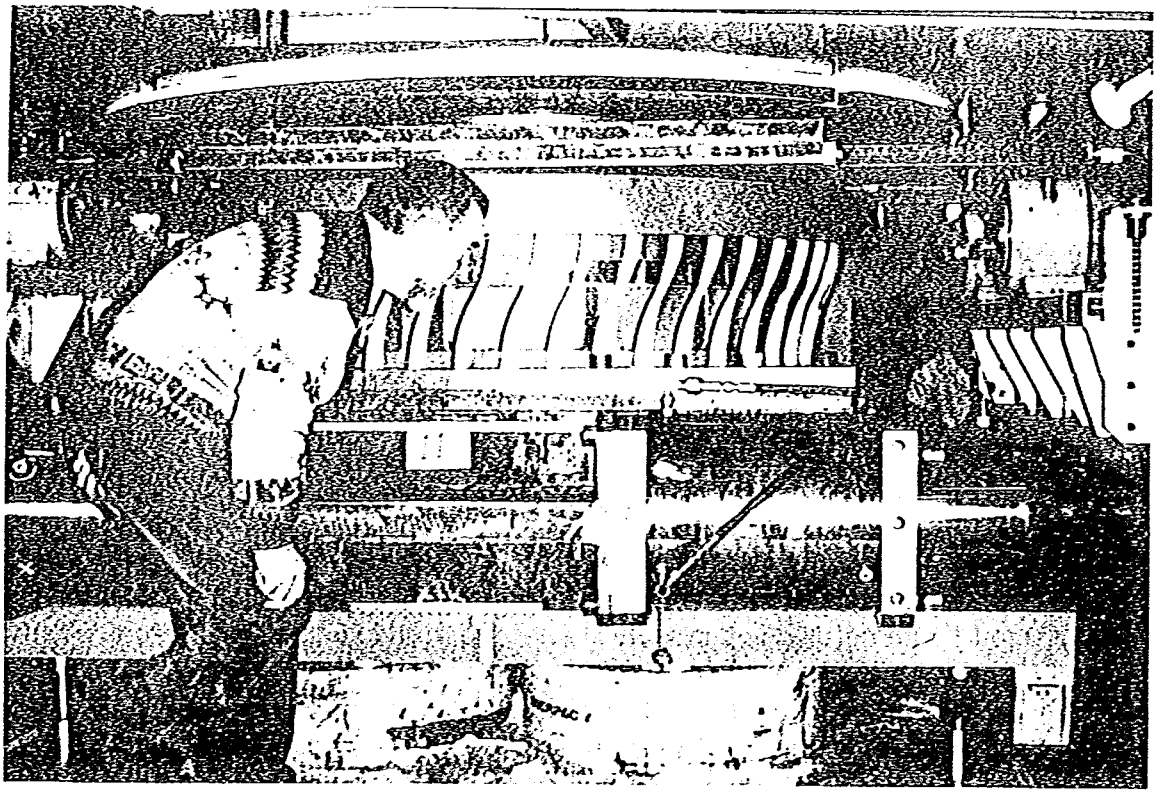


Figure 12. - Isolator VEP 5200 in Test Rig.

5.3.1 Vertical Static Load Test

The objective of the Vertical Static Load Test was to verify the load capacity of the seismic isolators in the presence of the maximum rotation.

Acceptance Criterion: The tested device shall show no indication of failure or other defects such as weld cracking, plate distorsions, extrusion of the elastomer or bearing material, or displacement of the elastomer seal while under load or subsequently upon disassembly and inspection.

Testing Procedure: A load equal to 150 percent of the design capacity of the tested device shall be applied for a period of one hour. The device shall be in rotated position during the test. Rotation shall be 0,015 radians or the design rotation, whichever is greater.

Test Results: This test involved the use of a tapered plate under the loading platen to achieve the required rotation of 0,015 radians.

The axial loads of the bearings are listed in Table 7 below.

Bearing Type	Specified Load (kN)	Test Load (kN)
VEP 1400/280-ST	9 345	9 438
VEP 5200	34 710	34 759

Table 7. - Loads of Vertical Load Test

No evidence of weld cracking, plate distorsion, extrusion of the elastomer and/or the bearing material or displacement of the elastomer seal was observed at any stage during or after the test.
It is worthy to note that the VET 5200, with its 23 140 kN load capacity, claims to be the largest type of high damping isolator installed to date.

5.3.2 Lateral Static Load Test

The primary objective of the lateral static load test was to evaluate the behaviour of the seismic isolators prior to the failure of the service load restrainers.

Testing Procedure: The devices shall be vertically loaded at the design dead load during lateral static testing. The devices shall be loaded laterally for 10 complete cycles of loading from 0 to F_1 to 0 to $-F_1$ to 0. The value of F_1 for each device shall be the lowest value from Table 8. The cycles of loading shall be at a uniform rate.
A continuous plot of the lateral load and deflection shall be recorded.

The deflection shall be measured on the first portion of the fifth cycle and be within the range specified in Table 5 (parameter S_1).
After the cycle load testing, the devices shall be loaded laterally to load restrainer failure while maintaining the vertical dead load.
Failure is defined to be the total fracture of the service load restrainers.
The lateral load at failure shall be within the range specified for parameter F_1.

Results: Table 8 below lists the results of the tests.

Type of Bearing	S_1 (mm)	Maximum Displacement (mm.)	F_1 (FN)	Lateral Load at Failure (kN)
VEP 1400/280-ST	0 - 5	2,0	757 - 1 024	877
VEP 5200	0 - 5	1,0	1 513 - 2 047	1 940

Table 8. - Target Parameters and Results of the Lateral Static Load Test.

5.3.3 Simulated Dynamic Load Test

The objective of the test was to evaluate the hysteretic performance of the devices.

Testing Procedure: The devices shall be vertically loaded at the design dead load during simulated dynamic testing. The devices shall be loaded laterally for 15 complete cycles of loading from 0 to 12 mm. to 0 to −12 mm. To 0. The cycles of loading shall be at a uniform rate. The value of the peak force shall be measured on the first portion of the fifth cycle.
The energy dissipated in one hysteretic loop shall be computed for the fifth cycle.

A continuous plot of the lateral load and deflection shall be recorded to permit an evaluation of the elasto-plastic and hysteretic performance of the device.

Acceptance Criteria: Peak force and hysteretic energy dissipation at the fifth cycle shall be within the respective ranges of the parameters F_2 and EDC (see Table 6 below).

Results: The results of the tests are listed in Table 9 on the next page.

Type of Isolator	F_2 (kN)	Measured Peak Force (kN)		EDC (kJ)	Hysteretic Energy (kJ)	
		5th cycle	15th cycle		5th cycle	15th cycle
VEP 1400/280-ST	1 179-1 602	1 600	1 424	700	551	493
VEP 5200	2 359-3 181	2 937	2 581		918	791

Table 6. - Target Parameters and Results of Simulated Dynamic Load Test.

The hysteretic loops of VEP 1400/280-ST and VEP 5200 devices are shown in Figures 13 and 14 respectively.

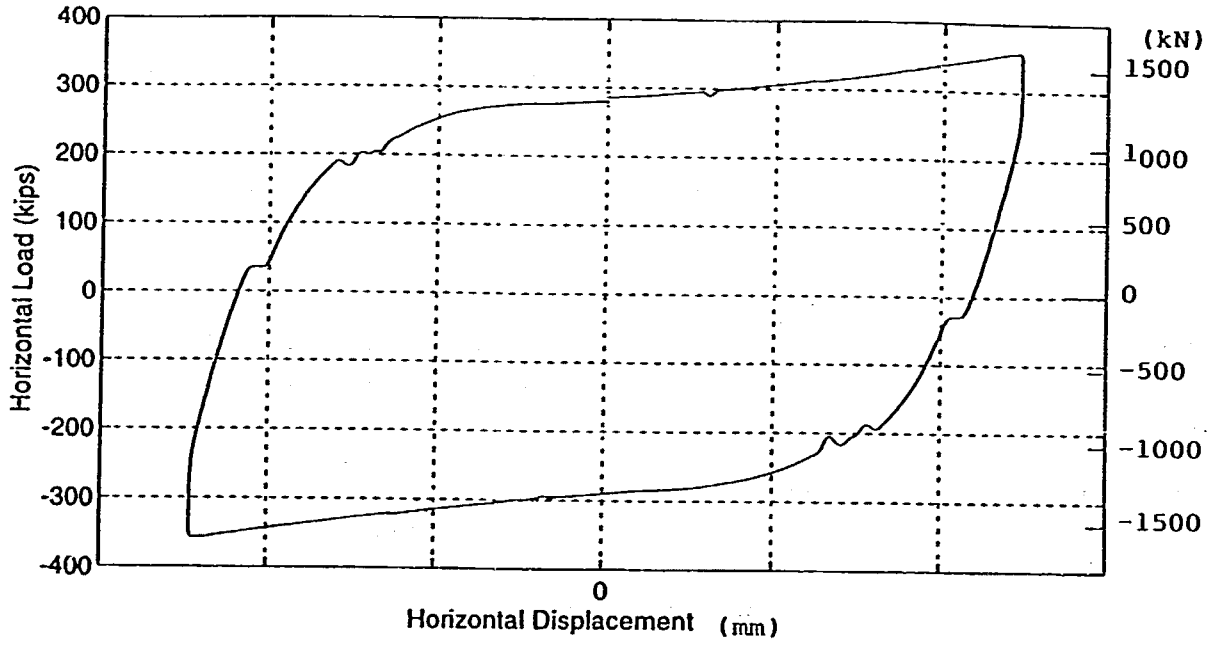


Fig. 13 - Hysteretic Loop of VEP 1400/280-ST at 5th Cycle.

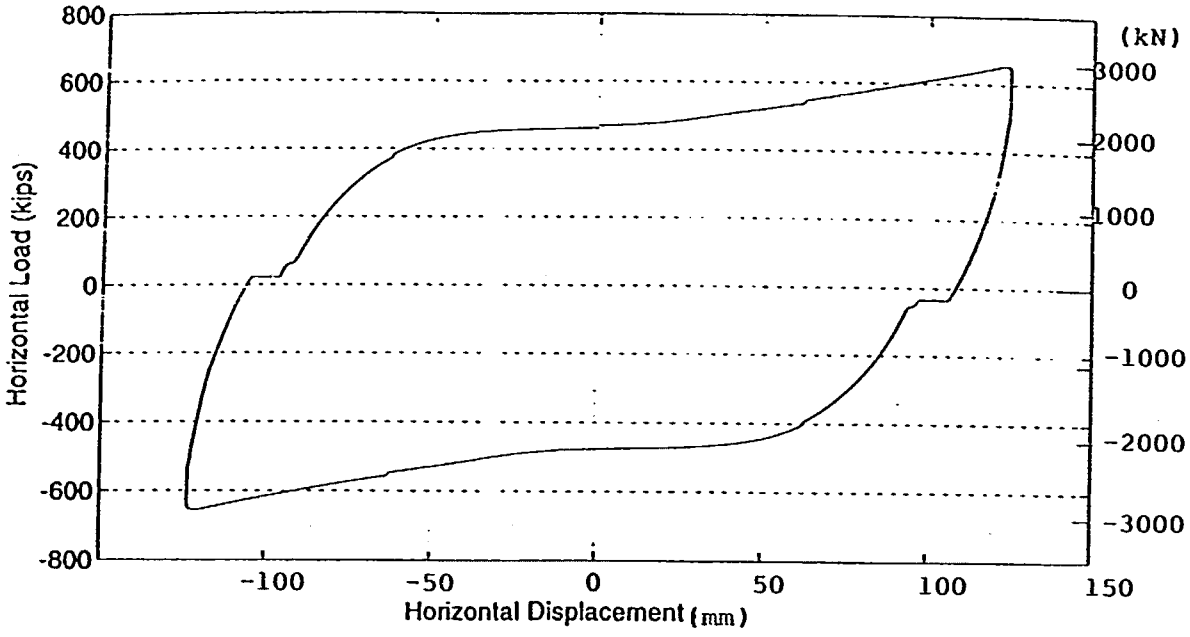


Fig. 14 - Hysteretic Loop of VEP 5200 at 5th Cycle.

6. CONCLUSIONS

The Marquam Bridge Retrofit Project represents the first case of application in the United States of high damping capacity sliding isolators in combination with shock absorbers.

Notwithstanding, this application has not consisted in the simple acceptance of an existing product, but rather, its adaptation to the American reality and its particular set of applicable rules and is thus the end result of a long cooperative effort of almost three years between US and Italian design engineers. As an example, the rigorous testing procedures as well as the protective coating of exposed surfaces carry an American brand. The pot bearings were designed according to AASHTO norms just as the anchorage system and other important details.

This marriage, fruit of cooperation between the Old and the New World has led to the birth of a new hybrid which, as it often happens in Botany, incorporates the best traits from both progenitors.

Other applications have already followed this first effort because American seismic engineers have immediately grasped the importance of the design instrument placed in their hands: the high dissipation of energy that ensures a high degree of protection to structures against natural phenomena such as earthquakes and even windstorms.

In conclusion, all the goals have been achieved with a minimum of effort; that is to say, with contained cost and, above all, without having to resort to the strengthening of the substructure.

The Marquam Bridge has regained a new youth. In the comfort of the positive experience matured in Italy, the good results of rigorous analysis and severe laboratory tests, one can reasonably count on this structure's capability to fully carry out its mission for still many decades despite even the probability of a Maximum Expected Design Earthquake.

SEISMIC DESIGN OF FADALTO BRIDGE

G. Furlanetto **M. Bruni**

Design department
Italstrade S.p.A.

ABSTRACT

Seismic design of Fadalto bridge was carried out by means of linear elastic analyses. Some finite element models of the structures where studied using the response spectra method.
The results of these analyses were confirmed by a non-linear study of the highest pier of the bridge. Such study showed safety factors larger than the ones deduced by response spectra analysis.

1 INTRODUCTION

The newly opened Fadalto bridge is possibly the most important structure of the Vittorio Veneto - Pian di Vedoia highway section, extension of the A27 Mestre - Vittorio Veneto highway.
The road cross section is made by two separated deck. Both carriageways, two lanes and hard shoulder each, are 11.75 m width.
The bridge total length is about 3600 m. The bridge alignment could be considered as divided into two parts.
Driving northwards from Vittorio Veneto towards Pian di Vedoia, the first part, about 2300 m long, runs, almost entirely straight, parallel to the mount Millifret slopes and to lake Morto shore. The two carriageways run side by side along this section. The deck structures of both carriageways are made up of pre-stressed concrete slabs, varying in thickness, on 55 m long spans. The two decks have separate piers, they share common foundations.
At the end of this section, placed about pier 42, the two carriageways deviate. The west one crosses the valley, passing over the Vittorio Veneto - Pieve di Cadore railway and the national road 51, while the east one goes on along the same side of the valley, crossing the detrital blocks of Fadalto saddle.
The final section of the west carriageway consists of a different structure, made by pre-stressed concrete box girder decks, varying in depth, spanning 115 m; while the final section of the east carriageway differs from the initial one only in the foundations.

1.2 District seismicity

Several earthquakes, some destructive, that occurred in the historic age, demonstrate the area seismicity. The most important one was the Alpago - Cansiglio earthquake, on June 29th 1873, whose epicentre was in the vicinity of lake S. Croce.
Italian seismic regulations provide a classification, where the area of the bridge is considered as seismical zone of II category.

2 SLAB DECK

2.1 General issues and design principles

This deck structure has been used to realize all the east way and two thirds of the west one, altogether forming eighty per cent of the bridge total length.
Requirements of the client, Autostrade, were in order to obtain a durable and easy to maintain structure and to shorten construction times. These requirements, together with constraints related to site geology and topography, made up the design basis.
The main conditions to be met where then identified.
The number of expansion joints and bearing devices had to be minimised, in order to reduce maintenance cost and traffic trouble consequent to their inspection and replacement. For the same reasons structural elements had to be thick enough to guarantee durability.
The construction system had to be fast enough to comply with time scheduled by the contract. It had to be completely independent of the terrain so as to go ahead without problems in the stretch running along the slopes, where the topography is quite rugged.
The superstructure had to be flexible enough to absorb without harm the foreseen differential settlement, due to the nature of the foundation soil, made up of heterogeneous fill material from the Fadalto paleoslide.

2.2 Structural behaviour

The superstructure is a full, variable-section slab of longitudinally pre-stressed concrete. The span is 55 m length. The piers comprise two r.c. walls, that are set at right angles to the viaduct and go down independently for the first 15.5 m from the deck soffit. Then they are connected together by two more walls so as to form a box section. The deck is rigidly connected to the walls.
Expansion joints absorb the displacements caused by temperature changes, shrinkage and concrete creep, they are installed every four spans at a section set 16 m from the pier axis, where the structural continuity is interrupted.
The structural scheme thus obtained is a series of frame structures, each made up of four spans monolithic with their piers. At the expansion joint a seat permits the transmission of only vertical loads through four pot-type sliding bearing devices.
The geometric proportions of the septa make the upper segment of the piers flexible enough to take horizontal displacements. The piers are thus able to absorb with limited increases in their stresses the longitudinal shifts arising from variations in deck length owing to temperature changes, shrinkage and creep. They furnish a considerable reaction to the bending forces arising from vertical loads, they acting as a "strut and tie scheme", set at 4.8 m spacing.

Moreover, the septa, because of their flexibility, act as isolating elements, and allow a reduction of the forces acting at the pier base because of the longitudinal component of a possible earthquake.
The overall behaviour of deck and piers enables the structure to stand up under seismic events, ensuring proper safety factors, without resorting to special devices to absorb and dissipate energy.
The framewise structural behaviour, owing to the fixed deck-pier joint and to the stiffness ratio between supports and middle span sections, made it possible to reach a clear span more than 50 m length. This is a considerable value in relation to the kind of structure and to the construction system used. The structure can stand differential settlements between the foundations with little stress increments because of the relative slenderness of the structure at middle span.

2.3 Construction method

The deck was poured in situ, using a self-supporting full span form carrier, where the running gears of the form carrier were placed below the bridge deck. Because of the terrain inaccessibility, the independence from it was an advantage for the self-supporting form carrier.
The whole reinforcement cage and the prestressing sheaths were assembled off site and brought in the form by a motor-driven carriage. The same carriage includes two ribbon conveyers that allowed the pouring of a full span within 6-7 hours. The production rate was one span every 4-5 days.

3 BOX GIRDER DECK

3.1 General issues and design principles

This deck structure has been used to realize the final stretch of the west carriageway, about 1300 m length, where the roadway reaches a considerable height from the valley floor. The height of the piers, almost 100 m, led to the choice of this structure, to maintain a harmonious proportion with the span length.
The requirements of the client in order to obtain a durable and easy to maintain structure made up the design basis of this bridge too

3.2 Structural behaviour

The superstructure consists of a prestressed concrete single-cell box girder. The depth of the girder varies from 2.5 m at middle span to 6 m at supports. The deck is longitudinally and transversally prestressed. The transversal prestressing is provided by vertical single bar tendons in the webs and horizontal strands in the top flange. The span is 115 m length. The piers have the same typology of the slab deck's one, but with increased dimensions in proportion to the larger forces they have to stand.
The deck is connected to the piers monolithically, and the structural behaviour of the piers is the same already explained in the paragraph dealing with the slab deck structure. Again, the upper part of the piers act as isolating element on case of seismic events.
Only four expansion joints, whose two at the abutments, are provided in the whole structure.

The joints are well spaced for the elasticity of the piers, due to their height and to the flexibility of the upper part, made by two parallel septa.
Two expansion joints are placed at middle span. Here the two cantilevers are shear connected by a steel beam placed inside the box girder.

3.3 Construction method

The erection of the superstructure was done using segmental balanced cantilever construction. The form carriers were placed below the bridge deck, to allow the bottom flange and wedges reinforcement cage to be assembled at the site and then placed into position.
The production rate was 10 m per week for each couple of carriages.
The cambering for the compensation of the construction deflections and the long-term plastic deformations was studied with care to obtain, on the basis of the project schedule, the right alignment of the cantilever ends before casting the closing end, and the right profile after long time.

4 FOUNDATIONS

We have already seen how it is possible to ideally divide the bridge in two stretches, and how in the first stretch the foundations are shared by the piers of the two carriageways.
In this stretch two different foundation typologies were realised, on the basis of the terrain topography. In the first part, where the slope of the ground is slight, the foundations are built on consolidated soil. The density of the jet injected columns grows with the terrain slope till it realize a real caisson made by consolidated soil.
Further on, where the foundations are placed on the steep slope of the Mount Millifret, the couple of piers is based on twin concrete caissons.
In the final stretch of the bridge, where the two carriageways deviate, the foundation of all the piers are circle concrete caissons, whose dimensions vary depending on the kind of superstructure supported.

5 SEISMIC ANALYSIS

5.1 Analysis methods

The seismic analysis of the bridge was carried out by the Italstrade design department, that developed the structural design of the bridge according to the Italian regulations ("NORME TECNICHE PER LE COSTRUZIONI IN ZONE SISMICHE", D.M. 24/01/1986).
The seismic stresses were evaluated by means of linear elastic analyses. According to the instruction quoted by the B.6 paragraph of the mentioned regulations, response spectra analyses were carried out for both structural type.
Further non-linear dynamic analysis was carried out at Padua University, with a research work led by professor Briseghella. The behaviour of the final stretch of the west way was studied, subject to the effect of the N-S component of El Centro Earthquake, this was appropriately scaled to be associated to the seismic intensity, in term of acceleration, provided for by the Italian regulations.

5.2 Modal analysis

This analysis was carried out using the SAP V finite element program.
Two models of the slab deck structure were realised, the first one representing the initial stretch, equal for both carriageways, the second one representing the final part of the east carriageway. Both models included a set of three frames, partially independent because of the expansion joints.
Another model was studied, representing the entire box girder deck structure, incorporating eleven piers and twelve spans. This model included 147 beam elements.
At least the first 20 normal modes were determined, to be sure of contemplating the first six modes for each of the three partially independent parts of structure included in the model.
The first normal period of each frame was always longer than 1.6 seconds, as a consequence of the piers elasticity. The structure has a favourable behaviour against the seismic actions contemplated in the Italian regulations.

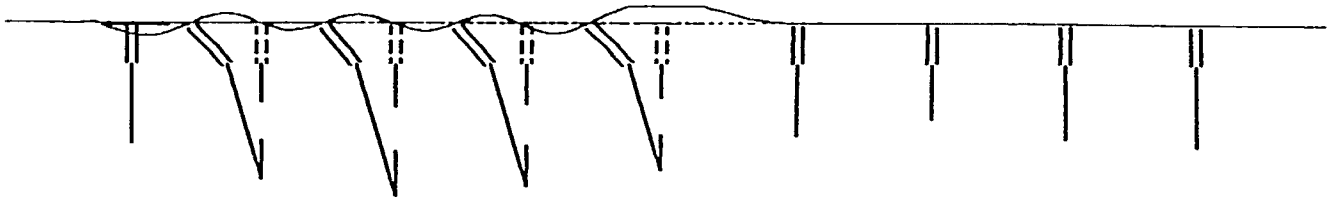


Fig. 1 *First longitudinal mode of the slab deck structure*

The displacements obtained by means of the dynamic analysis where multiplied by four, according to the instruction quoted by the B.9 paragraph of the regulations, to evaluate the joint movements. Further on the displacements of the two frame ends facing at the joint were added to consider the possibility that the structure movements were in opposite directions.

5.3 Non-linear analysis

The non-linear analysis was carried out using a simple model for the geometry, but much more complex for the constitutive laws of materials.
Two bi-linear constitutive model were associated to the elements modelling the highest pier. This elements represent respectively the lower part of the pier, having a box section, and the upper one, made by a double full rectangular section. The time-history analysis of the model was found by directly integrating the equation of motion, using the Central Difference Method.
The adopted structural model included the possibility of creating a plastic hinge at the pier base with linear constitutive law over the plasticity bending moment. In the same way a bilinear constitutive law, with the possibility of introducing damping, was defined for the element connecting the deck with the pier.
The analysis made showed that the whole structure remain in the elastic range with values of the a/g ratio corresponding to a 3rd category earthquake according to Italian regulations.

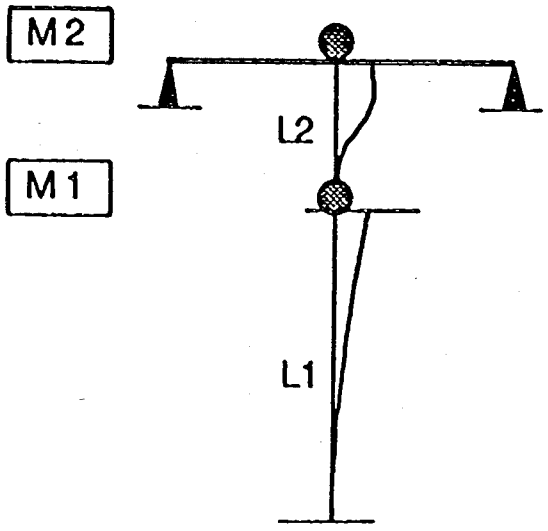


Fig. 2. *Model used for non-linear analysis*

For higher values of the acceleration the ductility required to the septa became more than one, while to the pier base grew slowly, remaining anyway less than one. For acceleration values corresponding to a 2nd category earthquake the ductility required to the septa was about 75% of the available one, while the pier base continued to stay in the elastic range. The resulting consideration is that the two septa act as isolating-dissipating devices, dissipating by histeresys the energy input.

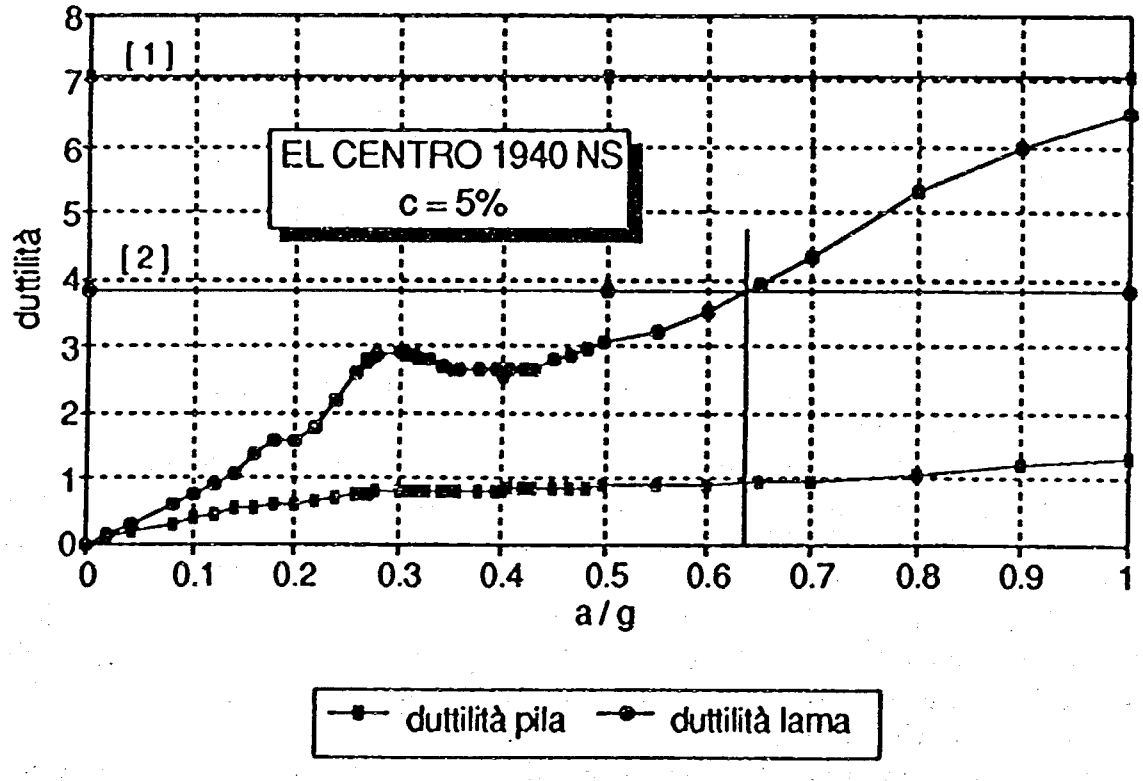


Fig. 3. *Ductility required to the structure*

Further increases of the seismic intensity did not involve a change of the structural behaviour. It seems that the structure is insensible to the increase of maximum soil acceleration, still remaining far away to collapse.

6 CONCLUSIONS

The scheme adopted for both the structural typologies of the Fadalto bridge allowed, as by means of the elasticity of the upper part of the piers, as for the frame behaviour of the whole structure, to obtain structures with the first natural modes long enough to have a favourable response to the seismic actions.
The non-linear analysis showed how the structure goes out of the elastic range if a violent earthquake occurs. This analysis, even tough its effectiveness is limited by the use of one accelerogram only, demonstrated that the structure have reserve factors larger than the ones deduced by the response spectra analysis.

PROGRAMMED MAINTENANCE OF MOTORWAY BRIDGES
ITALIAN EXPERIENCE IN THE USE OF "EXPERT SYSTEMS"

G. CAMOMILLA* - A. DRAGOTTI** - G. NEBBIA*** - M. ROMAGNOLO**
* Central Director, Autostrade S.p.A., Via A. Bergamini 50, Rome, Italy
** Autostrade S.p.A., Via A. Bergamini, 50 - Rome 00159 Italy
*** SPEA - Ingegneria Europea, Via Cornaggia 10, Milano 20123 Italy

ABSTRACT

The maintenance management program is designed to provide the motorway network manager the tools needed to program maintenance of an entire aggregate of structures of widely varying structural, environmental and "generational" characteristics. Using specially designed management software one can then develop overall assessments of structure reliability and thus obtain a classification on the basis of their state of conservation. The reliability assessment automatically expressed by the computer (the "expert" system) is of a global nature, i.e. aimed at creating an objective list of intervention priorities for the entire population of the structures under management.

INTRODUCTION

The Autostrade Company of the IRI-ITALSTAT Group, responsible for managing some 3,000 km of motorway containing around 3,000 bridges and viaducts exceeding 10 m in length, utilizes a series of control and maintenance systems coordinated within the framework of the partially automated SAMOA program (Surveillance, Auscultation, Maintenance of Structures). Under this program, which requires classification and recording of motorway structures according to their different structural components, one can obtain either a detailed analysis of their construction characteristics or an accurate survey of the defects present, selected according to ease of identification or their importance in assessing the state of health of the structure. To avoid subjective interpretations by different inspectors, data forms are compiled according to codified methods spelled out in special operator manuals, and then input into a system of compatible computers located throughout the territory covered by the Autostrade network.
The maintenance works are always of a preventive nature, ranging from ordinary "conservative" maintenance to more elaborate repair interventions. In some cases may be preferable to effect of complete restoration or a functional improvement, to upgrade the existing structure to cope with increased load conditions or to implement antiseismic protection utilizing

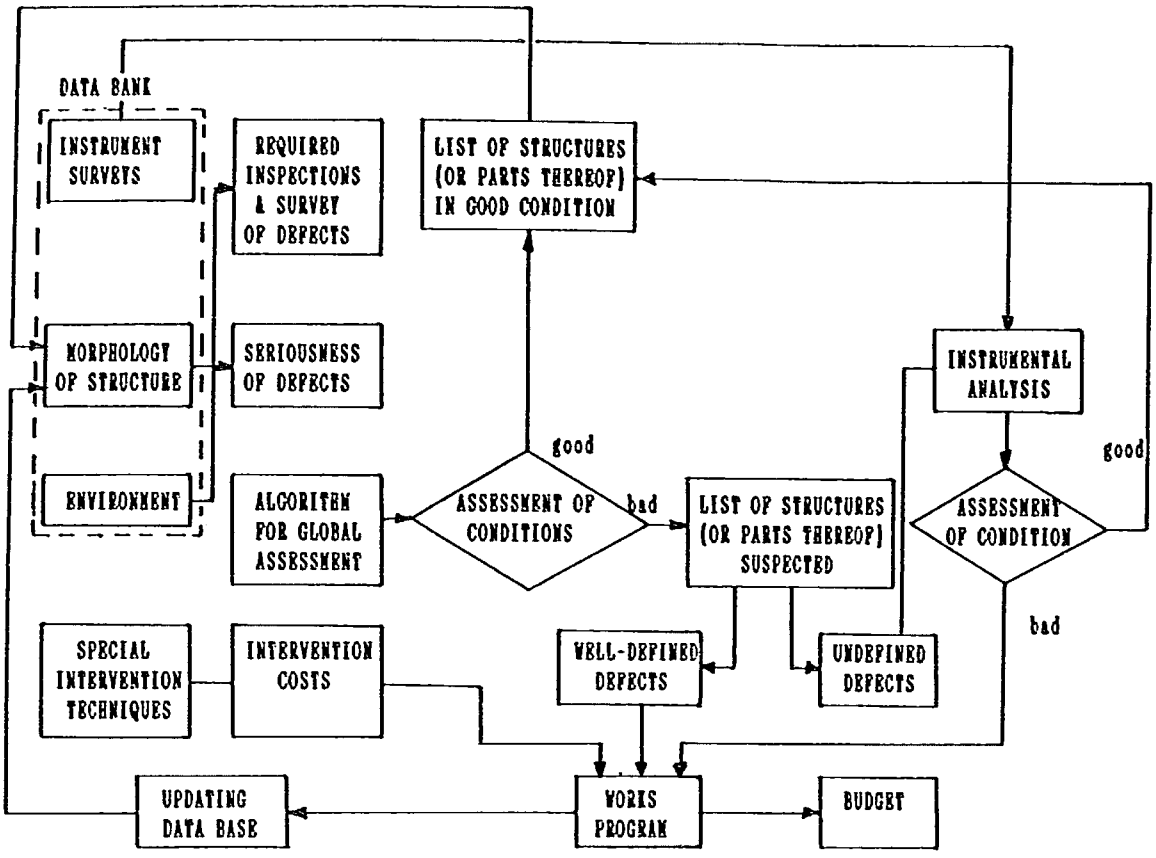
dissipative systems of more recent development. At this point one can also assess the advisability of modifying the original static configuration, with the advantage of extending the presumable working life of the structure.

AUTOMATED MANAGEMENT PROGRAM

The Autostrade Company has organized its maintenance of motorway bridges and viaducts within the framework of the so-called SAMOA project, which is aimed at developing the tools to achieve completely programmed operations.
The high average age of the structures and their growing numbers have reached such a point that surveillance based solely on visual inspection of the state of the structures and diagnosis based on individual inspector experience has become increasingly unreliable. It thus became necessary to devise specific criteria to ensure more uniform and sound assessment of the state of "health" of certain structures, but also to predict the probable evolution of this state over time.
Starting from this global assessment or diagnosis of the entire "population" of structures under surveillance, it is possible to extract three distinct sub-groups of structures (or structure components):
- certainly reliable;
- certainly requiring maintenance;
- not perfectly defined in terms of reliability.

The two sub-groups in precarious or suspect condition, presumably comprising a very limited number of items with respect to the total "population" are then subjected to more detailed inspection (and thence diagnosis) using instruments and tests more sophisticated than simple visual inspection.
The specific aims of the SAMOA program are as follows:
a) creation of a data base and related software for the management of the morphological data on the structures and the maintenance interventions performed on them;
b) research and development of rapid, non-destructive control systems for automatic acquisition of such data;
c) development of structural verification programs to assess the level of safety and need for intervention.

Implementation of this project permits, starting from the comparative analysis of the various data contained in the data base, the rational definition of intervention needs and priorities. The flow chart of this procedure (which constitutes the entire SAMOA project) is shown in the diagram on the following page.
The first part of management activity consisted in recording the registration data on all the structures on the network. Drawing on design and cost data from existing files, combined with information obtained on possible site visits, the next step was to compile special "morphological records" for each of the structural elements comprising the structure. Various type groupings were defined such as, for example, piers, foundations and all other elements making up the structures, indicating the dimensions and compositions occurring in the individual structure in question.
Each structure was thus subdivided into its constitutive elements and these latter reported, case by case, on the number of records required. General summary records refer to these latter and combine them with other information either pre-existing or acquired subsequently such as, for example, general data on the environment where the structure is situated, the con-



struction methods employed, static tests conducted, subsequent maintenance and repair interventions.
These data, subsequently memorized on computer, constitute the historical data base of the structures. Employing software able to select/sort on the basis of the historical data, the structures can then be classified on the basis of element types in such way as to visualize the appearance in the manner in which the human operator is more accustomed to viewing it.
As far as inspections are concerned, the surveillance is performed essentially by means of close visual examination or binoculars of the individual structural parts, to spot and take note of any defects which may be present, with particular care to observe the development of those already noted previously. Visual checks, despite their limitations with respect to the difficult but not always impossible task of identifying hidden defects or accessing parts concealed from view (e.g. parts below ground level, inaccessible heads of prestressed concrete beams, etc.), remains the fundamental method of surveillance able to provide at least general indications of the overall state of conservation of the structures.
In the case of those structures for which further detailed examination is considered advisable, however, recourse is had to more sophisticated methods based essentially on local and/or global non-destructive type tests. Considerable advances are occurring and are under study in this sector, but there already exist a number of different well known and widely utilized techniques which will be described in a following section.
In order to guarantee the greatest possible uniformity in classifying the different types of defects and the most important parameters for their description and control, use is made of "defect charts" on which such characteristics are defined in univocal fashion.

In fact, the inspections are conducted in accordance with a special manual on damage survey methods containing not just the record forms for recording the defects, but also detailed explanations of these defects (including descriptions and photos), as well as instructions on how to fill out the forms reporting the locations and extent of the deterioration observed.
By breaking down the structure into its individual structural components it is possible to conduct an accurate survey of all the defects present, using precise and codified methods such as to limit subjective interpretations by the inspectors.
The record forms, as can be seen from the example shown in Fig. 1 of a deck consisting of sliding cable prestressed reinforced concrete beams, are organized in such a way as to divide the structural parts into further specific elements to which the defects observed are referred.
In the case in question, the deck is first divided into its constitutive elements (beams, crossbeams and slab) and each of these is then divided into fields: for each beam, for example, a field consists of a section located between two consecutive crossbeams.
After the forms have been compiled in the field, the data is then entered into the computer, where they are processed according to special interpretative algorithms. The resulting output can take the form of an overall but at the same time objective assessment of condition of the single element, of the single structural component or of the structure as a whole, depending on the information desired.
The processing software contains defect assessments of varying degrees of seriousness in relation to the type of structure involved (supported beam, continuous beam, framework, arch, etc.), the component materials (reinforced concrete or prestressed reinforced concrete, steel, masonry, etc.), as well as the extent and location of the deterioration. This is combined with instrument measurements and/or considerations regarding the evolution of certain physical parameters measured geometrically (e.g. inertia moments) or instumentally (e.g. measuring vibration modes or using other non-destructive methods) on the structures themselves.
The processing criteria are such as to permit a "global assessment" of the state of the structure or of its single component parts, which serves as the basis for establishing criteria for intervention priority. In fact, the global assessment, which is quick to use and yet reasonably accurate, serves to separate the certainly reliable structures from those which require more detailed examination.
These latter must be examined with special attention (measurements, determination of restoration measures to be undertaken), and hence will be subject to more frequent surveillance or, if necessary, constant monitoring.
The reliable structures, on the other hand, will only be subjected to ordinary routine surveillance, save for the repetition every two years of the reliability inspection related to the "global assessment".
Before examining the data processing methods in detail, it would be advisable to look first at the special techniques employed in structure surveillance and the criteria employed in determining restoration interventions, so as to have a better understanding of the procedures followed in coping with the various problems of structure management.

SPECIAL TESTS

In presenting the surveillance methods it was mentioned earlier that, contrary to visual inspection procedures, the specialized control techniques are employed on an ad hoc basis when the need arises to have more

detailed information on a single structure or on those located on a particular section.
Such needs may be dictated by different circumstances:

a) visual inspection and subsequent data processing may leave room for various interpretations as to the actual state of the structure and the seriousness of the situation;
b) planning maintenance or restoration operations may require more specific measurements;
c) special research projects.

Examples of situations a) and b) are quite similar insofar as the problem is to define either the intervention priority or the manner of intervention; in the case of point c), however, the situation is much more varied, and we shall limit ourselves here simply to a few references. In all cases, however, it is advisable to deal with the subject starting from the single tests or, better, from the description of the criteria for the utilization of these in an integrated manner, without lengthy treatment of the single methods.
Proper integration of the various methods used is fundamental for valid interpretation of the data measured: indeed, only in this way is it possible to effect a type of iteration which, taking into account the various approximation factors proper to each of the systems, permits one to obtain a realistic "quantification" of the state of conservation.
In particular for type a) and type b) situations the following tests are normally conducted either on specific parts or sample areas:

- Ultrasonic: for the following purposes:
  . to supply indications of the homogeneity of the concretes by means of transparency and/or indirect tests;
  . to provide indications of the depth of cracks with indirect tests across the cracks or alongside them;
  . to determine, via correlation of the data obtained, the ultrasonic transmission velocities along with the recoil index obtained at the same points using sclerometric tests, concrete compression strength values;
- Sclerometer: this traditional non-destructive test provides information on the compression resistance correlated with the recoil index, but if used by itself it is limited to providing information tied very closely only with the "cortical" layer. For this reason it must always be used in conjunction with ultrasonic tests. Such integration has proven to be optimal in "filtering" the results from the influence of a number of variables (granulometry, moisture, binder dosage, type of aggregate) which in many instances register contrary values with the two methods.
- Pull-out: this is utilized mainly in cases where it is impossible to effect ultrasonic tests by transparency (on "chunky" elements), or where it is deemed useful to obtain compression strength data for comparison with that obtained from other non-destructive tests; these data are always combined with pacometer data regarding the position of the superficial reinforcing, so as to ensure that the piece is inserted in a suitable position such that extraction is not blocked by possible presence of reinforcing rods or mesh;
- Windsor probe test: in using this test the same applies as was said in the case of the pull-out test; the combination of this test with the preceding one is always useful, especially if there is a lack of information regarding the aggregate grain size and characteristics;
- Measurement of carbonation depth: this test is always employed, as it provides an important index of the aggressivity of a particular environment on a given composition of concrete, and thus provides extremely useful information for detailed studies of mix design for

durable concretes; it is superfluous to stress the value of a test which permits the designer to know whether or not one can still hypothesize passivation around the reinforcing.

- Measurement of chloride penetration: this is used generally only on exposed parts: pulvinos, heads of beams, heads of crossbeams. It may be direct (samples taken from the structure) or indirect, based on electrochemical potential measurements conducted on accessible structure surfaces and linked together by isopotential curves (mapping).

Obviously, this list of tests is far from complete, but mention is made here only of those which constitute part of the routine system which, as set out above, automatically comes into play once certain "alarm thresholds", defined in assembling the visual inspection data, are exceeded.
Besides these tests, which can be defined as "local", insofar as they provide punctual results on the state of the structure, we also utilize global type systems which yield information on the characteristics of the structure as a whole, obtained from static loading tests or measurements under dynamic excitation.
Dynamic analysis is the most commonly used test, aimed at determining the vibration modes of the various parts of the bridge under a known source of vibration. The method is not very sensitive to deterioration of the structure itself, and cannot, at the present time, be used to assess the actual state of structures. It can, however, be used to memorize the state of the structure at a certain moment, so as then to draw a comparison with the results of other dynamic tests conducted subsequently in time. Certain recent developments in survey systems and finite element modelling would seem to be promising for the practical use of this method.
Besides their use in maintenance design, these measurements can provide new criteria for assessing "sample defects", which can subsequently be incorporated in the global assessment and applied in expert systems to determine SAMOA intervention priorities.
In this way the bridge management system is continually improved over time: constantly increasing its data base and consequently improving the work of the human operators who continue to manage well the more traditional tasks; thus we have surveillance, auscultation and intervention as integrated moments of a single process, with the substantial but hardly "tyrannical" assistance of the computer.
In concluding this section, mention should be made of the various research objectives we will be aiming at in the use of the above tests and others. On the one hand we will be trying to understand better the limits of the various systems utilized and obtain more detailed information on those not routinely used, and on the other hand we will also attempt to develop hypotheses regarding the process of deterioration with respect to predetermined types of environment and structure.
In the case of the first of these two aspects we are already conducting careful analyses of the data as it is gathered, so as to improve design and programming of interventions, also by increasing the number and distribution of these tests and checking the results by means of destructive tests and controls employed during partial demolitions conducted in the course of repair operations.
So as to gain better understanding of other systems (e.g. potential mapping, release of tensions, etc.), trials are conducted in conjunction with both destructive and non-destructive tests on a case by case basis in specific situations.
Work continues toward the development of "deterioration curves over time" (a sort of measurement of the speed of deterioration under standard conditions - of crucial importance for a company responsible for the maintenance of such a large number of structures) in function of the environ

ment and the structural and technological characteristics. We have begun to conduct on site tests to determine the depth of carbonation on sample elements of selected structures of particular significance. These tests will naturally be repeated at regular intervals (around every two years, as already stated), so as to construct curves of the type indicated, also with a view toward future projections.

INTERVENTIONS ON STRUCTURES

Starting with the list of priorities provided automatically by the computer program, and following whatever specialized testing may be required, we proceed to the design of the intervention in accordance with defined general reference criteria.
Distinctions are made among different possible interventions, which can be grouped as follows:

- ordinary or extraordinary maintenance: these are distinguished according to the type and importance of the intervention to be performed, and are intended to maintain the structure at full efficiency in accordance with it original design characteristics;
- static restoration: when one wishes to restore the original bearing capacity of the structure;
- retrofitting (functional maintenance): when one decides to maintain unchanged the original geometry and static scheme, while at the same time permitting the structure to be subjected to actions either greater or differing from those for which it was initially designed;
- restructuration: this entails the alteration of the original static scheme of the structure and/or its geometric characteristics so as to restore or increase its bearing capacity.

Naturally, the last two items can be adopted also where the state of conservation of the structure is judged to be good.
At this point we shall illustrate several special intervention techniques employed on various parts of a bridge structure.
With regard to protective techniques (to restore the protective function of certain parts of the structure, which may have deteriorated or not have been supplied in the first place), the following may be employed:
For piers:

- plating with metal mesh and reoplastic mortars to restore protective covering of exposed reinforcing;
- light hooping where it is necessary to provide a certain additional strength to columns (the reinforcing is rendered continuous by suitable overlapping beyond the edges);
- localized repairs, followed by application of protective paint to prevent carbonation of the concrete cover layer over the reinforcing.

For slabs:

- surface repairs with stuccos or small castings and/or waterproofing of deck with synthetic membranes or other systems;
- more extensive repairs and waterproofing of specific points (drains, heads of prestressed beams, etc.);
- diffuse anode cathodic protection of outer reinforcing to eliminate chlorine ions present in the existing concrete.

For beams:

- application of protective paints with or without repairs of unfilled sheathes.

In the case of repairs to restore bearing or bonding function which has been lost or not suitably provided initially, on the other hand, operations might include the following:

For piers:
- substitute lining (new castings which by themselves support the total load on the pier) of columns with reinforcing and form casting using non-shrink reoplastic concretes;
- transversal strengthening of piers with additional septa;
- upgrading according to more strict criteria to better resist transversal seismic action.

For slabs:
- reconstruction of the upper layers of the slab, including elimination of degraded material by high-power hydrodemolition, application of new reinforcing and substitution with non-shrink reoplastic concrete;

For beams:
- strengthening with steel plate elements glued and/or bolted to the existing structure (thin plate reinforcing);
- addition of external cables to existing prestressed or non-prestressed structures to restore lost prestressing or provide it anew (positioning of the cables with respect to the beam cross-section, and that of anchor and drawing points will vary depending on the space available).

The preceding provides an overview of possible interventions normally adopted. It must be stressed, however, that in the majority of cases the aim is essentially to obtain a functional improvement of the structure as a whole, as well as of its component parts.
Types of intervention which could be cited as particularly successful examples are integral decks (jointing of decks), the introduction of special unidirectional and multi-directional bearing devices as well as seismic protection devices, and lastly the installation of breakthrough-proof guardrails capable of dissipating impact energy.
The problems faced by the designer of maintenance interventions on existing structures are considerably more complex than is the case with the design of new ones. Some of the additional constraints encountered include the need to operate in the presence of traffic; the need to select materials which yield reliable results within a very short period of time and in the presence of traffic-induced vibrations; the very strict limits on intervention time; the need to assess material strengths in situations where degradation is present; the need to achieve higher performance standards than those adopted in the original design of the structure.
It is easy to see from the above considerations that the concept of maintenance thus assumes the more "noble" connotations of the term "project" (i.e. that of "projecting the mind into the future so as to foresee in advance" what the work will require), thus superceding the rather simplistic notion of those who see no need for a specific design stage in the concept of maintenance.

DATA PROCESSING METHOD

At this point we would like to provide an example of how one goes about setting up an expert system of classification for purposes of controlling the state-of-the-art of the structures under management.
Given the fact that the assessment is conducted separately for each component part of the structure, we shall concentrate our attention on a specific application, in this case that of a deck.
As shown in the attached sample flow chart for decks, starting from the analysis of the morphological characteristics, the processing algorithm performs different specific tasks depending on the type of deck itself.
Selecting as our example the case of a deck consisting of simply supported

beams of prestressed reinforced concrete (form E3) with sliding cables (a structure quite common on the Autostrade network), we now proceed to a detailed description of the procedure.
The steps followed are not always the same, but will depend on the objective one wishes to achieve. The choice among the different analysis viewpoints takes the form of a selection from among the distinct "viewpoints" presented: structural safety, state of conservation, waterproofing, etc.
It is necessary to select the viewpoint (VP) at the very beginning, as in this way the processing operation can be carried out automatically without interruption.
At this selection level it is also possible to choose whether one wishes to have only the final output, or also the intermediate outputs corresponding to the various partial processing stages. The intermediate outputs constitute a partial processing of the codified defects reported on the forms compiled during the site inspections. These partial outputs, e.g. the "Table of Defects by Beam" (or by crossbeam or by slab element) provide, in the case of each element (beam, crossbeam or slab field) a "photograph" of the associated defects and related intensity/extent parameters.
The assemblies of the various elements are more complex, as they will differ for each of the above-mentioned viewpoints, and will provide data strings indicating a level of "seriousness" and function parameters of the intensity/extent of the defects for all of the beams, crossbeams or slab elements taken together.
Another important partial output useful for further assessment of a non-automatic nature is the schematic diagram, which summarizes the defect distribution of an entire span (beams plus crossbeams plus slab).
The final partial output consists of the aggregation of all the spans of a structure. These are subdivided into groups, each of which distinguished by appropriate separation thresholds. These latter serve to filter the parameters defined in processing each of the spans, even where these are not morphologically similar (simple reinforced concrete beams, prestressed reinforced concrete beams, box girders, etc.).
The groups associated with each span are organized according to two different output possibilities:

- aggregation of spans by single structure, with related indication of group;
- aggregation of spans by group, with related indication of the structure to which they belong.

These outputs provide a sufficiently complete indication of the state of the structure, always in accordance with the viewpoint selected. In this case, to obtain a more synthetic unit view, we have opted here for assembly of all the spans of each structure. In fact, the final output is represented by an overall assessment of the conditions of all the decks of a structure, and the ranking of this latter in a condition classification in relation to the condition ratings of various structures of a selected population.
The assembly operation takes into account spans having different structural characteristics, and hence different processing procedures. "Homogenization" of the spans in achieved by attribution of thresholds which are different for each type of record form; the thresholds thus constitute the point of equivalence in comparing spans of different types.
The operation proceeds as follows for the different viewpoints:
"Safety": The group of spans of a structure is classified in a determined order equivalent to the preceding groups. If at least one span is classed as group 1, the whole group of spans is of 1st order, and so on. Furthermore, each order is attributed percentages relating to the spans contained in each group, with respect to the total number of spans in the structure as a whole.

CARD E3: DECK DEFECTS

PRESTRESSED DECKS WITH CONCRETE BEAMS Carr. R ☐ L ☐ B ☐

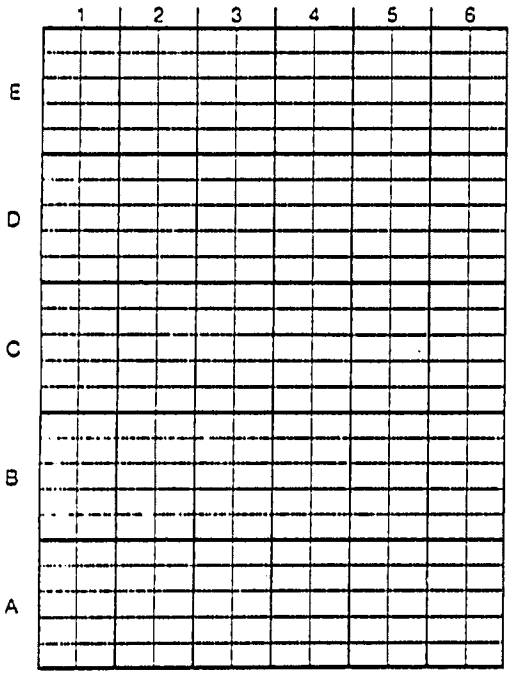
Viaduct code ☐☐☐☐☐☐☐☐☐☐ Date ☐☐ ☐☐ ☐☐

Element ☐☐ Span ☐☐ Page ☐

Beams number ☐☐

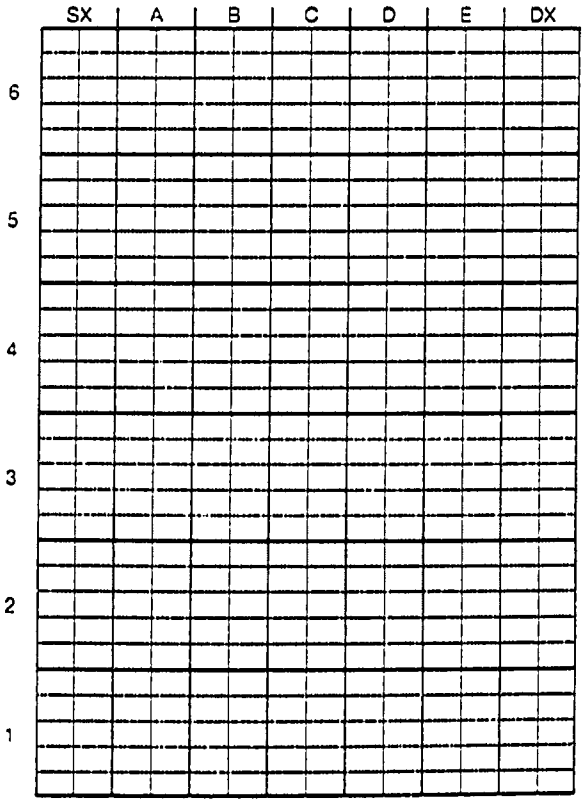
Cross beams number ☐☐

BEAMS



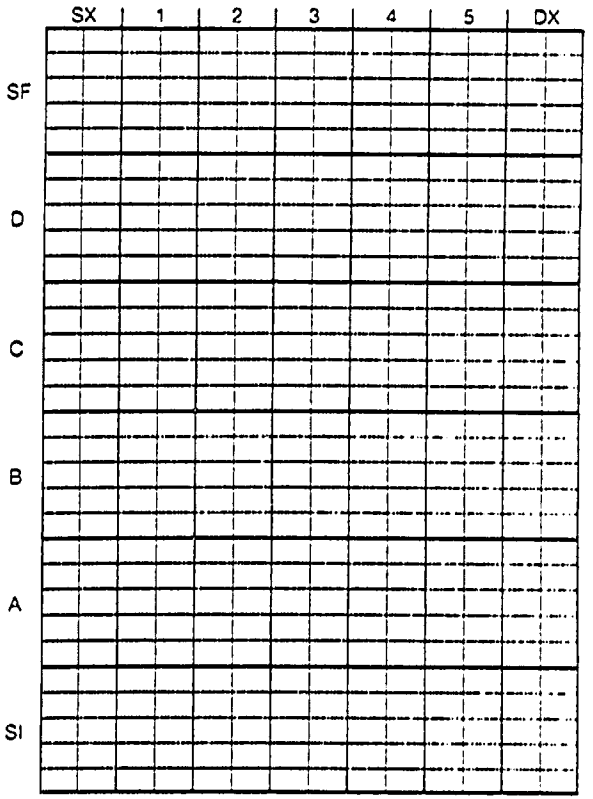
BEAMS DEFECT CODES

CROSS BEAMS



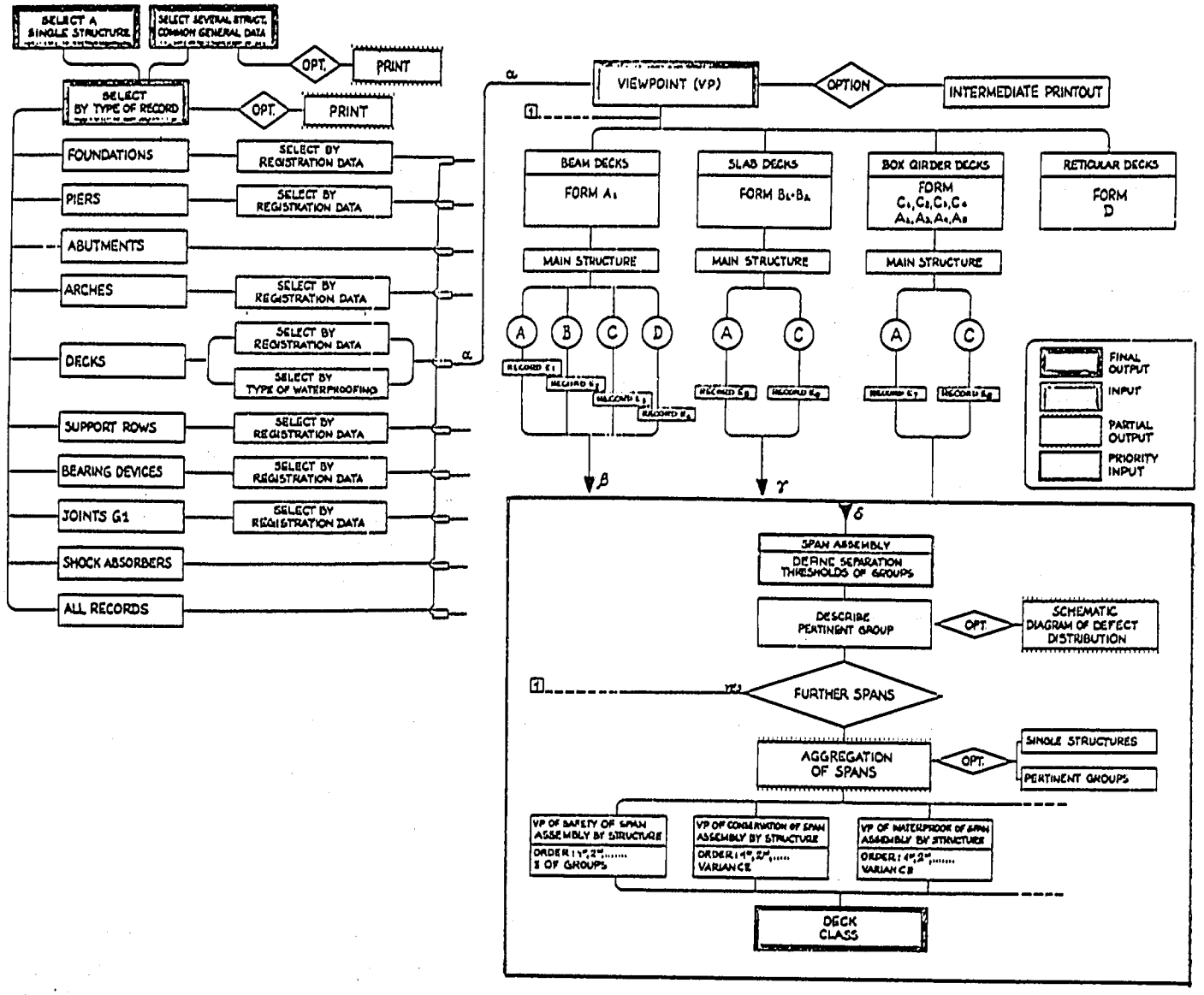
CROSS BEAMS DEFECT CODES

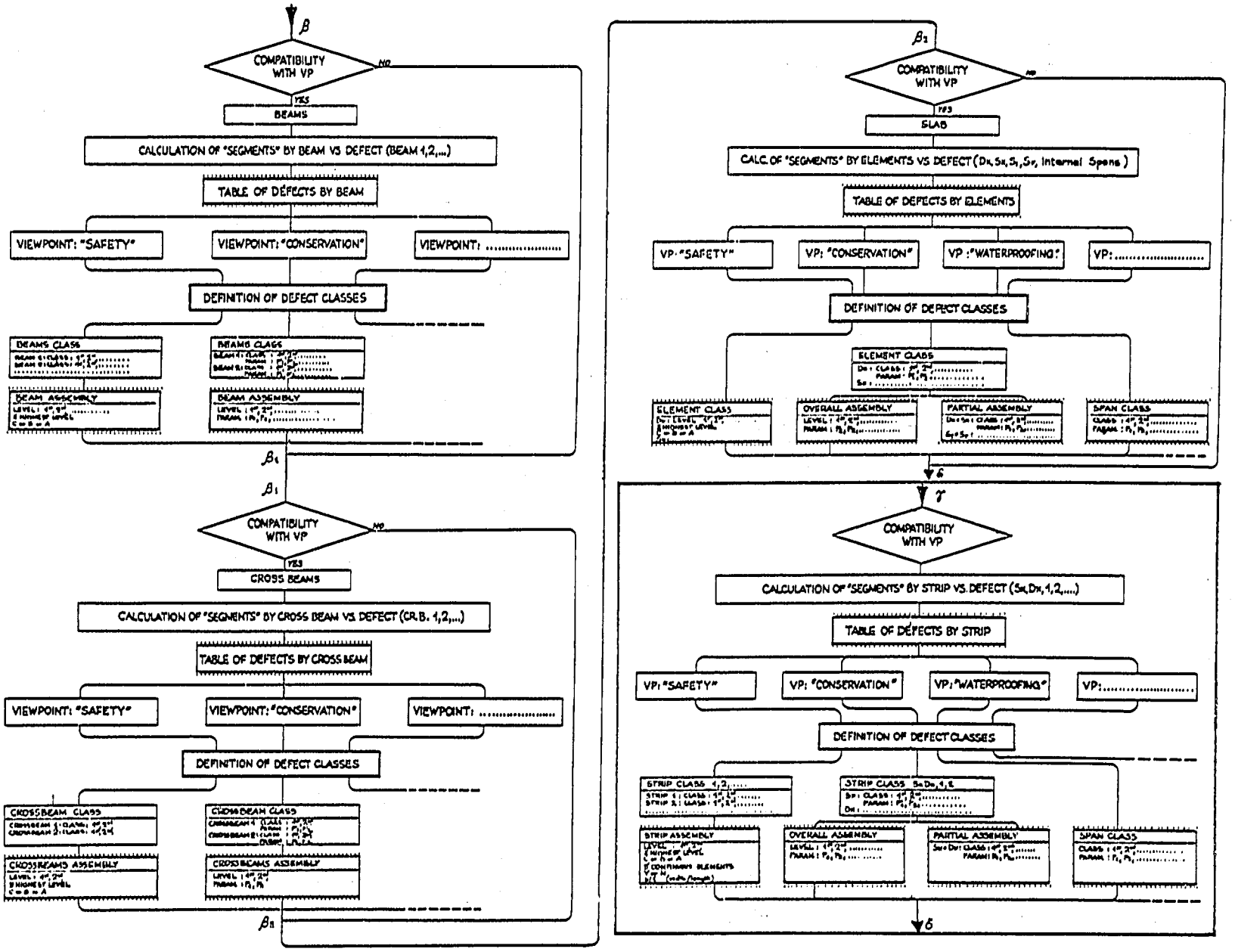
SLABS



SLAB DEFECT CODES

PICTURE 1


SELECT A SINGLE STRUCTURE
SELECT SEVERAL STRUCT. COMMON GENERAL DATA
OPT.
PRINT
SELECT BY TYPE OF RECORD
OPT.
PRINT
FOUNDATIONS
SELECT BY REGISTRATION DATA
PIERS
SELECT BY REGISTRATION DATA
ABUTMENTS
ARCHES
SELECT BY REGISTRATION DATA
DECKS
SELECT BY REGISTRATION DATA
SELECT BY TYPE OF WATERPROOFING
SUPPORT ROWS
SELECT BY REGISTRATION DATA
BEARING DEVICES
SELECT BY REGISTRATION DATA
JOINTS G1
SELECT BY REGISTRATION DATA
SHOCK ABSORBERS
ALL RECORDS
α
VIEWPOINT (VP)
OPTION
INTERMEDIATE PRINTOUT
BEAM DECKS
FORM A1
SLAB DECKS
FORM B1÷B4
BOX GIRDER DECKS
FORM C1,C2,C3,C4 A1,A2,A4,A5
RETICULAR DECKS
FORM D
MAIN STRUCTURE
MAIN STRUCTURE
MAIN STRUCTURE
A
B
C
D
A
C
A
C
RECORD E1
RECORD E2
RECORD E3
RECORD E4
RECORD E5
RECORD E6
RECORD E7
RECORD E8
FINAL OUTPUT
INPUT
PARTIAL OUTPUT
PRIORITY INPUT
β
γ
δ
SPAN ASSEMBLY
DEFINE SEPARATION THRESHOLDS OF GROUPS
DESCRIBE PERTINENT GROUP
OPT.
SCHEMATIC DIAGRAM OF DEFECT DISTRIBUTION
YES
FURTHER SPANS
AGGREGATION OF SPANS
OPT.
SINGLE STRUCTURES
PERTINENT GROUPS
VP OF SAFETY OF SPAN ASSEMBLY BY STRUCTURE
ORDER: 1°,2°,.....
Σ OF GROUPS
VP OF CONSERVATION OF SPAN ASSEMBLY BY STRUCTURE
ORDER: 1°,2°,.....
VARIANCE
VP OF WATERPROOF OF SPAN ASSEMBLY BY STRUCTURE
ORDER: 1°,2°,.....
VARIANCE
DECK CLASS


β
COMPATIBILITY WITH VP
NO
YES
BEAMS
CALCULATION OF "SEGMENTS" BY BEAM VS DEFECT (BEAM 1,2,...)
TABLE OF DEFECTS BY BEAM
VIEWPOINT: "SAFETY"
VIEWPOINT: "CONSERVATION"
VIEWPOINT: .....
DEFINITION OF DEFECT CLASSES
BEAMS CLASS
BEAMS CLASS
BEAM ASSEMBLY
BEAM ASSEMBLY
β1
β1
COMPATIBILITY WITH VP
NO
YES
CROSS BEAMS
CALCULATION OF "SEGMENTS" BY CROSS BEAM VS DEFECT (CR.B. 1,2,...)
TABLE OF DEFECTS BY CROSS BEAM
VIEWPOINT: "SAFETY"
VIEWPOINT: "CONSERVATION"
VIEWPOINT: .....
DEFINITION OF DEFECT CLASSES
CROSS BEAM CLASS
CROSS BEAM CLASS
CROSS BEAMS ASSEMBLY
CROSS BEAMS ASSEMBLY
βn
β2
COMPATIBILITY WITH VP
NO
YES
SLAB
CALC. OF "SEGMENTS" BY ELEMENTS VS DEFECT (Dx, Sx, Sy, Sr, Internal Spans)
TABLE OF DEFECTS BY ELEMENTS
VP: "SAFETY"
VP: "CONSERVATION"
VP: "WATERPROOFING"
VP: .....
DEFINITION OF DEFECT CLASSES
ELEMENT CLASS
ELEMENT CLASS
OVERALL ASSEMBLY
PARTIAL ASSEMBLY
SPAN CLASS
δ
γ
COMPATIBILITY WITH VP
CALCULATION OF "SEGMENTS" BY STRIP VS. DEFECT (Sx, Dx, 1,2,...)
TABLE OF DEFECTS BY STRIP
VP: "SAFETY"
VP: "CONSERVATION"
VP: "WATERPROOFING"
VP: .....
DEFINITION OF DEFECT CLASSES
STRIP CLASS 1,2,...
STRIP CLASS Sx Dx, 1, 2
STRIP ASSEMBLY
OVERALL ASSEMBLY
PARTIAL ASSEMBLY
SPAN CLASS
δ

"Conservation": The group of spans of a structure is classified in a determined order resulting from processing the data on the groups to which each span belongs. First, the frequencies of the groups are calculated. The order of a given structure corresponds to the mean of the groups present weighted according to their relative frequencies as in the following expression:

$$\bar{g} = \frac{\Sigma f \cdot g}{n} \qquad (1)$$

The order value is linked to a second parameter consisting of the variance of the frequency distribution, calculated as follows:

$$S^2 = \frac{\Sigma f (g - \bar{g})^2}{n} \qquad (2)$$

Depending on the viewpoint, each structure thus remains associated with an order and certain percentages or a variance.
In classifying all the structures of a selected population, these are first sorted in descending rank, from those of highest order to those of lowest order. In the case of the Safety VP the ranking is determined by relative percentages in reference to the order, whereas for the Conservation VP the position is determined by the variance, in inverse proportion to the value.

CONCLUSIONS

A structural programmed maintenance needs a data-base to give to a manager all the information about inspections and different choices of maintenance.

Data-base is the best right way to have all the elements in order to organize an objective list of intervention priorities, when the number of bridges is very large.

A good management software cannot become old; it always must be developped in order to obtain:

- new items of data-base (development of surveillaince methods of intervention techniques and special materials; etc)
- new outputs to use on time all the items of data-base to help better the manager in his choices.

A special management software will be always incomplete and needs to be improved to give step-by-step practical results.

SEISMIC RETROFITTING OF TWO LARGE SPAN BRIDGES

Mario P. Petrangeli Marco Petrangeli

Department of Structural & Geotechnical Engineering
University of Rome "La Sapienza"

ABSTRACT

The Ruiz and Stupino viaducts, spanning over 120 metres each, were built in the early '70^s by the cantilever method. With piers heights up to 150 metres, they are among the most significant structures along the 440 kilometres of the Salerno - Reggio Calabria motorway. Due to long term effects, large permanent deflections had developed at midspan. Therefore rehabilitation works had to be undertaken together with seismic retrofitting of these and other viaducts along the same motorway.
The paper describes the whole operation, now completed, from the numerical analysis, through the design, to the implementation of the proposed repair works.

1. INTRODUCTION

The Salerno - Reggio Calabria motorway was built in the early '70^s providing the southward extension of the main axis running from Milano through Bologna and Firenze to Roma and Napoli. This is still the main route connecting all the major cities in Italy, taking into account that Reggio Calabria, quite a large city itself, is the departure harbour for the ferries to Sicily and therefore to cities like Messina and Palermo.
The motorway is running mainly in mountainous regions Fig.1, for a total length of 440 km, 56 of which are on viaducts due to the orographic conditions. Most of these viaducts are made of simply supported prestressed concrete (pc) beams spanning over 35-40 metres. A number of different factors as the haste in the construction, the sometimes unsatisfactory quality of the materials and of the manufacturing and, last but not least, the extensive use of deicing salt has led to the situation that within less than twenty five years of lifetime, a significant percentage of these viaducts needed repairing. For this reason, in 1989 the government agency ANAS, in charge of the operation and maintenance of the Salerno - Reggio Calabria motorway, allotted 200 million US dollars on a comprehensive rehabilitation program.
The deterioration occurred to the pc viaducts can be ascribed to both the design and the construction phases of these structures. The first cause of deterioration was the above said quality of the construction amplified by the lack of accurate maintenance, especially with respect to the water drainage when deicing salt was used. This situation produced weathering of the beam concrete surfaces, with water and other external agents penetrating in to the concrete where diffuse beam cracking had occurred due to loss in the prestressing

force. In turn, some of the mortar injections were inaccurately made, when not missing at all, thus leading to cable corrosion as found in the site inspections.
The second cause for the deterioration was the insufficient understanding of the time dependent behaviour of concrete which yield high prestress losses and unacceptable deflections in the larger pc viaducts built by the cantilever method.

The paper will focus on the second aspect, describing the repair and strengthening of the two largest viaducts of this type, namely the Stupino and the Ruiz viaduct, which although showing a modest degree of deterioration in the concrete and in the prestressing bars, had developed deflections at midspan in excess of half a metre. The strengthening and repair works also focused on the seismic behaviour of these bridges, that although satisfactory in term of resistance and ductility demand, did not comply with the safety recommendations on the maximum displacements at the supports.

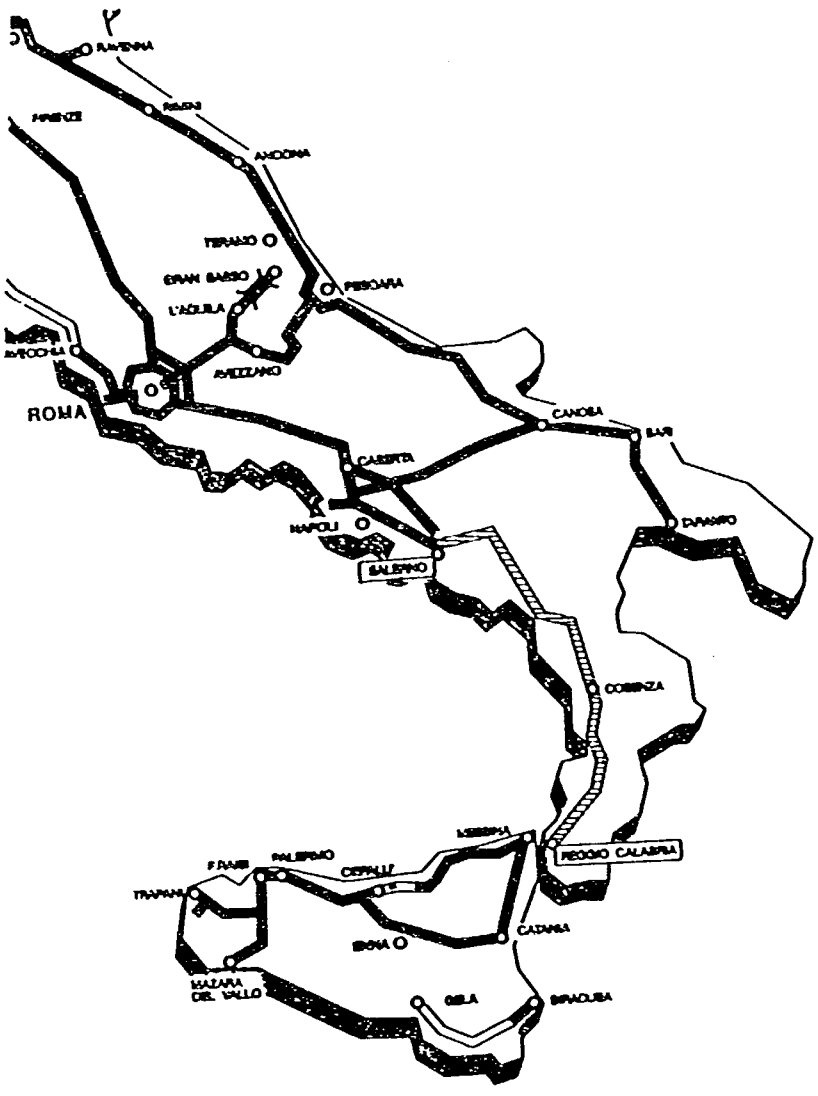


Fig.1 The Salerno - Reggio Calabria motorway

2. THE SITE SEISMIC HAZARD

The Salerno - Reggio Calabria highway runs along the south western italian coast mostly in mountainous regions with peaks in excess of two thousand metres above the sea level. This region is well known for showing a medium to strong seismic activity with experienced maximum magnitude of about 6.5.
Records of the past major earthquakes are available since since 1000 D.C., after 1600 D.C. these data are exhaustive and accurate even for the smaller events thus providing a reliable source of experience for the modeling of the seismic activity. A map showing the maximum intensity of the earthquakes registered so far, based on the MCS scale can be found in Fig.2.
The Ruiz and Stupino viaducts are situated adjacent to the Sila group, in a seismotectonic zone known as the *Alto Crati*, not far from the town of Cosenza. Based on the historical data on the previous seismic activity in the region and the seismotectonic information available today for this zone, an expected maximum ground acceleration of 0.31 g at the sites has been calculated using the Neumann and the Campbell relationships.

This ground acceleration has been multiplied by a factor of 1.3, as prescribede by the normative, to account for the slope effects in the sites where these viaducts stand.

Currently the official Italian code does not prescribe the use of the ground acceleration parameter to define either an equivalent static force or a design spectrum for dynamic analysis. The forces (seismic actions) are found based on a seismic coefficient which is used together with the allowable stress method for the structural verifications. With respect to this seismic coefficient, the Italian territory has been divided in four regions as shown in Fig.3. In the specific case, this coefficient is set to 7% of the gravity load.

Given the interest placed on the prediction of the maximum displacements of the two viaducts, a more sophisticated analysis was carried out in the time domain using realistic constitutive behaviours for the reinforced concrete members. In order to do this, a number of artificial accelerograms have been generated using the spectral shape for soil type S1 (stiff) as defined by the italian code. In a later stage of the project these analyses have also been repeated using the normalized accelerograms given by the european seismic code. All the accelerograms have been scaled to a peak ground acceleration of 0.403*g* as found from the seismic hazard study.

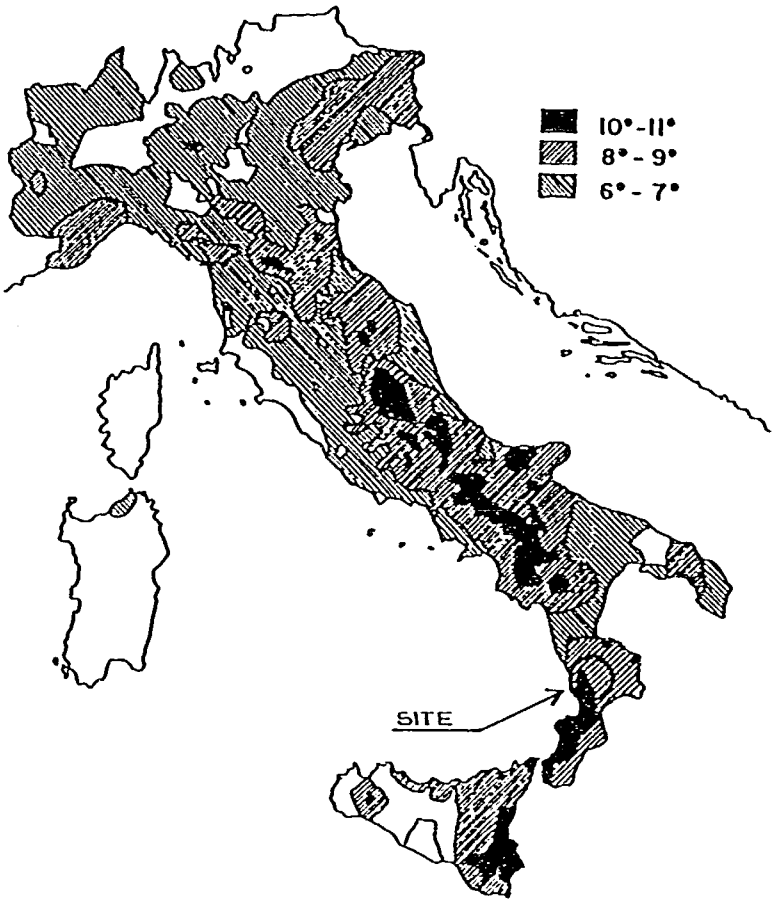


Fig.2 Maximum seismic intensity to 1968

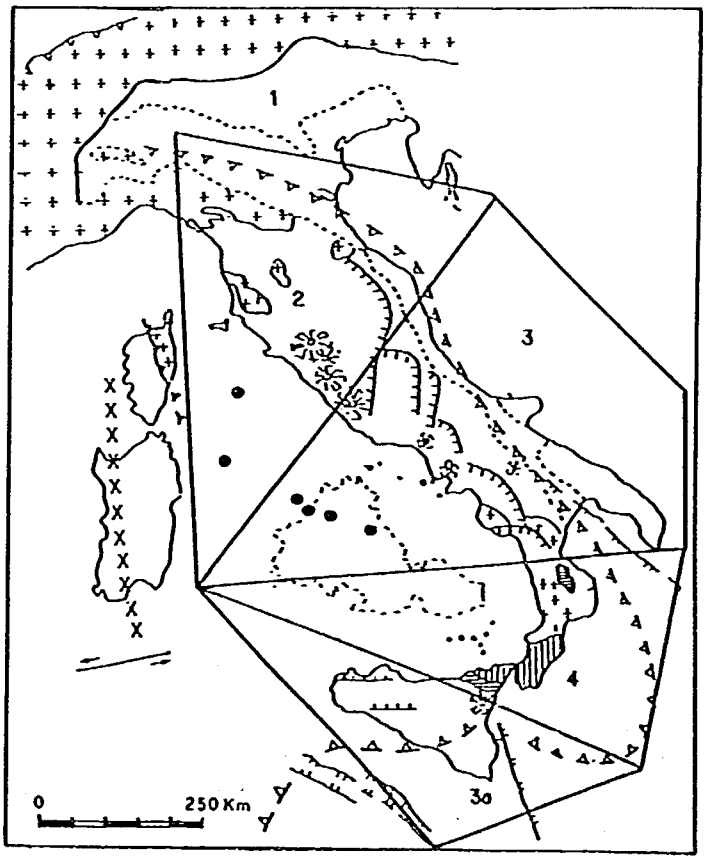


Fig.3 Italian official seismic zoning

3. THE STUPINO AND RUIZ VIADUCTS

These two pc bridges are among the first applications of the segmental cantilever construction in Italy, their design dating back to 1964. To this extent they represent the "first generation" of these bridges, a common feature being that the two adjacent cantilevers at midspan were not made continuous as normal practice in subsequent realizations. Prestressing in these bridges was achieved by means of high strength bars coupled at each cast-in-situ segment.

The Ruiz viaduct Fig.4 had a small dropped span between the adjacent cantilevers allowing relative rotation and horizontal displacement of the two sides. Due to creep the two piers had moved in towards the central span closing the expansion joints and enforcing compression in the dropped span which was therefore acting as a strut. Using hydraulic jacks, a compressive force of 1500 kN has been measured, to push back apart the two cantilevers. The profile of the bridge prior to the repairs is plotted in Fig.5. Obviously the profile refers to the structural concrete box, since the road geometry was realigned using filling material which added a considerable unbalanced moment on the structure and contributed to increase the creep process.

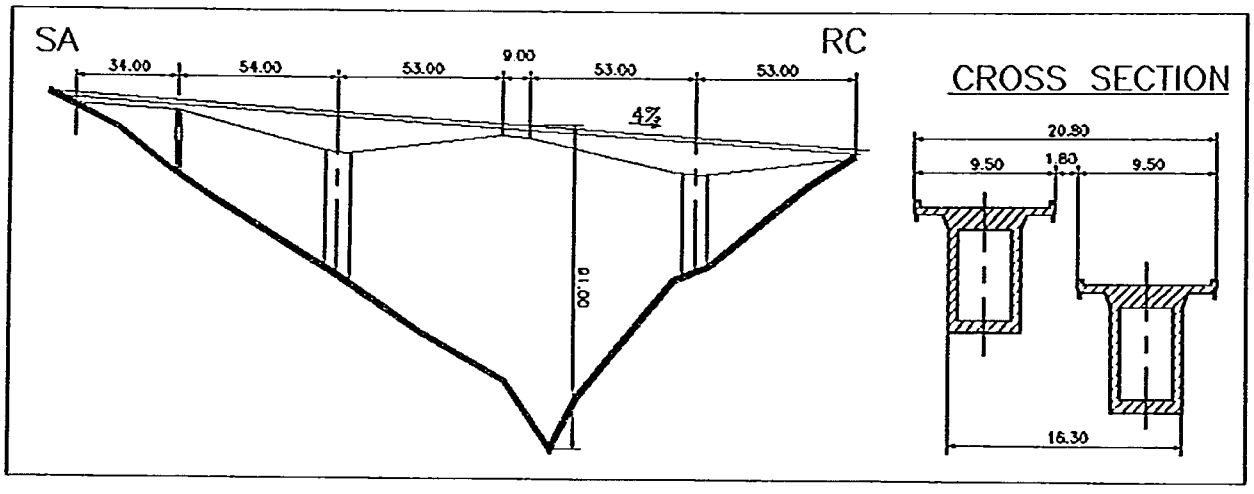


Fig.4 General scheme of the Ruiz viaduct

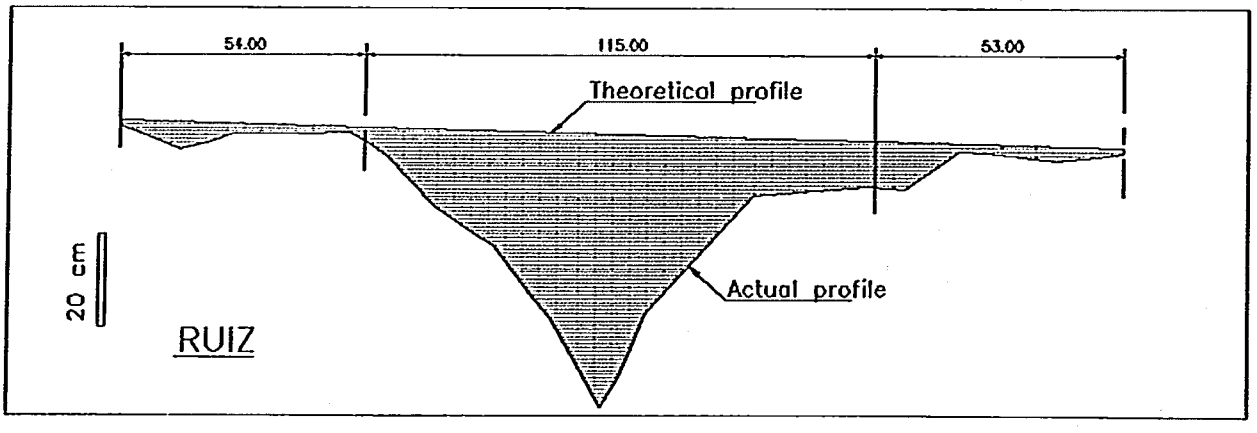


Fig.5 Ruiz deck profile prior to rehabilitation

On the Stupino viaduct instead, Fig.6, steel hinges allowing relative rotations and horizontal translations were placed to connect the adjacent cantilevers in the two main spans, These eight hinges, one in each web of the twin concrete boxes, were in bad conditions due to weathering and had to be changed. The profile of the bridge prior to the repairs is plotted in Fig.7.

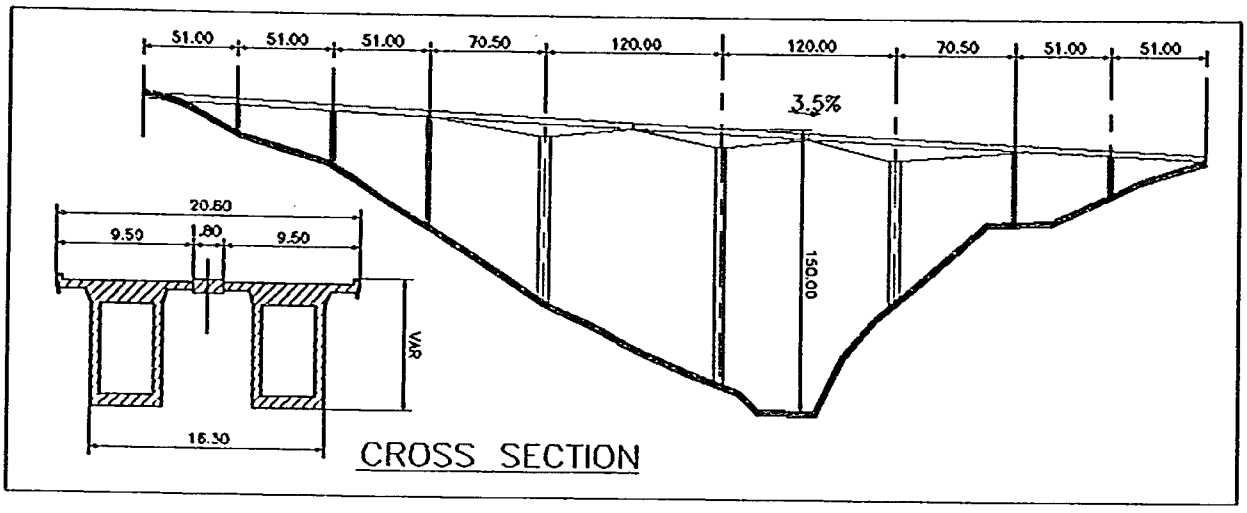


Fig.6 General scheme of the Stupino viaduct

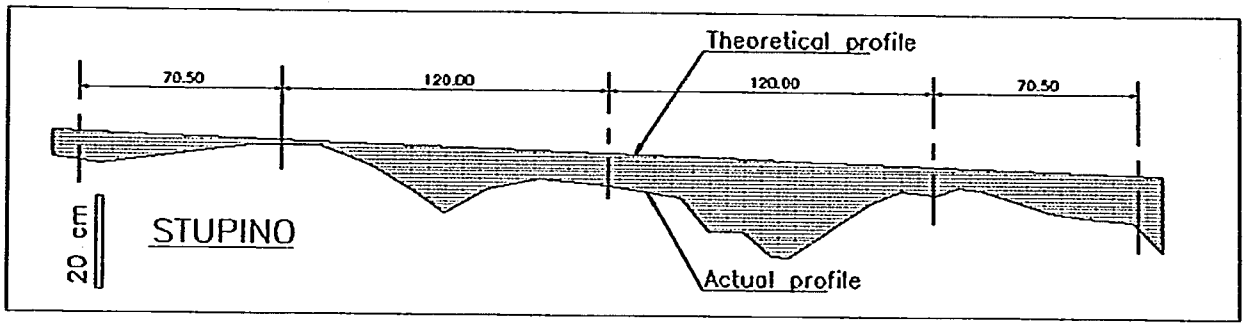


Fig.7 Stupino deck profile prior to rehabilitation

4. THE SITE INSPECTIONS AND TESTS

The main pourpose for the site inspections with regards to the concrete was to establish its mechanical properties and to check its deterioration (i.e. carbonation depth). An average compressive strength $f_c = 40MPa$ was found with carbonation depth ranging from 8 to 19 mm.

Another series of tests was carried out to asses the state of the prestressing bars with respect to corrosion. A number of prestressing bars were exposed by removing the concrete cover. The groutings of the ducts, probably due to their small diameter ($\phi 60mm$) for ($\phi 32mm$) bars, were almost unexisting but no evident signs of corrosion could be noticed.

Last but not least, a number of tests were carried out to asses the residual prestressing force in the structures and therefore find the explanation for the high permanent deflections accumulated during the structure lifetime. Stress-release tests carried out on bars near the pier showed these forces being only 60 to 70% of the theoretical values prescribed in the original design. This could have been caused by friction and high creep losses which were not accounted for at the design stage.

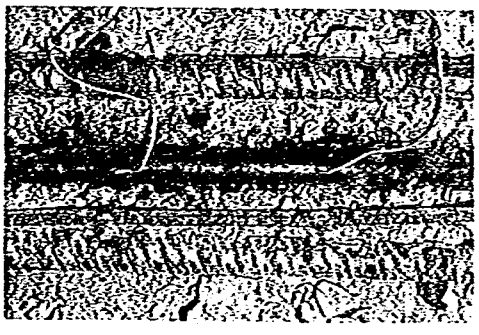


Fig.8 Prestressing bars. Stress-release tests

5. THE NUMERICAL ANALYSES

Two types of numerical analyses were carried out; a creep analysis to check the consistency of the experimental findings on the amount of prestress in the two structures with respect to the creep deformations accumulated during the previous 25 years and a nonlinear dynamic analysis of the structures subjected to a simulated numerical ground input motion so as to asses their behaviour under earthquake excitation.
The creep analyses, although very important for the calibration of the additional external prestress to be installed in the box girders, will not be discussed since the emphasis of the paper is in the seismic rehabilitations.
Under seismic excitation, in this kind of structures the deck remains normally elastic, while the plastic deformations concentrate at the pier bases, which was a cause for concern given the geometry of the two bridges with pier heights up to 150 metres.

The dynamic analyses were therefore carried out using a nonlinear finite element code (ANSR [2]) and a smeared plasticity beam element developed at the University of Rome [3] which is capable of accounting for the nonlinear cyclic behaviour of the pier cross sections.
2-D models were set up of the two bridges in the longitudinal direction, and a number of analyses were carried out with different accelerograms scaled to the same peak ground acceleration. The analyses showed that the ductility demand at the pier bases is very small, as can be seen for example in Fig.8 where the moment curvature response at the base section of the Stupino tallest pier is plotted.

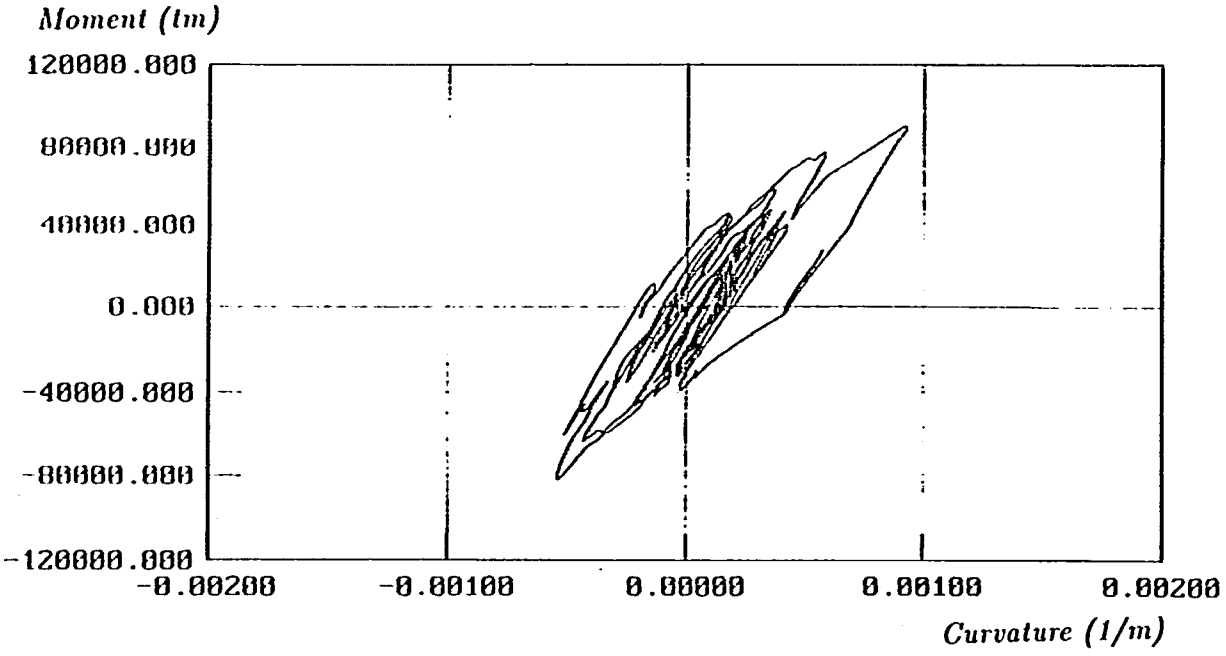


Fig.9 Moment curvature history for the Stupino central pier

Later during the project the analyses have been repeated using FIBER finite element program as developed by the second author as part of his doctoral thesis [4][5]. This program is based on a more sophisticated 3-dimensional fiber approach for the beam modelling, taking into account automatically the axial force-bending moment interaction. Some of the analyses were then repeated to double check the results obtained with the previous model and with the standard modal analysis as requested by the code.
A sample of the results which can be achieved with this tool can be seen in Fig.9 where the bending moment-curvature response is plotted for the base section of the short pier at the transition between the simply supported approach span and the north cantilever of the Ruiz viaduct. This pier, given its higher frequency has come out to be the most

within acceptable limits.

The diagram refers to a direction of the ground excitation acting at a 45° angle with the longitudinal axis of the bridge. The graph shows the moment curvature relationship in two orthogonal directions, the dashed lines being the one parallel to the bridge longitudinal axis. Generally, due also to the limited nonlinearity found in the analysis, the results of the two models showed good agreement, especially with regards to the maximum displacement of the structures.

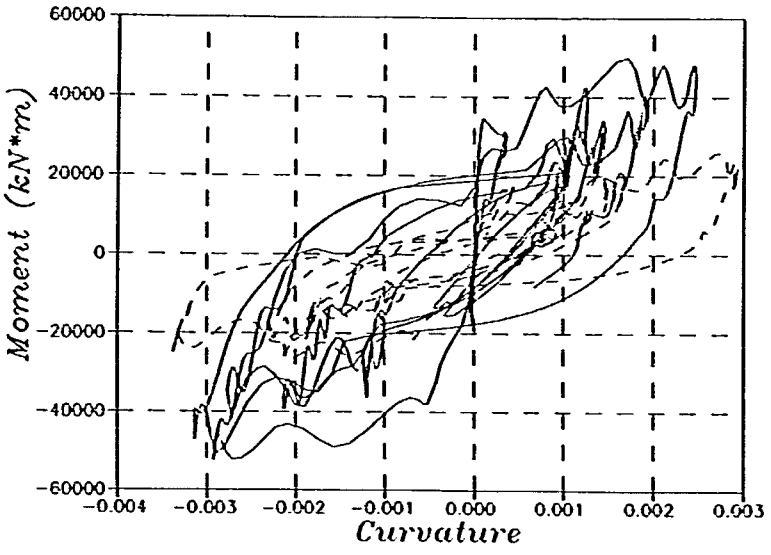


Fig.10 Moment curvature history using FIBER program

The longitudinal displacement at the pier top for the two structures are summarized in the table below; the seismic retrofit of all the bearings and joints of the two bridges has been decided according to these values. Where *Pier 2* is the central pier for the Stupino viaduct and the shorter one in the Ruiz viaduct. Displacements are in millimitres.

STUPINO		
	Abs. Max.	Aver. Max.
Pier 1-3	222	168
Pier 2	273	202

RUIZ		
	Abs. Max.	Aver. Max.
Pier 1	143	111
Pier 2	107	73

These results are also in good agreement with the estimate of the displacement which can be obtained from the modal analysis as follows: the first period of the two bridges in the longitudinal direction for the taller piers is $T_s = 2.73sec.$ for the Stupino viaduct and $T_r = 1.67sec.$ for the Ruiz viaduct. The response coefficient of the italian GNDT [6] spectrum type S1 (the one used to generate the accelerograms) for the two periods being:

$$R_s = \frac{2.5}{T_s/0.35} = 0.321 \tag{1}$$

$$R_r = \frac{2.5}{T_r/0.35} = 0.524 \tag{2}$$

Therefore the two expected displacements can be found according to the expression:

$$D_s = \frac{R_s * a_g}{\omega_s^2} = 239mm \tag{3}$$

$$D_r = \frac{R_r * a_g}{\omega_r^2} = 146mm \tag{4}$$

which are in good agreement with the values found with the nonlinear analysis.

6. THE STATIC AND SEISMIC RETROFIT

Under a *static* point of view, both viaducts needed to be strengthened with respect to the ultimate load factor. This was mainly a consequence of the lack of bond between the prestressing bars and the concrete section.
Another objective of the remedial work was to reduce the permanent deflections although only the elastic part of them could be recovered given the age of the structures with no residual creep to exploit in order to reverse the accumulated deformations.
Both tasks were achieved via additional external prestressing tendons placed inside the box girder Fig.11, calibrated to restore the original prestressing force. This technique has proved to be a powerful means in many retrofitting problems [7]. On the Ruiz viaduct, a further improvement has been achieved via the substitution of the heavy concrete dropped span with a orthotropic steel deck about 900 kN lighter.
The remaining permanent deflections were neutralized using a special lightweight filling material which allowed for substantial weight savings with respect to the previous bituminous filling (see also [8]).

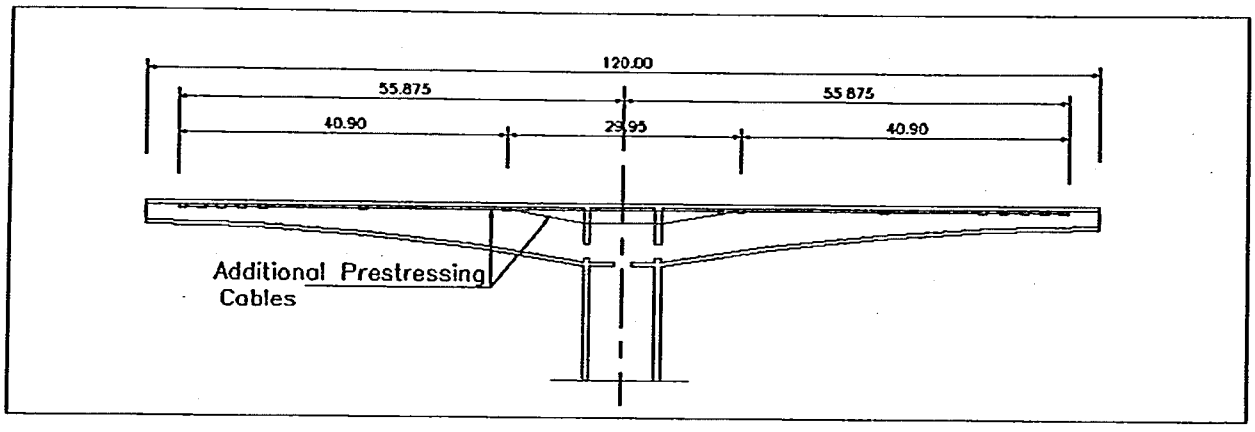


Fig.11 Typical layout of the external prestressing cables

The *seismic retrofitting* focused mainly on the maximum displacements at the bearings and joints of the two structures (cfr.[9]).
On the *Ruiz* viaduct the seats for the dropped span between the two cantilever had to be widened both in the longitudinal and in the transverse direction according to the results of the numerical study. In order to do that, the new steel beams replacing the old concrete ones have been shortened and the Gerber seats extended with cast in situ rheoplastic concrete (Fig.12 and Fig.13). Some of the external prestressing tendons has been therefore prolonged to fasten these new concrete blocks to the extremities of the existing cantilevers.

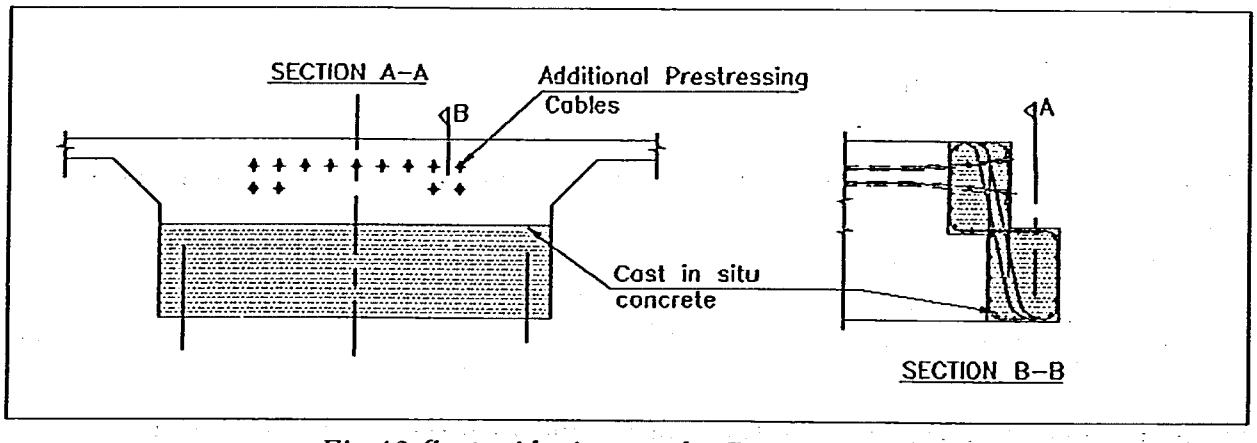


Fig.12 Seat widening on the Ruiz cantilevers

On the *Stupino* viaduct the old hinges connecting the adjacent cantilevers where in bad shape due to weathering and with inadequate run according to the above mentioned calculations. This hinges have been replaced with new ones Fig.14 in steel-teflon with the required specifications.

Also the longitudinal expansion joints placed at the extremities of the cantilevers towards Salerno and towards Reggio Calabria for both the Stupino and the Ruiz viaducts were under dimensioned and had to be replaced with new ones of longer run. This operation required the enlargement of the transition pier tops with cast in situ rheoplastic concrete connected with steel bars glued with epoxy resin to the existing structure (Fig.15).

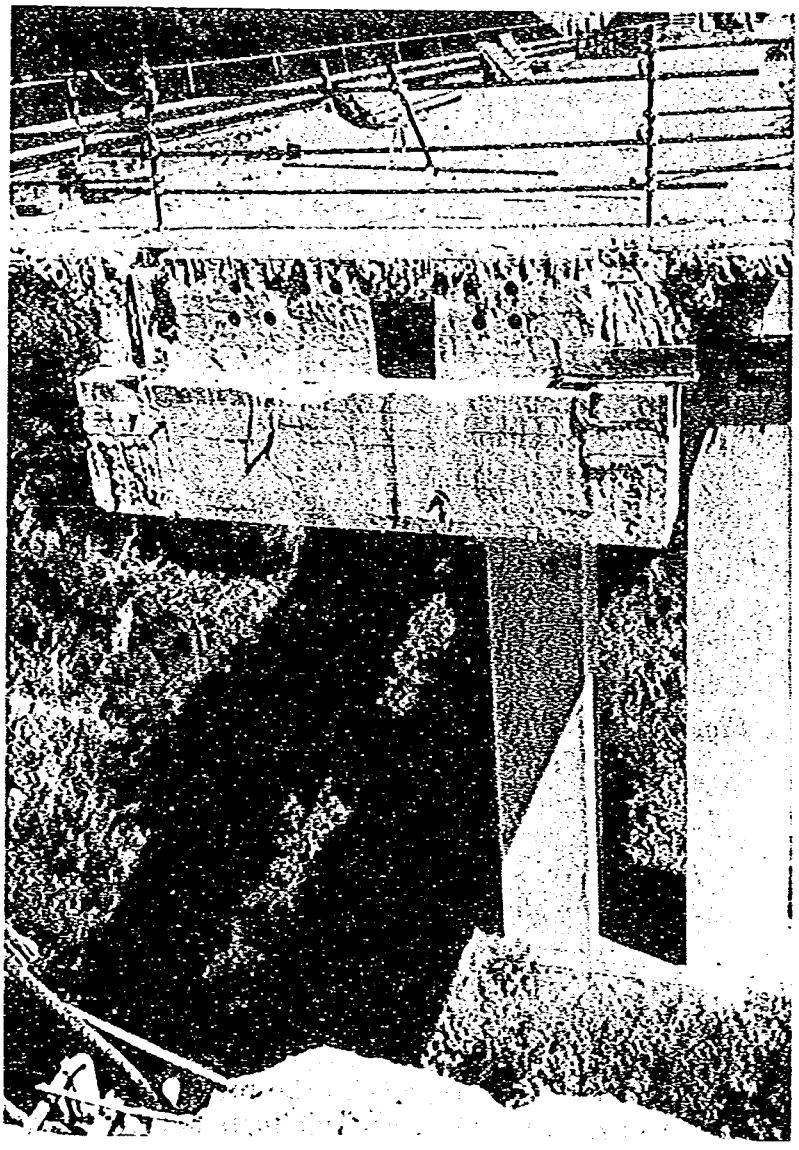


Fig.13 The existing seat on the Ruiz cantilevers

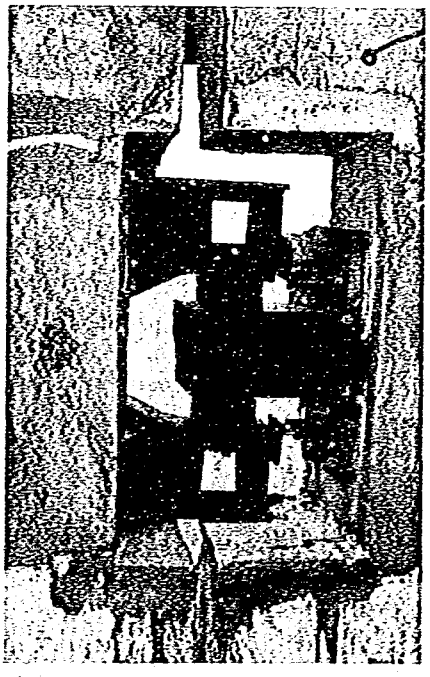


Fig.14 The Supino new hinges

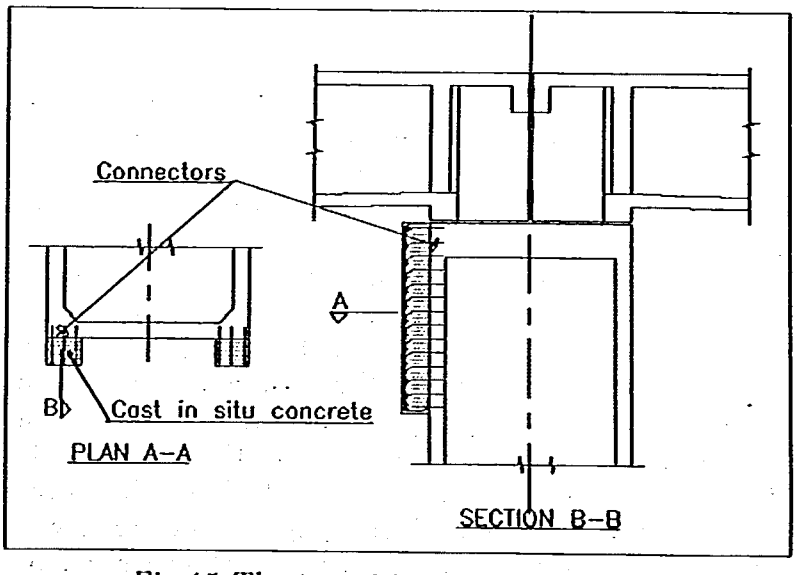


Fig.15 The transition pier enlargement



Fig.16 Steel stopper used for the Ruiz and Stupino

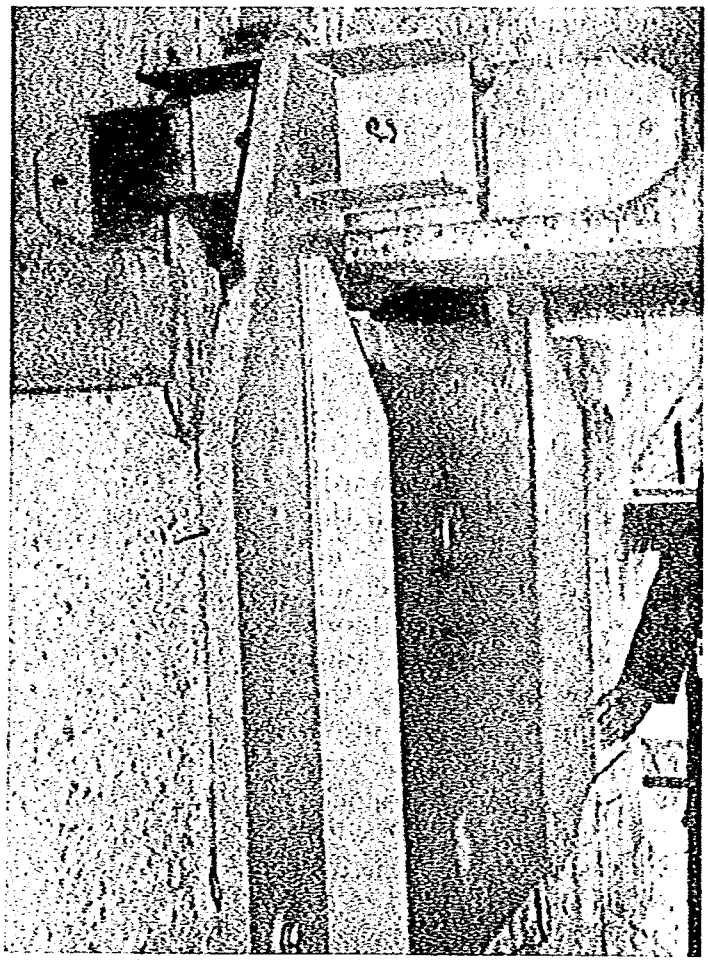


Fig.17 Steel stopper used for the standard viaducts

On the same piers, the transmission of the transverse actions coming from the cantilevers has been obtained via steel stoppers with neoprene bearings, specifically designed for the purpose and fastened vertically to the pier tops via bars glued into the existing concrete has shown in Fig.16. On nearby viaducts along the Salerno Reggio Calabria motorway, which were part of the same assignement, a different solution to the same problem has been used given the different geometry of the deck and the piers has shown in Fig.17.

7. CONCLUSION

In Italy, as well as in Europe, the large majority of the road and railway bridges date back to the '60 and the '70. In these years of economic expansion, in the process of reconstructing the infrastructures destroyed during the war, most of the present roadway and railway network was constructed without the possibility of relying on previous similar experiences.

Many of these bridges need now to be repaired because of two main reasons: (i) after 30 years lifetime these structures show, to various degrees, a justifyiable ageing and deterioration effects; (ii) the knowledge in seismic design acquired in recent years, namely the deeper understanding of the seismic actions and of the structural response, clearly demonstrate the inadequacy of the design criteria used at that time and therefore the need to upgrade the seismic performance of the structures built according to those criteria.

At the same time new materials and technologies have been developed such as the epoxy resins and the high-strength rheoplastic concrete as well as the external prestress and the fastening technique. Thanks to them we can carry out today these repair and retrofit works in a clean, fast and reliable way.

REFERENCES

[1] Mario P. Petrangeli (1990). *Inspection and Repair of some Highway Bridges in Italy.* Bridge Management, Inspection, Maintenance and Repair. Guilford, Surrey, UK. Ed. J.E.Harding et al. Elsevier, London.

[2] D.P.Mondkar, G.H.Powell (1975). "Static and dynamic analysis of nonlinear structures", Earthquake Engineering Research Center University of California Report No.75/10 March

[3] Ciampi V., Carlesimo L., *A Nonlinear Beam element for Seismic Analysis of Structure* 8th Europ. Conf. on Earth. Eng., Lisbon, September 1986

[4] Petrangeli M., Ciampi V., *A flexibility based 3-dimensional fiber beam element.* VIII Convegno Italiano di Meccanica Computazionale, Torino 15-17 Giugno 1994.

[5] M. Petrangeli and P.E. Pinto (1994) *Example A. Modern multispan bridge seismic response and assessment. Nonlinear and Linear models.* 2ND Int. Workshop on Seismic design of bridges, Queenstown, New Zealand.

[6] CNR - Gruppo Nazionale per la Difesa dai Terremoti (1984). *Norme tecniche per le costruzioni in zone tecniche.* Coord. Paolo E. Pinto (in italian)

[7] Mario P. Petrangeli (1993). *The use of external prestressing in the bridge rehabilitation and retrofitting.* L'Industria Italiana del Cemento N.680 September 1993. (in italian)

[8] M. Del Papa, M.P. Petrangeli and A. Bajo (1992). *Rehabilitation of prestressed concrete bridges built by the cantilever method in Italy.* Bridge Management 2, inspection, maintenance and repair. Guilford, Surrey, UK. Ed. J.E.Harding et al. Thomas Telford, London.

[9] K. Kawashima, S. Unjoh and H. Iida (1991). *Seismic Inspection and Seismic Strengthening of Highway Bridges in Japan.* 4th U.S.-Japan Workshop on Earthquake Disaster Prevention for Lifeline System, Los Angeles, CA, U.S.A.

SEISMIC RETROFIT AND STRUCTURAL REHABILTATION OF THE AGLIO VIADUCT

M.ROMAGNOLO

SOCIETA' AUTOSTRADE S.p.A.

CENTRAL DIRECTORATE - MAINTENANCE AND STUDIES

ROMA

ABSTRACT

The Aglio Viaduct is located between Bologna and Florence on the A1 Motorway "Autostrada del Sole". The viaduct was placed in service in 1960. The substructure consists of a double arch of reinforced concrete with a 163.4 m chord, and 18 access spans, for a total bridge deck length of 440 m. The repair works involved both substructure and deck. Repair to the substructure included: a) coating the full height of the piers with a rheoplastic cement mixture 0.15 m thick; b) coating the piers over the arches supporting the decks; c) repairing localized deteriorated concrete on the arches; d) protecting the concrete on the surfaces most exposed to aggressive agents. The 35 simply supported spans were linked to obtain three continuous multi-span decks. To fulfill current seismic requirements, the three decks were seismically isolated through the use of special PTFE/steel sliding and dissipating bearings. Step-by-step dynamic analysys has shown a 50% reduction in seismic response. Construction works were so programmed as to avoid disruption to road traffic, except for some limited closures of one lane.

1. DESCRIPTION OF THE STRUCTURE

The Aglio Viaduct is situated in the Apennine mountain range between Bologna and Florence. It is a structure (see Fig. 1) comprising a double arch of reinforced concrete with a chord of 163 m and a rise of 43.65 m crossing the Aglio stream with 18 access spans, 5 of which 18 m on the Bologna side, whereas the Florence side has 7 with a span of 18 m and 6 with a span of 9.5 m. The arch,pier and abtument foundations sit upon spread footings. The structure follows a straight line for 332.6 m and takes a horizontal bend 106.5 m long with a radius of 350 m on the Florence side. The longitudinal motorway gradient is 2.9%.

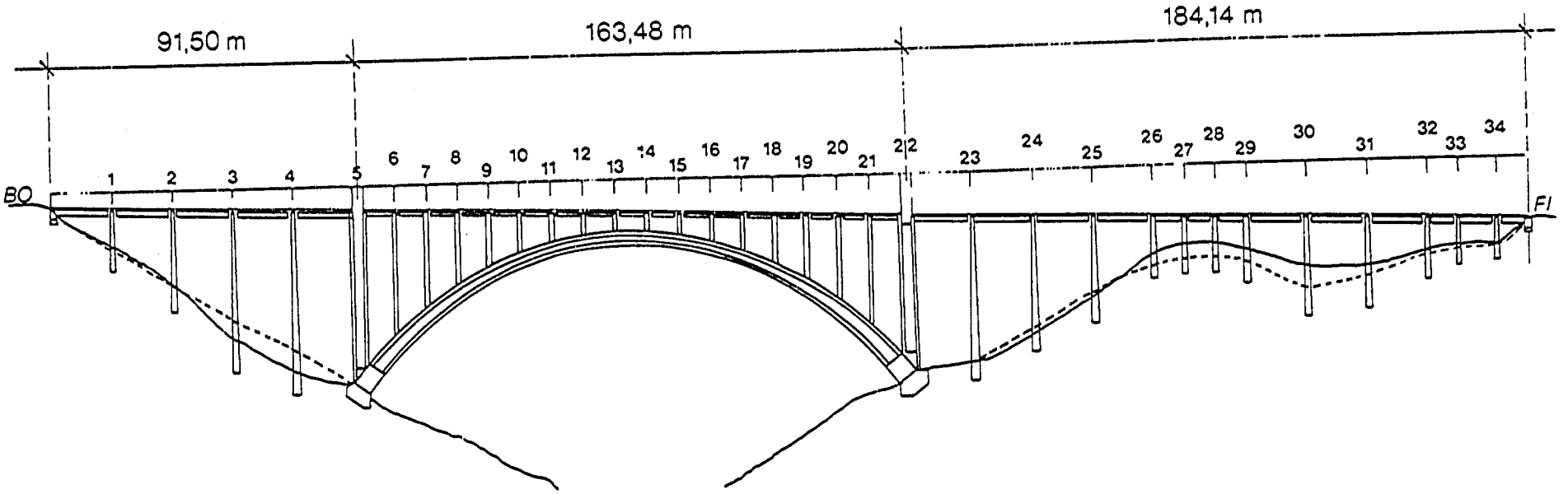


FIGURE 1 - AGLIO VIADUCT : LONGITUDINAL PROFILE

2. DETERIORATION OF THE PIERS AND ITS CAUSES

The viaduct was placed in service in 1960 and has undergone only two repair operations; one on a pier and another on a slab. Periodical inspections showed the piers resting on the arch as well as those carrying access spans to be badly deteriorated - with disintegrating concrete, damaged edges and widespread rusting of the reinforcement. In many cases, the pier stirrups had been sheared through and the main reinforcement was misaligned and badly rusted.
The portal beams were also badly damaged and the arches showed signs of efflorescence on the intrados as well as some modest honeycombing. In addition, both the fixed and movable bearings were rusted as well as seized. Finally, the water drainage system as well as the expansion joints proved to be inadequate.
Deterioration was mainly due to the chemical and mechanical effects of chlorides in the water runoff from the road surface that percolated through the joints in the bridge deck and ran down the underlying load bearing structures. To a lesser extent, part of the deterioration was due to traffic - which is particularly intense in this stretch of road.

3. REPAIRS TO THE PIERS

Repair work concerned a series of operations carried out first in the substructures and then on the deck. Repair of the piers included the following processes:

1) coating the full height of the access span piers and the two piers at the base of the arch with a 0.15 m thick layer of a rheoplastic cement mixture made with a highly adhesive binder and suitably reinforced.

2) Coating the piers over the arches with rheoplastic, shrinkproof, ready-mixed fine concrete to a thickness of 0.12 m and suitably reinforced.

3) Coating the portal beams supporting the deck with same previously decribed method for the access and arch spans respectively. This stage of the works also provided for the construction of brackets projecting from the supporting beams to serve as a base for the jacks which were subsequently needed to lift the deck.

4) Creating metal inspection platforms on the 7 piers.

5) Repairing localized deteriorated concrete on the arches.

6) Protecting the concrete of the surfaces most exposed to aggression through the application of epoxy and polyurethane base products.

4. REPAIR WORK AND TRAFFIC INTERACTION

Two alternative solutions were suggested in terms of methodology of repair their difference residing on whether the works were to be carried out with or without restriction of motorway traffic.
The chosen solution involved the creation of a temporary access road about 600 m long and 4.5 m wide along the slopes underlying the viaduct connecting to the normal road network and provided with suitable access junctions to all piers and arch springers. This was needed for the continuous supply of material and equipment coming from the central jobsite depot.
In addition, a structure was built onto the extrados of the arch to remove materials and handling work site equipment that comprised a rack with moto-driven trolleys mounted on rails. For the substructures alone - including seasonal work stoppages - it took 36 months to perform all work, including work site plants and the laying of a temporary access road.
An alternative solution, which was rejected, called for the handling of scaffolding and material exclusively from the motorway, which would have made the repair works - and thus interference with traffic - to last 4 years. Considering the obvious cost-effectiveness difference of the two solutions, a comparative study was conducted on the extra cost of the jobsite with respect to the reduced expense to the road user so as to verify which solution would be more advantageous for the general economy.
On this occasion, the study also included data processing with a program to calculate the cost of the road user's discomfort caused by the diversion involving a change of traffic lanes. Clearly, it wasn't easy to translate this into monetary terms and a certain amount of approximitation was called for. However, fuel consumption, travel time, road safety, and driving comfort were all taken into account, bearing in mind that the user of this road pays a toll. The variables represented by traffic volumes, road grade, car truck ratios, and the working week were also added.
With these elements, it proved possible to analytically evalutate the cost (to the user) of delays due to the road works as compared to the cost of the project, or rather, to that part of the project cost concerned with reducing the obstruction of the road itself during the works - which was justified by the reduction in disturbance to the user - also in terms of economy. Is was found that the extra expense for the works was a little over 1/3 of the cost to the user, and thus, to the community. In the specific case in point, in line with Società Autostrade policy - which aims to promote corporate image - the decision to keep the works off the road proved to be amply justified.

5. DETERIORATION OF THE DECK

So as to briefly describe the damage to the deck - in addition to those

aspects already discussed - mention must be made of the deterioration to the underside of the beams and the ends of the cross beams over the arch and those of the access ramps.
The state of the deck slab gave an amount of efflorescence and water permeation into the intrados, therefore significant deterioration had been already occurred.

6. REPAIRS TO THE DECK

Regarding deck work, the repair project called for the retrofit of the structure so as to conform to current seismic standard, which - quite apart from the reinforcement of the piers discussed earlier - made necessary the construction of two reinforced concrete walls 0.30 m thick up to the height of the lower cross-beams which connect the bulbs of the two main pillars forming piers no. 5 and 22 (i.e.: those at the base of the arch).
All this was done to stiffen the structure as the stresses determined by non linear step by step dynamic analysis led to very high strains, both at the base and in the linking cross-beams.
Seismic action on the masses of the decks were decreased by 50% thanks to the adoption of a special type of bearing which allowed the creation of a "base isolation system" and thus a significant reduction in seismic response (in fact, these bearings enable an increase in the structure's period of vibrations).
For a better cooperation between all structural elements and so as to cause as little driving discomfort as possible to the road user by reducing the number of expansion joints, the rigid linking of the decks was preferred. That's why the abutments and piers no. 5 and 22 had to be reinforced to withstand the extra seismic action coming to bear on them.
The static layout of the deck as a whole was thus modified, passing from the original 35 simply supported spans arrangement to that of 3 continuous beams resting upon several supports:

1) from the Bologna-side abutment to pier no. 5, with a fixed bearing on the abutment
2) from pier no. 5 to pier no. 22, with a fixed bearing on pier no. 22
3) from pier no.22 to the Florence-side abutment, with a fixed bearing on the abutment.

7. ASEISMIC BEARINGS

The seismic retrofitting of the Aglio Viaduct was completed through the adoption of special aseismic bearing of the elasto-plastic type. The "bearing system" comprises the following:

. "fixed aseismic bearing" at one end of each continuous section;
. regular guided bearing on the intermediate piers;
. "movable aseismic bearing" at the other end of the continuous sections.

"Fixed" and "movable" refer to conditions of normal service, as all bearings behave as mobile when a seismic event takes place, at least in the longitudinal direction.

The "fixed aseismic bearings" essentially comprise a classic PTFE guided pot bearing whose sliding plate is connected to the pot by means of special butterfly-shaped elements.

In the presence of normal actions (braking) or moderate earthquake, these elements show elastic behavior, thus making the bearing self-centering.

In the event of a severe seismic action, said elements undergo plastic deformation providing high dissipation (efficiency in excess of 70%) which afford total aseismic protection to the viaduct.

The "movable aseismic bearing" are similar to the type described above, save for the fact that the connection between the pot and the dissipating elements has been completed by means of 2 oleodynamic shock transmitters at both sides of the pot (see Fig. 2).

The last type accomodates thermal displacements without appreciable resistance, while becoming perfectly rigid in the presence of dynamic actions like those induced by earthquakes or abrupt braking forces.

In this fashion, this type of bearing behaves in essentially the same manner as the "fixed aseismic bearing" causing seismic actions to be equally distributed amongst all the bearings equipped with dissipating elements.

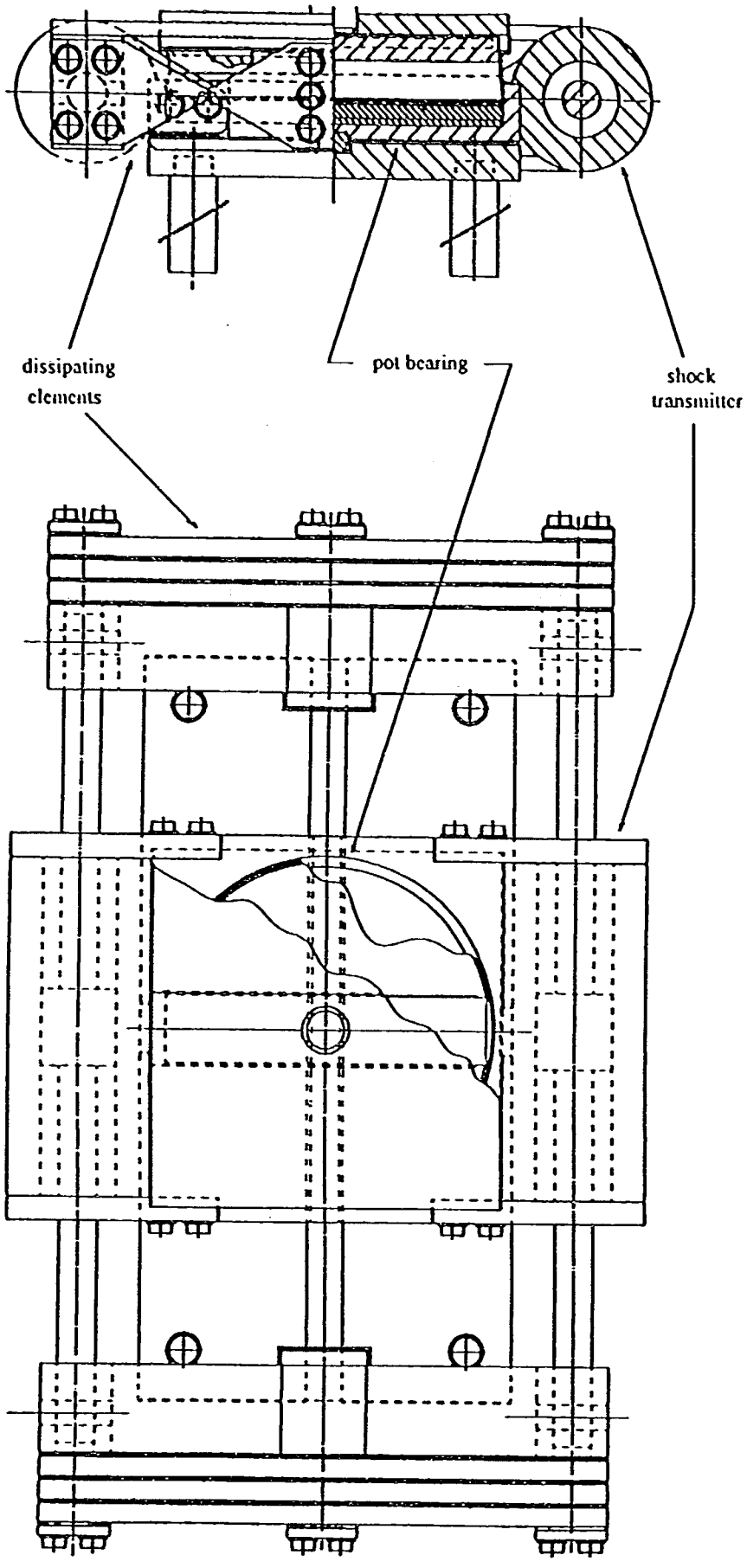


FIGURE 2 – "MOVABLE ASEISMIC BEARING"

8. SEQUENCE OF REPAIR WORKS TO THE DECK

The following series of operations summarizes the repair works - not necessarily in the specific order in which they were carried out:

1) reconstruction and reinforcement of the abutments and piers no. 5 and 22 (where the aseismic bearings are installed) to resist earthquake forces.
2) Rehabilitation and reinforcement of the outer beams by means of rheoplastic concrete coating.
3) Reconstruction of the ends of some of the curved beams.
4) Rehabilitation of the beam undersides at each bearing site given the state of severe deterioration in those critical locations.
5) Reinforcement of the end span cross-beams at the abutments and piers no. 5 and 22 and cross post-tensioning by means of dywidag bars.
6) Sequential jacking of deck sections under traffic.
7) Reconstruction of all end cross-beams with the exception of those already completed (see par. 5) and strengthening of the same so as to allow the longitudinal linking of deck section with dywidag bars.
8) Linking of the decks in order to create 3 multi-span sections.
9) Sequential installation of regular and aseismic bearings as required.
10) Surface rehabilitation of the intrados of the lateral cantilevers.
11) Reconstruction of pier tops.
12) Installation of expansion joints at the abutments and at pier no. 5 and 22.
13) Installation of joints providing continuity and impermeability at the deck points of linkage.
14) Completion of the rain water drainage system.

In terms of the time sequence adhered to, the works were completed as follows:

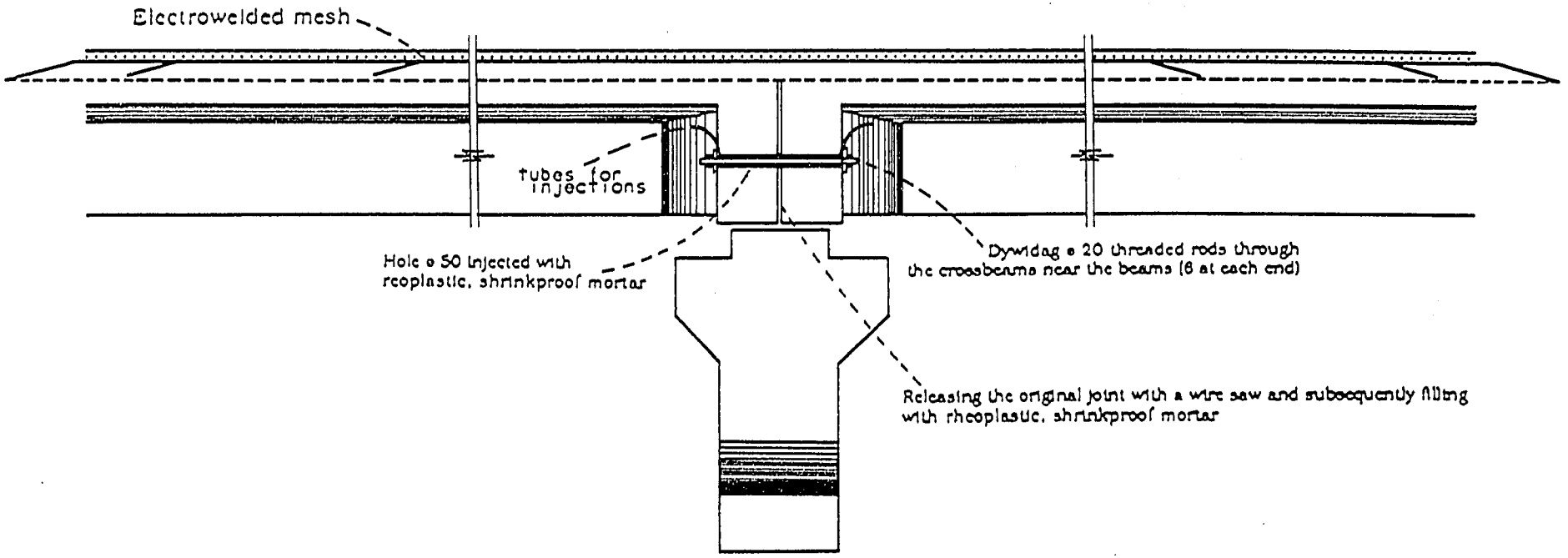
a) demolition of the Florentine side gravel guard
b) Jacking the first spans up and placing the same on PTFE temporary rocker bearings upon flame-cutting of the connecting studs between super and substructures (what had up to now passed for "aseismic protection").Said bearings were equipped with a special mechanical device permitting the adjustment of their height.
c) Reconstruction of the abutment up to the new height, 0.25 m taller than the previous one, while an independent team proceeded with the flame-cutting of the connecting studs of all the remaining spans.
d) While a third work team took care of the sequential jacking of the spans (always placing them upon temporary PTFE rocker bearings) a fourth team managed the rebuilding of the bearing seats as well as the installation of the permanent bearings. This same team managed the linking of the adjacent spans. The load transfer to the permanent bearings was effected simultaneously with the removal of the temporary PTFE rocker bearings.

e) A fourth team completed the installation of the espansion and continuity joints.

These operations of lifting and repositioning of the spans, as well as the connections and installation of the structural joints, were then repeated on the remaining viaduct spans. Finally, the continuous structure was completed by operations on the extrados slab, at the end crossbeams, adding the integrating reinforcement (see Fig. 3).

The rehabilitation works on the deck of the northbound lane were completed within 9 months (between March and November 1992) and carried out in the presence of traffic, detouring the same onto the two opposite traffic lanes and closing the entire northbound stretch for a total of only 60 days, in the 4 stages needed to demolish and reconstruct the two abutments and piers no. 5 and 22.
The project anticipated the availability of a "quick-install" mobile bridge in situ to be placed in the demolition area in the event of an emergency so as to keep the entire viaduct open to traffic. A situation of this nature developed only once during the November national All Saints Day festivities.

FIGURE 3 - INTEGRATED REINFORCEMENT AND RIGID LINKING - LONGITUDINAL SECTION



9. CONCLUSIONS

The Aglio Viaduct Rehabilitation Project represents one of the most demanding undertakings up to now faced by the Italian Motorway Administration. In fact, it has demonstrated that:

- seismic retrofitting of existing bridges conforming to the most recent seismic codes is always possible through the use of adequate aseismic devices even though said structures may be of outdated conception.

- Works can ben carried out in the presence of traffic with minimal disturbance of the same owing to the coordinated nature of a program and the adoption of specifically designed expedients.

- Costs of a rehabilitation are clearly lower than those of a structure replacement project, above all, when user incovenience is factored in.

DESIGN CRITERIA FOR BRIDGES OF THE ITALIAN HIGH SPEED RAILWAY SYSTEM

F. Braga,(1) F. Brancaleoni,(2) M. Colella,(3) G. Traini (4)

(1) Dept. DiSGG, University of Basilicata
(2) Dept. DiSSAR, University of Chieti "G. D'Annunzio"
(3) ITALFERR Sis. T.A.V. - Rome
(4) FS - Ferrovie dello Stato - Rome

ABSTRACT

This paper reports on the activities undertaken in order to define aseismic design criteria for the bridges and viaducts of the Italian High Speed Railway system. Specialised models of the seismic action have been defined accounting for seismicity levels and different site conditions. Actual acceleration records, complying with the above models, have been selected and used together with a sample set of representative bridge structures to study in detail the seismic response. Performance levels and indicators of the structural behaviour have been defined and computed via a wide numerical investigation, including soil-structure interaction and isolating devices presence. The correlation between the computed values of the performance indicators and the seismic intensity levels has allowed to assess the seismic risk of the railway line. Indications for further generalisation of the derived design criteria are also supplied.

1. INTRODUCTION

The Italian High Speed Railway system develops along two main lines crossing the country from Nort to South (Milan - Neaples line) and from East to West (Venice - Turin line) for a total length of about 1200 Km, a large part of which runs on bridges or viaducts. Some limited sections of the lines are already been constructed and presently in operation, but the main portion of the lines is scheduled for construction in the next years and is presently in the final design stage.

Aiming to obtain a uniform protection level of the entire railway system, homogeneous design criteria must be established. This is particularly true when the seismic action is involved, because of its random nature and its spatial variation. Due to the high seismicity of the Italian country, a wide scope study as been devoted to the above problem in order to estimate the seismic risk of the railway system and to make it as uniform as possible through the adoption of suitable design criteria. In particular, the paper reports on the activities undertaken and the main results obtained, focusing the attention on measures to be taken to comply with the relevant performance requirements.

This work is concerned with a numerical investigation, carried out on a number of structures, representative sample of the whole set of bridges and viaducts. Initially, performance and

seismicity levels have been defined according to proper indicators. Subsequently, the values attained by the seismicity levels have been computed using a seismic model specialised to the Italian country, adopted also for the derivation of the seismic actions. The performance indicators have been computed processing of the seismic response of structural models specifically devised to account for cracking, plasticization and other peculiar effects of bridge constitutive members when subjected to repeated loading. Different possible situations have been considered including soil-structure interaction, aseismic devices presence and different behaviour of the pier due to cracking. Finally, the correlation between the performance levels and the seismic intensity levels has allowed to draw general lines to be coplied with towards a safe structural design.

2. PERFORMANCE LEVELS AND INDICATORS

The design philosophy followed is primarily targeted towards the railway line operability, so that different service conditions are defined according to the attainment of correspondent limit state by the structure under consideration [1]. In other words, it is required that under small intensity earthquakes the line should guarantee no service break-downs, whereas for moderate earthquakes service should be continued with possible short interruptions for simple repairs and, finally, for strong earthquakes the line might be closed, allowed for significant repair works.
Aiming to establish design criteria it is therefore necessary to relate the above three performance levels to the earthquake intensity, in order to find out the intensities associated to the various line operability conditions excedence. Two different sets of parameters must hence be introduced and correlated, the former aimed at provideng a simple and synthetic measure of the structural behaviour, the second at providing a simple and synthetic measure of the seismic intensity.

2.1 Performance levels and structural indicators

Regarding the structural behaviour, the performance levels are introduced to represent respectively so called normal, exceptional and extreme conditions. Each performance level is divided into two limit states, one corresponding to safety requirements and the other corresponding to serviceability requirements. These two limit states must be simultaneously satisfied in order to comply with the selected operability level of the line. The limit states are defined as follows:

LEVEL 1 - normal conditions

SAFETY REQUIREMENTS:	no structural damage
	allowable stresses not exceeded
SERVICEABILITY REQUIR.:	no damage to ballasted track
	service tolerances not exceeded by track deformations

LEVEL 2 - exceptional conditions

SAFETY REQUIREMENTS:	only secondary structural elements damaged
	elastic limit stresses attained
SERVICEABILITY REQUIR.:	slight damage to the ballasted track
	no train derailment

LEVEL 3 - extreme conditions

SAFETY REQUIREMENTS:	structural damage allowed
	no collapse (either global or local)
SERVICEABILITY REQUIR.:	ballasted track severely damaged
	possible train derailment

The above performance levels are quantified by means of the so called performance indicators, chosen as appropriate dimensionless measures of the seismic structural response, with the following definition:

- χ/χ_y - structural ductility
- δ/δ_y - sectional ductility

The structural ductility is herein defined as the ratio between the maximum horizontal displacement of the top of the pier and the same displacement at the conventional elastic limit, whereas the sectional ductility is defined as the ratio between the maximum curvature and the curvature in the same section at the conventional elastic limit.
The performance levels are defined according to the following table 1, where the safety requirements are expressed in terms of the sectional ductility and the serviceability requirements are expressed in terms of the top pier displacement *d*:

Table 1. *Performance levels and indicators.*

Performance level	safety sectional ductility	serviceability maximum displ. (cm)	serviceability residual displ. (cm)
1	≤ 1/3	≤ 5	≤ 1
2	≤ 1	≤ 10	≤ 5
3	≤ 10	≤ 20	≤ 10

It is worth noting that the attention has been primarily focused on the above quantities since the structural safety can be measured directly in terms of the sectional ductility, whereas the serviceability requirements can be checked against the maximum top pier displacements that are immediately computed from the structural ductility. Moreover, the residual displacement has been used together with the maximum displacement because of the plasticizations effects.
Aiming to get a more detailed information on the structural behaviour the above indicators have been integrated with the behaviour factors defined as follows:

- qT - behaviour factor in terms of the shear force
- qM - behaviour factor in terms of the bending moment

qT is the ratio between the maximum shear force at the pier base evaluated from a linear elastic model and the maximum shear at the same section from nonlinear analyses; while qM is the ratio between the maximum bending moment at the pier base evaluated from a linear elastic modela and the maximum bending moment at the same section from nonlinear analyses.

2.2 Seismic intensity levels and indicators

As regard the seismic intensity, three levels have been considered, i.e.: low, moderate and strong earthquakes. A single synthetic indicator as been selected to quantify the levels. For simplicity, it has been related to the maximum peak ground acceleration and defined by the dimensionless quantity: a/g, where g is the gravity acceleration.

3. SEISMIC BEHAVIOUR

3.1 Structural types

A layout of the Italian National High Speed system network is given in fig. 3, where the solid line represents the section actually under consideration (Milan to Neaples via Rome). Part of this section is already in operation (the line from Rome to Florence), whereas the construction of the main part is scheduled for construction in the next years. Based on this observation, it has been decided to keep the investigation separated for the two, "existing" and "new", sections. In fact the "new" one is presently in an advanced design stage, whereas the "existing" one was designed almost 15 years ago and does not take into account the most recent progresses achieved in seismic design.
Furthermore, since the total railway line length is about 800 Km and a large percent runs on bridges or viaducts, it was necessary to restrict the investigation to the more representative structural configurations. The definition herein adopted to define a structural type and its representativeness is the following:

- a structural type is defined as a model structure, whose behaviour can be well defined and uniquely associated to a set of characteristics, that are: constitutive materials, structural shapes and dimensions, loading conditions and supports;
- a structural type is assumed to be representative when both its relative frequency of occurrence in the line and its vulnerability are higher than average.

Based on the above definitions the structural configurations selected as appropriate structural types and representative samples are listed in table 2, respectively for the "existing" and "new" lines. In the table the identification code refers to the code used throughout the paper to address that particular bridge type. Typical deck and pier cross sections are given respectively in fig. 1 and fig. 2, from which can also be derived the meaning of the other labels of table 2.

Table 2. *Structural types - (a) "existing" line, (b) "new" line.*

id code	pier height (m)	deck type	deck span length (m)	deck weight (t)
(a) (*)				
1P	15	G	35	1225
2P	15	B	25	750
3P	37	G	35	1225
4P	37	B	25	750
(b) (**)				
A	7	B-1	25	819
B	14	B-1	25	819
C	21	B-1	25	819
D	14	B-1	30	1027
E	21	B-1	30	1027
F	28	B-1	30	1027
G	21	B-2	35	1361
H	28	B-2	35	1361
L	35	B-2	35	1361
K	28	G	40	1848
M	35	G	40	1848

(*) construction materials: concrete 35 MPa, reinforcing steel 380 MPa
(**) construction materials: concrete 35 MPa, reinforcing steel 440 MPa

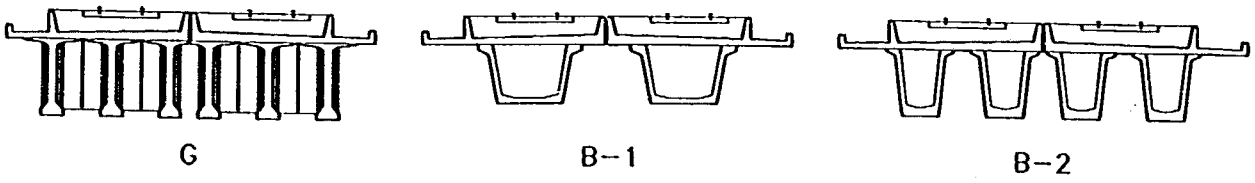


Fig. 1. *Typical deck sections: (a) G, (b) B-1, (c) B-2.*

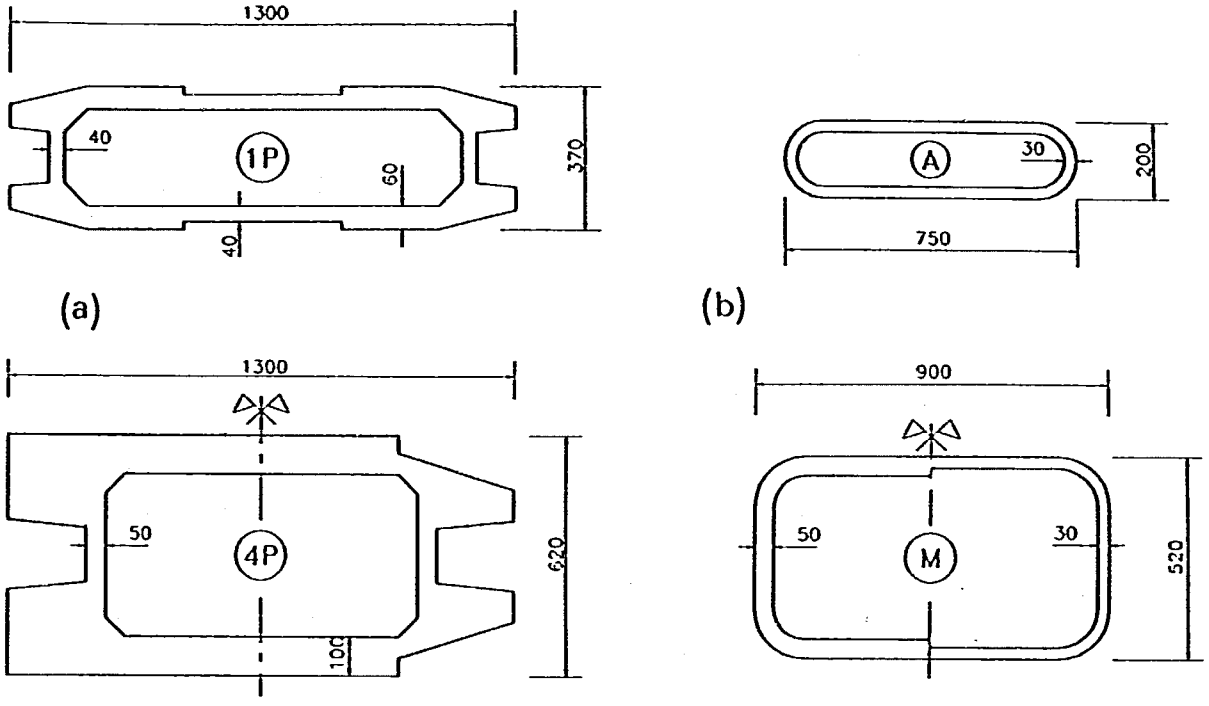


Fig. 2. *Typical pier sections: (a) "existing" line, (b) "new" line*

3.2 Seismicity model and seismic action

The seismic hazard of the entire NA-MI railway line, see fig. 1, has been evaluated following the scheme initially proposed by Trifunac [2]. The maximum spectral accelerations have been estimated via a three step procedure: (i) definition of a suitable seismic model, (ii) selection of the attenuation law, (iii) evaluation of the peak ground accelerations for several return periods. To this end, a map of the seismic history of the region has been defined and seismogentic zones have been characterised on the assumption that, within each zone, the occurrence rate of the seismic event should be approximately uniform or, with identical meaning, that the seismic event could occur with equal probability anywhere within the zone, fig. 4. Recent developed statistical methods have been used, together with the method proposed by Cornell [3], to account for the seismic catalog incompleteness, Van Dyck [4], and the spatial distribution of the historical seismic intensity, Mc Guire [5]. The attenuation law has been specialised to the Italian territory according to a formulation given by Sabetta [6], making use of empirical coefficients to account for epicentral distance, magnitude and site soil conditions. Using the above seismicity model and attenuation law the peak ground accelerations have been computed along the entire NA-MI railway line and the results are given in fig. 5, where the curves for several return period are shown. From the figure it is possible to observe that even for the highest return period (Tr = 2000 years) the maximum acceleration does not exceeds 0.325g.

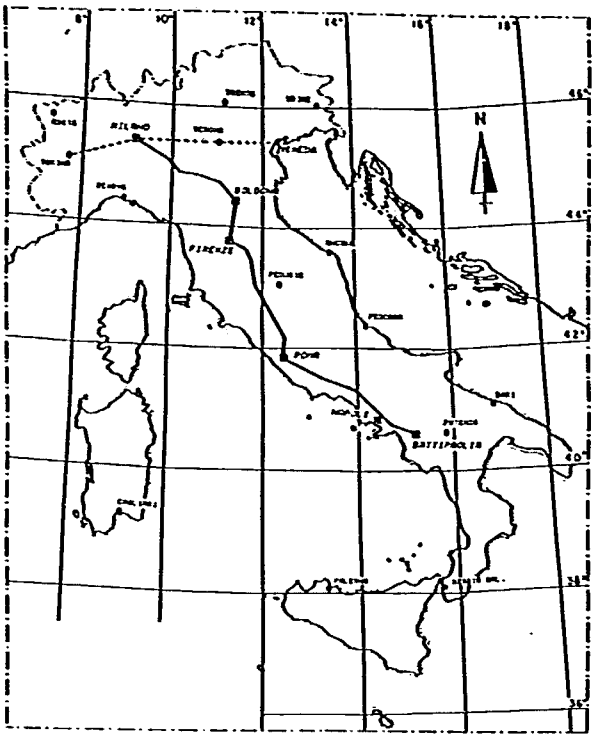


Fig. 3. *Italian high speed system (solid line = NA-MI line)*

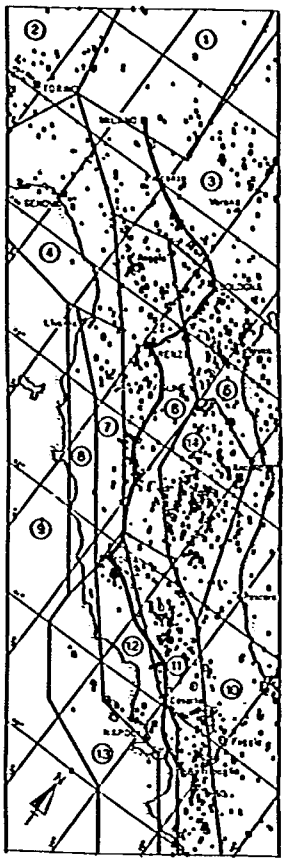


Fig. 4. *Map of seismic events M ≥ 4, period 1000 - 1980*

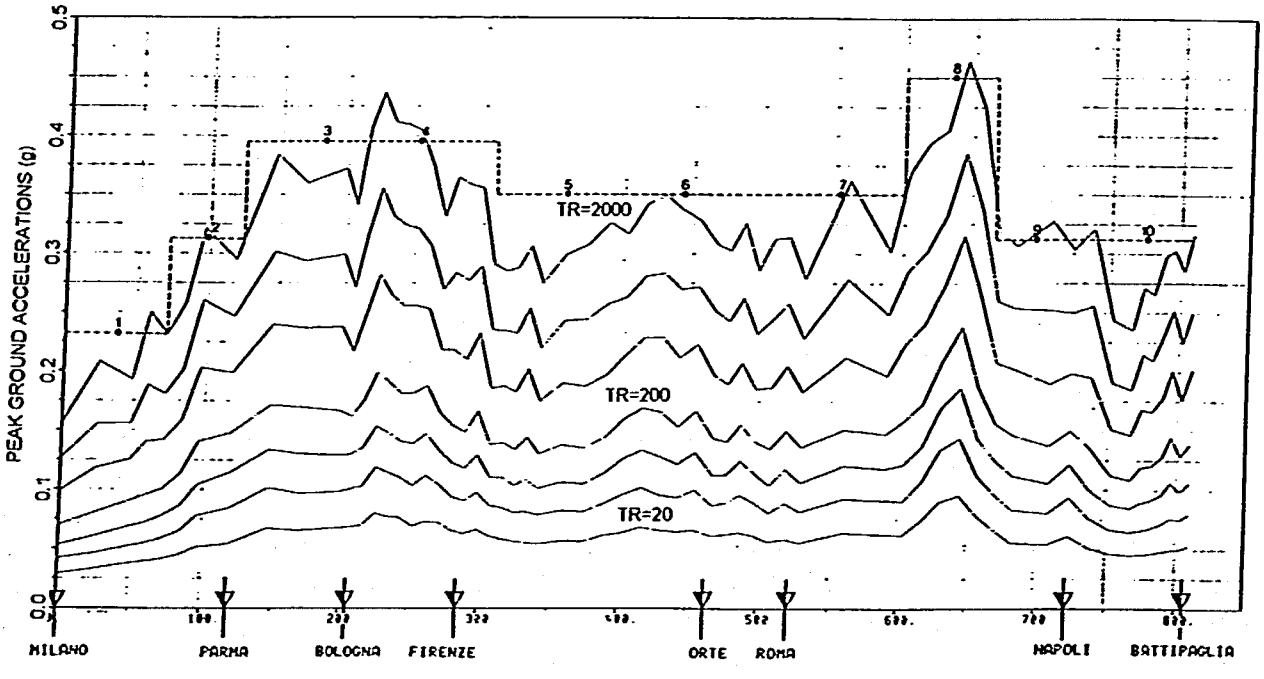


Fig. 5. *Peak ground acceleration along the NA-MI line for different Tr. (dashed line = sections with homogeneous seismicity)*

According to Trifunac [2], the acceleration spectra of the ten sections with homogeneous seismicity in fig. 5 have been computed. Three different soil conditions (DA - deep alluvium, SA - shallow alluvium and R - emerging bedrock) have been considered, together with a damping value of 5% of critical. The acceleration spectra have been subsequently normalised to unitary peak ground acceleration, aiming at comparing the spectral shapes, and a large scatter has been observed. However, if the same comparison is limited to the same soil conditions some degree of homogeneity emerges, see e.g. fig. 6, also if different return period are considered (Tr = 20, 200, 2000 years). For the present purposes it has been assumed to associate a single spectral shape to each soil condition, independently of the site location and the return period considered. The selected design spectra are shown in fig. 7, superposed for the three soil conditions.

Finally, a large screening of the Italian acceleration records has been performed in order to extract records whose normalised spectra adequately matching the proposed ones. In particular, three actual accelerograms have been selected for each design spectra and used as the input motion for the subsequent non-linear structural analyses.

To this end, they have been properly scaled on the basis of the results of the seismicity model of fig. 5. A close analysis of the figure led to conclude that three peak ground acceleration levels were sufficient to reproduce the effects of low, moderate and strong earthquakes. These levels, listed in table 3, are assumed identical for all of the three soil conditions, R, DA and SA.

Table 3. *Seismicity levels - normalised and absolute peak ground accelerations*

seismic intensity level	normalised peak ground accel. a/g	maximum peak ground accel. (m/sec^2)
1	0.1	0.981
2	0.2	1.962
3	0.3	2.943

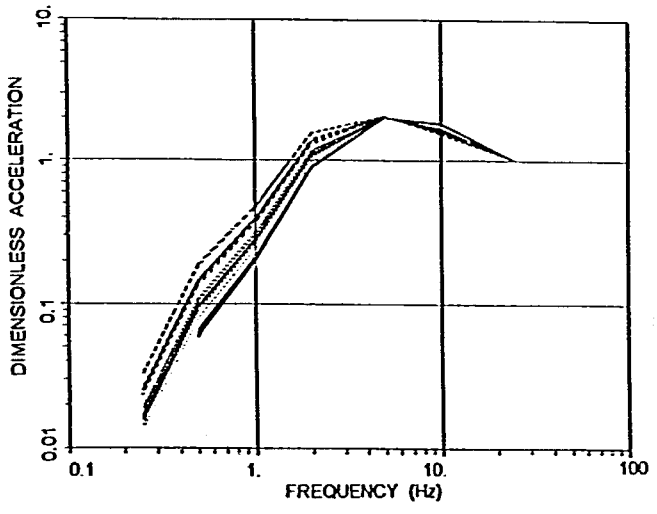


Fig. 6. *Normalised acceleration spectra*
shallow alluvium
solid - Tr = 20 years
dotted - Tr = 200 years
dashed - Tr = 2000 years

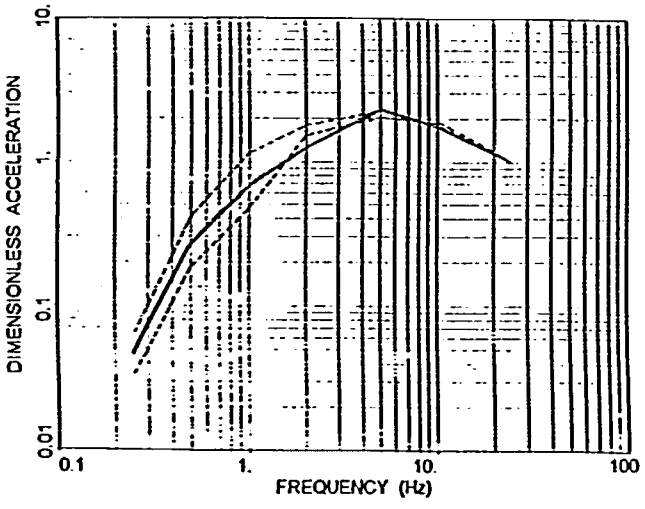


Fig. 7. *Design spectral shapes*
solid=rock
dashed=shallow alluvium
dotted=deep alluvium

3.3 Structural analyses

For the construction of the numerical models the following procedure has been followed: first, a local model simulating the nonlinear response of the cross section of typical structural members has been defined according to the prevailing force resultants in the member, then a global model of the whole structure, incorporating the local models, has been used for the structural analyses.

3.3.1 Local models

The local model should account for the actual behaviour of a beam section subjected to repeated, amplitude varying loads. Different models have been proposed in the literature with different degree of sophistication; however, in the present case, the leading feature in selecting a proper model was based on the primary consideration of the huge computer time requested by the very large number of analyses to be carried out. In fact, such analyses must be repeated for the different soil condition, the different acceleration levels and the different structural types, including also the soil-structure interaction and the addition of isolating devices.
It has been therefore preferred to adopt a very efficient model from a computational viewpoint, Brancaleoni [7], and to pay this choice in terms of the addition of a further step necessary to estimate, within the required accuracy, the constitutive parameters of the model. The procedure adopted is as follows: (i) a very simple, but also very time consuming model, has preliminary been used to obtain a pseudo-experimental behaviour of a beam section subjected to prescribed axial force and bending moment. The model is based on a fibre discretization of the section, allows for an exact reproduction of the section geometry and accounts for the concrete and reinforcing steel interaction, Capecchi [8]. The main advantage of this kind of model is that only the basic mechanical properties of the constitutive materials are requested. In the present case they are given by the elastic moduli and the bilinear stress-strain curve, table 4.

Table 4. *Mechanical properties of the constitutive materials*

material	compressive strength (MPa)	tensile strength (MPa)	elastic modulus (MPa)	strain elastic limit (%)	strain rupture limit (%)
concrete	35	0	33600	0.1	1
steel	440	440	210000	0.2	1

The number of the member cross sections modelled by the fibre-model is given by the number of structural typologies times the number of section variations along the pier height, see table 2 and fig. 2. Each model has been subjected initially to a monotonic loading until collapse occurred and then to a cyclic loading (3 cycles) with increasing amplitude up to a certain amount of the ultimate curvature, approx 60%. A typical result is shown in fig. 8, in terms of bending moment (M) and curvature (χ) relations where the monotonic as well as the cyclic responses are plotted for the case "M" of table 2.
From the monotonic behaviour the initial elastic branch and the subsequent cracking branch can be evaluated, whereas from the cyclic behaviour a strong pinching effect can be observed, together with a stiffness variation from the first loading branch to the repeated loading ones. All these feature can be reproduced using a synthetic model derived from the endochronic theory of plasticity available from Brancaleoni [7]. Main features of the model are a continuous transition from elastic to inelastic states, modelling of hardening, softening and pinching-like

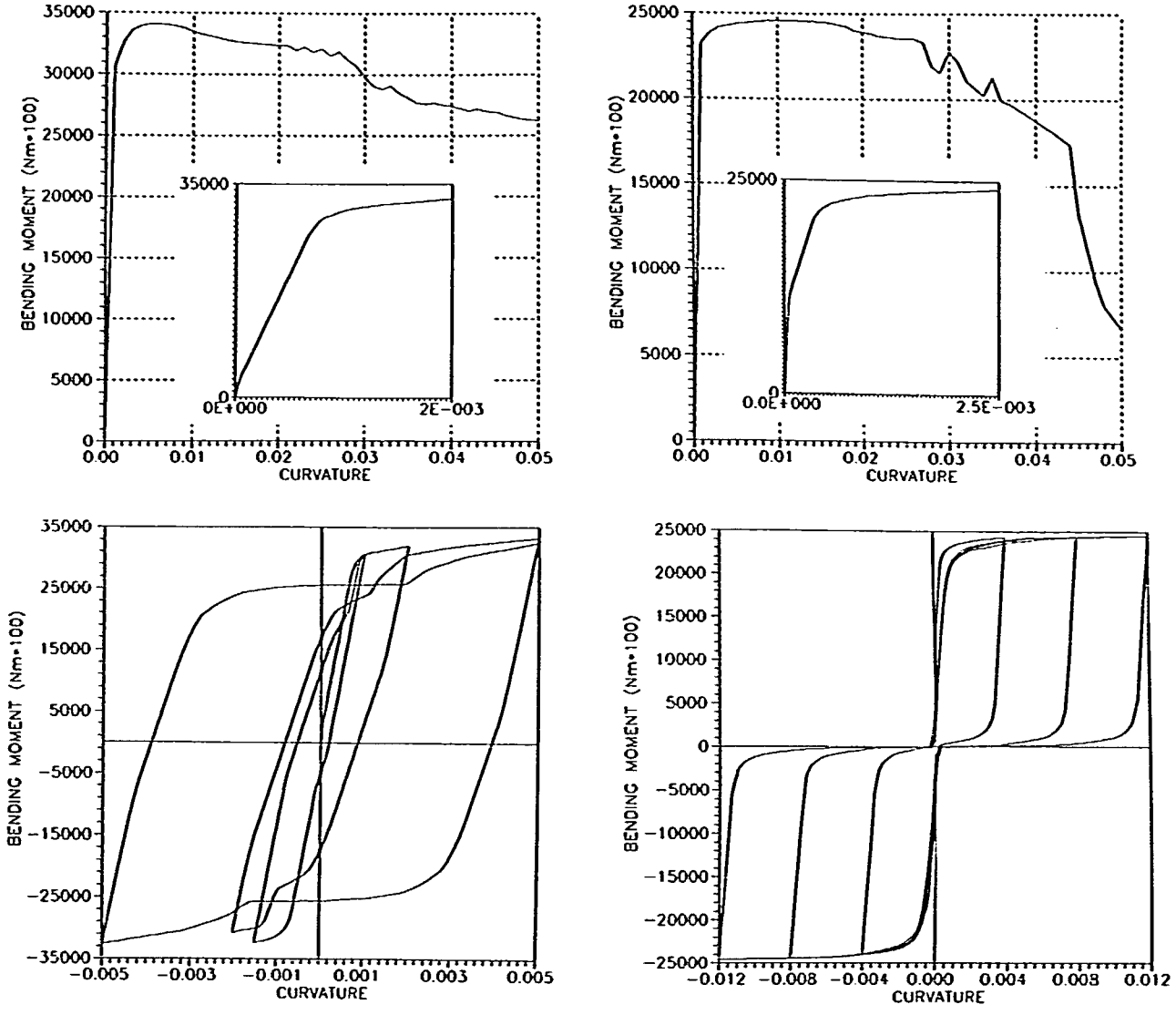


Fig. 8. *Monotonic and cyclic M - χ relation - (a) case 1P, (b) case 3P.*

behaviour, material degradation, different unloading and reloading patterns, nonsymmetric behaviour. However, the model, formulated using a single non-linear differential equation, depends on more than 15 parameters, that can vary with the loading history: hence, a non linear minimisation procedure was performed to estimate the optimal values to adopt for the said parameters, Ciampi [9]. To this end the response of the fibre-model has been assumed as "true" result and fitted by the synthetic model.

3.3.2 Global models

The bridges have been treated as plane structures lying in the vertical plane containing the longitudinal bridge axis. In this plane, they present the static scheme of simply supported beams, with the decks acting simply as dead masses at the pier top. The piers themselves are the critical elements during a seismic event and have hence been accurately modeled, using plane beam f.e. elements incorporating the local model discussed, Ciampi [10]. Moreover, the

4. DESIGN CRITERIA

The performance indicators apt to characterise the performance levels, table 1, have been computed from the results of the numerical analyses carried out and are plotted in fig. 9 for the "BASE" case and in fig. 10 and 11 respectively for the "DIS" and the "IN" cases. Each figure shows the results in terms of the average (avg.) and maximum (max.) values for the three acceleration levels considered. It is important, for a correct interpretation of the figure, to understand that maximum stands for the maximum absolute response computed within 9 analyses (3 soil conditions x 3 acceleration records), whereas average stands for the average value of the 9 maxima, one for each analysis. No distinction is made in the figure between the average and maximum curves, however no confusion should arise since the average values are consistently smaller than the maximum ones. Finally, a break in the curves indicates the separation between the "existing" and the "new" structural types.
The highest values attained by the sectional ductility, by the horizontal displacement at the pier top and by the behaviour factors are listed in table 6 and 7, regardless the case considered. The sectional ductility relates to the structural safety, while the horizontal displacements relate to the serviceability conditions and, finally, the behaviour factors help for a better understanding of the structural performance.

Table 6. *Maximum values attained by the safety and serviceability indicators.*

seismic intensity a/g	χ/χ_y avg	χ/χ_y max	δ maximum avg (cm)	δ maximum max (cm)	δ residual avg (cm)	δ residual max (cm)
0.1	0.26	0.65	3.18	4.29	0.37	2.08
0.2	4.13	12.90	3.89	6.62	2.02	4.77
0.3	5.80	22.80	5.13	14.03	4.02	11.82

Table 7. *Maximum values attained by the behaviour factors.*

seismic intensity a/g	qT avg	qT max	qM avg	qT max
0.1	1.494	2.610	1.560	2.733
0.2	1.911	3.031	2.003	3.104
0.3	2.336	3.617	2.500	3.742

The comparison between table 6 and table 1 allows to establish guidelines towards the sought design criteria. In the case of the structural safety, the average values attained by the sectional ductility are within the limits given by the performance levels; this applies also to the maximum values if adequate consideration is given to the large response scatters that are typical in the seismic case. In conclusion all the considered typologies, and in particular the "new" ones, are able to sustain the seismic excitation even in the case of extreme events (Tr = 2000 years), therefore it can be stated that the piers do not need a detailed verification against the seismic action if the longitudinal reinforcement is at least 0.6% of the gross section. Major detailing necessitates the stirrups at least in special cases, a/g =0.3 case IN2, so as to guarantee the ductility requirements.

beam elements have been tuned from the base to the top to account for the cross section variations along the pier vertical axis, in terms both of geometry and reinforcing steel.

3.3.3 Numerical analyses

Using the seismic action defined in chapter 2 and the structural models discussed in paragraph 3.3.2 a series of numerical analyses have been performed to compute the seismic responses of the structural types listed in table 2. The analyses have been carried out using the f.e. program ANSR [11], on which the f.e. model described in 3.3.2 has been implemented. Because of the plane scheme assumed for the structure, only one of the two horizontal components of the acceleration records has been considered; between the two the one presenting the maximum peak ground acceleration has been chosen and then scaled to the acceleration levels of table 3. The seismic action was supposed to act in a direction parallel to the longitudinal bridge axis and no train presence has been considered. A set of 27 analyses (3 soil conditions x 3 acceleration records x 3 seismic intensities) have been performed for each one of the 15 structural types of table 2. Moreover, the analyses have been repeated according to different hypotheses for the structural behaviour. The total set of cases is listed in the table below:

Table 5. *Performed analyses*
"Y" means a complete set of 27 analyses for that case - "-" means no analyses

id code	BASE	RS	IN1	IN2	DIS
1P	Y	-	-	-	-
2P	Y	-	-	-	-
3P	Y	-	-	-	Y
4P	Y	-	-	-	-
A	Y	Y	Y	Y	Y
B	Y	-	-	-	-
C	Y	Y	-	-	Y
D	Y	Y	Y	Y	Y
E	Y	Y	Y	Y	Y
F	Y	Y	Y	Y	Y
G	Y	Y	-	-	Y
H	Y	Y	-	-	Y
L	Y	-	-	-	-
K	Y	Y	-	-	Y
M	Y	Y	Y	Y	Y

The label BASE in table 5 stands for basic case that fully agrees with the above descriptions for the seismic actions and the structural models. The other labels refer to modified structural models to account for loss of stiffness in the pier due to cracking (RS), soil-structure interaction (IN) and isolating device presence (DIS). In particular, in the "RS" case no modification has been made to the structural model and only a revised set of material parameters for the endochronic model has been re-computed. In the "IN" case pile foundations have been assumed and two different types of interaction have been considered between the pile group and the soil, point resistance (IN1) and shaft resistance (IN2); in this case sway and rocking elastic springs have been added to the structural model at the pier base, the IN2 values are one half of the corresponding values for IN1. In the "DIS" case an elastic-perfectly plastic spring has been inserted between the pier top and the deck mass to simulate the presence of a isolating device; the device stiffness has been taken 10 times the pier stiffness and the device max. force has been taken 1.5 times the braking force of the train.

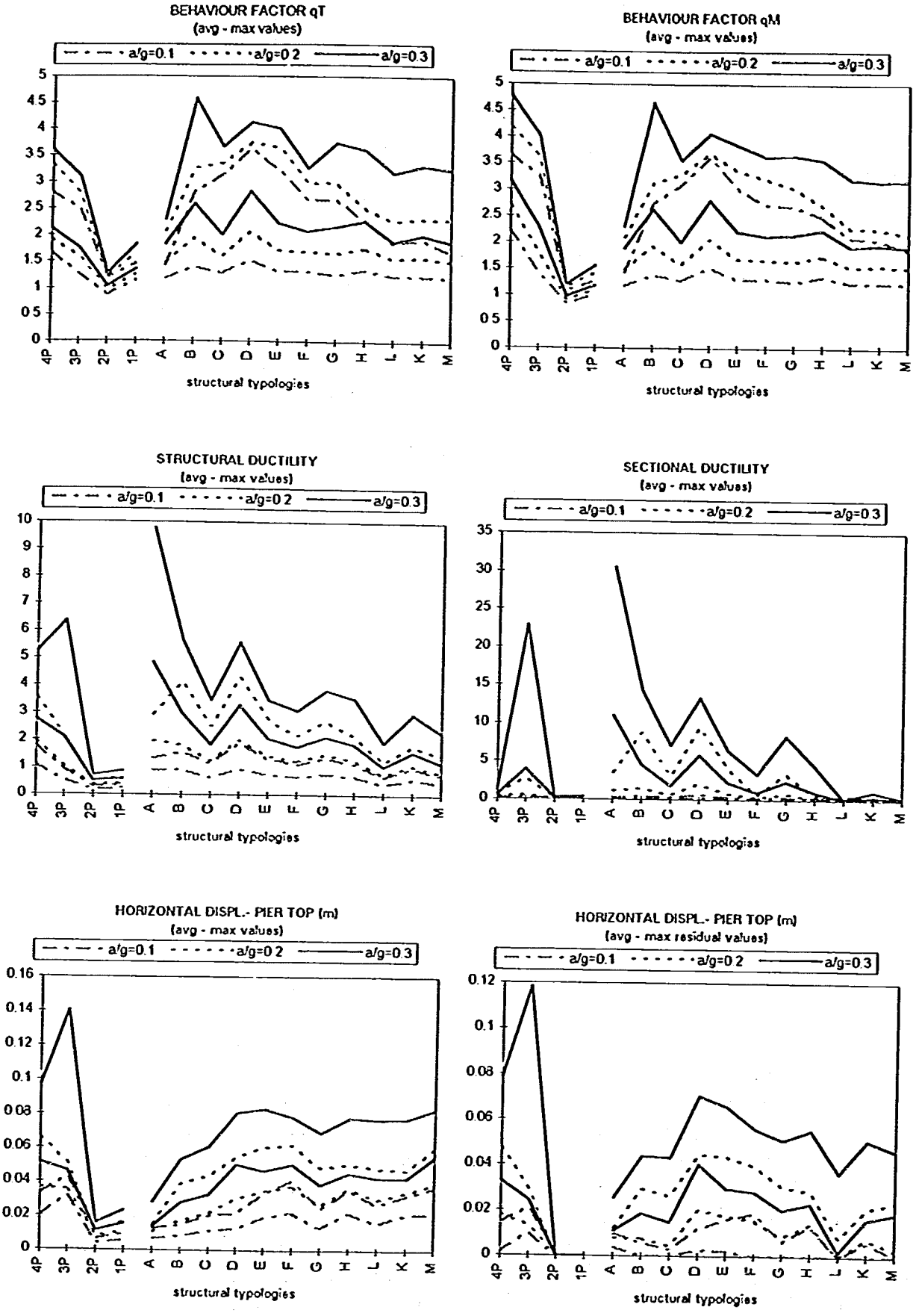


Fig. 9. *Performance indicators vs. acceleration levels and structural types - BASE case*

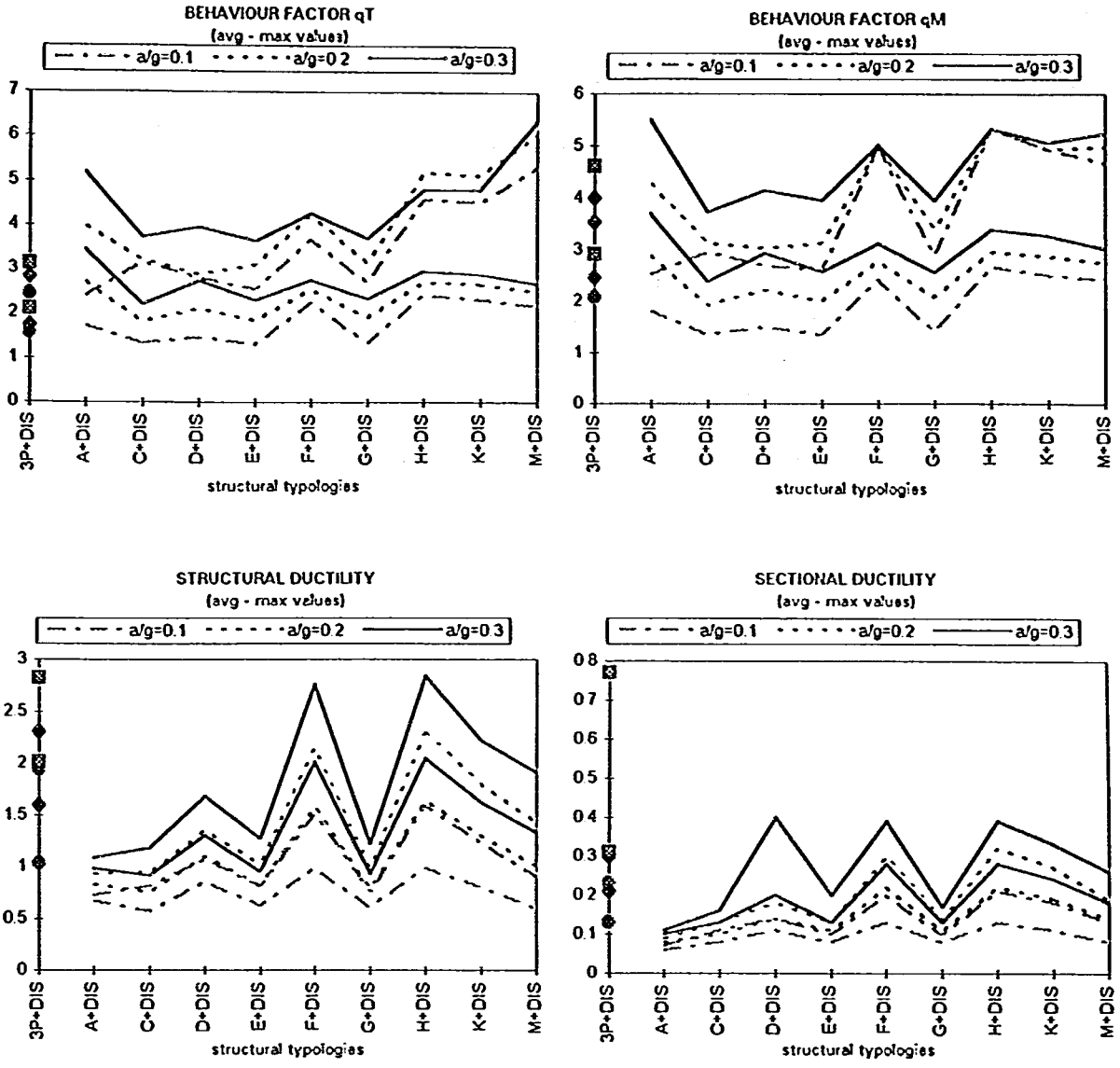


Fig. 10. *Performance indicators vs. acceleration levels and structural types - DIS case*

In the case of the serviceability conditions, the same considerations do apply, but in the present case it appears exaggeratedly conservative to associate in a one to one correspondence the three seismic intensity levels to the three performance levels. In fact, with the only exception of the a/g = 0.3 - 3P case, all the other computed values are well below the accepted limits. The same results hold if the "RD" instead of the "BASE" case is evaluated. In this instance, the horizontal displacements increase up to 130% of the corresponding values in the "BASE" case, therefore it appears acceptable to associate the seismic intensity level 3 (a/g = 0.3) to the performance level 2, so that also in the case of extreme events (Tr = 2000 years) train derailment and damage to the ballasted tracks are not probable.

The analysis of the behaviour factors can help to understand deeply the above results and also to give light on some important modelling assumptions. Preliminary it is possible to note that both qT and qM are always greater than unity, therefore some cracked region in the piers should appear already in the case of small seismic intensity, a/g = 0.1. This is confirmed by the relative values attained by the structural and sectional ductility; in fact, as long as a/g = 0.1, the structural ductility is greater than the sectional ductility and this confirms the spread of cracking, on the contrary as long as a/g increases up to its maximum, a/g = 0.3, both the

ductilities increase, but the sectional ductility becomes more and more pronounced with respect to the structural one. This means that a plastic hinge has been forming and developing in a cross section of the pier. In conclusion, the structural model adopted should account for a proper definition of the reduced stiffness due to cracking effects and should be used solely together with a dynamic analysis, so as to be able to cope with the reduction of the seismic response as long as the reduced structural stiffness progresses. Moreover, the dynamic analysis should allow for the inclusion of a convenient number of modes, since the relation qM > qT, indicating clearly the importance of the higher order modes, holds true systematically.
Finally, the effectiveness of the isolating devices has been assessed through a cost-benefit analysis. The results indicated that the use of the isolating devices would be justified only if the seismic actions capable to induce severe damage to the bridges (structural ductility > 4) would have return period in the range 1 to 10 years. Since in the present case such seismic intensities are related to return period of the order of 1000 years, it can be stated that it is not economically beneficial to fit up aseismic devices in the bridges.

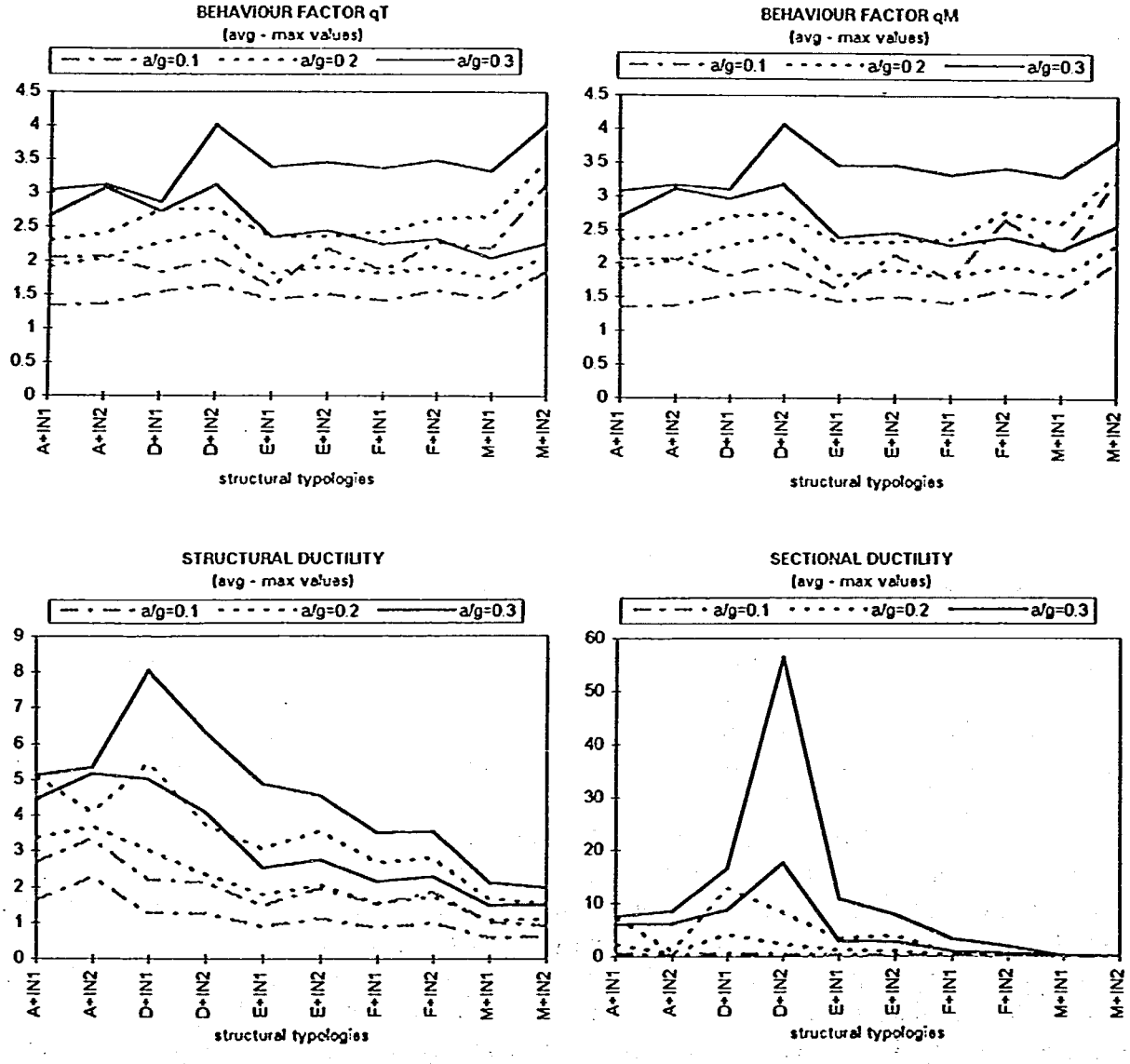


Fig. 11. *Performance indicators vs. acceleration levels and structural types - IN case*

5. CONCLUSIONS

All the points discussed are intended to draw preliminary design criteria for the assessment of the seismic performance of the Italian High Speed Railway system. Even if they originate from a large study carried out on the most representative structural typologies and hence maintain their own importance, it must be said that they necessitate to be confirmed by further, more comprehensive, analyses aiming to point out possible unexpected effects due to some limitations of the present investigation, i.e.: (i) no live load on the bridge, that is no train presence, (ii) absence of interaction between the structure and the ballasted tracks, (iii) plane model of the structure instead of a full tridimensional scheme.
Nonetheless general conclusions can be traced since now and they mainly concern the correlation between the seismicity levels and the performance levels that can be established on the basis of the structural types studied.
About the safety requirements, it has been found that one can establish a direct correspondence between the performance levels I, II and III and the peak ground acceleration 0.1g, 0.2g and 0.3g related respectively to return periods of 20, 200 and 2000 years. However, the more hazardous bridge members, the piers, do not need verifications against the seismic action as long as the cross sections maintain the assumed geometry, needing only a proper detailing of the reinforcing steel with particular attention to the transverse reinforcement in order to guarantee the ductility requirements.
Regarding the serviceability requirements, it has been assessed that also in the case of extreme events (Tr = 2000 years), train derailment and damage to the ballasted tracks are not probable.
The effectiveness of aseismic isolation devices was showns by a cost-benefit analysis to be low, indicating that they do not result economically beneficial convenient in the situation examined.
Finally, regarding the numerical models and analyses it has been found that adequate provisions must be made for the cracking behaviour of the pier and that dynamic analyses, including higher order mode contributions, are advisable to take into account the reductions of the seismic forces induced by the stiffness reductions due, in turn, to the cracking propagation.

REFERENCES

[1] FS - Italian National Authority for the Railway System: *Aseismic Design Criteria for Bridges of the New High Speed Railway System* (in italian), 1993.

[2] Trifunac M.D. "Effects of Site Geology on Amplitudes of Strong Motion", Proc. of the 7th World Conference on Earthquake Engineering, Istanbul, 1980.

[3] Cornell, C. A.: "Engineering Seismic Risk Analysis", *Bulletin of the Seismological Society of America*, Vol. 58, No. 5, 1968.

[4] Van Dyck, J.: "Statistical Analysis of Earthquake Catalogs", *Thesis submitted in partial fulfillment for the degree of Doctor of Philosophy*, Massachusetts Institute of Technology, Dept. of Civil Engineering, Cambridge, MA, 1986.

[5] Mc Guire, R.K.: "FORTRAN Computer Program for Seismic Risk Analysis", *U.S. Geological Survey Open File*, Report 76-67, Washington D.C., 1976.

[6] Sabetta, F., Pugliese, A.: " Attenuation of Peak Horizontal Acceleration and Velocity from Italian Strong Motion Records", *Bullettin of the Seismological Society of America*, Vol. 77, No. 5, 1987.

[7] Brancaleoni, F., Ciampi, V., Di Antonio, R.: "Rate-Type models for Nonlinear Hysteretic Structural Behaviour", *Inelastic Structures under Variable Loads*, Proc. of the EUROMECH Colloquium n. 174, Palermo, Italy, october 1983.

[8] Capecchi, D., Ciampi, V., Vestroni F.: "A model for reinforced concrete beam elements subjected to repeated load cycles" (in italian), *CEB Bullettin* n. 132, International AICAP - CEB Symposium, Rome, Italy, May 1979, pp. 105-113.

[9] Ciampi, V., Nicoletti, M.: "Parameter Identification for Cyclic Constitutive Models with Stiffness and Strength Degradation" *Proc. of the 8th European Conference on Earthquake Engineering*, Lisbon, Portugal, 1986.

[10] Ciampi, V., Carlesimo, L.: "A Nonlinear Beam Element for Seismic Analysis of Structures" *Proc. of the 8th European Conference on Earthquake Engineering*, Lisbon, Portugal, 1986.

[11] *ANSR: Static and Dynamic Analysis of Nonlinear Structures*, A computer program by NISEE/Computer Applications, Report No. EERC 75-10, Berkeley, California, march 1975.

JAPAN SIDE

Effect of Geological Irregularities on Ground Motion Characteristics

by
Ryoji Hagiwara[1] and Riki Honda[2]

[1] Head, Ground Vibration Division, Public Works Research Institute, Ministry of Construction, Japan
[2] Researcher, ditto.

ABSTRACT

In the recent studies, it has been said that the ground motion is amplified on the ground which has irregularity in layer configuration or soil properties, causing severer damage on various structures or ground itself than it would on the horizontally layered ground.

In this study, amplification characteristics of ground motion on the various grounds with relatively simple irregularity are investigated through the finite elements method analyses (FLUSH) to seize how ground condition's irregularity affects. In order to see the amplification purely due to the irregularity of ground condition, amplification is evaluated by the comparison of the results of the two dimensional analyses by FLUSH and the one dimensional analyses by the multiple reflection method (SHAKE), in which the effect of ground condition irregularity is not considered.

Based on the results of these investigation, method to evaluate the amplification is presented and, to check its applicability, ground motion amplification in several other cases are calculated and compared with the value estimated by the proposed method.

INTRODUCTION

Through the investigation of damage caused by earthquakes, it has been found that on the ground which has geological or topographical irregularity, the seismic ground motion is amplified and causes severer damage. Based on the acceleration records, various studies (1) have been conducted based on the recorded accelerograms to clarify the mechanism how such amplification occurs.

Analytical approach through numerical computations, in which usually ground with simple irregularity are assumed, are also carried out by many researchers(2). Some of these studies have their aims in proposing computational methods for accurate computation of wave deflection, reflection, propagation etc. However, studies conducted from the view point of proposing the method to evaluate the amplification to be considered in practical seismic design of various structures, such as the study by Ejiri and Goto (3), are not so great in number.

It is certainly quite difficult to propose a precise method to estimate such ground motion amplification, because so many factors affects in various ways. The method to estimate the ground motion amplification to be considered in seismic design, however, is necessary, even if it does not give perfectly correct estimation, because, without such method, structures must be designed with unnecessary large safety factors, or insufficient seismic resistance.

OBJECTIVE

As is mentioned above, it is observed that on the ground with irregularity in topographical or geological condition, the ground motion is amplified and therefore a method to estimate such amplification of seismic waves on the irregular grounds is in urgent need so that such amplification can be taken into consideration in seismic design of various structures.

Considering this, the objective of our study is set to propose a method to evaluate the ground motion amplification to be considered in the seismic design on the irregular grounds.

Our final goal should be proposal of a method that can evaluate the ground motion amplification on any irregular ground with rational accuracy. However, the ground motion amplification is affected by so many factors including the size of the irregularity and the input motion characteristics, and it is almost impossible to carry out analyses that take all possible factors into consideration. Therefore in our study, the ground with rather simple irregularity is considered, as the initial step toward the final goal.

CONDITIONS FOR ANALYSIS

Ground Models Considered

The ground models considered in the two dimensional and one dimensional analyses are shown in Figure 1.

For the two dimensional analyses, ground models are made by changing the three following parameters: the inclination of the hard layer (θ), the thickness of the soft layer (H), and the impedance ratio (Ir). Among the three parameters, θ and H are shown in Figure 1. As the value for the inclination θ, $\tan\theta$=1/2, 1/4, 1/8 are assumed, and as the soft layer thickness, H=10m, 20m, 30m are assumed. The impedance ratio Ir is the ratio of impedance of soft layer to that of hard layer and it is defined as:

$$Ir = \frac{\rho_1 \cdot Vs_1}{\rho_2 \cdot Vs_2}$$

where

ρ_1 :unit weight of soft layer

ρ_2 :unit weight of hard layer

Vs_1 :shear wave velocity of soft layer

Vs_2 :shear wave velocity of hard layer, and as the value of it, assumed are Ir= 0.31, 0.48, 0.66 (Each corresponds to the shear wave velocity in the surface layer Vs_1=100, 150, 200m/s respectively.).

Changing these three parameters gives 3x3x3=27 types of ground models. One additional model, in which $\tan\theta$=infinity, H=30m and Ir=0.31 are assumed, is also considered. In total, twenty-eight models listed in Table 1 are considered. For all cases, the height of the ground model (H + H2) is 60m.

Soil constants assumed for the soft and the hard layer are shown in Table 2. The non-linearity of soil behavior is considered by equivalent linear method for the soft and the hard layers. As the equivalent linear soil property curve of the soft layer and the hard layer, the curve presented by Iwasaki, Tokita et al.(4) for the alluvial clay and the one presented by Iwasaki, Tatsuoka et al.(5) for the diluvial sand are employed respectively. The equivalent linear soil property curves are shown in Figure 2.

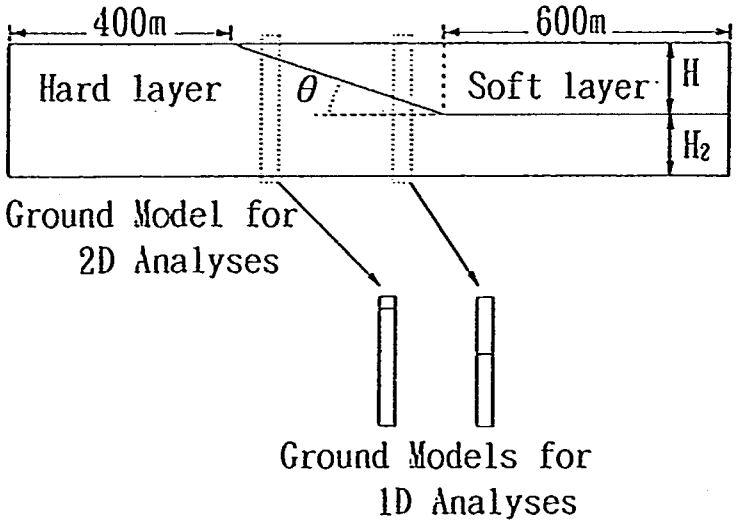


Figure 1 Gound Models for One and Two Dimensional Analyses

TABLE 1 ANALYSED GROUND MODELS

Model No.	Thickness of soft layer H (m)	Thickness of hard layer H_2 (m)	Inclination angle of hard layer θ tan θ	Shear wave velocity (m/s)		Impedance ratio
				Soft layer	Hard layer	
1	30		∞ (6.0)	100	270	0.31
2	10	50	1/2	100		0.31
3				150		0.48
4				200		0.66
5			1/4	100		0.31
6				150		0.48
7				200		0.66
8			1/8	100		0.31
9				150		0.48
10				200		0.66
11	20	40	1/2	100		0.31
12				150		0.48
13				200		0.66
14			1/4	100		0.31
15				150		0.48
16				200		0.66
17			1/8	100		0.31
18				150		0.48
19				200		0.66
20	30	30	1/2	100		0.31
21				150		0.48
22				200		0.66
23			1/4	100		0.31
24				150		0.48
25				200		0.66
26			1/8	100		0.31
27				150		0.48
28				200		0.66

TABLE 2 SOIL CHARACTERISTICS

	Soft Layer	Stiff Layer
Soil Type	Alluvial Clay	Diluvial Sand
Unit Weight(gf/cm^3)	1.55, 1.60, 1.65	1.85
Shear Wave Velocity (m/sec)	100, 150, 200	270
Poisson's Ratio	0.45	0.40
Soil Property	Non-linear *1	Non-linear *2

*1, *2 Nonlinearity of the shear moduls and damping ratio of the soil is accounted for by using the equivalent linear soil properties.

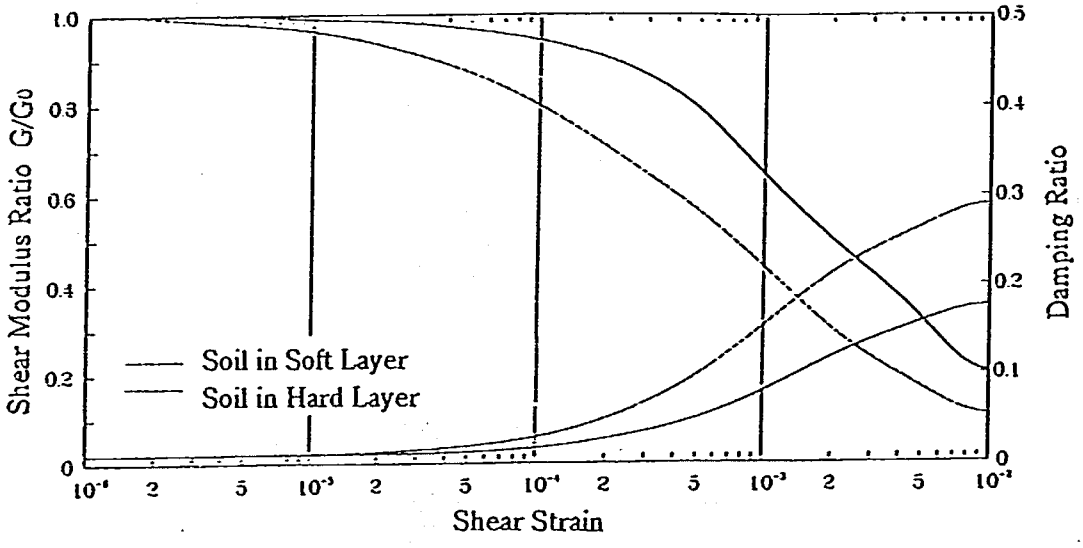


Figure 2 Assumed Dynamic Property Curves of Soils

Vertical displacement is fixed to zero for all nodal points on the both side ends and both vertical and horizontal displacement for the points on the bottom are fixed to zero.

In the one dimensional analyses to see the ground motion on the horizontally layered ground, as is shown in the Figure 1, the vertical section of the two dimensional model is employed as the ground model and all conditions such as soil properties, thickness of the soft and the hard layers are set equal to those of corresponding two dimensional ground model. The computation using these one dimensional models gives the ground motion which can be evaluated by the data obtained by vertical boring. Therefore, by comparing the results of the two dimensional analyses with these one dimensional cases, the amplification purely due to the irregularity condition can be observed.

Analysis Methods

Two dimensional seismic response analyses of the ground were carried out by FLUSH. One dimensional analyses to see the ground motion on the horizontally layered ground were carried out by SHAKE. Both are based on the equivalent linear method.

Input Ground Motion

Two incident seismic waves are employed for all ground models. One was recorded in the 1978 Miyagiken-oki Earthquake on the very hard ground near the Kaihoku bridge, and the other was recorded in the 1983 South Ibaraki-ken Earthquake on the relatively hard ground in the Public Works Research Institute. Figure 3 shows their time histories, Fourier spectra and response acceleration spectra for damping ratio of 5%. In the seismic response analysis, both waves multiplied by constants to adjust their maximum acceleration to 100gal, are employed. The input motion is assumed to be spatially uniform along the bottom line of the ground model.

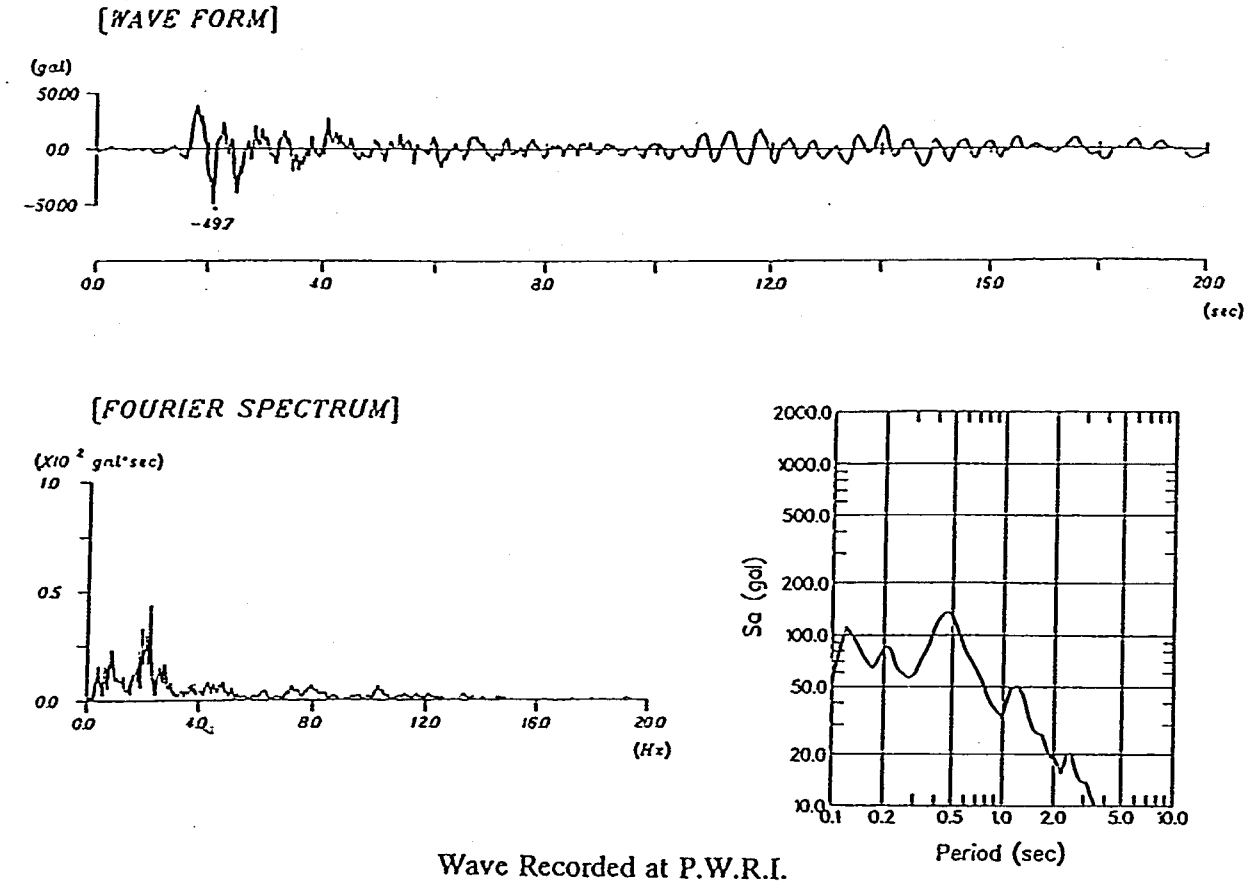
AMPLIFICATION DUE TO IRREGULARITY

Amplified Ground Motion on the Irregular Ground

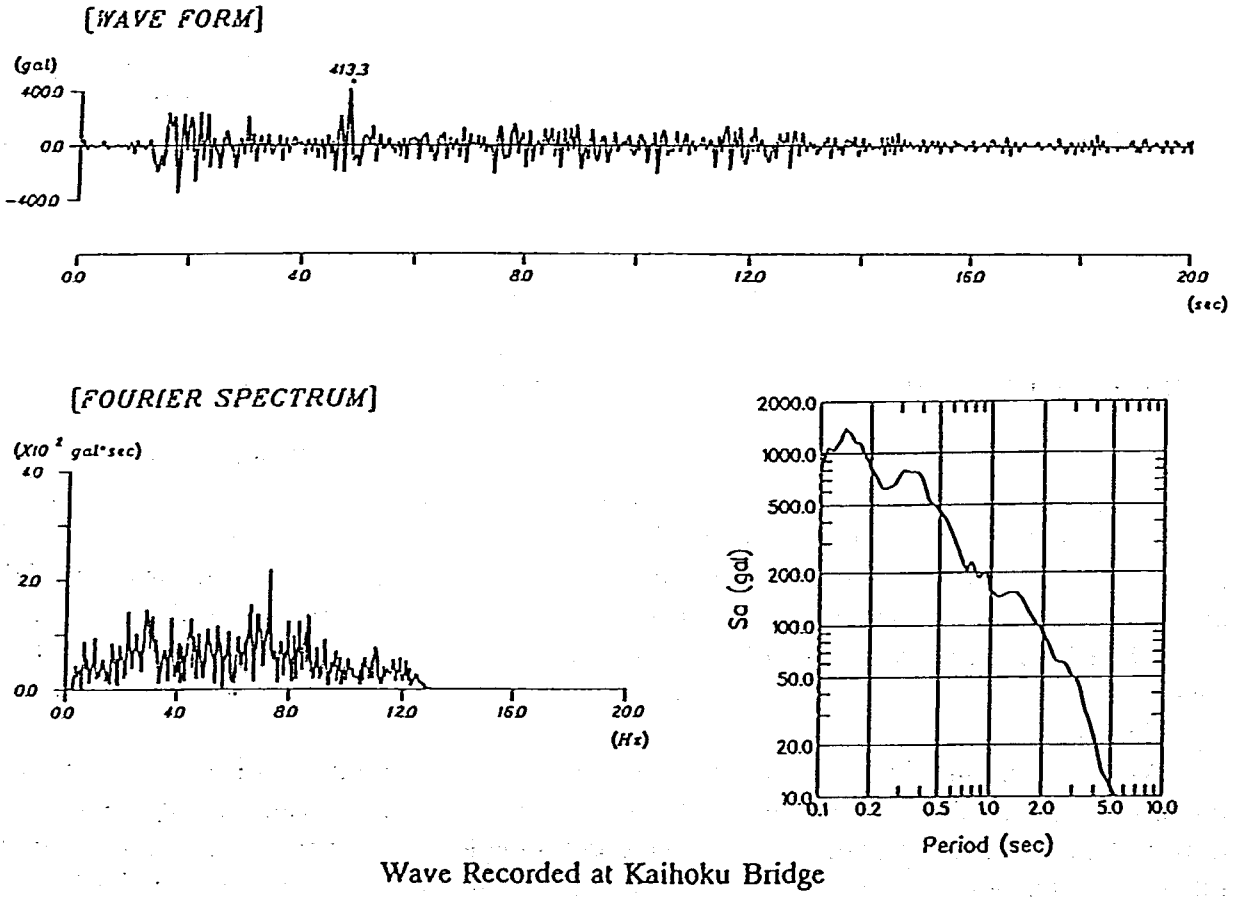
Ground motion on the irregular ground differs considerably for different models.

Figure 4 shows, as examples, the distribution of the maximum acceleration on the ground model 2, 4 and 23. Tangent of the inclination of the hard layer θ is 1/2, for the model 2 and 4, and 1/4 for the model 23. The thickness of the soft layer H is 10m for the model 2 and 4, and 30m for the model 23. The shear wave velocity in the soft layer of the model 2 and 23 is 100m/s (i.e. Impedance ratio Ir=0.31), and 200m/s (Ir=0.66) for the model 4. In these figures, the area between the two vertical dotted lines corresponds to the area where the hard layer inclines.

As is seen in this figure, the amplification of the ground motion is different for different models. On the model 23, for example, the maximum acceleration reaches 240gal while it is only 120gal on the horizontally layered area such as the left edge of the ground model. On the other hand, it should be also noted that only slight amplification is seen on the model 4.

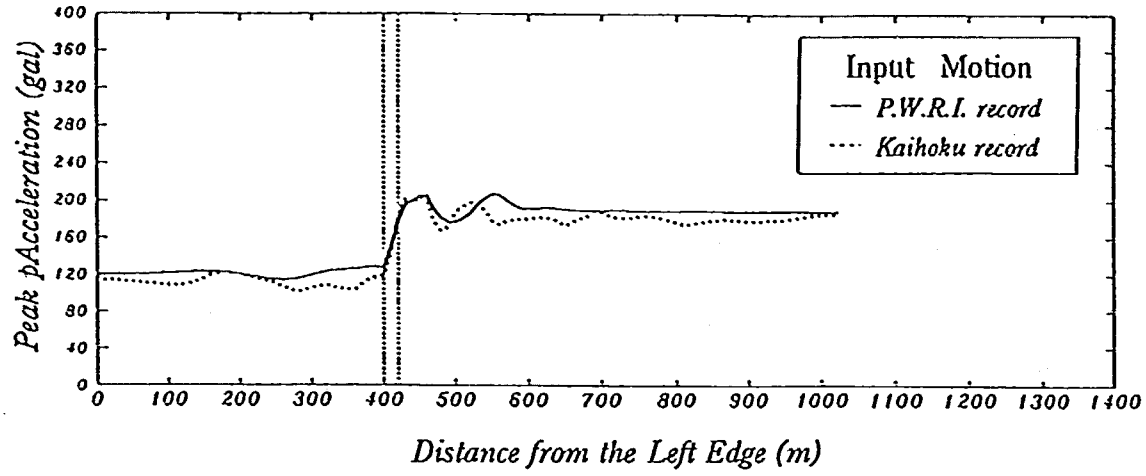


Wave Recorded at P.W.R.I.

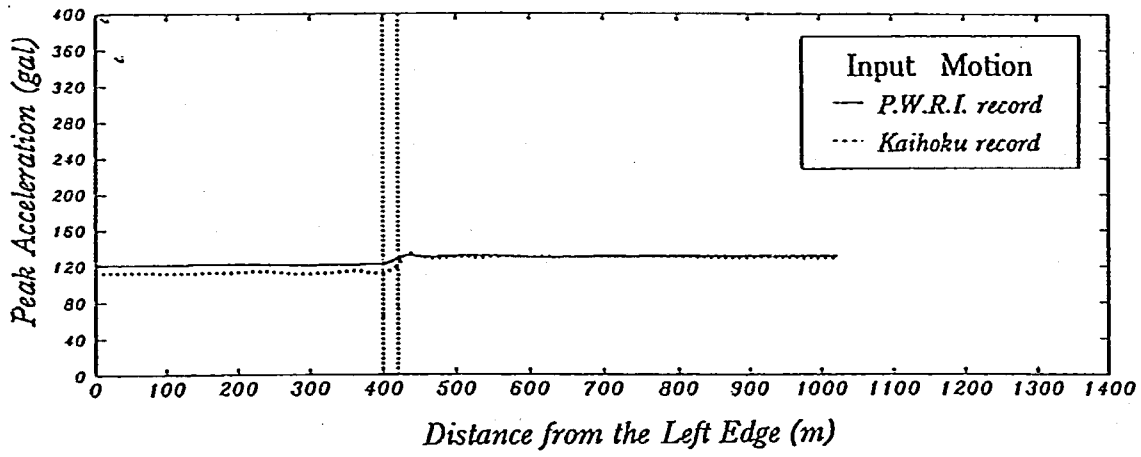


Wave Recorded at Kaihoku Bridge

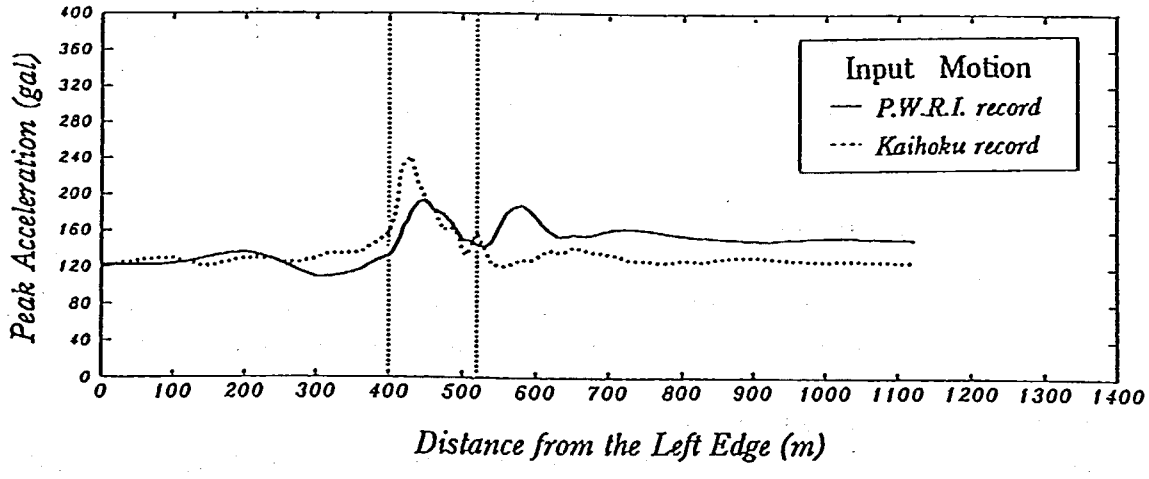
Figure 3 Time history, Fourier Spectra and Acceleration Spectra of Input Motions



(a) Model 2



(b) Model 4



(c) Model 23

Figure 4 Distribution of Peak Acceleration

It is not adequate, therefore, to assume a large seismic design force for every irregular ground. It is required to estimate how much ground motion amplification should be expected, so that it can be considered properly in seismic design.

Estimation of Amplification

In order to see the amplification purely due to the ground condition irregularity, amplification factor was measured by the ratio of the response acceleration of the ground motion computed by two dimensional analysis, to the response acceleration of that by one dimensional analysis. The latter can be regarded as the acceleration evaluated from the boring data of that site.

The amplification factor R(Sa) is defined in the following manner.

Let $Sa(T,x)_{2D}$ be the 5% damped response acceleration of the linear SDOF system with natural period of T for the ground motion at a certain point x calculated by two dimensional analysis. In the similar manner, let $Sa(T,x)_{1D}$ be defined as the response acceleration of the ground motion calculated by one dimensional analysis conducted on the vertical section of the two dimensional analysis model at the corresponding point x. Here, $Sa(T,x)_{2D}$ is calculated for every node on the ground model surface. But $Sa(T,x)_{1D}$ is calculated for seven vertical models. The thickness H of surface layers in these seven models are 0m, 5m, 10m, 15m, 20m, 25m, 30m. $Sa(T,x)_{1D}$ for the ground which is different in the thickness of layers from these seven models, is linearly interpolated. This does not affect the results so much because the configuration of the ground model is quite simple, consisting of only two layers.

Using these two response acceleration, R(Sa,T) is defined as:

$$R(Sa,T)=Sa(T,x)_{2D}/Sa(T,x)_{1D}.$$

Although R(Sa,T) is the function of x, for simple expression, it is not written explicitly. R(Sa) is the maximum value of R(Sa,T) in the range of natural period T from 0.1 second to 5.0 seconds (frequency = 0.2 to 10Hz). It can be regarded as the coefficient to adjust the seismic design force on the normal ground to the one on the irregular ground.

Two input motions are employed for each ground model and, because the soil property dependent on strain is assumed in the equivalent linear method, different input motion gives different amplification spectra. Tokita et al.(6), shows that the standard deviation of amplification factors for different four input motions, including the two used in this study, is about 10–15%. In this study, therefore, the amplification factor for each ground model is defined as the average of those for two different input motions.

Effect of Factors Considered

The effect of three factors considered in this study, H, Ir and θ are described below.

The maximum value of R(Sa) over the ground surface is defined as Rmax(Sa). The effect of factors is evaluated by investigating how each factor affects Rmax(Sa).

i) H : Thickness of the soft surface layer

The thickness of the soft layer plays important role in determining the amplification factor at the ground surface. Figure 5 shows the relation of the thickness of the soft layer H and the maximum amplification factor Rmax(Sa) for the cases in which the impedance ratio

Ir=0.31 (shear wave velocity in the soft layer is 100m/s) is assumed. It shows clearly that ground motion is amplified largely on the ground with the thick surface layer.

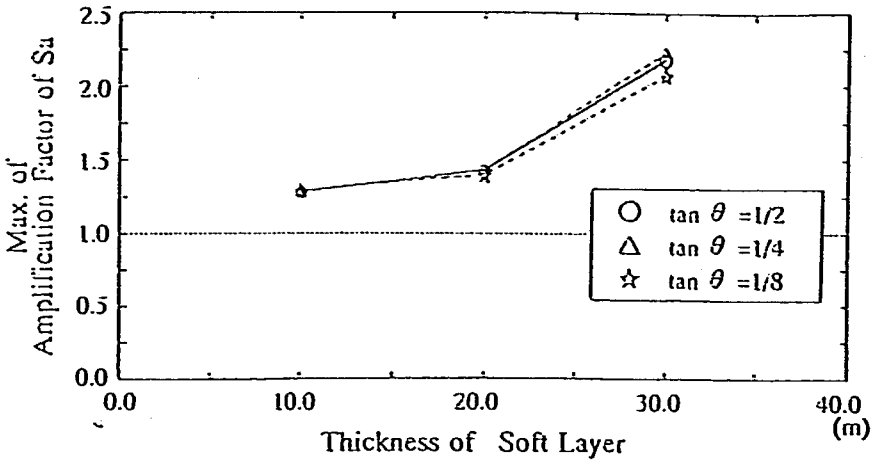


Figure 5 Relationship of the Surface Layer Thickness H
and the Maximum Amplification Factor Rmax(Sa)

ii) Ir : Impedance ratio

The impedance ratio is also important in determining the amplification factor. The relation of the maximum amplification factor and the impedance ratio for the cases with surface layer thickness H = 30m, is shown in Figure 6, which indicates that the softer the surface layer is, the larger amplification should be expected. The same trend is observed in the cases for which thinner surface layer (H = 10m and 20m) is assumed.

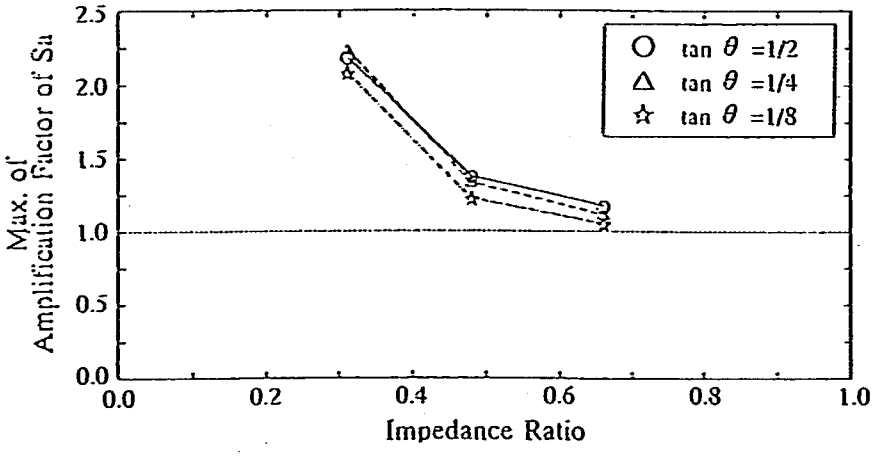


Figure 6 Relationship of the Impedance Ratio Ir
and the Maximum Amplification Factor Rmax(Sa)

iii) θ : Inclination of the hard layer

The inclination angle θ does not affect the amplification significantly. As is shown in Figure 5 and Figure 6, the amplification factor is almost same for different inclination angle θ.

The same tendency is also observed in the cases with different impedance ratio or different surface layer thickness.

Method for the Estimation of the Ground Motion Amplification

The results mentioned in the preceding section indicates that the amplification on the ground with the variation of surface layer thickness should be evaluated based on the index which involves the softness of the surface ground and its thickness. Our aim being to present the practical method to evaluate such amplification, the index must be easy to calculate and the data required for the calculation of the index must be easy to obtain. T_G, which is referred to as the traits of the ground in the specification for highway bridge design in Japan(7) satisfies these condition, because it has been used for long in designing to decide the ground type and can be evaluated from the data which is available from the ground boring data by a simple formula. T_G is defined as :

$$T_G = 4 \cdot \sum_{i=1}^{n} \frac{H_i}{V_i}$$

where

n : number of layers above the base.

H_i : thickness of the i–th layer.(m)

V_i : average shear wave velocity of the i–th layer. (m/sec)

T_G represents the fundamental natural period of the ground under the conditions that the displacement is fixed to zero at the upper surface of the underlying base and that the ground behaves elastically. It can be regarded as the fundamental natural period in the small strain range.

First, the maximum value of the amplification factor Rmax(Sa) is estimated based on T_G. ΔT_G is defined as the difference of the T_G at the point with the thickest surface layer and that at the point where no soft layer lies. Figure 7 shows the relation of ΔT_G and Rmax(Sa). There is close correlation among them. Regression analysis of them gives the formula to estimate the maximum amplification factor Rmax(Sa):

$$Rmax(Sa) = 0.885 + 1.481\Delta T_G \qquad \cdots(1)$$

which is also shown in the Figure 7 by a broken line.

Secondly, distribution of the amplification factor is considered. The distance from the origin to the point at which the maximum amplification is observed is referred to as L. The origin is set 100m left from the point at which the underlying hard layer reaches the ground surface, because amplification starts rising near that origin in most cases. Ls is the length of the area in which thickness of the soft layer varies. The definition of L and Ls is shown in Figure 8. The relation of the ratio of L to Ls and Ls is shown in Figure 9. Regression analysis of the data gives the formula to estimate the ratio L/Ls:

$$L/Ls = 116.590/L + 0.778 \quad \cdots(2)$$

which is also shown in Figure 9 with a broken line.

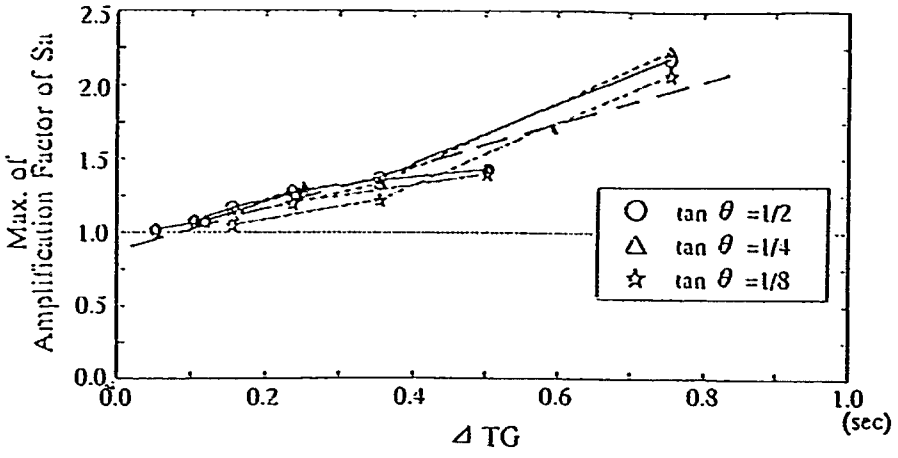


Figure 7 Relationship of the Maximum Amplification Factor Rmax(Sa) and ΔT_G

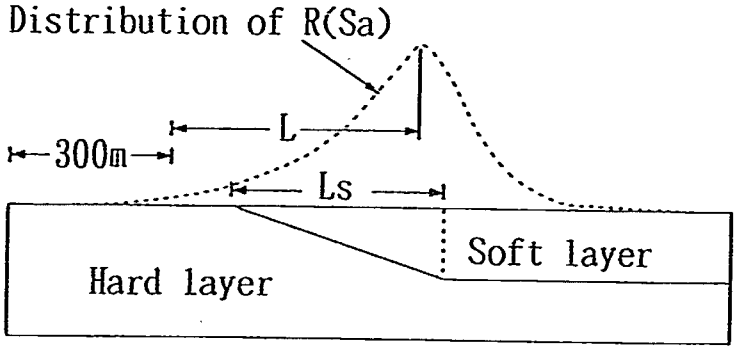


Figure 8 Definition of L and Ls

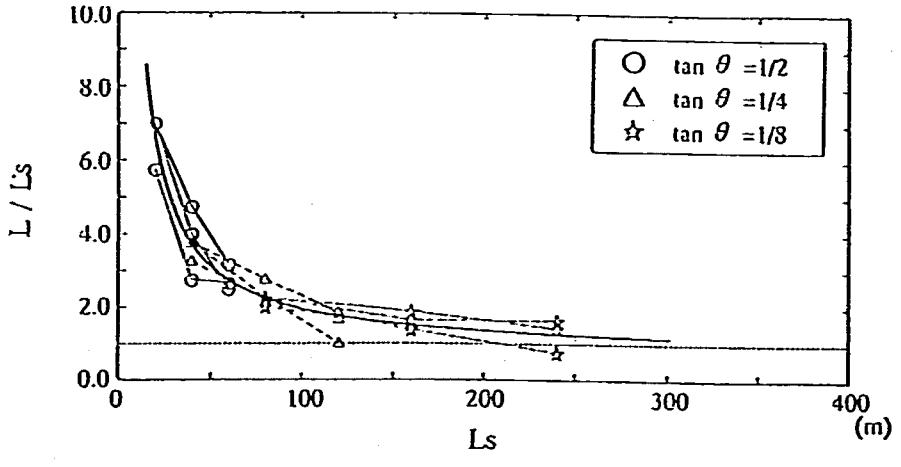


Figure 9 Relationship of L/Ls and Ls

Thirdly, the spatial variation of the amplification factor is considered. Judging from the results of the twenty-eight ground models, a function of the formula to estimate the amplification factor (R(Sa)) at point x, is assumed as:

$$R(Sa) = A \cdot (x/\beta)^{\alpha} \cdot \exp(1 - x/\beta) + 1.0 \quad \cdots(3)$$

where

A : (Rmax(Sa)−1)/(α^{α}•exp(1−α))

α : constant set to 10.

β : L/α

L : the point which gives the maximum of R(Sa). Given by equation(2).

Rmax(Sa) : Maximum of R(Sa). Given by equation (1).

where α is a constant to determine the sharpness of the distribution form.

In Figure 10, the estimated distribution of the amplification factor (by a rigid line) and the distribution of the calculated R(Sa) (by circles) for the model 2, 20, 23 and 24 are shown. The surface layer thickness H=10m for model 2 and H=30m for model 20, 23 and 24. The inclination of the hard layer tanθ=1/2 for model 2 and tanθ=1/4 for model 23 and 24. The impedance ratio is Ir=0.31 (shear wave velocity in the surface layer is 100m/sec) for model 2 and 4, and Ir=0.48 (shear wave velocity in the surface layer is 150m/sec). The estimated distribution show a reasonable agreement with the distribution of the computed values.

APPLICABILITY OF THE PROPOSED METHOD

Amplification factor on eight additional ground models are computed to see the applicability of the formula (3). In the additional cases, variables such as impedance ratio, shear wave velocity, thickness of the underlying hard layer, are changed from those of the original twenty-eight cases. The ground models analyzed are shown in Table 3 and the soil characteristics additionally assumed are shown listed in Table 4.

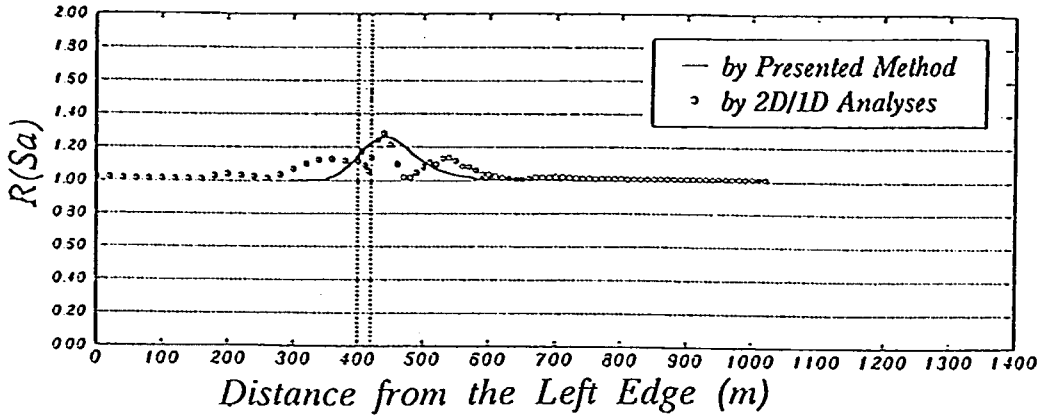
Model 29 and 30 are computed to see the effect of the thickness of the hard layer, and model 31 is to see the applicability of the presented method to the ground with the thicker surface layer.

In the analyses of the models 32 to 36, the shear wave velocities in the hard layer are adjusted so that the impedance ratio is equal to the values employed in the preceding twenty-eight cases. These are the cases to verify whether the method can evaluate correctly the effect of shear wave velocity even when the impedance ratio is not changed. In models 32 and 33, the surface layer thickness of 20m is assumed, and in models 34 to 36, the surface layer thickness of 30m is assumed.

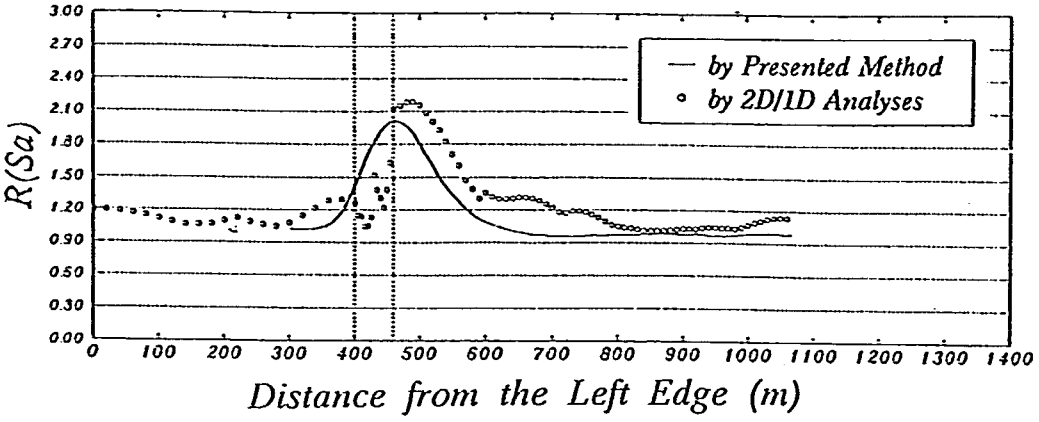
For all cases, the inclination of the hard layer is set as tanθ=1/2, because the preceding investigation indicates that the amplification is almost independent of the inclination angle.

The same soil type (alluvial clay for the surface layer and diluvial clay for the underlying layer), the same equivalent linear soil property curves and the same input motions are employed for these cases.

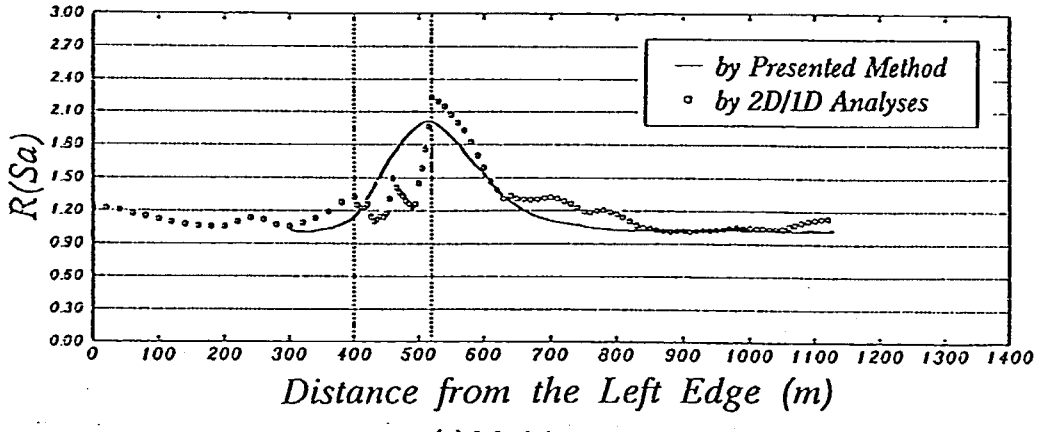
In Figure 11, the maximum amplification factors Rmax(Sa) for these eight models are



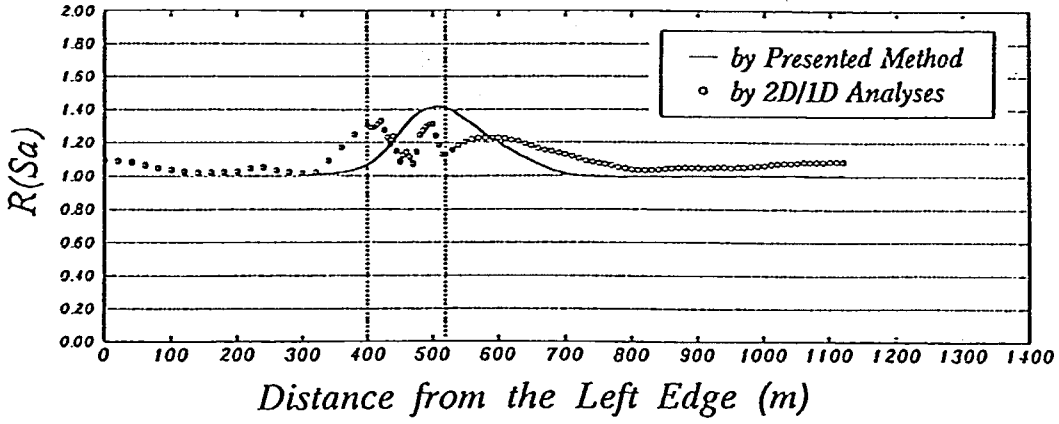
(a) Model 2



(b) Model 20



(c) Model 23



(d) Model 24

Figure 10 Distribution of Amplification Factor R(Sa)

plotted with the estimated value indicated by dotted line. Good agreement is seen for most cases, but model 31 is widely apart from the estimated value. This indicates that the amplification on the irregular ground whose soft surface layer is 40m thick or more requires further investigation.

TABLE 3 ADDITIONAL GROUND MODELS

Model No.	Thickness of soft layer H (m)	Thickness of hard layer H_2 (m)	Inclination angle of hard layer θ tan θ	Shear wave velocity (m/s)		Impedance ratio
				Soft layer	Hard layer	
29	20	100	1/2	100	270	0.31
30		200				
31	40	40				
32	20	40		100	180	0.47
33				150	405	0.32
34	30	30		125	270	0.40
35				100	180	0.47
36				150	405	0.32

TABLE 4 SOIL CHARACTERISTICS ASSUMED FOR ADDITIONAL CASES *1

	Soft Layer	Stiff Layer
Soil Type	Alluvial Clay	Diluvial Sand
Unit Weight(gf/cm³)	1.58	1.85
Shear Wave Velocity (m/sec)	125	180, 405
Poisson's Ratio	0.45	0.40
Soil Property	Non-linear *2	Non-linear *3

*1 As for the layer whose shear wave velocity is the same as those listed in Table 2, same condition is assumed.

*2, *3 Nonlinearity of the shear moduls and damping ratio of the soil is accounted for by using the equivalent linear soil properties.

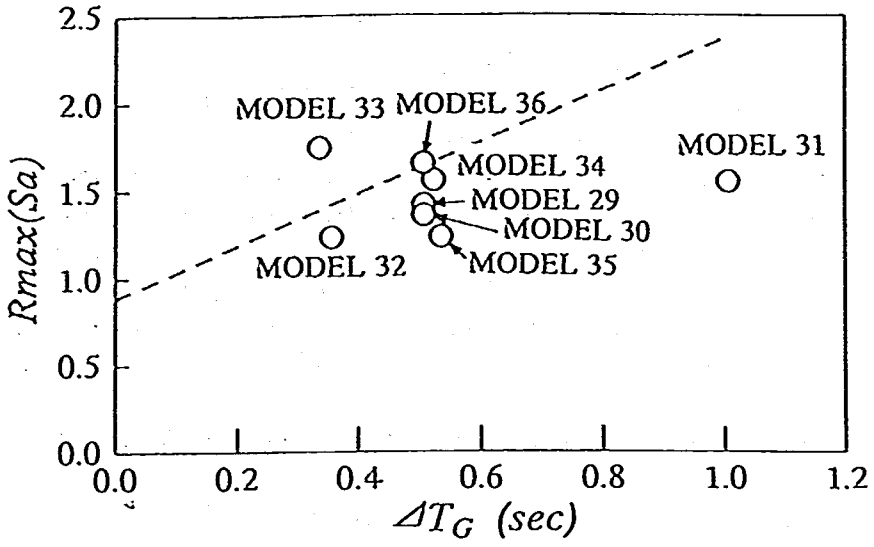


Figure 11 Comparison of the Maximum Amplification Factor Rmax(Sa) estimated by the Presented Method and that by the Analyses of Models 29-36

CONCLUSION

A practical method to estimate the amplification factor of the response acceleration on the irregular ground which has spatial variation of the surface layer thickness, is presented. The estimation formula is made based on the comparison results of the two dimensional and one dimensional computation conducted for the various ground models. The irregularity of the ground condition is measured by the variation of the traits of the ground T_G, which corresponds to the fundamental natural period in the small strain range. Usage of T_G makes the method more practical, because T_G can be easily calculated from the boring data and has been used in seismic designing. The presented method show good agreement with the twenty-eight cases dealt with in the first part. It also shows reasonable agreement for the additional cases, which are analyzed to see the applicability of the presented method.

Further study, however, is required to investigate the frequency band in which amplification is relatively large. The definition of the irregularly conditioned ground also remains to be determined, because the presented method indicates that the ground motion amplification is independent of the inclination angle of the surface layer, which means the amplification should be always taken into consideration in seismic design no matter how slightly the hard layer may incline. It is also required to investigate the amplification on the ground with the surface layer whose thickness varies in the different (usually more complex) manner.

REFERENCE

1) *for example,* Bard,P-Y et al.: "The Mexico Earthquake of September 19, 1985- A Theoretical Investigation of Large- and Small-scale Amplification Effects in the Mexico City Valley", Earthquake Spectra, Vol.4, No.3,(1988)
2) Takenaka,H: "Computational Methods for Seismic Wave Propagation in Complex Subsurface Structures", Jishin No.46 (1993) ,(in Japanese)
3) Ejiri,J and Goto,Y: "Introduction of Topographical Effects on Site Response for Design Spectra", J. of Japan Society of Civil Engineers. No.501/I-209 (1994), (in Japanese)
4) Iwasaki,T et al.: "Experimental Study on Dynamic Deformation Characteristics of soils", Report of Public Works Research Institute No.153(1980), (in Japanese)
5) Iwasaki,T et al.: "Dynamic deformation and Strength Characteristics of Alluvial Clay", 15th Japan National Conference on Soil Mechanics and Foundation Engineering (1980), (in Japanese)
6) Tokida,K et al.: "Effects of Geological Irregularities on Ground Motion Characteristics", Proc. of 10th WCEE, (1992)
7) Japan Road Association : "Specifications for Highway Bridges",(1990)

CONSIDERATION OF SOIL LIQUEFACTION POTENTIAL IN SEISMIC DESIGN OF HIGHWAY BRIDGE FOUNDATION

by

Yasuyuki KOGA [1], Yoshio NINOMIYA [2] and Masuo KONDO [3]

1)Director, Earthquake Disaster Prevention Department, Public Works Research Institute
2)Senior Research Engineer, Ground Vibration Division, ditto
3)Chief,International Cooperation Division, ditto

SUMMARY

This paper presents the efforts to mitigate the liquefaction-induced hazard for highway bridges in Japan. Firstly described briefly is a few examples of liquefaction-induced damage to bridges caused in past earthquakes. Secondly presented is the history of the development of soil liquefaction evaluation in the seismic design method of highway bridges, which includes current method in the latest version of Seismic Design Specifications of Highway Bridges issued by the Ministry of Construction in 1990. Thirdly assessment procedure of the safety of existing highway bridges against soil liquefaction is presented and some examples of strengthened highway bridges considering soil liquefaction are described. Finally some of the research themes currently undertaken by the PWRI to improve the design practice concerning soil liquefaction are introduced.

INTRODUCTION

It has been deeply recognized since the 1964 Niigata Earthquake that soil liquefaction causes extensive damage to various enginnering structures such as buildings, bridges, highways, railways, river dikes and lifeline facilities. Since then considerable efforts have been made to mitigate the liquefaction-induced damage to these engineering structures. Consequently practices to consider the effect of soil liquefaction have been introduced in the design of many engineering facilities.

This paper presents the consideration of soil liquefaction potential in seismic design of highway bridges in their construction, and practice for assessing the safety of existing bridges is also presented.

EFFECTS OF SOIL LIQUEFACTION ON STRUCTURE/FOUNDATION SYSTEM

The mechanism of soil liquefaction occurrence is now well understood. Furthermore the effects of soil liquefaction on structure and foundation system are:

1)The bearing capacity of liquefied subsoils decreases and their deformability increases.

2)Liquefied soils surrounding the foundation give additional force to the foundation.

3)Liquefied soils under some surface inclination or nonuniform overburden pressure show very large deformation.

4)The natural period of the ground is lengthened as the stiffness of liquefied soils decreases.

5)As the pore water pressure of liquefied deposit finally dissipates, the deposit consolidates and consequently its surface settles.

Strutures and foundations are damaged by one of or the combined effects above mentioned that liquefaction causes.

DAMAGES TO HIGHWAY BRIDGES INDUCED BY SOIL LIQUEFACTION IN THE PAST EARTHQUAKES

Table 1 shows the number of highway bridges which experienced seismic damages in the past from the Kanto Earthquake of 1923 to the Sanriku−haruka−Oki Eathquake of 1994 [1) 2)] . Table 1 indicates that over 3,000 highway bridges experienced seismic damages since 1923 till 1994 and 15 of these fell down.

According to the survey of the damaged bridges, major factors to cause damages to bridges are [1)] :

a) weakness of substructure,

b) weakness of bearing supports,

c) weakness of surrounding subsoils.

Reflecting on newly obtained engineering views from respective earthquake damages, seismic design practices of highway bridges in Japan have been occasionally improved.

After the experience of the Kanto Earthquake, the requirements for seismic design of highway bridges were first included in the "Details of Road Structures(Draft)" issued by the Ministry of Internal Affairs in 1926.

It was first recognized in the Niigata Earthquake of 1964 that not only strong earthquake motion but soil liquefaction of the subsoils causes extensive damages to bridge foundations. Wide areas of Niigata city, especially those along Shinano and Agano River which flow through the city, was underlain by loose sandy deposits with high groundwater level. Soil liquefaction occurred in such subsoils and caused extensive damages to many engineering structures such as buildings, bridges, embankments and lifeline facilities. The decks of the Showa Bridge, which had been constructed over the Shinano River, fell−off. This bridge [3)] was a 303.9 m long simple girder bridge with 12 spans, which had been completed just one month before the

earthquake. The design seismic coefficient for the substructure was 0.2. Two abutments and 11 piers were supported respectively by a row of nine steel piles of 609 mm in diameter and 22–25 m in length. Almost no damage occurred to the east side abutment and five piers. Conversely the west side abutment moved one meter toward the river center, adjacent four piers from 1st to 4th tilted to the same direction and two piers, 5th and 6th, completely fell down into the water. Consequently, movable shoe sides of five girders, from 3rd to 7th span from west side, and one total girder of 6th span fell down into the water. The reasons for this were assumed: 1)the bearing capacity of subsoils decreased because of liquefaction, 2)a landslide occurred near the west side abutment, 3)a large relative displacement occurred at the bearings of both ends of respective girders due to phase difference which might be caused because of small stiffness of pile foundations, and 4)all main girders were simple girders, whose ends had not been connected with each other and especially two girder ends placed on the 6th pier had been movable bearings, therfore they were quite likely to fall down. Reflecting on the experience of such damages to Showa Bridge a device to prevent bridges from falling off was developed.

On the contrary, Bandai Bridge [3] which had been also constructed over Shinano River experienced very little damage, which served effectively for the restoration of the area. It was a six span arch deck bridge, which had been constructed in 1929. Although it had considered the experienee of the Kanto Earthquake, it had not taken the seismic coefficient into account in its design. While two abutments settled 1.4 and 0.4 m respectively, small permanent deformation and slight cracks occurred for six central arch portions. Such a high seismic resistance despite of no earthquake resistant design was considered due to strong arch structures which connected girders adjacently and to the substructure.

Prior to the Niigata Earthquake of 1964, almost no studies had been conducted concerning soil liquefaction. But after this earthquake many past earthquake reports were reviewed from the view point of liquefaction. The survey clarifed that soil liquefaction did occur in many sites in past earthquakes and they were supposed to have contributed to many damages to engineering structures including the falling–off of the bridges in the Kanto Earthquake.

Even after the 1964 Niigata Earthquake, soil liquefaction ocurred repeatedly in major earthquakes such as the 1978 Miyagi–ken–Oki and 1983 Nihonkai–Chubu Earthquake. However soil liquefaction solely did not cause such critical damage to bridegs as falling–off. For example an approaching bank to Gomyoko Bridge in Hachirogata Lagoon, in Akita Prefecture settled excessively in the 1983 Nihonkai–Chubu Earthquake. It was observed that those settlements were caused by liquefaction of supporting sandy layers, however, Gomyoko Bridge itself had only very minor damages to reinforced concrete piers.

DEVELOPMENT OF SOIL LIQUEFACTION ASSESSMENT PROCEDURE IN THE SEISMIC DESIGN OF HIGHWAY BRIDGES

After experiencing serious damage due to soil liquefaction during the Niigata Earthquake of

1964, extensive studies have been made on assessment procedures of liquefaction potential by a number of researchers and organizations. As a consequence of these studies liquefaction assessment methods have been included in most seisimic design guidelines in Japan.

After the Niigata and the Tokachioki Earthquake in-situ SPT N-values were collected and several criteria assessing liquefaction potential based on critical N-value and soil gradation characteristics were proposed. This critical N-value method was first proposed right after the Niigata Earthquake based on the N-value records for buildings in Niigata city [4) 5)] . The concept of critical N-value was introduced into seismic design guidelines for many engineering structures such as harbour structures, highway bridges, buildings, railways in early 1970s.

In the 1971 version of Seismic Design Specifications of Highway Bridges, soil liquefaction was assessed on the basis of N-value:

a)sandy soil vulnerable to liquefaction:

Saturated sandy layers which have N-value less than 10, uniformity coefficient less than 6 and D_{50} between 0.04-0.5 mm are vulnerable up to a depth of 10m below the ground surface.

b)treatment of soil layers judged to liquefy:

Soil layers which were judged to liquefy in the above evaluation shall be neglected in calculating the bearing capacity of the foundation. Liquefied soil layers are assumed to work as an overburden pressure for the underlying layers.

On the other hand, Seed et al. proposed a procedure to assess liquefaction by comparing the liquefacton strength obtained from laboratory tests and shear stress calculated from dynamic analysis right after the Niigata Earthquake [6) 7)] . Furthermore collecting many SPT data for liquefied and non-liquefied sites and laboratory data, Seed et al. proposed another simple liquefaction assessment procedure [8)] . These procedures have been modified by many investigators in several points to produce quite a few different procedures although the principle is the same. They are included in many revisions of seismic design guidelines for such as highway bridges, buildings and railways.

Since the above 1971 version of Seismic Design Specifications of Highway Bridges, a more rational and quantitative method was pursued for soil liquefaction assessment. For this purpose dynamic shear strength of undisturbed samples were investigated by use of cyclic triaxial tests and its simple assessment procedure on the basis of SPT N-value and soil gradation characteristics was proposed [9)] . Besides simple method to estimate the dynamic shear stress in the ground from the surfacial design acceleration was also proposed. As a whole in the 1980 version liquefaction potential assessment procedure is summarized as follows.

1)Soil layers to be checked for liquefaction

Saturated alluvial sandy layers which have the water table within 10 m from the ground surface and have D_{50} values between 0.02 to 2.0 mm are vulnerable to liquefaction up to a depth of 20m below the ground surface, and liquefaction potential of these layers is to be

estimated according to item 2).

2)Estimation of liquefaction

For those soil layers which were judged to be vulnerable to liquefaction, liquefaction potential of these layers is estimated based on the liquefaction resistance factor F_L defined as

$$F_L = R / L \tag{1}$$

where

F_L :liquefaction resistance factor

R :resistance of soil elements against dynamic load defined as

$$R = R_1 + R_2 \tag{2}$$

$$R_1 = 0.0882\sqrt{\frac{N}{\sigma_v' + 0.7}} \tag{3}$$

$$R_2 = \begin{cases} 0.19 & (0.02\ \text{mm} < D_{50} \leqq 0.05\ \text{mm}) \\ 0.225\,\text{Log}_{10}(0.35 / D_{50}) & (0.05\ \text{mm} < D_{50} \leqq 0.6\ \text{mm}) \\ -0.05 & (0.6\ \text{mm} < D_{50} \leqq 2.0\ \text{mm}) \end{cases} \tag{4}$$

L :dynamic load induced in soil elements during an earthquake defined as

$$L = r_d \cdot k_s \cdot (\sigma_v / \sigma_v') \tag{5}$$

$$r_d = 1.0 - 0.015 \cdot z \tag{6}$$

$$k_s = \nu_1 \cdot \nu_2 \cdot \nu_3 \cdot k_{so} \tag{7}$$

z : depth from the ground surface(m)

k_s : seismic coefficient for evaluating liquefaction

k_{so} : standard design horizontal seismic coefficient for check of liquefaction(=0.15)

ν_1, ν_2, ν_3 : modification factors for zone, ground condition and importance

σ_v : total overburden pressure(kg/ cm^2)

σ_v' :effective overburden pressure(kg/ cm^2)

Soil layers with liquefaction resitance factor F_L Smaller than 1.0 are judged to liquefy during an earthquake.

3)Treatment of soil layers judged to liquefy

For those soil layers which were judged to liquefy in the above estimation the spring stiffness is reduced in seismic design by multiplying the original spring stiffness by the reduction factor D_E which is determined in accordance with F_L and tabulated in Table 2.

Following the revised version, a new version of the Seismic Design Specifications was issued in 1991. As to the liquefaction potential assessment, the estimation method for dynamic

strength R was changed reflecting on the recent research knowledge.

R is a resistance of soil elements against dynamic load defined as

$$R = R_1 + R_2 + R_3 \tag{8}$$

R_1 and R_2 are the same as in the 1980 version.

$$R_3 = \begin{cases} 0.0 & (0\% \leqq F_c \leqq 40\%) \\ 0.004F_c - 0.16 & (40\% \leqq F_c \leqq 100\%) \end{cases} \tag{9}$$

F_c :fine content

The rest are the same as those of 1980 version.

More new attempts for the future revision of the specificaton will be described in the later section.

SEISMIC INSPECTION AND STRENGTHENING BRIDGE FOUNDATION FROM THE VIEW POINT OF SOIL LIQUEFACTION

The nationwide seismic inspection and seismic strengthening of highway bridges were made in 1971, 1976, 1979, 1986 and 1991 by the Ministry of Construction. Liquefaction vulnerability of the supporting ground is one of the most important factors to be taken into account. Only the assessment procedure of the liquefaction vulnerability in 1991 inspection is presented here. Although the assessment procedure for liquefaction vulnerability is already included in the seismic design specification, seismic inspection for existing bridges has following difficulties through which assessment procedure for seismic design cannot be applied directly.

a) in−situ soil profile data are not sufficient for existing bridges
b) insufficient soil constants
c) influence of subsoil liquefaction on the structures must be adequately considerd
d) detailed seismic design of bridges cannot be conducted for a number of exisiting bridges

Considering such difficulties past cases of the bridges which were affected by the subsoil liquefaction were analyzed and a new simple procedure applicable to existing bridges was proposed.

Fig.1 shows the outline of inspection procedure of the bridges with emphasis of liquefaction estimation. It can be seen that liquefaction estimation is done in the 2nd and 3rd stage inspection. Liquefaction estimation is conducted gradually more in detail as described in the following. Fig.2 shows the inspection procedure for liquefaction and Table 3−5 are

inspection sheets in different stages for liquefaction evaluation.

More than 30,000 highway bridges have been investigated in 1991 seismic inspection of highway bridges. During this inspection, above procedure has been used to estimate the vulnerability of bridges against liquefaction. Following the stages of the procedure shown in Fig.2 in order, bridges necessary for more detailed inspection have been selected, and finally those which need countermeasures have been selected.

Although only the procedure used in 1991 seismic inspection was described above, some bridges had already been selected in the previous inspection which needed some measures against liquefaction. For the bridges which needed reinforcement against liquefaction, some countermeasures were to be sought. Some examples are described below.

First general countermeasures for the existing highway bridges against liquefaction are summarized in Table 6, which indicates that while only structural reinforcement can be applied for most of existing bridges, ground improvement can be used in combination for new construction of bridges.

Two case histories are illustrated in the following. One is a bridge that had experienced liquefaction-induced damage and then was rehabilitated. The other also is of a bridge that was strengthened against liquefaction based on seismic inspection.

1)Strengthening of a bridge damaged by an earthquake, Showa Bridge [10]

Showa Bridge which had been damaged by liquefaction in the 1964 Niigata Earthquake was strengthened by driving additional piles.

Fig.3(a) shows foundation dimensions before and after the strengthening, subsoil conditions and the liquefaction resistance factor F_L against design earthquake. The figure indicates that the factor F_L of the soil is less than 1.0 within about 10 meter below the riverbed. The post-earthquake study also revealed that the piles had been bent within the almost the same length. Thus liquefaction of the soil was presumed to have occurred within the depth.

The effectiveness of additional piles was examined according to the procedure of the Specifications for Highway Bridges, and the result is shown in Fig.3(b). The figure shows that the displacemnet decreaes significantly after strengthening. This result proves the effectiveness of additional piles.

2)Strengthening of an old bridge [11]

The bridge foundation was originally constructed with wooden piles with a diameter of 180 mm and a length of 7 m. Following enlargement works of the superstructure, prestressed concrete piles with a diametre of 300 mm and a length of 7 m were added, and the footings were enclosed by steel sheet piles of 10 m length to prevent scouring.

The seismic study conducted later had revealed that the soil within a depth of about 10 m was alluvial sand with SPT N-value of 10 to 30, and the liquefaction resitance factore F_L was around 0.6 to 0.9 against anticipated earthquake, resulting in insufficient bearing capacity of the

RC piles in terms of pull-out force and bending moment. In order to improve earthquake resistance of the pile foundation several countermeasures were compared, including grouting, cut-off steel sheet piles, cut-off steel sheet pipe piles and additional piles. As a result additional cast-in-place piles method was selected and their diameter and number were designed. In the desugn, following points were taken into consideration.

a) It is more economical to adopt large diameter piles than to use large number of piles.

b) Adoption of large diameter piles makes it easier to drill down gravel layers.

Fig.4 shows the strengthened foundation. 14 additional piles (ϕ =1000 mm, l= 23 m) were placed between the existing sheet piles and footing, and the original footing was enlarged so as to fix the newly constructed piles head.

CURRENT RESEARCH THEMES CONCERNING SOIL LIQUEFACTION IN PWRI

Fortunately we have not experienced catastrophic damages to highway bridges induced solely by soil liquefaction in recent earthquakes since provisions regarding soil liquefction were included in the 1971 Seismic Specifications for Highway Bridges and preventing devices for falling-off have been equipped to most bridges, however, there are still some points to be improved to reduce the possible liquefaction-induced damages in the future. In fact, a number of highway bridges were severely damaged by the latest strong Hyogoken-nanbu Earthquake of 1995 [12] , and some new problems of current Seismic Specifications concerning soil liquefaction were revealed, which proved continuous works on soil liquefaction are needed. Some of the research themes concerning soil liquefaction that have been undertaken in the PWRI are described below.

(1)Evaluation of liquefaction resistance of sandy soils [13]

The standard design seismic coefficient for liquefaction assessment, ks=0.15, was determined by considering the acceleration observed during the Niigata Earthquake, however, there have been some opinions that this value should be higher considering very high accelerations observed in recent earthquakes. This is especially the case where very important bridges are considered. In such cases liquefaction resistance of soils against large load or in a dense state is required. Fig.5 shows the comparison of liquefaction strength on the basis of several guidelines including highway bridges. This figure indicates that Specifications of Highway Bridges gives smaller resistance than other guidelines as the soil become denser. Originally the resistance curve for highway bridges was obtained from the results of loose to medium dense sand, threfore it has been necessary to investigate the liquefaction resitance of sand in a denser state.

As the first stage of investigation a series of cyclic triaxial tests have been conducted changing the density of reconstituted samples for Toyoura sand. The test results are formulated as

$$R_L = 0.22 \left(\frac{Dr}{100}\right) + \left(\frac{Dr}{100}\right)^{15} \qquad (10)$$

for the double amplitude of cyclic triaxial test,DA = 5%, and the number of cycles, N = 20.

This equation is shown in Fig.5 together with the equations of Specifications of Highway Bridges and Kokusho's [14] . Eq.(10) gives smaller values when relative density D_r is small while Eq.(10) and Kokusho's result increase rapidly when relative density D_r is greater than 70 to 80 % then become greater than the equation of Specifications of Highway Bridges. The discrepancy between the result of this experiment and the value by Specifications of Highway Bridges in the range of small relative density is considered due to the discrepancy of assumed value of D_r from Meyerhof's equation [15] , which is not included directly in the Specifications of Highway Bridges. Furthermore investigations of undisturbed samples are to be conducted to establish new formula to be used for wide density range.

(2)Soil reaction coefficient for foundation in liquefied ground [16]

In the Specifications for Highway Bridges, the effect of liquefaction of the subsoils on the foundation is taken into account by reducing the subgrade reaction evaluating from liquefaction resistance factor F_L and the depth from the surface as shown in Table 2. The value D_E in Table 2 was based on the static plate loading tests in the vertical direction with a container, 30 cm in diameter, applying overburden pressure and excess pore water pressure. The result was arranged to relate coefficient D_E and excess pore water pressure ratio. Besides horizontal loading tests of model piles in liquefied soil layer have been conducted in various scales, which give generally more steeply decreasing tendency against excess pore water pressure ratios than those included in the Specifications. Then a series of model horizontal plate loading tests in liquefied soils have been started in the PWRI. Fig.6 describes test apparatus. Fig.7 shows the relationship between normalized soil reaction coefficient and excess pore water pressure ratio.

(3)Effect of lateral ground flow by soil liquefaction [17]

It has been known that a large ground flow occurred as a consequence of soil liquefaction where there was some surface inclination. This was demonstrated by comparing air photos before and after the earthquakes [18] . Furthermore excavation investigations conducted almost 20 years after the Niigata Earthquake revealed that some piles supporting buildings were broken by the ground flow induced by the liquefaction [19] . Therefore the effect of such phenomena on bridge foundations should be evaluated. For this purpose two stage studies have been started. In the first stage the method to predict the amount of ground movement was studied by conducting a series of large scale model shaking table tests. In addition a theory to predict the flow displacement of the ground was developed considering the liquefied ground as liquid. After confirming that the theoretical estimation agrees fairly well with above test results and observed displacements in the fields during past earthquakes, a parametric study changing several factors

was conducted. Then a regression formula to predict the flow displacement of liquefied ground was derived as follows.

$$D=1.73\times10^{-5}L^{1.94}H_L^{0.298}H_{NL}^{-0.276}\theta_s^{0.963}$$
when $L=10\sim100$m (11)
at the center of the slope

where D:flow displacement of liquefied ground, L:length of liquefied ground, H_L :thickness of liquefied ground, H_{NL}: thickness of surface nonliquefied ground, θ_s :gradient of ground surface.

In the second stage the force to act the foundation in such a liquefied ground is required. A series of another shaking table tests of model flowing ground where model piles are embedded in the ground are now being conducted in the PWRI for this purpose.

CONCLUSION

Many efforts to mitigate the liquefaction-hazard have been done since the 1964 Niigata Earthquake. Then soil liquefaction assessment procedure has been improved a few times in many seismic design guidelines including Specifications of Highway Bridges. As a consequence of the efforts incorporated in the Seismic Design, we have experienced very few bridges falling-off solely because of soil liquefaction. Besides the brief history of the Seismic Design Specifications of Highway Bridges regarding soil liquefaction, the inspection method of existing highway bridges to consider the effect of soil liquefaction are reviewed. Some of the research themes concerning soil liquefaction undertaken in the PWRI is briefly described as well..

REFERENCES

1)Kawashima,K.: Seismic design, seismic strengthening and repair of highway bridges in Japan, Proc.of 1st U.S.-Japan Workshop on Sesimic Retrofit of Bridges, PWRI, 1990.

2)Miscellaneous reports of earthquake damage investigation.

3)Ohmachi,T.: *in* "Handbook of earthquakes", *ed.*T.Utsu, Asakura Book Publising Company, 1987 (in Japanese).

4)Ohsaki,Y.: NiigataEarthq1uake, 1964-- Building damage and soil condition, Soils & Foundations,1966,JSSMFE, 6, 2.

5)Koizumi,Y.: Changes in density of sand subsoil caused by Niigata Earthquake, Soils & Foundations, 1966, JSSMFE, 6, 2.

6)Seed,H.B. and Idriss,I.M.: Analysis of Soil Liquefaction: Niigata Earthquake, Proc.of ASCE, 1967, 93, SM3.

7)Seed,H.B. and Idriss,I.M.: Simplified procedure for evaluating soil liquefaction potential, Proc.of ASCE, 1971, 97, SM9.

8)Seed,H.B. et al.: Evaluation of soil liquefaction potential using field performance data, Jour.of Geotech., ASCE, 1983, 102, GT4.

9)Iwasaki,T. et al.: A practical method for assessing soil liquefaction potential based on case studies at various sites in Japan, Proc. 5th Japan Symp.on Earthquake Engineering, 1978 (in Japanese).

10)Iwasaki,T. et al.: Investigation of earthquake resistance of ground and substructure at Showa Bridge(in Japanese), PWRI Technical Memorandum, No.1591, 1980.

11)Tokida,K.: *in* "From survey and design to execution of liquefaction mitigation work" (in Japanese), JSSMFE, 1994.

12)Iijima,T. et al.: Infrastructure damage by the 1995 Hyogoken Nanbu Earthquake, Proc.of 27th Joint meeting of U.S.–Japan Cooperative Program in Natural Resources Panel on Wind and Sesimic Effects, PWRI, 1995.

13)Ohtsuka,H. et al.: Cyclic triaxial test on liquefaction characteristiucs of dense sand (in Japanese), Civil Eng.Jour., PWRI, 36, 7, 1994.

14)Kokusho,T. et al.: Liquefaction assessment of dense sand deposit based on SPT N–value, Proc.of 16th Japan National Conf.on Soil Mech. & Found.Eng., JSSMFE, 1981.

15)Meyerhof,G.G.: Discussion of sesion 1, Proc.4th ICSMFE, 1957.

16)Hagiwara,R. et al.: Model test on the horizontal liquefied–subgrade reaction in pile–foundation ground, Proc.of 4th U.S.–Japan Workshop on Soil Liquefaction, PWRI, 1994.

17)Tokida,K. et al.: Study on prediction of lateral ground flow by soil liquefaction and its influence on piles, Proc.of 24th Joint meeting of U.S.–Japan Cooperative Program in Natural Resources Panel on Wind and Sesimic Effects, NIST SP 843, 1992.

18)Hamada,M. et al.: Study on liquefaction induced permanent ground displacements, Assoc. Develop.Earthq.Predic.in Japan, 1986.

19)Kawamura,S. et al.: Damage to piles observed by the excavation of 20 years after the earthquake (in Japanese), Nikkei Architecture, 1985.7.29.

Table 1 Damage of Highway Bridges in the Past (1923-1994)

DATE	EARTHQUAKE	MAGNITUDE	NUNBER OF BRIDGES DAMAGED	NUMBER OF BRIDGES WHICH FELL DOWN
1923. 9. 1	KANTO	7.9	1,785	6
1946.12.21	NANKAI	8.1	346	1
1948. 6.28	FUKUI	7.3	243	4
1949.12.26	IMAICHI	6.4	1	0
1952. 3. 4	TOKACHI-OKI	8.1	128	0
1962. 4.30	MIYAGI-KEN-HOKUBU	6.5	187	0
1964. 6.16	NIIGATA	7.5	98	3
1968. 2.21	EBINO	6.1	10	0
1968. 5.16	TOKACHI-OKI	7.9	101	0
1978. 1.14	IZU-OHSHIMA	7.0	7	0
1978. 6.12	MIYAGI-KEN-OKI	7.4	95	1
1982. 3.21	URAKAWA-OKI	7.1	5	0
1983. 5.26	NIHON-KAI-CHUBU	7.7	176	0
1984. 9.14	NAGANO-KENN-SEIBU	6.8	14	0
1993. 1.15	KUSHIRO-OKI	7.8	63	0
1993. 7.12	HOKKAIDO-NANSEI-OKI	7.8	24	0
1994.10. 4	HOKKAIDO- TOHO-OKI	8.1	40	0
1994.12.28	SANRIKU-HARUKA-OKI	7.5	13	0
TOTAL			3,331	15

Data Source : (1923-1984) [1] (1933-1994) [2]

Table 2 Reduction Factor D_E of Soil Constants Depending on F_L Value

F_L-VALUE	DEPTH FROM GROUND SURFACE	D_E
$F_L \leqq 0.6$	$0m \leqq x \leqq 10m$	0
	$10m < x \leqq 20m$	1/3
$0.6 < F_L \leqq 0.8$	$0m \leqq x \leqq 10m$	1/3
	$10m < x \leqq 20m$	2/3
$0.8 < F_L \leqq 1.0$	$0m \leqq x \leqq 10m$	2/3
	$10m < x \leqq 20m$	1

Table 3 Inspection Sheet for Liquefaction Vulnerability of Highway Bridge (Crude Inspection)

<table>
<tr><th>Inspection Item</th><th>Factors of Inspection</th><th>Result</th></tr>
<tr><td>(1)Design Specifications</td><td>Specifications after 1971</td><td>Yes, No</td></tr>
<tr><td>(2)Bridge Type</td><td>Bridge type of Insusceptible of Liquefaction
(Arch Deck Bridge, Frame Type Bridge, Culvert Type ridge)</td><td>Yes, No</td></tr>
<tr><td rowspan="4">(3)Possibility of Liquefaction</td><td>Sites of Low Possibility of Liquefaction</td><td rowspan="4">Yes, No</td></tr>
<tr><td>Boring Data for the Bridge (Available, None)</td></tr>
<tr><td>a) Boring Data for Objective Bridge : Available
Saturated Sandy Layers (Yes, No)</td></tr>
<tr><td>b) Boring Data for Objective Bridge : None
<table>
<tr><th rowspan="2">Inspection Item</th><th>Data</th><th></th><th rowspan="2">Judgement Reason</th></tr>
<tr><th>Low Possibility</th><th>High Possibility</th></tr>
<tr><td>① Ground Condition</td><td>Group I</td><td>Group II , III</td><td>Design Documents
Site Condition
Foundation Type</td></tr>
<tr><td>② Microtopography Land Condition Map</td><td>B, C</td><td>A</td><td>(Type of Microtopography)</td></tr>
<tr><td>③ Saturated Sand Layers in Adjacent Boring Data</td><td>No</td><td>Yes</td><td>(Type of Applied Data)</td></tr>
</table></td></tr>
<tr><td rowspan="2">(4)Corrected Thickness Ratio of Liquefiable Layers</td><td>Name of Typical Substructure ( )</td><td></td></tr>
<tr><td>Corrected Thickness Ratio of Liquefiable Layers, $r_{HL} < 0.2$. r_{HL}= ( )
<table>
<tr><th colspan="2">Boring Data</th><th>Available or None</th></tr>
<tr><td colspan="2">At Objective Site</td><td></td></tr>
<tr><td rowspan="10">Adjacent site</td><td>Other Road Administrator</td><td></td></tr>
<tr><td>River Administrator</td><td></td></tr>
<tr><td>Railway Administrator</td><td></td></tr>
<tr><td>Sewage Administrator</td><td></td></tr>
<tr><td>Water Work Administrator</td><td></td></tr>
<tr><td>Industrial Water Administrator</td><td></td></tr>
<tr><td>Gas Administrator</td><td></td></tr>
<tr><td>Electricity Administrator</td><td></td></tr>
<tr><td>Telephone Administrator</td><td></td></tr>
<tr><td>Others</td><td></td></tr>
</table></td><td>Yes, No</td></tr>
</table>

Table 4 Inspection Sheet for Liquefaction Vulnerability of Highway Bridges (Detailed Inspection)

Inspection Item	Factors of Inspection		Result
(1) Abutment	Bridge Name ( )		
I_C, Falling-off Prevention Device	Fixed Abutment : 0.0 S_E and Falling-off Prevention Device : 0.5 S_E or Falling-off Prevention Device : 1.0 None : 1.5		
I_J, Bearing Type	Movable : 0.0 Fixed : 1.0		
I_F, Foundation Type	Pile Foundation (Except Wooden Pile and Pile Bent Pier) or Caisson : 1.0, Wooden Pile or Pile Bent Pier : 2.0		
I_{FS}, Foundation Supporting Condition	Complete Support : 1.0 Incomplete Support : 5.0 Supported at Shallower Layer than Liquefiable Layer : 6.0		
I_{HB}, Back Fill Height (H_B)	$5.0m > H_B$: 1.0, $5.0m \leqq H_B$: 1.2		
I_{HL}, Corrected Thickness Ratio for Liquefaction (r_{HL})	$0.4 > r_{HL}$: 1.0, $0.4 \leqq r_{HL}$: 1.5		
	$P\ I = (I_C + I_J + I_F + I_{FS}) \times I_{HB} \times I_{HL}$ Total Point P I Calculated from Above Formula < 6.0	P I =	
		Evaluation	Yes, No
(2) Pier with Movable Bearin	Name of Pier ( )		
I_C, Falling-off Prevention Device	Pier at Continuous Deck : 0.0 S_E and Falling-off Prevention Device : 0.5 S_E or Falling-off Prevention Device : 1.0 None : 1.5		
I_F, Foundation Type	Pile Foundation (Except Wooden Pile and Pile Bent Pier) or Caisson : 1.0, Wooden Pile or Pile Bent Pier : 2.0		
I_{FS}, Foundation Supporting Condition	Complete Support : 1.0 Incomplete Support : 5.0 Supported at Shallower Layer than Liquefiable Layer : 6.0		
I_{HL}, Corrected Thickness Ratio for Liquefaction (r_{HL})	$0.4 > r_{HL}$: 1.0, $0.4 \leqq r_{HL}$: 1.5		
I_{GC}, Ground Type	Group II : 1.0 , Group III : 1.2		
	$P\ II = (I_C + I_F + I_{FS}) \times I_{HL} \times I_{GC}$ Total Point P II Calculated from Above Formula < 6.0	P II =	
		Evaluation	Yes, No
(3) Pier with Fixed Bearing	Name of Pier ( )		
I_F, Foundation Type	Pile Foundation (Except Wooden Pile and Pile Bent Pier) or Caisson : 1.0, Wooden Pile or Pile Bent Pier : 2.0		
I_{FS}, Foundation Supporting Condition	Complete Support : 1.0 Incomplete Support : 5.0 Supported at Shallower Layer than Liquefiable Layer : 6.0		
I_{HL}, Corrected Thickness Ratio for Liquefaction (r_{HL})	$0.4 > r_{HL}$: 1.0, $0.4 \leqq r_{HL}$: 1.5		
	$P\ III = (I_F + I_{FS}) \times I_{HL}$ Total Point P III Calculated from Above Formula < 4.5	P III =	
		Evaluation	Yes, No

Table 5 Inspection Sheet for Liquefaction Vulnerability of Highway Bridges (3rd Stage Inspection)

Inspection Item			Evaluation	Need for Mearsures	Proposed Measures
Abutment	Name of Bridge ( )				
	Ground Data		(Available, None)	(Yes, No)	
	Structural Dimension Data		(Available, None)	(Yes, No)	
	Pile Foundation	Pile Stress	(O.K, N.G.)	(Yes, No)	
		Vertical Bearing Capacity	(O.K, N.G.)	(Yes, No)	
	Caisson Foundation	Vertical Bearing Capacity	(O.K, N.G.)	(Yes, No)	
		Sliding Resistance	(O.K, N.G.)	(Yes, No)	
Pier with Movable Bearing	Name of Bridge ( )				
	Ground Data		(Available, None)	(Yes, No)	
	Structural Dimension Data		(Available, None)	(Yes, No)	
	Pile Foundation	Pile Stress	(O.K, N.G.)	(Yes, No)	
		Vertical Bearing Capacity	(O.K, N.G.)	(Yes, No)	
	Caisson Foundation	Vertical Bearing Capacity	(O.K, N.G.)	(Yes, No)	
		Sliding Resistance	(O.K, N.G.)	(Yes, No)	
Pier with Fixed Bearing	Name of Bridge ( )				
	Ground Data		(Available, None)	(Yes, No)	
	Structural Dimension Data		(Available, None)	(Yes, No)	
	Pile Foundation	Pile Stress	(O.K, N.G.)	(Yes, No)	
		Vertical Bearing Capacity	(O.K, N.G.)	(Yes, No)	
	Caisson Foundation	Vertical Bearing Capacity	(O.K, N.G.)	(Yes, No)	
		Sliding Resistance	(O.K, N.G.)	(Yes, No)	

Table 6 Countermeasures Against Liquefaction for Existing Highway Bridges

Fundamentals	Principle		Method	Applicability	Applicability for Existing Highway Bridges
I .Prevention of occurrence of liquefaction or reduction of degree of generation	Ground improvement	Increase of density	Sand compaction pile, Vibro rod compaction	Applicability depends on the size of construction equipment	B
			Vibroflotation		
			Surcharge	Permanent settlement, restrained by right-of-way	D
			Dynamic consolidation, Blast compaction	Difficult to apply for surrounding environment	D
		Lowering of degree of saturation	Well point, Deep well	Ground subsidence, difficult to maintain	D
		Adjustment of grain size distribution and solidification	Replacement	Difficult to execute	D
			Injection	Difficult execution control, questionable for durability	D
			Mixing consolidation	Applicability depends on the size of construction equipment	B
		Dissipation of pore water pressure	Gravel drain	Applicability depends on the size of construction equipment, reliability of long life has not been confirmed yet	B
	Restraint of shear deformation		Steel sheet pile or RC diaphram wall enclosure	Applicability depends on the size of construction equipment, difficult evaluation of effectiveness	C
II .Reduction of liquefaction induced damage to facilities by structural reinforcement	Increase of foundation stiffness		Increase of piles	Applicability depends on the size of construction equipment, difficult evaluation of effectiveness	A
			Increase of foundation stiffness by RC diaphram wall or steel sheet pipe pile for surrounding area	Applicability depends on the size of construction equipment, difficult evaluation of effectiveness	A

Legend: A: most applicable, B: applicable, C: little possibility, D: not applicable
Evaluation of countermeasures will be made from methods marked A or B. In fact methods "A" are basically considered advantageous from the viewpoint of secureness of effectiveness and degree of design accuracy.

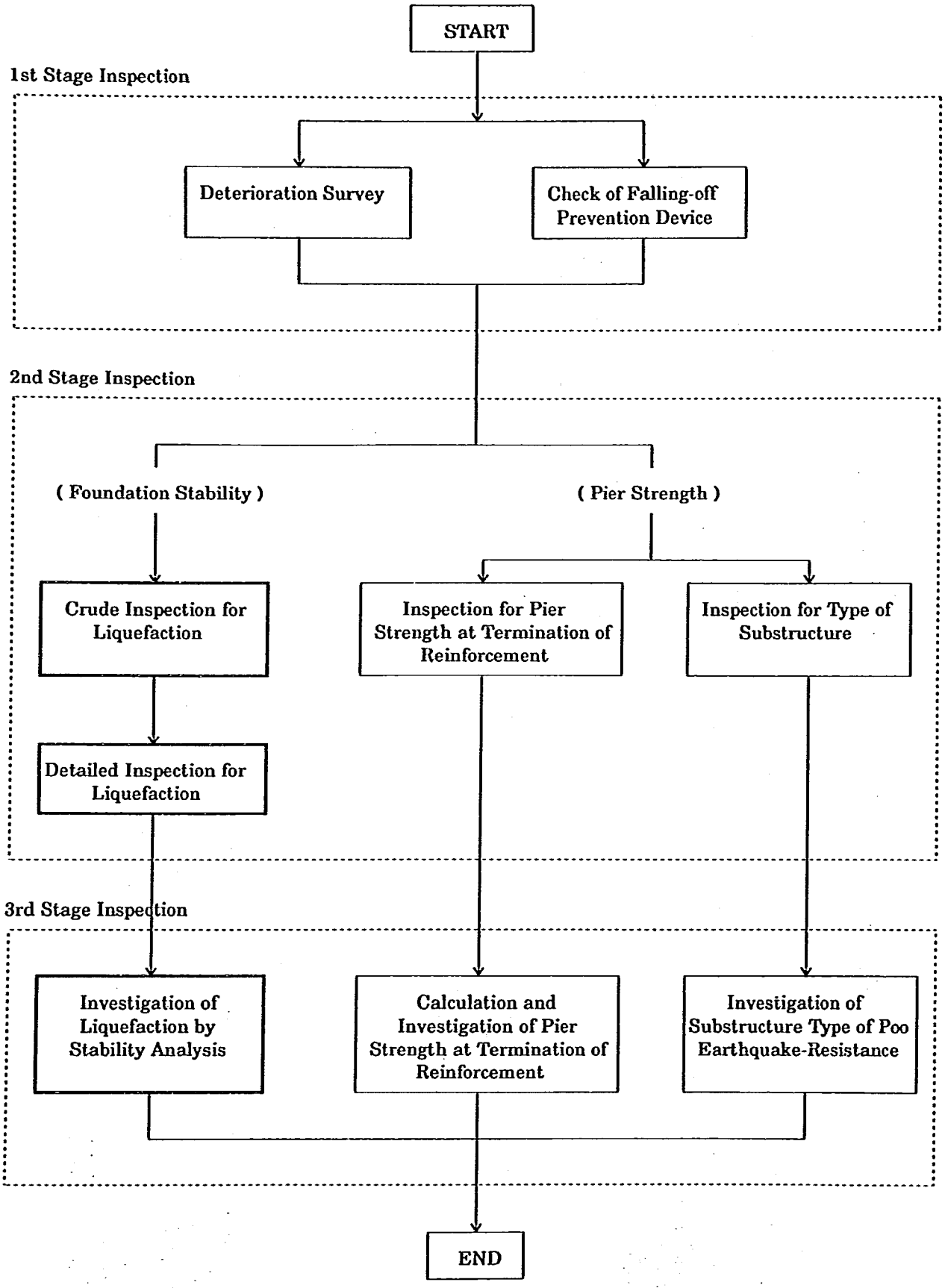


Fig.1 Outline of Inspection Procedure of Highway Bridges Including Inspection for Liquefaction

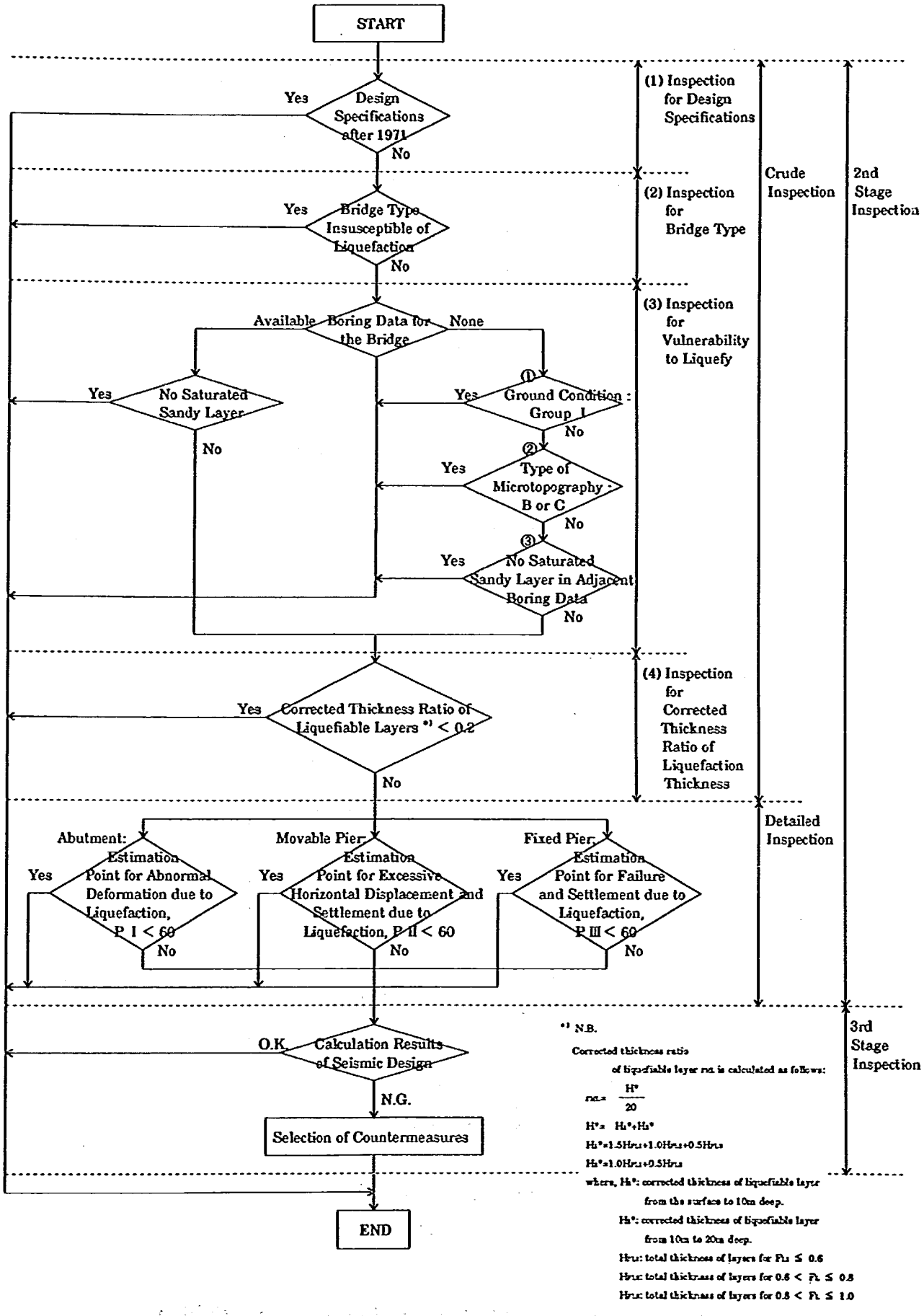
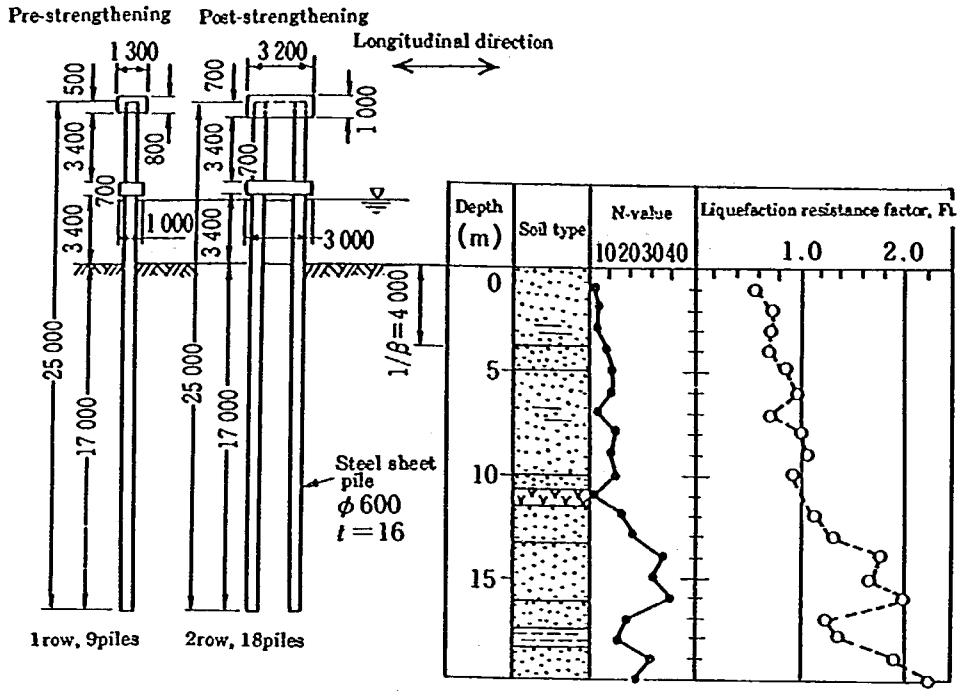
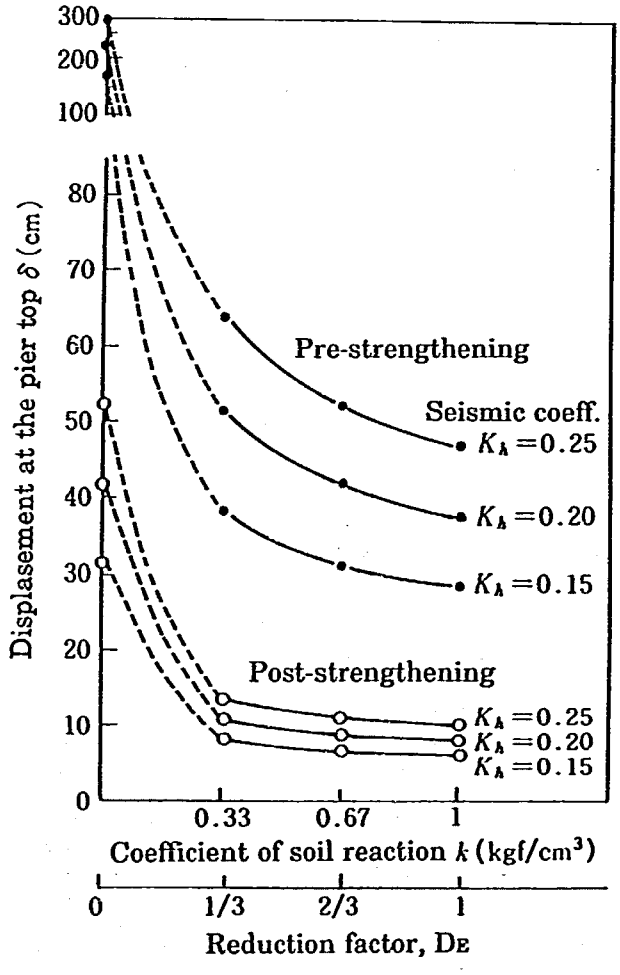


Fig.2 Inspection Procedure for Liquefaction Vulnerability



(a) Evaluaion of liquefaction and pile foundation structure



(b) Response displacement

Fig.3 Strengthening of Pile Foundation of Showa Bridge and Its Response Characteristics (No.5 Pier)

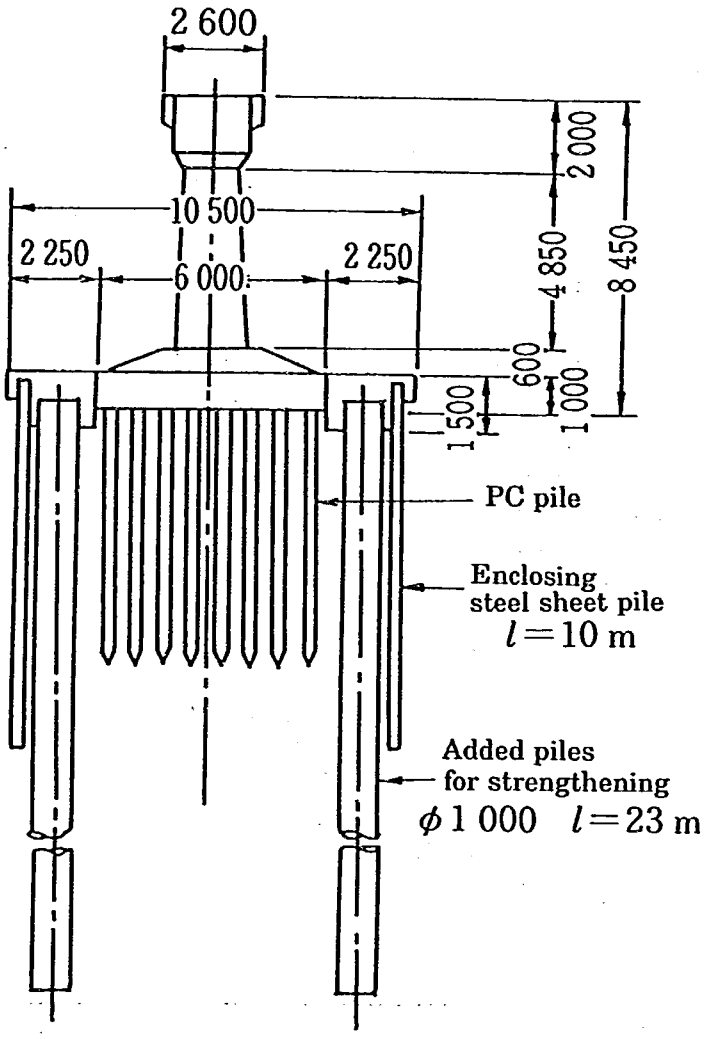


Fig.4 Example of Strengthening of Piers of Existing Highway Bridge against Liquefaction

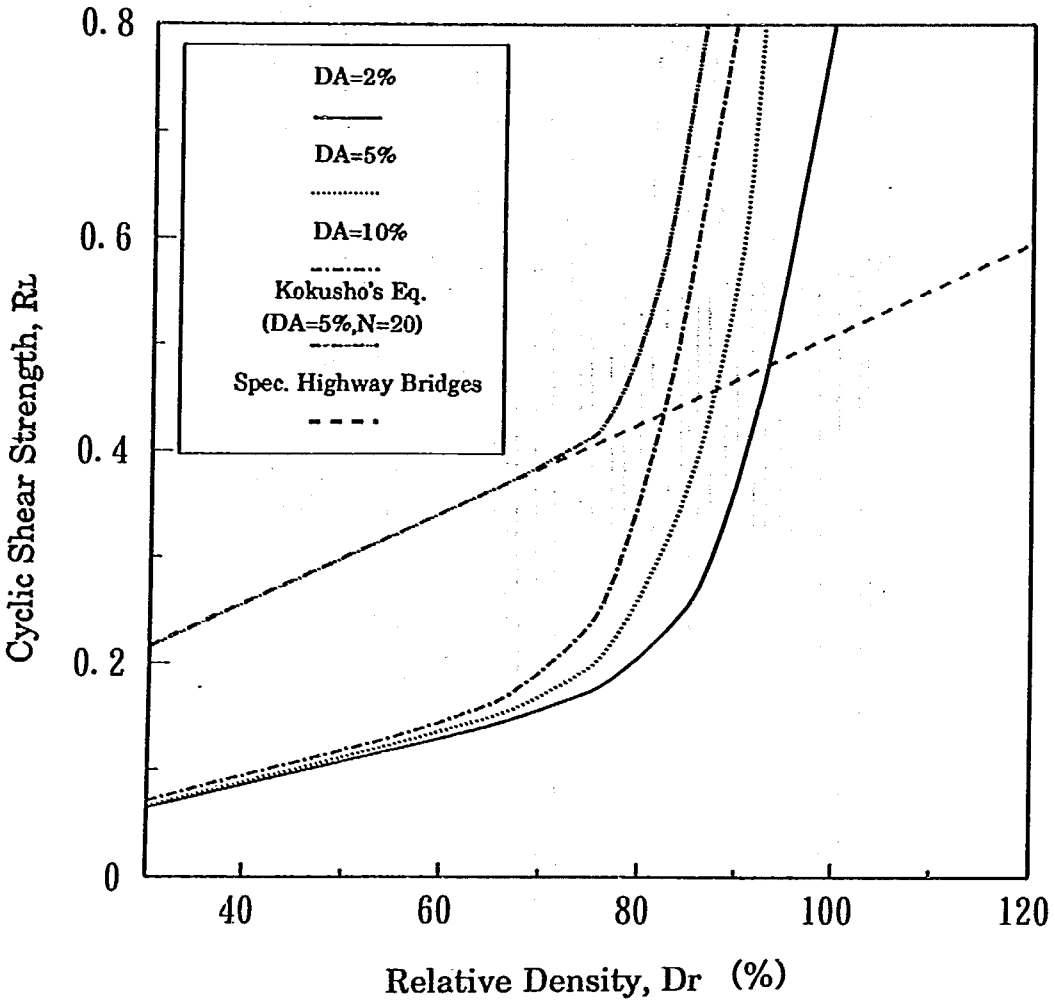


Fig.5 Relation between Cyclic Shear Strength RL and Relative Density Dr

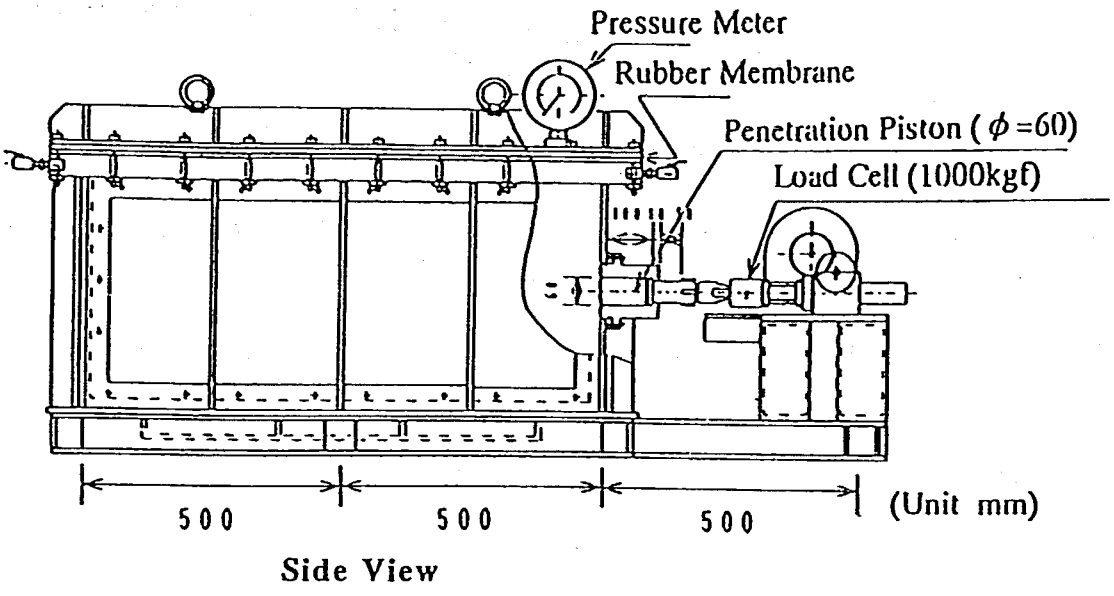


Fig.6 Test Apparatus

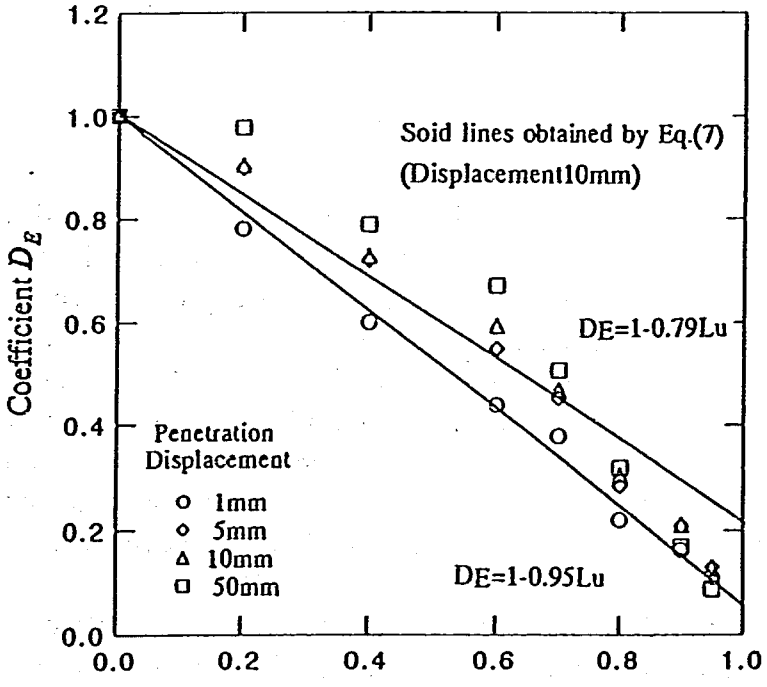


Fig.7 Relationship between Coefficient, D_E and Excess Pore Wtater Pressure Ratio, Lu
(σ v'=1.0kgf/cm^2)

A STRESS–STRAIN MODEL FOR CONFINED REINFORCED CONCRETE IN BRIDGE PIERS

J. Hoshikuma[1], K. Kawashima[2], K. Nagaya[3]

1)Research Engineer, Earthquake Engineering Division, Public Works Research Institute, Ministry of Construction, Tsukuba Science City, Ibaraki–ken, Japan, 305

2)Research Coordinator for Geospace Use, Planning and Research Administration Department, ditto

3)Assistant Research Engineer, Earthquake Engineering Division, ditto

ABSTRACT

In this paper, a stress–strain model of concrete which takes confinement effects into account is developed, based on the results of a series of compression loading tests of reinforced concrete column specimens. The specimens have circular, square and wall–type cross sections, with various arrangements of hoop reinforcement. The stress–strain model was formulated by evaluating the relationship between several key parameters and the stress–strain behavior observed in the experiments. It is shown that the predicted stress–strain relation provides better agreement with the experimental results than previous models.

INTRODUCTION

Reinforced concrete bridge piers subjected to large seismic lateral forces exhibit inelastic response. It is well known that the confinement associated with hoop reinforcement increases the ductility and the energy absorption capacity of reinforced concrete bridge piers. It is, therefore, important to incorporate the effects of hoop reinforcement into seismic design when evaluating the strength and ductility of reinforced concrete bridge piers. This paper proposes a stress–strain model for confined reinforced concrete in bridge piers. To study the effects of confinement on the stress–strain relation, a series of compression loading tests of small and large scale confined concrete columns were conducted, and a model of the stress–strain curve was developed.

Various studies on the confinement effects of lateral reinforcement in column have already been conducted, and stress–strain models of confined concrete were proposed as given in Table 1.

Reinforced concrete bridge piers constructed in Japan have larger concrete sections and thus lower hoop reinforcement volumetric ratios than those constructed in the United States and New Zealand. In Japan, reinforced concrete bridge piers generally have a volumetric ratio of 0.3% to 0.5% of hoop reinforcement, and hoops with a yield stress of 295 MPa or 345 MPa. The models described above were developed based on data from the loading tests shown in Table 2. Although a few specimens containing a volumetric

Table 1 Summary of Previous Stress–Strain Models for Confined Concrete

Researcher	Stress–Strain Model for Confined Concrete			Applicable Cross Sectional Shape
	Ascending Branch	Falling Branch	Residual Stress	
Kent and Park	$f_c = K f_{co}\left\{\frac{2\varepsilon_c}{0.002K} - \left(\frac{\varepsilon_c}{0.002K}\right)^2\right\}$	$f_c = K f_{co}\{1 - Z_m(\varepsilon_c - 0.002K)\}$	20% of $K f_{co}$	Square
Sheikh et al.	$f_c = K f_{cc}\left\{\frac{2\varepsilon_c}{\varepsilon_{s1}} - \left(\frac{\varepsilon_c}{\varepsilon_{s1}}\right)^2\right\}$	$f_c = f_{cc}\{1 - Z(\varepsilon_c - \varepsilon_{cc})\}$	30% of f_{cc}	Square
Mander et al.	$f_c = \frac{f_{cc} x r}{r - 1 + x^r}$ where $x = \frac{\varepsilon_c}{\varepsilon_{cc}}$, $r = \frac{E_c}{E_c - E_{sec}}$			Circle Square Wall-type
Saatcioglu et al.	$f_c = f_{cc}\left\{2\left(\frac{\varepsilon_c}{\varepsilon_{cc}}\right) - \left(\frac{\varepsilon_c}{\varepsilon_{cc}}\right)^2\right\}^{1/(1+2K)}$	$f_c = f_{cc} - \frac{0.15 f_{cc}}{\varepsilon_{85} - \varepsilon_{cc}}(\varepsilon_c - \varepsilon_{cc})$	20% of f_{cc}	Circle Square Wall-type
Muguruma et al.	$f_c = E_i \varepsilon_c + \frac{f_{co} - E_i \varepsilon_m}{\varepsilon_m^2}\varepsilon_c^2$ and $f_c = \frac{f_{co} - f_{cc}}{(\varepsilon_{co} - \varepsilon_{cc})^2}(\varepsilon_c - \varepsilon_{cc})^2 + f_{cc}$	$f_c = \frac{f_{cu} - f_{cc}}{\varepsilon_{cu} - \varepsilon_{cc}}(\varepsilon_c - \varepsilon_{cc}) + f_{cc}$	——	Circle Square
Fujii et al.	$f_c = E_i \varepsilon_c + \frac{f_{co} - E_i \varepsilon_{co}}{\varepsilon_{co}^2}\varepsilon_c^2$ and $f_c = \frac{f_{co} - f_{cc}}{(\varepsilon_{co} - \varepsilon_{cc})^3}(\varepsilon_c - \varepsilon_{cc})^3 + f_{cc}$	$f_c = f_{cc} - E_{des}(\varepsilon_c - \varepsilon_{cc})$	20% of f_{cc}	Circle Square

Table 2 Test Specimens in Previous Research Programs

Researcher	Cross Sectional Shape	Size of the Section in Specimen (cm)	Volumetric Ratio of Hoop Reinforcement(%)
Kent and Park	Rectangle	10×15	0.35~1.87
	Square	12.8×12.8	2.07~2.39
		10×10	1.09~1.81
Sheikh et al.	Square	30×30	0.76~2.40
Mander et al.	Circle	ϕ50	0.60~2.50 (Spiral)
	Square	45×45	1.86~1.97
	Wall-type	15×70	1.62~7.87
Saatcioglu et al.	Square	16×16	1.34~2.78
Muguruma et al.	Circle	ϕ15	0.76~2.79 (Spiral)
	Square	19.4×19.4	0.40~3.13
Fujii et al.	Circle	ϕ15	0.62~4.02
	Square	15×15	0.62~2.50

ratio of hoop reinforcement less than 0.5% have been tested previously, they must be considered special cases, because high tensile strength steel was used for the hoop reinforcement, and some of the specimens were subject to eccentric loading. Therefore, the previous models may not adequately represent confinement effects in the range of low hoop reinforcement ratios. It is also pointed out that only Mander's and Saatcioglu's models can be directly applied to concrete bridge piers with wall-type cross sections. It is, therefore, necessary to study the confinement effects for wall-type sections as well.

In this research, a series of compressive loading tests were conducted to study several effects of the confinement on the stress-strain behavior. In these tests, hoop volumetric ratio, hoop spacing and configuration of the hook in the hoop reinforcement were varied as parameters. It is the main purpose of this research to propose a stress-strain model of confined concrete which is applicable to a wider range of hoop reinforcement ratios than previous models.

COMPRESSION TEST OF CONFINED CONCRETE COLUMNS

The test specimens are described in Table 3. The first symbol of the specimen name is used to describe the scale of the specimen: S and L stand for small scale and large scale. The second symbol is used to describe the cross sectional shape: C, S and W stand for circular, square and wall-type section. Thirty one specimens, with circular, square and wall-type sections as shown in Fig. 1, were constructed to evaluate the confinement effect in terms of volumetric ratio, spacing and configuration of the hook of the hoop reinforcement. The strength of unconfined concrete is usually determined by uniaxial loading test for a concrete cylinder with 20cm height and 10cm diameter. On the other hand, it is often pointed out that the scale effect on the strength of unconfined concrete can be considerable. To avoid such an effect, the strength of unconfined concrete was determined from tests of Specimens SC0, SS0, LC0 and LS0, with the same geometry,

Table 3 Test Specimens

Specimen			Dimension of Section and Height (mm)	Strength of Unconfined Concrete (MPa)	Longitudinal Reinforcement Ratio (%)	Hoop Reinforcement				Aspect Ratio of Section
						Material / Diameter(mm)	Spacing (cm)	Volumetric Ratio (%)	Anchorage Type	
S	C	SC0	φ200 h=600	18.5	0	–	–	–	–	–
		SC1				SR235 φ6	15	0.39	Weld	
		SC2					10	0.58		
		SC3					5	1.17		
		SC4					2.5	2.33		
		SC5					1.25	4.66		
	S	SS0	200 × 200 h=600	23.2	0	–	–	–	–	1.0
		SS1				SR235 φ6	15	0.39	Weld	
		SS2					10	0.58		
		SS3					5	1.17		
		SS4					2.5	2.33		
		SS5					1.25	4.66		
L	C	LC0	φ500 h=1500	28.8	1.01	–	–	–	–	–
		LC1				SD295 D10	30	0.19	Weld	
		LC2					15	0.39		
		LC3					10	0.58		
		LC4					5	1.16		
		LC5				SD295 D13	30	0.34		
		LC6				SD295 D16	30	0.54		
		LC7				SD295 D10	10	0.58	90° Hook	
		LC8							135° Hook	
		LC9							180° Hook	
	S	LS0	500 × 500 h=1000	24.3	0.95	–	–	–	–	1.0
		LS1				SD295 D13	6	1.73	Weld	
		LS2				SD295 D16	7.5	2.19		
		LS3				SD295 D13	4	2.60		
		LS4				SD295 D16	4	4.10		
	W	LW1	350×700		0.97	SD295 D13	6.5	1.72		2.0
		LW2	300×900		1.03		6.7	1.74		3.0
		LW3	250×1000		0.95		7.5	1.77		4.0
		LW4						2.45		

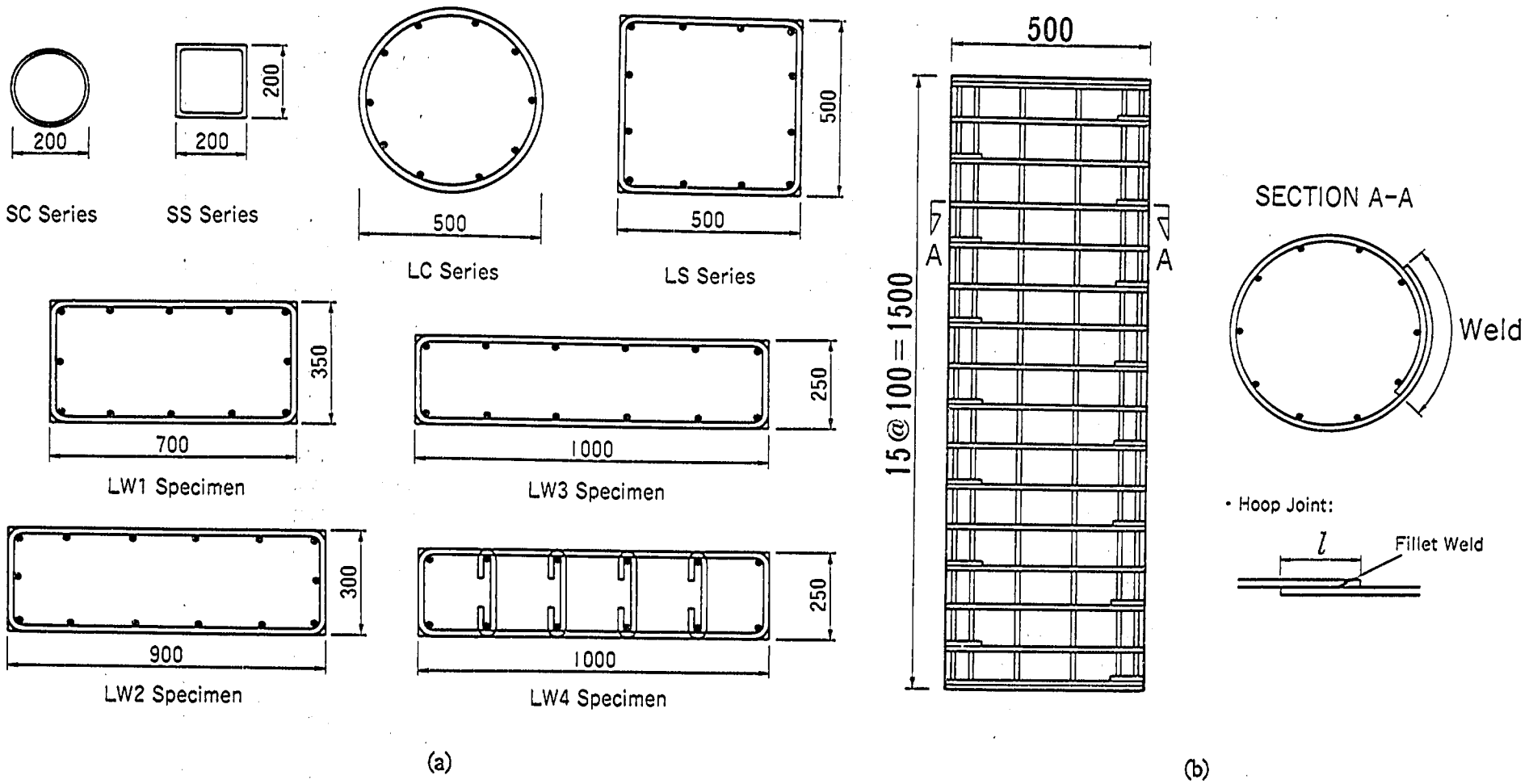


Fig. 1 Construction Details of Specimens: (a) Cross Sections; and (b) Details for Specimen LC3

size, and concrete casting practice as those of the confined concrete columns, as given in Table 3.

Portland cement and aggregates with maximum size of 13mm were used in the specimens. The water/cement ratio was set as 0.50 to 0.65. Round bars were used for hoop reinforcement in the SC and SS Series, and deformed bars were used for longitudinal and hoop reinforcement in the LC, LS and LW Series. The yield stress of the bars was 235 MPa for round bars and 295 MPa for deformed bars. Only hoop reinforcement was provided in the SC and SS Series, so that the effect of confinement could be isolated. The longitudinal reinforcement ratio was set at approximately 1% in the LC, LS and LW Series, because that is the typical value for bridges in Japan. The volumetric ratio of hoop reinforcement was varied in the range of 0.19% to 4.66%. The hoop reinforcement was anchored by hooks or by welding, and the joints were staggered over the specimen height as illustrated in Fig. 1. Specimens LC7, LC8 and LC9 used hoop reinforcement with 90, 135 and 180 degree hooks, respectively, as shown in Fig. 2 (Japan Road Association 1991). In the remaining specimens, the hoop reinforcement was anchored by a fillet weld, as illustrated in Fig. 1. The lap length was calculated as;

$$l = \frac{f_{yh} A_h}{\tau_a a} \qquad (1)$$

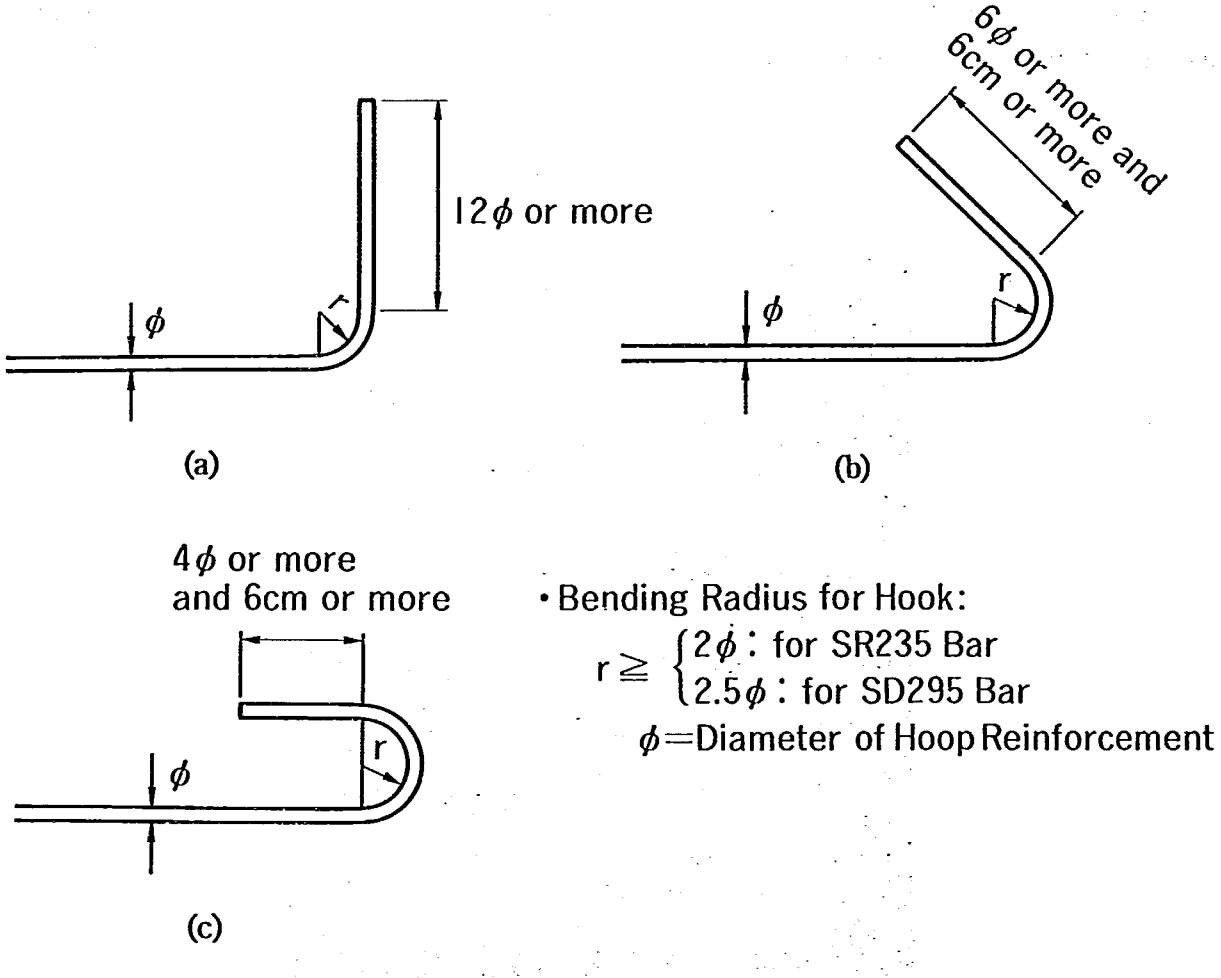


Fig. 2 Configuration of Hook in Hoop Reinforcement: (a) 90 Degree Hook; (b) 135 Degree Hook; and (c) 180 Degree Hook

where, l = lap length for fillet weld; f_{yh} = yield strength of hoop reinforcement; A_h = area of hoop reinforcement; τ_a = allowable shear stress for weld metal; and a = throat thickness of weld.

To examine the effect of cross sectional shape on confinement, specimens of various shapes were tested. In the wall–type piers, it may not be possible to achieve effective confinement with hoop reinforcement alone. Therefore, four cross ties were installed across each hoop in Specimen LW4. The volumetric ratio of hoop reinforcement in Specimen LW4, including the cross ties, is 2.45%.

Fig. 3 shows the experimental setup in a 30MN capacity universal testing machine at the Public Works Research Institute. All specimens were subjected to uniaxial compressive loading under displacement control, at a rate of 1mm/min. The axial deformation of the specimen, between the top and bottom load heads, was measured by two linear jpotentiometers placed on opposite sides of the specimen. The longitudinal strain was calculated by dividing the measured axial deformation by the total height of the specimen. Because failure of the concrete did not occur over the whole height of the specimen, but only over part of the height, the question is raised as to what length should be assumed in calculating the longitudinal strain. One option is to use the height over which the failure of the concrete occurs. However, measurement of this height may be made only after the failure of the concrete is initiated. On the other hand, before concrete failure occurs, the total height contributes to the deformation. Thus, it is difficult to evaluate the

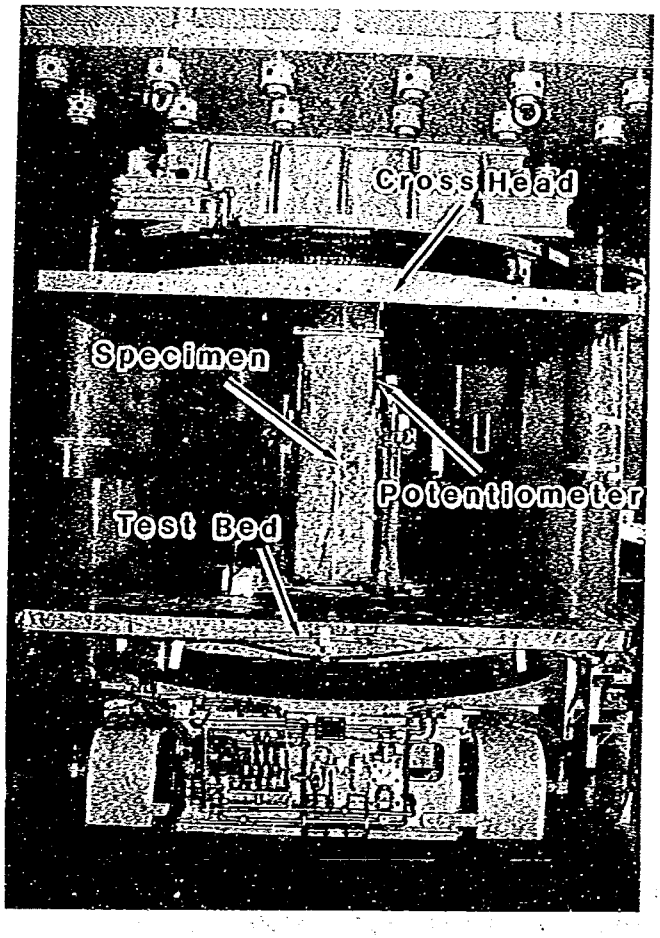


Fig. 3 Experimental Setup with 30MN Universal Testing Machine

appropriate total height for whole loading sequence. Based on these considerations, it was decided to use the total height of the specimen to evaluate longitudinal strain over the entire loading sequence.

EFFECTS OF CONFINEMENT

Failure Mode

Fig. 4 shows the failure mode of the Specimens LC1 through LC6, LW3 and LW4. Diagonal cracks were developed in the specimens with circular sections. The Specimens LC1, LC5 and LC6 suffered serious buckling of longitudinal reinforcement and the deterioration of the core concrete. The spacing of 30cm between the hoops is obviously too large to prevent such serious failure. The damage in the specimens becomes less as the hoop reinforcement ratio increases. It is also observed that the hoop reinforcement deformed outward in Specimen LW3 providing very little confinement, and buckling of the longitudinal reinforcement occurred. On the other hand, such significant deformation was not developed in Specimen LW4, because the cross ties worked effectively.

Effect of Hoop Reinforcement ratio

Fig. 5 shows stress–strain curves for circular and square cross sections with various volumetric ratios of hoop reinforcement. A predicted relation, which will be described later, is also presented for comparison in Fig. 5. It should be noted that the initial stiffness is independent of hoop reinforcement ratio. As the volumetric ratio of hoop reinforcement increases, both the peak stress and the strain at the peak stress increase, and severe deterioration of concrete after the peak stress is prevented. It is also clear that the confinement effect is highly dependent on the cross sectional shape.

Effect of Spacing of Hoop Reinforcement

Fig. 6 illustrates the effect of changing hoop reinforcement spacing, while maintaining the same volumetric ratio of hoop reinforcement. It can be seen that even if the same amount of hoop reinforcement is provided, deterioration after the peak stress is considerable when the spacing of hoop reinforcement is increased. As shown in Fig. 4, severe outward bucklings of longitudinal reinforcement and deterioration of the core concrete were observed in Specimens LC1, LC5 and LC6, which had a hoop spacing of 30cm. Therefore, for a given volumetric ratio of hoop reinforcement, confinement is improved by placing the hoop reinforcement at smaller intervals.

Effect of Configuration of Hook

Fig. 7 shows the effect of the confining reinforcement hook configuration on the stress–strain curve. Although the peak stress is approximately the same for all four anchorage types, the post–peak deterioration rate for Specimen LC8, which used the 135 degree hook, is slightly smaller than the others. The reason for this is not clear. However, Specimens LC7 and LC9, which used the 90 degree and the 180 degree hook, respectively, show similar stress–strain relations as Specimen LC3, which used welded

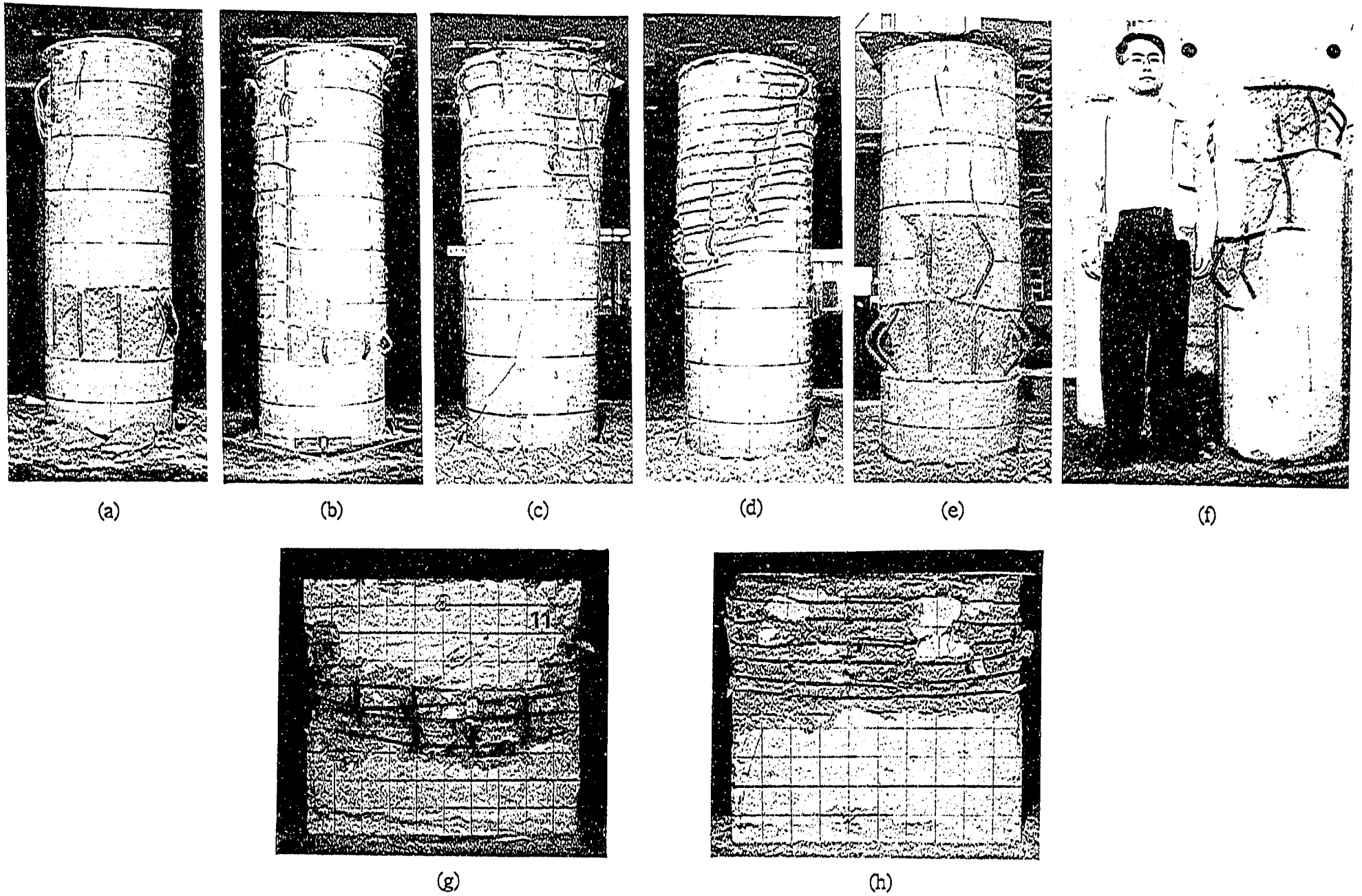


Fig. 4 Failure Mode of Specimens: (a) Specimen LC1; (b) Specimen LC2; (c) Specimen LC3; (d) Specimen LC4; (e) Specimen LC5; (f) Specimen LC6; (g) Specimen LW3; and (h) Specimen LW4

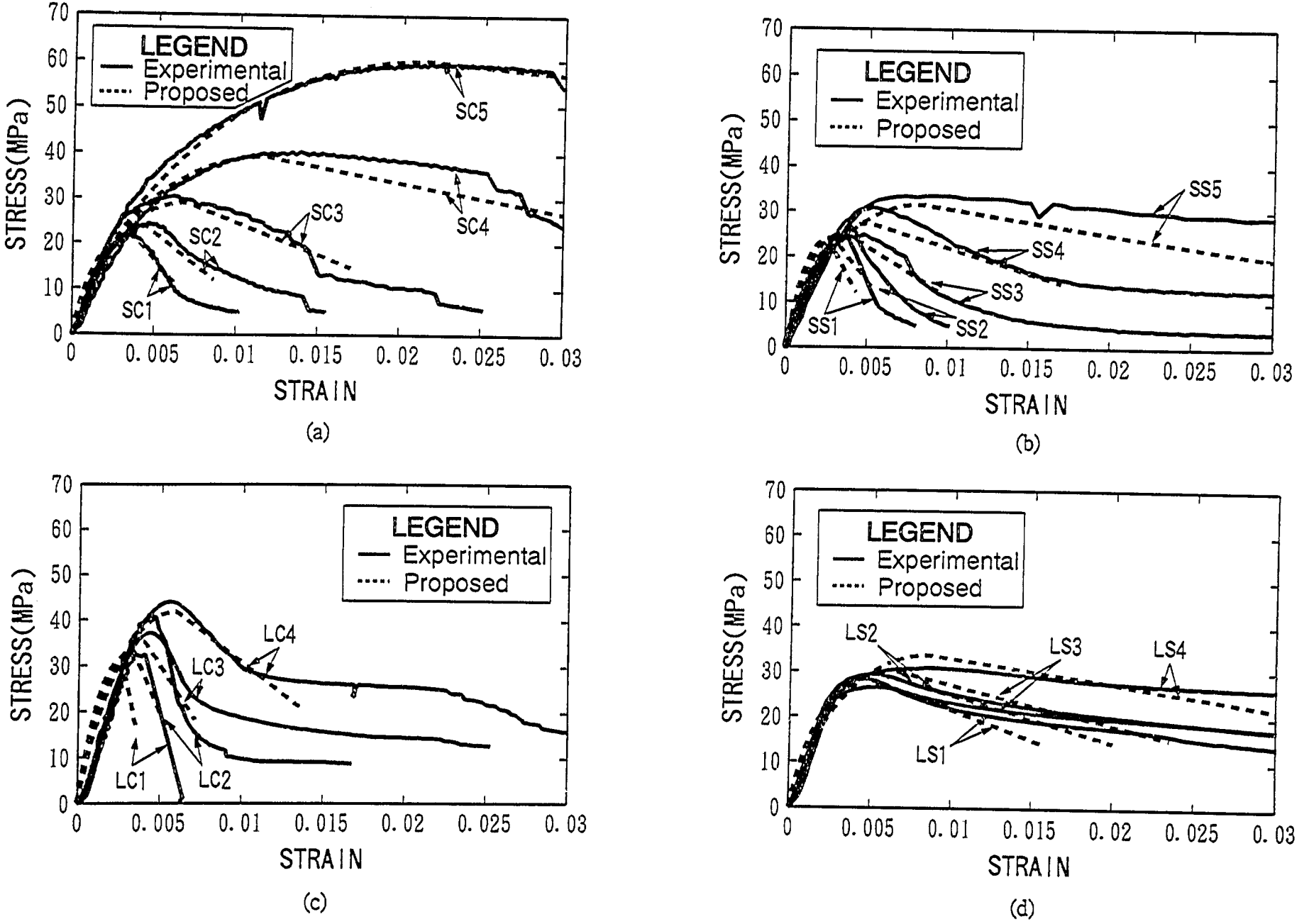
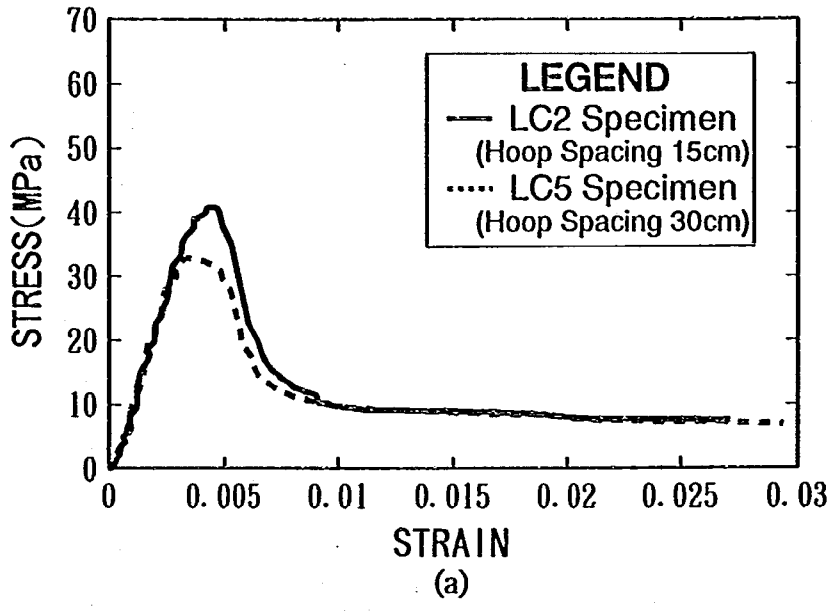
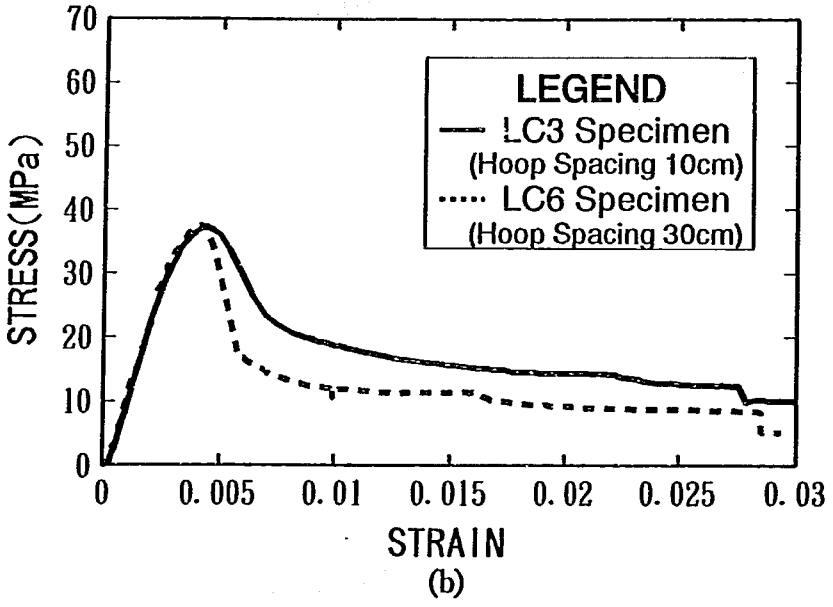


Fig. 5 Comparison of Stress–Strain Relation from Test Results, and from Predictions by (8) and (10): (a) SC Series; (b) SS Series; (c) LC Series; and (d) LS Series



(a)



(b)

Fig. 6 Effect of Spacing of Hoop Reinforcement: (a) ρ_s Approximately 0.35%; and (b) ρ_s Approximately 0.55%

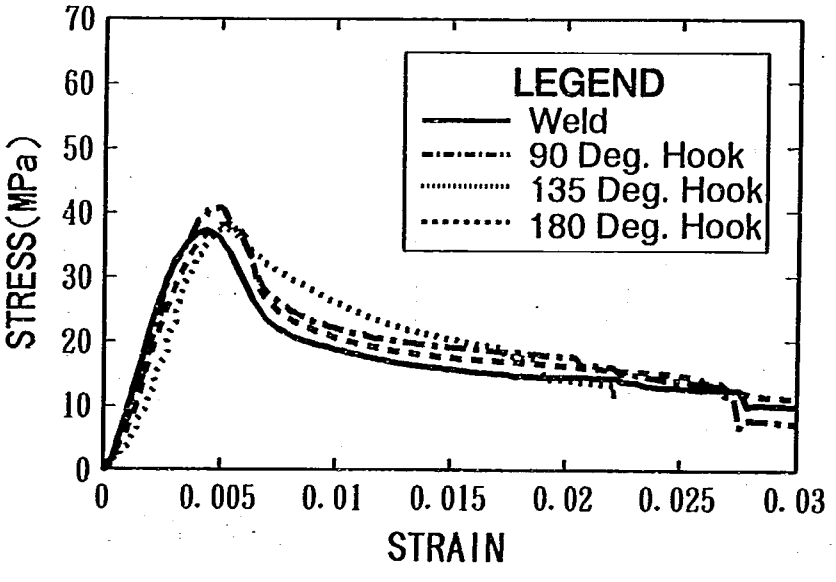


Fig. 7 Effect of Configuration of Hoop Reinforcement

hoop reinforcement. In all specimens, failure of the hoop reinforcement did not occur near the hook. It may be said, therefore, that for the three types of hooks tested in this series the stress–strain behavior was insensitive to hook configuration.

Effect of Aspect Ratio of the Section

Fig. 8 shows the effect of aspect ratio of the cross section for 5 specimens with the same volumetric ratio of hoop reinforcement of 1.75%. It can be seen that when a constant amount of hoop reinforcement is provided, the peak stress and the ductility deteriorate as the aspect ratio of the section increases. The stress–strain relation of Specimen LW3 is quite close to that of unconfined concrete. It is apparent that confinement can not be effectively achieved using rectangular hoop reinforcement in a section with an aspect ratio of the section of 4.0. On the other hand, the stress–strain relation of Specimen LW4, with cross ties, shows significantly improved performance over Specimen LW3. Therefore, the effect of cross ties is significant in increasing the ductility of concrete piers with wall–type cross sections.

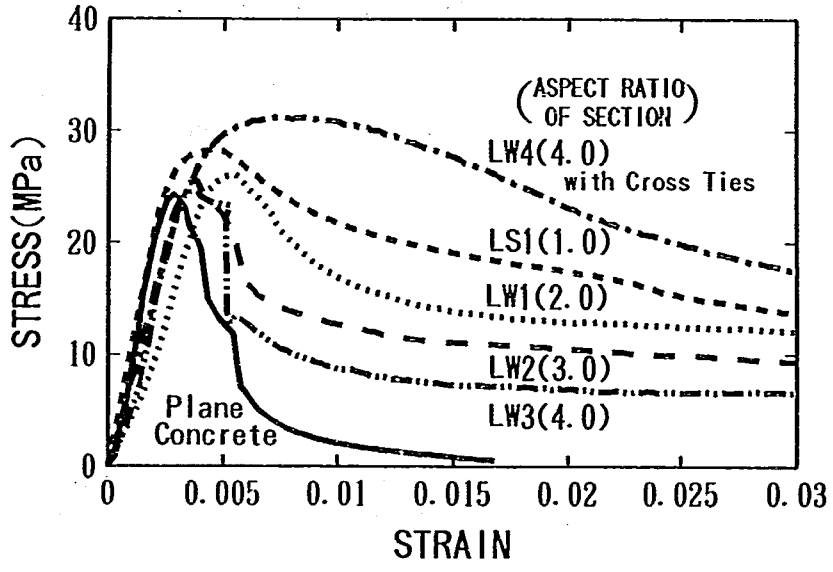


Fig. 8 Effect of Aspect Ratio of Section

MODELING OF THE STRESS–STRAIN RELATION

It can be seen in Fig. 5 that the stress–strain curve consists of three parts, i.e., an ascending branch, falling branch and sustaining branch. In most of the stress–strain models proposed previously, the ascending branch has been formulated by a second order parabola as shown in Table 1. This is because a second order parabola is a simple mathematical expression and it represents well the stress–strain relation. However, it should be noted that the second order parabola can reflect only three boundary conditions, even though the stress–strain model for the ascending branch of confined concrete should reflect the following four boundary conditions.

a) initial condition : $f_c=0$ at $\varepsilon_c=0$ (2)

b) initial stiffness condition : $df_c/d\varepsilon_c=E_c$ at $\varepsilon_c=0$ (3)

c) peak condition : $f_c=f_{cc}$ at $\varepsilon_c=\varepsilon_{cc}$ (4)

d) peak stiffness condition : $df_c/d\varepsilon_c=0$ at $\varepsilon_c=\varepsilon_{cc}$ (5)

where, f_{cc} = peak stress; ε_{cc} = strain at peak stress ; and E_c = initial stiffness. By disregarding (3), the second order parabola is expressed as

$$f_c = f_{cc}\left\{\frac{2\varepsilon_c}{\varepsilon_{cc}} - \left(\frac{\varepsilon_c}{\varepsilon_{cc}}\right)^2\right\} \tag{6}$$

The initial stiffness $2f_{cc}/\varepsilon_{cc}$ in (6) is an implicit function of the volumetric ratio of hoop reinforcement, since both f_{cc} and ε_{cc} depend on the hoop reinforcement content. However, test results show that the initial stiffness is essentially independent of the volumetric ratio of hoop reinforcement, as illustrated in **Fig. 5.** To avoid such an inconsistency, Mander et al. (1988a) adopted a fractional function, which includes the initial stiffness as one of four boundary conditions. Muguruma et al. (1978, 1980) and Fujii et al. (1988) considered (3) as well as (2) and (4) in their second order parabola expressions. However, they needed to use two equations to represent the stress–strain relation of the ascending branch.

To include (3), and avoid having to adopt two equations for the ascending branch, it is proposed here to assume that the stress of concrete is represented by the function

$$f_c = C_1\varepsilon_c^n + C_2\varepsilon_c + C_3 \tag{7}$$

in which C_1, C_2, C_3 and n are constants to be determined from (2) to (5). Eq.(7) enables simplification of the stress–strain expression, while at the same time satisfying the four boundary conditions. By substituting (2) through (5) into (7), one obtains

$$f_c = E_c\varepsilon_c\left\{1 - \frac{1}{n}\left(\frac{\varepsilon_c}{\varepsilon_{cc}}\right)^{n-1}\right\} \tag{8}$$

where, n is a coefficient, and is given as

$$n = \frac{E_c\varepsilon_{cc}}{E_c\varepsilon_{cc} - f_{cc}} \tag{9}$$

A standard values of E_c , provided by Japanese Specifications (Japan Road Association 1991) is used here, and is shown in **Table 4.** It is assumed E_c is not influenced by confinement.

Table 4 Initial Stiffness

Strength of Unconfined Concrete (MPa)	20.6	23.5	26.5	29.4	39.2	49.0
Initial Stffness (MPa)	2.30×10^4	2.45×10^4	2.60×10^4	2.75×10^4	3.04×10^4	3.24×10^4

The falling branch of the stress–strain curve is idealized here by a straight line, as indicated by the test results shown in **Fig. 9,** and is formulated as

$$f_c = f_{cc} - E_{des}(\varepsilon_c - \varepsilon_{cc}) \tag{10}$$

where, E_{des} = deterioration rate, which is developed from regression analysis of test data in the range of ε_{cc} to ε_{cu} . The definition of ultimate strain, ε_{cu} , is important. In the tests, crushing of core concrete and buckling of longitudinal

reinforcement were observed when the compressive stress dropped to less than $0.5f_{cc}$. Because such damage is excessive and unrepairable, the strain corresponding to 50% of the peak stress f_{cc} is assumed as the ultimate strain ε_{cu}.

By substituting $f_c=0.5f_{cc}$ into (10), the ultimate strain ε_{cu} is obtained as

$$\varepsilon_{cu}=\varepsilon_{cc}+\frac{f_{cc}}{2E_{des}} \tag{11}$$

Kent and Park, Sheikh et al., Saatcioglu et al., and Fujii et al. considered the sustained stress after the falling branch to be 20% or 30% of the peak stress. In the proposed model, a special effort was not made to develop a formulation of the sustaining branch, since that region is not critical in the seismic design of bridges.

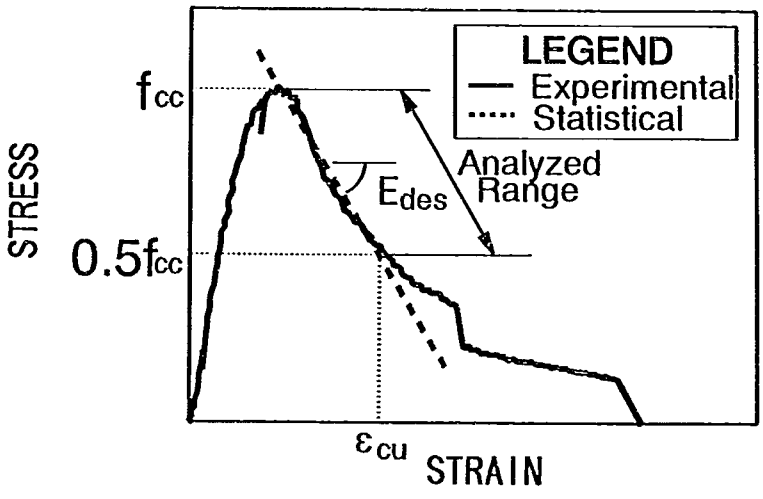


Fig. 9 Definition of Ultimate Strain and Deterioration Rate

EVALUATION OF CONFINEMENT EFFECTIVENESS

Parameters for Confinement Effect

In the proposed model, expressed by (8) and (10), factors for controlling the stress–strain relation of confined concrete are the peak stress, the strain at the peak stress and the slope of the falling branch. The effect of confinement on these three parameters was determined based on the test results, as described below.

The main parameters which are likely to influence the confinement effect are the volumetric hoop reinforcement ratio, the spacing between hoops, hook configuration, the yield strength of hoop reinforcement, core concrete shape, and the strength of the unconfined concrete. Based on the tests presented, it was shown that the hook configuration and the spacing between hoops are less significant on the confinement effect if the hoop reinforcement is placed with reasonable hook configuration and spacing, as is usually the case for bridge columns designed for earthquakes. Therefore, it was determined that the volumetric ratio, the yield strength of hoop reinforcement, the strength of unconfined concrete and core concrete shape were the four most important parameters.

Peak Stress

Fig. 10 shows the relation between a confinement effectiveness factor, $\rho_s f_{yh}/f_{co}$, and the ratio of peak stress to the strength of unconfined concrete, f_{cc}/f_{co}, for the circular and square specimens of the test series. It can be seen that the peak stress f_{cc} is proportional to the volumetric ratio ρ_s and the yield strength f_{yh} of hoop reinforcement, and is inversely proportional to the strength of unconfined concrete f_{co}. The relation may be approximated by a linear function, with the slope depending on the cross sectional shape. It is interesting to note that the slopes of the linear approximation for the SC Series and the SS Series seem to be very close with those for the LC Series and the LS Series, respectively. This implies that the contribution of the longitudinal reinforcement to the confinement effectiveness is limited.

From regression analyses for each section, the relations are written as

$$\frac{f_{cc}}{f_{co}}=\begin{cases}1.0+3.83\dfrac{\rho_s f_{yh}}{f_{co}} & \text{: for circular sections} \quad R^2=0.98\\[2ex] 1.0+0.73\dfrac{\rho_s f_{yh}}{f_{co}} & \text{: for square sections} \quad R^2=0.55\end{cases} \tag{12}$$

where, R^2 is the regression coefficient. It is noted that the slope of the linear approximation for the square section is approximately 20% of that for the circular section. This clearly shows the dependence of confinement on the cross sectional shape, and the efficiency of circular hoops in confining the core concrete.

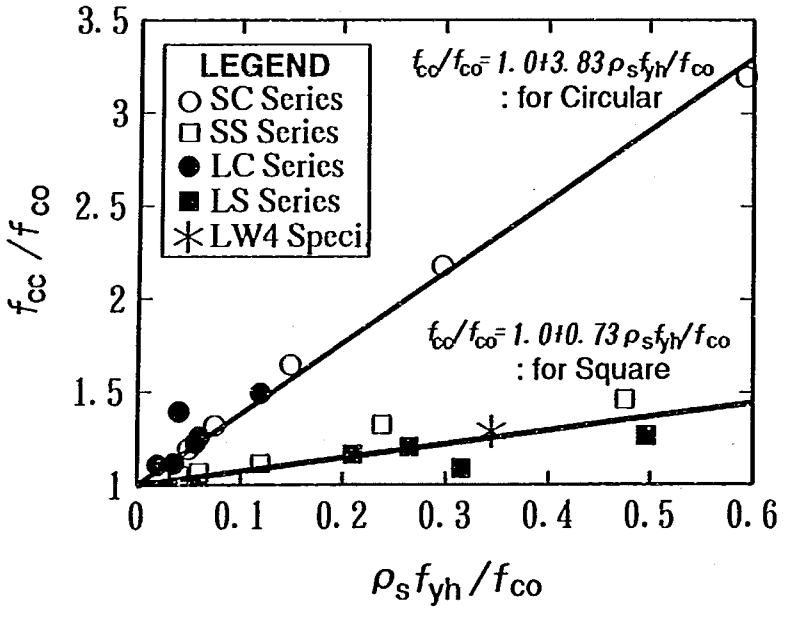


Fig. 10 Relation between Confinement Effectiveness Factor and Peak Stress

Strain at Peak Stress

Fig. 11 shows the confinement effectiveness factor $\rho_s f_{yh}/f_{co}$ vs. the strain ε_{cc}. Clearly the $\rho_s f_{yh}/f_{co}$ vs. ε_{cc} relation may be approximated by a linear function. The following relations are obtained from regression analyses.

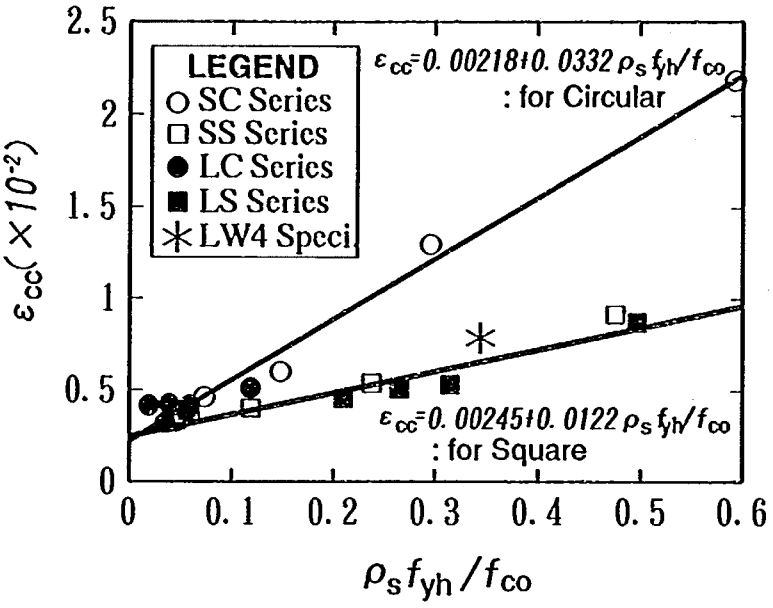


Fig. 11 Relation between Confinement Effectiveness Factor and Strain at Peak Stress

$$\varepsilon_{cc}=\begin{cases}0.00218+0.0332\dfrac{\rho_s f_{yh}}{f_{co}} & \text{: for circular sections} \quad R^2=0.98 \\ 0.00245+0.0122\dfrac{\rho_s f_{yh}}{f_{co}} & \text{: for square sections} \quad R^2=0.92\end{cases} \tag{13}$$

The confinement effectiveness on ε_{cc} for square sections is approximately 40% of that for circular sections.

Deterioration Rate

Fig. 12 shows a confinement effectiveness factor $\rho_s f_{yh}/f_{co}^2$ vs. the deterioration rate, E_{des}. The deterioration rate seems to be inversely proportional to $\rho_s f_{yh}/f_{co}^2$. It is apparent from the data that the effect of cross sectional shape does not significantly influence the deterioration rate. Therefore, a single expression can approximate to test data for both circular and square sections, and the approximate relation is written as

$$E_{des}=\frac{11.2}{\rho_s f_{yh}/f_{co}^2} \tag{14}$$

From (12) to (14), the confinement effectiveness for circular and square sections may be represented as

$$\frac{f_{cc}}{f_{co}}=1.0+3.8\alpha\frac{\rho_s f_{yh}}{f_{co}} \tag{15}$$

$$\varepsilon_{cc}=0.002+0.033\beta\frac{\rho_s f_{yh}}{f_{co}} \tag{16}$$

$$E_{des}=11.2\frac{f_{co}^2}{\rho_s f_{yh}} \tag{17}$$

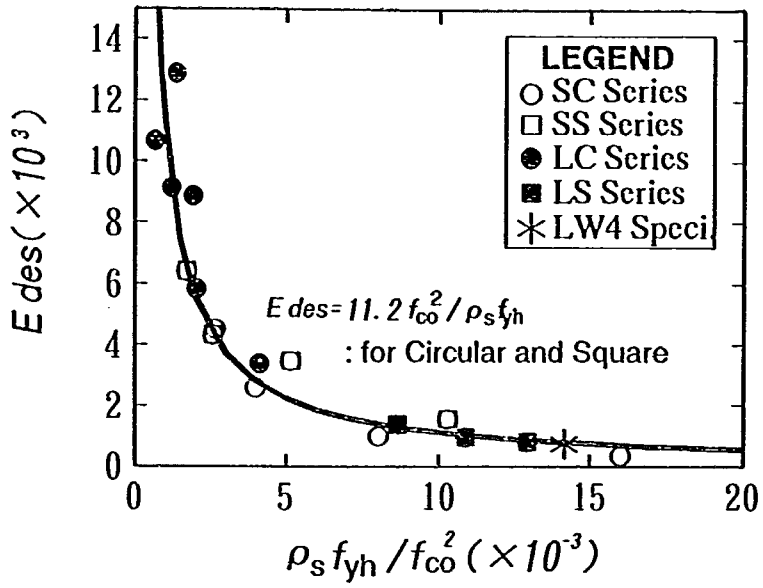


Fig. 12 Relation between Confinement Effectiveness Factor and Deterioration Rate

in which α and β are modification factors depending on cross sectional shape: for circular sections $\alpha=1.0$ and $\beta=1.0$; for square sections $\alpha=0.2$ and $\beta=0.4$.

Estimation of Stress–Strain Relation

Based on (15) to (17), the stress–strain relation was computed for the test specimens shown in Table 3. Analytical results are compared with the test data in Fig. 5. The computed stress–strain relations are in good agreement with the test results. It should be noted that because all four boundary conditions (2) through (5) were included in the proposed stress–strain model, it is possible to reflect the observed phenomenon that the slope of the ascending branch is independent of the hoop reinforcement ratio.

Evaluation of Effect of Cross Ties

To evaluate the confinement effectiveness in wall–type columns with cross ties, Mander et al. (1988a) reported a theory that accounts for the horizontal arching action of the concrete, which occurs between longitudinal reinforcing bars. In Mander's model, the arches were represented by second order parabolas with an initial tangent slopes of 45°.

To study the confinement effect of cross ties, Specimen LW4 was analyzed. It is assumed herein that the whole section with cross ties can be divided into five confined areas, and that each confined area is equivalent to a concrete column of 25cm x 25cm square cross section as shown in Fig. 13. The volumetric ratio of hoop reinforcement, ρ_s, in the equivalent confined section is thus calculated as 2.85%. Therefore, the relations between the confinement effectiveness and three factors f_{cc}, ε_{cc}, E_{des} are obtained as shown in Figs. 10 to 12. It is apparent that the test data of f_{cc}, ε_{cc}, and E_{des} in Specimen LW4 are very close to the prediction by (15), (16) and (17) for square sections. Therefore, based on the test results, the confinement effect for wall–type sections with cross ties may be simply evaluated using equivalent confined sections, as illustrated in Fig. 13.

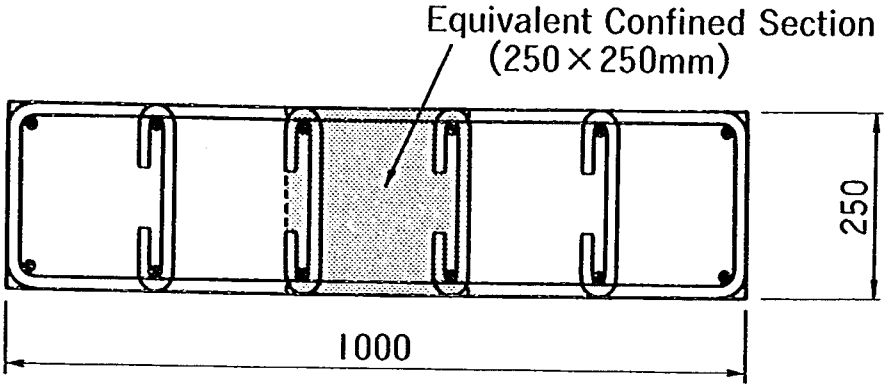


Fig. 13 Equivalent Confined Section

COMPARISON WITH PREVIOUS MODELS

To show the effectiveness of the proposed model, the stress–strain relation predicted by previous models was computed for the test specimens, and compared with the experimental results, as shown in Figs. 14 to 17. Only the comparisons with the models of Kent and Park, of Mander et al., Saatcioglu et al., and of Muguruma et al. for the LC and LS Series are presented in Figs. 14 to 17 as examples. Similar results were found for the other stress–strain models shown in Table 1, and for the SC and SS Series, but these are not presented here due to space limitations.
The previous models generally predict the slope of the ascending branch to be larger than the experimental results. By comparing Fig. 5 with Figs. 14 to 17, it can be seen that the proposed model predicts the peak stress, the strain at the peak stress and the deterioration rate more accurately than the previous models.

The deterioration rate of the LS Series, in which ρ_s is in the range of 1.73% to 4.10%, shows good agreement between the experimental data and prediction by the previous models. However, there are some discrepancies in the previous models for the LC Series. Specimens in the LC Series have lower volumetric ratios of hoop reinforcement (0.19% to 1.16%) than in the LS Series. Therefore, it is concluded that the previous models may not be able to accurately model confinement effects for such low volumetric ratios of hoop reinforcement. The deterioration rate predicted by the proposed model approximates the experimental results somewhat better than the previous models, because the effect of low hoop reinforcement ratio is incorporated into the model.

From the above comparisons, it may be said that the proposed model generally provides better agreement with the stress–strain relation of confined concrete over a wider range of hoop reinforcement ratios than previous models.

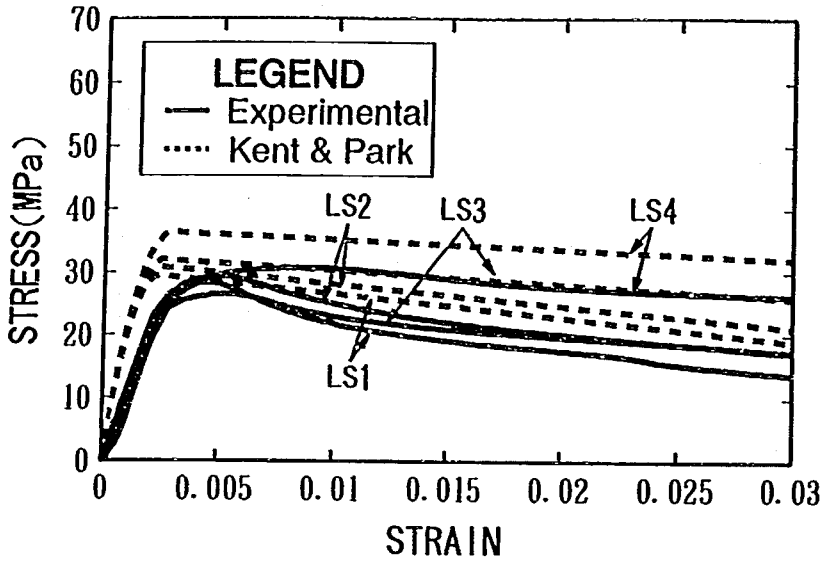
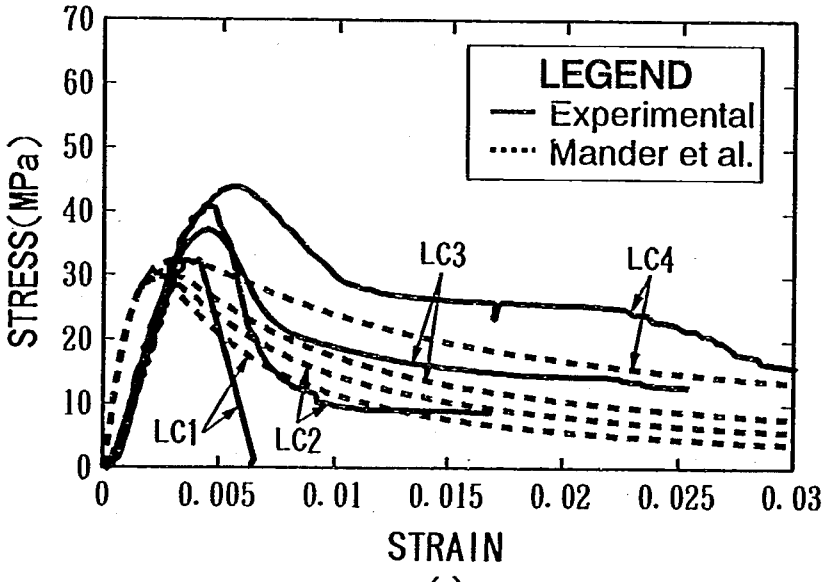
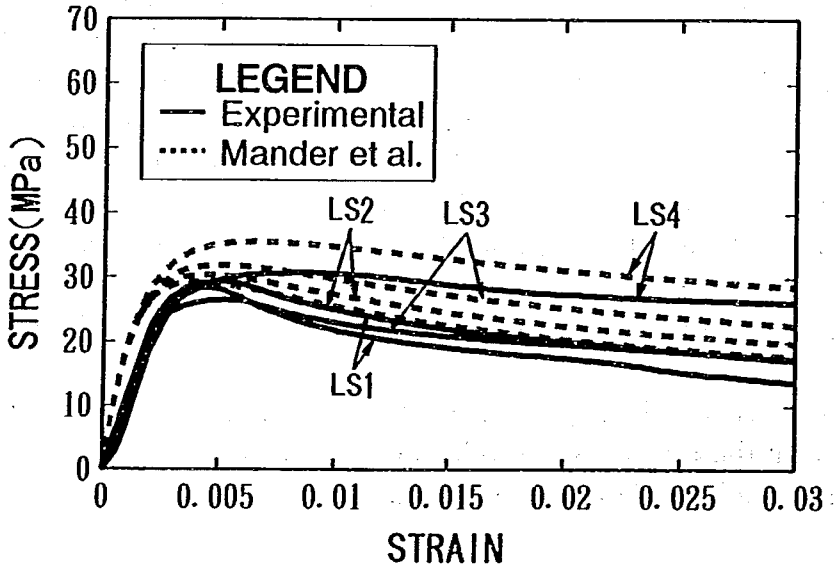


Fig. 14 Stress–Strain Relation by Kent and Park

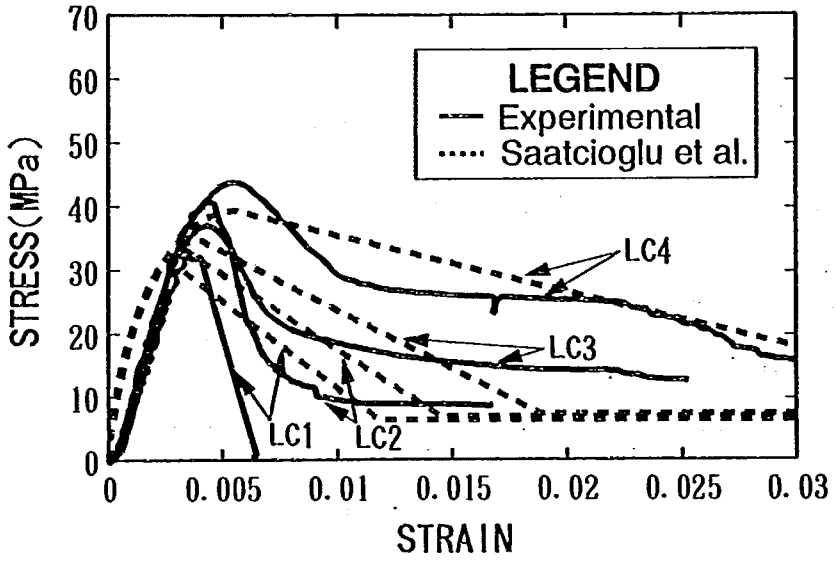


(a)

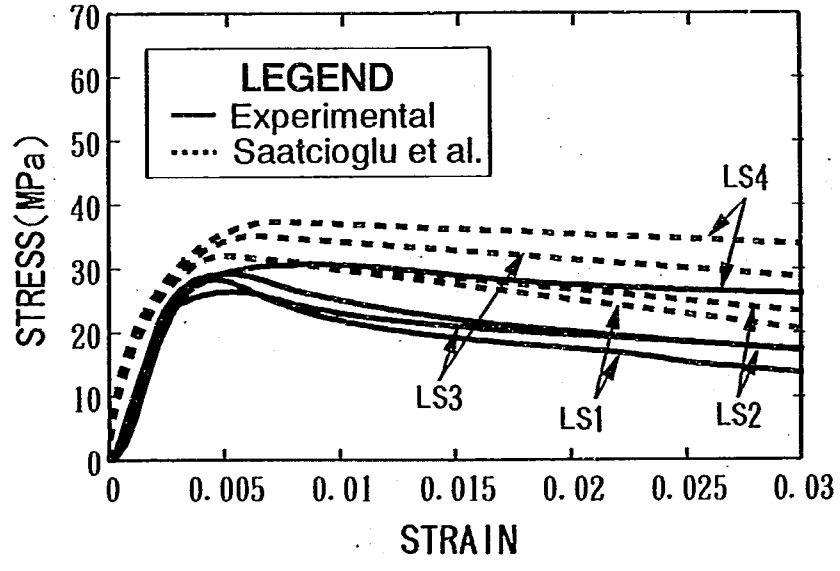


(b)

Fig. 15 Stress–Strain Relation by Mander et al.: (a) LC Series; and (b) LS Series

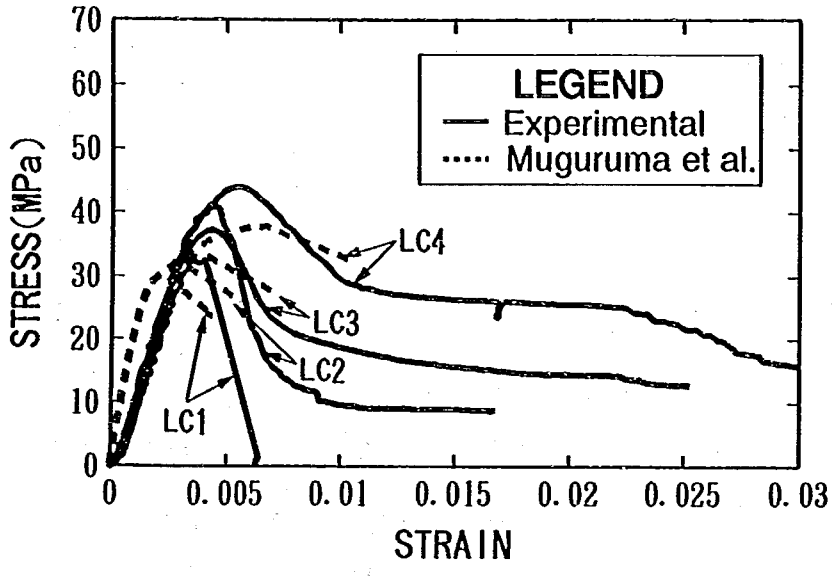


(a)

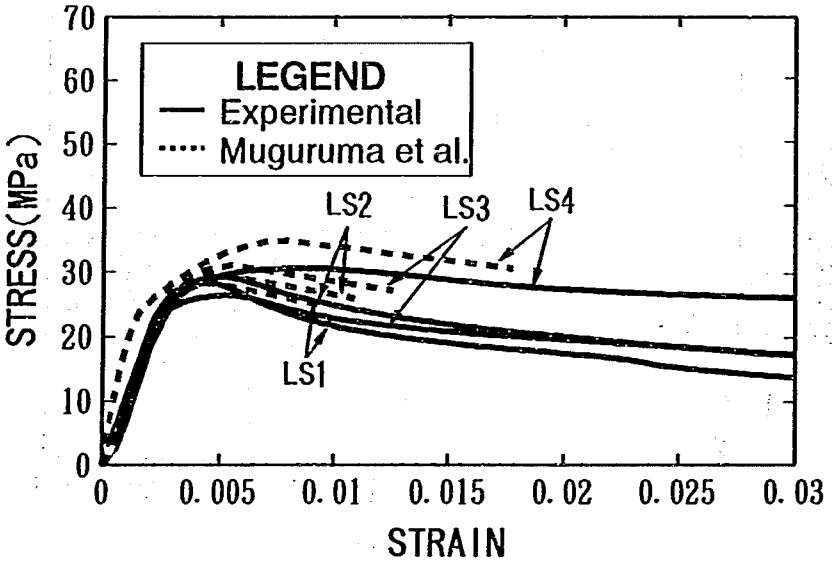


(b)

Fig. 16 Stress–Strain Relation by Saatcioglu et al.: (a) LC Series; and (b) LS Series



(a)



(b)

Fig. 17 Stress–Strain Relation by Muguruma et al.: (a) LC Series; and (b) LS Series

CONCLUDING REMARKS

To propose a reliable and practical stress–strain model for confined concrete, which includes the effects of low confining reinforcement ratios, a series of loading tests were conducted for 31 concrete column specimens. The conclusions from the study are as follows.

1) To consider four boundary conditions by (2)–(5) in the stress–strain relation of concrete, formulation of (8) and (10) is proposed.
2) The ultimate strain ε_{cu} is defined in this study as the strain corresponding to 50% of the peak stress, since knowledge of behavior beyond ε_{cu} is not significant in the seismic design, due to excessive and unrepairable damage.
3) It is proposed to evaluate the peak stress, the strain at the peak stress, and the deterioration rate according to (15) to (17). These expressions were derived based on the test results for specimens with a cross sectional dimension of 20 to 50cm and a volumetric ratio of hoop reinforcement of 0.19 to 4.66%.
4) Cross ties in the wall–type section have a significant effect on increasing ductility. The confinement effectiveness of cross ties can be evaluated by assuming an equivalent confined section, as shown in Fig. 13.
5) The proposed model provides better agreement with the test results, particularly for the confined concrete with low hoop reinforcement ratios, than the previous models.

REFERENCES

"Part IV, Design of Foundations, Design Specifications of Road Bridges." (1991). Japan Road Association

Fujii, M. et al (1988). "A study on the application of a stress–strain relation of confined concrete." *JCA Proceedings of Cement and Concrete*, Japan Cement Association, Vol.42, Tokyo, Japan, pp.311–314

Kent, D. C. and Park, R. (1971). "Flexural members with confined concrete.", *Journal of the Structural Division*, ASCE, Vol.97, No.ST7, pp.1969–1990

Mander, J. B., Priestley, M. J. N and Park, R. (1988a). "Theoretical stress–strain model for confined concrete." *Journal of the Structural Division*, ASCE, Vol.114, No.ST8, pp.1804–1826

Mander, J. B., Priestley, M. J. N and Park, R. (1988b). "Observed stress–strain behavior of confined concrete." *Journal of the Structural Division*, ASCE, Vol.114, No.ST8, pp.1827–1849

Muguruma, H. et al (1980). "A stress–strain model of confined concrete." *JCA Proceedings of Cement and Concrete*, Japan Cement Association, Vol.34, Tokyo, Japan, pp.429–432

Muguruma, H. et al (1978). "A study on the improvement of bending ultimate strain of concrete." *Journal of Structural Engineering*, JSCE, Vol.24, Tokyo, Japan, pp.109–116

Park, R. et al (1982). "Ductility of square–confined concrete columns." *Journal of the Structural Division*, ASCE, Vol.108, No.ST4, pp.929–950

Razvi, S. R. and Saatcioglu, M. (1989). "Confinement of reinforced concrete columns with welded wire fabric." *ACI Structural Journal*, 86(6), pp.615–623

Saatcioglu, M. and Razvi, S. R. (1992). "Strength and ductility of confined concrete." *Journal of the Structural Division*, ASCE, Vol.118, No.ST6, pp.1590–1607

Sheikh, S. A. and Uzumeri, S. M. (1980). "Strength and ductility of tied concrete columns." *Journal of the Structural Division*, ASCE, Vol.106, No.ST5, pp.1079–1102

Sheikh, S. A. and Uzumeri, S. M. (1982). "Analytical model for concrete confinement in tied columns." *Journal of the Structural Division*, ASCE, Vol.108, No.ST12, pp.2703–2722

RESIDUAL DISPLACEMENT RESPONSE SPECTRA AND ITS APPLICATION

Kazuhiko Kawashima[1], Gregory A. MacRae[2], Jun-ichi Hoshikuma[3] and Kazuhiro Nagaya[4]

1: Professor, Civil Engineering Department, Tokyo Institute of Technology, Meguro-ku, Tokyo, 152, Japan
2: Assistant Professor, University of Washington, Seattle, Washington, USA
3: Research Engineer, Public Works Research Institute, Ministry of Construction, Tsukuba Science City, Ibaraki-ken, 305, Japan
4: Assistant Research Engineer, Public Works Research Institute, Ministry of Construction, Tsukuba Science City, Ibaraki-ken, 305, Japan

INTRODUCTION

When a structure is subjected to a strong ground shaking, the structural members may exhibit nonlinear behavior. If enough ductility is available in structural members with stable hysteretic energy dissipation, the structure will not collapse during the strong shaking. For this reason, the lateral strength level considered in seismic design is generally less than the elastic response force level for structures with stable nonlinear behavior. The level of strength provided depends on the ductility capacity.

It should be noted however that a limitation for the maximum amount of force reduction from the elastic force level may be required even if enough ductility is secured for structural members. It has been pointed out that residual displacements may be associated with large nonlinear behavior after an earthquake (for example, Kawashima, MacRae and Hasegawa, 1992, Kawashima and Hasegawa, 1994). This causes various problems for repair and reconstruction. It is important to consider an appropriate combination of lateral strength and residual displacement developed in structures after earthquakes.

Various studies have been made on the nonlinear behavior of structures and it is well known that the residual displacement increases as the ductility of structures increases. However, the dependence of the residual displacement on the ductility and strong ground motion has not yet been precisely investigated.

This paper proposes a residual displacement response spectrum, which describes the residual displacement developed in a one-degree-of-freedom

oscillator with various natural periods of structures, damping ratio, ductility and bilinear factors, and presents an application of the residual displacement response spectra.

RESIDUAL DISPLACEMENT RESPONSE SPECTRUM

A one-degree-of-freedom oscillator is assumed to be supported by a spring with a nonlinear hysteretic restoring force characteristic. The oscillator is subjected to a ground shaking at its base. Although any hysteretic restoring force models can be assumed in the spring, a bilinear model as shown in Fig. 1 is assumed here for simplicity of analysis.

The spring changes its stiffness from an initial (elastic) stiffness k_1 to a second (post-yielding) stiffness k_2 at a yield displacement u_y. The bilinear factor r and the ductility factor μ are defined as

$$r = k_2 / k_1 \qquad (1)$$

$$\mu = u_{max} / u_y \qquad (2)$$

where u_{max} is the maximum displacement of the oscillator.

To represent the energy dissipation contributed from sources other than the hysteretic energy dissipation such as radiation of energy from a foundation to surrounding soils, a viscous damping ratio h is considered in the analysis in addition to the hysteretic damping associated with the nonlinear spring stiffness.

When an oscillator is subjected to a ground motion at its base, a residual displacement u_r may be developed after the shaking has finished. The magnitude of residual displacement u_r depends on various factors such as the ductility factor μ, natural period T, damping ratio h, bilinear factor r and the intensity of ground shaking. Because the residual displacement sometimes oscillates even at the end of ground accelerations, some zero accelerations were added at the end of the ground motions to compute the final rest point of the residual displacement.

Thus the residual displacements can be computed from each strong motion record for oscillators with various values of ductility factor μ, natural period T, damping ratio h, and bilinear factor r. The residual displacement plotted against natural period T, damping ratio h, bilinear factor r and ductility factor μ is proposed here to be defined as a *residual displacement response spectrum* S_{RD} from its analogy to the original definition of the response spectrum (Housner 1959).

Target ductility factors μ_T of 2, 4 and 6 were selected, and the yield force F_y was obtained in order that the ductility factors μ computed corresponded to the target ductility factors μ_T. This requires some iterations as shown in Fig. 2. First one assumes F_y to compute $u_{\max}$ for a given strong motion acceleration. If the ductility factor μ computed by (2) is not close to μ_T, a new value of F_y is chosen to compute $u_{\max}$ until the difference between μ and μ_T becomes sufficiently small. Generally 5 iterations is sufficient to have a convergence with an error of less than 0.1%.

For any hysteretic curve, there is a maximum possible value of the residual displacement. As shown in Fig. 3, the residual displacement takes its maximum value when oscillator unloads from the maximum displacement $u_{\max}$. Assuming that the motion of oscillator comes to rest when the restoring force becomes zero, the maximum residual displacement may be written as

$$u_{r\max}=\begin{cases}(\mu-1)(1-r)u_y \text{----} r(\mu-1)<1\\ \{(1-r)/r\}u_y \text{----} r(\mu-1)\geq 1\end{cases} \qquad (3)$$

Because the motion of oscillator does not necessarily stop on the hysteresis loop immediately after the oscillator experienced the maximum displacement $u_{\max}$, (3) represents the maximum possible value of the residual displacement u_r. Therefore, $u_{r\max}$ is defined as the maximum possible residual displacement.

It is convenient to normalize the residual displacement u_r by $u_{r\max}$ as

$$S_{RDR}=u_r/u_{r\max} \qquad (4)$$

S_{RDR} is designated here as a residual displacement ratio. The plots of S_{RDR} against natural periods T, damping ratio h, bilinear factor r and ductility factors μ are defined as the *residual displacement ratio response spectra.*

In the following, the natural period T is computed from the initial stiffness k_1 and the mass of the oscillator. The viscous damping ratio h is assumed to be 0.05 for typical structures.

RESIDUAL DISPLACEMENT RESPONSE SPECTRA FOR A TYPICAL RECORD

Fig. 4 shows a residual displacement u_r computed for an oscillator with natural period $T=1s$ subjected to a strong motion acceleration recorded in the vicinity of Itajima bridge during the Hyuga-nada earthquake in 1968 (Iwasaki

et al, 1982). The magnitude of earthquake was 7.2 and the record was obtained 195 km from the epicenter. It is seen in Fig. 4 that the residual displacement is developed approximately when the ground motion takes its peak value. It is important to note that u_r increases as the bilinear factor r decreases.

By computing the residual displacement in the same manner for oscillators with various natural periods, the residual displacement ratio response spectrum S_{RDR} for the Itajima record is obtained as shown in Fig. 5. The acceleration response spectrum S_A is also presented in Fig. 5. It is seen from S_A that the predominant period of ground motion is about 0.2s and 1.0s. It is interesting to note that the residual displacement ratio response spectrum S_{RDR} takes peak values at those natural periods. This may be due to the fact of resonance.

ANALYSIS OF RESIDUAL RESPONSE SPECTRA

The residual displacement ratio response spectrum S_{RDR} was evaluated for 63 components of strong motion acceleration records triggered by earthquakes with magnitude ranging from 6.5 and 7.9. They were recorded at free-field ground surface, and any records obtained at basement and first floor of buildings were excluded.

Fig. 6 shows the earthquake magnitude and epicentral distance of the data set. About 71 % of the records were induced by the earthquakes with magnitude larger than 7. The ground condition was classified into three groups as shown in Table 1 based on the natural period of ground T_g (JRA 1990, Kawashima and Hasegawa 1994). The number of the records at Group I (stiff), II (medium) and III (soft) sites are 13, 37 and 13, respectively. Fig. 7 shows the peak acceleration of strong motion records used in the analysis. About 1/3 of the total records have peak accelerations larger than 60 gal (cm/s^2).

Effect of Earthquake Magnitude and Epicentral Distance

Fig. 8 is a typical example to show how the residual displacement ratio response spectra S_{RDR} changes with the earthquake magnitude M and epicentral distance Δ of the records. The S_{RDR} for $T=1s$ and $\mu=4$ are presented here, because other conditions show similar results. The earthquake magnitude is classified into $6.5 \leq M < 7$, $7 \leq M < 7.5$, and $7.5 \leq M$.

It is apparent from Fig. 8 that the residual displacement ratio response spectra S_{RDR} do not consistently depend on the earthquake magnitude and epicentral distance.

Soil Condition, Natural Period and Ductility Factor

Therefore, the residual displacement ratio response spectra S_{RDR} which are in the same combinations of the natural period T, ductility factor μ and soil conditions GC were analyzed using oscillators with the bilinear factor of -0.05, 0.0 and 0.1. Figs. 9 and 10 show the mean value m and the standard deviation σ which were computed for specific combinations of T, μ and GC.

The dependence of the mean value m of residual displacement ratio response spectra on the bilinear factor r is considerable. This effect will be precisely discussed later.

It is interesting to note that the soil condition is less significant for the residual displacement ratio response spectra S_{RDR}. The effect of natural period on S_{RDR} is generally small, in particular for r=-0.05 and r=0. At r=0.1, S_{RDR} seems to have slightly smaller values at specific natural periods. The natural periods where S_{RDR} is slightly smaller at r=0.1 is about 0.1-0.2s in Group I and 0.5-1s in Groups II and III. This may be related to the predominant period of ground motions. However it may be considered that the dependence of the residual displacement ratio response spectra S_{RDR} on natural period is less significant from a practical point of view.

The mean value m of residual displacement ratio response spectra is also less sensitive to ductility factor at r=0. However, it increases as ductility factor increases at $r>0$ while vice versa at $r<0$.

The standards deviation σ of residual displacement ratio response spectra increases as ductility factor increases. But it is almost independent of ductility at r=0, and is about 0.3 regardless of natural period and ground condition. It is also about 0.3 for μ=2 at r=-0.05 and r=0.1.

Effect of Bilinear Factor

As was described in the previous sections, it is apparent that the bilinear factor r is the most significant parameter controlling the residual displacement ratio response spectra S_{RDR}.

Fig. 11 shows the effect of soil condition on the S_{RDR} vs. r relation. The result for a combination of T=1s and μ=4 is presented here, because other cases exhibit similar results. Although S_{RDR} is about 0.2 or less at $r\geq$0.1, it

suddenly starts to increase as r approaches zero. S_{RDR} is almost 1.0 at $r \leq -0.05$. Although S_{RDR} is slightly larger at the Group *I* sites than the Group *II* and *III* sites at $r>0$, the effect of soil condition is less sensitive, as described in the previous section.

Fig. 12 shows the effect of natural period T on the S_{RDR} vs. r relation. Because the effect of soil condition was less sensitive, S_{RDR} averaged over all ground conditions is presented here. It is apparent from Fig. 12 that the effect of natural period on the S_{RDR} vs. r relation is less significant.

Fig. 13 shows the effect of ductility factor on the S_{RDR} vs. r relation. The effect of ductility factor is not necessarily less sensitive. S_{RDR} becomes slightly larger as μ decreases to about 2 at $r>0$ and vice versa at $r<0$. The variation of S_{RDR} between $\mu=2$ and $\mu=6$ is the largest at r from -0.01 to 0.05. The effect is however limited to formulate the general trend of the residual displacement ratio response spectra S_{RDR} vs. bilinear factor r relation.

S_{RDR} PROPOSED FOR SEISMIC DESIGN

As shown previously, the residual displacement ratio response spectra S_{RDR} depends on various factors, and bilinear factor r is the most significant factor controlling the residual displacement ratio response spectra S_{RDR}. The scatter of S_{RDR} for records is large.

Based on those findings, for evaluating the residual displacement ratio response spectra for seismic design, it was decided to ignore the effect of natural period, ground condition and ductility factor on S_{RDR} and to consider only the effect of bilinear factor. Because the scatter of the residual displacement ratio response spectra around the mean value m is considerable, one standard deviation σ from the mean value is included for design. Fig. 14 shows the residual displacement ratio response spectra S_{RDR} thus evaluated, and this is proposed to be used in design.

APPLICATION OF RESIDUAL DISPLACEMENT RESPONSE SPECTRA

The residual displacement response spectra of Fig. 14 can be used for any structure where the hysteresis lop shape may be reasonably approximated by a bilinear model.

An example of the application of this method is given for thirteen reinforced concrete bridge piers as shown in Table 2. They were designed in accordance with the equivalent static seismic design method with the lateral force coefficient of 0.2 and the allowable stress design approach (JRA 1990,

Kawashima and Hasegawa 1994). The pier height was varied from 5m to 20m and the deck length was varied from 20m to 40m. The deck was assumed to be a simply supported plate girder with 7m (2 lanes) in wide. The piers were assumed to have rectangular cross section with 7m wide in transverse direction. Shear span ratios range between 5 and 9 in longitudinal direction. These are assumed to be subjected to earthquake excitation in longitudinal direction with approximately the same amount of displacement in each direction.

From the Takeda model of the reinforced concrete column (Takeda, Sozen and Nielsen, 1970) , it may be seen that after the initial cycle, the behavior of the lateral force vs. displacement relationship is bilinear with the initial stiffness k_1 and the post-yield stiffness k_2 as shown in Fig. 15. These parameters may be evaluated based on the monotonic force vs. displacement curve of the cracked columns. The equivalent bilinear factor for the this model is $r = k_2 / k_1$.

The monotonic curve is evaluated according to the Seismic Design Specifications of Bridges of the Japan Road Association (JRA, 1990), and the yield force F_y, ultimate force F_u, yield displacement u_y, and the ultimate displacement u_u of the columns were obtained. From those values, the monotonic initial stiffness k_{1m} and the monotonic second stiffness k_{2m} were obtained as

$$k_{1m} = \frac{F_y}{u_y} \qquad (5)$$

$$k_{2m} = \frac{F_u - F_y}{u_u - u_y} \qquad (6)$$

In order that the displacement capacity u_u is not reached during an earthquake, the maximum ductility μ which may be used in design is reduced below u_u / u_y as (JRA, 1990)

$$\mu = 1 + \frac{u_u - u_y}{\alpha u_y} \qquad (7)$$

where α is a factor of safety of 1.5.

The displacement demand is therefore μu_y. The stiffnesses of the bilinear loop k_1 and k_2 are obtained as

$$k_1 = \frac{k_{1m}}{\sqrt{\mu}} \qquad (8)$$

$$k_2 = \frac{F_m}{2\mu u_y - F_m / k_1} \qquad (9)$$

where

$$F_m = F_y + \frac{\mu u_y - u_y}{u_u - u_y}(F_u - F_y) \qquad (10)$$

The natural period T was computed from the initial stiffness k_{1m} of cracked section due to nomotonic loading and the mass M_D given as

$$M_D = M_1 + 0.3M_2 \qquad (11)$$

where M_1: mass of the deck supported by the pier and M_2: mass of the pier.

Table 3 shows k_1, k_2 and natural period T for the thirteen piers.

Residual displacements at the pier top were computed from

$$u_{r\max} = \mu u_y - F_m / k_1 \qquad (12)$$

together with (4) and Fig. 14 as shown in Table 4 for different ductilities specified by JRA 1990 according to (7) and 10. The bilinear factor r for the system was in the range of 0.19 to 0.43. It tended to be larger at lower ductilities. The residual displacement ratio response spectra S_{RDR} from Fig. 14 range between 0.19 and 0.32 considering the standard deviation factor of safety. This gave the maximum likely residual displacement u_r. These displacements range from 4.3mm to 90mm which is from 0.08 to 0.21 of the peak displacement μu_u and are larger in the more flexible columns with large u_y and high ductility. For critical structures, the post earthquake serviceability should be able to be guaranteed with these levels of residual displacement.

It should be noted that reinforced concrete columns which are subjected to a pulse type motion and which do not deform approximately the same amount in each direction may have larger residual displacements because its hysteresis loop does not match the bilinear approximation.

Also, structures with lower bilinear factors r or eccentrically loaded reinforced concrete cantilever columns are likely to have significantly greater residual displacements.

CONCLUSIONS

For evaluating the residual displacement developed at structures subjected to large ground motions, a residual displacement response spectrum was proposed, and its characteristics were clarified based on the 63

components of free-field strong motion records. An application of the residual displacement response spectra was also presented. Based on the results presented herein, the following conclusions may be deduced:

(1) The residual displacement ratio response spectrum S_{RDR} , which is defined as a residual displacement response spectrum S_{RD} normalized by the maximum possible residual displacement $u_{r\max}$ given by (3), is almost independent of earthquake magnitude, epicentral distance and soil condition.

(2) The residual displacement ratio response spectra S_{RDR} depends significantly on the bilinear factor r. The residual displacement ratio response spectra is small at $r>0$, but it suddenly starts to increases as r approaches to 0 and becomes negative. It is almost 1.0 at $r<-0.05$.

(3) The dependence of natural period and ground condition on the residual displacement ratio response spectra S_{RDR} vs. bilinear factor r relation is not very significant. Ductility factor has slight effect on this relation. A design residual displacement ratio response spectra S_{RDR} vs. bilinear factor r relation was proposed as shown in Fig. 14 by taking average of the residual displacement ratio response spectra for 63 components of strong motion records. To consider the scatter around the mean value, one standard deviation from the mean value was included in the proposed relation.

(4) Residual displacement developed at the crest of reinforced concrete bridge piers was computed based on the residual displacement ratio response spectra proposed. The maximum residual displacement at the pier crest is 56.3cm for the pier with 20m high, if ductility factor is 10.

(5) The residual displacement response spectrum is very effective to evaluate residual displacement developed in structures subjected to strong ground motions.

REFERENCES

Housner, G. W. (1959), "Behavior of structures during earthquakes." Proc. ASCE, 85, Em4

Iwasaki, T., Kawashima, K., Takagi, Y. and Aizawa, K. (1982), "Dynamic soil-structure interaction of Kaihoku bridge." Proc. Japan Society of Civil Engineering, 322, 15-24

Japan Road Association (1990), "Part V Seismic design, Design specifications of highway bridges."

Kawashima, K. and Hasegawa, K. (1994a), "Experimental investigation on nonlinear seismic response of bridge columns and accuracy of equal energy assumption." Proc. Japan Society of Civil Engineering, 483/I-26, 137-146

Kawashima, K. and Hasegawa, K. (1994b), "New seismic design specifications of highway bridges in Japan." Earthquake Spectra, 10 (2), 333-356

Kawashima, K., MacRae, G. A. and Hasegawa, K. (1992), "The strength and ductility of steel bridge piers based on loading tests>" Journal of Research, 29, Public Works Research Institute, Tsukuba, Japan.

Takeda, T., Sozen M. A. and Nielsen N. N. (1970), "Reinforced concrete response to simulated earthquakes," Journal of Structural Engineering, ASCE, 96-12, 2557-2573

Table 1 Definition of Ground Condition

Ground Condition	Natural Period T_G	Geological Definition
Group I	$T_G<0.2s$	Tertiary or older rock, or diluvium with H<10m
Group II	$0.2s \leq T_G<0.6s$	Diluvium with H≥10m, or alluvium with H<25m including soft layer with H<5m
Group III	$0.6s \leq T_G$	Other than the above, usually soft alluvium or reclaimed land

Table 2 Bridge Piers Analyzed

Case	Hight of Pier (m)	Shear–Span Ratio	Width of Pier (m)	Span Length (m)
1	5	6	0.83	20
2				30
3				40
4	10	7.1	1.4	30
5				40
6		9	1.11	30
7				40
8	15	7.1	2.1	30
9				40
10		9	1.67	30
11				40
12	20	7.1	2.8	40
13		9	2.22	40

Table 3 Yield Displacement, Natural Period and Bilinear Factor

Case	u_y (cm)	u_u (cm)	F_y (tf)	F_u (tf)	k_{1m} (tf/cm)	k_{2m} (tf/cm)
1	0.56	8.96	54.2	62.1	96.79	0.94
2	0.96	8.13	67.1	76.3	69.90	1.28
3	1.43	6.89	91.8	103.3	64.20	2.11
4	1.93	24.7	85.5	98.1	44.30	0.55
5	2.85	22.2	109.5	125.8	38.42	0.84
6	4.60	23.7	85.9	96.3	18.67	0.54
7	5.30	23.6	108.5	123.3	20.47	0.81
8	2.94	53.5	124.2	145.8	42.24	0.43
9	4.12	47.2	152.8	180.2	37.09	0.64
10	6.03	50.0	112.1	129.7	18.59	0.40
11	7.00	48.4	137.1	159.5	19.59	0.54
12	4.98	70.68	181.6	220.3	36.47	0.59
13	9.40	70.9	177.5	212.1	18.88	0.56

Table 4 Residual Displacement Developed at Top of Piers

Case	Ductility Factor μ Specified by JRA (1990)	μ =5	μ =10
1	4.12	1.50	3.67
2	3.18	2.50	6.06
3	2.15	3.53	8.44
4	10.80	5.12	12.51
5	8.39	7.32	17.71
6	7.68	11.51	27.64
7	6.99	12.78	30.28
8	25.06	7.86	19.26
9	19.82	10.76	26.16
10	19.22	15.51	37.54
11	17.34	17.62	42.36
12	30.98	13.04	31.76
13	25.81	23.48	56.30

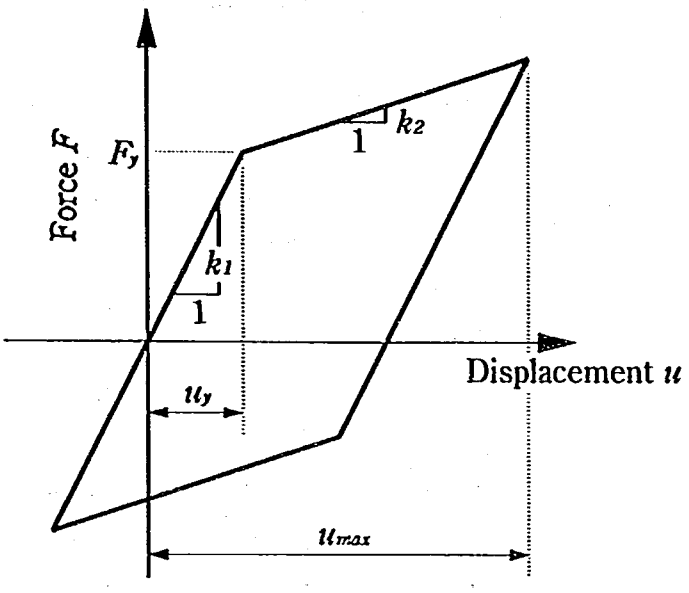


Fig. 1 Definition of Bilinear Hysteresis Model

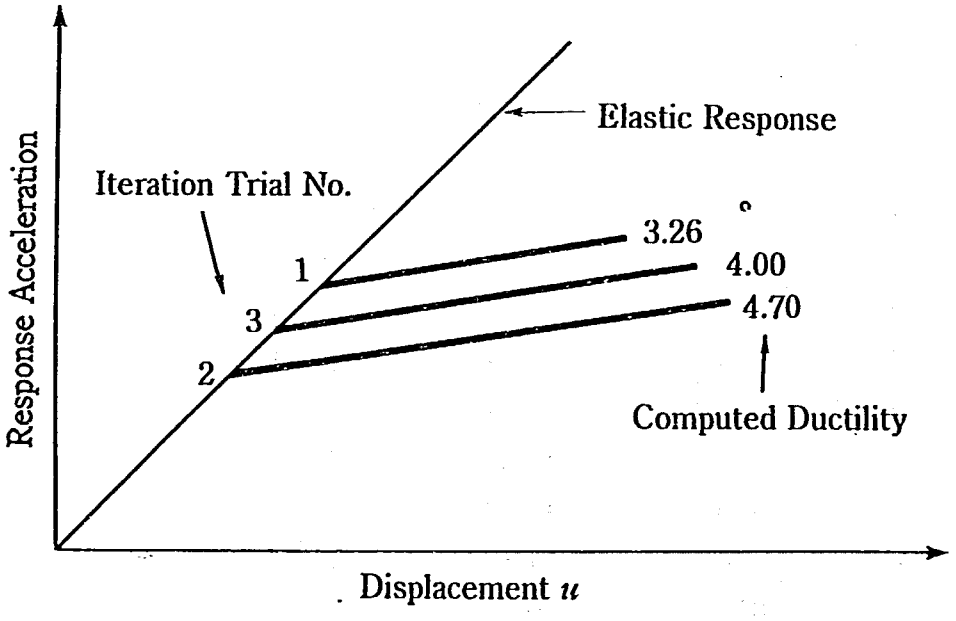
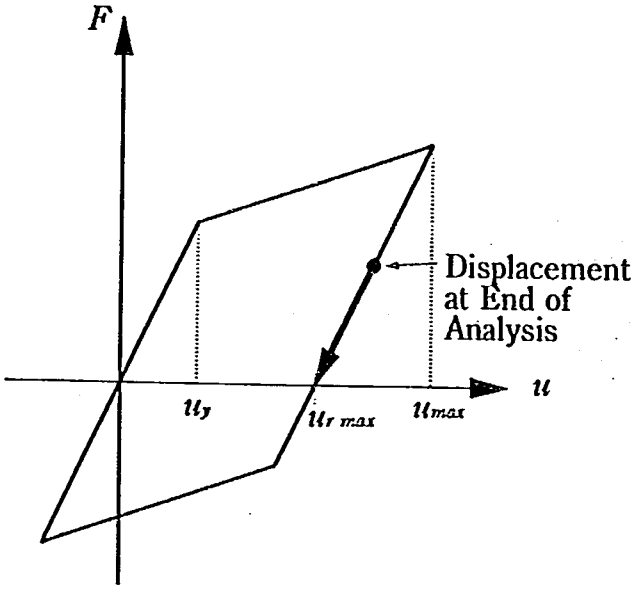
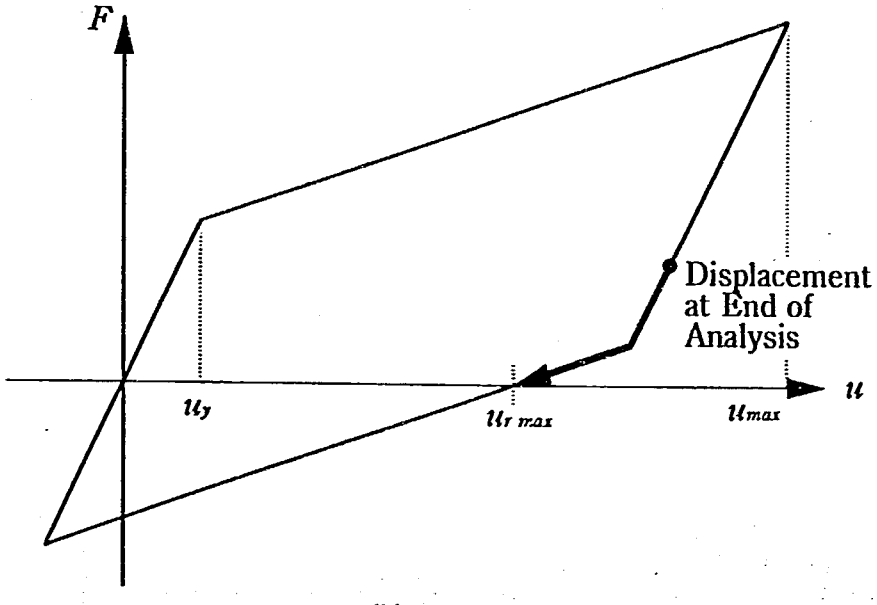


Fig. 2 Iteration Required to Achieve Target Ductility Factor

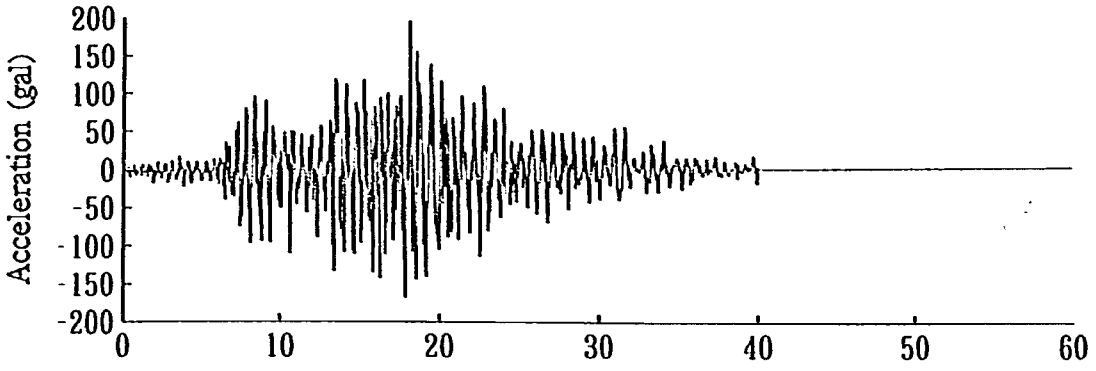


(a) $r(\mu-1)<1$

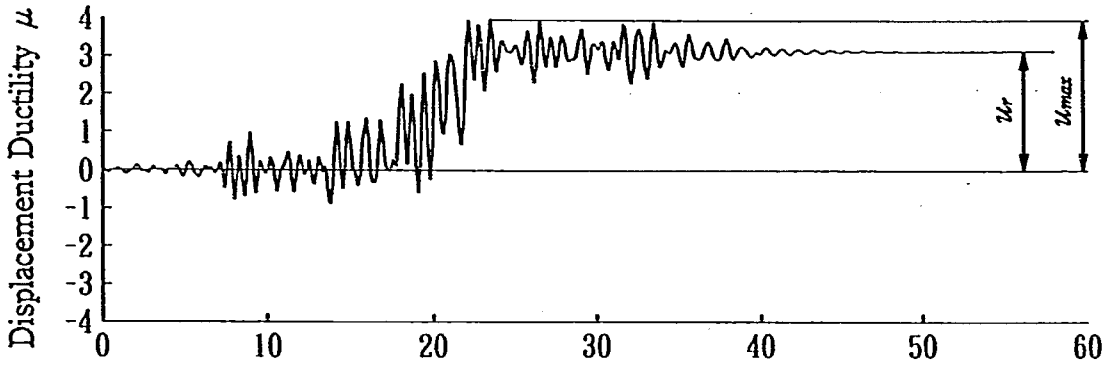


(b) $r(\mu-1)\geqq 1$

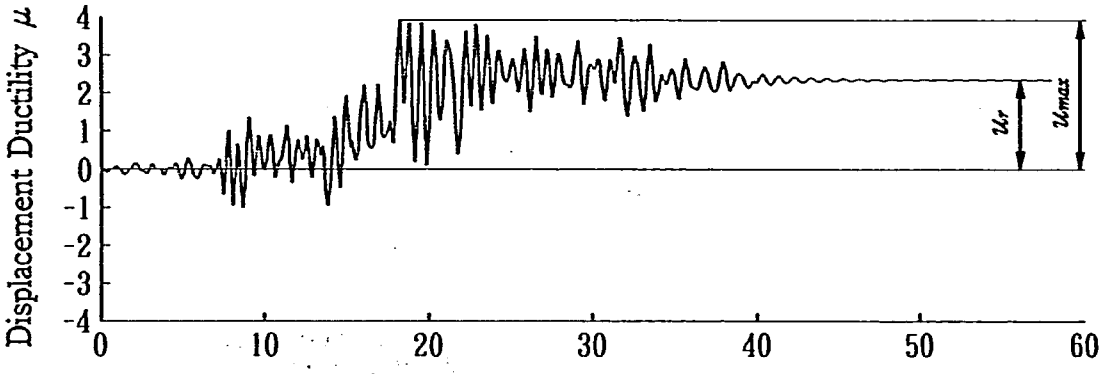
Fig. 3 Maximum Possible Residual Displacement



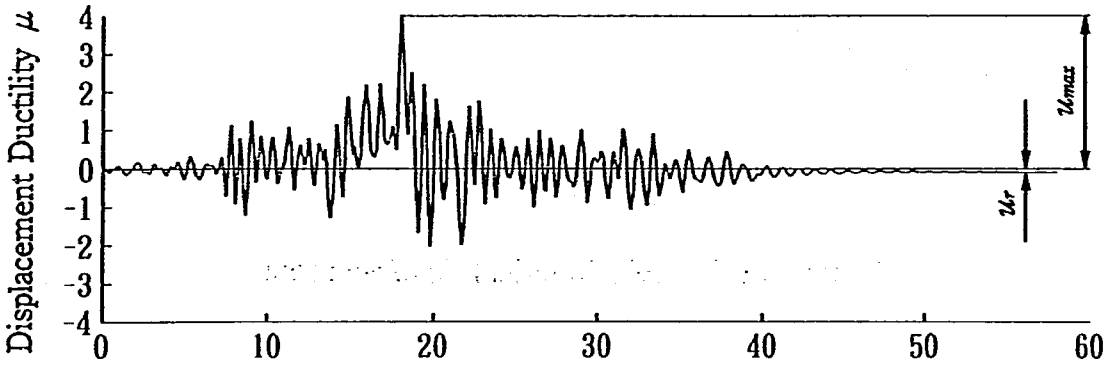
(a) Input Acceleration



(b) $r=-0.05$

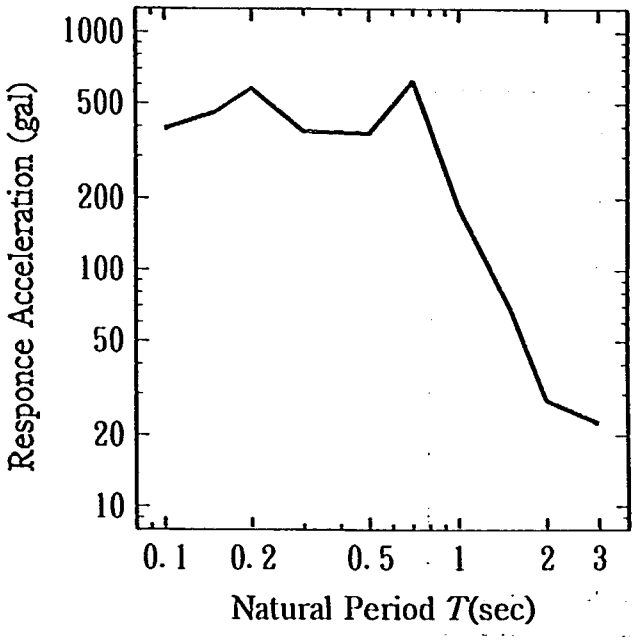


(c) $r=0$

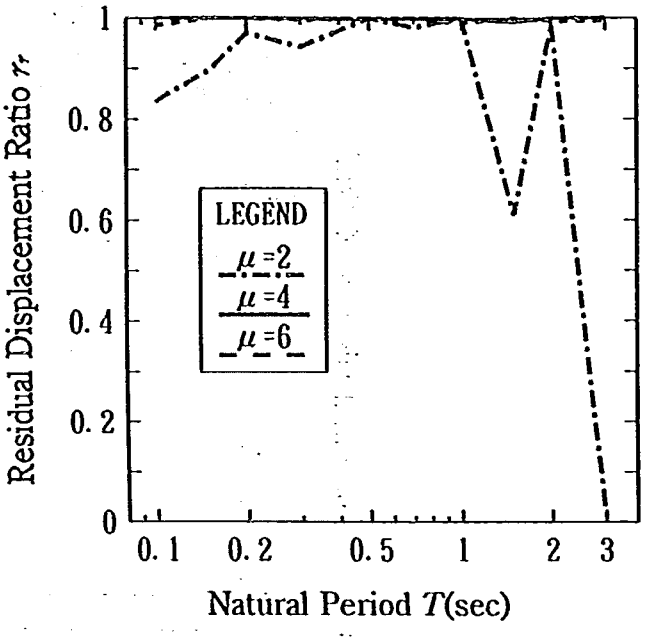


(d) $r=0.1$

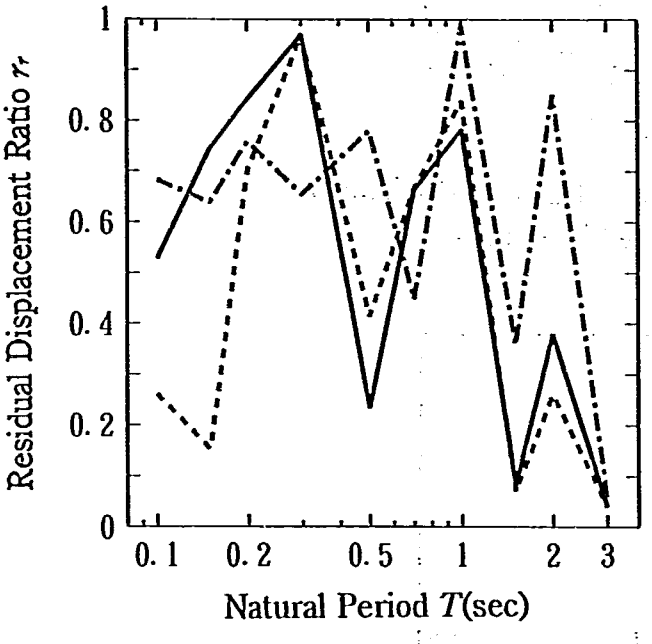
Fig. 4 Residual Displacement for Itajima record (T=1s)



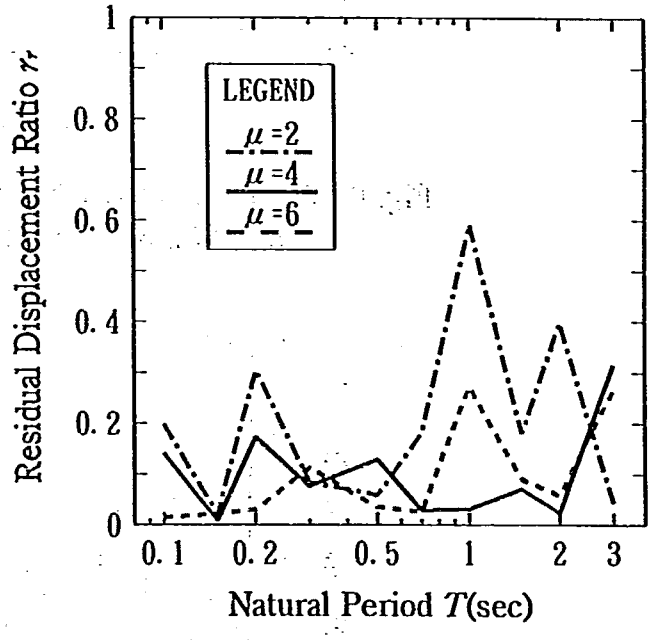
(a) Acceleration Response Spectra (h=0.05)



(b) r=−0.05



(c) r=0



(d) r=0.1

Fig.5 Residual Displacement Ratio Response Spectra for Record

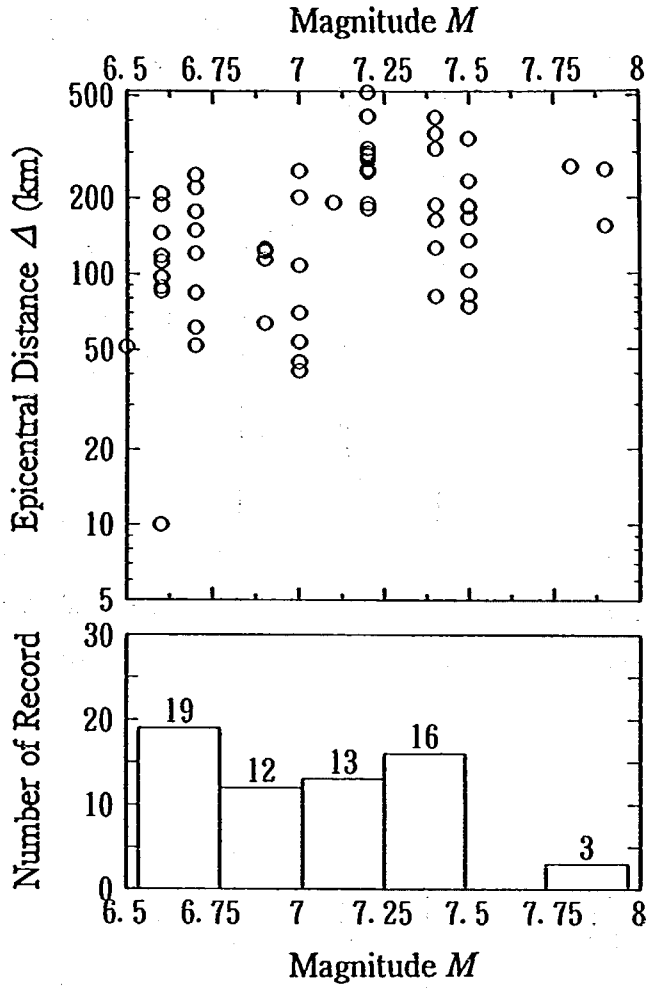


Fig. 6 Magnitude of Earthquake and Epicentral Distance for Strong Motion Records Used in Analysis

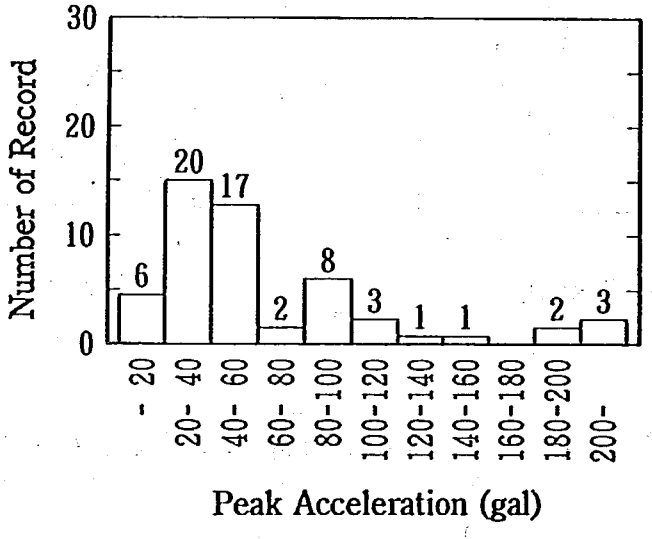
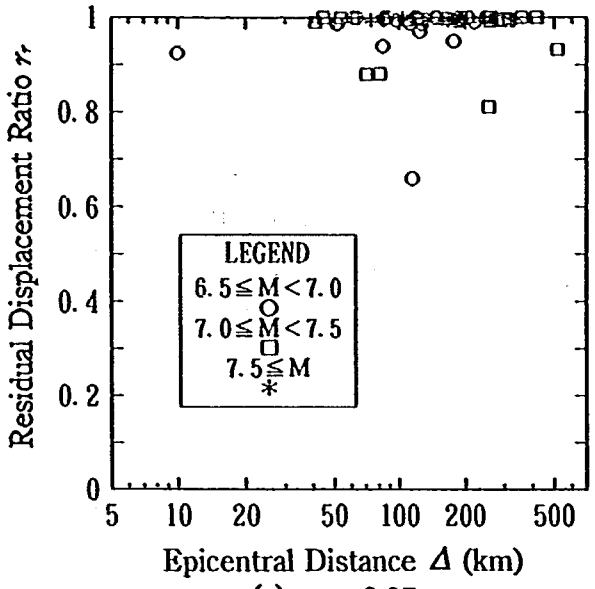
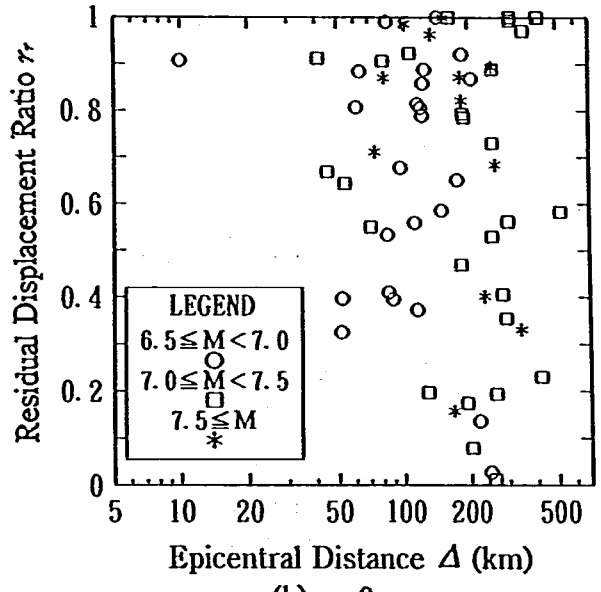


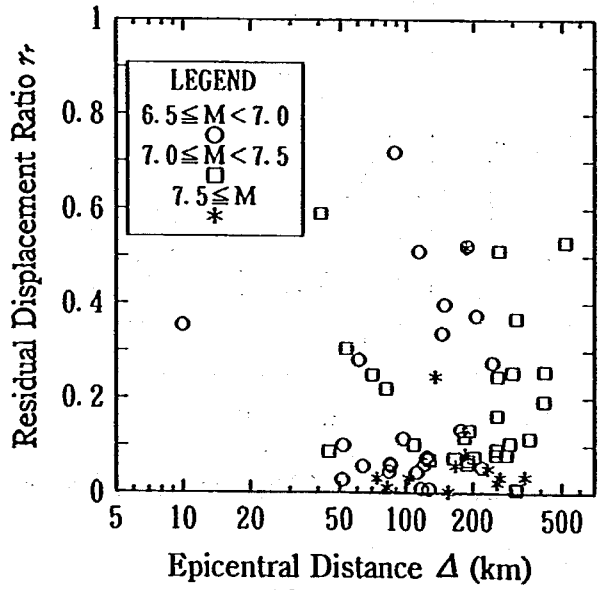
Fig. 7 Peak Ground Accelerations



(a) $r=-0.05$



(b) $r=0$



(c) $r=0.1$

Fig. 8 Effect of Earthquake Magnitude and Epicentral Distance on Residual Displacement Ratio Response Spectra

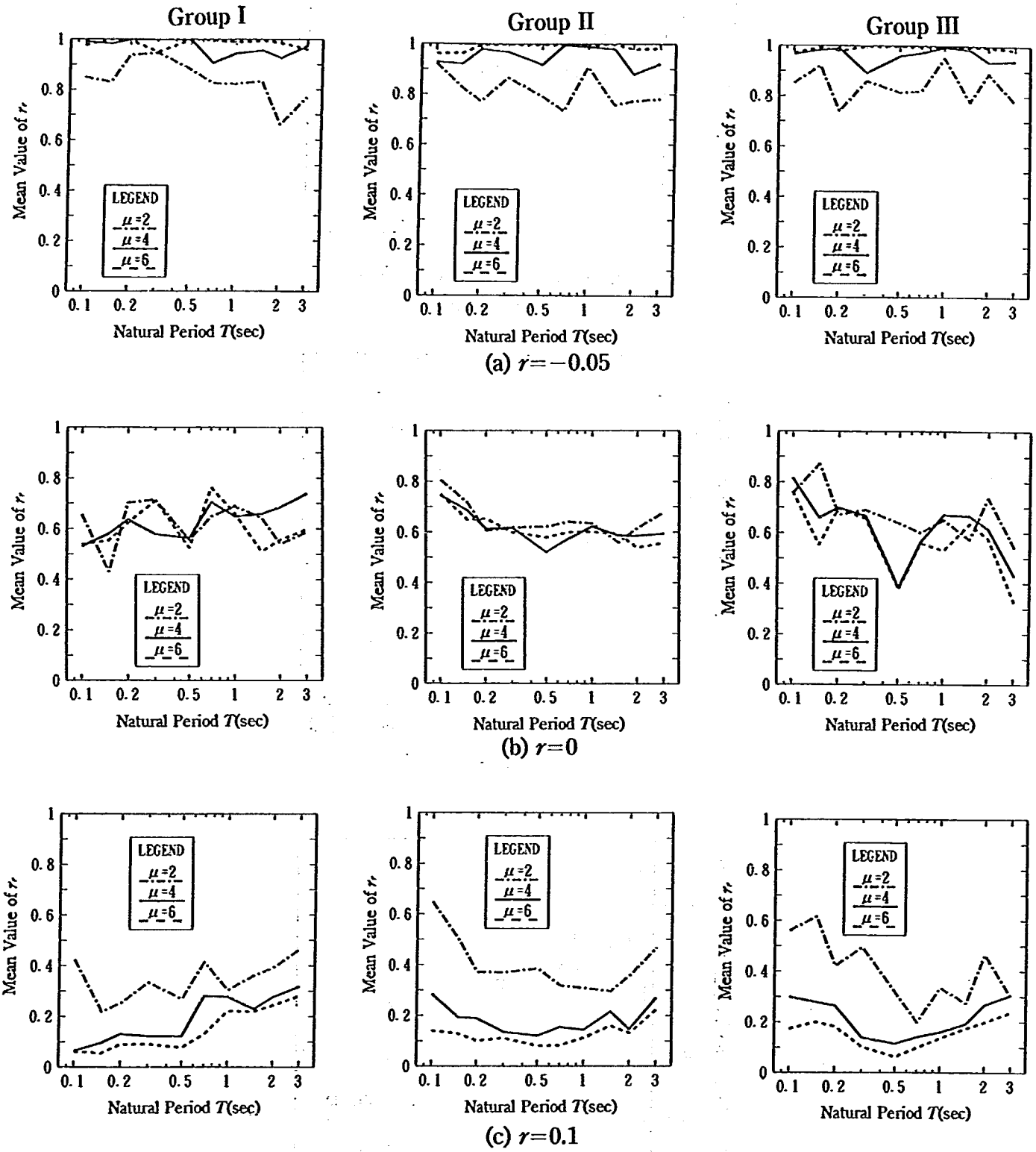
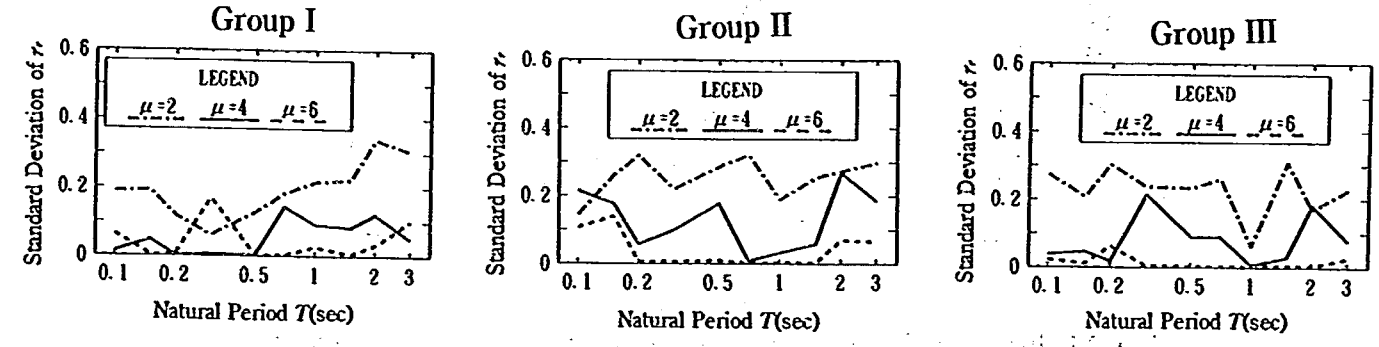
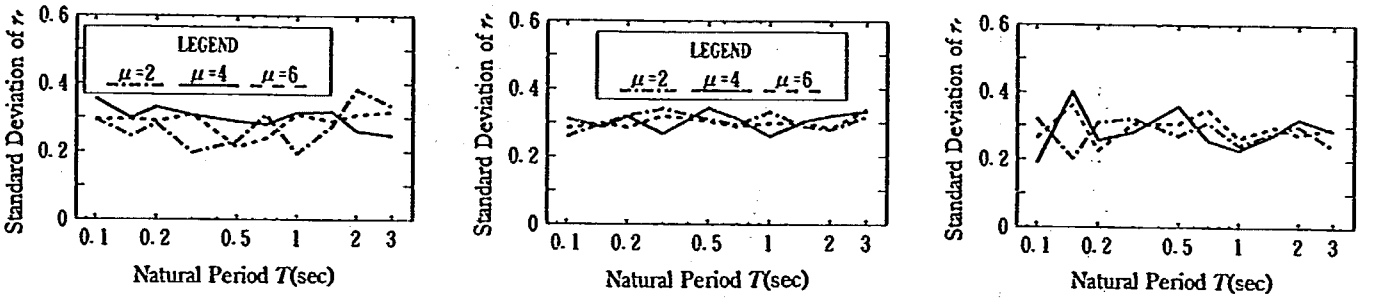


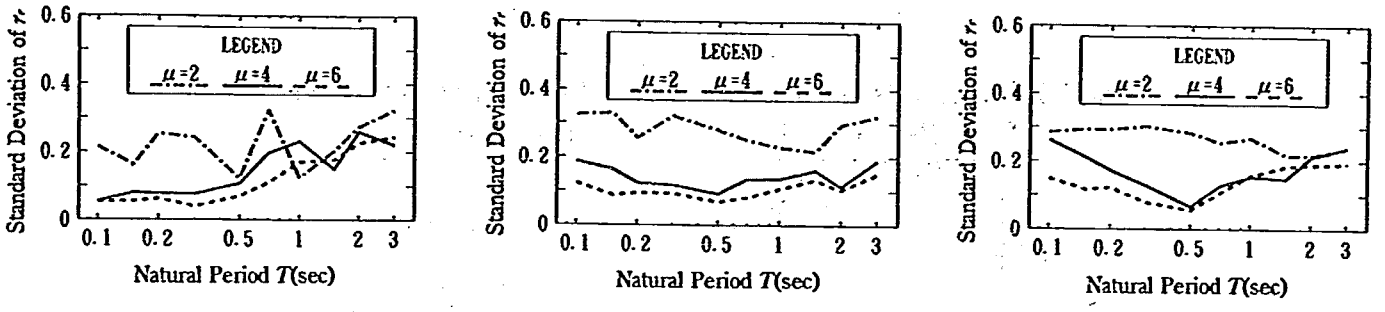
Fig. 9 Mean Value of Residual Displacement Response Spectra



(a) $\gamma=-0.05$



(b) $\gamma=0$



(c) $\gamma=0.1$

Fig. 10 Standard Deviation of Residual Displacement Response Spectra

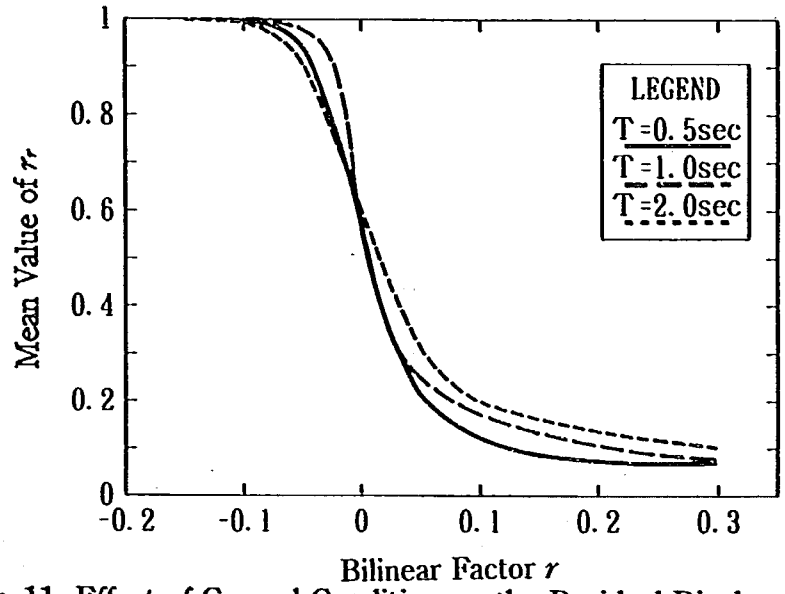


Fig. 11 Effect of Ground Condition on the Residual Displacement Ratio Response Spectra vs. Bilinear Factor

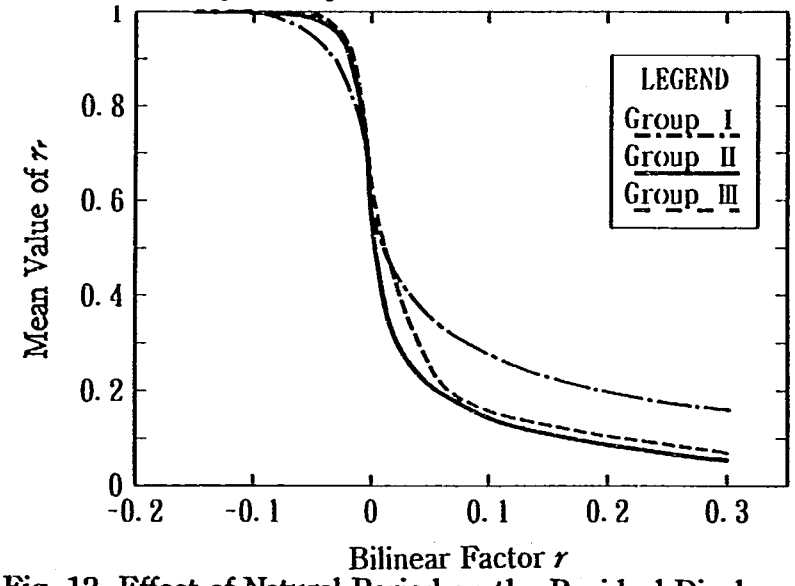


Fig. 12 Effect of Natural Period on the Residual Displacement Ratio Response Spectra vs. Bilinear Factor

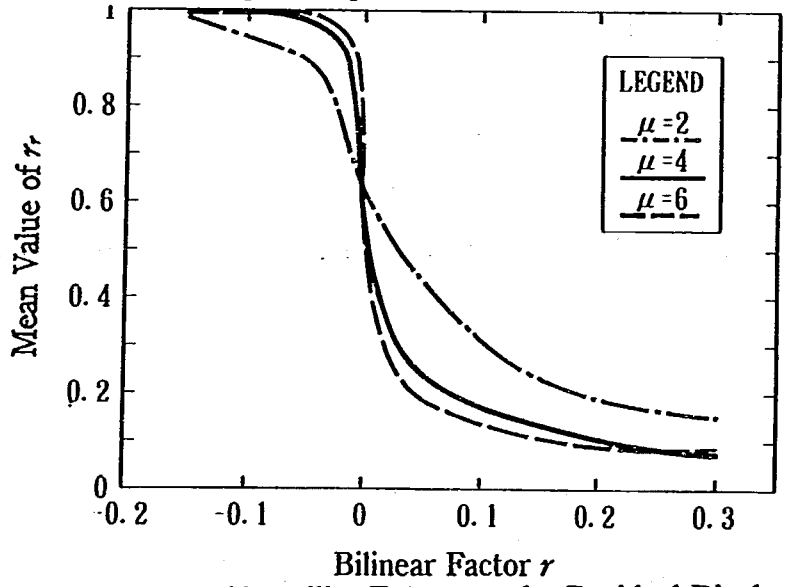


Fig. 13 Effect of Ductility Factor on the Residual Displacement Ratio Response Spectra vs. Bilinear Factor

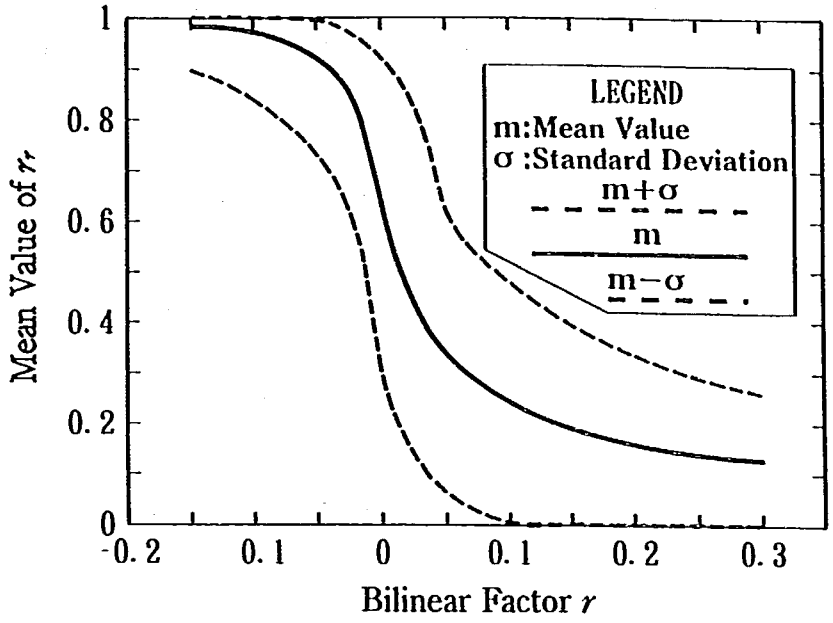


Fig. 14 Residual Displacement Ratio Response Spectra vs. Bilinear Factor Proposed for Design

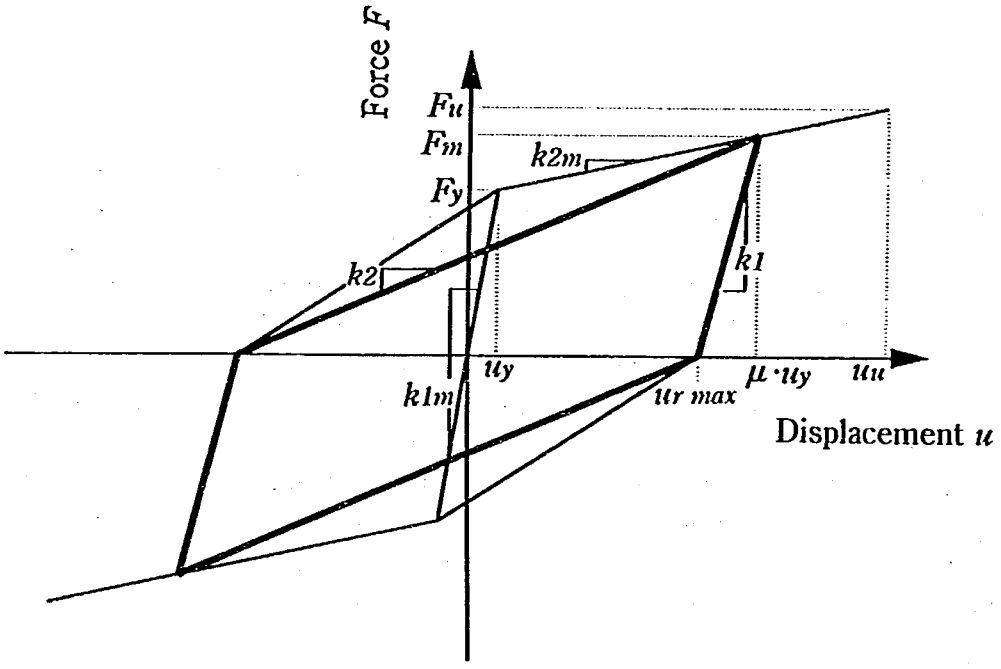


Fig. 15 Takeda Hysteresis Loop for Reinforced Concrete Structure

STRENGTH AND DUCTILITY CHARACTERISTICS OF STEEL BRIDGE PIERS WITH CONCRETE FILLER

by

Kazuo YAMAZAKI

Manager of Design Reseach Division, Metropolitan Expressway Public Corporation, Kasumigaseki, Chiyoda-ku, Tokyo, 100 Japan.

Shinnichi EGAWA

Assistant Manager of Design Reseach Division, Metropolitan Expressway Public Corporation, Kasumigaseki, Chiyoda-ku, Tokyo, 100 Japan.

Kiyokazu KUBOTA

Chief of Design Reseach Division, Metropolitan Expressway Public Corporation, Kasumigaseki, Chiyoda-ku, Tokyo, 100 Japan.

ABSTRACT

There are many steel bridge piers on expressways constructedin densely populated urban areas. In these piers the lower column-part is usually filled with concrete. Up to this time such piers are so designed that they do not produce more than yield stress under earthquake of medium scale. It is, however, important to confirm that they do not come to a collapse even under a strong earthquake of magnitude 8. In the present study a stiffened thin-walled box specimen simulating as close as possible configuration, structural and welding details of a real pier column was submitted to shaking table tests repeating inputs of acceleration waveforms corresponding to a strong earthquake. As a result it was made clear that the stiffened box section is free from local buckling on account of the filled concrete, but it ultimately results in a fracture of the column through fatigue cracks propagating from the column lower end-base plate weld toe.

INTRODUCTION

There are many steel bridge piers as shown in Fig. 1 on expressways constructed in densely populated urban areas, because unlike reinforced concrete bridge piers, steel bridge piers, permitting the pier column section to be small and the pier beam overhang to be long, contribute to more effective utilization of the space under the expressway. The cross-sectional shapes of steel bridge piers are stiffened thin-walled box sections or unstiffened pipe

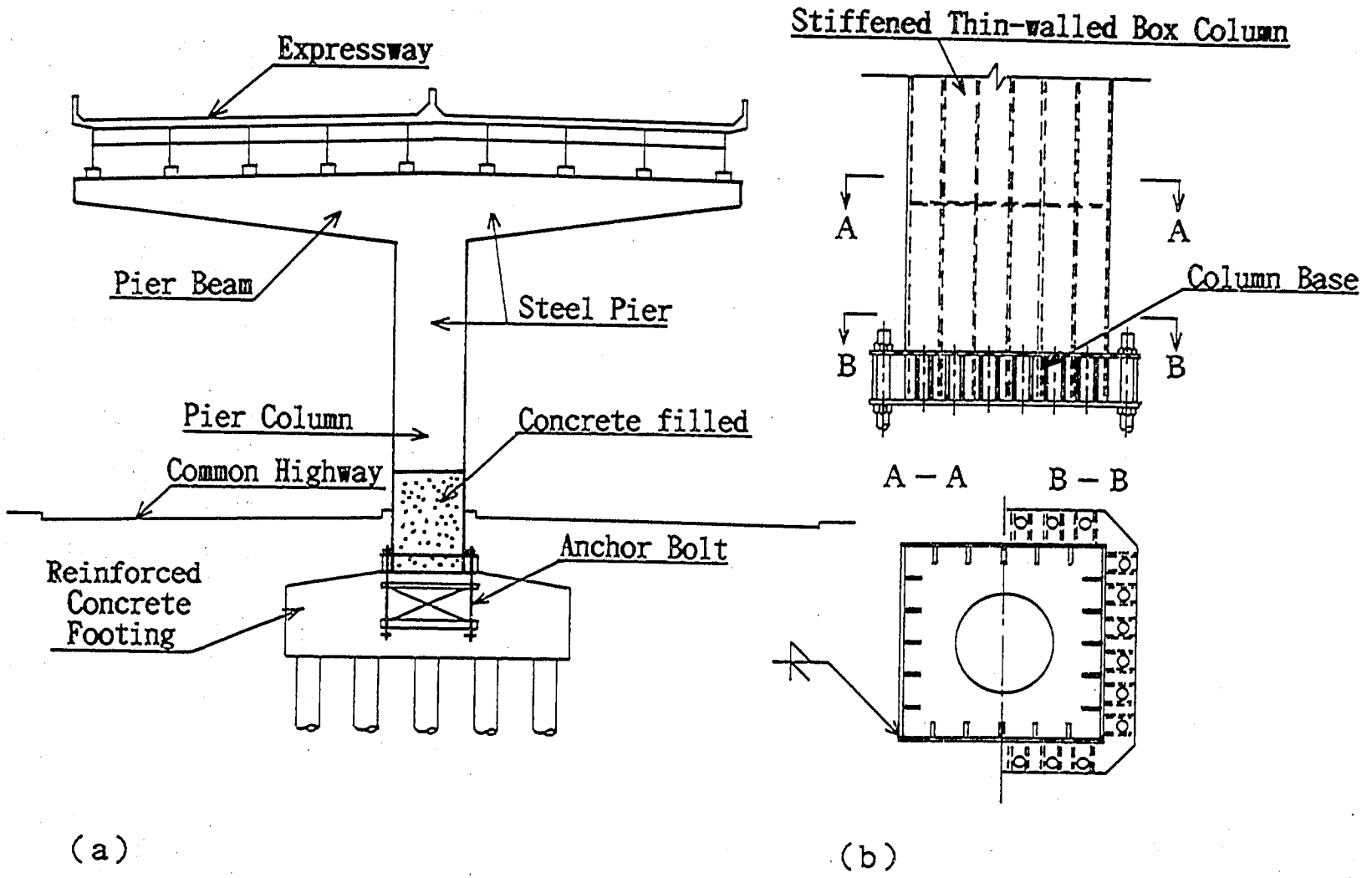


Fig. 1 Steel Bridge Pier: (a) General Elevation; and (b) Details of Column Bottom

sections. In most of pier columns, which are usually installed adjacent to common highways in existence, the lower column-part is filled with concrete (though design resistance may not consider it) so that the column section may not be deformed in collision with automobiles running on the common highway. The steel column base is anchor-bolted to the reinforced concrete footing.

It is a matter of great significance that in densely populated urban areas the expressway bridges can stand without a collapse even under a strong earthquake of magnitude 8 which seldom hits, because once the bridge collapses, it is likely that the traffic even on the common highways is disrupted resulting in a catastrophe. However, so far the steel bridge piers have been constructed by such a design that the working stress produced in them by a medium-scale earthquake of relatively high probability of occurrence must not surpass yield stress and nothing has been done to check the collapse probability of steel bridge piers under a strong earthquake.

Cyclic lateral load tests (Usami et al. 1994) are known to have been executed using small column-specimens which are filled with concrete in the lower part.

According to the results of preliminary tests which the authors have conducted by cyclic lateral loading, it is made clear that the failure mode differs between the lower column-part with concrete and the upper column-part without concrete and since the two kinds of failures happen independently of one another, the resistance of the whole structure is determined by the strength which is lower (Private Report, 1989).

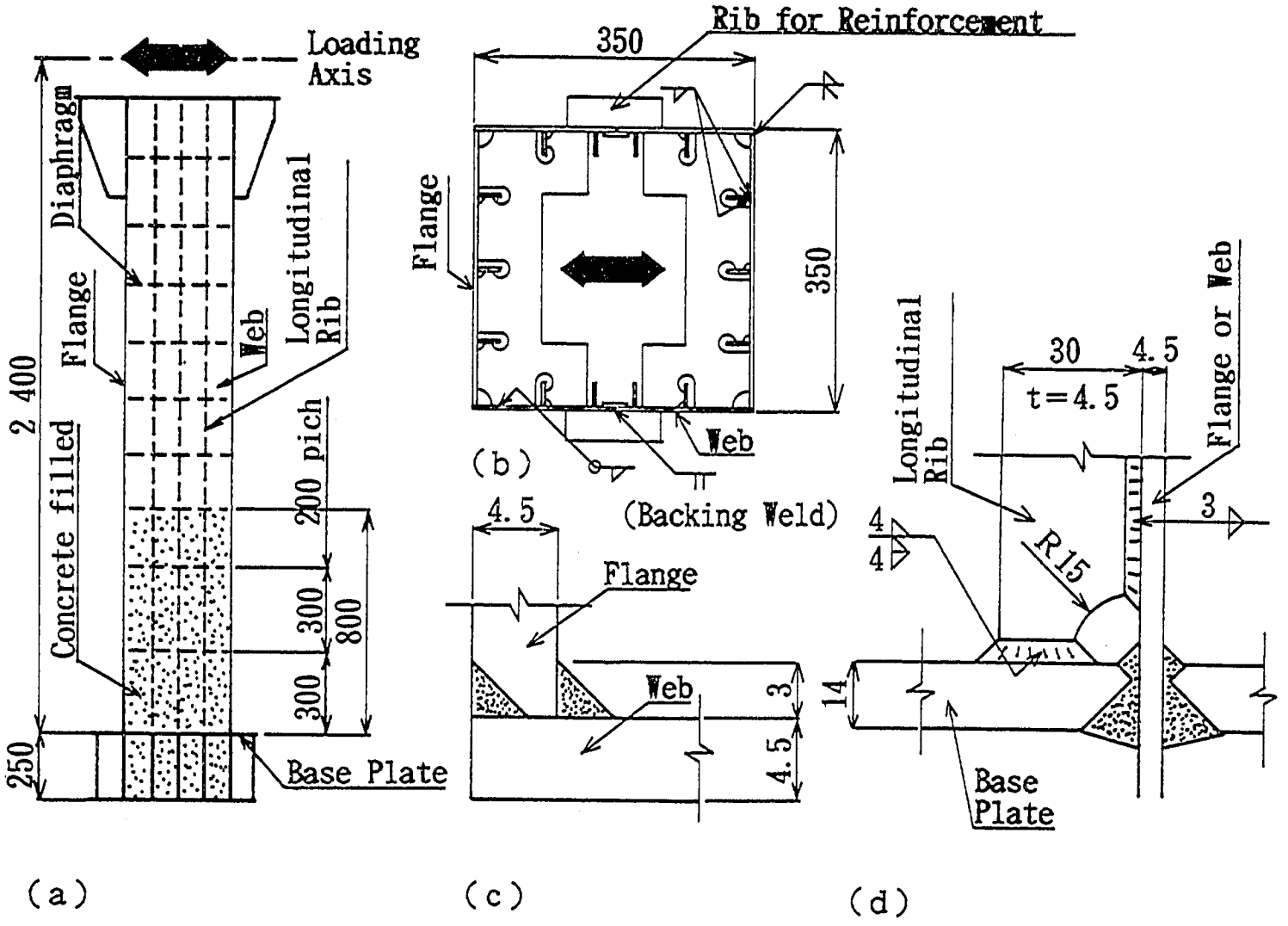
In the present study, using an about 1/5 scale specimen which simulates as far as possible the shapes, the structural and welding details of real steel bridge piers, shaking table tests were conducted with cyclic inputs of acceleration waveform equivalent to a strong earthquake, thereby revealing the behavior and failure mode of steel bridge piers with concrete under a strong earthquake.

EXPERIMENTAL PROCEDURE

DESIGN AND FABRICATION OF SPECIMEN

The shape and dimensions of the steel stiffened box column specimen with filled concrete are shown in Fig.2. The shape and dimensional proportion simulate the real bridge piers as closely as possible. The dimensions are on a scale of about 1/5. The specimen made of SM490Y (normal yield stress = 355 MPa, normal tensile stress = 590 MPa) with filled concrete (design strength = 14.7 MPa, 28 days strength = 17.5 MPa) is designed for the severest conditions in accordance with the JRA 90 specification ("JRA90" 1990) and the ME 91 design code ("ME91" 1991) as follows:

1. Maximum working stress produced by design seismic inertia force [i.e., product of design response acceleration (270 Gal, see Fig.3)


Loading Axis
Diaphragm
Flange
Web
Longitudinal Rib
2 400
Concrete filled
200 pich
300
800
300
250
Base Plate
(a)
Rib for Reinforcement
350
Flange
350
Web
(b)
(Backing Weld)
4.5
Flange
Web
3
4.5
(c)
30
4.5
t=4.5
Flange or Web
Longitudinal Rib
3
4
4
R15
14
Base Plate
(d)

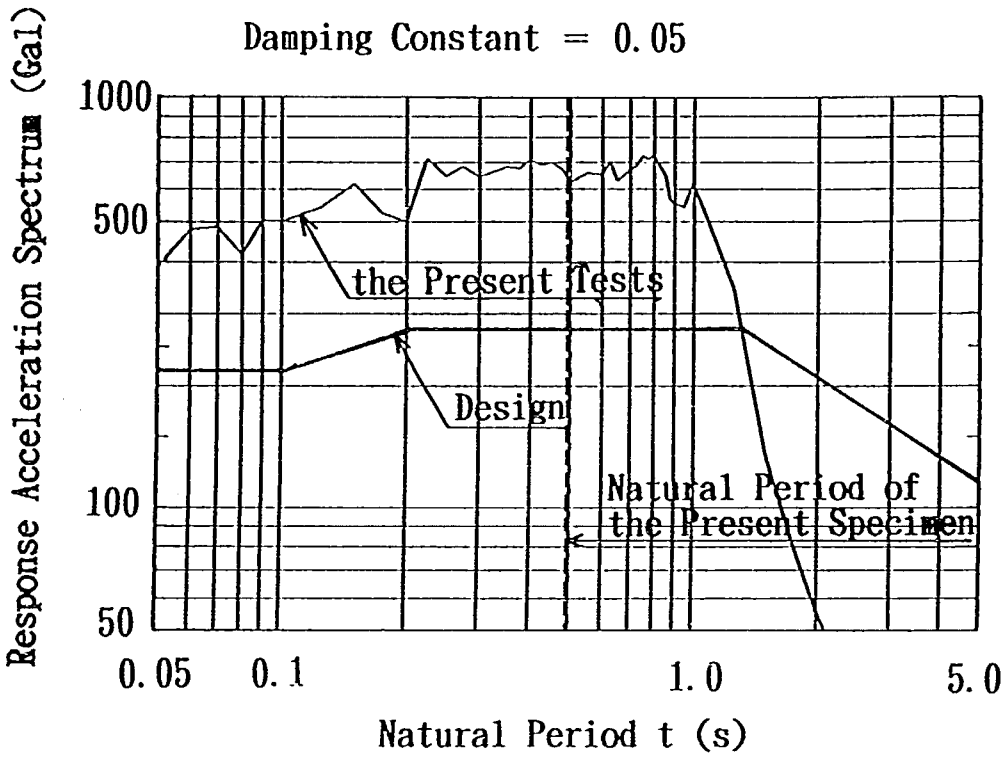


Fig. 3 Response Acceleration Spectrum and Natural Period of Specimen

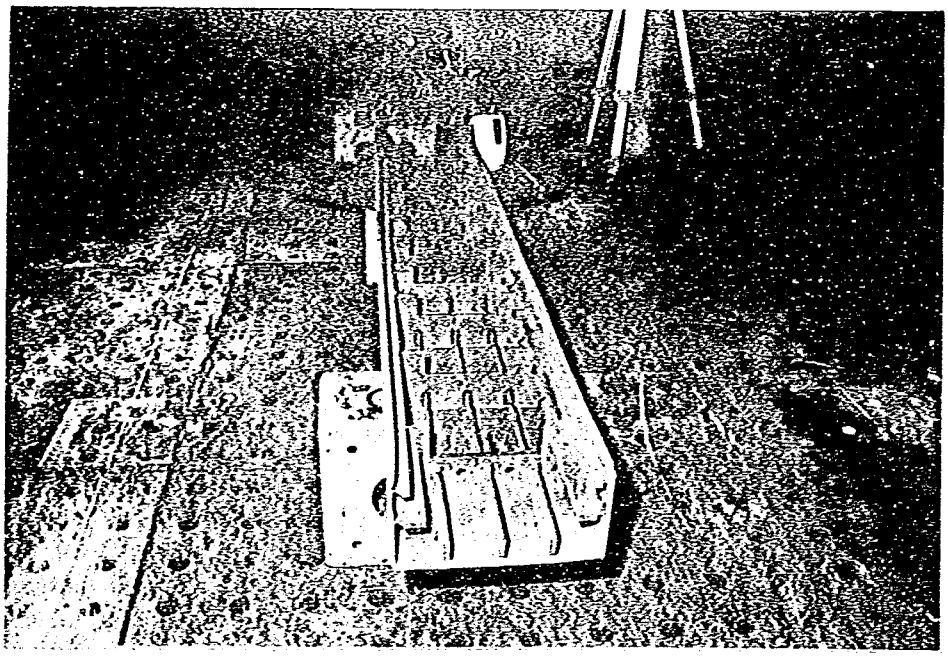


Fig. 4 Fabrication of Specimen

and mass of superstructure] and dead load is approximately equal to nominal yield stress.

2. Relative flexural rigidity of one longitudinal rib (γ_l) is approximately equal to optimal value of γ_l ($\gamma_l *$) obtained from the linear buckling theory ("DIN4114" 1953). In the case of the upper column-part without concrete, however, the diaphragm spacing is set half that of the lower column-part with concrete so that the stiffened plate of the upper part is less liable to local buckling. Because originally the purpose of testing is to investigate about a failure of lower-column part with concrete.

As shown in Fig.2, the specimen simulates as closely as possible the structural and welding details of the real bridge piers, but for the convenience of welding inside the box, as indicated in Fig.4, two split parts of a channel mold were built and then back-welded. Since the diaphragms inside the box were separated, reinforcing ribs were welded outside of the box [see Fig. 2(b)].

EXPERIMENTAL METHOD

Fig.5 shows the test device. The specimen was fixed on a frame attached to the shaking table. Two simple beams were placed between

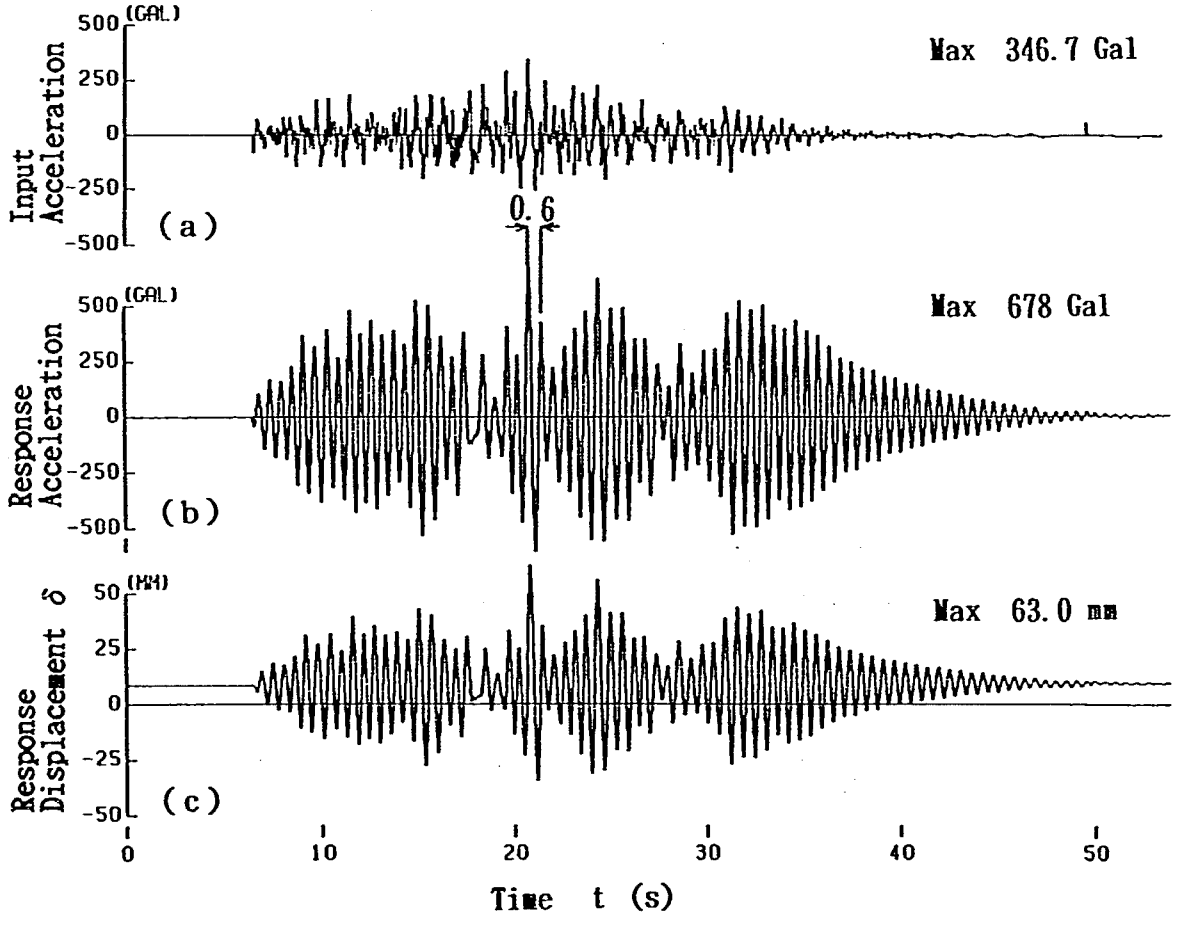


Fig. 6 Condition and Results of the 5th Test: (a) Input Acceleration; (b) Response Acceleration; and Response Displacement (δ)

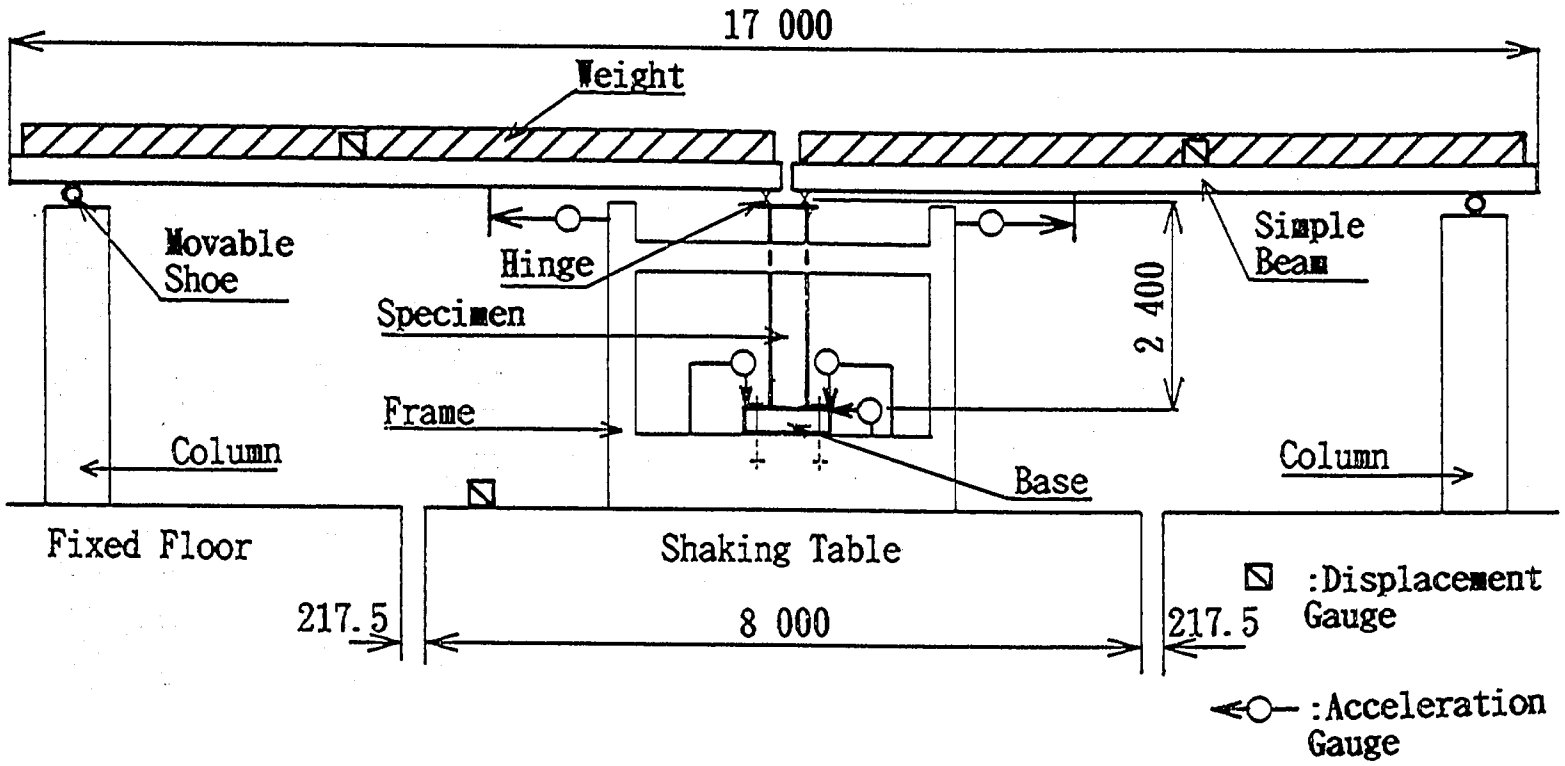


Fig. 5 Test Device

the specimen and the two columns on fixed floor. The specimen and the beams were hinge-coupled, while the columns and the beams were in contact with movable shoes. Weights were mounted on the beams. The mass of superstructure (i.e., sum of beams and weights) was 40.8 t.

In this state an input of an acceleration waveform equivalent to a strong earthquake as shown in Fig.6(a) was applied to the shaking table by an electric oil pressure servo (capacity = 700 Gal to 980 kN, maximum displacement = 75 mm), and after application of one input a magnetic particle test was conducted to check for cracking in the specimen. This is one cycle of testing and the same cycle was repeated until the testing became impossible. On condition that the damping constant is 0.05, the response acceleration spectrum which corresponds to the input acceleration waveform [see Fig.6(b)] is shown in Fig.3. The response acceleration spectrum is made considerably low when the natural period exceeds 1.0 s, because in this range the displacement of the shaking table is likely to surpass the allowable value for the test device. Nevertheless, since the calculated natural period of the specimen was about 0.5 s, it was assumed that even in testing, the vibrational period would not exceed 1.0 s. As a matter of fact, as

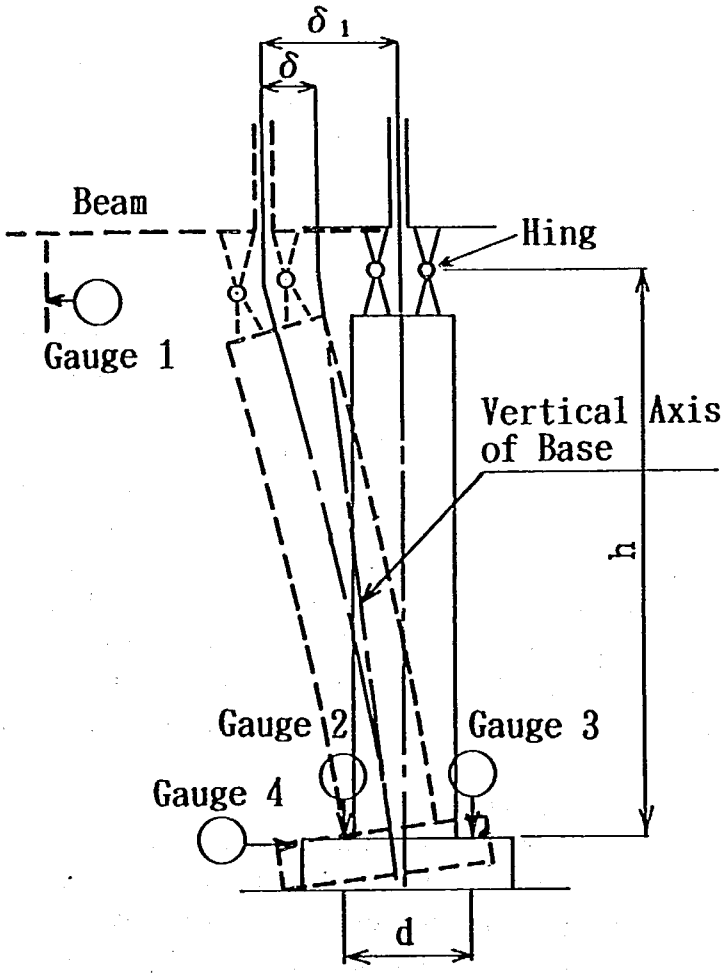


Fig. 7 Relative Displacement (δ) of Specimen at Transmitted Position of Superstructure Inertia Force

indicated in Fig.12, even in the 10th test, which was the last one, the vibrational period turned out equal to about 0.7 s.

The accelerations of the shaking table and the beams were measured by acceleration gauges. The relative displacements of the beams and specimen base to the frame were measured by displacement gauges (minimum displacement = 1/500 mm). The relative displacement (δ) of the specimen at the transmitted position (i.e., the hinges) of the superstructure inertia force, to the vertical axis of the specimen base was determined as follows (see Fig.7):

$$\delta = \delta_1 - \{\delta_4 - \frac{(\delta_3 - \delta_2)\cdot h}{d}\} \qquad (1)$$

in which δ_1 = the horizontal displacement of the beam measured by gauge 1; δ_2 and δ_3 = the vertical displacements of the specimen base measured respectively by gauge 2 and gauge 3; δ_4 = the horizontal displacement of the specimen base measured by gauge 4; h = distance between the transmitted position of the superstructure inertia force and the specimen base; and d = distance between gauge 2 and gauge 3.

EXPERIMENTAL RESULTS

RESPONSE BEHAVIOR

Upon completion of the 10th test, fatigue cracks were found to have so largely propagated that the authors sensed a probability of specimen collapse if the testing was continued and accordingly they decided to terminate the testing, but they recognized no local buckling of the steel stiffened box section.

Fig.6 shows the input acceleration (measured by the acceleration gauge on the shaking table), the response acceleration of the beam and the response displacement (δ) in the 5th test. As indicated in Fig. 6(c), before start of the 5th test there is a residual displacement of about 10 mm which has been caused by the last four tests; namely, the specimen column is inclined to the vertical axis of the specimen base. The residual displacement at the end of the 5th test remains practically the same as the residual displacement at the start of it. The vibrational period, as indicated in Fig. 6(b), is about 0.6 s, which is slightly higher than 0.48 s, i.e., the calculated natural period. Meanwhile, the maximum response acceleration is 678 Gal, which is nearly equal to the response acceleration spectrum indicated in Fig.3.

Fig. 8 shows the relation between the force of inertia (P = response acceleration x superstructure mass) and the displacement (δ) (i.e., P - δ hysteretic curves). As indicated in Fig. 8(a), in the 1st test there are two groups of curves which overlap each other and look like two solid black bundles (hereafter to be called "black bundles"). The left-side black bundle, surrounding the origin, represents a response at the early stage of repetition where the deterioration of filled concrete has not so far advanced. On the

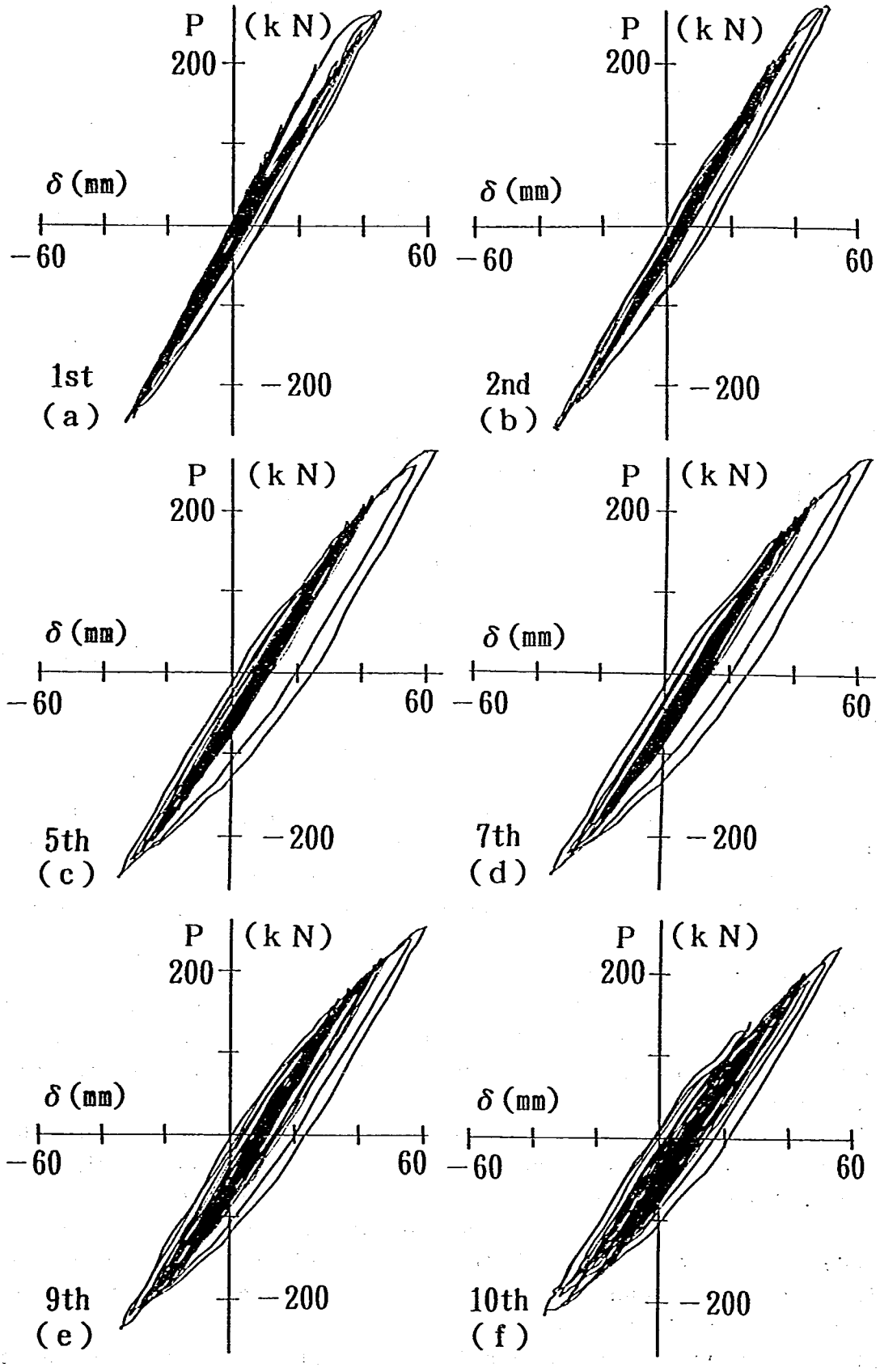


Fig. 8 Force of Inertia (P) versus Displacement (δ) Hysteretic Curves

contrary, the right-side black bundle has a rather mild slope (i.e., the bending stiffness of the specimen decreases), the cause being that the concrete deterioration was suddenly promoted by a single heavy deformation suffered at the late stage. Following the 2nd test, there happened no sudden progress in deterioration of the concrete; this is because, as seen from Fig. 8(b) ~ (f), there is only a single black bundle. After the 9th test, the overlapping of curves is considerably less complicated, probably because after the 9th test the fatigue cracks suddenly propagated, as explained later.

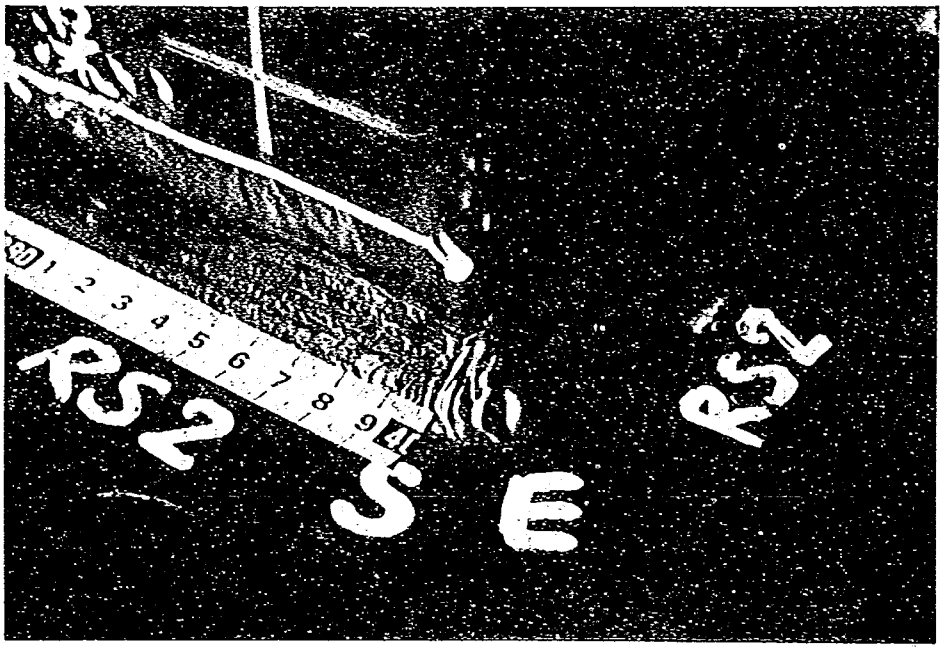
PROPAGATION OF FATIGUE CRACKS

When all the tests finished, the steel box section was gas-cut; the filled concrete was removed; and the crack state was surveyed from within the box section to see whether the crack had penetrated the plate or not. Fig. 9(a) shows fatigue cracks which penetrate the plate. Fig. 9(b) indicates the extent of penetrating cracks and the crack shapes as observed from outside of the box section. Penetrating cracks occurred invariably centering around the box sectional corners. At the flanges the penetrating cracks propagated to an extent of about 1/2 of the width of all the flange plates. Near the corners all the cracks ran along the weld toe, but they often deviated from the weld toe as they separated farther from the corners [see lateral elevation in Fig. 9(b)].

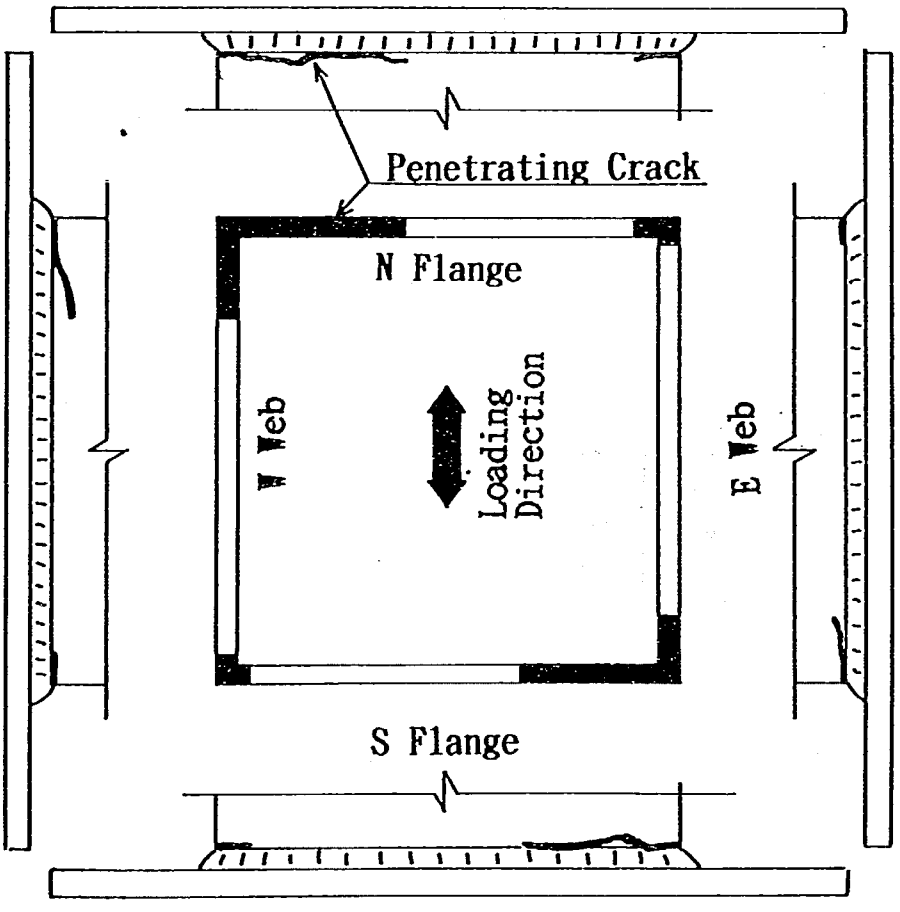
Fig. 10 summarizes the results of investigations from outside of the specimen about initiation and propagation of fatigue cracks through magnetic particle test and visual inspection at the end of each test. The numerals appearing in the figure indicate the test number in which cracks were discovered. At the end of the 3rd test, for the first time fatigue cracks were discovered at the weld toe of all the flanges in sectional corners. At the end of the 4th test, cracks were found at the weld toe of all the webs in the sectional corners. In the tests thereafter, cracks gradually propagated toward the center of the plate. After the 9th test, the propagation was abrupt and at the end of the 10th test cracks covered virtually the whole flange.

The penetrating cracks are cracks which propagate from the weld toe near the corner, because for the first time cracks originate near the corner and as they separate farther from the corner, they often deviate from the weld toe. Most of the non-penetrating cracks are regarded as cracks which individually originated at the weld toe unlike the ones propagating from the corner, because they are found only after the 10th test; they are so shallow that they can be identified in the magnetic particle test but can never be recognized by the naked eye; and they are discontinuous.

Thus it can be said that what mainly causes a fracture of the box section column is a crack originating from the weld toe at the corner.



(a)



(b)

Fig. 9 Penetrating Cracks: (a) S Flange-E web Corner; and (b) Cross-section and Lateral Elevation

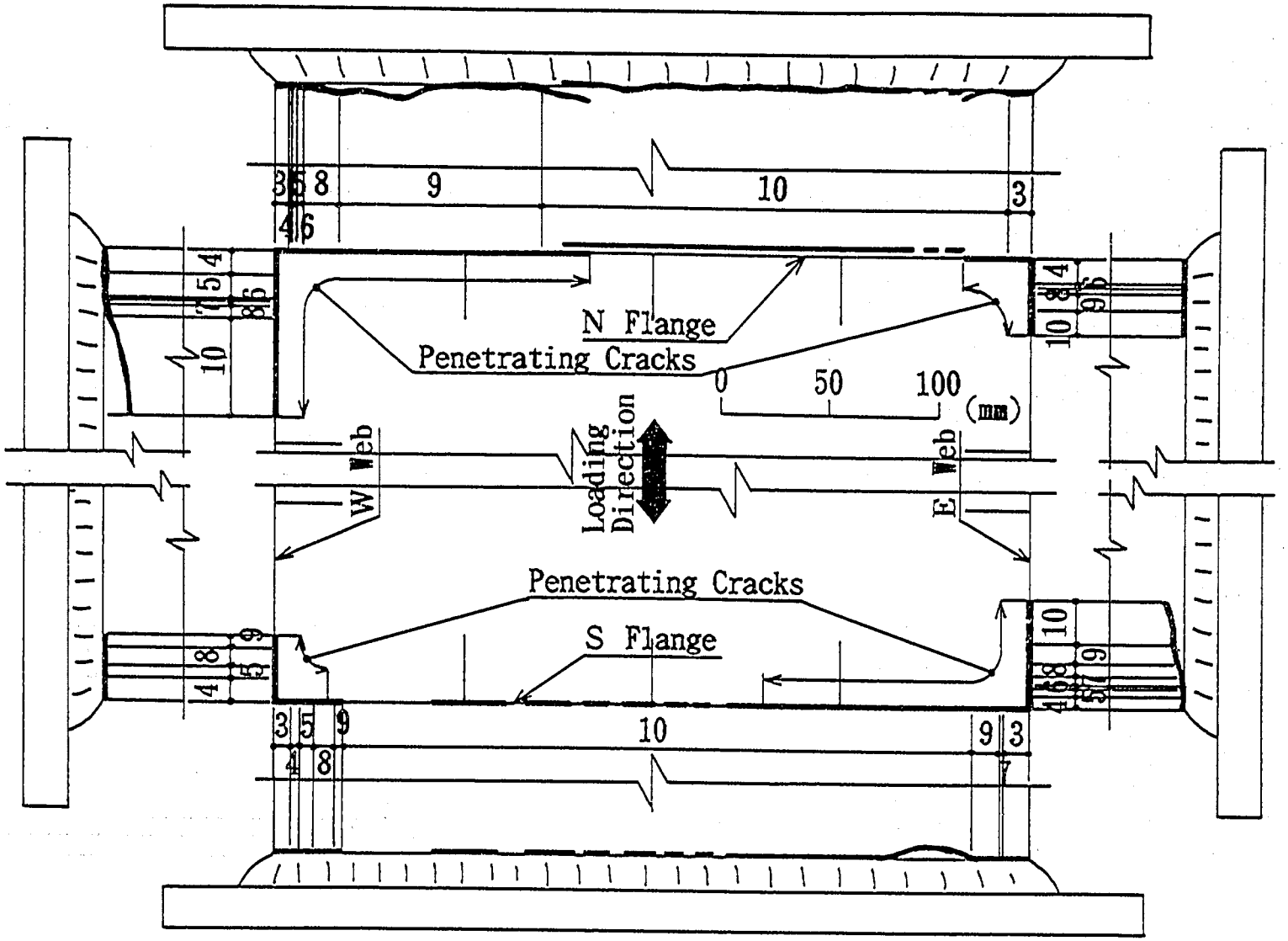


Fig. 10 State of Crack Propagation

RESIDUAL DISPLACEMENT AND ULTIMATE LIMIT STATE

Fig. 11 shows the residual displacement (δ) to the vertical axis of specimen base at the end of each teat. Initially the displacement increases, but in the 6th test and thereafter it settles nearly constant. Finally it is about 10 mm and the inclination of the specimen column to the vertical axis of the specimen base is 0.23 degree (0.23°) which is visually unperceivable (see Fig. 12) so that there is structurally no problem.

Fig. 13 shows the maximum input acceleration measured on the shaking table, the maximum response acceleration on the beam, and the

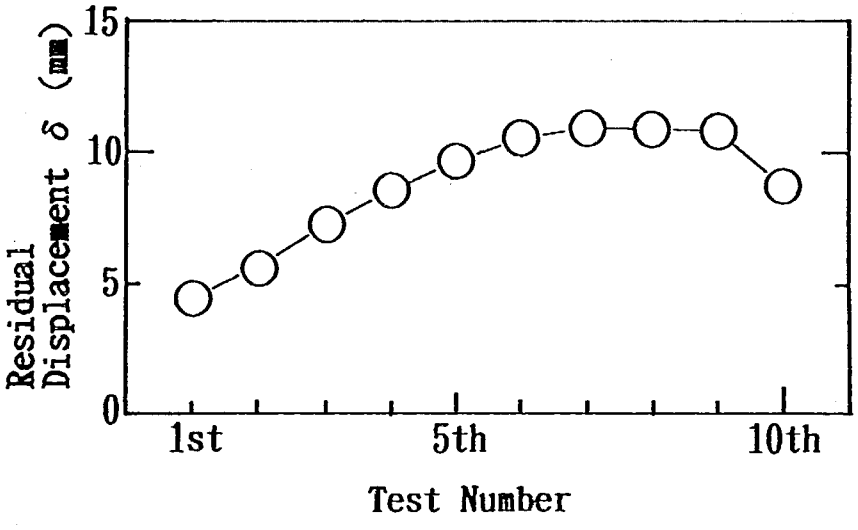


Fig. 11 Residual Displacement versus Test Number

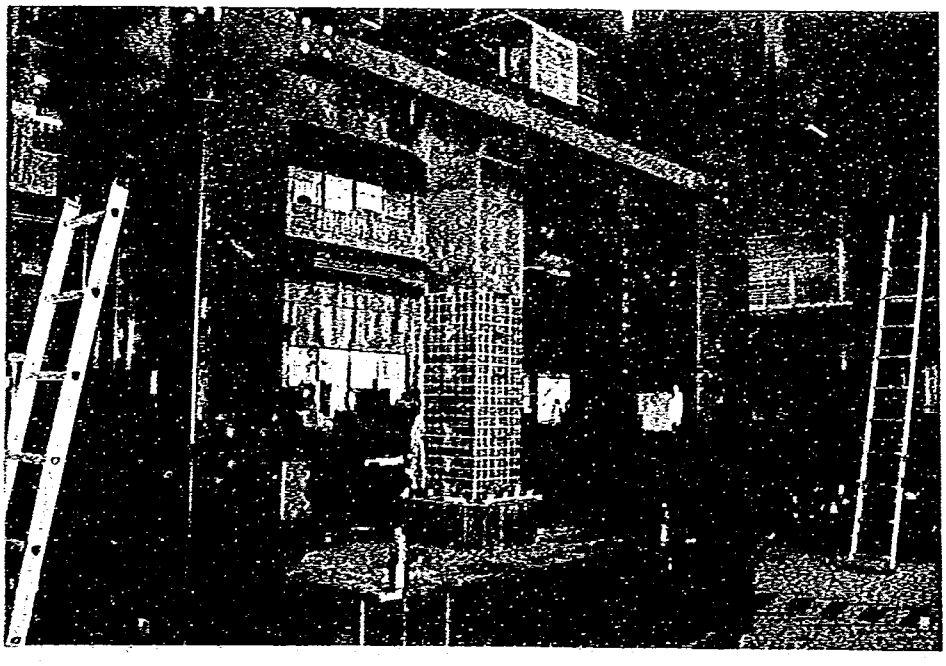


Fig. 12 State of Specimen after finishing all the Tests

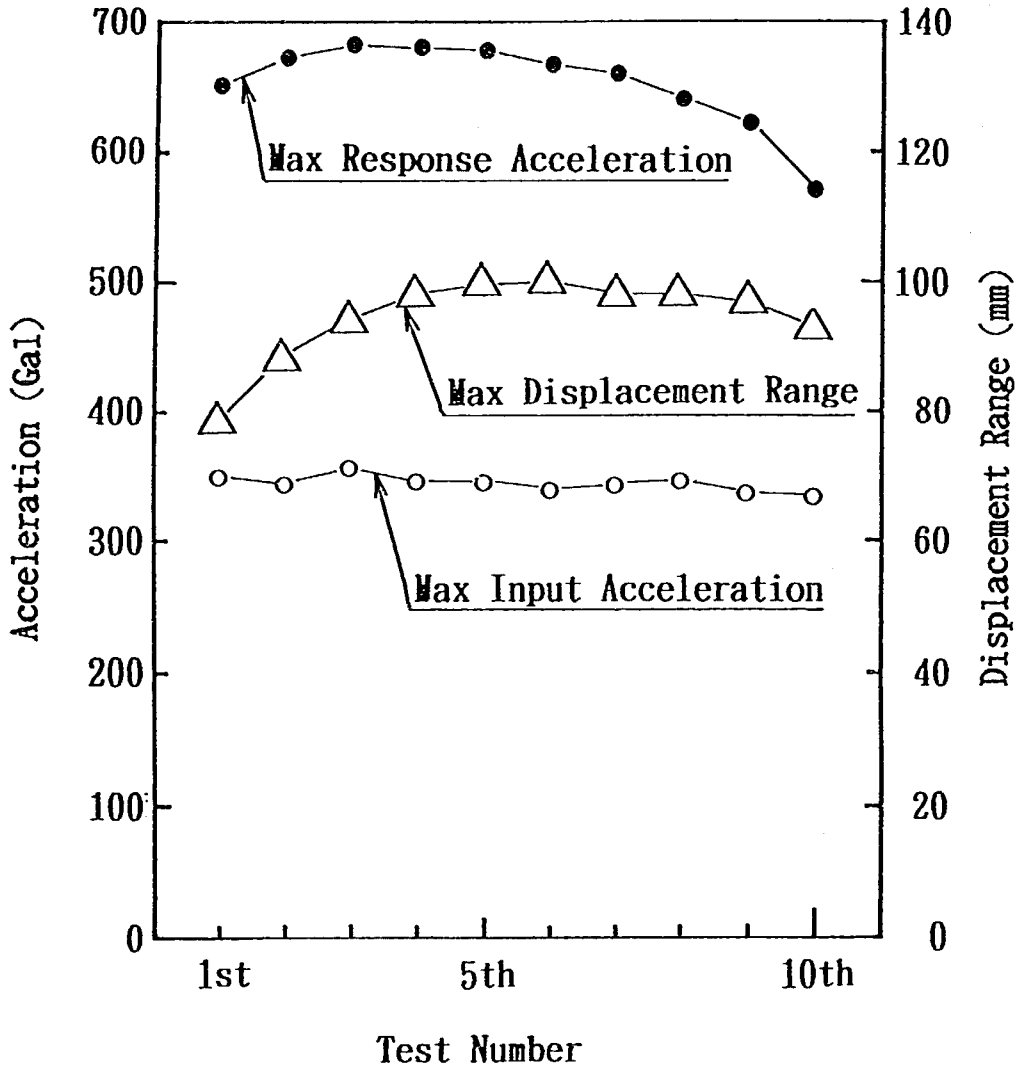


Fig. 13 Max Response Acceleration, Max Displacement Range and Max Input Acceleration versus Test Number

maximum displacement range (i.e., maximum displacement - minimum displacement) in each test. In spite of the maximum input acceleration hardly changing, the maximum response acceleration and the maximum displacement range change as the tests are repeated.

The maximum response acceleration is smaller in the first test and the latter tests than in the middle tests, in spite of range of vibrational period being constant response acceleration spectrum in all the tests [see Fig. 3, even in the 10th test the natural period is about 0.7 (see Fig. 14)]. It is considered that this is caused by energy-damping effect which is produced by the deterioration of the filled concrete and the propagation of fatigue cracks, respectively in the first test and the latter tests. The maximum displacement in the first test is considerably small. This is because the maximum response acceleration is small and the column bending stiffness which includes concrete is larger than in the other tests. In the latter tests, in

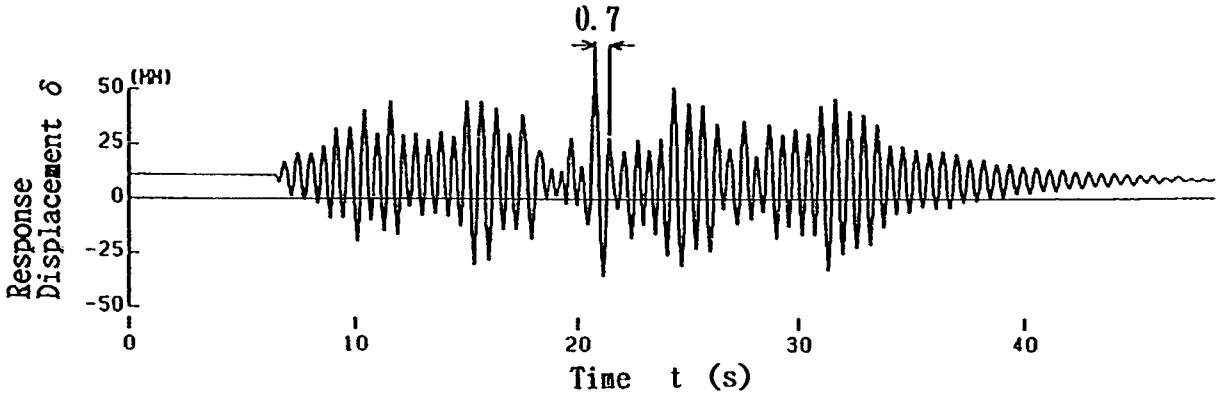


Fig. 14 Response Displacement on the 10th Test

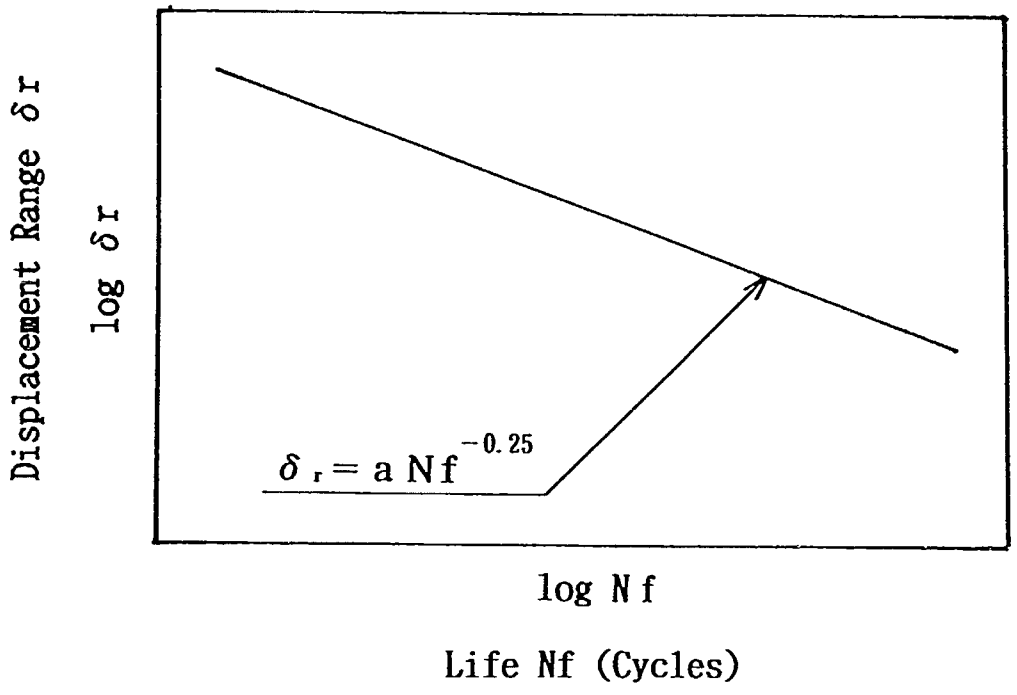


Fig. 15 Displacement Range versus Life

spite of the maximum acceleration being small, the maximum displacement is not small. The cause is that the column bending stiffness has dropped as the cross section decreases with propagation of cracks.

As explained in the above, the failure of concrete-filled steel column is caused by fatigue. Then, the extent of fatigue damage to the concrete-filled steel column in each test is calculated under the following assumptions:

1. Relation between life (Nf) and the displacement range (δr) can be expressed by the following equation(see Fig. 15).

$$\delta r = a \cdot Nf^{-0.25} \qquad (2)$$

in which a = constant.

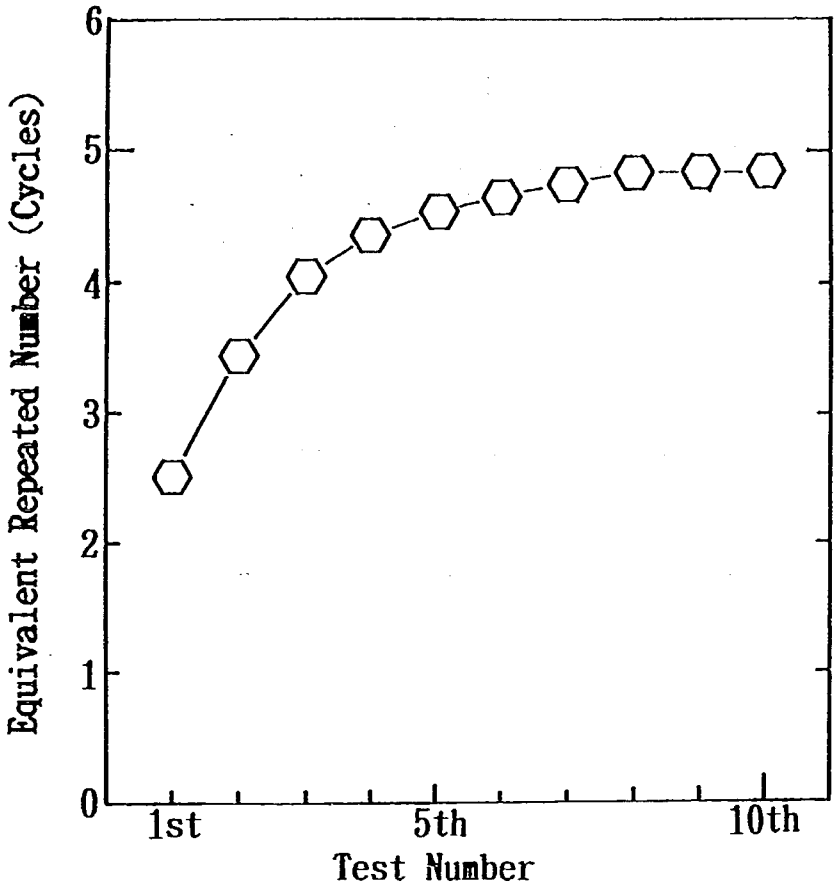


Fig. 16 Equivalent Repeated Number versus Test Number

2. The equivalent repeated number (Ne) to a given displacement range [(δe)r] is calculated by Palmgren-Miner rule (BS5400, 1980).

3. Frequency distribution (Ni) of displacement range [(δi)r] is calculated by rain flow rule (BS5400, 1980).

Under these assumptions the equivalent repeated number to a given displacement range [(δe)r] can be calculated as follows:

$$Ne = \Sigma(Ni \cdot \frac{(\delta i)r}{(\delta e)r}) \qquad (3)$$

Fig. 16 shows the equivalent repeated number (i.e., magnitude of fatigue damage accumulated in one test) to 100 mm of displacement range in each test. The damage in the first test is very small. This implies that the effect of energy-damping produced with progress of the deterioration in the filled concrete is very large.

If one more test were done, the specimen column would fracture, because it is speculated that in the 10th test the fatigue cracks have already made a considerably wide propagation and that, as shown in Fig.16 in the additional test the specimen column is likely to suffer the same fatigue damage as in the latter tests.

As the result of performing shaking table tests of a specimen simulating the shape , the structural and welding details of real steel bridge piers, the following trends in the behavior and the failure mode of the concrete-filled steel bridge pier column in the case that inputs of an acceleration waveform corresponding to a strong earthquake were repeated were made clear:

1. On account of the concrete filling it, the stiffened box section is free from local buckling. However, fatigue cracks propagate from the column lower end-base plate weld toe at the box corner and ultimately bring about a fracture of the column.
2. In the early input, the effect of energy-damping produced with progress of the deterioration in the filled concrete is very large.
3. The column suffers such a small residual displacement that it poses no structural problem just up to its fracture.

REFERENCES

"BS 5400." (1980). Steel, concrete and composite bridges, Part 10.Code of practice for fatigue, British Standard Institute, U.K."DIN 4114, Blatt2." (1953). Stahlbau, Stabilitatsfalle (Knickung, Kippung, Beulumg), Berechnungsgrundlagen,Richtlinien, Berlin, Germany (in German).

"JRA 90." (1990). Specification for highway bridges. Part 11 :steel bridges. Japan Road Association, Tokyo, Japan (in Japanese).

Private report. (1989). Metropolitan Expressway Public Corp., Japan (in Japanese).

"Me 91." (1990). Code for metropolitan expressway bridges. Metropolitan Expressway Public Corp., Japan (in Japanese).

Usami , T., and Ge, H. (1994). "Ductility of concrete-filled steel box column under cyclic loading." J. Engrg. Struc., ASCE 120(7), 2021-2040.

NONLINEAR RESPONSE EVALUATION OF SHALLOW FOUNDATIONS AGAINST EARTHQUAKE GROUND MOTIONS

Hisanori OTSUKA [1], Shigeki UNJOH [2] and Hidetoshi MUKAI [3]

1) Head, Earthquake Engineering Division, Earthquake Disaster Prevention Department, Public Works Research Institute, Ministry of Construction, Tsukuba City, Japan 305
2) Senior Research Engineer, ditto
3) Assistant Research Engineer, ditto

ABSTRACT

This paper presents a nonlinear response evaluation method for sliding of a shallow foundation subjected to earthquake ground motions. An analytical model which takes account of sliding and rocking motions of a shallow foundation is presented. The proposed analytical method is verified through simulation analyses of the shake table test results of foundation models.

KEYWORDS : Seismic Design, Shallow Foundation, Nonlinear Analysis, Sliding, Shaking Table Test, Simulation Analysis

INTRODUCTION

In the current seismic design codes in Japan [1], the seismic stability of a shallow foundation against an earthquake ground motion is evaluated based on a combination of the equivalent lateral force method and the allowable design approach. This combination of the methods is called as the "seismic coefficient method" in Japan. This method generally assumes a 20% – 30% of gravitational force as the lateral seismic force. The seismic stability of a shallow foundation is evaluated in terms of 1)vertical soil bearing capacity at the base, 2)overturning, and 3)sliding.

To evaluate the seismic safety for sliding of a shallow foundation, the horizontal (shear) force applied at the base of the foundation is computed. The shear force is developed by the seismic lateral force of a superstructure, a pier, and a foundation. The stability of the foundation for sliding is then made in terms of the "safety factor S_F " as

$$S_F = H_u / H \geqq 1.2 \tag{1}$$

where

S_F : safety factor for sliding

H : horizontal (shear) force at the base of a foundation (KN)
H_u : horizontal shear resistance of underlying soils (KN)

The horizontal shear resistance H_u of underlying soils at the base of a foundation is defined as

$$H_u = c_B A' + V \tan \phi_B \quad (2)$$

where

c_B : cohesion between the base of a foundation and underlying soils (KN/m^2)
ϕ_B : friction angle between the base of a foundation and underlying soils (degree)
A' : efective area of the base of a foundation (m^2)
V : vertical load of a foundation (KN)

The vertical load V is contributed from the dead weight of a superstructure, a pier and a foundation. The effective area A' of the base of a foundation is computed in consideration with the separation between the base and the underlying soils caused by the rocking motion.

The "seismic coefficient method" assumes a 20% – 30% of gravitational force as the lateral seismic force as above mentioned, the width of a foundation is designed so that the safety factor of the seismic stability for sliding be within allowable range. However, when a large earthquake with magnitude of 8 occurs close to the site of a bridge, the acceleration response may exceed the designed value. Therefore, the horizontal (shear) force at the base of the foundation exceeds the allowable horizontal shear resistance of soils and then the sliding may occur. Therefore, it is required to develop a rational design method for a shallow foudnation against a large earthquake.

This paper presents a nonlinear response evaluation method for sliding of a shallow foundation subjected to earthquake ground motions. An analytical model which takes account of sliding and rocking motions of a shallow foundation is presented. The proposed analytical method is verified through simulation analyses of the shake table test results of foundation models.

AN ANALYTICAL MODEL FOR SLIDING AND ROCKING OF SHALLOW FOUNDATIONS

Analytical Model

To precisely analyze the nonlinear sliding and rocking response of a shallow foundation, an analytical model as shown in **Fig. 1** is developed [2) 3)] . Because foundations support piers and a superstructure, they also need to be idealized. If a foundation is subjected to a large ground motion, a sliding response with residual displcament, a rocking response including a separation (uplift) from the underlying soils may be developed. If the uplift occurs, a concentration of the vertical load at the other edge of the foundation may be developed. This

sometimes causes the yielding of the underlying soils. **Fig.2** shows the idealization of the restoring forces of the surrounding soils. Uplift and contact between the base and the underlying soils causes energy dissipation. The separation/contact and yielding are also developed at the side of a foundation.

Based on those considerations, it is assumed that a footing is idealized by one mass (three degrees-of-freedom) system, and that a pier and a part of superstructure are idealized by a beam-mass system. Assuming that the node n represents the foundation, the equations of motion for a foundation/pier/superstructure system are written as

$$\begin{aligned} \underline{m_X}\,\ddot{\underline{X}} + \underline{F_X}^D + \underline{F_X}^M &= \{0,0,\cdots\cdots,0,\ F_X{}^B + F_X{}^S\}^T \\ \underline{m_Y}\,\ddot{\underline{Y}} + \underline{F_Y}^D + \underline{F_Y}^M &= \{0,0,\cdots\cdots,0,\ F_Y{}^B + F_Y{}^S - F_Y{}^G\}^T \\ \underline{J}\,\ddot{\underline{\theta}} + \underline{M}^D + \underline{M}^M &= \{0,0,\cdots\cdots,0,\ M_X{}^B + M_X{}^S + M_Y{}^B + M_Y{}^S\}^T \end{aligned} \tag{3}$$

where

$\underline{m_X}$, $\underline{m_Y}$, $\underline{J}$: mass matrices in lateral and vertical directions and inertia moment of nodal points ($i = 1 - n$)

$\underline{X}$, $\underline{Y}$, $\underline{\theta}$: absolute lateral, vertical and rotational displacements vectors of nodal points ($i = 1 - n$)

$F_X{}^D$, $F_Y{}^D$, M^D : horizontal, vertical and rotational damping forces vectors acting at nodal points ($i = 1 - n$)

$F_X{}^M$, $F_Y{}^M$, M^M : horizontal, vertical and rotational member forces vectors acting at nodal points ($i = 1 - n$)

$F_Y{}^G$: the gravity force of a footing

$F_X{}^B$, $F_Y{}^S$: restoring forces of soil at base and sides of a footing in tangential direction

$F_Y{}^B$, $F_X{}^S$: restoring forces of soil at base and sides in normal direction

$M_X{}^B$, $M_Y{}^S$: moments by restoring forces of soil at base and sides of a footing in tangential direction

$M_Y{}^B$, $M_X{}^S$: moments by restoring forces of soil at base and sides of a footing in normal direction

Restoring Force of Soil

To represent nonlinear restoring force $F_X{}^B$, $F_Y{}^B$, $F_X{}^S$ and $F_Y{}^S$ at the base and side of a foundation, the base and the side in contact with soil are divided into discrete segments. From the restoring force at j-th segment, the restoring force at the base and side may be written as

$$\begin{aligned} F_X{}^B &= \sum_j f_{Xj}{}^B \\ F_Y{}^B &= \sum_j f_{Yj}{}^B \\ F_X{}^S &= \sum_j f_{Xj}{}^S \\ F_Y{}^S &= \sum_j f_{Yj}{}^S \end{aligned} \tag{4}$$

where

f_{Xj}^{B} : horizontal restoring force of j–th segment at base
f_{Yj}^{B} : vertical restoring force of j–th segment at base
f_{Xj}^{S} : horizontal restoring force of j–th segment at side
f_{Yj}^{S} : vertical restoring force of j–th segment at side

The moment by restoring forces M_X^B, M_Y^B, M_Y^S and M_X^S may be written as

$$\begin{aligned} M_X^B &= -\sum_j f_{Xj}^B \cdot d_{Yj} \\ M_Y^B &= \sum_j f_{Yj}^B \cdot d_{Xj} \\ M_X^S &= -\sum_j f_{Xj}^S \cdot d_{Yj} \\ M_Y^S &= \sum_j f_{Yj}^S \cdot d_{Xj} \end{aligned} \tag{5}$$

where

d_{Xj} : horizontal distance at j–th segment from the gravity point of a footing
d_{Yj} : vertical distance at j–th segment from the gravity point of a footing

The restoring force at the base of a foundation are assumed as

$$f_{Yj}^{B} = \begin{cases} 0 & (y_j > 0) \\ K_{Yj}^{B1} \cdot y_j + C_j^B \cdot \dot{y}_j & (y_j^Y \leqq y_j \leqq 0) \\ K_{Yj}^{B1} \cdot y_j^Y + K_{Yj}^{B2} \cdot (y_j - y_j^Y) + C_j^B \cdot \dot{y}_j & (y_j^Y < y_j) \end{cases} \tag{6}$$

$$f_{Xj}^{B} = \begin{cases} -|\mu_d f_{Yj}^B| & (-|\mu_s f_{Yj}^B| > K_{Xj}^B \cdot x_j) \\ K_{Xj}^B \cdot x_j & (-|\mu_s f_{Yj}^B| > K_{Xj}^B \cdot x_j > |\mu_s f_{Yj}^B|) \\ |\mu_d f_{Yj}^B| & (K_{Xj}^B \cdot x_j < |\mu_s f_{Yj}^B|) \end{cases} \tag{7}$$

where

K_{Yj}^{B1}, K_{Yj}^{B2} : initial and second stiffness in vertical compression at j–th segment
K_{Xj}^{B} : stiffness in lateral direction at j–th segment
y_j^Y : yield displacement at j–th segment
y_j : displacement at j–th segment
x_j : lateral displacement of j–th segment
C_j^B : damping coefficient which represents energy dissipation due to impact between a foundation and underlying soil
μ_s, μ_d : static and dynamic friction coefficient between a foundation and underlying soil

The restoring force of the side springs are similarly assumed as

$$f_{Xk}^{S} = \begin{cases} 0 & (x_k > 0) \\ K_{Xk}^{S1} \cdot x_k & (x_k^Y \leqq x_k \leqq 0) \\ K_{Xk}^{S1} \cdot x_k^Y + K_{Xk}^{S2} \cdot (x_k - x_k^Y) & (x_k^Y < x_k) \end{cases} \tag{8}$$

$$-|\mu_d f_{Xk}^S| \quad (-|\mu_s f_{Xk}^S| > K_{Yk}^S \cdot y_k)$$

$$f_{Yk}^{S} = \begin{cases} K_{Yk}^{S} \cdot y_k & (-|\mu_s f_{Xk}^{S}| > K_{Yk}^{S} \cdot y_k > |\mu_s f_{Xk}^{S}|) \\ |\mu_d f_{Xk}^{S}| & (K_{Yk}^{S} \cdot y_k < |\mu_s f_{Xk}^{S}|) \end{cases} \quad (9)$$

where

K_{Xk}^{S1}, K_{Xk}^{S2} : initial and second stiffness in lateral direction at k–th segment
K_{Yk}^{S} : stiffness in vertical direction at k–th segment
x_k^{Y} : yielding displacement at k–th segment
x_k : lateral displacement at k–th segment
y_k : vertical displacement at k–th segment

Energy Dissipation due to Impacting at Base

Energy dissipation is made due to the impact developed at the base of a foundation when the foundation causes uplift. Because the energy dissipation is not considered in the idealization by **Eq.(2)**, it needs to be included in the analysis in terms of damping. If one represents the velocity of a foundation before and after the contact with the underlying soils as v and v', the impact coefficient "c" is defined as

$$c = -v'/v \quad (10)$$

In a single–degree–of–freedom system, the "c" may be written as

$$2\pi h/\sqrt{(1-h^2)} = \ln(v'/v) \quad (11)$$

where

h : damping ratio of critical of a system

Substituting **Eq.(10)** into **Eq.(11)**, one can have

$$h = \sqrt{\{(\ln c)^2/((\ln c)^2 + \pi^2)\}} \quad (12)$$

The damping coefficient C_j^{B} is assumed as

$$C_j^{B} = 2h\sqrt{(m_{Yn} \cdot K_{Yj}^{B1})} \quad (13)$$

The damping force acting at the members of a superstrucutre and a pier is assumed to be computed using given modal damping coefficients. It should be noted here that since simulation analyses which will be discussed later are made for the shake table test results of a simple rigid mass foundation, the analytical model without a superstructure nor a pier is used.

SHAKE TABLE TESTS

A series of simulation analyses were made for the shake table test results of a ridid mass foundation made of concrete mortar. **Fig. 3** shows the set–up of the shake table tests of the foundation models [4]. The foundation model was set on the plywood plate with thickness of 3cm which is the model of soil and is fixed at the shake table. To control the friction coefficient between the foundation base and the plywood plate, a teflon plate with thickness

of 1cm and a vinyl chloride plate with thickness of 1cm were fixed at the plywood plate using bolts and a epoxy resin type bonding agent, respectively.

Two types of foudnation models with circular and rectagular sections were used for the shake table tests. **Table 1** shows the detaied conditions of the foundation models. The friction coefficient between the foundation base and the friction control plates was measured by the sliding tests of the models. The measured static friction coefficient was about 0.24 for the teflon plate, 0.49 – 0.57 for the vinyl chloride plate. Measured dynamic friction coefficients were smaller by about 20% than the static ones, respectively. Impact coefficient between the foundation and base was measured by free fall tests of a concrete block with diameter of 30cm and thickness of about 3cm. The block was fallen from the height of about 30cm and the impact coefficients was estimated by the heights before and after the impact.

Table 2 shows the shake table test cases. The harmonic and earthquake excitations were made. The shaking parameters for the harmonic excitation tests were assumed as frequency and acceleration amplitude. On the other hand, the shaking parameters for the earthquake excitation tests were assumed as ground motion type (ground condition type) and acceleration amplitude. As shown in **Table 2**, three type of earthquake ground motions recorded in the past earthquakes in Japan are used. These records correspond to the standard earthquake ground motions recorded on stiff, moderate and soft grounds, respectively. It should be noted here that the time axis of the earthquake acceleration time histories is assumed as half the original ones so that the necessary acceleration be obtained for the used shake table.

Measuring instrumentation system was provided for the shake table tests. The accelerations of the shake table and the foundation model were measured by the acceleration sensors. The displacements of the shake table and the foundation model were measured by a video camera and the visual analysis system for the harmonic excitation tests. For the earthquake excitation tests, the displacement responses were computed from the accelerations.

SHAKE TABEL TEST RESULTS AND THE SIMULATION ANALYSIS

A series for simulation analyses corresponding to the shake table tests are made. In the shake table tests, the shape of foundation models (circular and rectangular sections), the friction coefficient (teflon and vinyl chrolide plates), and the excitation motions are varied as test parameters. Since the results of the simulation analyses agree well with those of the tests, the simulation analyses for the foundation model with circular section on the tefron plate are shown in the following.

Date used for the simulation analyses is based on the test condition as shown in **Table 1**. Since the restoring forces of soil at the base of the foundation is modelled as discrete springs, it is essential to give the appropriate spring coefficient for the simulation analyses. The spring coefficient of vertical restoring forces was obtained from the elastic modulus of the teflon plate. However, the spring coeffcient thus obtained was 2.65×10^{6} (N/cm) then the

divergence was found in some cases of the numerical simulation analyses. Therefore, the spring coefficient of the vertical restoring forces was reduced to 1/100 the above. Although the displacement response tends to be larger as the spring decreases, the displacement response does not significantly varied in the range of the spring coefficient above mentioned. The spring at the base is assumed to be divided into 10 discrete segments. This is because it is verified that the rocking motion with uplift (separation) at the base can be accurately analysed if the base spring is divided into 10 or greater number of discrete segments. It should be noted here that the time step of numerical integlation is assumed as 1/1,000 second in the simulation analyses.

Harmonic Excitation

Fig. 4 shows time histories of the acceleration and displacement responses of the foundation model subjected to harmonic excitation with acceleration amplitude of 400cm/s ^{2} and frequency of 3Hz. It is found from the shake table tests that when the sliding of the foundation occurred the acceleration response exceeding that obtained by the corresponding frcition coefficient was cut. This phenomena was accurately simulated in the analyses.

On the other hand, with regard to the relative displacement response of the foundation model, the sliding and the accumulation of the sliding displacement was found in one direction. The final residual displacement was found to be about 5cm after 13 cycles of the shaking. Although the residual displacement is computed in the same direction as that in the tests, it is about 1cm and correponds to 1/5 the measured. The accumulation of the residual displacement is never computed in one direction on the ideal condition when the rigid mass on the rigid base with certain friction condition is subjected to the harmonic excitations. Therefore, the residual displacement measured in the tests may be affected by the slight inclination of the shake table and the base plates, antisymmetric acceleration amplitude of the shake table, the variation of friction coefficient from place to place. Although the antisymmetric acceleration amplitude is considered as an input excitation in the simulation analysis, the inclination of the shake table and the base plates and the variation of friction coefficient from place to place can not be considered in this analysis. However, if one pays attention to the sliding amplitude of each cycle of the shaking, the good agreement was found between the measured and computed ones, which are 2cm and 2.2cm, respectively.

Fig. 5 shows the same time histories as shown in **Fig. 4** when the foundation model is subjected to harmonic excitation with acceleration amplitude of 400cm/s ^{2} and frequency of 5Hz. Good agreement was found between the measured and the computed sliding amplitude of each cycle of the shaking as similar with the case shown in **Fig. 4**. The measured and computed ones are 0.7cm and 0.8cm, respectively. However, it is similar with the case shown in **Fig. 4** that the residual displacement is accumulated in one direction and that the difference between the measured and computed final residual displacement is found. The reason of the difference may be the same as discussed in the above.

Earthquake Excitation

Fig. 6 to **Fig. 8** show time histories of the acceleration and displacement responses of the foundation model subjected to three earthquake excitations, which are the Kaihoku Bridge Record (recorded at stiff ground), the Itajima Bridge Record (recorded at moderate ground) and the Tsugaru Bridge Record (recorded at soft ground), respectively. The peak accelerations of the three record were adjusted as 500cm/s ^{2} . **Table 3** shows the comparison between measured and computed peak responses.

When the foundation model is subjected to the Kaihoku Bridge Record, the major sliding of the foundation model is found twice at time of about 4 second and 6 second. These major sliding of the foundation is precisely simulated in the analysis. The good agreement between the measured and computed responses is found. The measured and computed residual displacement are 0.48cm and 0.34cm, respectively.

When the foundation model is subjected to the Itajima Bridge Record, a major sliding of the foundation is found once at time of 5 second. The measured and computed residual displacement are 0.53cm and 0.41cm, respectively. The good agreement is found between the test and the simulation as simiar to the case when the foundation was subjected to the Kaihoku Bridge Record.

On the other hand, when the foundation model is subjected to the Tsugaru Bridge Record, the several times sliding of the foundation is found. Although the simulation analysis shows good agreement with the test results on the time when the sliding occurs, the computed residual displacement is half the measured. This may be because since the several times sliding occured in the response of the foundation subjected to the Tsugaru Bridge Record the analytical errors in each sliding cycle is accumulated. The analytical error of each sliding cycle may be developed by the same reason as the cases in which the foundation was subjected to the harmonic excitation discussed in the previous section.

CONCLUDING REMARKS

A nonlinear response analysis method for sliding of a shallow foundation was proposed and the analysis method was verified through the simulation analyses of the shake table test results of the foundation models. Based on the results presented herein, the following conclusions may be deduced:

1) When the sliding of the foundaton model occured in the shake table test, the acceleration response of the foundation was observed to be cut at the acceleration exceeding the corresponsding sliding acceleration determined by the friction coefficient between the foundation and the base. The simulation analysis precisely showed the cut of the acceleration response of the foundation.
2) In the harmonic excitation, the sliding amplitude of an each cycle showed good agreement between the shake table tests results and the simulation analysis. However, residual displacement after the shaking did not show good agreement between those. This may be because of slight inclination of the shake table and the base and the variation of

friction coefficient from palce to place of the base, which did not take consideration in this simulation analysis.

3) When the foundation model was subjected to earthquake ground motions with the Kaihoku Bridge Record (Ground Conditon : Stiff) and the Itajima Bridge Record (Ground Condition : Moderate), a few times of the sliding were found in the shake table tests and the simulation analyses showed good agreement with the test results. When the foundation model was subjected to the Kaihoku Bridge Record, the measured and computed final residual displacements are 0.48cm and 0.34cm, respectively. On the other hand, when the foundation model was subjected to the Itajima Bridge Record, they are 0.53cm and 0.41cm, respectively.
4) When the foundation model was subjected to the Tsugaru Bridge Record (Ground Conditon : Soft), the several times sliding of the foundation were found. Although the simulation analysis showed good agreement with the test results on the time when the sliding occurs, the computed residual displacement was half the measured. This may be because since the several times sliding occured in the response of the foundation subjected to the Tsugaru Bridge Record the analytical errors in each sliding cycle was accumulated. The analytical error of each sliding cycle may be developed by the same reason as shown in 2).
5) Based on the sliding displacement and the residual displacement of a shallow foundation using the proposed nonlinear analytical method, a displacement-based evaluation method for the stability against the sliding of a shallow foundation will be developed.

REFERENCES

1. Japan Road Association : Design Specifications for Highway Bridges, Part IV : Substructures and Part V : Seismic Design, 1990 (in Japanese)
2. Kawashima, K. and Unjoh, S. : Analysis of Rocking Vibration of Rigid Foundations, 8th U.S.-Japan Bridge Engineering Workshop, UJNR, Chicago, U.S.A., 1992
3. Kawashima, K., Unjoh, S. and Mukai H. : Rocking Response of Direct Foundations, 10th U.S.-Japan Bridge Engineering Workshop, UJNR, Lake Tahoe, U.S.A., 1994
4. Otsuka, H. and Hosokawa, M. : Shake Table Tests on Sliding of Caisson Foundation Model subjected to Earthquake Ground Motion, Technical Memorandom of the Public Works Research Institute, No.3303, August 1994 (in Japanese)

Table 1 Details of Foundation Models

Foundation Model		Foundation with Circular Section	Foundation with Rectangular Section
Height (cm)		30	30
Diameter (cm)		41.5	–
Width (cm)		–	30 × 45
Area of Base (cm^2)		1,352	1,350
Weight (N)		848.3	853.2
Static Friction Coefficient	Teflon	0.24	0.24
	Vinyl Chloride	0.49	0.57
Dynamic Friction Coefficient	Teflon	0.20	0.20
	Vinyl Chloride	0.40	0.40
Impact Coefficient	Teflon	0.38	
	Vinyl Chloride	0.63	

Table 2 Shake Table Test Cases

Motion of Shake Table	Test Condition	
Harmonic Excitation	• Shaking Parameter : Frequency and Acceleration Amplitude	
Earthquake Excitation	Kaihoku Bridge Record (1978 Miyagi–ken–oki Earthquake) (Ground Condtion : Stiff)	• Shaking Parameter: Peak Acceleration • Time Axis : Half The Original
	Itajima Bridge Record (1968 Hyuganada–oki Earthquake) (Ground Condition : Moderate)	
	Tsugaru Bridge Record (1983 Nihonkai–chubu Earthquake) (Ground Condition : Soft)	

Table 3 Comparison between Measured and Computed Peak Responses of the Foundation Models subjected to Earthquake Excitations

Earthquake Excitation	Peak Acceleration of Shake Table (cm/s^2)	Peak Acceleration (cm/s^2)		Peak Relative Displacement (cm)		Residual Displacement (cm)	
		Measured	Computed	Measured	Computed	Measured	Computed
Kaihoku Bridge Record	521	257	203	0.48	0.34	0.40	0.31
Itajima Bridge Record	513	240	203	−0.53	−0.41	−0.50	−0.40
Tsugaru Bridge Record	513	207	204	3.01	1.35	2.90	1.19

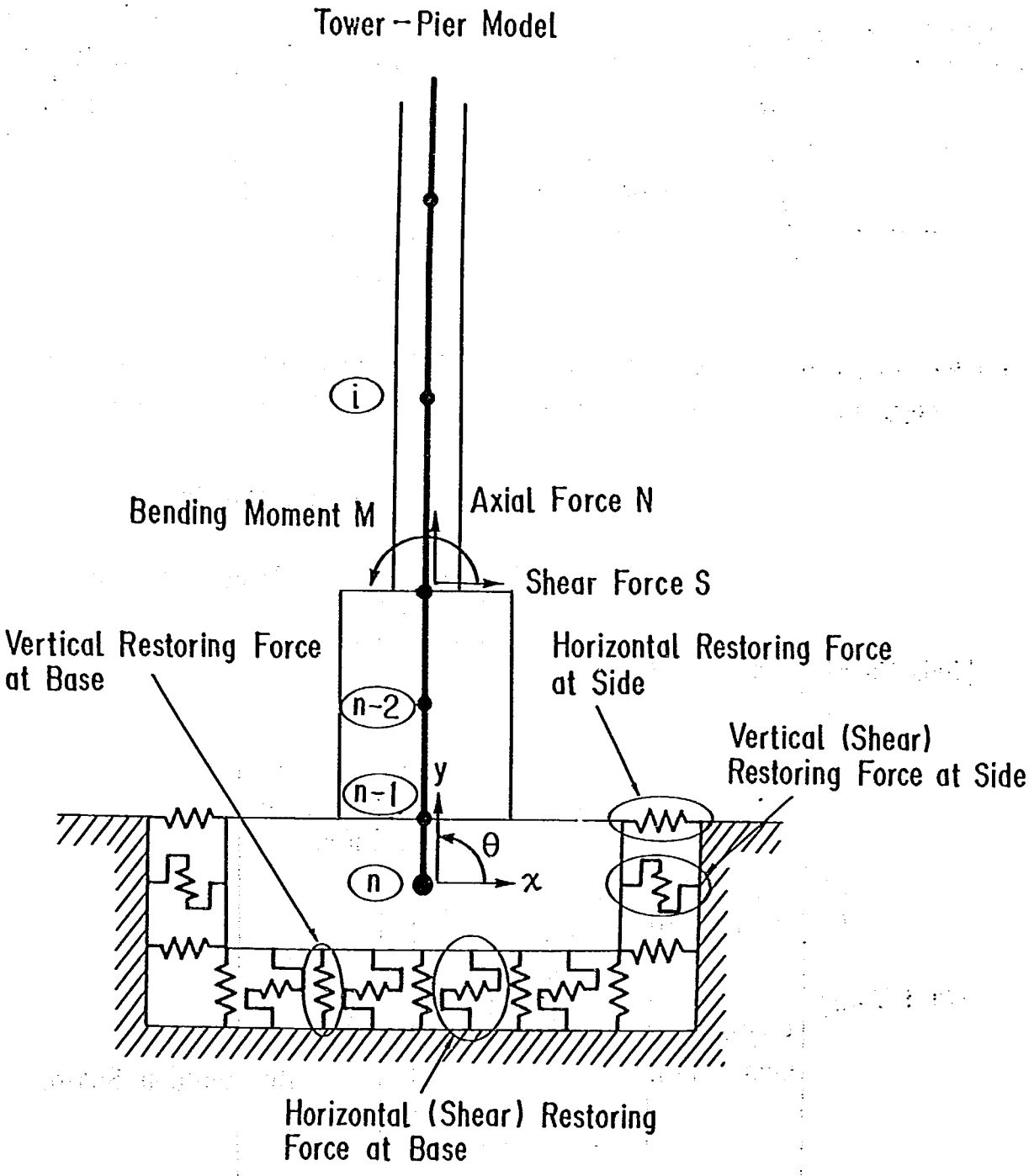
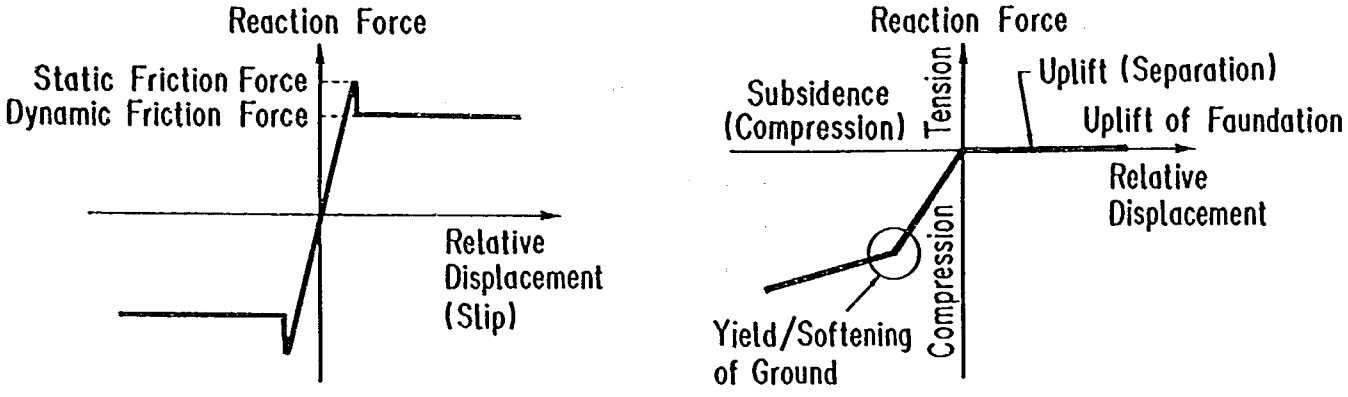


Fig.1 Analytical Model for Sliding and Rocking Motions of Foundations



(1) Restoring Force in Normal Direction (2) Restoring Force in Tangential Direction

Fig.2 Model of Restoring Forces of Soil at Base and Sides of A Foundation

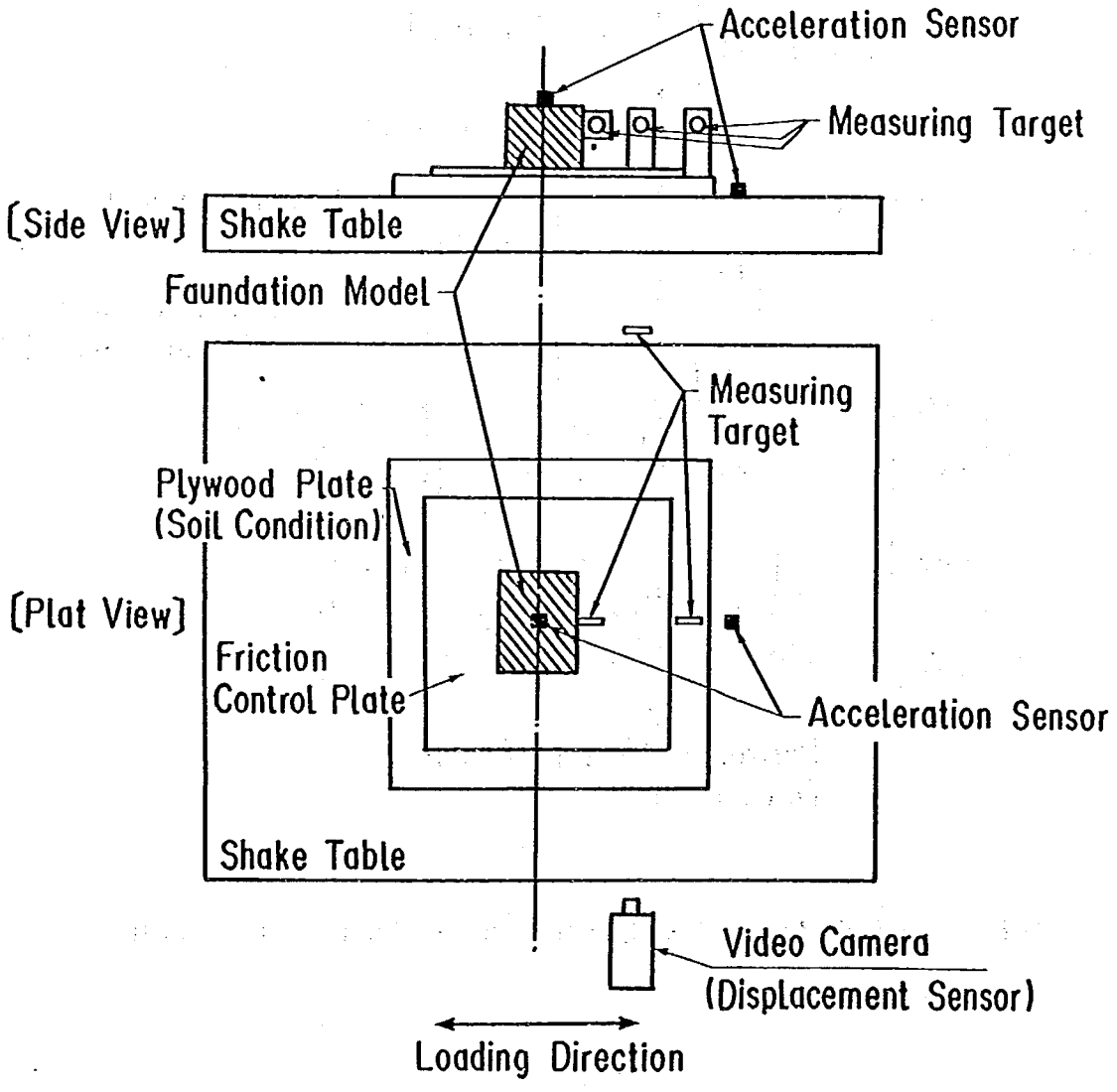
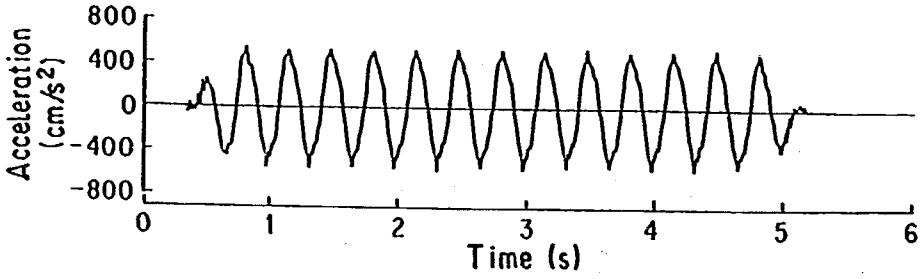
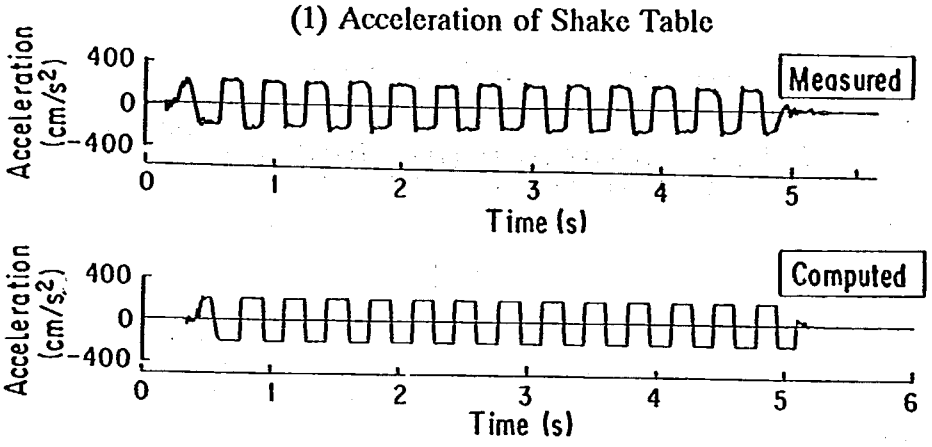


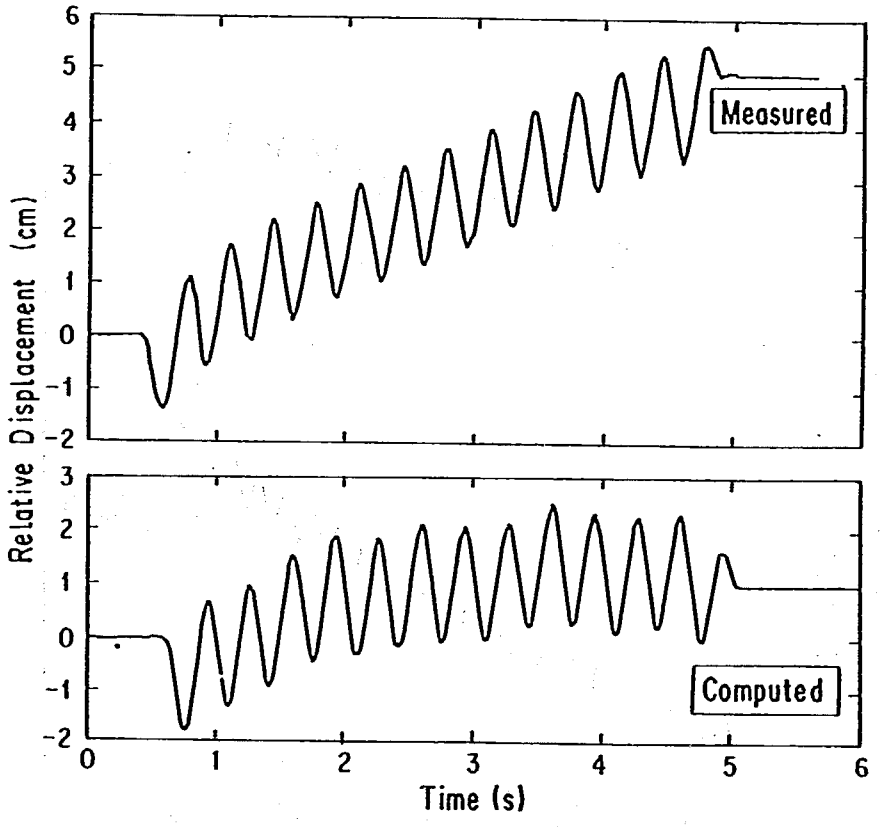
Fig.3 Set-up of Shake Table Tests of Foundation Models



(1) Acceleration of Shake Table

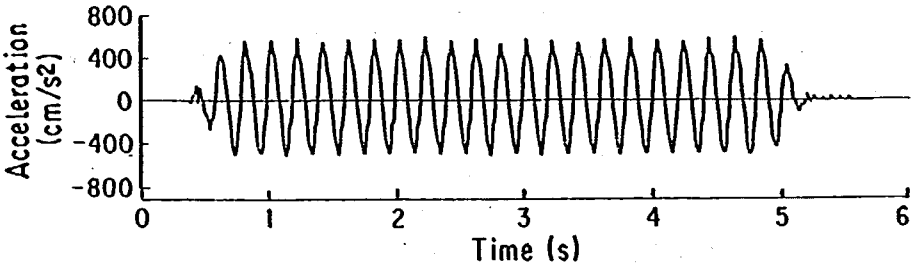


(2) Acceleration of Foundation

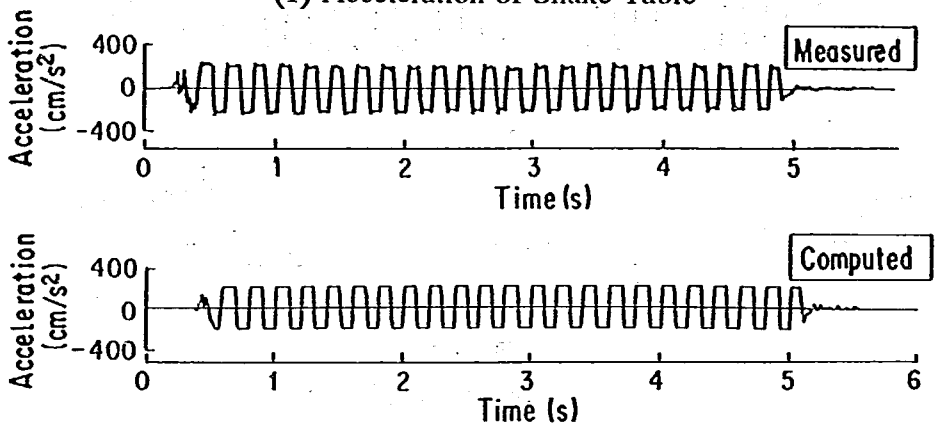


(3) Relative Displacement of Foundation

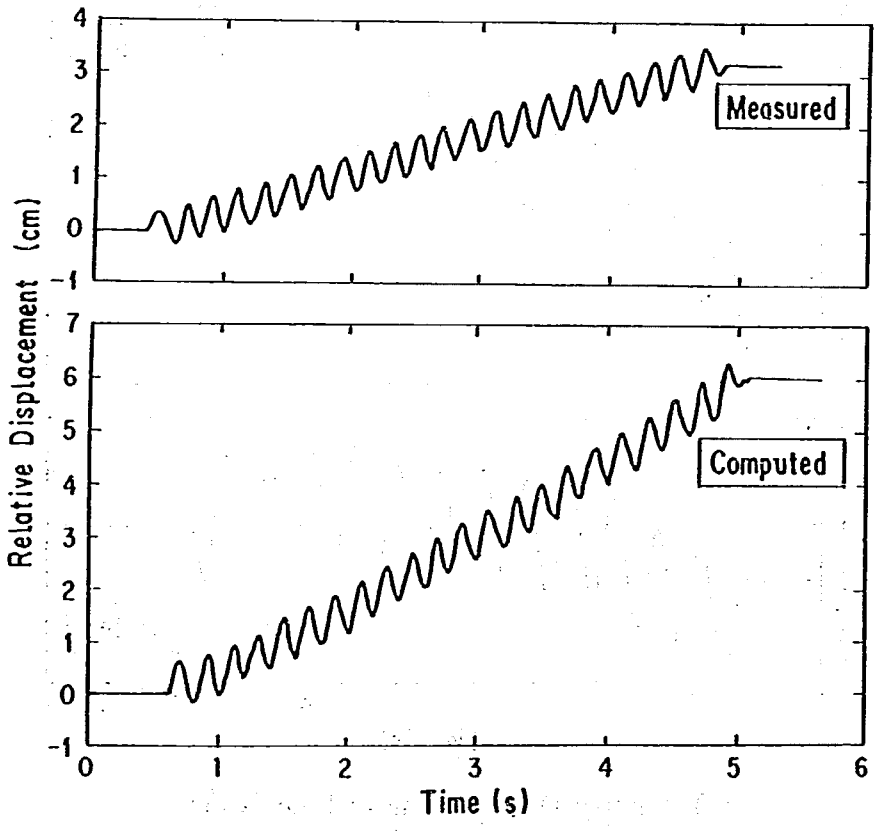
Fig.4 Shake Table Test Results and the Simulation Analysis of the Responses of Foundation subjected to Harmonic Excitation
(Acceleration Amplitude : 400cm/s ^{2} , Frequency : 3Hz)



(1) Acceleration of Shake Table

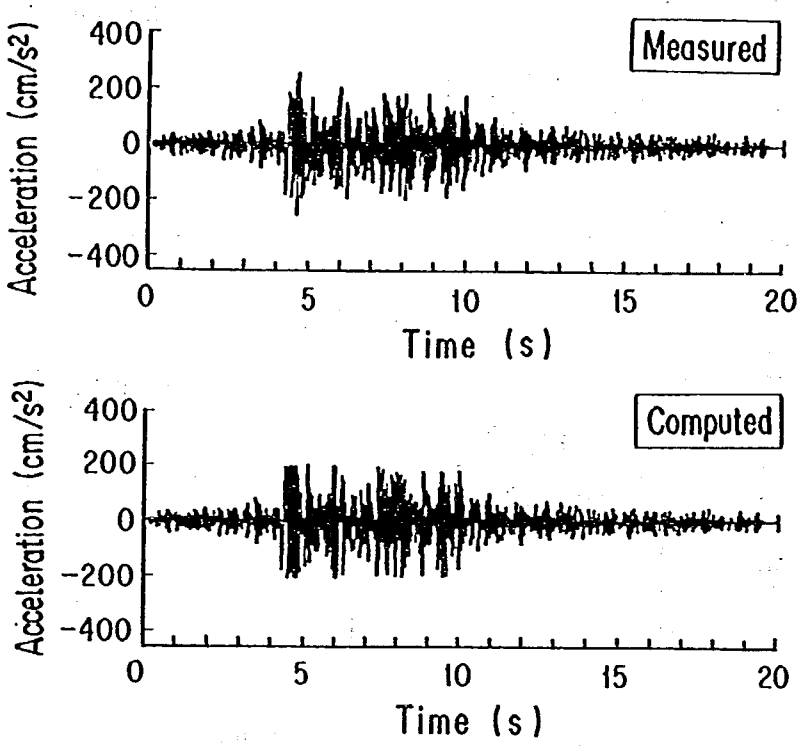


(2) Acceleration of Foundation

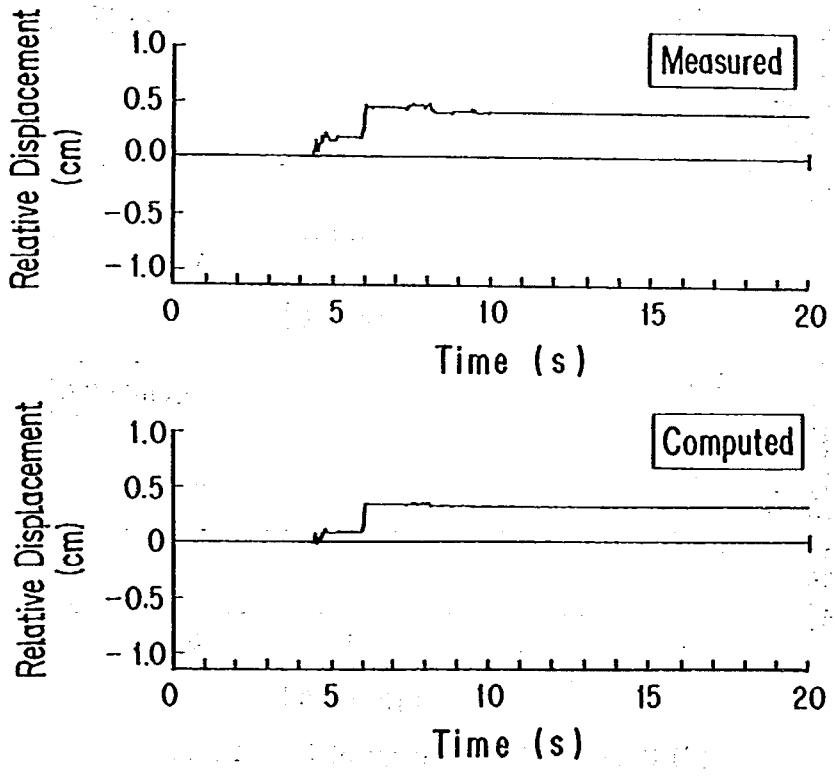


(3) Relative Displacement of Foundation

Fig.5 Shake Table Test Results and the Simulation Analysis of the Responses of Foundation subjected to Harmonic Excitation
(Acceleration Amplitude : 400cm/s^2, Frequency : 5Hz)

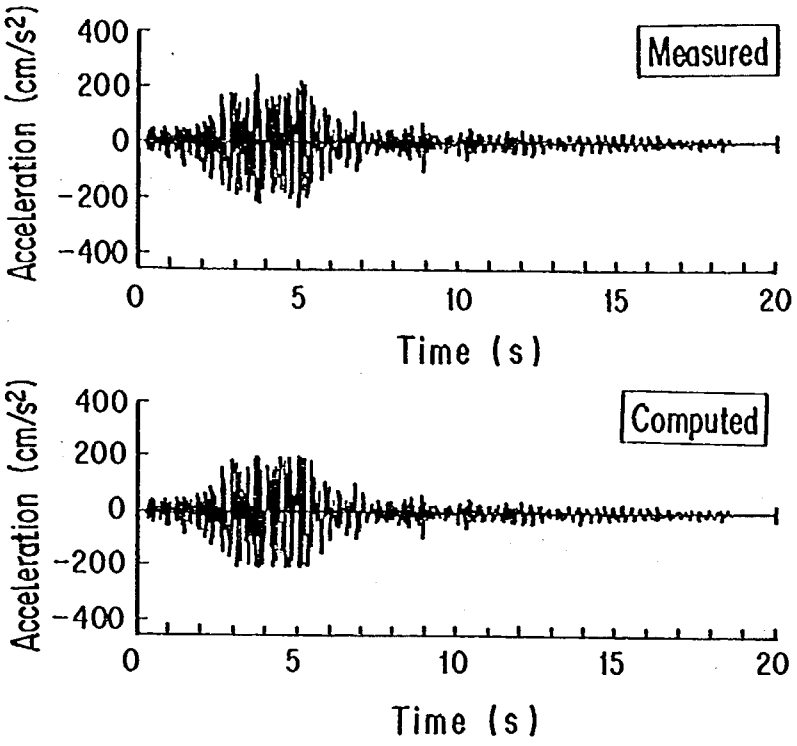


(1) Acceleration of Foundation

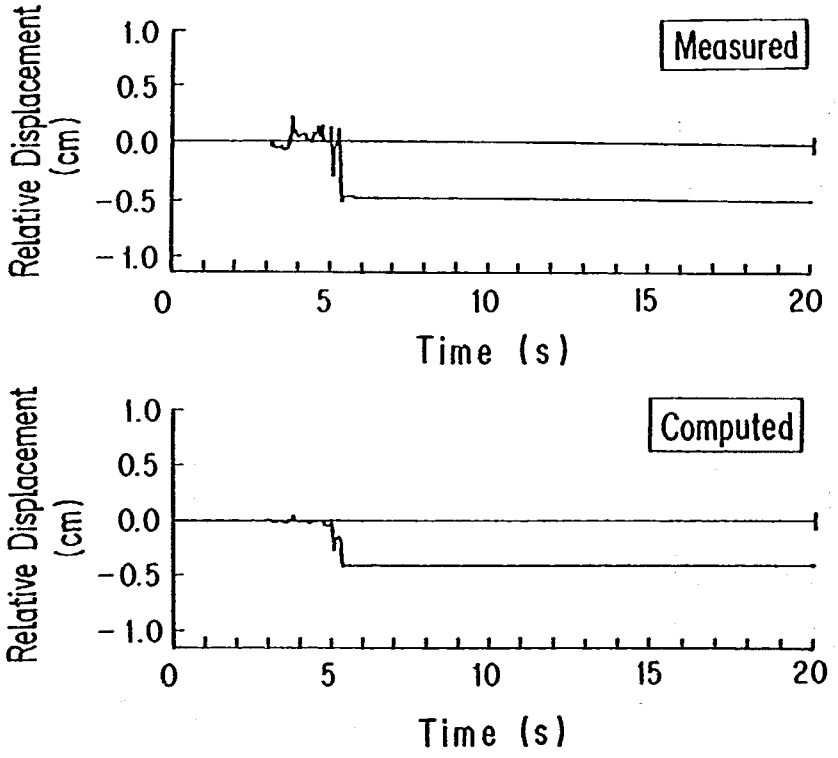


(2) Relative Displacement of Foundation

Fig.6 Shake Table Test Results and the Simulation Analysis of the Responses of Foundation subjected to Earthquake Excitation
(Kaihoku Bridge Record, Peak Acceleration : 521cm/s ^{2})

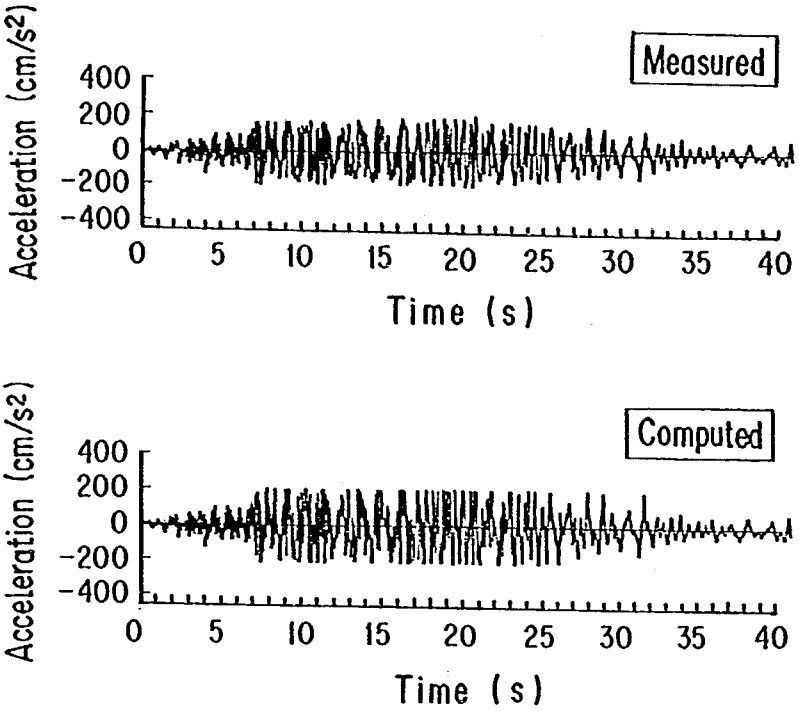


(1) Acceleration of Foundation

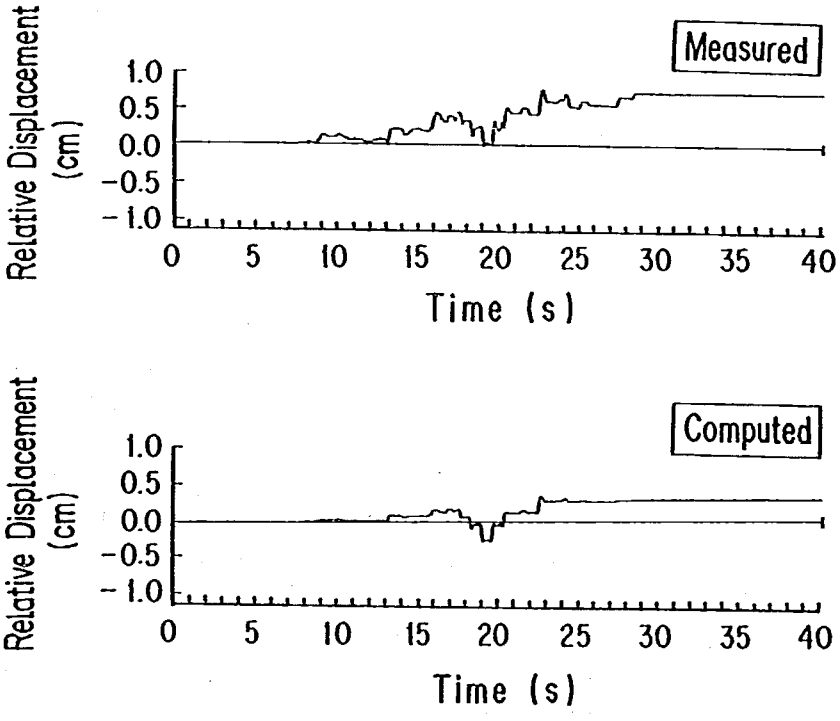


(2) Relative Displacement of Foundation

Fig.7 Shake Table Test Results and the Simulation Analysis of the Responses of Foundation subjected to Earthquake Motion
(Itajima Bridge Record, Peak Acceleration : 513cm/s ^{2})



(1) Acceleration of Foundation



(2) Relative Displacement of Foundation

Fig.8 Shake Table Test Results and the Simulation Analysis of the Responses of Foundation subjected to Earthquake Motion
(Tsugaru Bridge Record, Peak Acceleration : 513cm/s ^{2})

A STUDY ON THE DEFORMATION CHARACTERISTICS OF PRECAST HOLLOW PIERS DURING EARTHQUAKES

Masanori NAKANO[1], Shigeru TAKAGI[2], Moriyuki OKOSHI[3] PWRI

1)Head, Foundation Engineering Division, Structure and Bridge Department, Ministry of Construction, Tsukuba Science City 305 Japan
2)Research Engineer, ditto
3)Assistant Research Engineer, ditto

ABSTRACT

More high piers are likely to be constructed in the future, and construction techniques therefore need to be developed to make effective use of precast technology in order to reduce labor, preserve the natural environment and improve the infrastructure as society develops.

As a part of a fundamental study on the design technology for high piers using precast concrete, we carried out loading tests to determine the factors which affect earthquake resistance, since these are usually difficult to concrete body. In these tests, parameters included the method used to join precast members, the arrangement and shape of reinforcement bars, and the amount of prestress and so forth. We successfully determined the deformation characteristics, sheared gaps between blocks, fracture properties and toughness of the annular (hollow) pier.

INTRODUCTION

Recently in Japan, the slow progress of construction work, a sharp rise in building costs due to aging and the shortage of laborers have become a serious social problem. In addition, construction conditions are becoming more demanding, for example, bridges requiring high piers in mountainous regions will increasingly be required in the future, while demands for environmental preservation are growing. To solve such problems, studies are underway to reduce the effort and labor involved, and to rationalize construction work. Such measures include the use of precast members for structures, and automated, mechanized construction techniques. This study investigates experimentally the lower structure of bridges, particularly the use of precast piers in above-ground portions.

There have been a number of studies on reinforced concrete piers, yet almost none on hollow prestressed reinforced concrete piers and prestressed concrete piers, and their characteristics remain unclear. We therefore conducted repeated tests on static horizontal positive and negative alternating loading to determine the earthquake resisting properties of precast piers, using parameters such as whether or not there

are block joints and shear keys, the amount of prestress and the arrangement and shape of reinforcement bars. This study included the following evaluation.

1. Evaluation of (fracture properties,)
2. Evaluation of R(range of plastic hinge generation by strain distribution in axial reinforcements,)
3. Evaluation of (restraining effect of hoop tie by its strain distribution,)
4. Evaluation of (proof stress and deformation capacity by load displacement, deformation angle,) etc.
5. Evaluation of (behavior of joints portions by changes in displacement angle, crack width, etc. in joint portions,)
6. Evaluation of energy absorbing power by historical absorbed energy, equivalent viscous damping constant and cumulative absorbed energy,
7. Comparison of amount of slip-out of axial reinforcements obtained by the conventional computation method and our empirical values, and
8. Comparison of ductility factor obtained by the conventional computation method and our empirical values.

OUTLINE OF EXPERIMENTS

Specimens

The structure hypothetically tested in this study consisted of hollow rings piled up one on another, prestressed by PC steel bars and joined as shown in Fig.1. We chose this structure since it is frequently used for the underground base and has established manufacturing and construction methods, and also because we considered it relatively easy to apply to piers.

The specifications of the specimens are listed in Table 1.
Specimens Nos. 2 and 3 are PRC structures using PC steel bars joined by low-level prestressing, their axial reinforcements continuing through the joints from the footing to the upper end of the pier to act ordinarily as tension reinforcements (i. e., not during earthquakes). Specimen No. 4 was also made from precast rings joined by PC steel bars but discontinued reinforcements were used in each block and so only the PC steel bars and prestressing offered resistance to bending tension. Thus, this specimen needed more prestressing than Nos. 2 and 3.

Figure 1 shows the shape and size of the specimens and reinforcement bar arrangement. All specimens were of a similar external shape and size. Specimen No. 1 was a conventional one piece structure of reinforced concrete and was tested for comparison with the others. Specimens Nos. 2, 3 and 4 were precast structures as noted above and no adhesive was applied on their joint surfaces. To prevent shear, shear keys were installed on the joint surfaces of No. 3. The quantities of vertical steel materials were determined so that all the specimens had an equal ultimate proof stress due to bending. For circumferential reinforcements, double, i.e., inner and outer hoop ties per cross section, were placed in specimen Nos. 1 to 4, but the

lowermost block of No. 3 was provided with interlaced hoop ties while No. 4 was provided with U-shape reinforcement bars to restrain the inner and outer axial reinforcements. Hoop ties were placed in all the specimens as required to prevent prior shear failure.

The design reference strength of the concrete was set at 400 kgf/cm2 and commercialise available PC steel bars with a diameter of 9.2 mm (yield strength: 125 kgf/mm3; tensile strength: 140 kgf/mm3) and D10·D6 deformed bars (SD295D) were used.

Loading Patterns and Loading History

Figure 2 shows of the loading patterns. The strain produced in the primary reinforcement on the outermost edge of the pier was measured. The horizontal displacement (excluding the displacement caused by rotation of the footing) produced on the upper end of the pier when the primary reinforcement yielded at its base was used as the yield displacement (hereafter, δ y), positive and negative alternating loading was repeated five times in displacement amplitudes of n δ y (integral multiples of δ y, n= 1, 2, ...).

The displacement due to rotation of the footing was obtained by measuring the angle of rotation using two displacement meters installed on the lower end of the footing and converting it into a horizontal displacement at the upper end of the pier (See Fig. 1). On No. 3, the loading was increased gradually and monotonously by controlling the load until the cracking load was reached. Loading was regarded as complete when it fell to approximately 40% of the maximum load. The height between the pier base and the point of loading (effective height) was 2.6 m and the shear span ratio (ratio of effective height to outside diameter of pier) was 3.25.

TEST RESULTS

The drawings and tables shown below were prepared by using values obtained when the maximum deformation occurred for the positive load at each δ y in each of the fifth cycle.

Fracture Properties

Figure 3 shows the cracks that were produced. In all the specimens, cracks appear in the positions of the hoop ties (at intervals of 10 cm). In specimen No. 1, cracks are seen across the whole area of the pier whereas cracks are distributed in an area between the base and 1.7 to 2.0 m above it in each of specimens Nos. 2 and 3.

No. 3 has a slightly wider distribution than No. 2, due to dispersion of the shear force owing to the shear keys, dispersion of the plastic hinge range owing to the interlaced reinforcements, and also due to residual prestress. The cracks in No. 4 are concentrated in the base area due to the larger axial prestress. The inside and outside axial reinforcements of specimen No. 1 mostly buckled and broke to the direction of the concrete covers, but the inside axial reinforcements of Nos. 2 and 3 buckled and broke outwardly with respect to the rings. Table 2 shows the proof stresses and deformation properties.

Distribution of Strains of Axial Steel Materials

The strains shown in Figs. 4 and 5 do not include initial strain due to prestressing.

Distribution of Strains for Axial Reinforcements

Figure 4 shows the strains of axial reinforcements at $3\delta y$ in specimens Nos. 1, 2 and 3. (In No. 4, no existence of contiuece axial reinforcement Nos. 1 and 2 had a substantially similar distribution, that is, the reinforcements in their base areas yielded at about 20 cm considering the formation of plastic hinges there. Specimen No. 3 showed that plastic hinges formed in a wider range than the base area and that there was less strain in the base area.

Distribution of Strains for PC Steel Bars

Figure 5 shows distributions and changes of strains of PC reinforcement bars at the similar respective upper end displacements in specimens No. 2, 3 and 4. The PC steel bars have higher yield points than the reinforcement bars and their strain distributions are smoother. Specimen No. 2 tends to have larger strains compared to No. 3. In specimen No. 4, strains of about 5,000 μ were uniformity produced at $1\delta y$ and above, considering that the grout was cut in all portions.

Distribution for Strains of Hoop

In this study, hoop were placed between the inside axial reinforcements and the cover concrete in anticipation of reduced toughness of the members due to exfoliation of the concrete, and the effects of the ties were studied. Interlaced hoop ties (No. 3) and U-shape reinforcements (No. 4) were placed and their effects on suppressing buckling of the axial reinforcements were monitored.

Figure 6 shows the strain distributions with the upper end displacement in the respective specimens. In all of them, the inside hoop ties have greater strains. Compared with specimens Nos. 1 and 2, strains in the lowest block of No. 3 are distributed over a smaller area, due to the interlaced reinforcements which restrained the deformation of the axial reinforcements resulting in less strain in the hoop ties. The maximum strains were 534 μ (NO. 1), 455 μ (NO. 2) and 424 μ (NO. 3) respectively in specimen Nos. 1, 2 and 3.

In the distribution of 11 δ y of No. 3, the maximum strain of the inside hoop ties was 814 μ and the strains of the outer ones increased sharply at 12 δ y in the area less than 45 cm from the base and the gauge stopped functioning normally. The strains produced in the interlaced reinforcements corresponded with those of the hoop strain.

In specimen Nos. 1, 2 and 3, the strains in the inside hoop ties remained similar to the positive and negative alternating loads (under tension and under compression), and the highest strains occurred in the outside hoop ties under compression, which tended to decrease under tension.

Deformation Capacity

Envelope Line

Figure 7 shows envelope lines which represent the relation between the load and the horizontal displacement. In specimen No. 1, peeling off of the inside and outside concrete started at 9 δ y and major exfoliation and breaking occurred at 11 δ y. In specimen No. 2, the reinforcement bars began to swell at 11 δ y; concrete broke at 12 δ y; and inside concrete conspicuously peeled off at 13 δ y. In specimen No. 3, exfoliation of concrete and breaking of reinforcement bars started at approximately the same value of 16 δ y. As for specimen No. 4, in the tested range of displacements, no clear point of decrease was found although the load began to reduce little by little at 10 δ y. This was believed to be the result of very localized breaking of concrete and the slow progress of exfoliation.

Figure 8 shows envelope lines representing the relation between the load and the displacement angle (δ /2.6m*100). All the specimen reached their ultimate loads at 1% displacement angles and the loads started to reduce at 2%.

Behavior of Joint Portion

The shear magnitude and width of cracks which developed in joint portions under loading were compared in specimen No. 1, which was a one-piece structure of reinforced concrete, and specimen Nos. 2, 3 and 4, which were precast structures, and the different behaviors of the joint portions were analyzed.

Shearing gaps of Joint Portion

The amount of shearing gaps is obtained by averaging the measurements read from a cantilever type displacement meter and deducting the displacement produced due to bending of the member from the average. Measurements were taken on both sides of each specimen at right angles to the direction of loading.

Figure 9 shows the relation between the amount of shearing gaps and the upper end displacement. The largest shearing gaps were: 0.04 mm in specimen No. 1, 0.17 mm in No. 2, 0.08 mm in No. 3 and 0.2 mm in No. 4. The shearing gaps of No. 3 which was smaller than that of No. 2 is thought to have been due to the shear keys installed in the joint portions. Specimen No. 4 had the largest shear presumably because it had no axial reinforcements piercing through the blocks and the only frictional force was provided by prestressing. Shearing gaps was the largest in the second block from the top in each of specimen Nos. 1 and 2 while the shear was also large in the top block in No. 3. In No. 4, the values for all blocks varied little.

Crack Width

In each joint, the width of cracks was measured by a π gauge on both sides of the specimen in the direction of loading. Figure 10 shows the relation between crack width and the upper end displacement, both when the load was the maximum and when the load was removed. Comparing the specimens at their maximum deformation, No. 1 had the largest crack width of 1.33 mm and the value was the largest in the lowest block (third from the top). Crack width became narrower as the displacement increases to a certain extent. The amount of displacement starts to decrease approximately when the residual displacement begins to stabilize. The maximum width in specimen No. 2 was 1.06 mm and there is a clear trend similar to No. 1. The amount of residual displacement was also smaller than that of No. 1 probably because of the effect of prestressing. In specimen No. 3, both the lowest and the second lowest blocks had wide cracks, the largest being 1.36 mm. Openings of No. 4 were far narrower compared with those of specimen Nos. 1, 2 and 3.

When there was no load, the crack width in the lowest block of No. 1 started to increase sharply when the upper end displacement was 25 mm, reaching approximately 0.8 mm. In specimen Nos. 2 and 3, the values were similar to or less than those of No. 1. Specimen No. 3 had slightly larger values than No. 2 and residual cracks were scattered in the lowest block and the second block from the top. In No. 4, the residual displacement scarcely increased, indicating the remarkable effect of prestressing.

Energy Absorbing Power

Figure 11 shows load-displacement curves of the various specimens at $3\delta y$, $6\delta y$, $9\delta y$ and the ultimate δy. The ultimate δy of specimen No. 1 had a substantial residual load as the experiment ended with a much smaller displacement compared to the other specimens. The proof stress of specimen No. 4 fell less than Nos. 1, 2 and 3 despite its displacement.

Figure 12 shows the historical absorbed energy, equivalent viscous damping constant and cumulative absorbed energy. Since each specimen had its own $1\delta y$ value, the gradients shown in the respective graphs are different. However, specimen Nos. 1, 2 and 3 begin to show a decrease in historical absorbed energy at almost the same displacement (about 66 mm) and there was no sharp fall before it. On the other hand, the energy absorbed in No. 4 is

conspicuously lower than in the others.

The specimens display the same tendency with regard to their equivalent viscous damping constants and cumulative absorbed energy. It is noticeable that the cumulative absorbed energy of specimen No. 1 was slightly higher compared to that of the others. Because of its large displacement per δ y, No. 4 was loaded fewer times and thus did not show much difference from the others in the experimental range of this study.

Computation of Slip-out Length of Axial Reinforcement

To compute the displacement due to slip-out, formulae 1 and 2 given in the Railway Structure Design Standards and Guidelines [Concrete Structures] (hereinafter, "the standards") were used. Values thus obtained were compared with those obtained by integrating the strain distributions of the respective axial reinforcements. In this process, the highest value of strain was set at 2000 μ which was the yield strain.

$$\Delta l_y = 0.070 - 0.0054(D/\phi) + 0.00017(D/\phi)^2$$
$$\Delta l_u = 0.083 - 0.0054(D/\phi) + 0.00015(D/\phi)^2 \qquad \text{(Formula-1)}$$

Δl_y: Length of slip-out at yield(cm)
Δl_u: Length of slip-out at the end (cm)
D : Distance between the centers of bars (cm)
ϕ : Diameter of bars (cm)

Δl_y and Δl_u obtained from formulae 1 and 2 were 0.511 mm and 0.638 mm respectively. Figure 13 compares these with the empirical values of the specimens. The empirical values when all the specimens yielded were considerably smaller, about 20%, than the computed ones. For the ultimate slip-out, the empirical value of No. 1 was nearly the same as the computed one, whereas specimen Nos. 2 and 3 gave similar values which were smaller than the computed ones.

Computation of Ductility Factor

The ductility factor of the members was computed by using the following formula given in the Railway Structure Design Standards and was compared with the empirical values.

$$\mu = \delta_u / \delta_y = (\mu_o \cdot \delta_{yo} + \delta_{ui}) / (\delta_{yo} + \delta_{yi}) \qquad \text{(Formula-2)}$$

μ : Ductility factor of member,
δ_u: Ultimate displacement,
δ_y: Yield displacement,
μ_o: Ductility factor of body,
δ_{yo}: Displacement due to body deformation at yielding,
δ_{yi}: Displacement due to rotation caused by slipping out of axial reinforcements at yielding,
δ_{ui}: Displacement due to rotation caused by slipping out of axial

reinforcement at the end

μ of specimen Nos. 1, 2 and 3 obtained by using formula 3 was 7.6, which was less than the empirical values.

SUMMARY

The main results obtained from this study are summarized as follows:

1. The proof stresses of specimens No. 2 and 3 were approximately equivalent to that of specimen No. 1 RC pier, and computation using the existing formula appears to be valid. Specimen Nos. 2 and 3 were confirmed to have a slightly higher toughness than No. 1.

2. In the specimens reinforced by the arrangement and shape of hoop ties, the inside concrete peeled off less quickly and toughness was increased. Interlaced reinforcement bars thus appear to effectively increase the rigidity of the base.

3. Although prestressed piers absorbed less energy due to the restoring force of the prestressing, the effectiveness of prestressing in suppressing cracks was confirmed.

4. The loading pattern used in this study did not produce conspicuous shear in the joint portions of the PRC piers which had reinforcement bars placed crossways and were not coated with an adhesive, although the specimen with shear keys exhibited a somewhat smaller shear.

These results show that the effects of reducing the shear span ratio and the axial reinforcement ratio, and of increasing or decreasing the amount of prestressing need to be investigated.

REFERENCES

1) Kawashima, K.: Dynamic Proof Stress and Deformation Capacity of Hollow Circular RC Piers, Civil Engineering Technical Materials 34-10, pp. 34-39, 1992

2) Nakai, M., Shima, H. and Abe, M.: Study on Shear Keys of Post-installation Mortar Filling Type, The 48th annual symposium of the Civil Engineering Society, Section 5, pp. 672-673

3) Japan Road Association: Highway Bridge Specifications V, Earthquake Resistant Design Section, 1993.2

4) Japan Railway Construction Corporation: Railway Structure Design Standards and Guidelines [Concrete Structures]

Table. 1 Description of Specimens

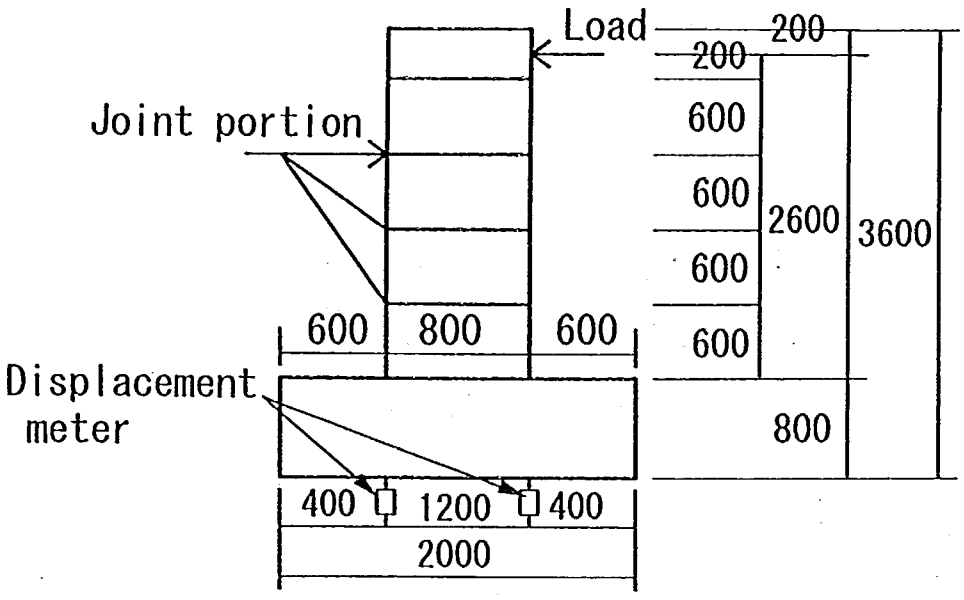
Type of Sample	Structure Type	Sear Key	Axial reinforcement ratio	Traverse reinforcement ratio
NO. 1	RC One piece driving	-------	1.9%	0.63%
NO. 2	PRC Without Key	Without	1.4%	0.63%
NO. 3	PRC With Key	With	1.4%	0.63%
NO. 4	PC Without Key	Without	0.58%	0.63%

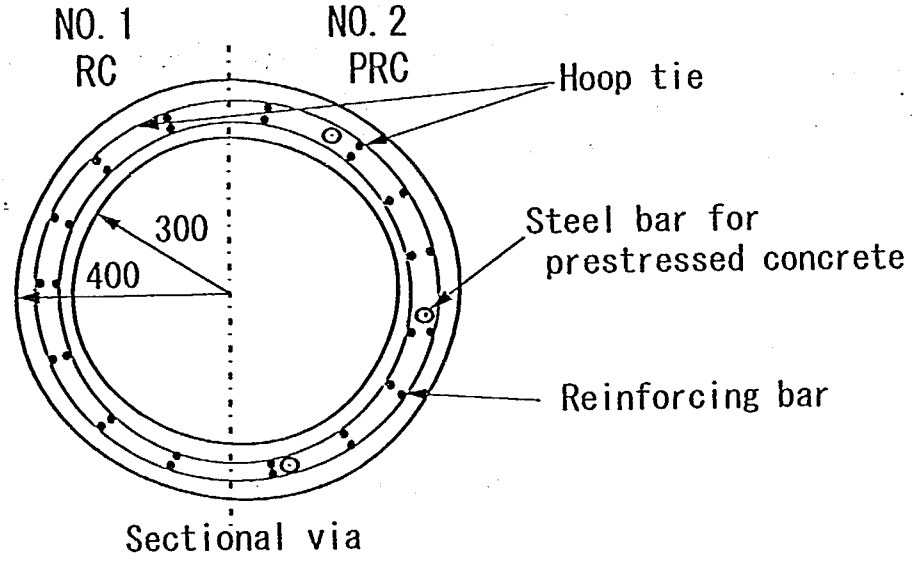
Note: Amount of prestress=Total prestress force÷ Total sectional area

Table. 2 Description of Specimens

Name of Sample		NO. 1	NO. 2	NO. 3	NO. 4
Proof stress	Yielding proof stress	12.1	13.4	10.5	14.8
	Maximum proof stress	19.7	20.6	19.6	17.2
	Pm/Py	1.63	1.54	1.87	1.16
Deformation capacity	Yielding displacement	6.0	5.5	4.3	20.0
	Ultimate displacement	72.0	77.0	68.8	160.0
	Ductility factor	12	14	16	8

Note: Horizontal displacement when loading lowered to about 80% of maximum load was regarded as ultimate displacement δu





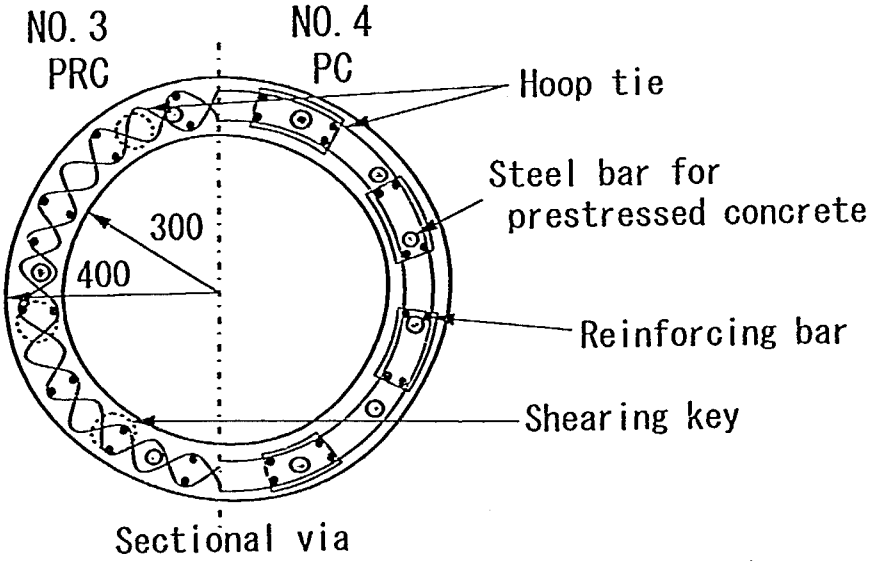


Fig. 1 Shape and Size Specimens

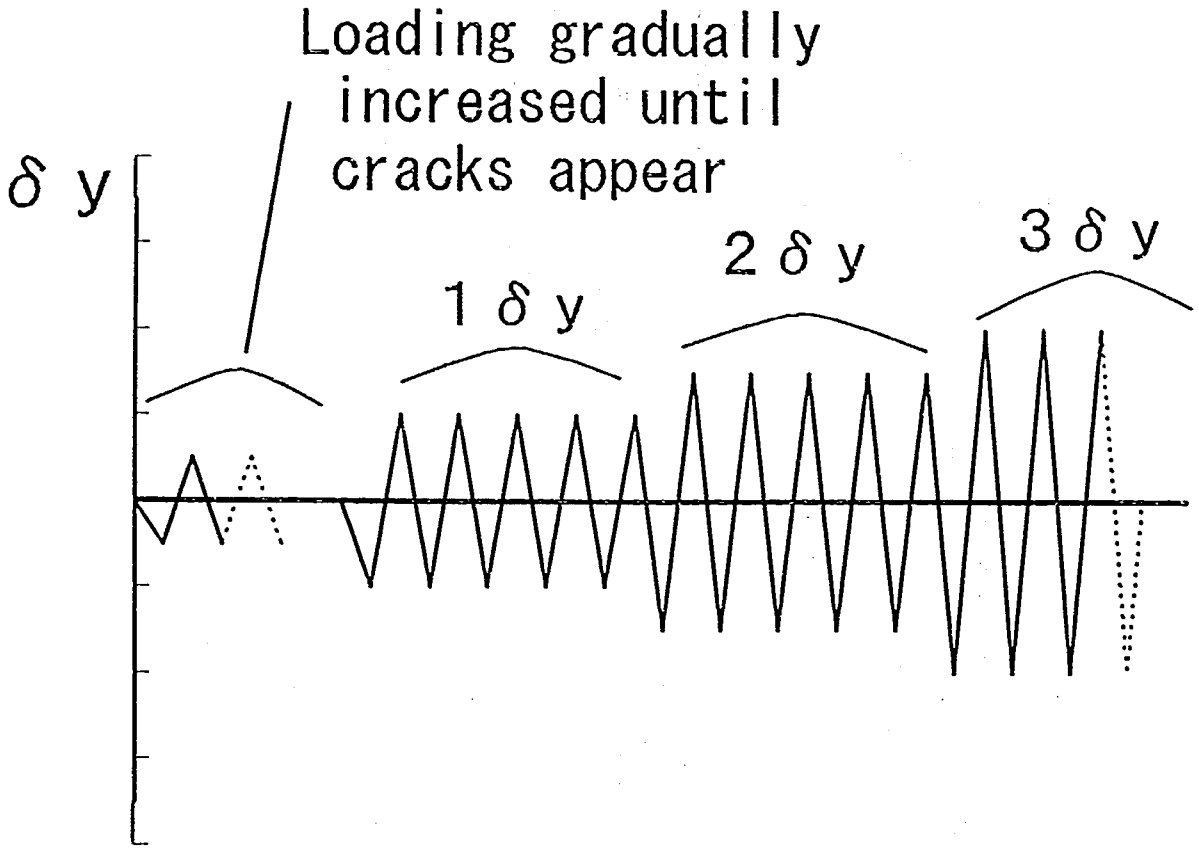
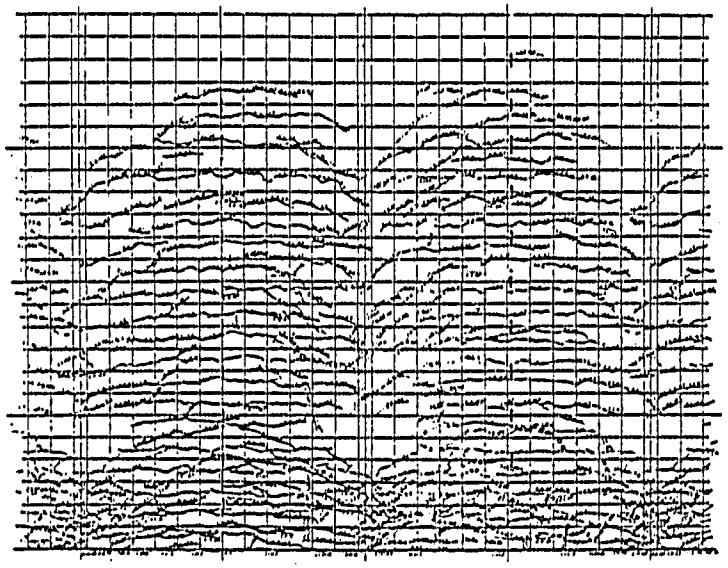
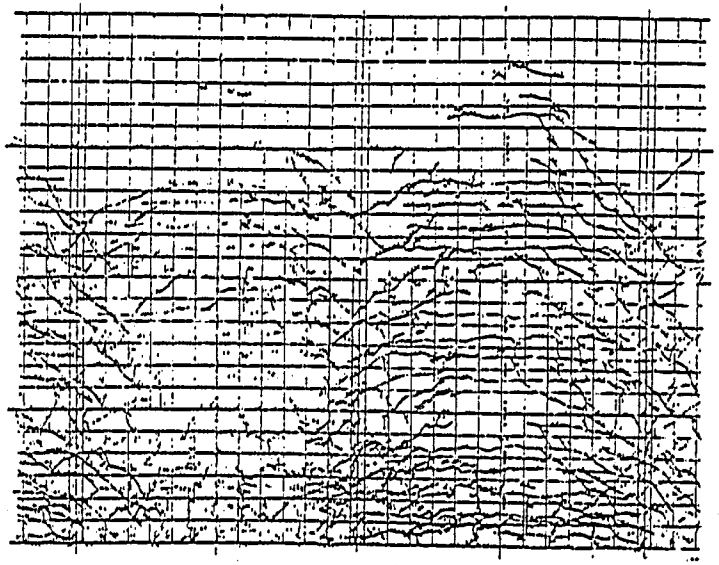


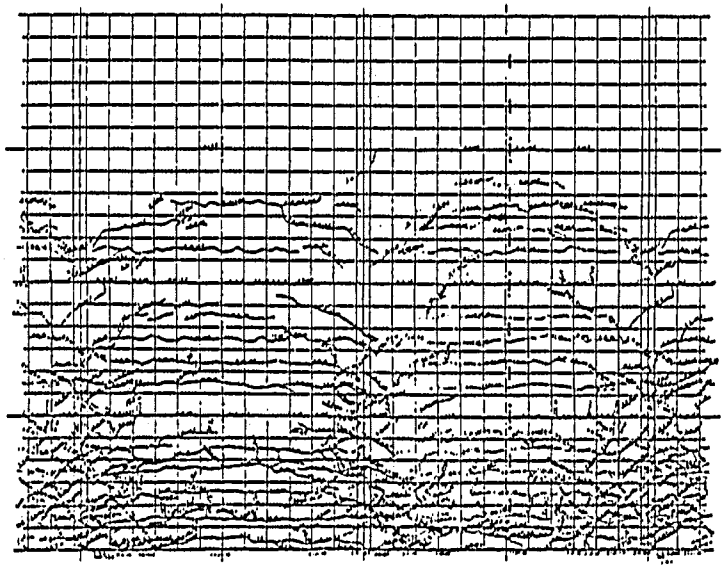
Fig. 2 Type of Loading



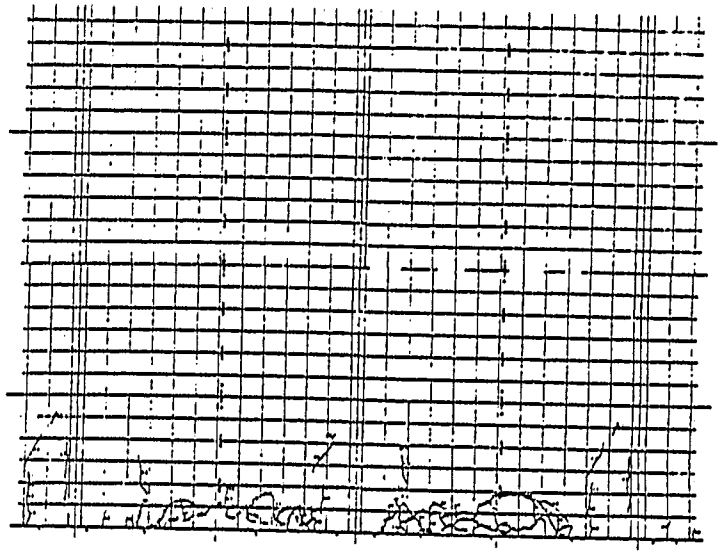
NO. 1



NO. 3

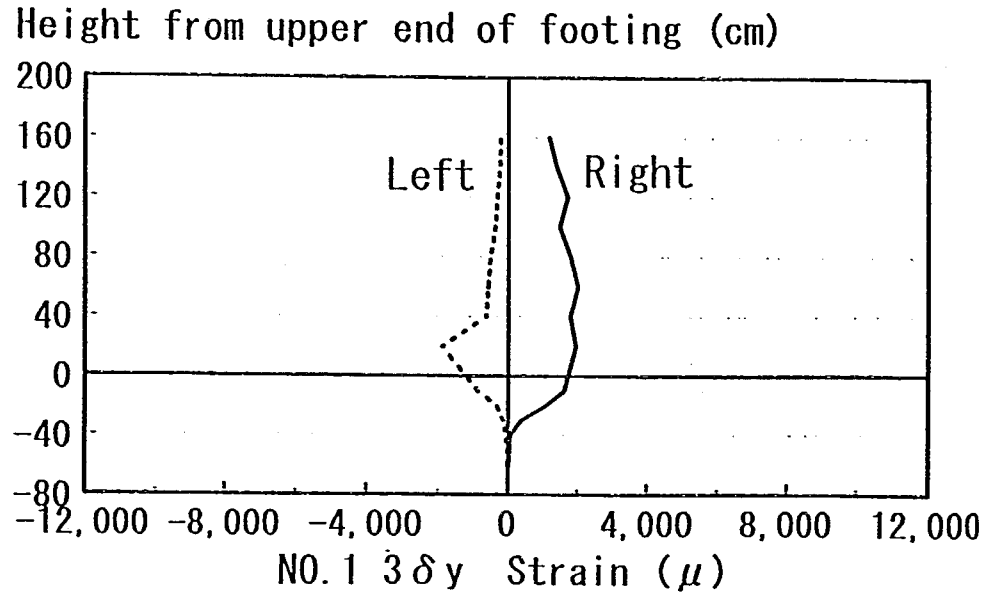


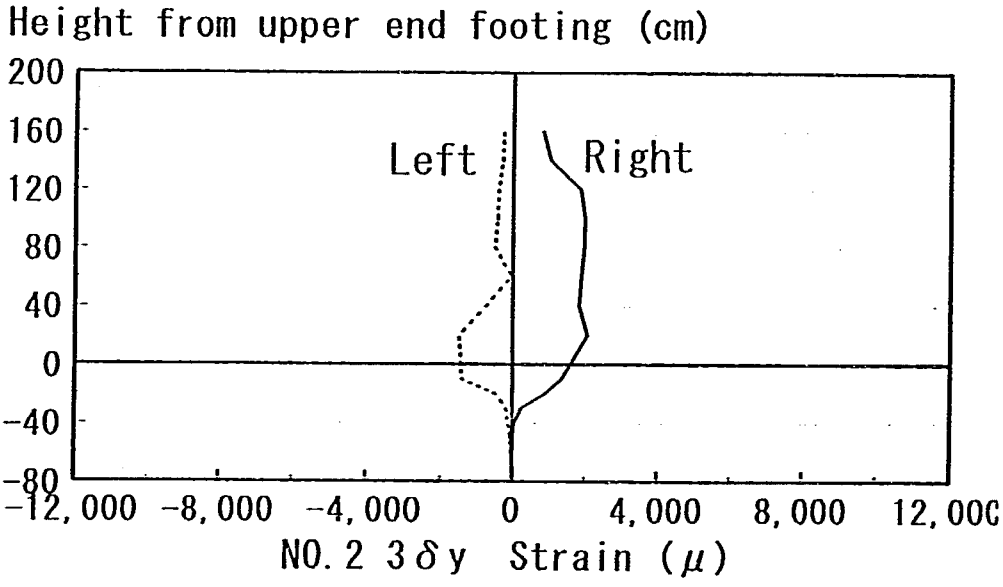
NO. 2



NO. 4

Fig. 3 Cracks





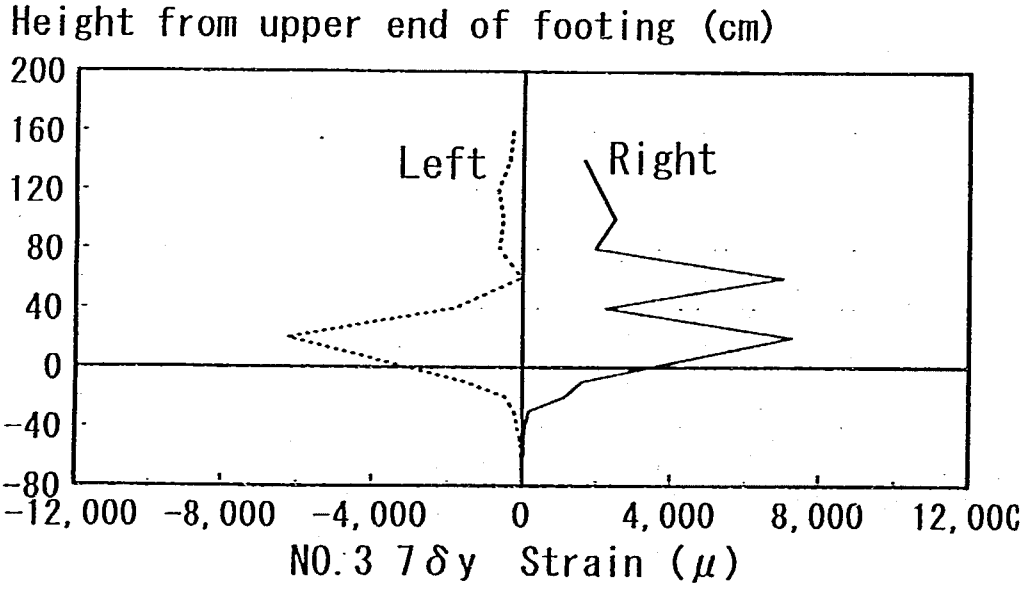
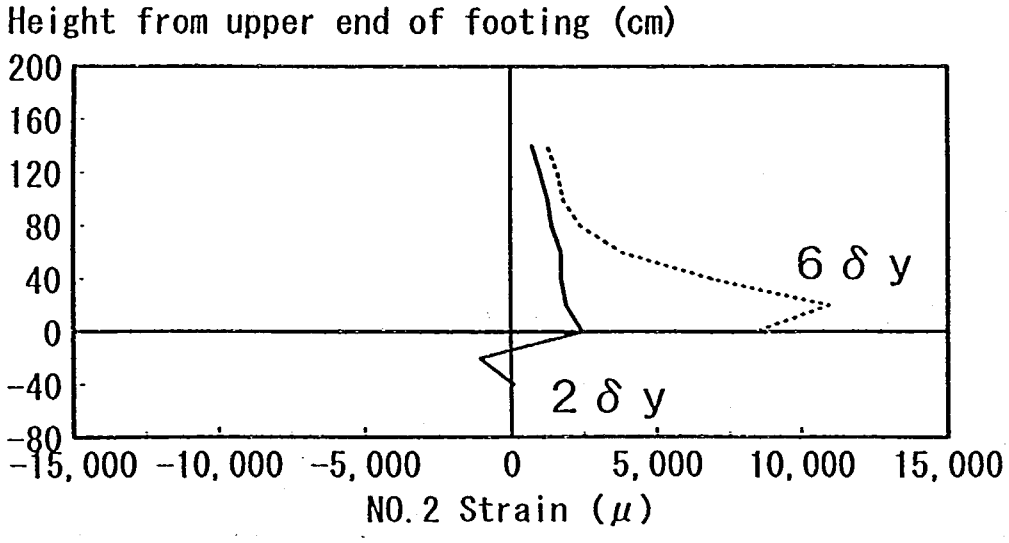
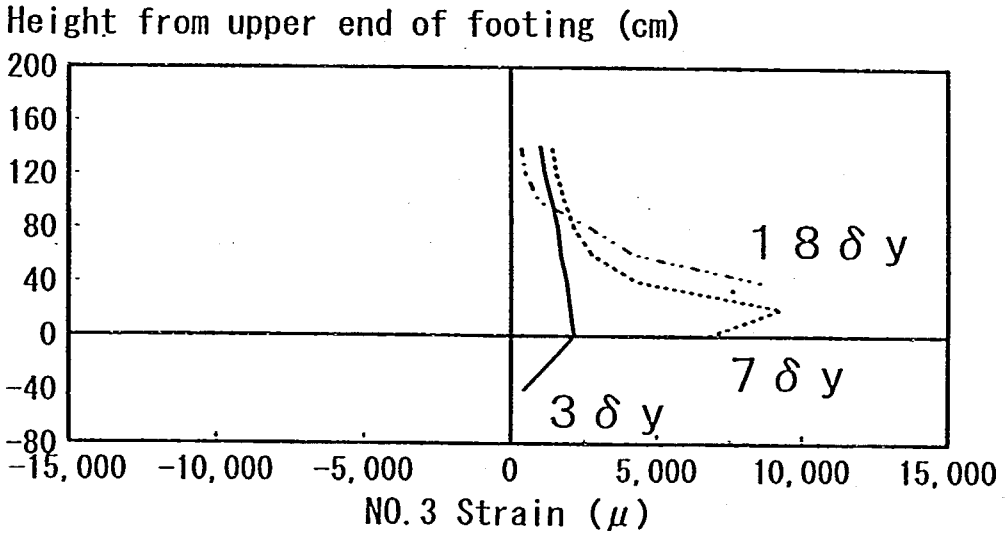


Fig.4 Strain Distribution of Axial Reinforcement





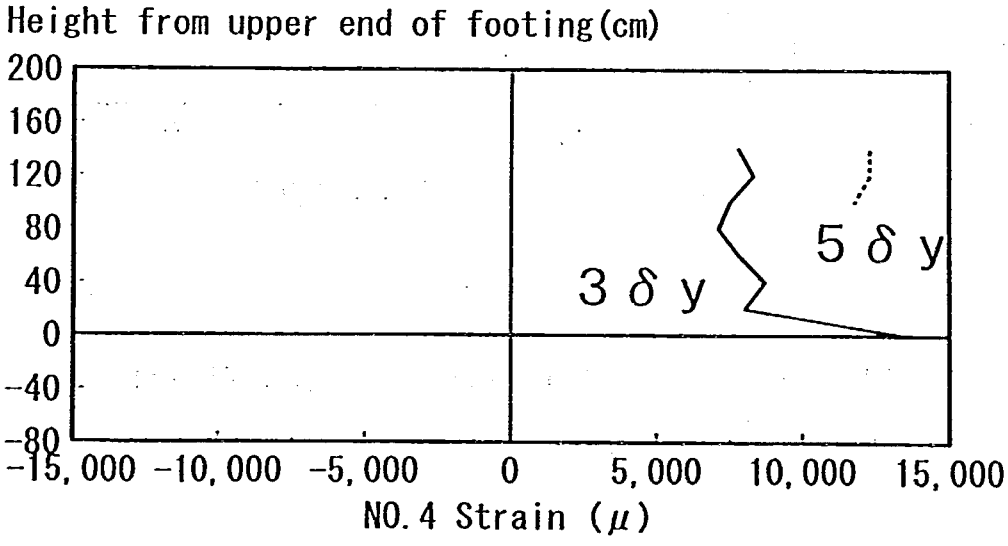
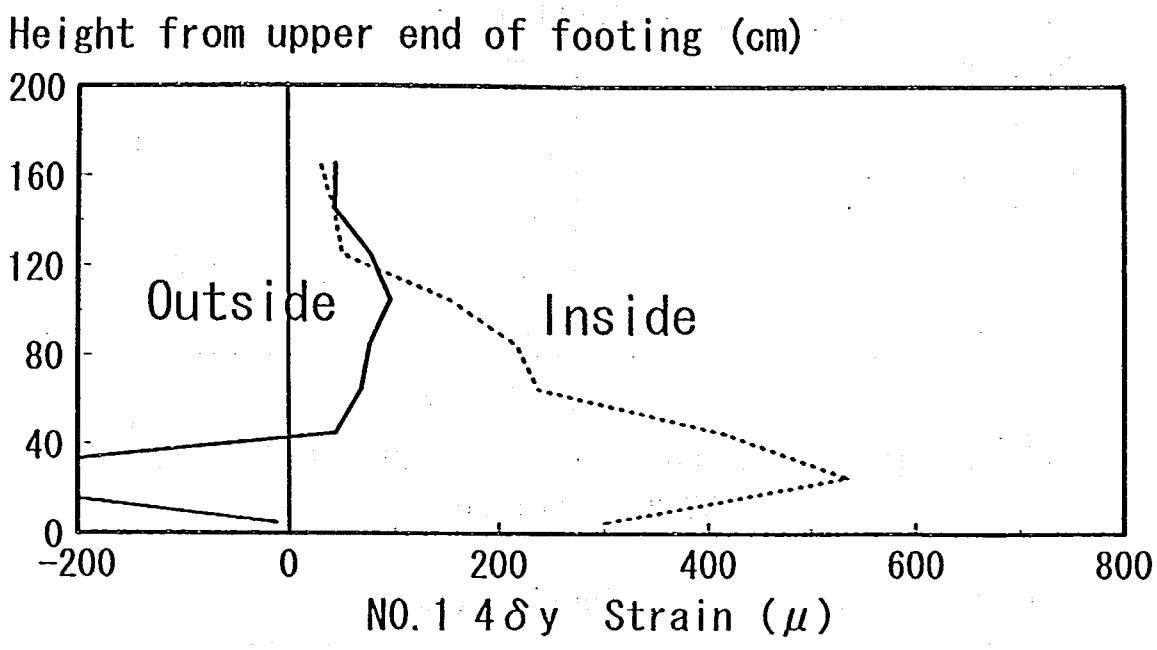


Fig.5 Strain Distribution of PC Steel Bar



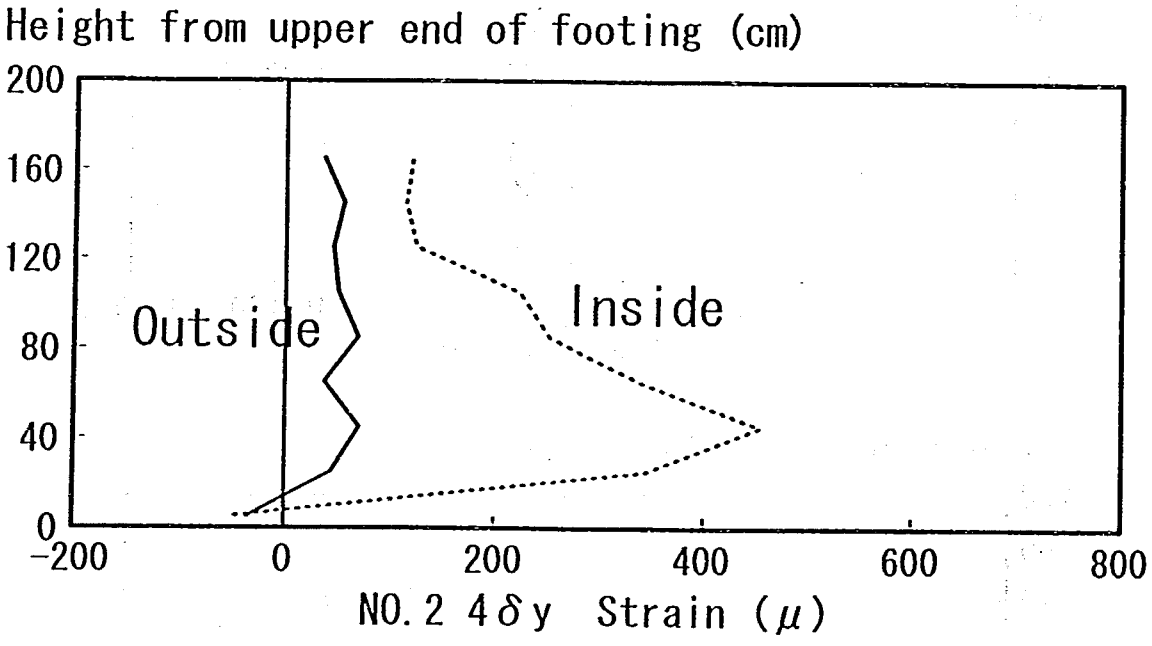
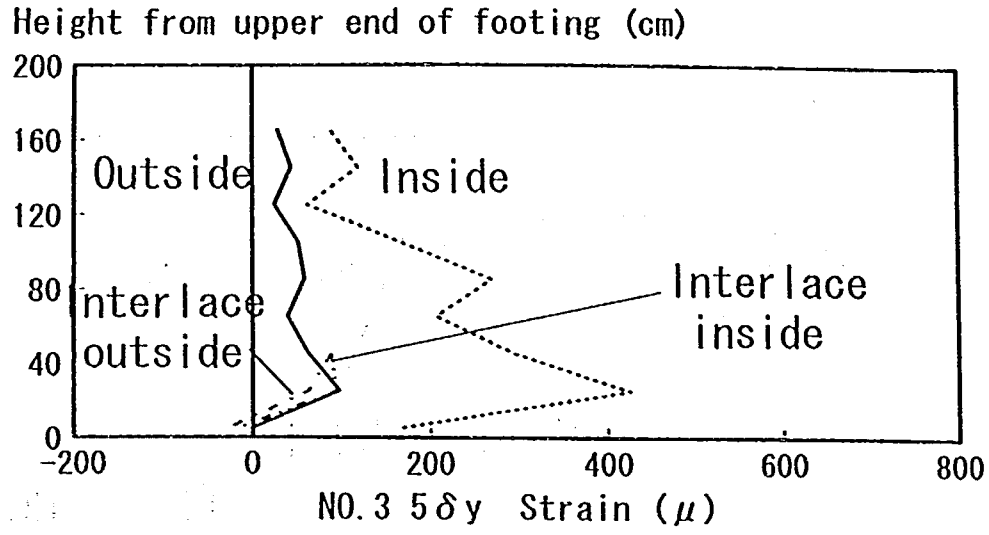
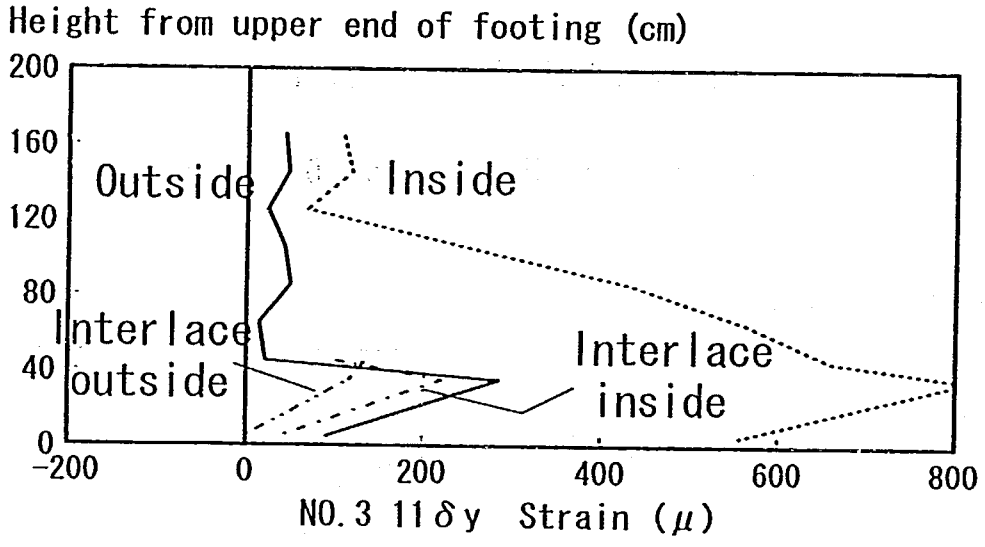


Fig.6 Strain Distribution of Hoop Tie(1)





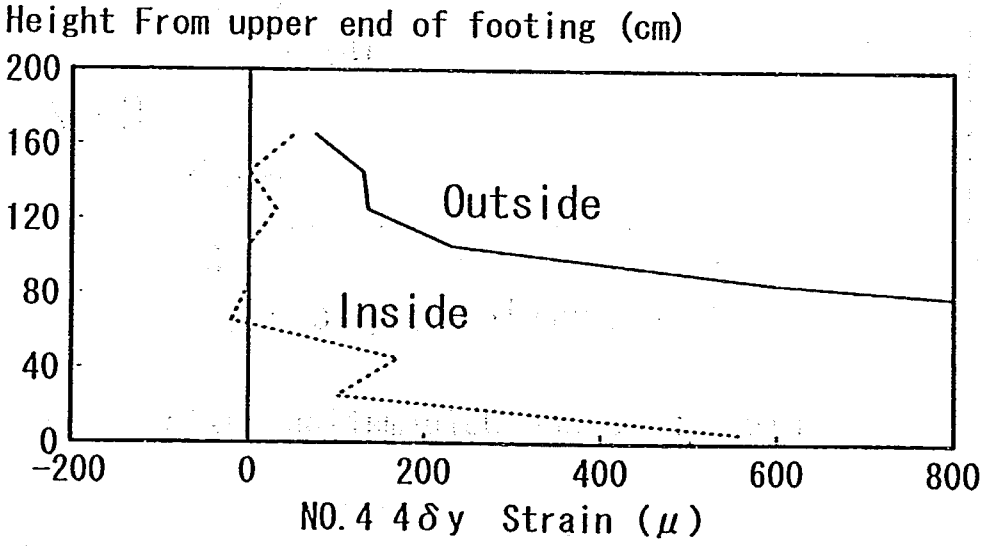


Fig.6 Strain Distribution of Hoop Tie(2)

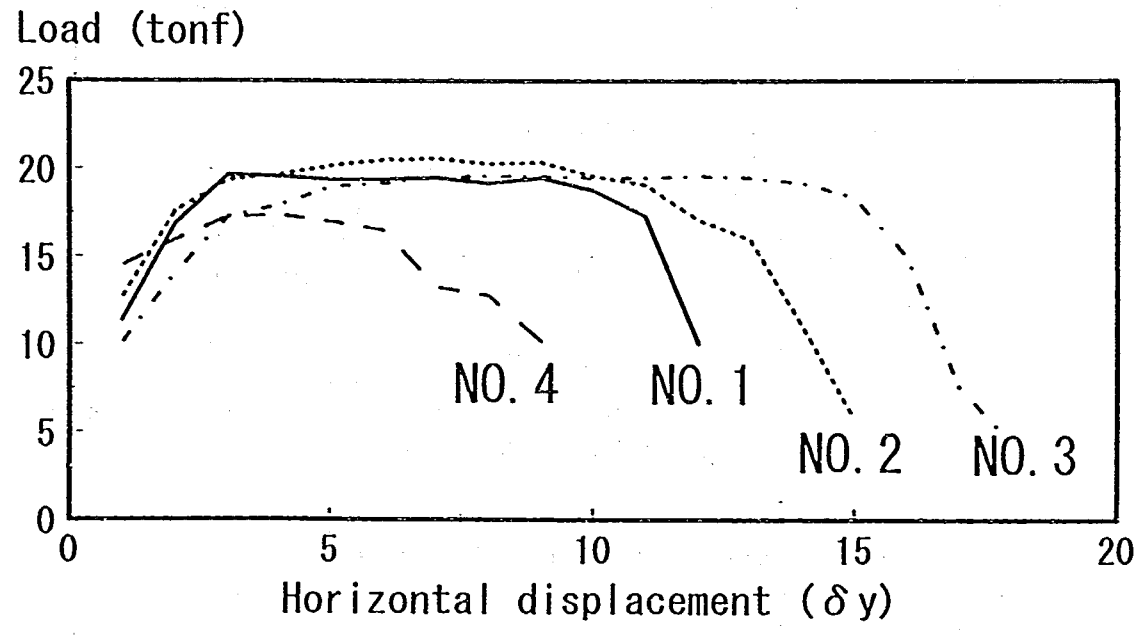


Fig. 7 Load and Horizontal Displacement

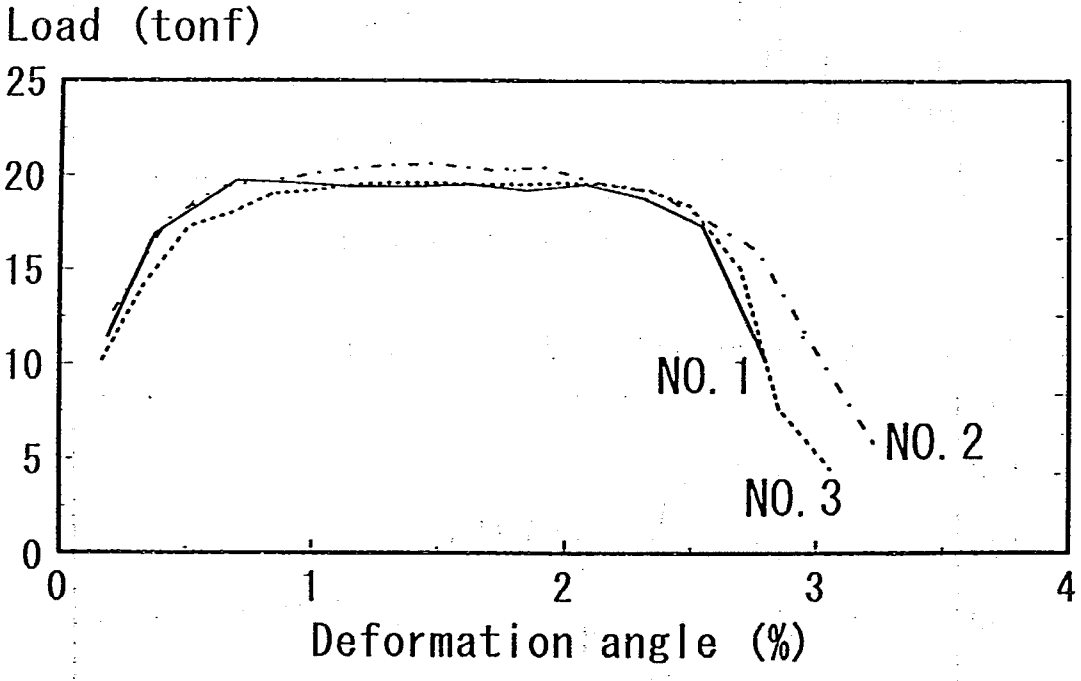


Fig. 8 Load and Deformation Angle

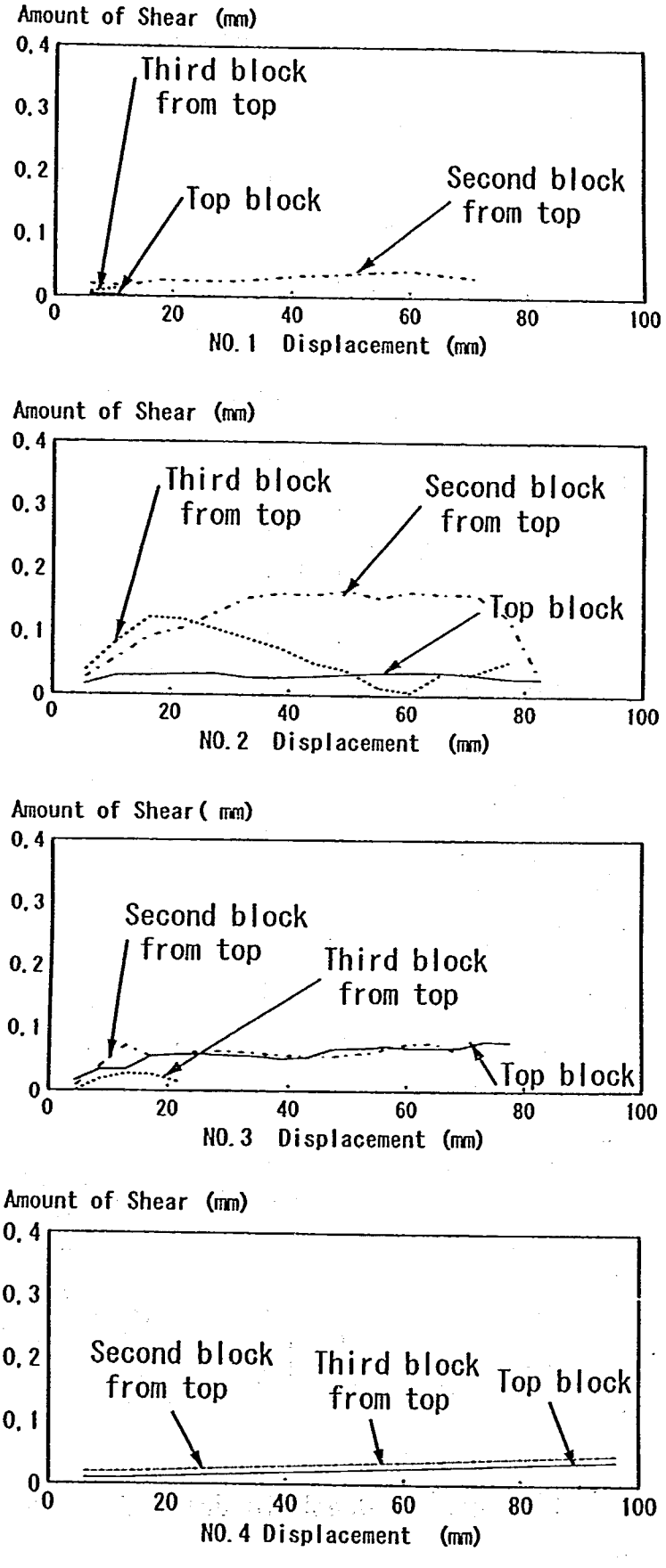


Fig. 9 Amount of Shear in Joint Portion

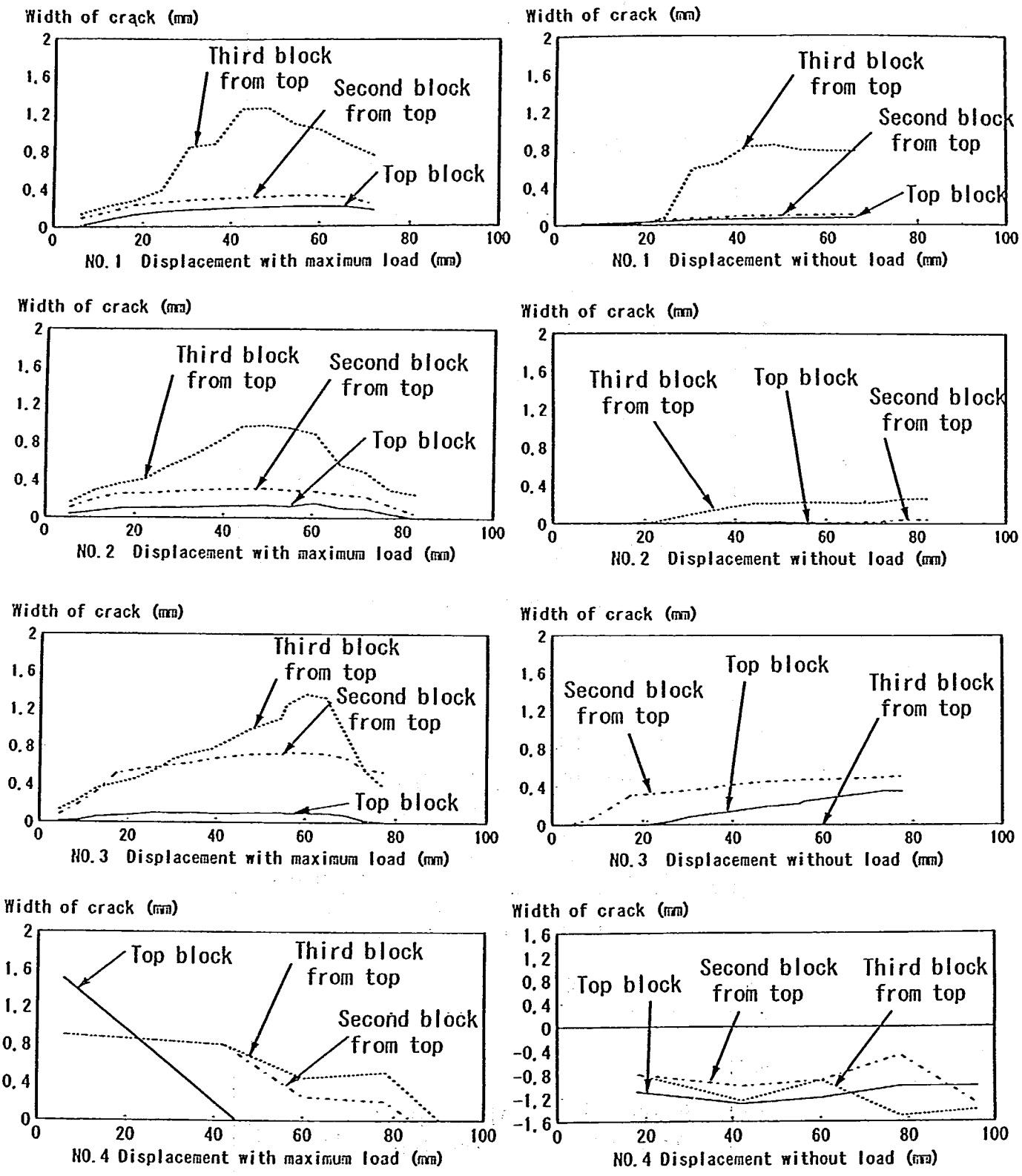


Fig. 10 Width of Crack in Joint Portion

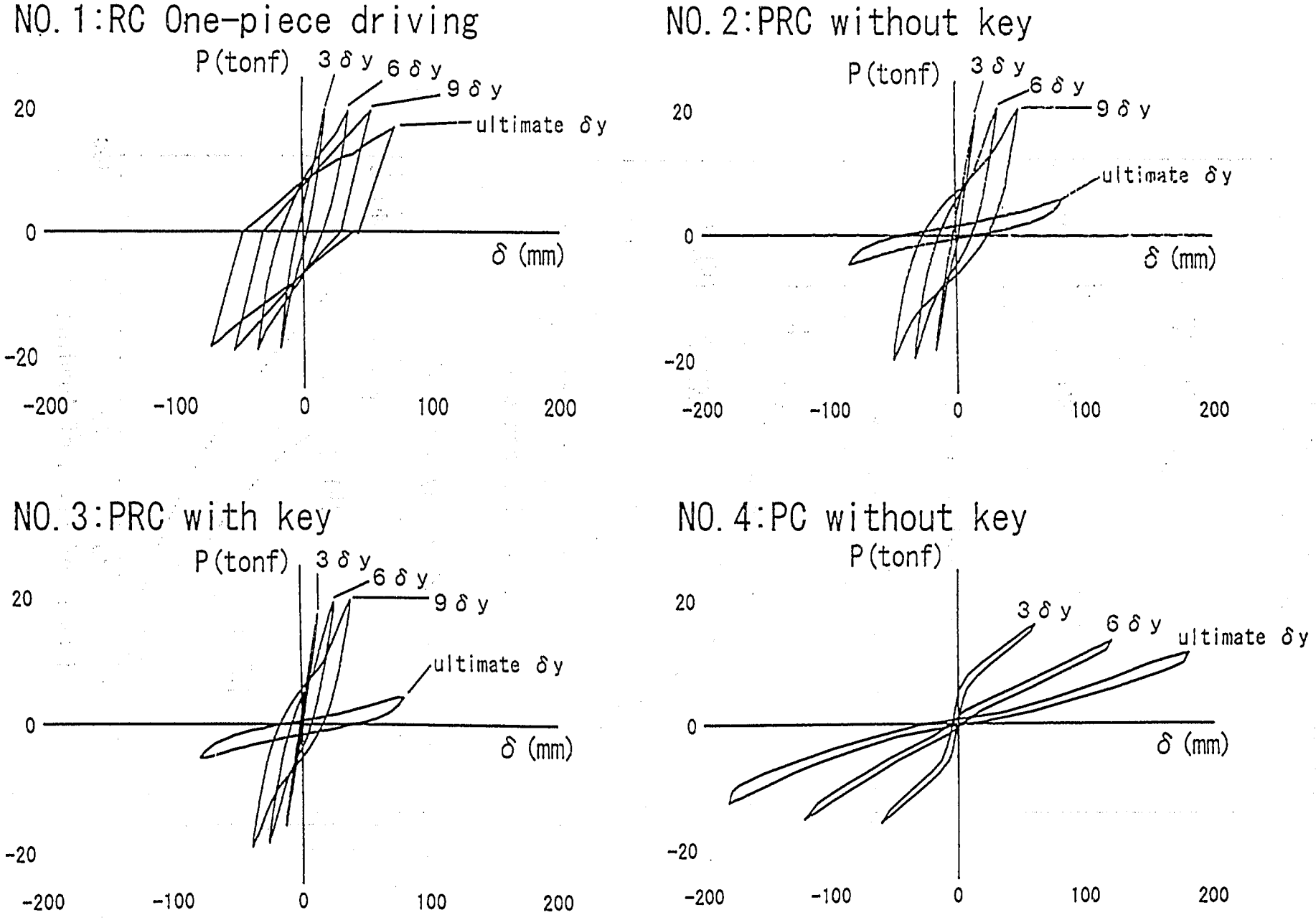


Fig.11 Load-Displacement Curve

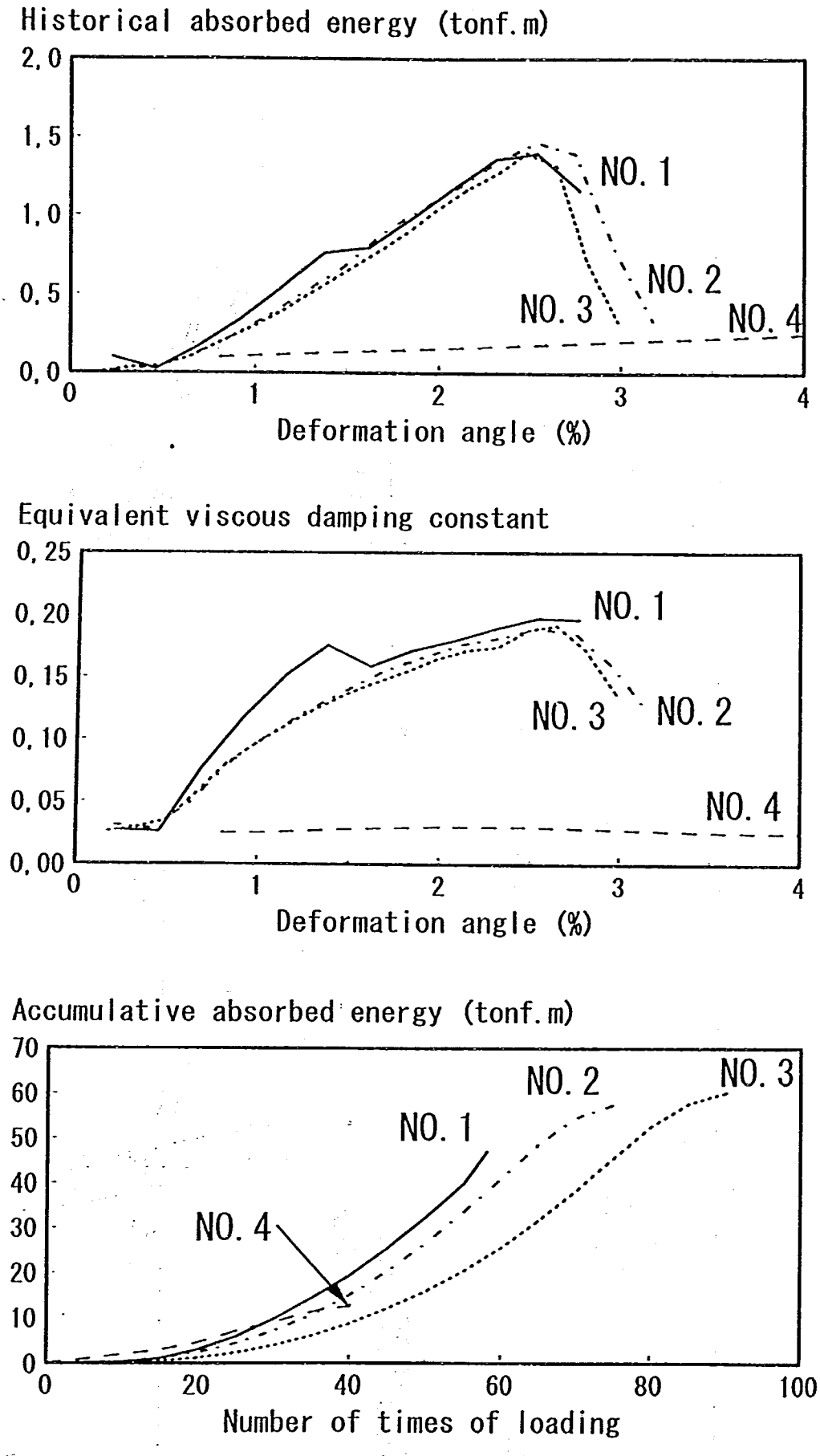


Fig. 12 Energy Absorbing Power

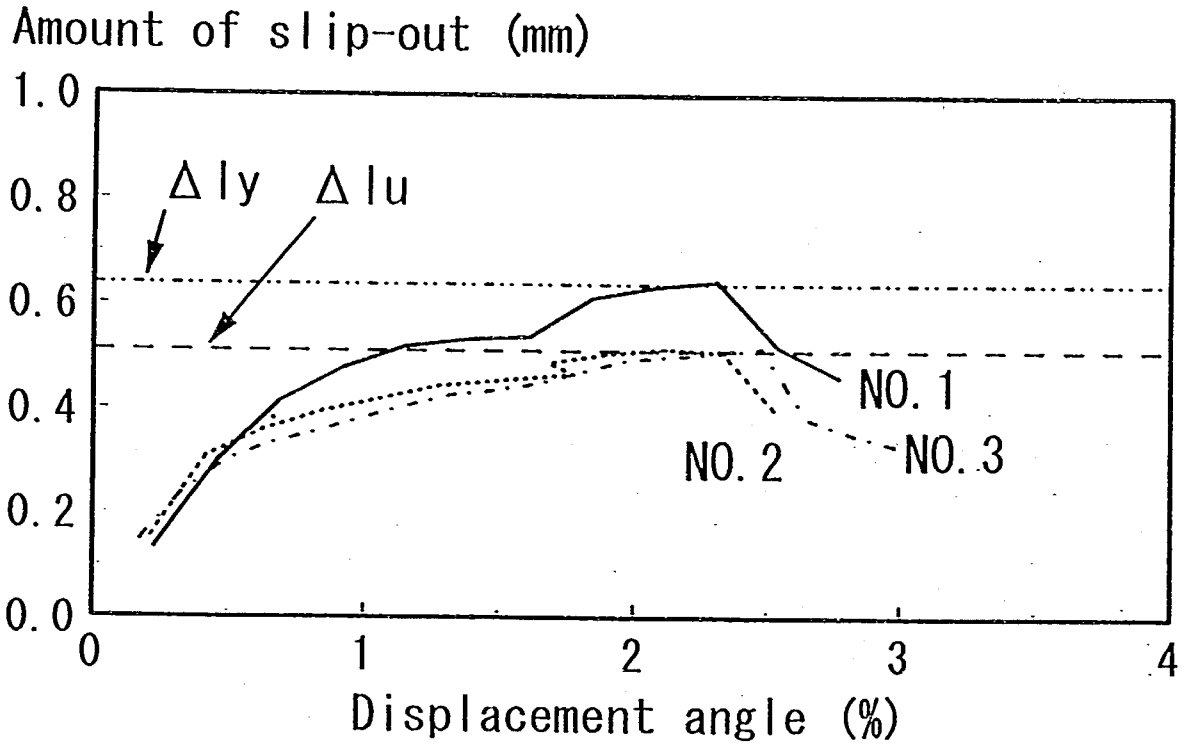


Fig.13 Amount of Slip-out

PLANNING OF THE NEW TOMEI EXPRESSWAY AND DESIGN/CONSTRUCTION OF HIGH-RISE BRIDGE PIER

by

Kazuyuki MIZUGUCHI

Senior Engineer, Bridge Engineering Division, Engineering Department, Japan Highway Public Corporation (JH), Shin-kasumigaseki Building, 3-3-2 Kasumigaseki, Chiyoda-ku, Tokyo 100, Japan

ABSTRACT

In Japan, the total length of expressways which are operated in 1995 reaches about 5,600km. However, this is only half length of whole national expressway plan. From now on,transverse expressways which cross the Japanese Archipelago and new planning routes such as the New Tomei Expressway will be mainly constructed. These roads are often planned through rugged mountainous regions, so the percentage of tunnels and bridges is very high and a lot of high-rise bridges are planned in these route. Hence, it is necessary for JH that rational and simple seismic design methods and efficient construction methods for these high-rise bridges are developed. This paper introduces bridge plan of the New Tomei & Meishin Expressways at first, and then presents "Equivalent Lateral Force Method for earthquake" and design/construction method of composite bridge column with steel tubes combined with reinforced concrete, which are examined in JH.

PLANNNG OF THE NEW TOMEI EXPRESSWAY

National Plan of Expressways in Japan

Fig-1 shows the network of nationals expressway in Japan. The first construction of expressway in Japan started from "Primary Five-year Road Improvement Program" in 1954. At that time, Japan revived from the defeat of World WarII and rearrangement of domestic economy was the most urgent task. Therefore, the transportation network such as highways and railways was most important for Japan, but Japanese government needed special fund and organizations for constructing new expressways because of luck of budget. It was for this purpose that JH was established for constructing and managing expressways as toll roads.

After that, the first expressway in Japan (the Meishin Expressway; between Ritto and Amagasaki) was opened in 1964, and then, through high economic growth, the total length 5,600km of expressways have been constructed and operated at present. The plan of national expressway in Japan has been reexamined with growth of domestic economy. Now a total length of 14,000km high-graded trunk road network shown as Fig-1 are scheduled by the law . The purpose of this plan is "an exchange network scheme "for forming a multipolar dispersion-type development toward the 21th century and making it possible to reach exprssways within one hour drive from the local cities.

The total of 5,600km of expressways constructed so far are the major longitudinal expressways running through the Japanese Archipelago, and this length have not reached the half length of the whole plan yet. This means that Japanese expressway network is still an incomplete stage in spite of high level economy in the world. Therefore, JH has a plan of completing the network, i.e. constructing the transverse expressways, ring-roads around large cities for getting rid of traffic jam and the New Tomei & Meishin Expressways.

Outline of The New Tomei & Meishin Expressway

The Tomei Expressway and the Meishin Expressway, which run through big cities; Tokyo, Nagoya and Osaka, were completely opened in 1969. These expressways extending about 500km have supported the rapid economy growth from 60's to 70's and now act an important role in Japan's physical distribution. The one day traffic flow volume through the Tomei and Meishin is over 100,000, so that the traffic congestion often occur here and there in addition to the damage of structures from overweight vehicles. Therefore, JH has been reconstructing roads or restoring bridges and another structures for adjusting the increase of traffic, but it has been difficult to keep the serviceability.

For solving these problems in the existing Tomei & Meishin, the New Tomei & Meishin Expressway is planned as the new network of high speed transportation. It is expected that completing the New Tomei & Meishin will not only solving the traffic congestion of the existing Tomei & Meishin, but also reduce the transporting time which causes the activation of domestic economy and decrease noise and vibration of traffic.

Fig-3 shows the difference of cross section and alignment between the New Tomei and ordinary expressways including the existing Tomei. The New Tomei has more gentle vertical alignment and horizontal curves than other expressways for making vehicles possible to run over 140km/hr. Thus straight road, which is located on the mountainous side of the existing Tomei, is mainly formed by bridges and tunnels,and has 60% of high structural ratio to entire length. Over 40% of proportion of bridges in the New Tomei is very high in comparison with that of ordinary highways; about 15%. This means that the most important problem for constructing the New Tomei efficiently is how to construct bridges rationally and economically.

Planning Bridges of The New Tomei Expressway

As mentioned above, the New Tomei is planned by bridges which applies 40% of entire length. Most of these bridges have high-rise piers because of running through steep mountains, and some of pier height are over 100m. Fig-4 shows a general view of typical high-rise bridge on the New Tomei.

In seismic design of Japan, such high-rise bridges should be examined by both static analysis considering fundamental natural period (Seismic Coefficient Method) and dynamic analysis. However, applying dynamic analysis to all high-rise bridges needs considerable time and labor. Hence, in seismic design of bridges of the New Tomei JH needs simplified analysis method which captures dynamic behavior in earthquakes.

SEISMIC DESIGN METHOD FOR HIGH-RISE BRIDGE PIERS

Seismic Coefficient Method and Equivalent Lateral Force Method (ELFM)

In the seismic design of Japan, ordinary bridges are required to keep function without structural damage against moderate earthquakes, and to avoid critical failure against significant earthquakes such as the 1923 Kanto earthquake. To be more concrete, the static analysis based on the allowable stress design approach(Seismic Coefficient Method) is applied to moderate earthquakes, and the ductility analysis (Check of Bearing Capacity),is applied to significant earthquakes for avoiding critical failure of RC piers. Seismic Coefficient Method is a seismic design approach considering classification of ground condition or fundamental naturalperiod of structures. (Please refer to "Seismic Design force of Bridges" K. Kawashima, Second International Workshop on the Seismic Design of Bridges).

In this method, at first, static lateral force coefficients are calculated depending on classification of ground conditions and fundamental natural period of each bridges. And then, static lateral force which is obtained by the coefficient and weight of members, is loaded to whole bridges uniformly and examined by allowable stress.

Seismic Coefficient Method is simple and useful in designing small or moderate class bridges because of corresponding with dynamic response analysis. However, Seismic Coefficient Method can not be applied to high-rise bridges of the New Tomei for reasons much as follows.

1) In Seismic Coefficient Method, the design lateral force is uniformly loaded to whole bridges. However, the acceleration response in earthquakes are generally high on the top of piers and low on the bottom of piers. The gap of acceleration response between top and bottom of piers, are expected to be very large in high-rise bridge piers.

2) The design seismic lateral force is calculated by considering only fundamental natural vibration mode in Seismic Coefficient Method. But, in seismic design of continuous rigid frame bridges which are planned in the New Tomei, fundamental natural period of bridges are generally very long. Therefore influence of high degree vibration is expected to be great to high-rise bridge piers.

Dynamic response analysis might be applied to high-rise bridges which have complicated movement in earthquakes. However, applying dynamic response analysis to all high-rise bridges is expected to need much time and labors. So JH has been trying to develop "Equivalent Lateral Force Method (ELFM)" as seismic static approach considering dynamic movement of bridges in earthquakes. The relationship between ELFM and dynamic response analysis (Response Spectrum Method: RSM) is presented as follows.

Examination of Equivalent Lateral Force Method

"Equivalent Lateral Force" means design seismic lateral force which is equal to a result of dynamic analysis with response spectrum. In determining equivalent lateral force,

following types of methods are reviewed.

Method-1: Uniform lateral force is loaded to whole bridge. (Equal to Seismic Coefficient Method)
Method-2: Lateral force is calculated by acceleration of each point in RSM.
Method-3: Lateral force is calculated by dynamic shear force.
Method-4: Lateral force is calculated by dynamic bending moment.
Method-5: Lateral force is calculated by static displacement which is obtained by horizontally loading weight of bridges.

Lateral forces calculated by each method above are loaded to two types of model bridges shown in Fig-5, and the results of each analysis are compared with the result of RSM. Fig-6 and Fig-7 shows the results of comparison summarized as follows.

1) Shear force in Method-1 is smaller on the top of pier and larger on the bottom of pier than RSM.
2) Dynamic maximum acceleration is SRSS of response of each degree vibration mode,and is not considered in relationship of plus and minus of each vibration mode. Therefore, both shear force and bending moment by Method-2 drastically exceed the results of RSM.
3) Equivalent lateral force by Method-3 shows a tendency to differ between longitudinal direction and perpendicular direction to the bridges axis.
4) In seismic design of rigid frame bridges whose bending moment of middle of column changes from positive to negative, Method-4 is not suitable for practical seismic design,because design lateral force of Method-4 changes drastically with bending moment.
5) The distribution of design lateral force by Method-5 are similar to Method-3, and the sectional force of Method-5 almost correspond with RSM.

From the results of examination above, Method-3 or Method-5 are suitable for the way to calculate equivalent lateral force. The static displacement obtained by horizontally loading weights of the superstructures and the substructures are always calculated when natural period is calculated by "Seismic Design" of "Design Specification of Highway Bridges" (JRA). Therefore, Method-5 is expect to be applied to "Equivalent Lateral Force".

How to Calculate Equivalent Lateral Force

Fig-8 shows analytical flow of ELFM.In this method, the static displacement obtained by horizontally loading weight of superstructures and substructures is regarded fundamental natural vibration mode and distribution of horizontal displacement is considered to be in proportion to vibration mode. Equivalent lateral force coefficient Khi is calculated by Eq.(1), (2) and (3).

$$k_{hi} = \beta \cdot u_i \cdot k_h \qquad (1)$$

$$\beta = \frac{\int w(s) \cdot u(s)\ ds}{\int w(s) \cdot u(s)^2\ ds} \qquad (2)$$

$$k_h = c_z \cdot c_G \cdot c_I \cdot c_T \cdot k_{ho} \qquad (3)$$

where, u_i : displacement at point i in an inertia force acting direction when horizontal force equivalent to weights of the superstructure and the substructure; β : a stimulus coefficient when considering u_i as vibration mode; c_z, c_G and c_I : modification coefficients for zone, ground condition and importance; c_T : modification coefficient factor depending on natural period in Seismic Coefficient Method; k_{h0} : standard lateral force coefficient in Seismic Coefficient Method.

Comparison of ELFM and RSM

ELFM and RSM are compared by designing model bridges which have following conditions.

Requirements:
Case-1: Not only spread foundations on the hard ground(I) but also pile and caisson foundation on the soft ground(II).
Case-2: Both spread and pile foundations exist in one bridge.
Case-3: End substructures of bridges are not abutments, but piers.
Case-4: Gaps between each height of piers are very large.
Fig-9 ~ Fig-11 shows the typical results of calculations of 27 types of bridges and presents following conclusions of analysis.

(1) In bridges whose fundamental natural vibration is dominant in RSM, the result of ELFM corresponds with that of RSM, because fundamental natural period are considered in calculating equivalent lateral force.
(2) The distribution of shear force and bending moment in case of spread foundations on the hard ground are similar to that of pile foundations on the soft ground. This means that ELFM can be applied to practical seismic design. When both spread and pile foundations exist in one bridge, the result of analysis shows same pattern.
(3) When end substructures are not abutment,but piers, ELFM can be applied to practical seismic design in longitudinal direction to the bridge axis. However, in case of perpendicular direction, ELFM shows different distribution pattern from RSM, because vibration mode of piers are effected by high degree vibrations.
(4) When difference of pier height are over 50m, distributions of sectional force in ELFM are greatly different from that of RSM.

From the results of examination above, ELFM is expected to be applied to practical seismic design of these of bridges whose fundamental natural vibration is dominant in dynamic movement and in which difference of pier height are relatively small.

DEVELOPMENT OF NEW CONSTRUCTION METHOD OF HIGH-RISE BRIDGE PIERS

General

High-rise bridge piers whose height are over 100m have difficulty in construction method in addition to seismic design method. Usual construction method of ordinary high-rise pier in Japan has been cast in place method with steel bars reinforced concrete and sliding

forms. Such construction method is economical for existing circumstances, but reqires much labors and time.

JH has been developing composite bridge column with steel tubes combined with reinforced concrete for establishing new construction method of high-rise bridge piers such as the New Tomei bridges. This type of composite bridge column has specific features in the followings.

1) Multiple Steel tubes are utilized not only as support for hanging slip form but also interval form for concrete pouring and also useful as longitudinal reinforcement.
2) Prestressing strand is wound in stead of lateral rebars.
3) Steel tubes with spiral rib induced on its external surface(STSR) is utilized in the anchorage section.

Fig-12 Shows the general view of Composite Bridge Column. Practical movement of steel tubes and concrete in earthquakes and bearing capacity in significant earthquakes of this type of bridge column is not clearn. Next section presents the results of basic test for Composite Bridge Column.

Bond Strength of STSR

At the bottom of steel tubes, STSR is used aiming at increasing bond strength between steel tubes and concrete. Spiral rebars are arranged around actual tubes for avoiding decrease of bond strength from bond splitting cracks. In this test, two types of test specimen, with(B-R) and without spiral rebar(B-O) around STSR are prepared as shown Fig-14. Bond strength of STSR and effect of spiral rebars are measured by cyclic bending test with these types of test specimen.

Fig-15 and 16 show bond stress-slip relationships. After circumferential cracks along STSR around 200N/cm ^{2} of bond strength, considerable cracks appear in the stab around 550N/cm ^{2}. Immediately after these bond splitting cracks, B-O specimen reaches maximum loading capacity 560N/cm ^{2}, while B-R specimen provides some increase in loading capacity. This difference means confinement effect of spiral rebars. B-R specimen provides 6.6MPa in ultimate strength, 20% more than 5.49MPa for B-O specimen and also 2.8times the allowable stress of 2.35MPa employed in the practical design.

Horizontal Bearing Capacity of Composite Bridge Column

A steel tube-reinforced concrete composite column(H-SRC) and reinforced concrete column (H-RC) for comparison which has similar flexural strength and lateral reinforcement, are prepared as test specimen. Layout of specimen are shown in Fig-17and 18. With combination of constant force of Pa = 1,410 KN(σ o= 1.47MPa: design axial stress), horizontal force is repeatedly applied for drift of R=1/200, 1/100, 2/100, 3/100, 4/100, and 5/100
respectively with two loaded cycles each and finally up to failure in the positive loading.

Fig-19 and 20 show load-displacement hystereses obtained by test. In the case of H-SRC

specimen, pre-yielding behavior is flexural and flexural shear cracks appearance in the range of R=1/200. After yielding in the cycle of R=1/100, maximum loading capacity is reached at the 1st cycle of R=3/100 with concrete crush in the column base. Concrete spalling appears in the R=4/100 cycle followed by longitudinal rebar buckling and partially rapture of prestressing stand in the R=5/100 cycle. However under further loading, 71% of maximum loading capacity can be held at the final displacement range (R=7.9/100) which is limited by the hydraulic jack stroke capacity.

On the other hand in the case of H-RC specimen, failure process is similar but wider range of concrete spalling appears with longitudinal rebar buckling in the R=4/100 cycle. For further loading, load resistance capacity rapidly decreases with large extent of damages. Maximum horizontal force 825KN of H-SRC specimen corresponds with predicted valve based on beam theory.

Fig-21 represents absorbed energy variation which is defined as the area of load-displacement curve shown in Fig-19 and 20. From the figure, it is observed that absorbed energy decreases beyond R=4/100 range in the H-RC specimen, while still increases even in the ultimate range in the H-SRC specimen, that verifies superior seismic resistant characteristics of composite type column.

Concluding Remarks of Composite Bridge Column Test

The present study provides following conclusions.

1) Bond strength of 6.7MPa of STSR is 2.8times as large as allowable design stress of 2.4MPa used in practice. Bond strength is improved by spiral ring round steel tubes.

2) H-SRC specimen, composite column provides quite good agreement in load-displacement relationship with predicted value based on beam theory with plane section assumption.

3) H-SRC specimen provides superior result in ductility and energy absorption characteristics in comparison with H-RC specimen.

4) The present horizontal loading test would be for preliminary study to investigate potentially superior seismic characteristics in the new type column in comparison with commonly used reinforced concrete column. For future work, usage of more actual model, i.e. with number of steel tubes arranged in the cross section is needed especially for ductility estimation.

CONCLUSION

Mountainous expressways including the New Tomei will be main target for construction of expressways in future. otherwise, not only completing networks of expressways is needed, but also constructing economical and profitable expressways is required. It is a great challenge for JH that high-rise bridges must be constructed rationally and immediately. Studies in this paper are a part of technical developments which JH has achieved so far, and expected to be established by further examinations in future. JH hope that these studies will be widely used by other organizations in addition to JH.

REFERENCES

Japan road association (1990) "Part V Seismic Design: Design specification of highway bridges"

Kawashima, K. (1994) "Seismic Design force of Bridges," Report of International Workshop on the seismic design of bridges, Queenstown, New Zealand.

Meta,T., Yamagata,K., Inokuma,Y., Ohuchi,K., Irisawa,K.and Kobatake,Y. (1994) "A horizontal Loading Test of Steel Tubes-reinforced Concrete Composite Bridge Column,"Report of International Workshop on the seismic design of bridges, Queenstown, New Zealand.

Expressway Technology Center (1990-1992) "The Examination of Seismic Design Method of High-rise Bridges in Expressway."

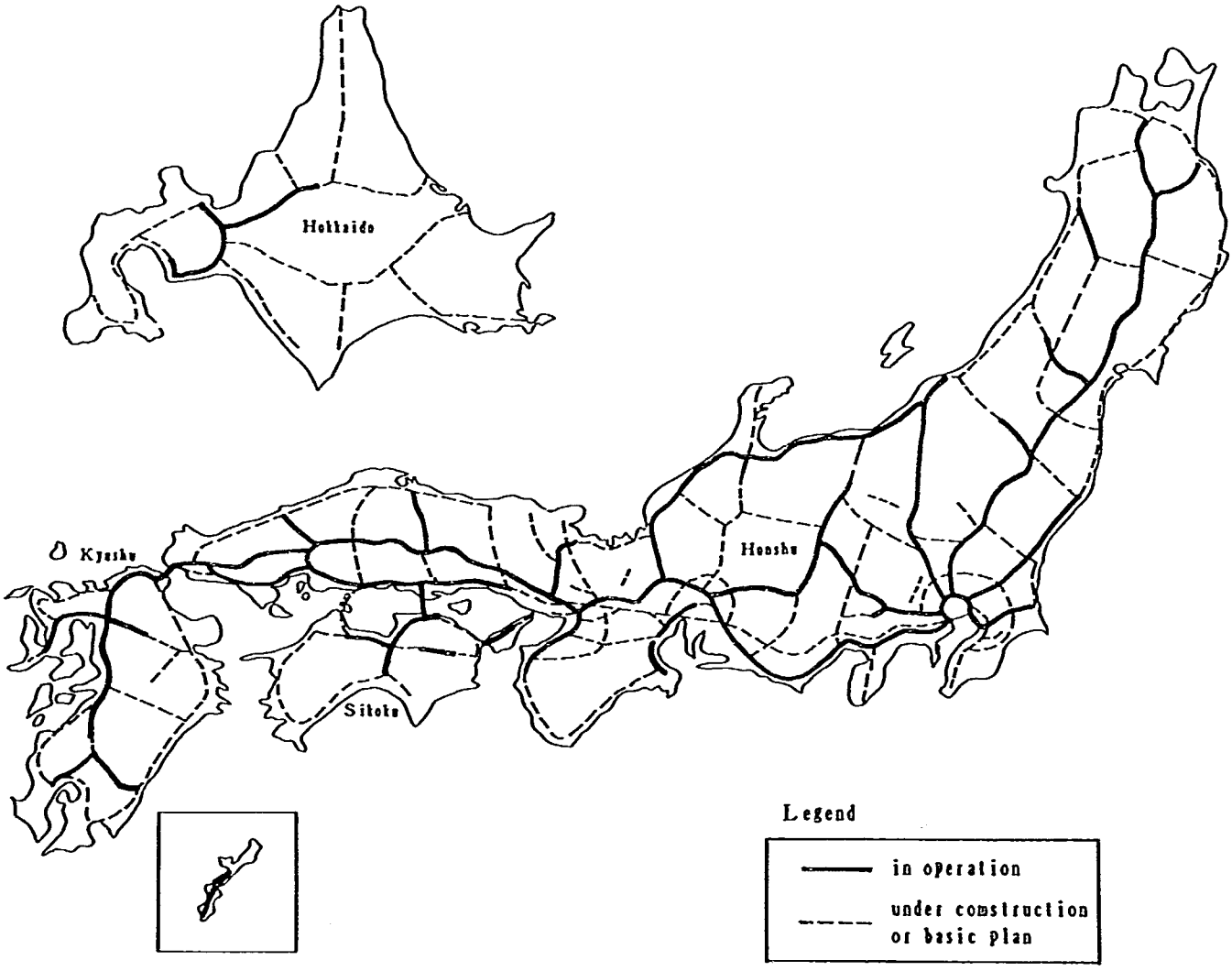
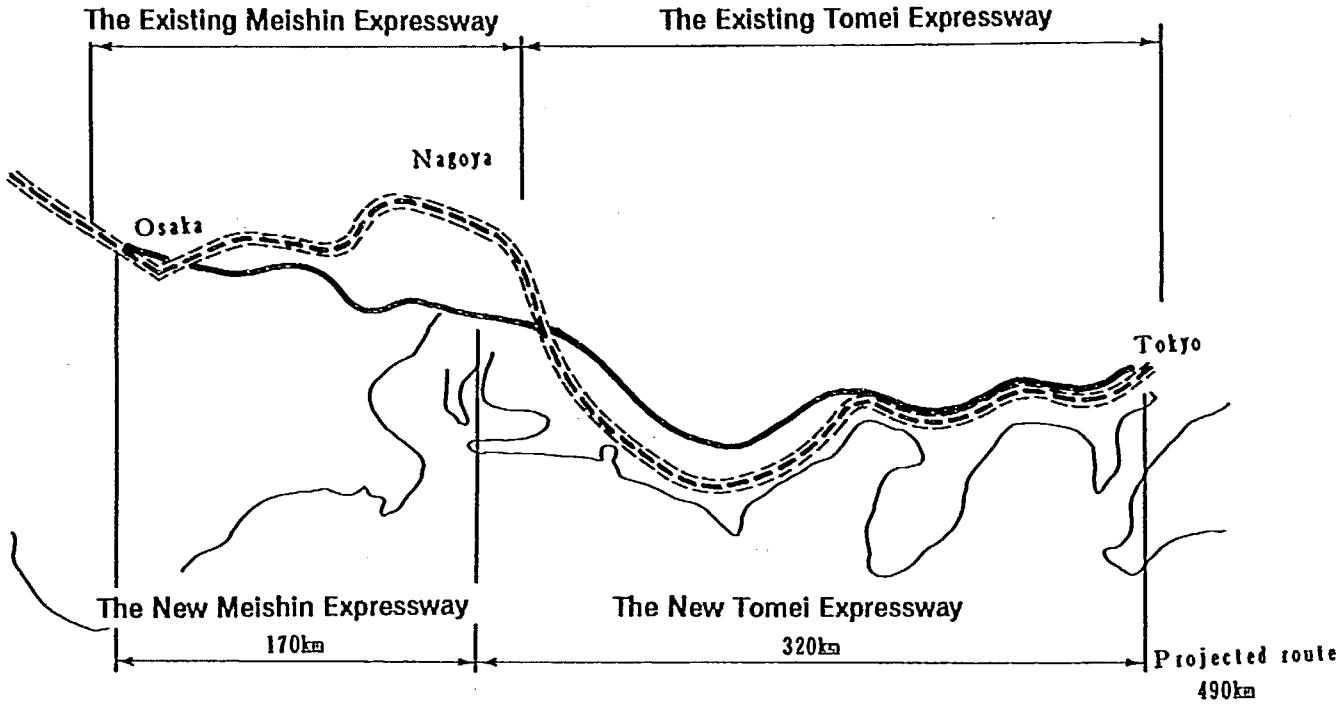


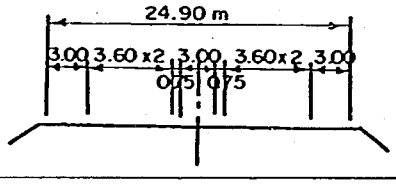
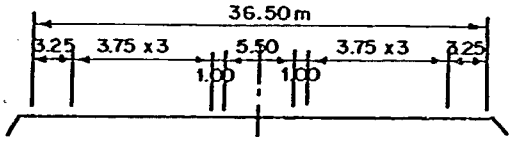
Fig-1 Road Networks in Japan
(High graded Trunk Road : 14,000km)



Fig–2 Location of New Tomei Expressway and Meishin Expressway

	Earthworks	Bridges	Tunnels
The New Tomei	35	40	25
The Present Tomei	81	16	3

Table–1 Proportions of structures to entire Length (%)

	Cross Section	Minimum Radius	Maximum Gradient
The Present Tomei		300m	5%
The New Tomei		3,000m	2%

Fig–3 Comparison of Cross Section and Alignment

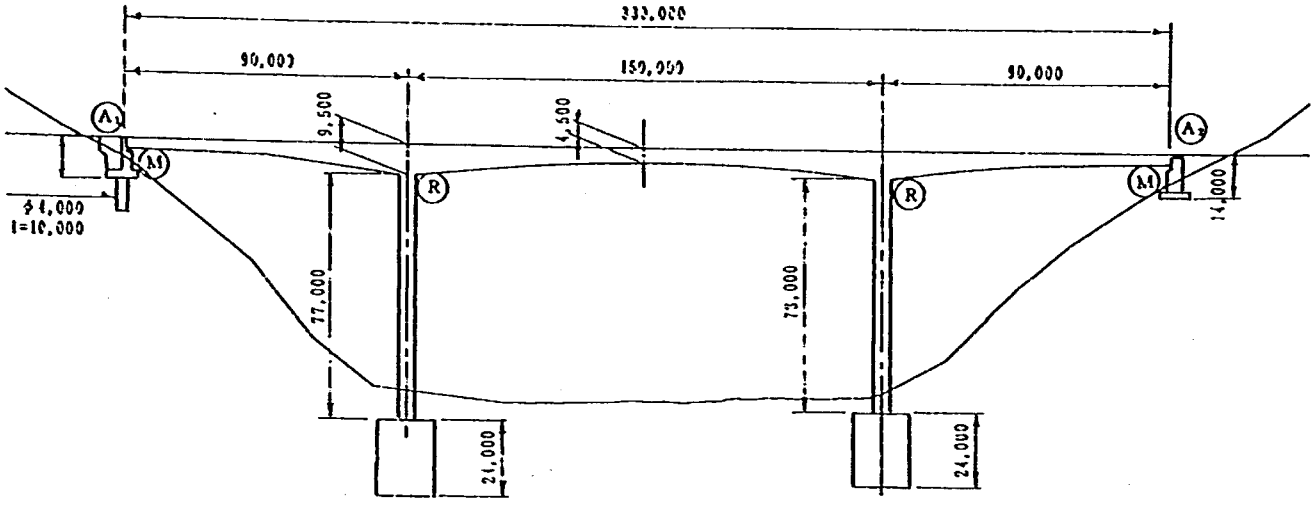
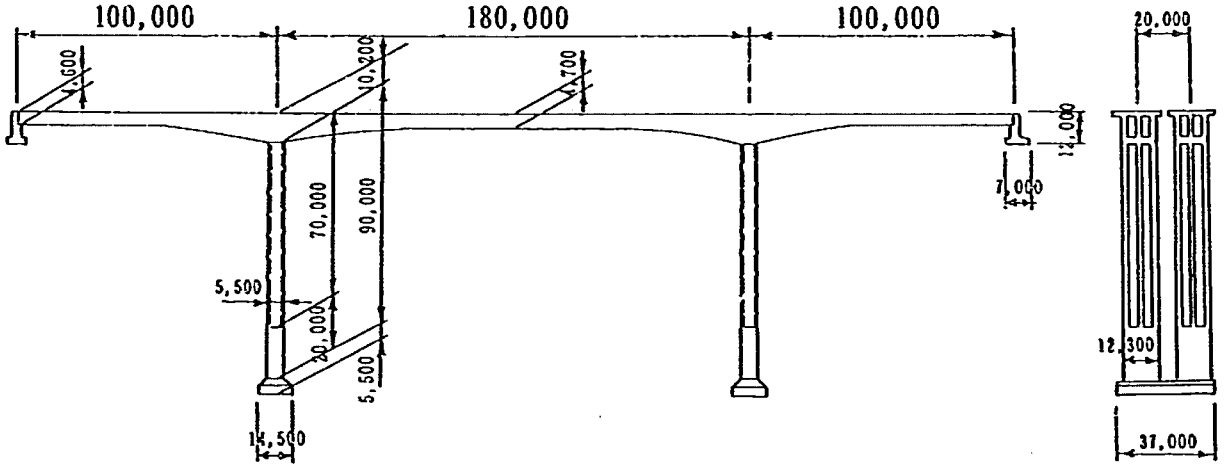
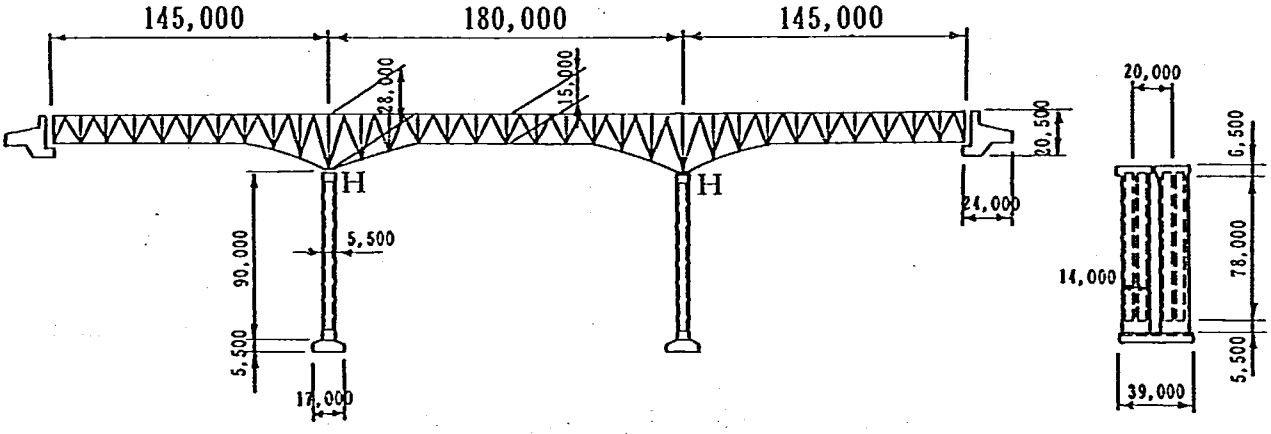


Fig--4 General View of Typical Bridges of the New Tomei
(Okitsugawa Bridges : Continuous Rigid – frame Bridge)

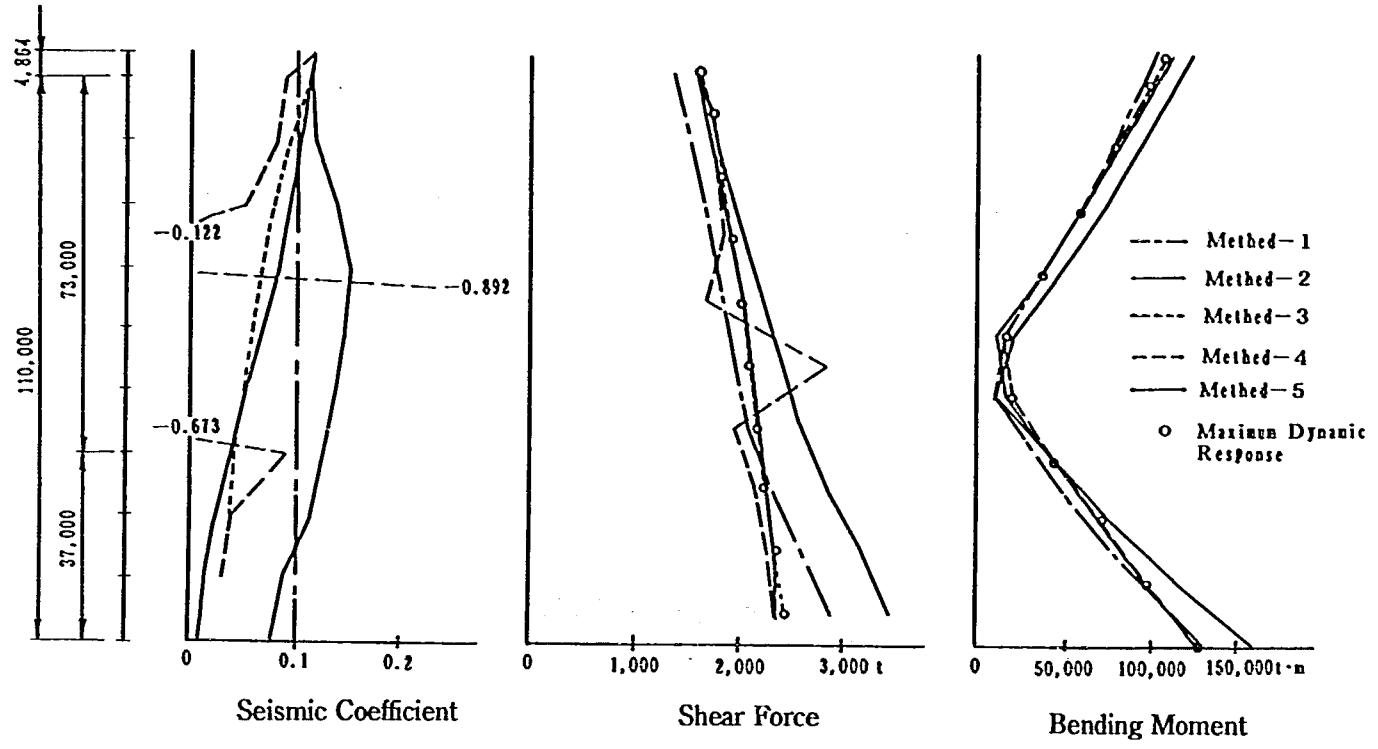


(a) Continuous Rigid – frame Bridge

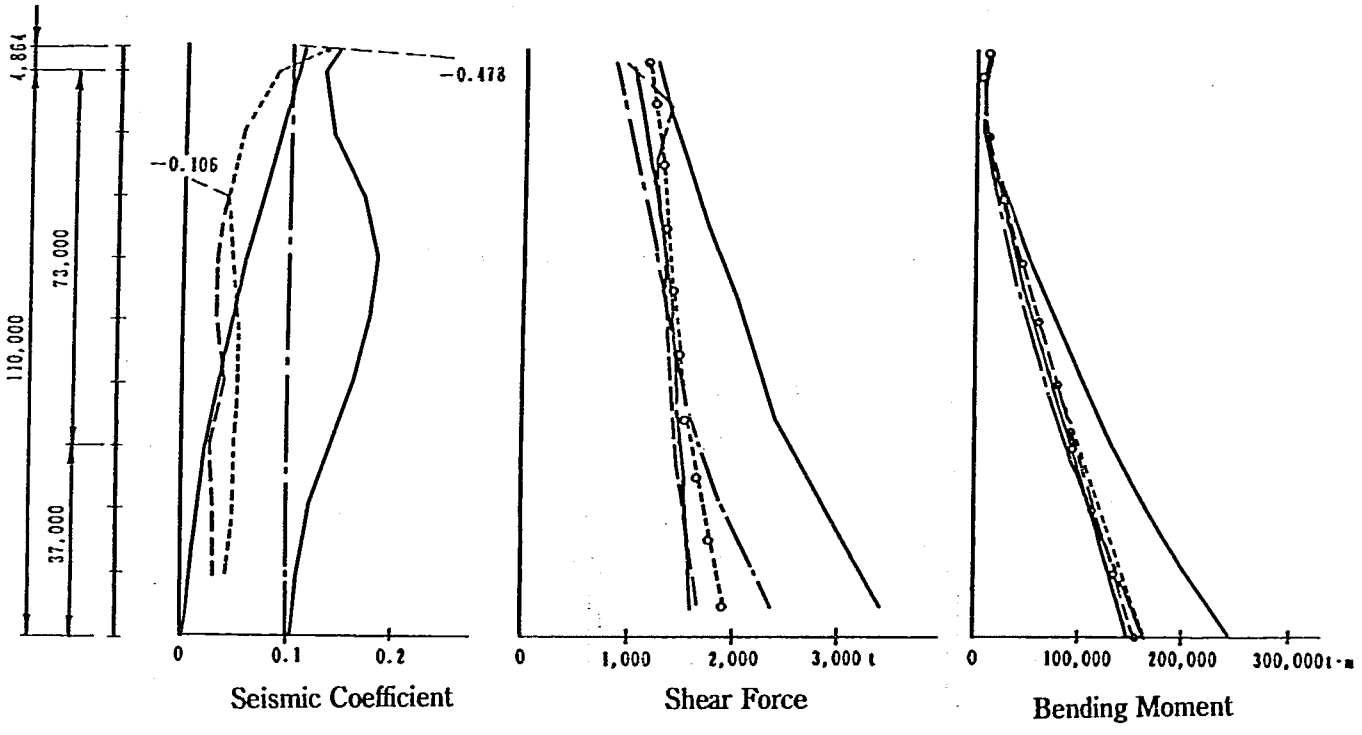


(b) Continuous Steel Truss Bridge

Fig–5 Model Bridges Used Examination of Equivalent Lateral Force Method

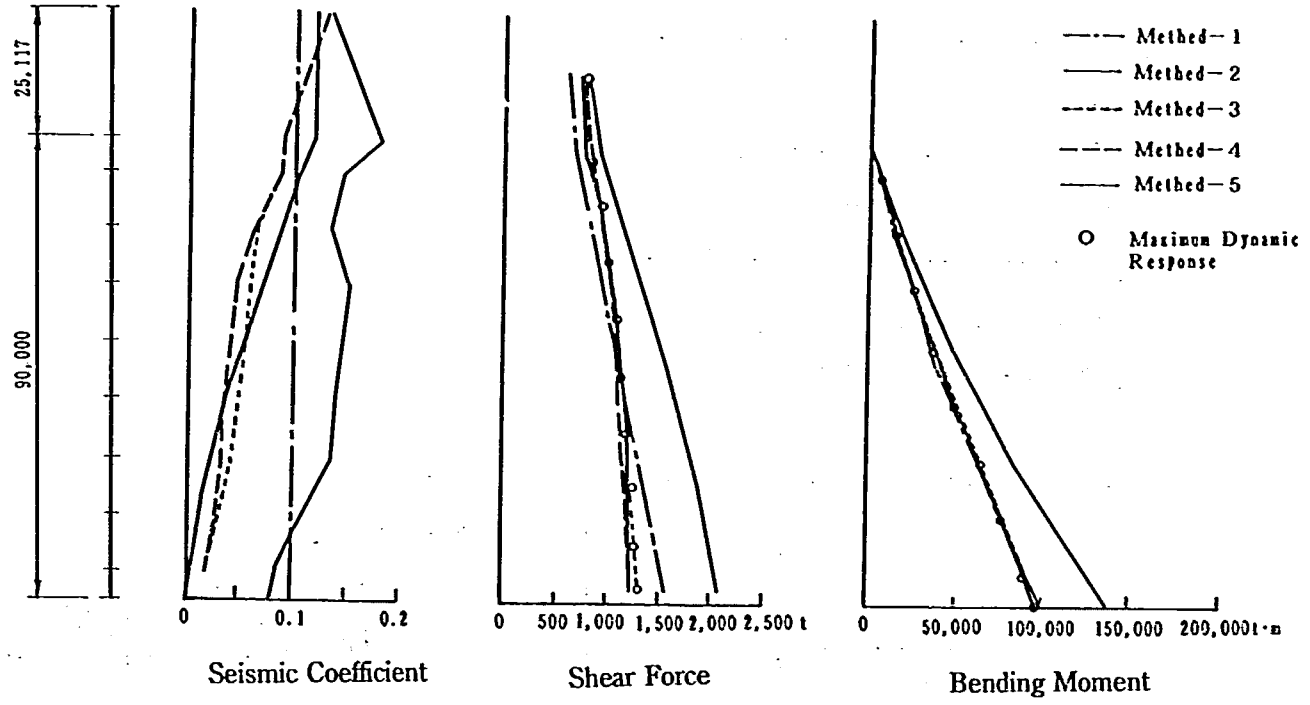


(a) Longitudinal Direction to the Bridge Axis

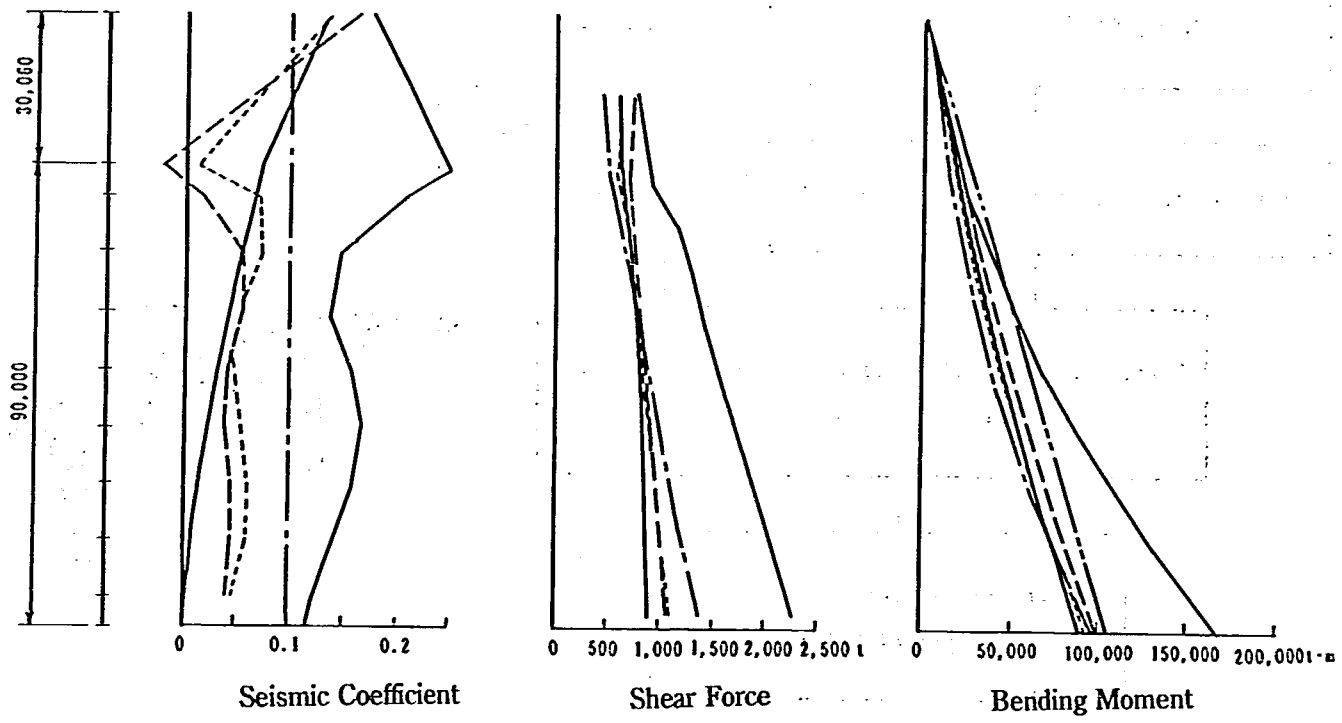


(b) Perpendicular Direction to the Bridge Axis

Fig-6 Distribution of Seismic Coefficieut and Sectional Force ; In Case of Continuous Rigid – frame Bridge

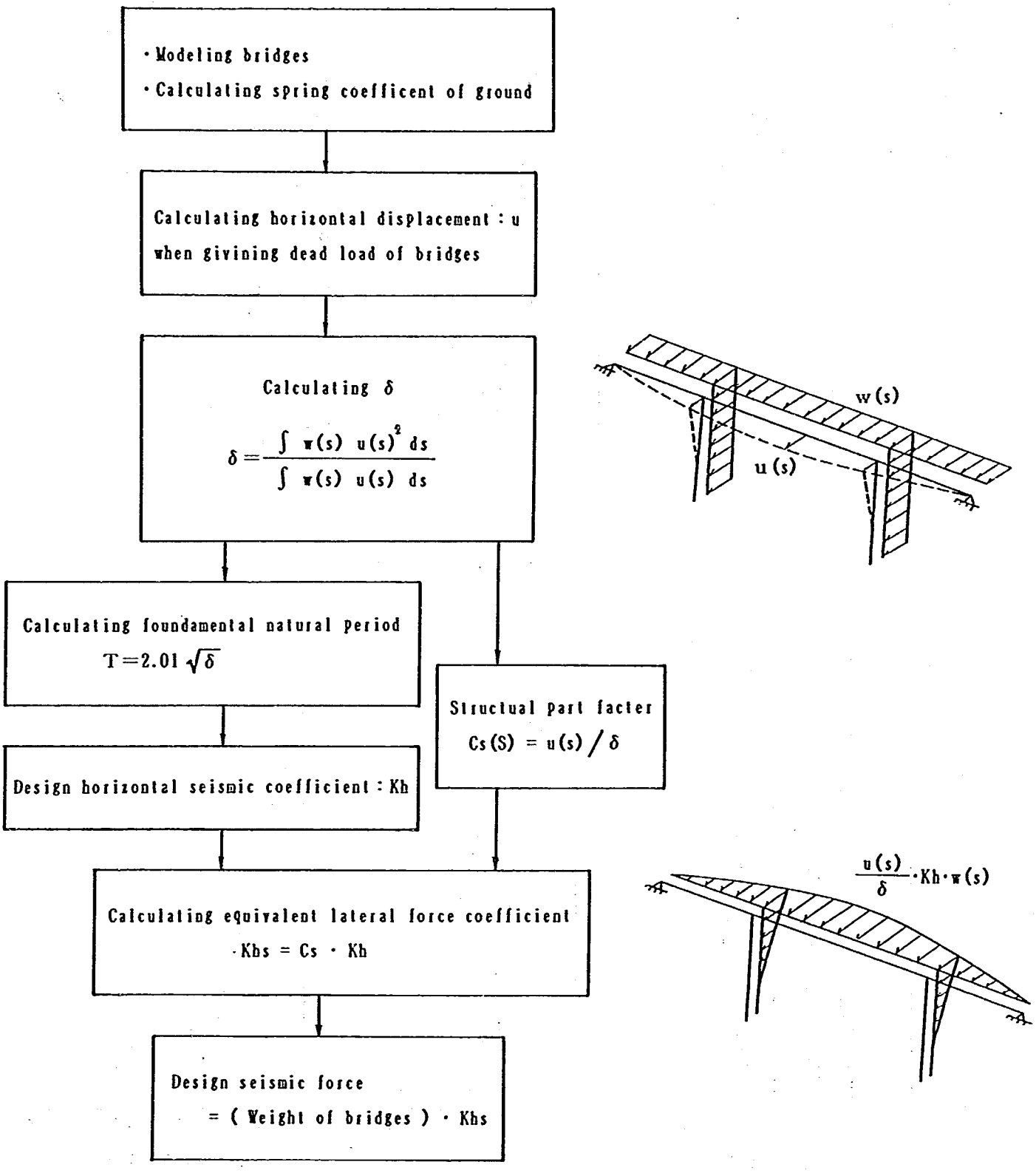


(a) Longitudinal Direction to the Bridge Axis

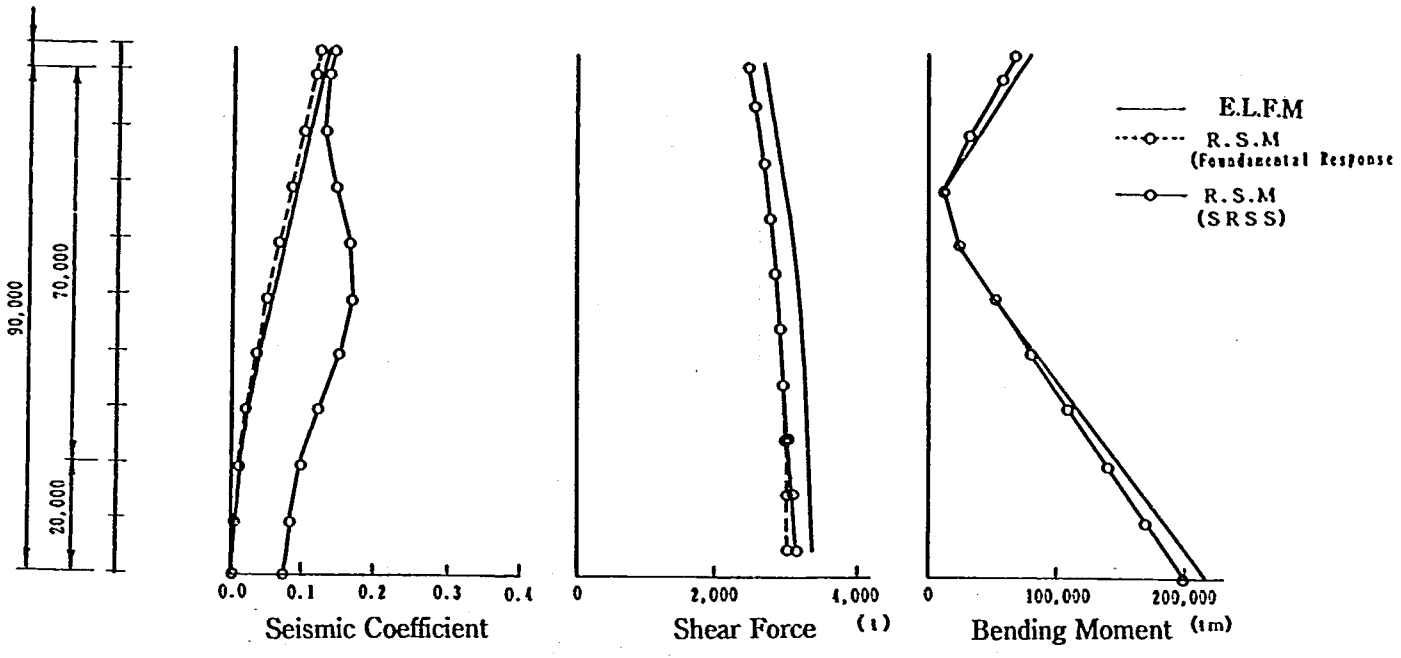


(b) Perpendicular Direction to the Bridge Axis

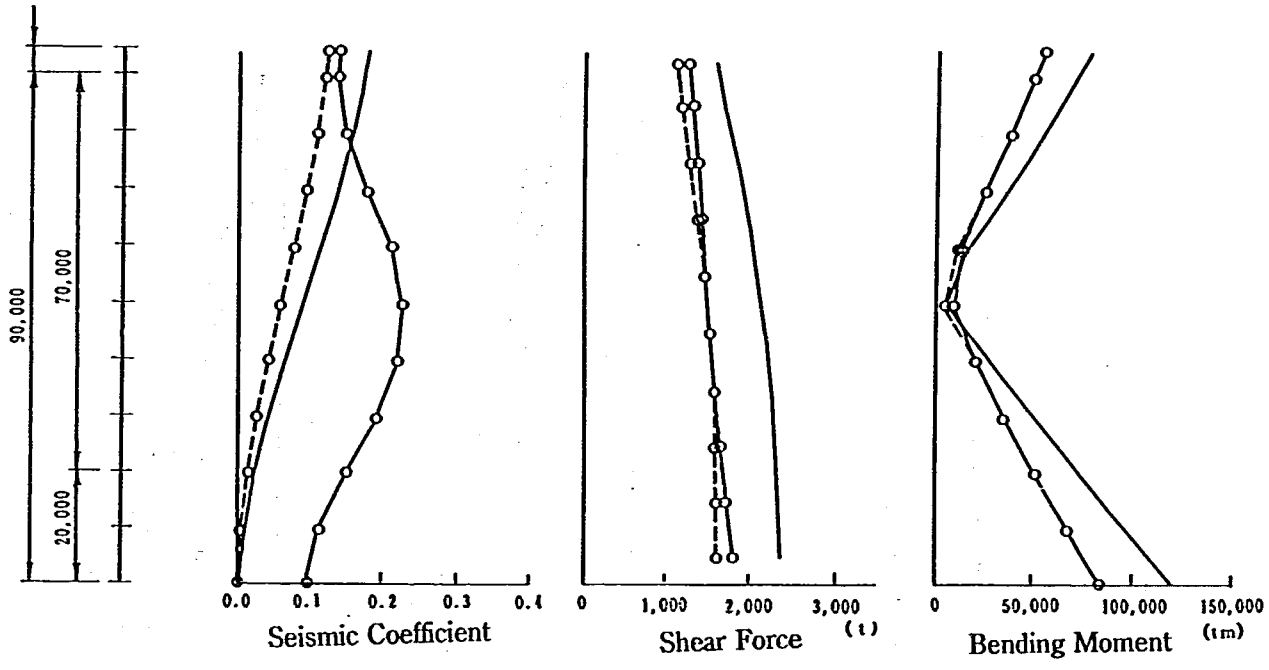
Fig－7 Distribution of Seismic Coefficient and Sectional Force
; In Case of Continuous Rigid － frame Bridge



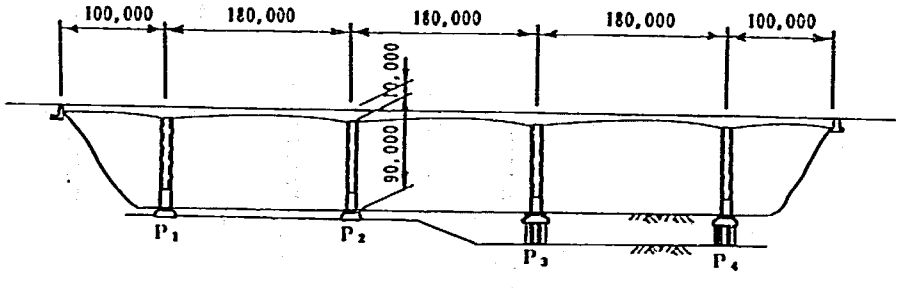
Fig—8 Flow of Equivalent Lateral Force Method



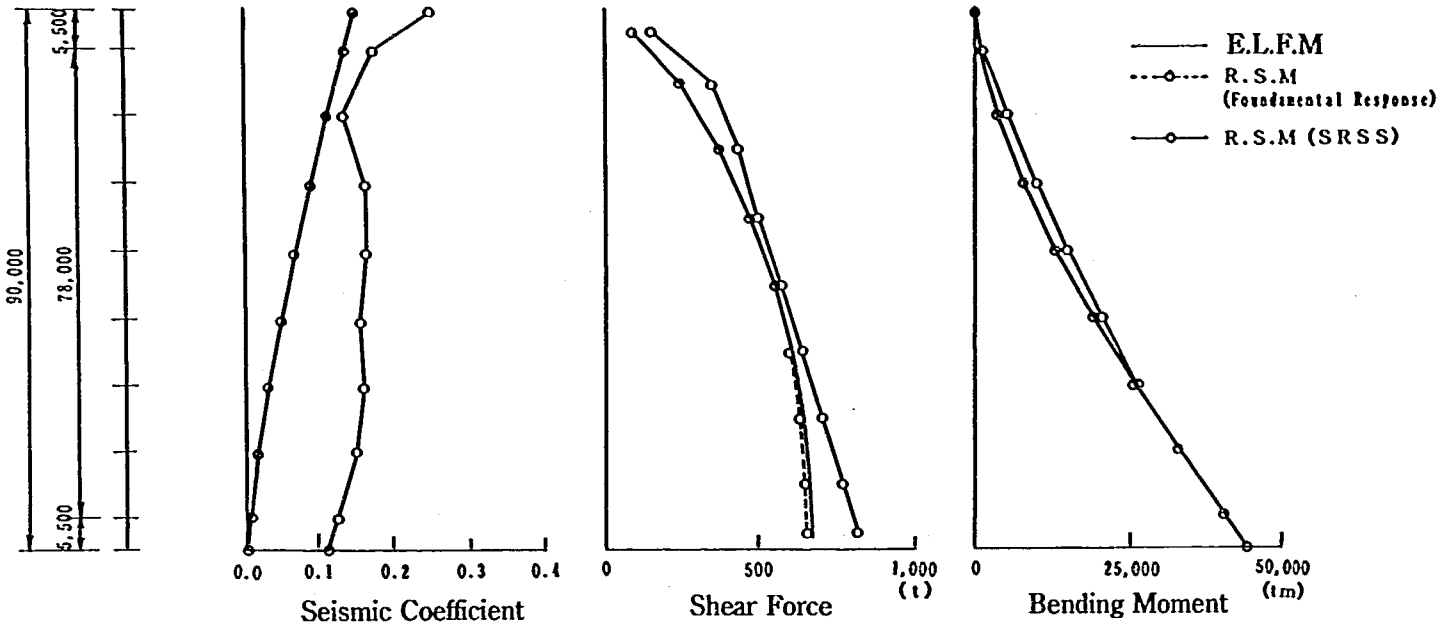
(a) Longitudinal Direction to the Bridge Axis (Spread Foundation : P_2)



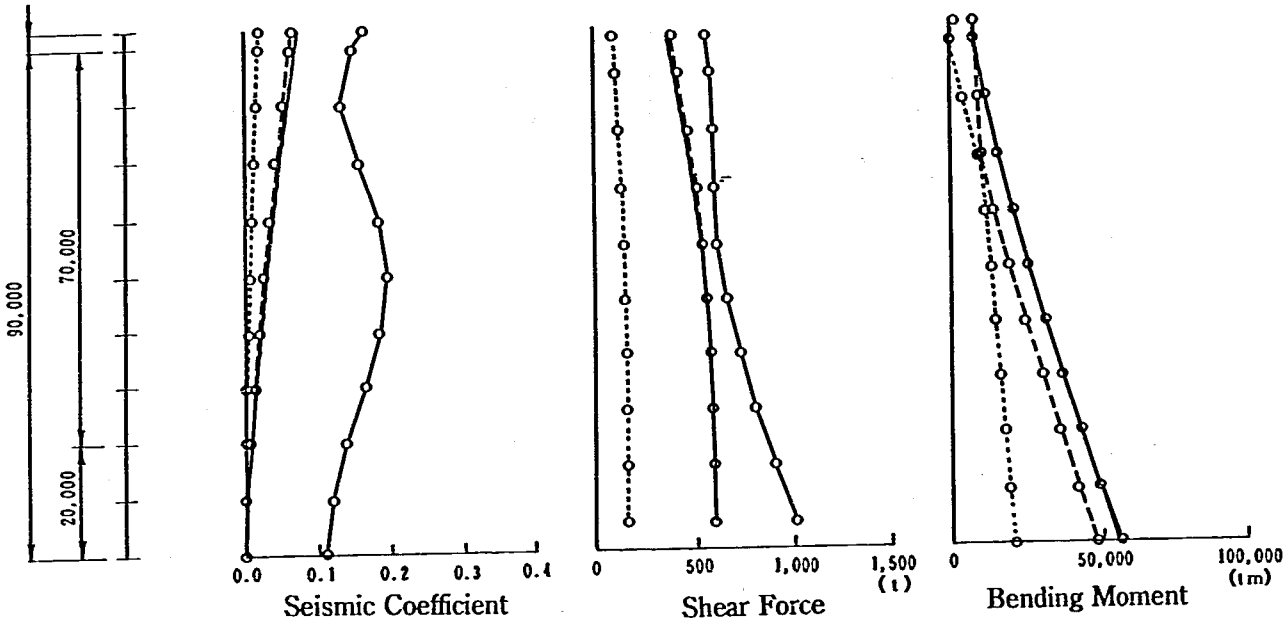
(b) Longitudinal Direction to the Bridge Axis (Pile Foundation : P_3)



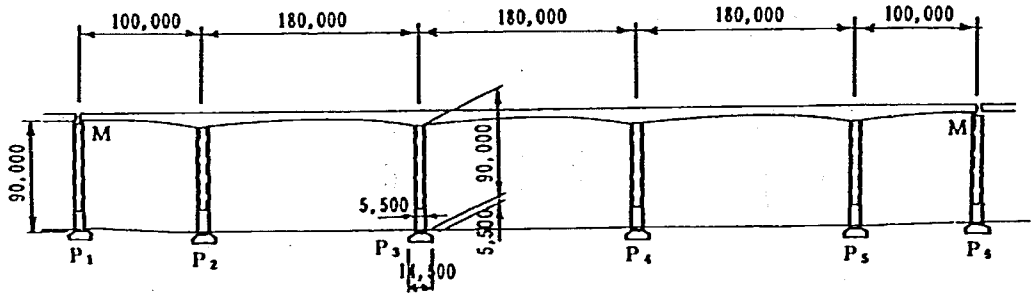
Fig–9 Comparison of E.L.F.M and R.S.M
(In Case of Existing Two types of Foundations in a Bridge)



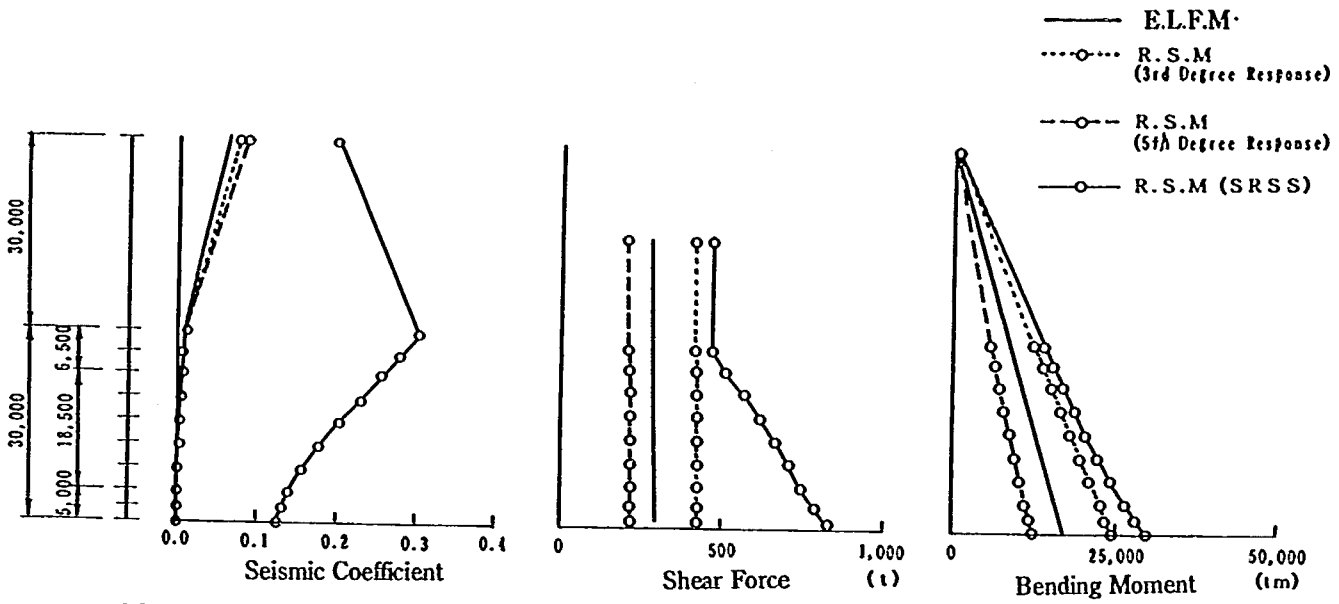
(a) Longitudinal Direction to the Bridge Axis (End Pier : P_1)



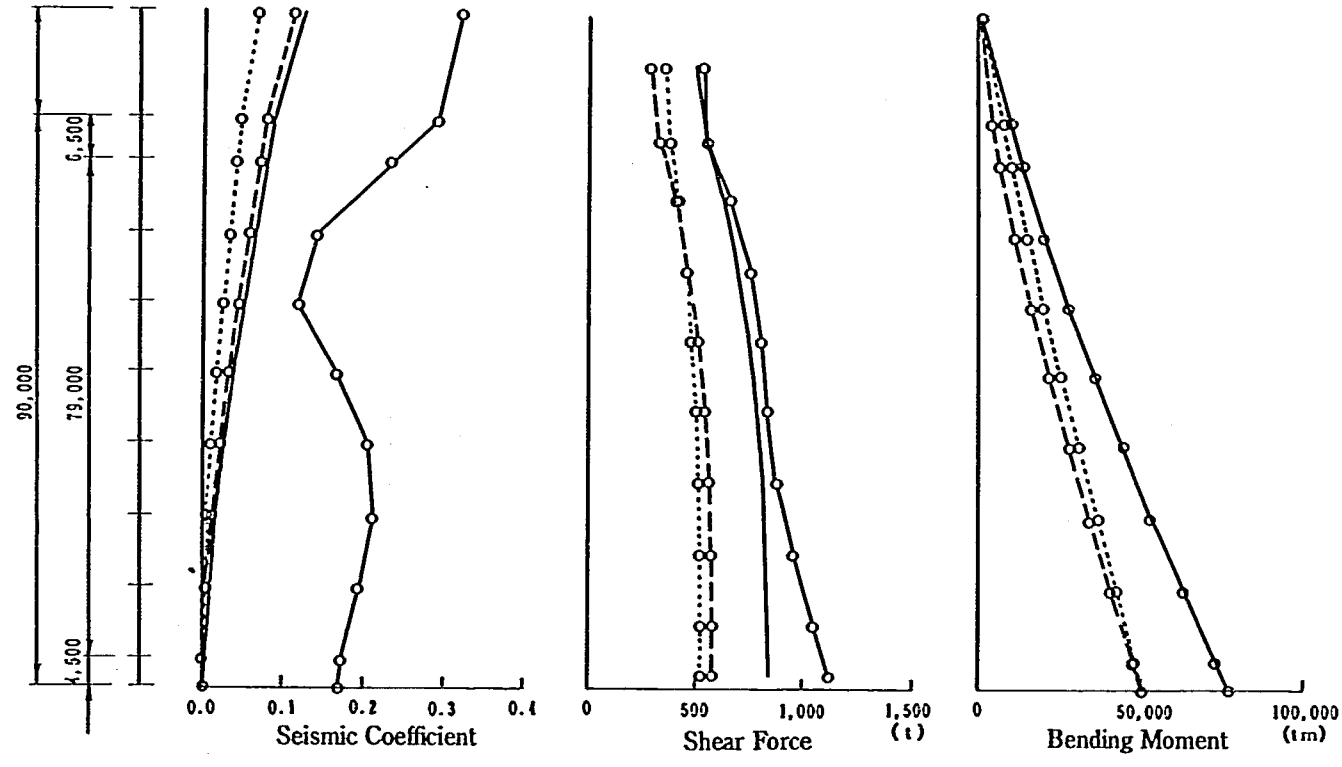
(b) Perpendicular Direction to the Bridge Axis (End Pier : P_1)



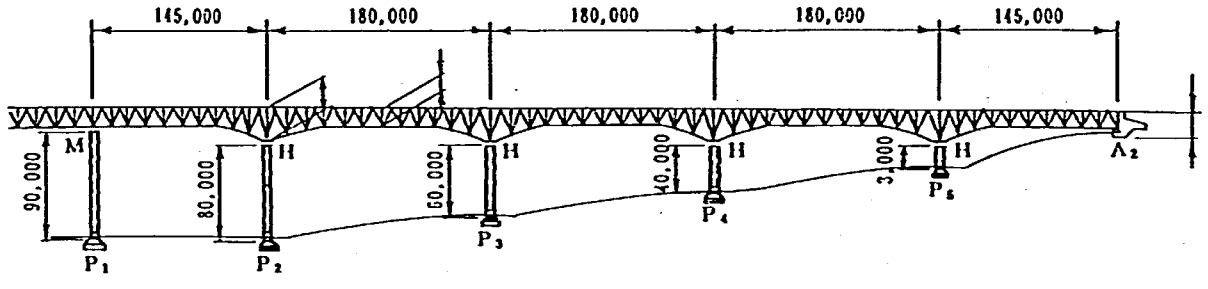
Fig–10 Comparison of E.L.F.M and R.S.M
(In Case that End Substractures are not Abutments, but Piers)



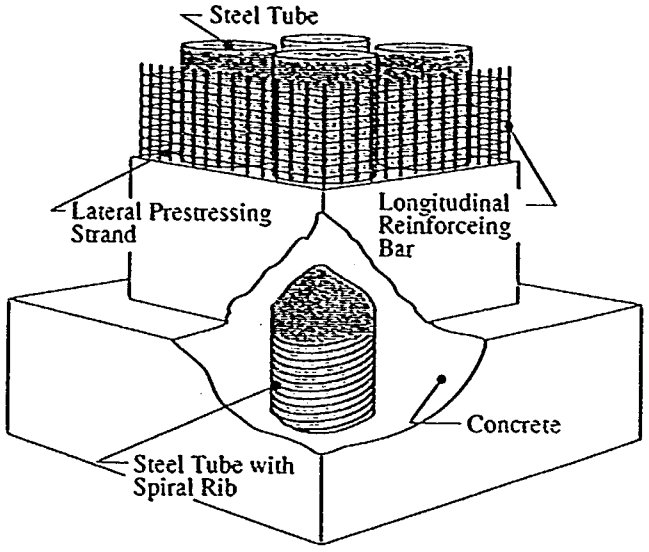
(a) Perpendicular Direction to the Bridge Axis (Pier Height = 30 m : P_5)



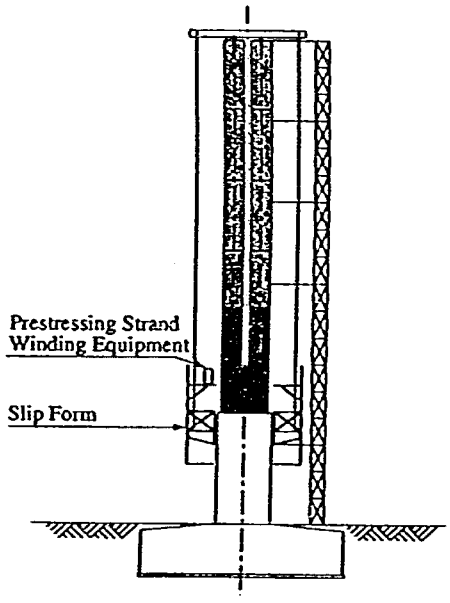
(b) Perpendicular Direction to the Bridge Axis (Pier Height = 90 m : P_1)



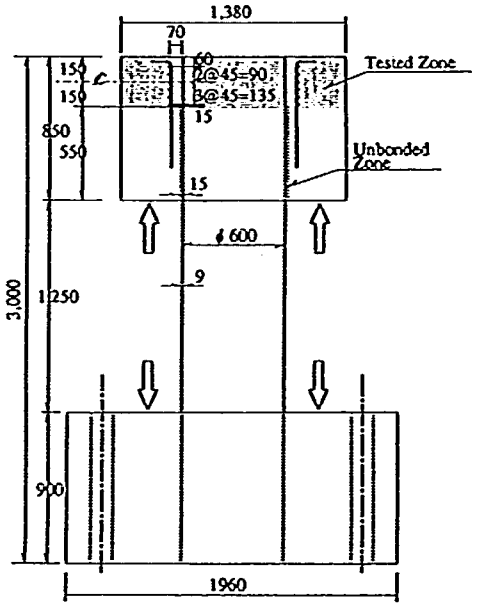
Fig–11 Comparison of E.L.F.M and R.S.M
(In Case that Difference of Each Height of Piers are Extremely Large)



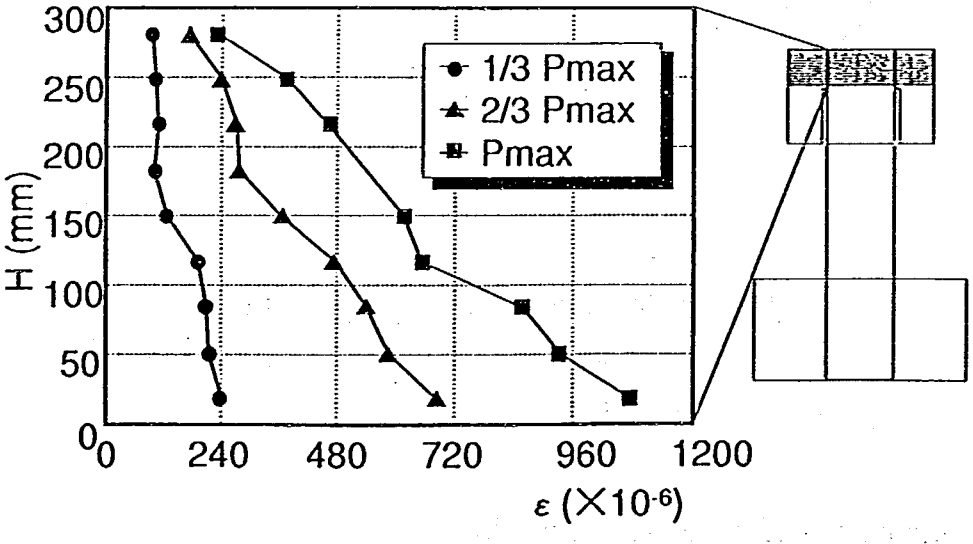
Fig–12 General View of Hybrid Bridge Column



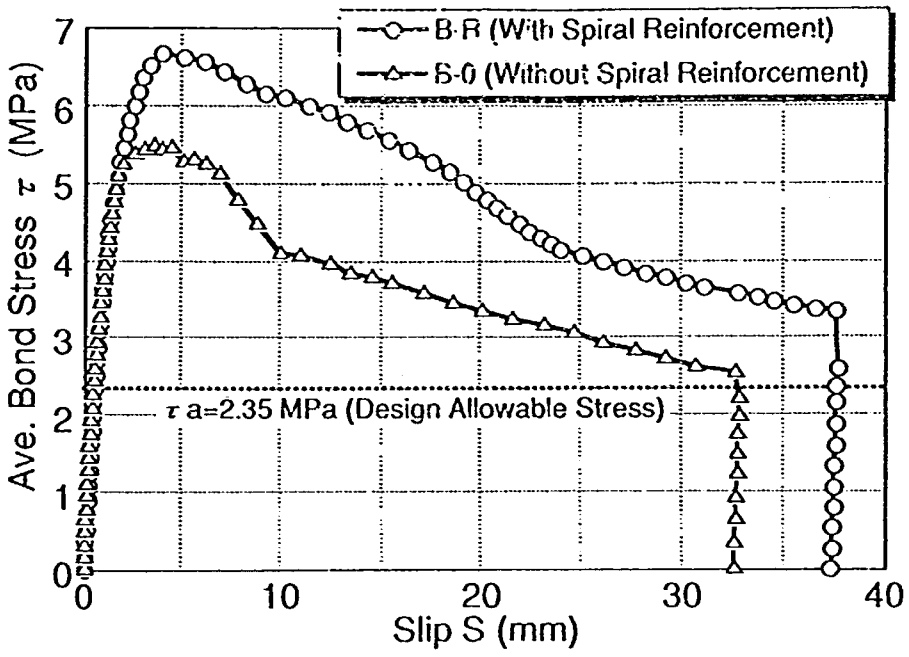
Fig–13 Hybrid Slip Form Method



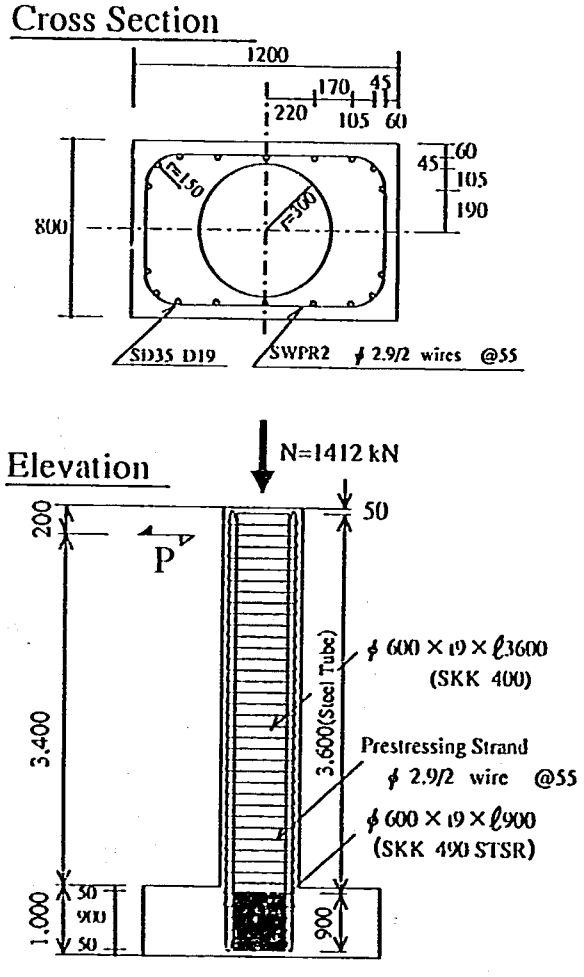
Fig–14 Test Specimen



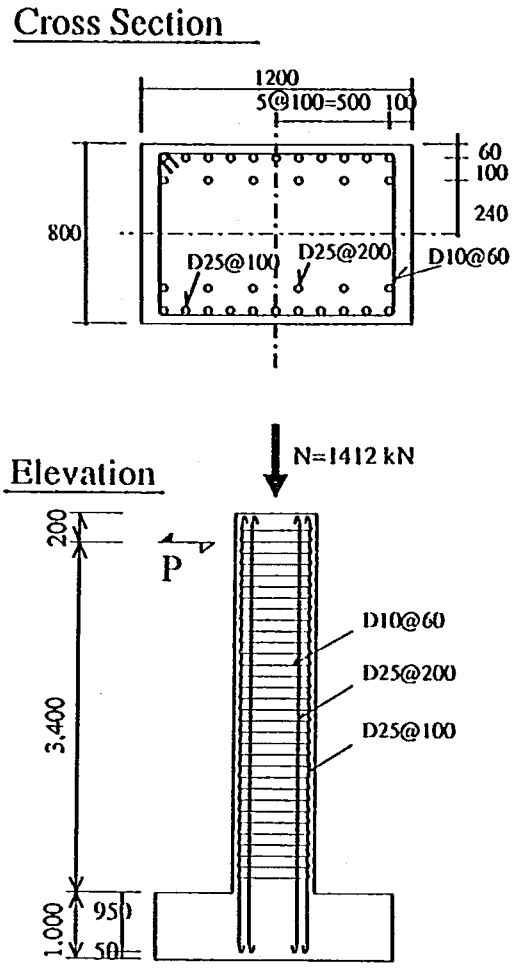
Fig–15 Vertical Strain Distribution of STSR (Specimen B–R)



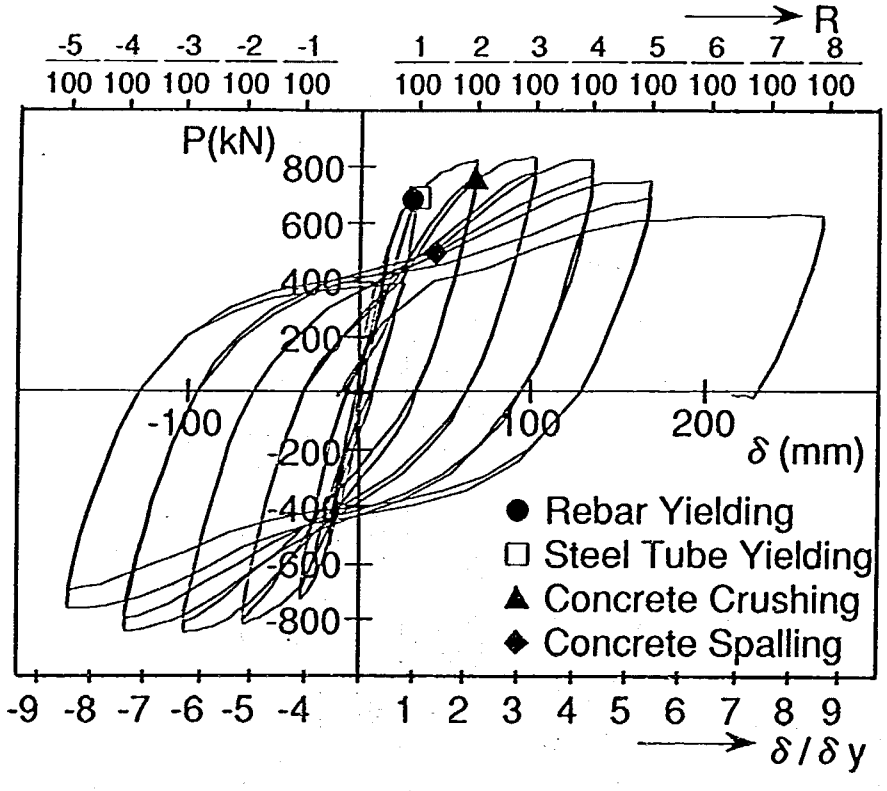
Fig−16 Bond Stress vs. Slip Relationship



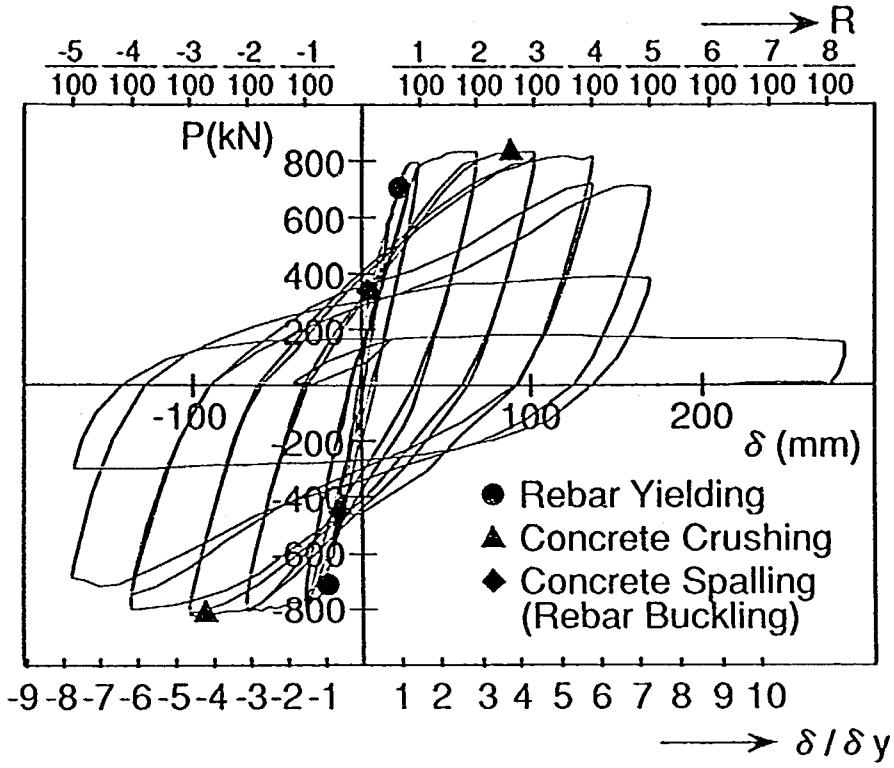
Fig−17 Specimen Layout and Reinforcement (Specimen H−SRC)



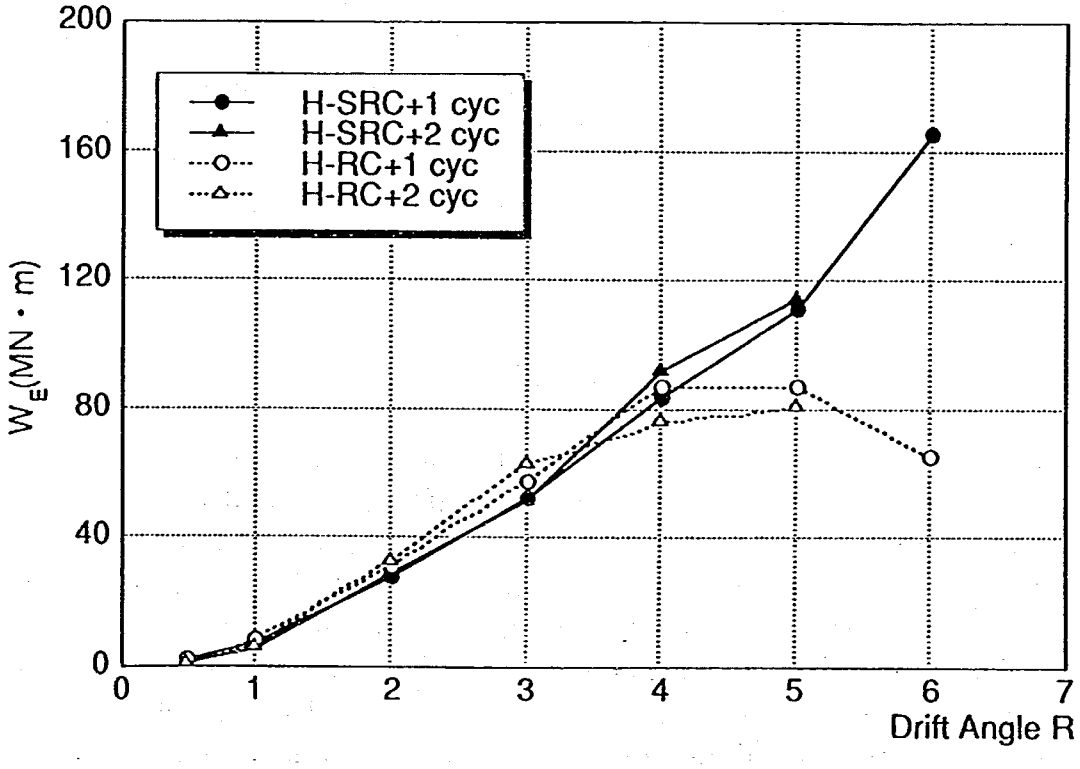
Fig—18 Specimen Layout and Reinforcement (Specimen H—RC)



Fig—19 Load — Displacement Relationship (Specimen H—SRC)



Fig–20 Load – Displacement Relationship
(Specimen H–RC)



Fig–21 Absorbed Energy – Drift Angle Relationship
for Positive Loading

Shaking Table Test for Large-Scale Seismic Isolated Structure using High Damping Rubber Bearings

by

Yoji SUIZU, Chiaki SUDO, Shigenobu SUZUKI, Kengo GODA
Bridgestone Corporation

Nobuyuki OGAWA
National Research Institute for Earth Science and Disaster Prevention

Yasuki OHTORI
Central Research Institute of Electric Power Industry

Abstruct

This paper describes the results of the shaking table test for the large-scale base-isolated structure supported by high damping rubber bearings, supposing a base-isolated bridge. In Japan, results of recerchin base isolation design of highway bridges were compiled in "Manual for Menshin Design for Highway Bridges (draft)" in 1992. The Manual requires the design considering both the Seismic Coefficient Method and the Bearing Capacity Method. The shaking table test was carried out for the base-isolated suructure using the bearings designed on the basis of the Manual, and seismic responses against the earthquake motion at the levelof the Seismic Coefficient Method and the Bearing Capacity Method were evaluated. Test results showed that the response accerelations at the superstructure were the same as or less than the designed values, and the effectiveness of the base isolated structure was obtained. Additionally, the restoring forces of the high damping rubber bearings were reduced when they were deformed largely, therefore, the effect of this phenomenon on the seismic responses was evaluated.

Introduction

In Japan, "Manual for Menshin Design of Highway Bridges (draft)" has been made, and the introduction of base-isolated structures into highway bridges has been progressing rapidly. High damping rubber bearings have been used for several base-isolated bridges including Yamaage Ohashi completed in 1992 (in Tochigi Prefecture), and those are spreading widely as the standard seismic isolation device.

In this study, seismic responces of the base-isolated structure using high damping rubber bearings were investigated, and the effectiveness of base-isolated structure was evaluated on comparison with the results of the design according to the Manual described before, trough the shaking table test for the large-scale base-isolated structure, to extend/enrich the design data on the base-isolated bridges using high damping rubber bearings. This shaking table test was carried out for the rigid model with the mass of

50ton supported by four bearings, keeping time, displacement, acceleration and so on as the values of the actual size system.

Specimens and experimental method

Specimens

The base-isolated structure used for the shaking table test is shown in Fig.1. The frame of 6 m x 4 m was assembled with H-shaped steels, and steel plates were piled on it, as the result, the superstructure was 50 tonf in weight. The superstructure was supported by four high damping rubber bearings. The specifications of the high damping rubber bearings and their design conditions are shown as below.

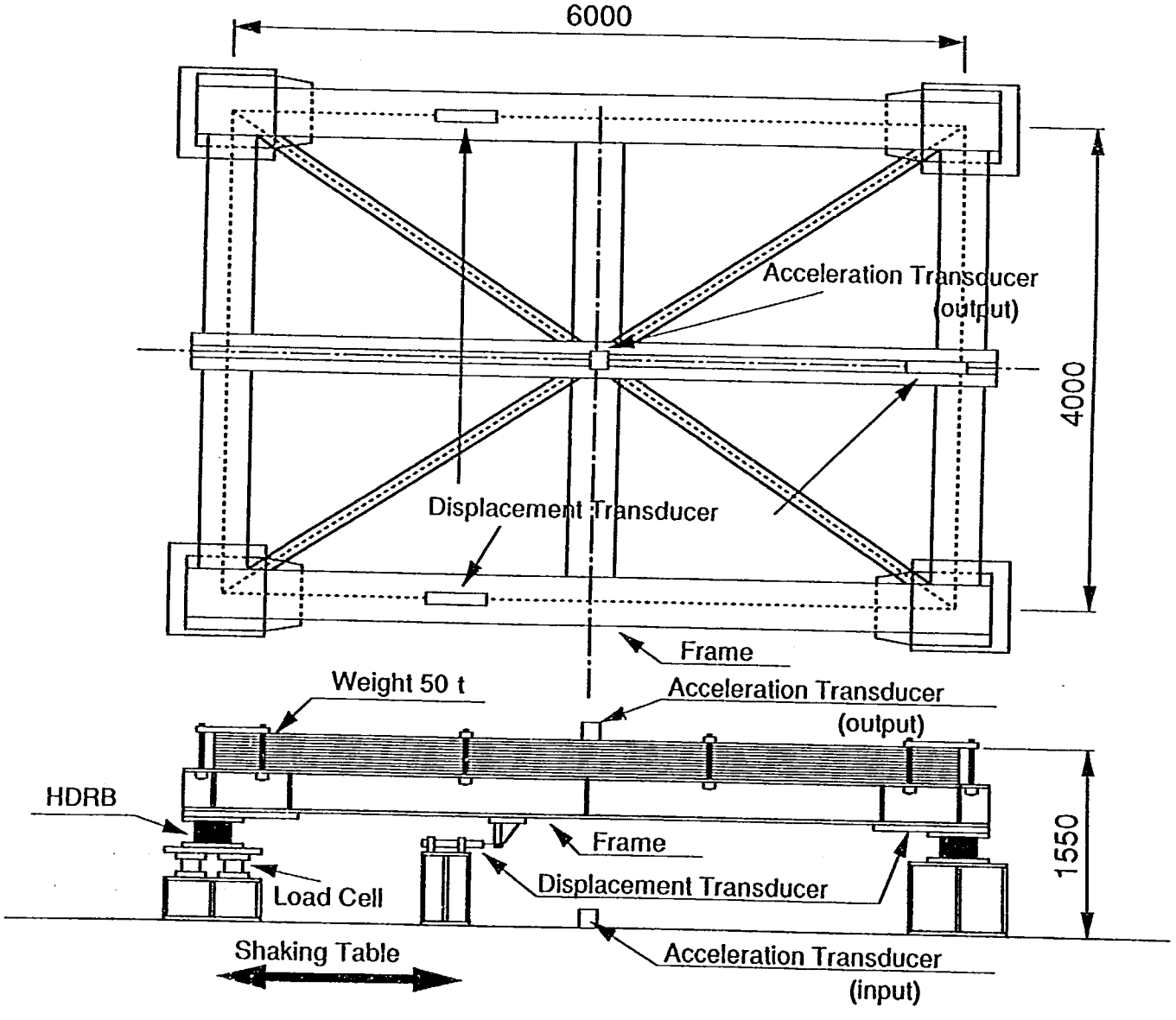


Fig.1 The Base-Isolated Structure

(1)Specifications

Effective dimensions : ϕ205mm x 4 mm x 10 layers
(Shape factor S = 12.8)

Rubber material : High damping rubber (HDR401)

(2)Design conditions

Ground group : I (C_G = 0.8, C_I = 1.0, C_Z = 1.0)

Weight of superstructure : 50 tonf

Number of bearings : 4

Stiffness of lower structure : Rigid

Where C_G is Modification factor for ground condition, C_I is Modification factor for impor-tance, and C_Z is Modification factor for zone. Those arestipulated in the "Part V Seismic Design" of "Specifications of the Design of Highway Bridges".

Measurement

The positions of installing acceleration transducers, displacement transducers, and load cells measuring bearing's restoring forces are as shown in Fig.1. Acceleration transducers were installed on the center of the shaking table and on the center of the superstructure, and their full-scale is 2 G. Displacement transducers were used for measuring deflection of the bearings, and their full-sale is ±100 mm. Besides, load cells measuring restoring force of the bearings were installed under two bearings, and their full -scale is 15tonf (7.5tonf x 4).

The measured data (accelerations, deflection and restoring foece of rubber bearings) were recorded in analog form, and were digitized with the sampling time of 8 ms.

Experimental method

In the test, the shaking table in Large-Scale Earthquake Simulator in National Recerch Institute for Earth Science and Disaster Prevention in Tukuba Science City was used. This shaking table has been used so far, for the studies on seismic efficiency of various structures, such as bridges, levees, trench tunnels, buildings, nuclear facilities and others. The main specifications of this shaking table are shown in Table 1.

As for the input seismic waves, supposing Ground Group I (the modified record for Kaihoku-bridge), the Seismic Coefficient Method Level (L1 : maximum acceleration 103 Gal) and the Bearing Capacity Method Level (L2 : maximum acceleration 360 Gal) were used.

The test was started from the condition in which bearings didn't kave experienced deformations. First, the seismic waves of L1 were inputted, and subsequently, the seismic waves of L2 were inputted. Additionally, the seismic waves of L1 were inputted again, in order to estimate the seismic responces when restoring forces werer diminished. The above mentioned experimental process is shown in Table 2.

Table.1 Specifications of Shaking Table

The Shaking Table	15.0×14.5(m) Weight 160tf
Driving System	Electro-Hidraulic servo Mechanism
Maximum Load Weight	500ton
Maximum Amplitude	±220(mm)
Maximum Velocity	75(cm/sec)
Maximum Acceleration	0.5G (500t) 0.94G (200t)
Range of Frequency	DC~50Hz
Waveforms of Excitation	Sine Wave, random Wave, Seismic Wave

Table.2 Turn of Experiment

Turn of Experiment	Condition of High Damping Rubber Bearings	Method of Experiment
1	Initial State	Shaking Table test L1
2	After Defomation of L1	Shaking Table test L2
3	After Defomation of L2	Shaking Table test L1

Experimental results

Time history responses

In Fig.2 ~ Fig.4, the waveforms of time history response and the load-displacement Lissajous' figures by L1 and L2 at the time of initial deformation and L1 after large deformation (after experenced the shearing strain of 173%) are shown.

When L1 at the time of initial deformation is compared with L1 after large deformation, it can be said that as to the response values of input seismic waves, judging from the waveforms of time history response of input seismic waves and the maximum and the minimum values of their acceleration in both L1 at the time of initial deformation and L1 after large deformation, the almost equivalent input seismic waves L1 were able to reproduce.

As for the response values of the acceleration of the superstructure, the maximum absolute value was 130 Gal in L1 at the time of initial deformation, but was reduced down to 115 Gal in L1 after large deformation.

As to the displacement, whereas the maximum absolute value was 6.57mm in L1 at the time of initial deformation, it increased up to 14.1mm in L1 after large deformation.

Judging from the waveforms of time history response of output acceleration and displacement, it is known that in L1 after large deformation, the period became longer as

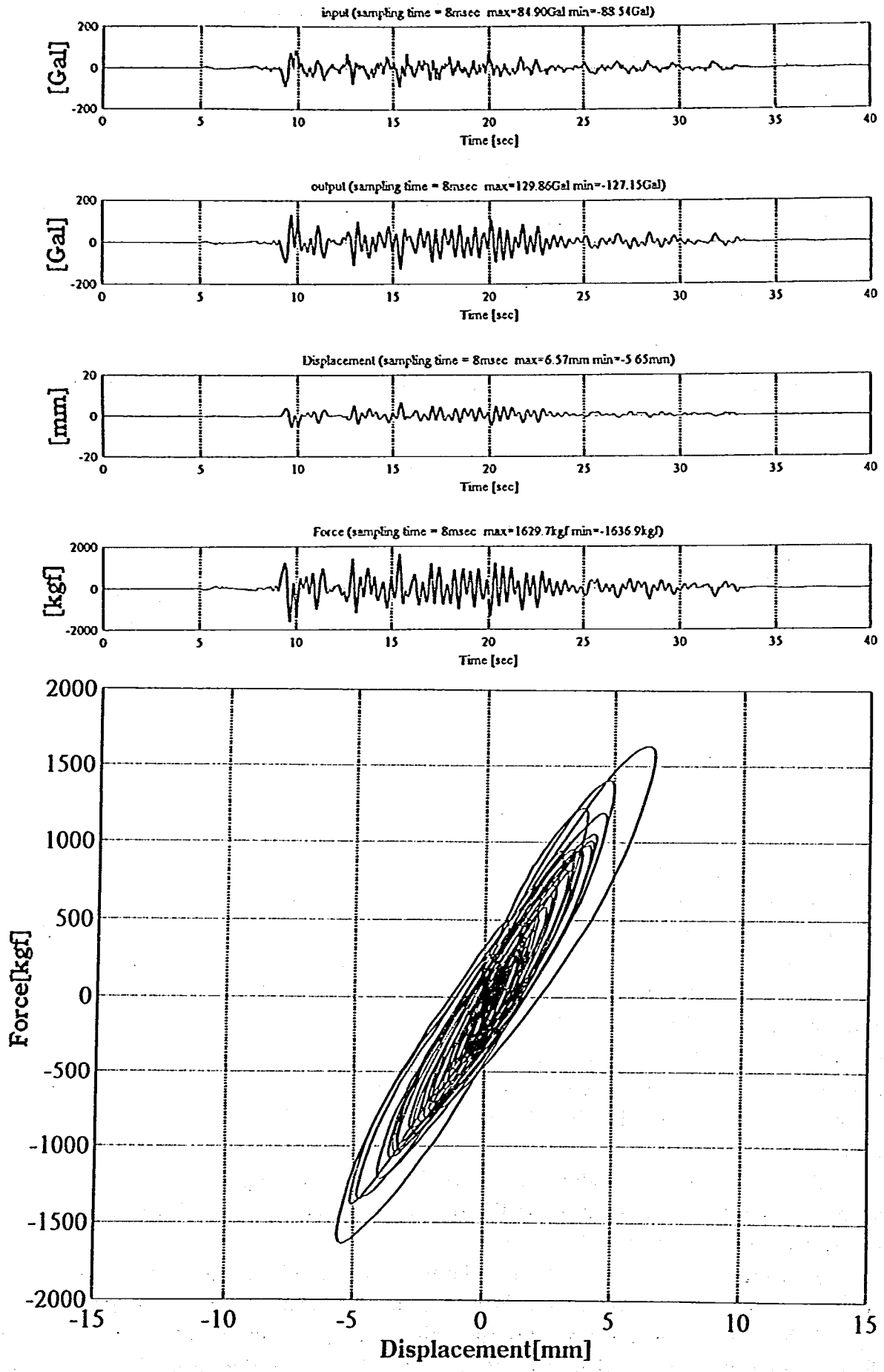


Fig.2 Time History response (L1 First)

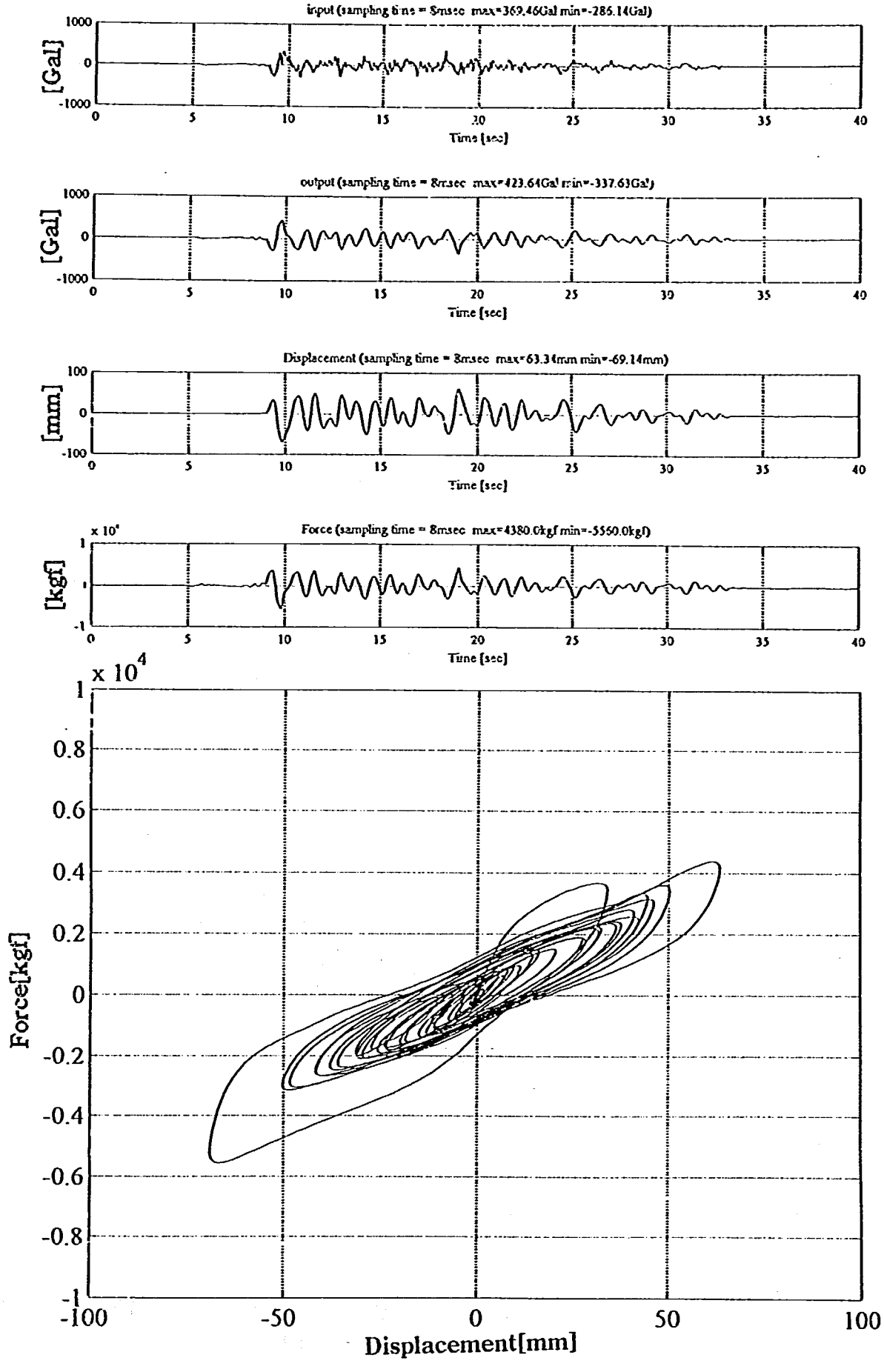


Fig.3 Time History response (L2)

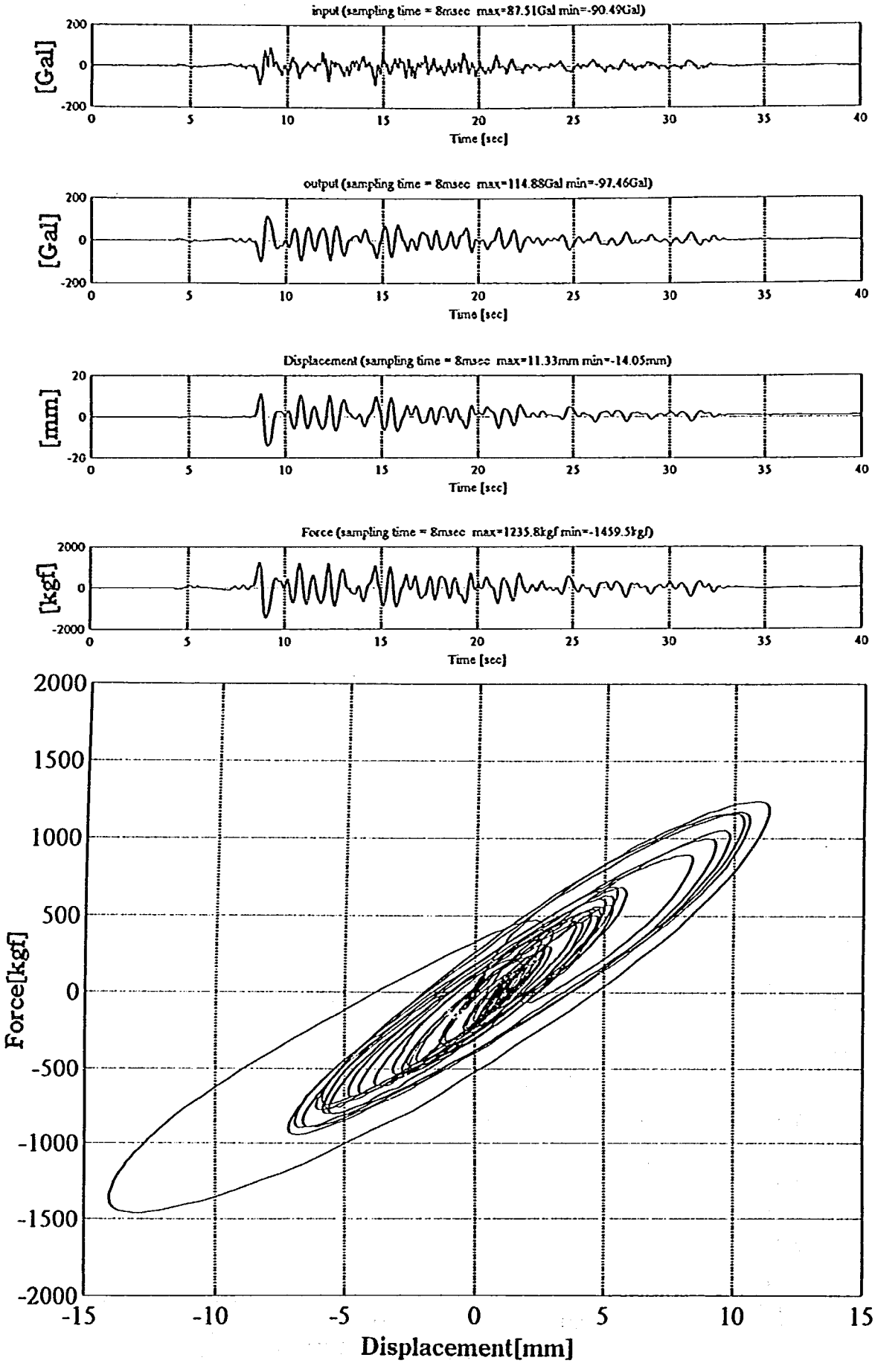


Fig.4 Time History response (L1 Second)

compared with L1 at the time of initial deformation.

When the Lissajous' figures of L1 at the time of initial deformation is compared with that of L1 after large deformation, it is known that in L1 after large deformation, the periodbecame longer and displacement became larger, but regarding the magnitude of load, both the magnitude of load of the former and that of the latter were nearly the same degree.

Fourier spectra and transfer function

As for L1 and L2 at the time of initial deformation and L1 after large deformation (after experienced the shear strain of 173%) , in the upper parts of Fig.5~Fig.7, the Fourier spectra of input seismic waves and the acceleration of the superstructure are shown with broken lines and continuous lines respectively. In the lower parts, the values ofthe Fourier spectra of the superstructure divided by the Fourier spectra of input seismic waves, namely transfer function are shown. In this case, all the Fourier spectra were smoothed with the Bartlett wind of 0.24 Hz band width. Judging from the Fourier spectra and transfer functions, the following matters can be said.

The natural frequency of L1 and L2 at the time of initial deformation and L1 after large deformation was 2.4 Hz, 1.3 Hz and 1.7Hz, respectively. Namely, it is known that in L1 after large deformation, the stiffness of the bearings lowered due to the effect of loading history, and the period became longer as compared with L2 at the time of initial deformation.

Dynamic magnification factor of transfer function has become less than 1 in the range larger than 3.4 Hz in L1 at the time of initial deformation, 1.8 Hz in L1 after large deformation, and 2.2 Hz in L1 after large deformation.

Effect of base isolation

Normally, high damping rubber bearings are installed to actual bridges after the restoring force characteristics are evaluated as the completed product inspection. Accordingly, it is necessary to consider earthquake response by taking the restoration characteristics of hysteresis restoring force in consideration. At present in the design, the average of the characteristic value of initial loading and the characteristic value immediately after initial loading (shear modulus G, equivalent damping constant heq) was calculated by anticipating the restoration characteristics, and these have been utilized as the characteristic formulas. Namely, the average values of two curves that characteristic value of initial loading andthe characteristic value immediately after initial loading are shown, that is to say, G– γ curve of average and heq– γ curve of average (γ : shear strain) have become the criteria for evaluating the stiffness and damping. Also in the results of this experiment, in L1 at the time of initial deformation and L1 after large deformation (after experienced the shear strain of 173%), the stiffness of the latter lowered, and the natural period of the latter became longer as compared with the former due to the effect of loading history.

Next, the results of the design values and the experimental values by the Seismic Coefficient Method Level are shown, and it is Table.2. The design conditions are as shown in Chapter of Specimens, As compared with the design displacement of 3.5 cm, in

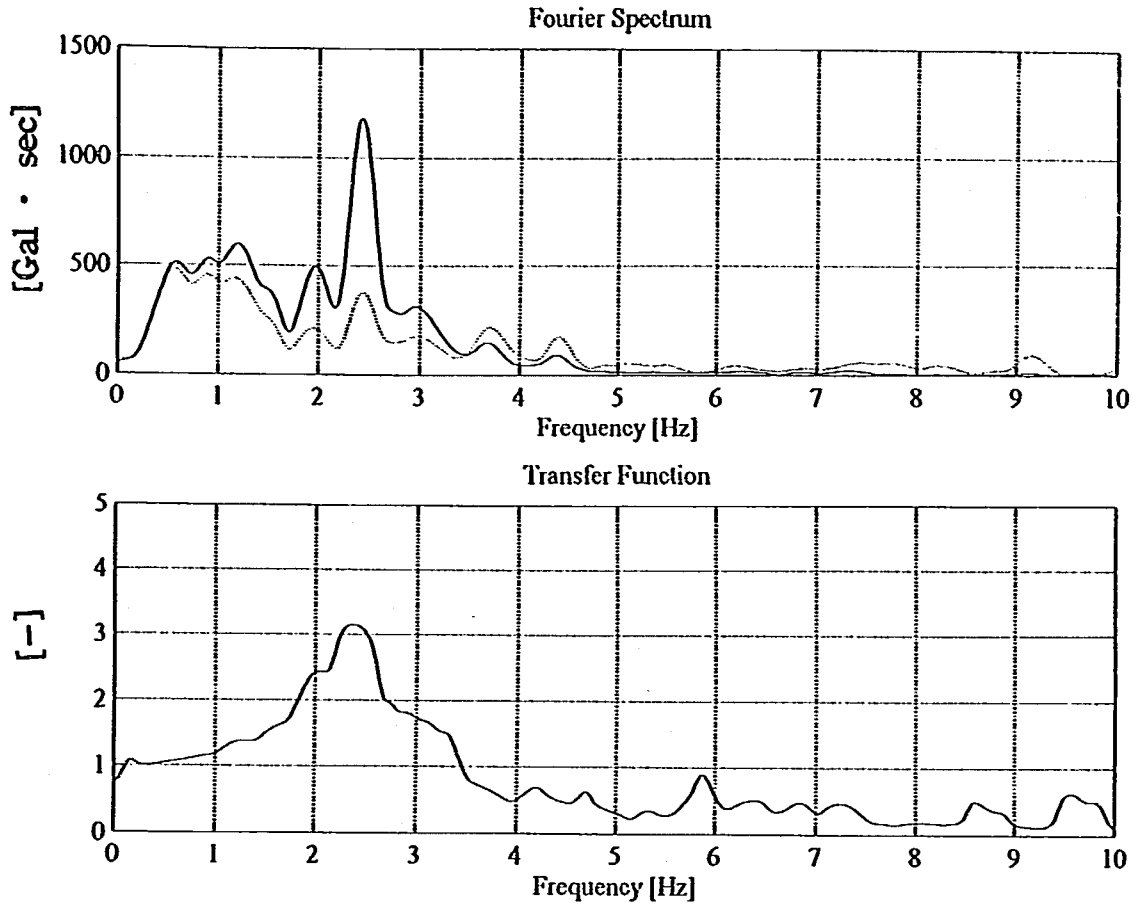


Fig.5 Fourier Spectrum (L1 First)

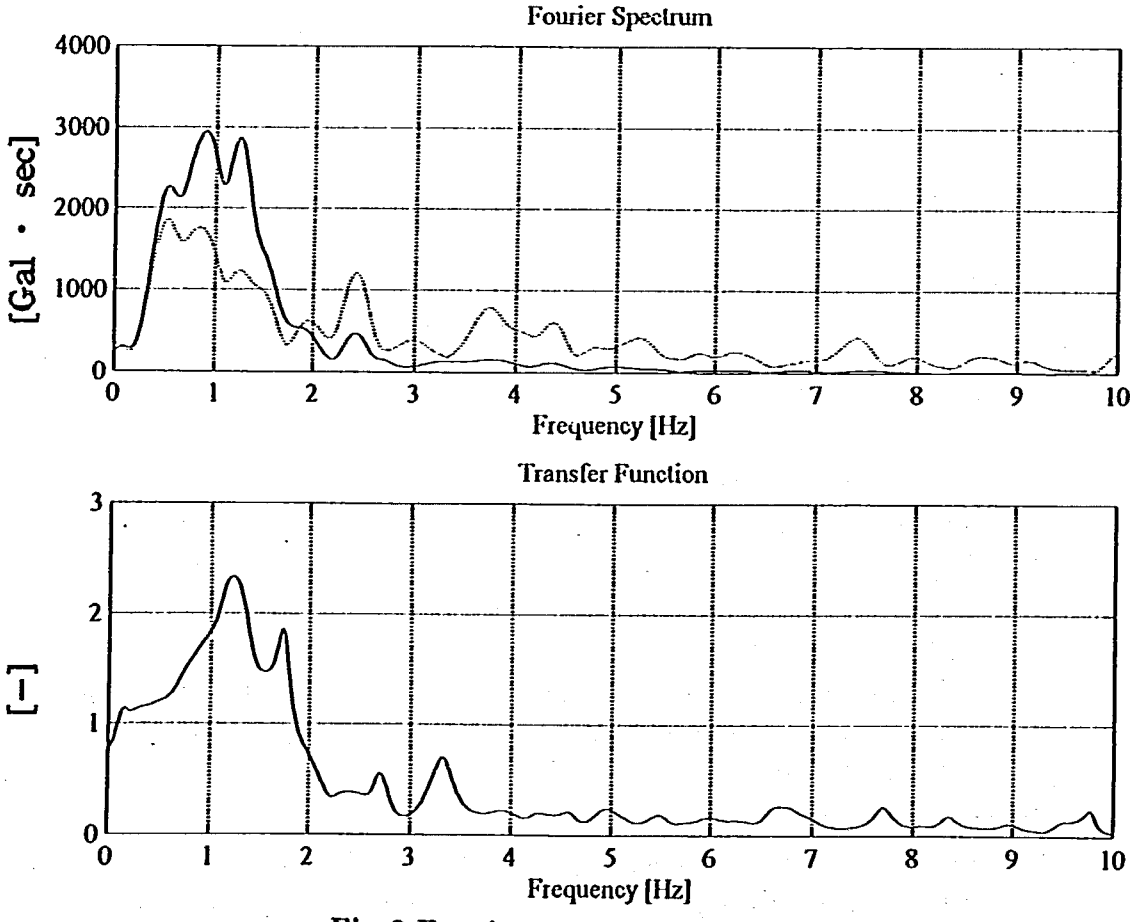


Fig.6 Fourier Spectrum (L2)

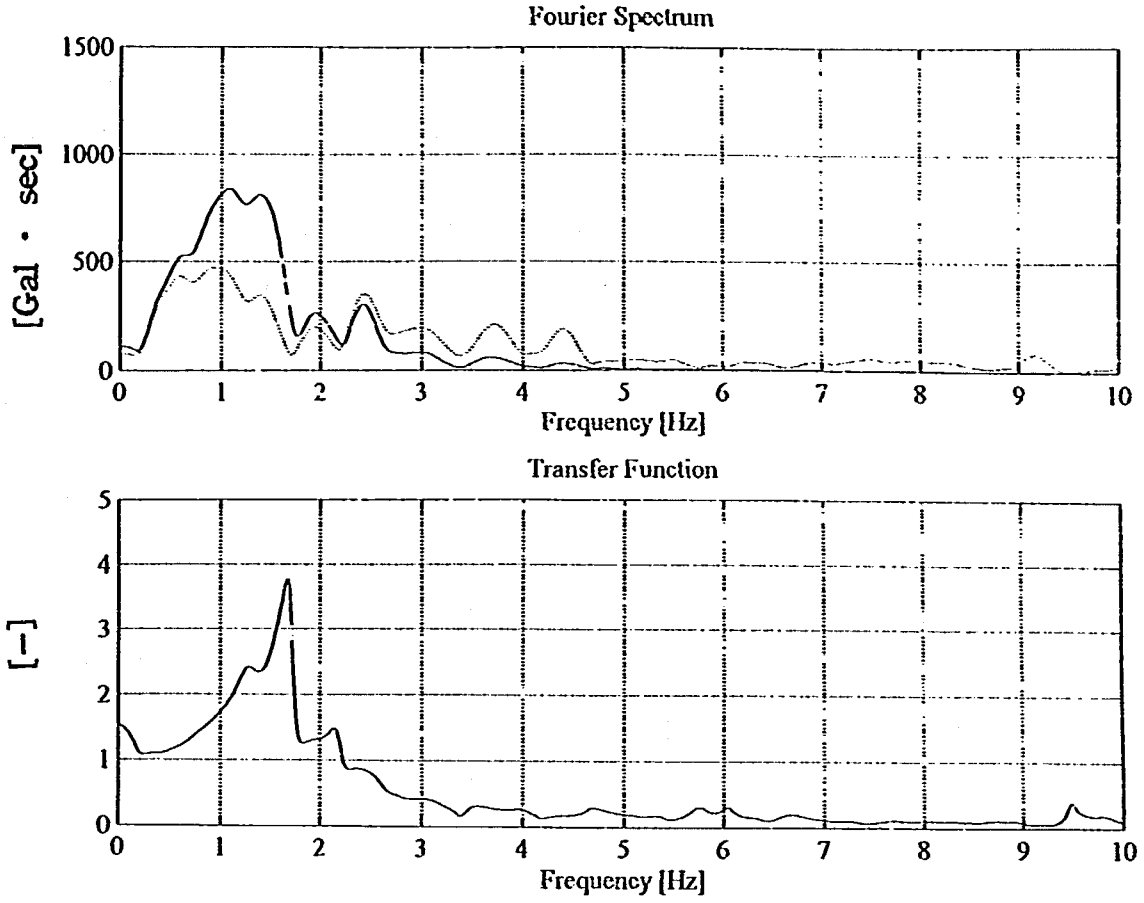


Fig.7 Fourier Spectrum (L1 Second)

the experiment, each displacement in both L1 at the time of initial deformation and L1 after large deformation bacomes smaller. Consequently, as compared with the design value of 1.3 Hz, also the natural frequency became 2.4 Hz in L1 at the time of initial deformation and 1.7 Hz in L1 after large deformation, and considering that the equivalent stiffness in the design values used the average value of that before experiencing the shea r strain of 200% (initial deformation) and that after experienced it (after large deformation), at the Seismic Coefficient Method Level, the stiffness of the bearings has been made stiffer than the design value, and the extension of the period as aimed at in the design has not been achieved. Moreover, as compared with the design horizontal seismic coeffi- cient of 0.2, the horizontal seismic coefficient was 0.13 (130 Gal) in L1 at the time of initial deformation, and 0.12 (115 Gal) in L1 after large deformation, and it is known that the large reduction from the design value has arisen. In the design of base isolation devices, the lowering ofseismic coefficient due to the damping effect at Seismic Coeffici- ent Method Level is notexpected, but actually this seems to arise because the lowering of seismic coefficient occurred due to the damping effect of high damping rubber bearings.

As to the Bearing Capacity Method, as compared with the design displacement of U_B=9.8 cm (shear strain γ_B=2.46), the displacement in L2 at the time of initial defor- mationin the experiment has become 6.9 cm (shear strain 1.73), and also as for the natural frequency, it has become 1.3Hz in the experiment whereas it was 1.05Hz in the design. The stiffness of experimental value was shown somewhat more rigidly than that of the design value, but considering that the equivalent stiffness in the design values uses the average value of stiffness before experiencing the shear strain of 200% (initial defo-

Table.3 The Seismic Coefficient Method Level

Item / Parameter		Design Value	L1 (First)	L1 (second)	Remarks Column
Design Displacement (Shear Strain)	u_B γ_B	3.46cm (0.864)	0.657cm	1.41cm	(≦1.5)
Effective Design Displacement (Shear Strain)	u_{Be} γ_{Be}	2.42cm (0.605)	(0.164)	(0.351)	0.7・u_B
Equivalent Stiffness	K_B	0.723tf/cm	—	—	u_B
Effective Equivalent Stiffness	K_{Be}	0.887tf/cm	—	—	u_{Be}
Equivalent Damping Ratio	h_B	0.172	—	—	u_{Be}
Natural Frequency	f_n	1.32Hz	2.4Hz	1.7Hz	k_{Be}
Modification Factor for Structural Response	C_T	1.25	—	—	
Hrizontal Seismic Coefficient	k_h	0.20	0.13	0.11	

rmation) and that after experienced it (after large deformation), it can be said that the almost proper results have been obtained for the design value and the experimental values. Moreover, as compared with the design horizontal seismic coefficient $K_{hc}=0.49$ (Modification factor forstructural response $C_R=0.7$, Modification factor for energy dissipation capability $C_E=0.7$), the horizontal seismic coefficient has become 0.432 (424 Gal) in the experiment, and it can be said that the base isolation effect as expected has been obtained.

Conclusion

In this study, the shaking table test at the Seismic Coefficient Method Level and at the Bearing capcity Level was carried out by using the high damping rubber bearings which were designed in accordance with "Manual for Menshin Design of Highway Bridges (draft)", and the results were put in order. Hereinafter, the results obtained by this study are summarized.

(1) At both the Seismic Coefficient Method Level and the Bearing Capacity Method Level, the horizontal seismic coefficient in the experiment became lower than the design horizontal seismic coefficient, and the base isolation effect as expected was able to be obtained.

(2) In base isolation design method, the lowering of seismic Coefficient due to damping effect at the Seismic Cefficient Method Level is not expected, but according to the experimental results, there is the possibility that the high damping rubber bearings

caused the lowering of seismic coefficient due to the damping effect.

(3) Since the restoring force characteristics of high damping rubber bearings have influence on the effect of loading history, as compared with the stiffness the time of initial deformation, that after large deformation became lower and the period after large deformation became longer. Though there is the dependence on loading history in the restoring force characteristics of high damping rubber bearings, it was able to be confirmed that this point has not become a big problem when base isolation bearings is designed.

Acknowledgement

The author expresses thanks to Professor Takafumi FUJITA of institute of Industrial Science,University of Tokyo, who gave appropriate guidance on the experiment when this research was carried out.

Reference

1. Public Works Research Institute : Manual for Menshin Design of Highway Bridges (draft), October 1992 (in Japanese)
2. Japan Road Association : Part V Seismic Design of the Specifications of the Design of Highway Bridges, February 1990 (in Japanese)
3. Nobuo MUROTA, Kengo GODA, Shigenobu SUZUKI, Chiaki SUDO, Yoji SUIZE : Recovery Characteristics of Dynamic Properties of High Damping Rubber Bearings, Third U.S.–Japan Workshop on Earthquake Protective Systems for Bridges, Berkeley Marina Marriott Hotel, Berkeley, Clifornia, January 24 and 25, 1994

Elasto-Plastic Earthquake Response of Prestressed Concrete Cable-Stayed Bridges with Hysteretic-type Bearing between Deck and Piers/Abutments

Hisanori Otsuka[1], Kazuyuki Mizutori[2], Yutaka Yamahana[3]

1)Head, Earthquake Engineering Division, Earthquake Disaster Prevention Department, Public Works Research Institute, Ministry of Construction, Tsukuba Science City, Ibaraki-ken 305, Japan
2)Chief Manager, Technical Research Institute, The Zenitka Corporation, 3-7-1, Nishi-Shinjuku, Shinjuku-ku, Tokyo 160, Japan
3)Assist. Chief, Civl Engineering Department, The Zenitaka Corporation, 31, Ichiban-cho, Chiyoda-ku, Tokyo 102, Japan

ABSTRACT

In order to investigate the earthquake response of PC cable-stayed bridges with Elasto-Plastic Shear Springs between Deck and Piers/Abutments, both elastic and elasto-plastic analyses for cable-stayed bridges with 200m center span subjected to two different seismic waves are carried out.
In the analysis, the effect of the following items on the seismic induced forces and displacements, crack propagation and member yield are investigated.
1) elastic versus elasto-plastic response,
2) effectiveness of the elasto-plastic shear bearings as energy dissipation devices,
3) response property for different seismic waves.

INTRODUCTION

Although girder bridges with hysteretic damping augmentation devices such as lead-rubber bearings have been constructed, possibility of application of this type of devices to long span bridges such as cable-stayed bridges has not been studied. Cable-stayed bridges are known to flexible structures with long natural period compared with ordinary girder bridges. Investigation of effectiveness of hysteretic-type bearing for this type of bridge subjected to seismic forces has not been conducted sufficiently yet.

Hysteretic damping-type rubber bearings, which are installed at deck-abutment and deck-pier connections, are expected to reduce the response of cable-stayed bridges during severe seismic events.

This paper presents the results of elastic and elasto-plastic seismic response analysis conducted for three spans continuous prestressed concrete cable- stayed bridges (a center span length of 200m) with various combinations of support conditions. Discussions on the results of numerical calculations are focused to the following items.

- difference between elastic and elasto-plastic response
- effectiveness of elasto-plastic shear bearings as hysteretic damping augmentation devices
- difference of seismic response due to different ground motions

ANALYTICAL MODEL

Structural general view of the model analysed in this study are shown in Figure 1, and material property is shown in Table 1. Profile of the model is summarized as follows.

type of structure: three spans continuous prestressed concrete cable–stayed bridges
span length: 100m + 200m + 100m
total width of deck: 10.3m
foundation: caisson type
pier: reinforced concrete with hollow section (height of 30m)
tower: framed type reinforced concrete (height of 52m)
deck : two–box prestressed concrete (height of 1.8m)
stay cable: double–plane, multi–cable (eleven), semi–harp system

As hysteretic damping augmentation devices, elasto–plastic shear bearings are adopted in this study. Combinations of support conditions treated here are summarized in Table 2. Location A and B show deck–abutment and deck–pier connection, respectively (Figure 2). Four different combinations are considered. Firstly, model 1 has rollers at the abutments and the deck is free on the piers. Model 2 has hysteretic–type bearing at deck–pier connections, while rollers are provided at deck–abutment connections. Model 3 has hysteretic–type bearings at abutments, while deck is free on the piers. Model 4 has hysteretic–type bearings at both deck–abutment and deck–pier connections.

All models are analysed by both elastic and elasto–plastic analyses. In elastic analysis 100 cm/sec^2 of maximum peak acceleration is used. For this acceleration all structural members and shearing spring remained within elastic region, therefore only first stiffness in hysteresis loop is used. The results are multiplied by 5 and shown in all figures to compare the results of elasto–plastic analysis conducted for 500 cm/sec^2 of maximum peak acceleration.

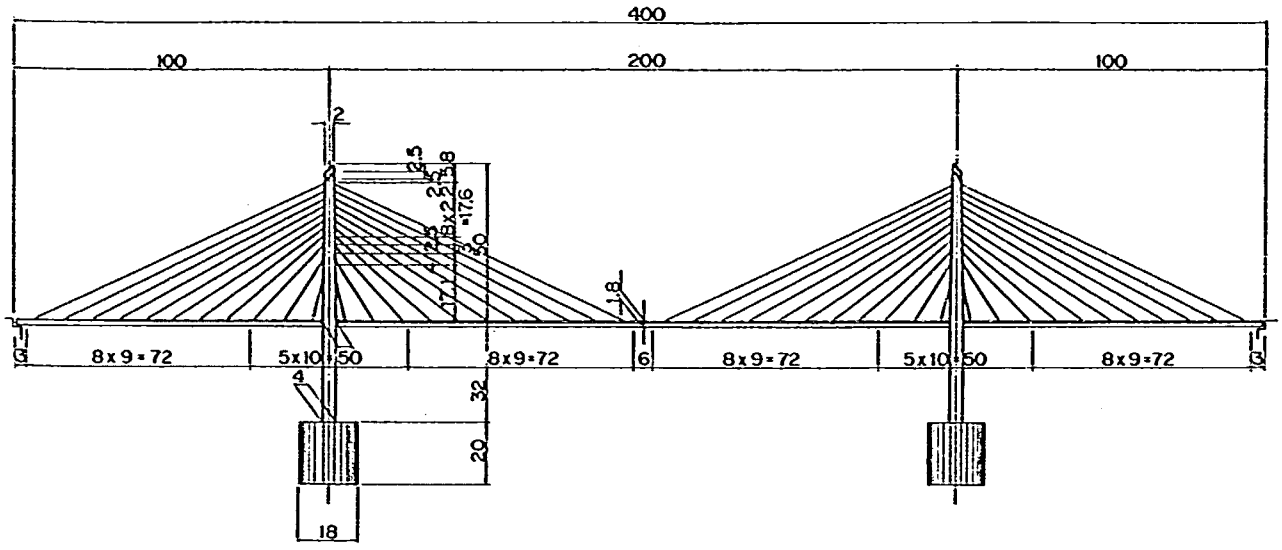
ANALYTICAL METHOD

Outline of Method

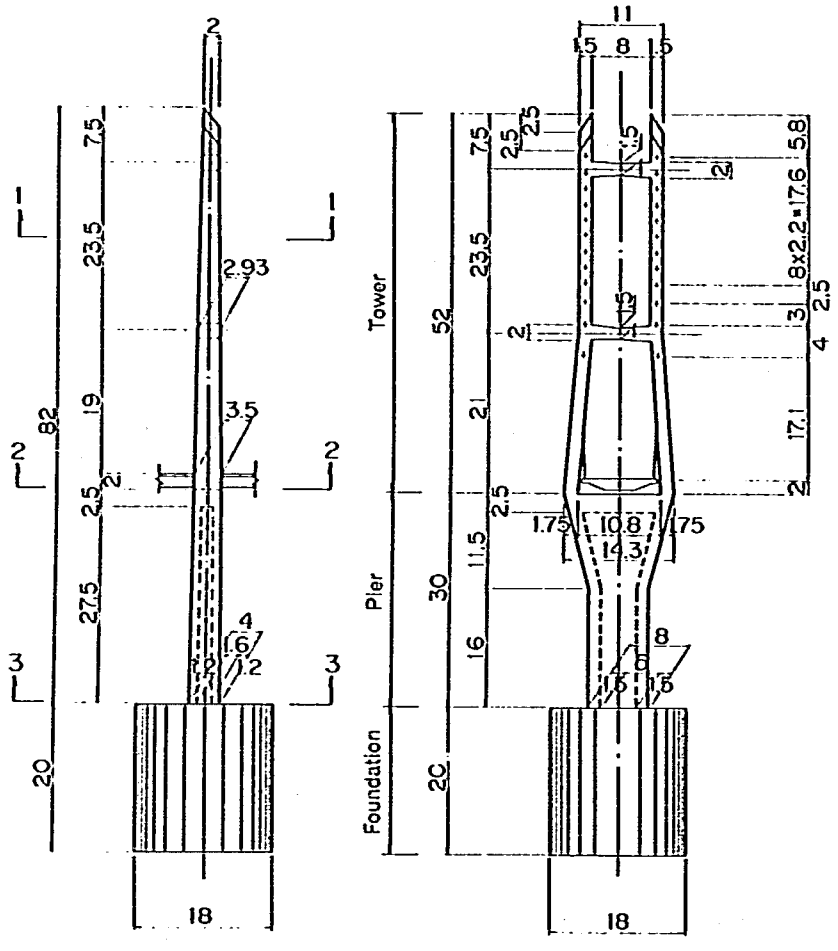
Direct integration method (Newmark β method) is used to solve the equation of dynamic equilibrium (1).

$$[M]\{\ddot{x}\}+[C]\{\dot{x}\}+[K]\{x\}+\{f\}=\{F\} \qquad \cdots\cdots\cdots(1)$$

Mass matrix $[M]$ is made using lumped mass modeling, and overall stiffness matrix $[K]$ is made assuming that the end of the element has non linear spring. Damping matrix $[C]$ is assumed to be Rayleigh type, therefore it is made from mass and stiffness matrices. The damping matrix is changed at the same time according to the change of the stiffness matrix. External force vector $\{F\}$ is assembled at each time period multiplied by earthquake wave. Vector $\{f\}$ is correction vector calculating the unbalanced stresses



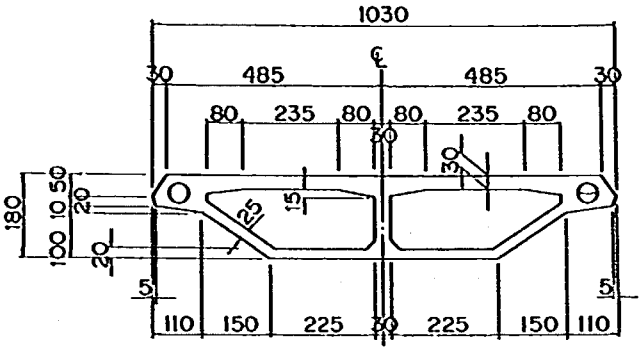
(a) Overall side view (unit: m)



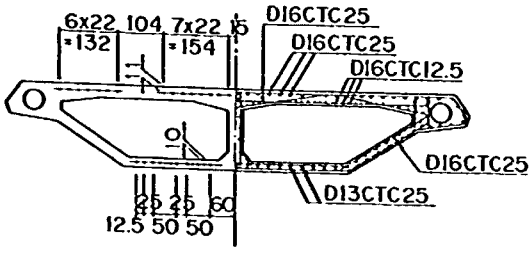
(b) Tower, pier and foundation (unit: m)

Figure 1 Structural model of prestressed concrete cable-stayed bridges (continned)

which occurs due to the changing of the stiffness and hysteretic property of members. The unbalanced stresses are harmonized by adding this vector to the term of external force vector at the next time step.

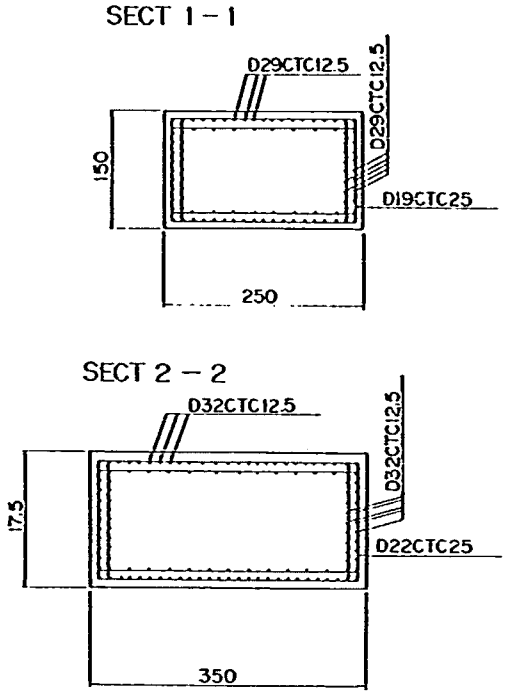


(c)Cross section of deck (unit: cm)

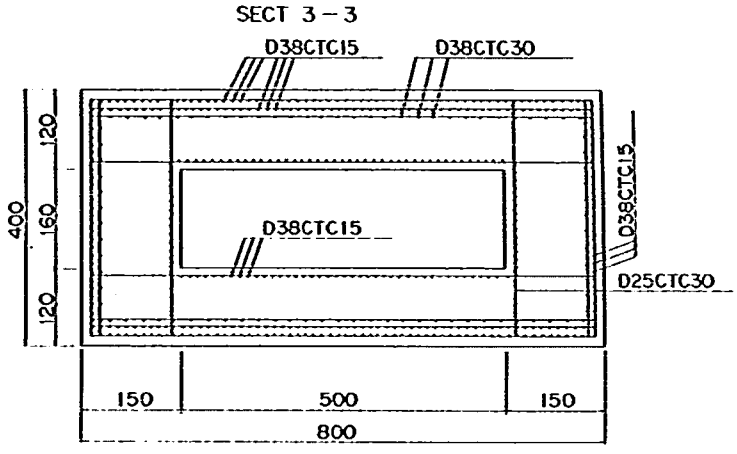


Prestressing bar Reinforcement bar

(d)Steel bar alignment in deck (unit: cm)



(e)Steel bar alignment in tower (unit: cm)

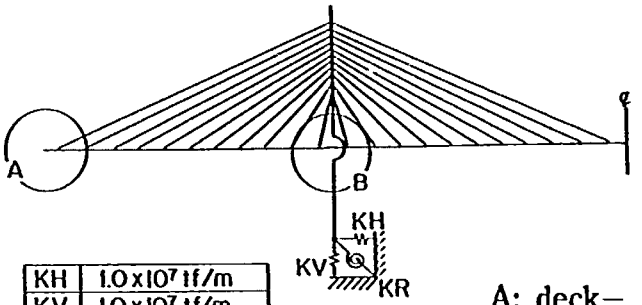


(f)Steel bar alignment in pier (unit: cm)

Figure 1 Structural model of prestressed concrete cable-stayed bridges

Table 1 Material property

Concrete	Deck : σ =400kg/cm^2	E=3.50× 10^{5}kg/cm^2
	Tower : σ =350kg/cm^2	E=3.25× 10^{5}kg/cm^2
	Pier : σ =270kg/cm^2	E=2.85× 10^{5}kg/cm^2
Reinforcedment	SD35	E=2.10× 10^{6}kg/cm^2
Prestressing bar	Stay cables : SWPR7B 12T15.2	E=2.00× 10^{6}kg/cm^2
	Deck : SBPR 95/120 ϕ32	E=2.00× 10^{6}kg/cm^2



KH	1.0x10⁷ tf/m
KV	1.0x10⁷ tf/m
KR	1.0x10⁹ tf·m/rad

A: deck– abutment connection
B: deck– pier connection

Figure 2 Locations of connections and spring of foundation

Table 2 Combination of bearing

Model	Location of Connection		National period of vibration (sec)
	A	B	
1	roller	free	4.484
2	roller	hysteretic–type bearing	2.786
3	hysteretic–type bearing	free	2.584
4	hysteretic–type bearing	hysteretic–type bearing	2.451

Hysteretic Property of Members

Figure 3 shows Degrading Tri–linear type hysteretic property adopted to the nonlinear structural members in this study. The slope in unloading process Kd is determined by equation (2), in which stiffness degrading coefficient γ is assumed to be 0.4 for all structural members in this study.

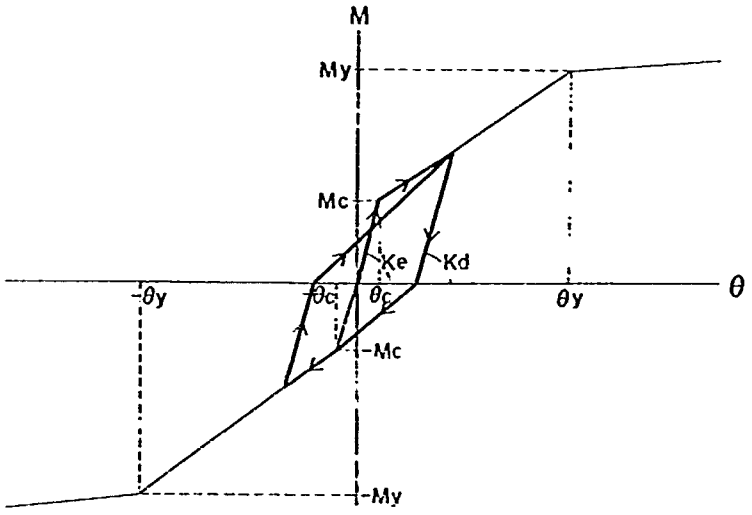
$$Kd=Ke\left|\frac{\pm\theta_{max}}{\theta_c}\right|^{-\gamma} \qquad \cdots\cdots\cdots\cdots(2)$$

in which Ke is initial slope, θ_c is rotation angle when cracksterts, θ_{max} is rotation angle when unloading starts.

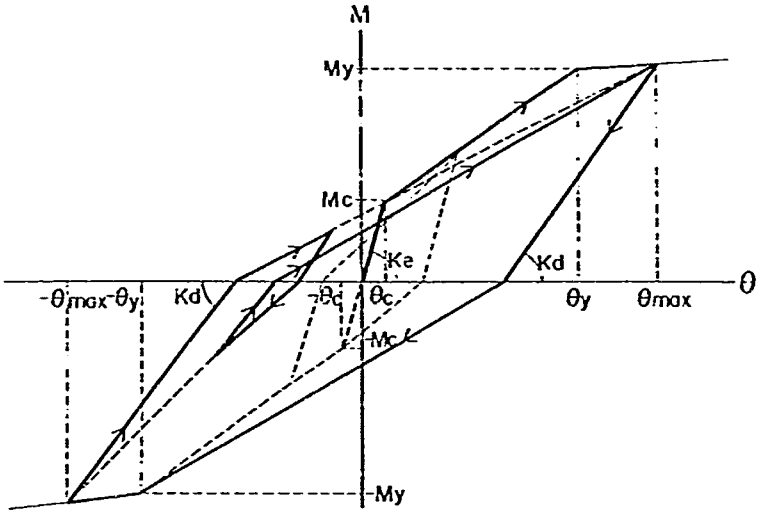
Outline of hysteretic property of structural members are as follows.

(1) Crack starting bending moment (*Mc*)

Crack is defined to start at the time bending tensile stress at the end fiber of member reaches to the concrete tensile strength.



(a) in case of $M<My$



(b) in case of $M>My$

Figure 3 Restoring force characteristics of Degrading Tri-linear type

(2) Reinforcement yielding bending moment (My)

Using the stress-strain curve for concrete and reinforcement bar shown in Figure 4, the moment reinforcement starts to yield is calculated.

(3) Ultimate bending moment(Mu)

Mu is defined as the ultimate moment in which maximum strain reaches to ultimate concrete strain $\varepsilon c=0.0035$. In this study the second stiffness of reinforcement bar after the yielding is assumed to be $\alpha 3Ke$, in which $\alpha 3=0.001$ and Ke is the initial stiffness.

(4) Rigid plastic spring of member end

$M-\theta$ relation at member end is expressed by considering both property of structural member and rotational characteristic of end springs shown in Figure 5. Ductility ratio μ is defined as shown in equation (3) using rotation angle of end spring of element.

$$\mu = \theta max / \theta y \qquad \text{.....(3)}$$

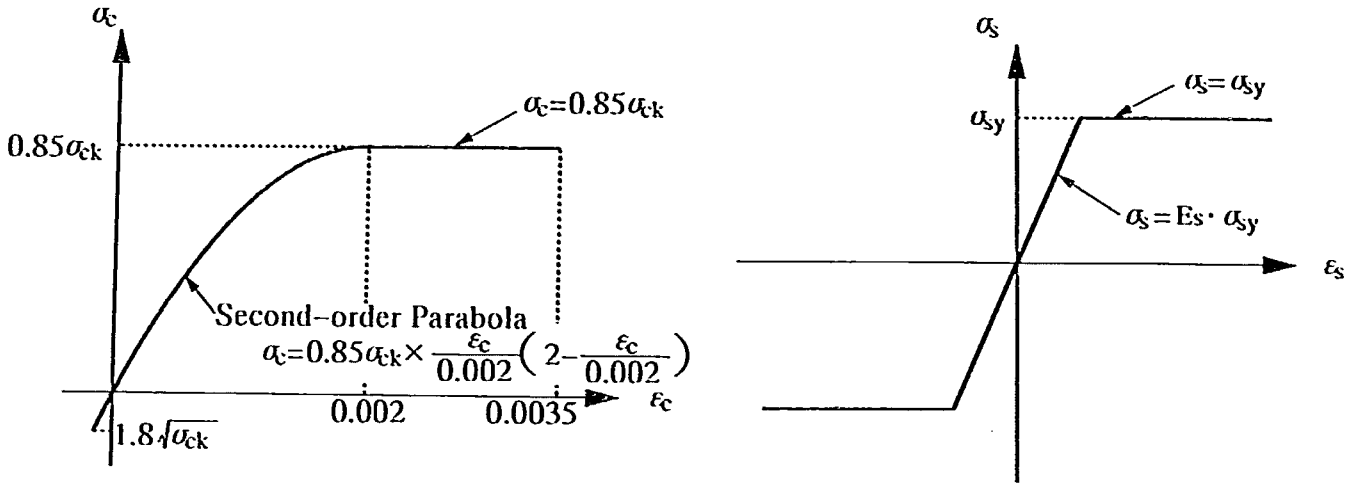


Figure 4 Stress–strain curve for concrete and reinforcement bar

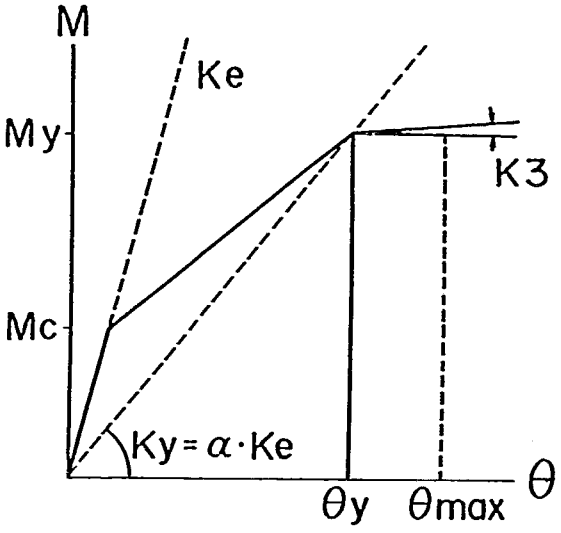


Figure 5 $M-\theta$ relation at member end

(5) Skelton of structural member

Skelton curves of structural member are illustrated in **Figure 6.** Pier and tower are divided into 8 and 11 different elements respectively. Deck is assumed to have the same cross section along the whole length of the bridge. Skelton curves are determined at the beginning of the numerical calculation, and assumed not to be changeable during the seismic excitation. Stay–cable is defined as elastic truss element because of considering the prestressing in the cable.

(6) Load–deflection relationship and skelton of shear bearing

The hysteretic property of shear bearing is assumed to be bilinear type as shown in **Figure 7(a),** hence the skelton curve is determined such as **Figure 7(b).** The shear bearing has initial stiffness of 20 t/cm, and after the relative displacement beyonds 3.5 cm the second stiffness decrease to twentieth of initial stiffness.

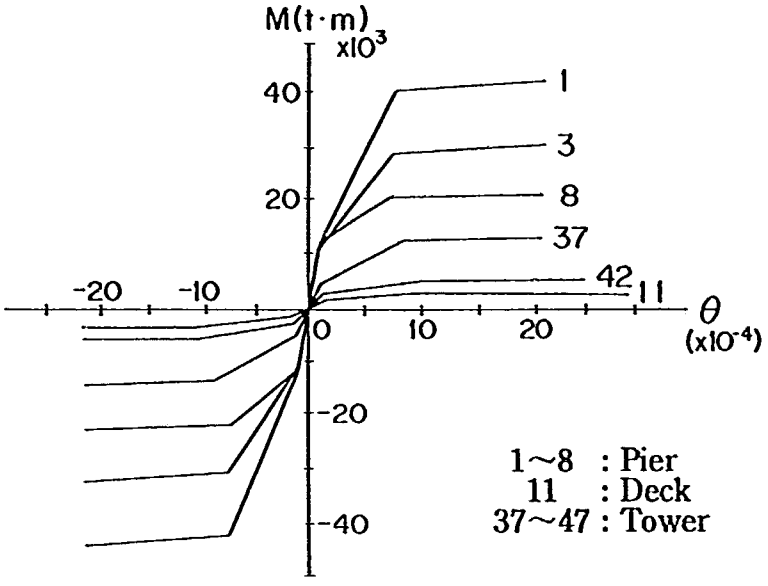
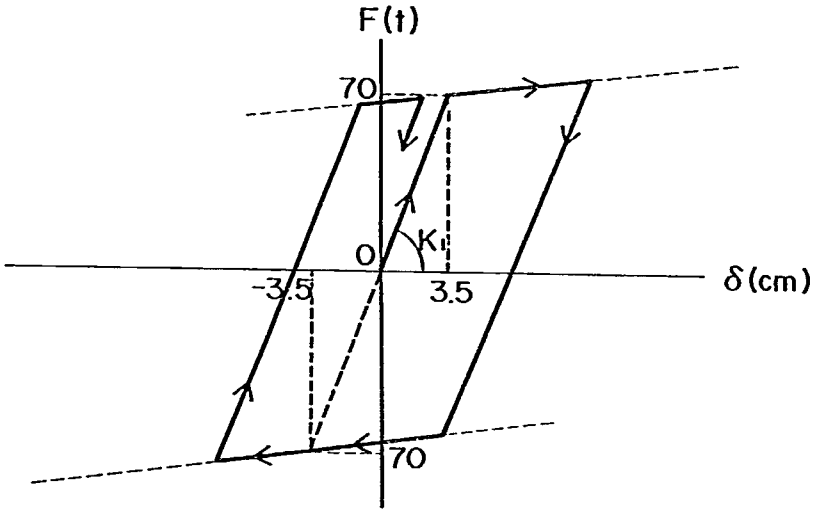
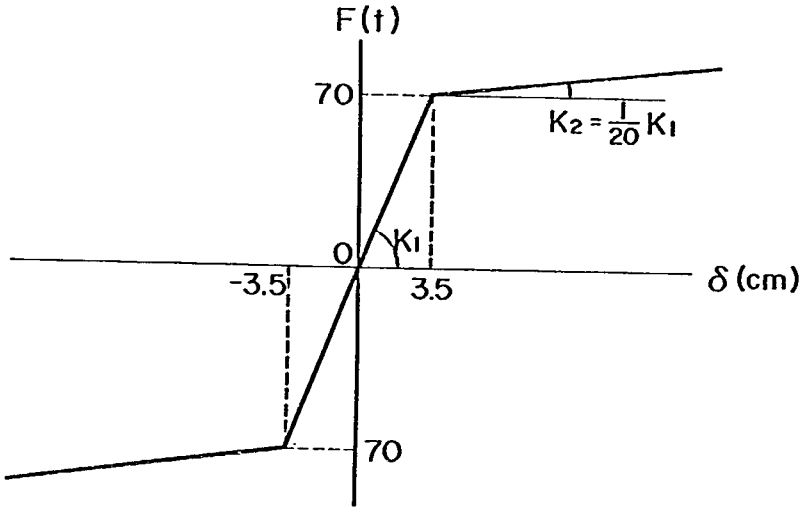


Figure 6 Skelton curves of structural member



(a) Hysteretic property



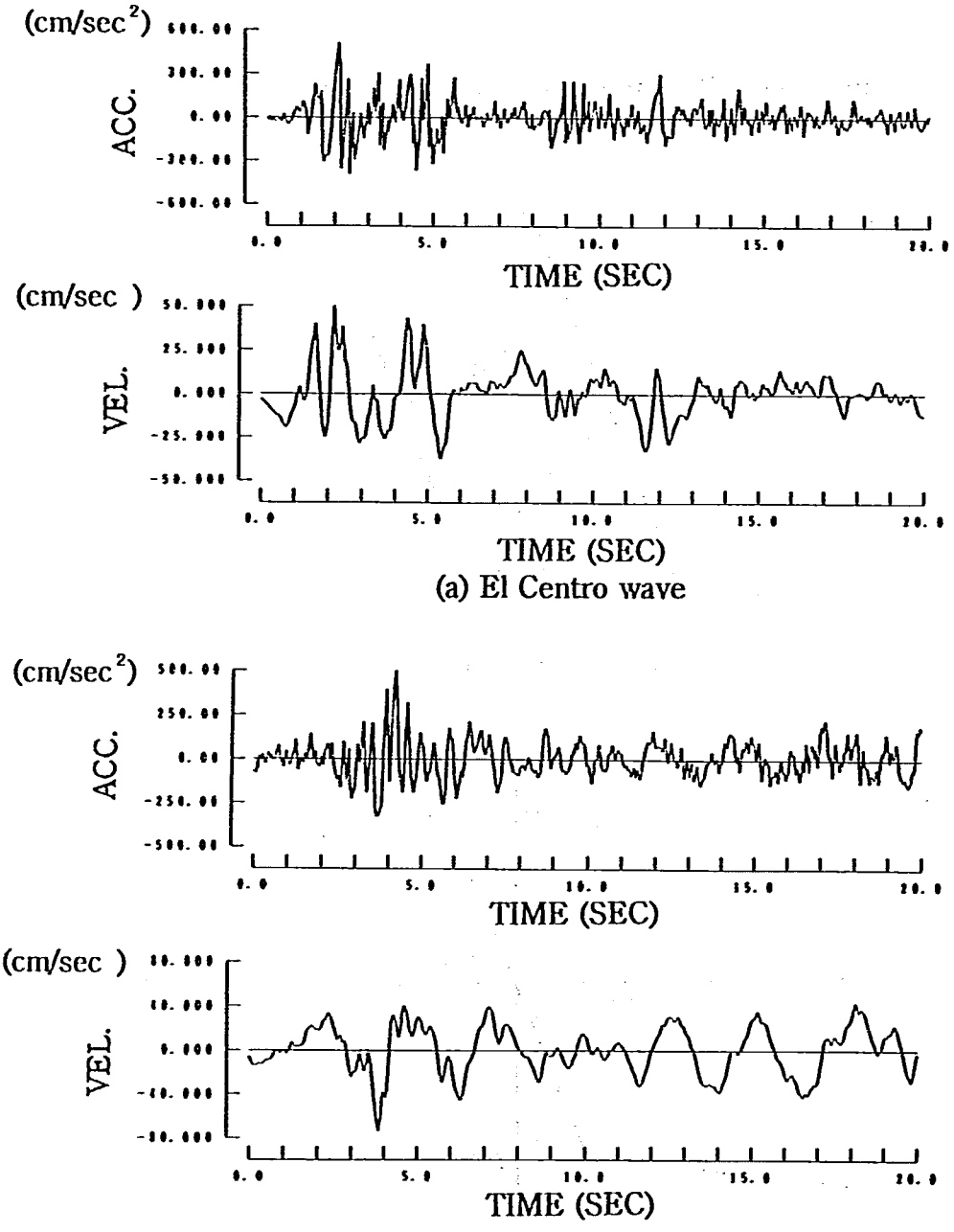
(b) Skelton curve

Figure 7 Hysteretic property and skelton curve of shear bearing

CONDITION AND CASE OF ANALYSIS

Damping assumed to be produced by inner viscosity. Damping ratio is 0.05 for elastic response analysis, while 0.02 of damping ratio is adopted for elasto–plastic analysis considering hysteretic damping effect.

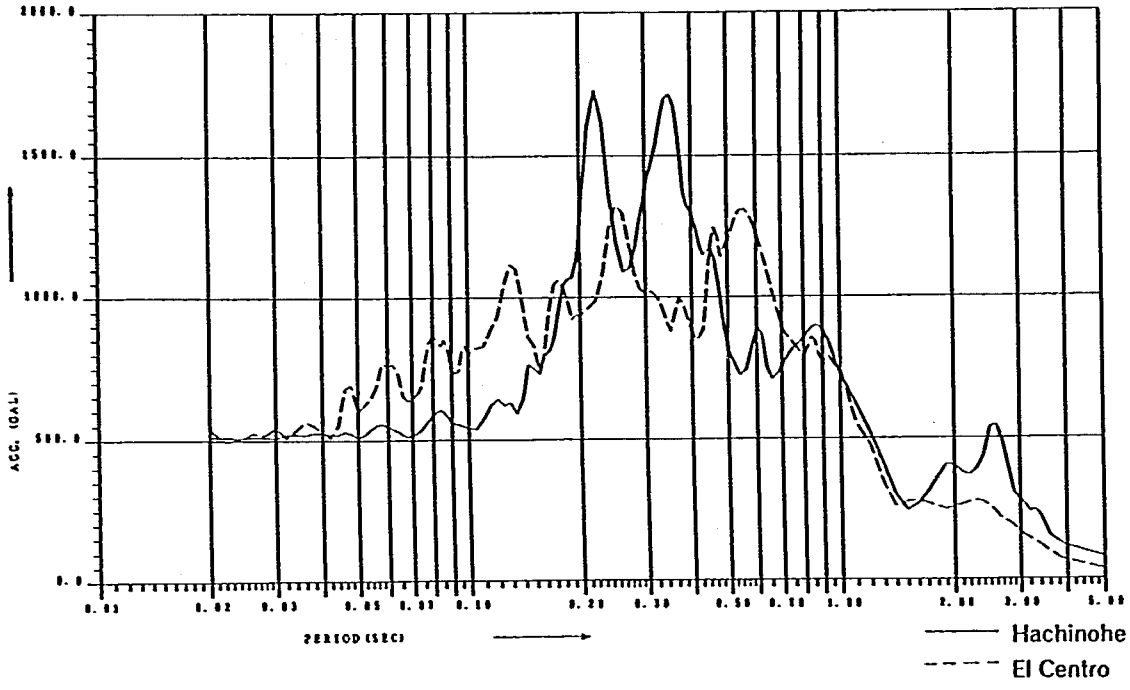
Seismic motions used in this analysis are El Centro NS wave of the 1940 Imperial Valley earthquake and Hachinohe NS wave of the 1968 Tokachi–oki earthquake. The peak acceleration are standardized to 500 cm/sec^2. At this level, El Centro wave has 48.8 cm/sec peak velocity, and Hachinohe wave has 74.8 cm/sec peak velocity. Therefore Hachinohe wave is larger than El Centro wave in energy aspect. Accelerograms and acceleration response spectra for both waves are shown in Figure 8 and 9 respectively.



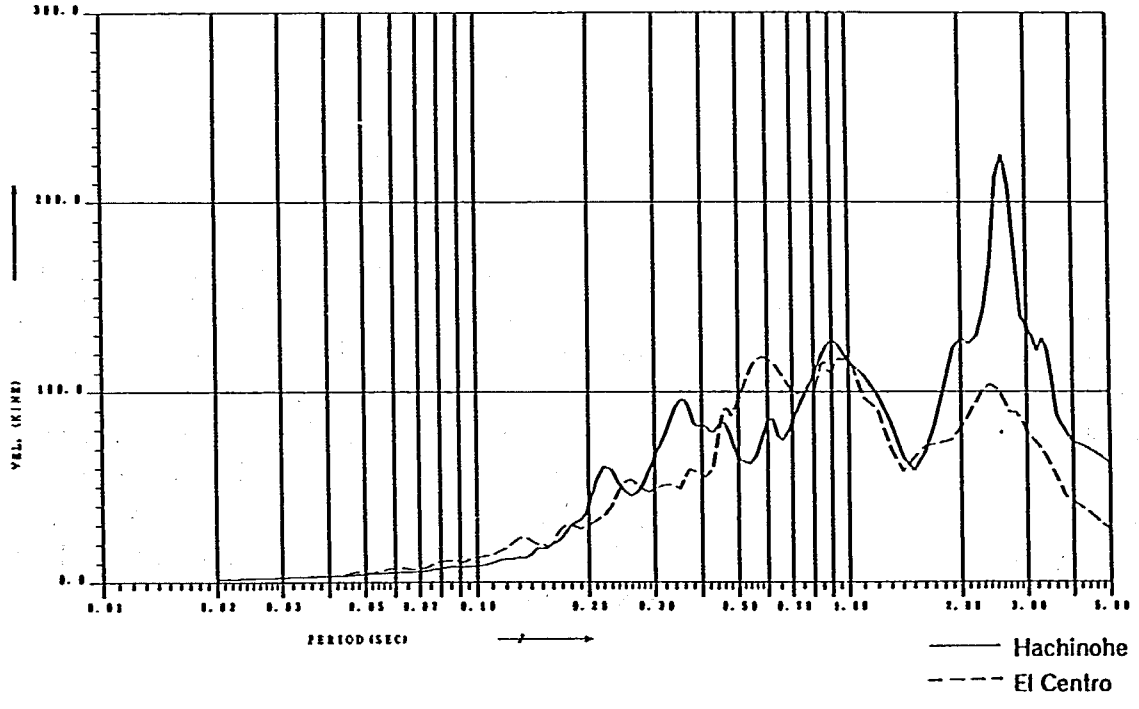
(a) El Centro wave

(b) Hachinohe wave

Figure 8. Accelerograms and velocity of El Centro and Hachinohe waves



(a) Acceleration response spectra



(b) Velocity response spectra

Figure 9 Acceleration and velocity response spectra

Time step for analysis is 0.01 second, and dynamic analysis is conducted for 12 seconds. Table 3 shows structural types, analytical methods, seismic motions, and case symbols used here. Four different structural types above mentioned, two different analytical methods: namely elastic and elasto–plastic analyses, and two different ground motion records are compared. Therefore total number of analytical case becomes 16.

Table 3 Structural types, analytical methods, seismic motions and case symbols

Structural type	Analytical Method	Seismic Motion	Case Symbol
Model–1	Elasticity	El Centro	M1EL–E
		Hachinohe	M1EL–H
	Elasto–Plasticity	El Centro	M1PL–E
		Hachinohe	M1PL–H
Model–2	Elasticity	El Centro	M2EL–E
		Hachinohe	M2EL–H
	Elasto–Plasticity	El Centro	M2PL–E
		Hachinohe	M2PL–H
Model–3	Elasticity	El Centro	M3EL–E
		Hachinohe	M3EL–H
	Elasto–Plasticity	El Centro	M3PL–E
		Hachinohe	M3PL–H
Model–4	Elasticity	El Centro	M4EL–E
		Hachinohe	M4EL–H
	Elasto–Plasticity	El Centro	M4PL–E
		Hachinohe	M4PL–H

RESULTS AND DISCUSSIONS

Natural periods and modes

Natural periods of vibration and corresponding natural modes are obtained by igenvalue analysis. **Table 4** shows natural periods until tenth mode for all models, and **Figure 10** shows natural modes until sixth for model 4. First and third modes are horizontal mode of deck and towers for all models, therefore the difference of natural periods among four models is noticeable. To put it more concretely, in first mode natural period of model 4 decrease to 55 percent of model 1. In third mode, only model three has different property. The natural period of model 3 decrease to about 76 percent of others. Other modes until tenth, except first and third modes, has almost same natural periods, because shear bearing has no effect on vertical vibration mode of the bridge.

Response time histories

Examples of hysteresis loops of concrete deck (nodal point 25) and shear bearing are shown in **Figure 11** for Hachinohe wave (peak acceleration of 800 cm/sec^2).

Nodal point number is indicated in **Figure 12.**

Figure 13 compares time histories of shear forces of shear bearing for model 2, 3, and 4. Top figure is plotted for elastic response, and bottom is plotted for elasto–plastic response. Shear forces in elasto–plastic analysis decrease and period of vibration becomes longer due to the hysteretic damping of bearing.

Table 4 Natural periods until tenth mode for all models

(sec)

Mode	Model 1	Model 2	Model 3	Model 4
1	4.484	2.786	2.584	2.415
2	2.358	2.331	2.342	2.358
3	1.592	1.590	1.203	1.575
4	0.999	0.994	0.996	0.999
5	0.824	0.824	0.824	0.824
6	0.697	0.693	0.695	0.697
7	0.579	0.572	0.575	0.579
8	0.504	0.501	0.503	0.504
9	0.459	0.459	0.459	0.459
10	0.417	0.413	0.415	0.417

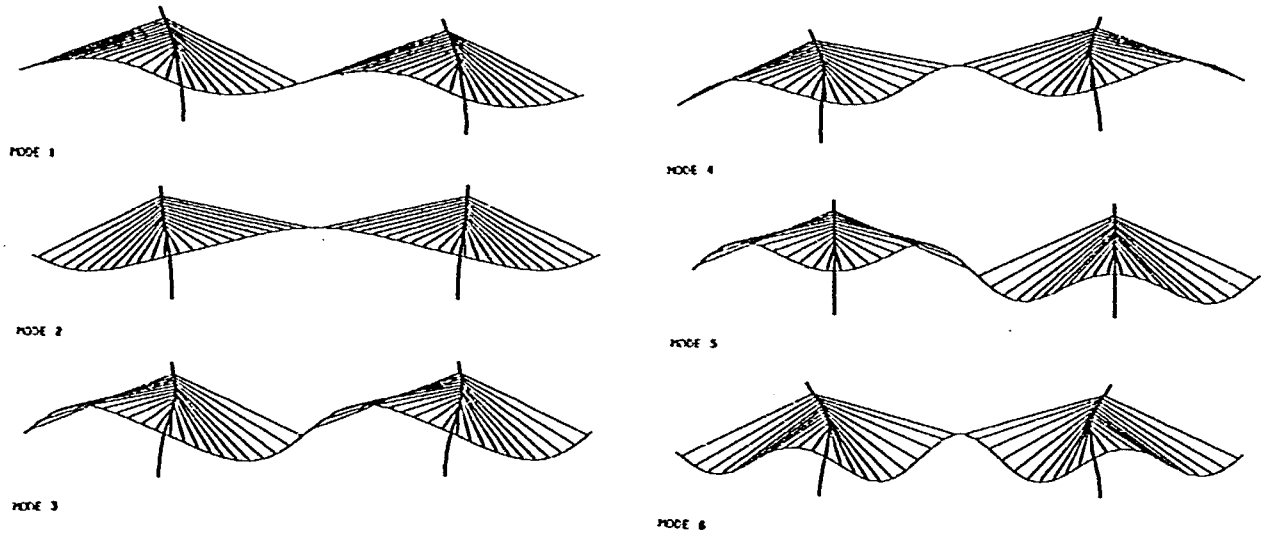
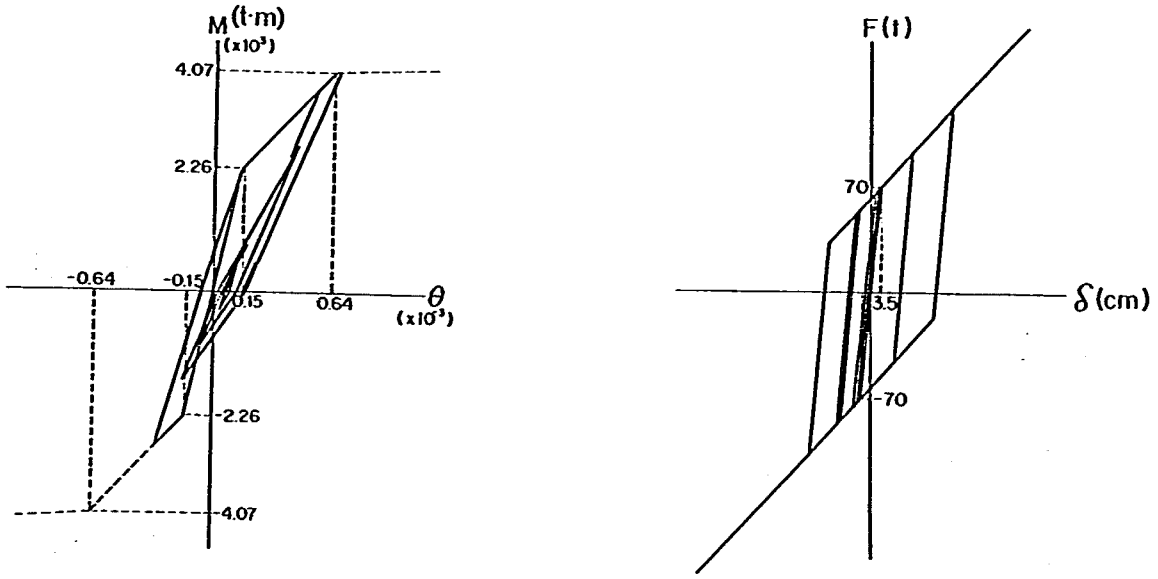


Figure 10 Natural modes until sixth for model 4



(a)Concrete deck NP.25 (b)Shear bearing

Figure 11 Examples of hysteresis loops

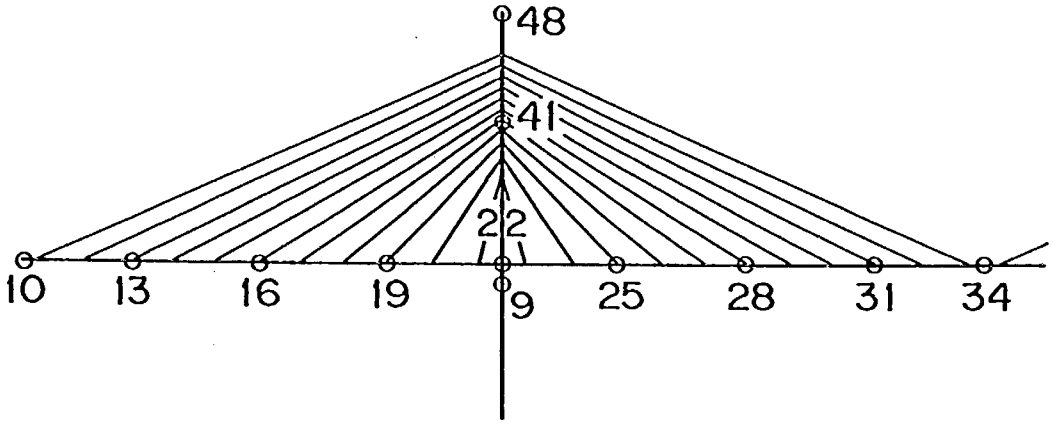
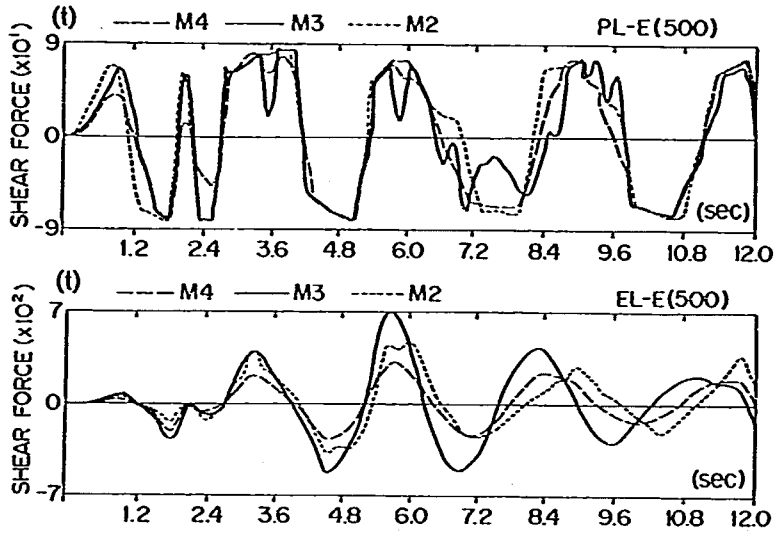


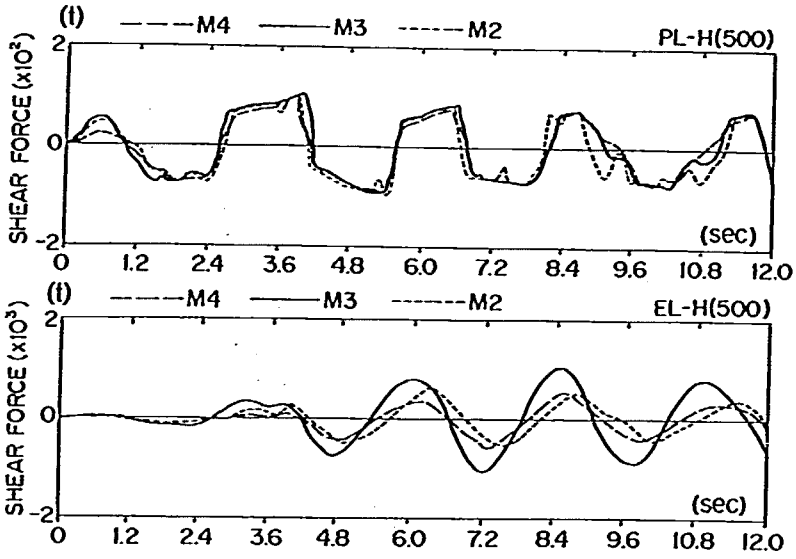
Figure 12 Numbering of nodal points of model



TOP : Elasto–plastic response

BOTTOM : Elastic response

(a) El Centro wave



TOP : Elasto–plastic response

BOTTOM : Elastic response

(b) Hachonohe wave

Figure 13 Time histories of shear forces of shear bearing

Time histories of horizontal displacements at the top of the tower (NP 48) and at the mid point of the deck in the center span (NP34), and vertical displacements at the deck in side span (NP19) are plotted in **Figure 14**. According to this figure it is very clear that, in elasto–plastic analysis, amplitudes of displacements decrease rapidly after the first period in all models, although in elastic analysis the amplitude reaches maximum at third period of vibration.

Seismic–induced maximum forces and displacements

(1) Response property of each model

Figure 15 shows maximum displacements and forces for all models subjected to El Centro and Hachinohe wave. **Figure 16** shows the distribution of these values along member axes for model 1 and 4. From these figures following consideration can be pointed out.

In the case of elastic analysis, maximum displacements and maximum axial forces of the deck in the model 3 is largest, and these decrease in the order of model 4, 2 and 1 for both earthquakes. Maximum bending moment of pier is largest in the model 2, and smallest in the model 1 among four models for both earthquakes. Therefore in the case of small earthquake and elastic behaviour, model 1 having longest first natural period has smallest seismic response. In other words, we may say that model 1 is most efficient supporting system for cable–stayed bridges.

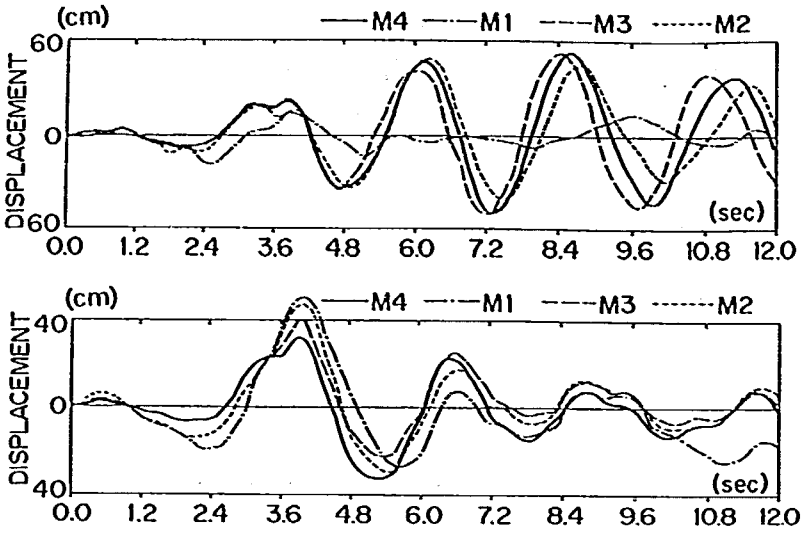
In the case of elasto–plastic analysis, maximum horizontal displacements becomes smaller in the order of model 1, 2, 3 and 4 for both earthquakes. Therefore effectiveness of shear bearing on decreasing maximum displacements is obvious. On the other hand maximum moment of piers in model 4 is smaller than that in model 1 for Hachinohe wave, but for El Centro wave model 4 produces largest maximum moment among four models. Therefore we cannot say that the seismic induced maximum forces in model 4 always become smallest among four models.

We may conclude at least that the object to decrease the horizontal displacement of deck would be accomplished by the shear bearing. Since the seismic induced response varies according to the hysteretic property of shear bearing, parametric study is necessary to find optimum selection of shear bearing.

(2) Difference between elastic and elasto–plastic analyses

Figure 17 shows maximum displacements and forces calculated by elastic and elasto–plastic analyses for model 1 and 4. **Figure 18** shows the distribution of these values along member axes for model 4. From these figures following points can be summarized.

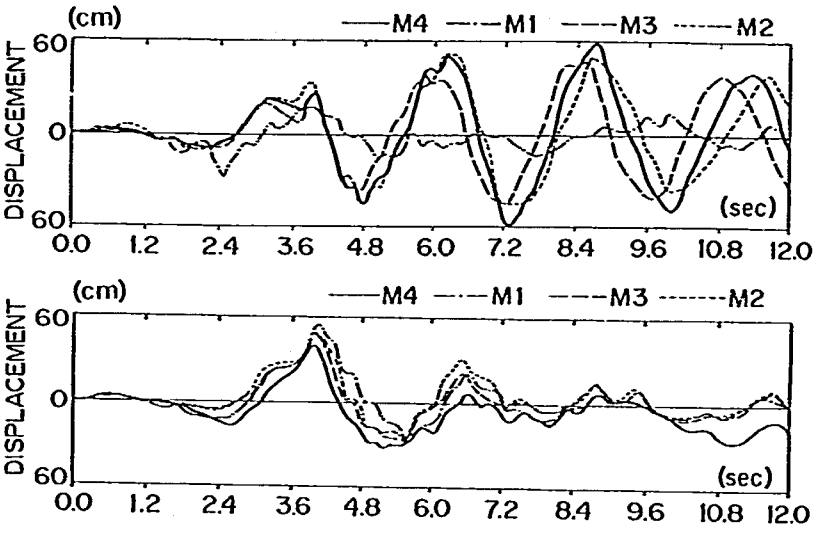
In model 1 the difference of response between two analyses is small. Especially horizontal displacements are almost same, and the difference of forces is also very small. This reason is that model 1 has no shear bearing, therefore the difference of response comes from only material properties of structural members. In addition to that the few structural members yield for maximum acceleration of 500 cm/sec^2.



TOP : Elastic response

BOTTOM : Elasto−plastic response

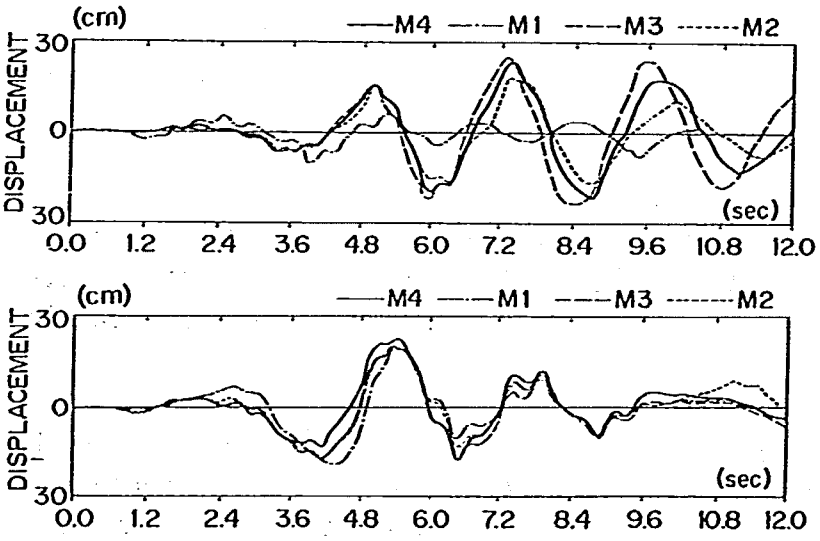
(a) Horizontal displacement (NP.48)



TOP : Elastic response

BOTTOM : Elasto−plastic response

(b) Horizontal displacement (NP.34)



TOP : Elastic response

BOTTOM : Elasto−plastic response

(c) Vertical displacement (NP.19)

Figure 14 Time histories of displacements

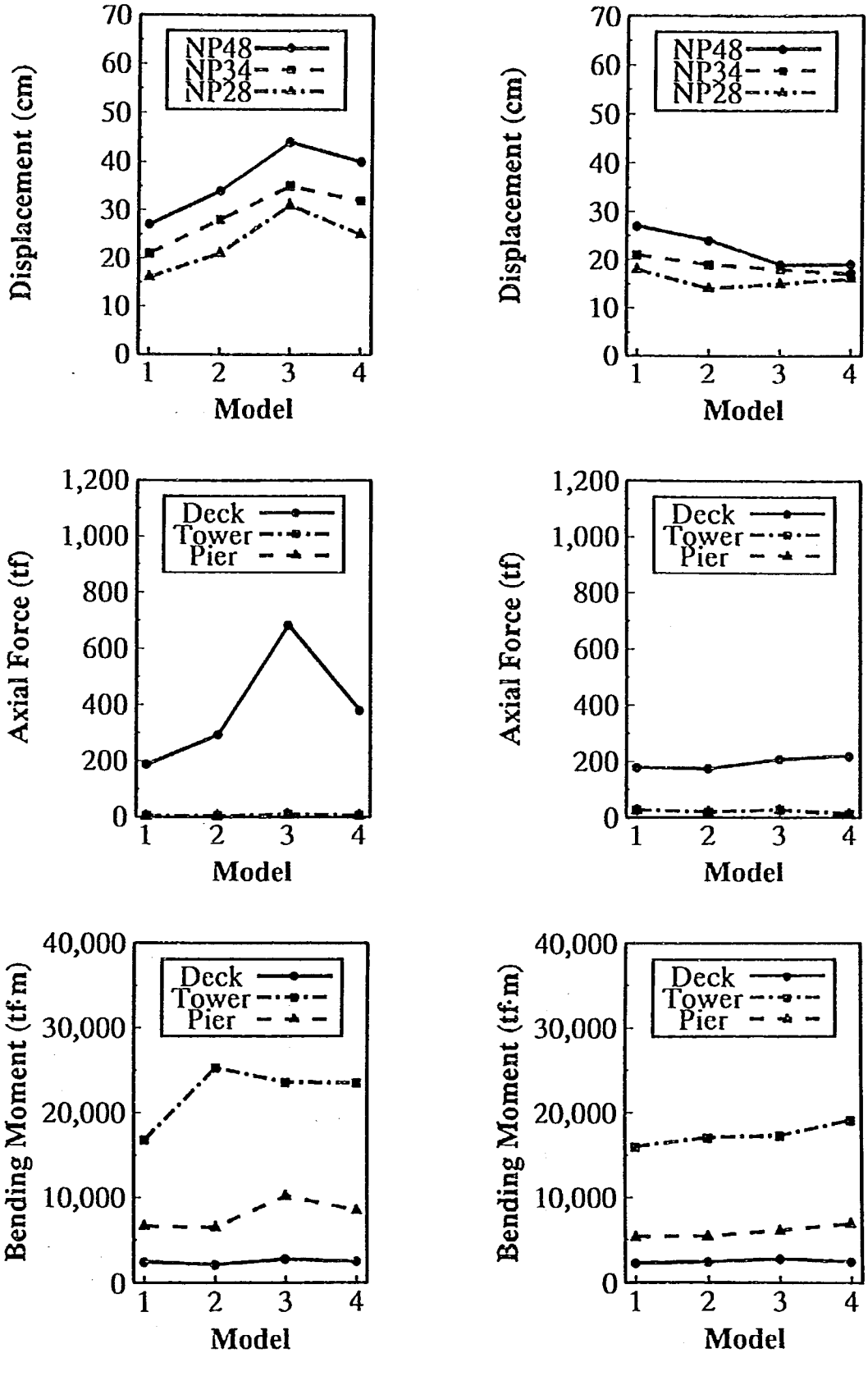
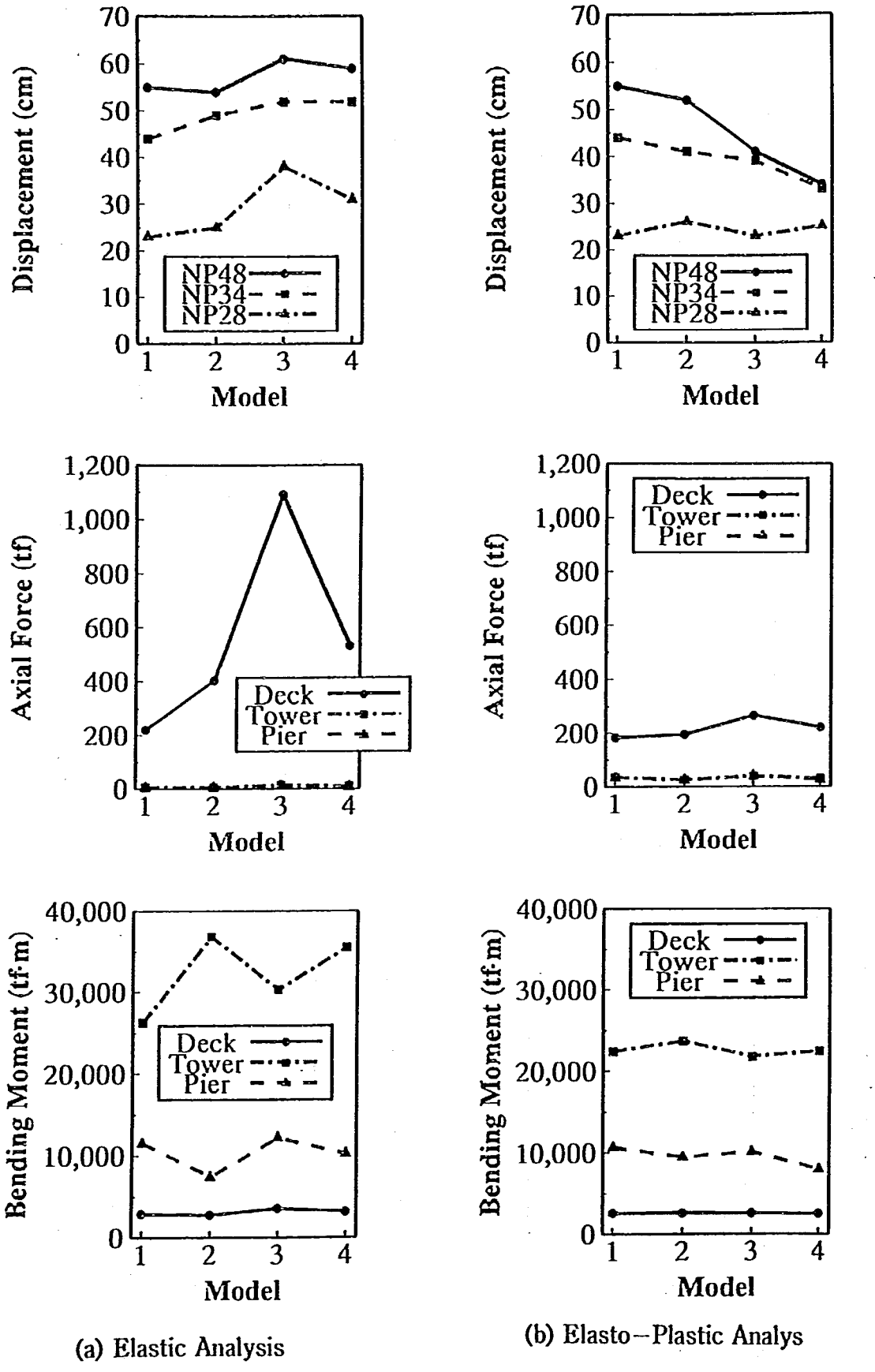


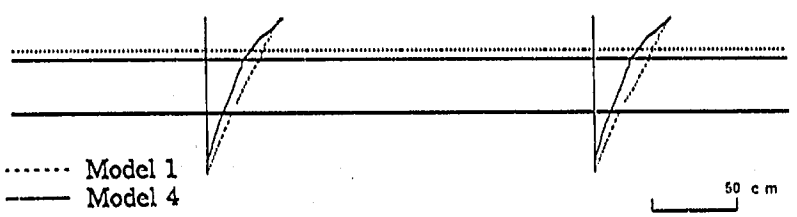
Figure 15–1 Difference of maximum response among four models (El Centro wave)



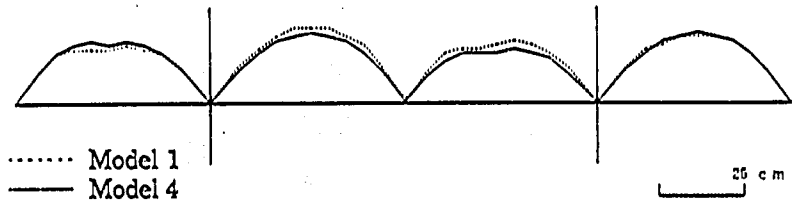
(a) Elastic Analysis

(b) Elasto−Plastic Analys

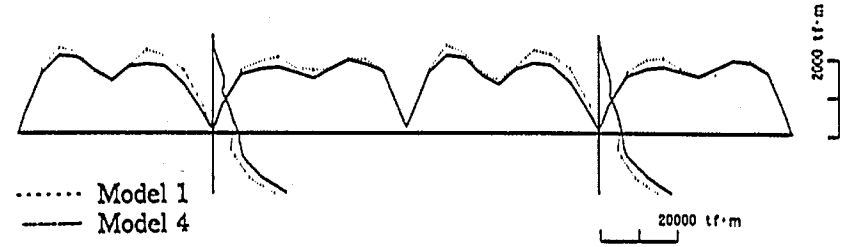
Figure 15−2 Difference of maximum response among four models (Hachinohe wave)



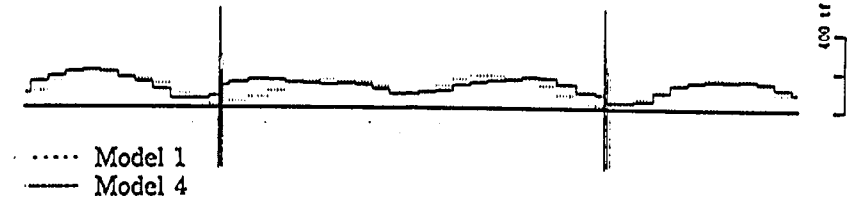
(1) Horizontal displacement



(2) Vertical displacement

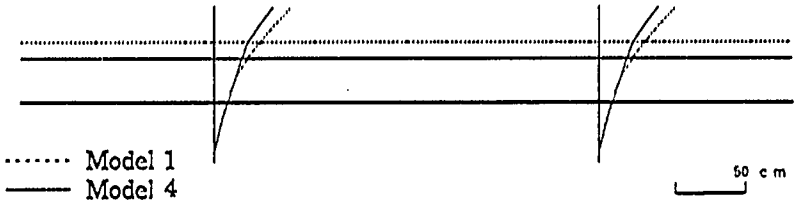


(3) Bending moment

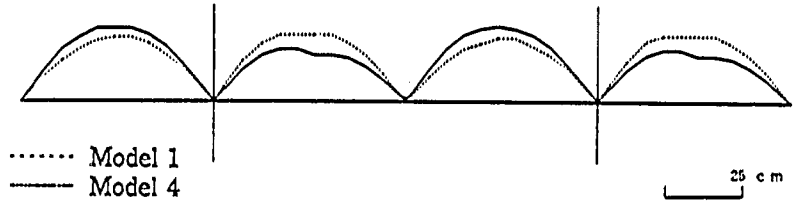


(4) Axial force

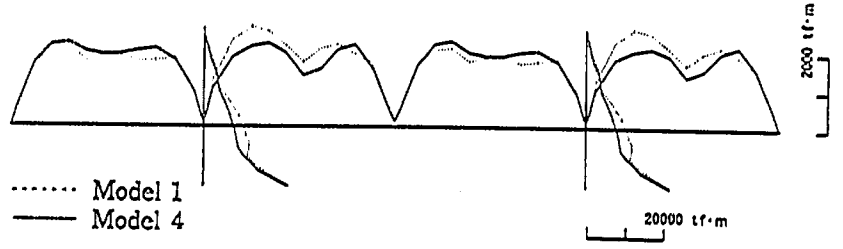
(a) El Centro wave



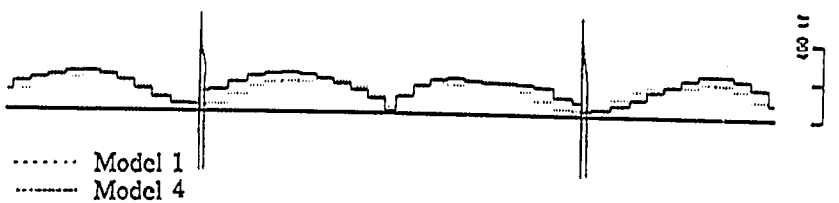
(1) Horizontal displacement



(2) Vertical displacement



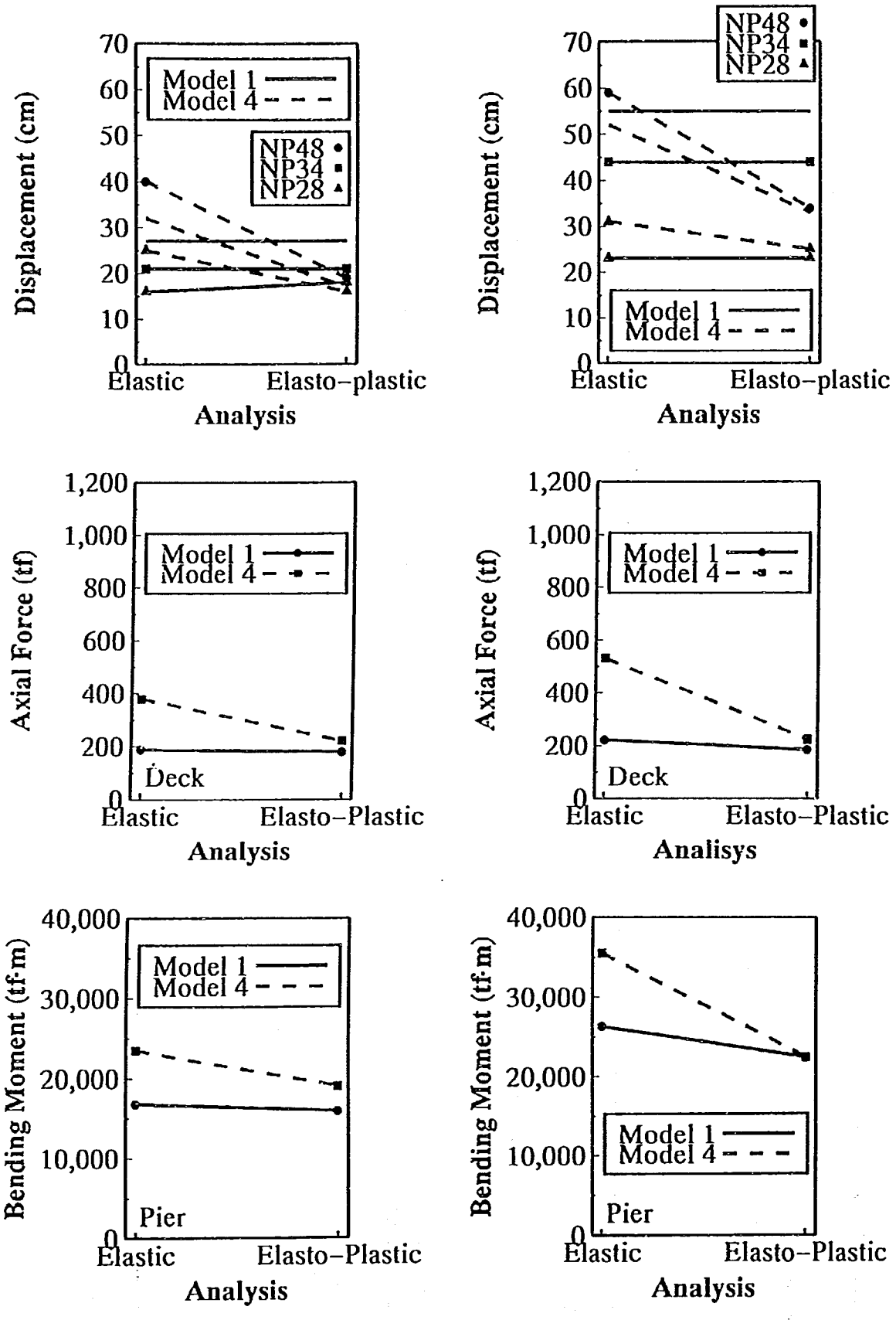
(3) Bending moment



(4) Axial force

(b) Hachinohe wave

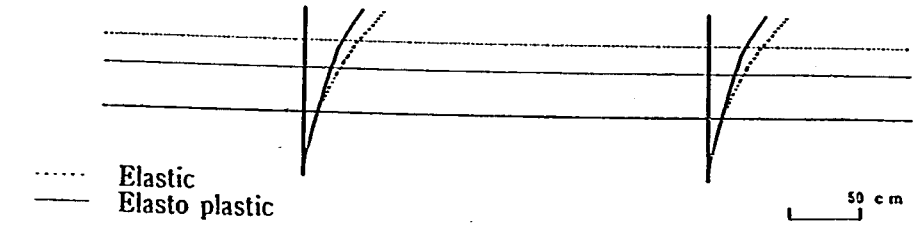
Figure 16 Comparison between model 1 and 4 for displacements, moments and axial forces analysed by elasto−plastic analysis



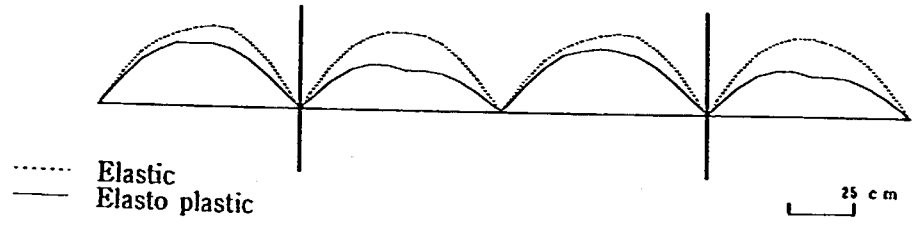
(a) El Centro wave

(b) Hachinohe wave

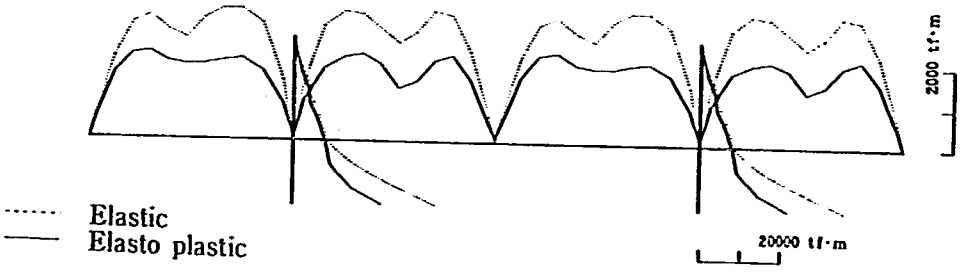
Figure 17 Difference of response between two analyses



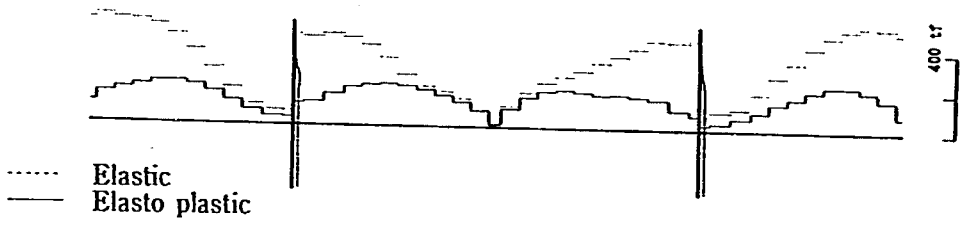
(1) Horizontal displacement



(2) Vertical displacement



(3) Bending moment



(4) Axial force

Figure 18 Comparison between elastic and elasto-plastic analyses (model 4. Hachinohe wave)

In model 4 the response of elasto-plastic analysis is rather smaller than that of elastic analysis, because the energy is absorbed by the hysteretic damping of shear bearing. Therefore it is clear the effectiveness of shear bearing.

(3) Difference due to seismic waves

Figure 19 shows maximum displacements and forces for model 1 and 4 subjected to El Centro and Hachinohe wave. **Figure 20** shows the distribution of these values along member axes for model 4. From these figures following remarks can be pointed out:

Both displacements and forces due to Hachinohe wave is larger than those due to El Centro wave. It may come from that Hachinohe wave has larger peak velocity than El Centro wave.

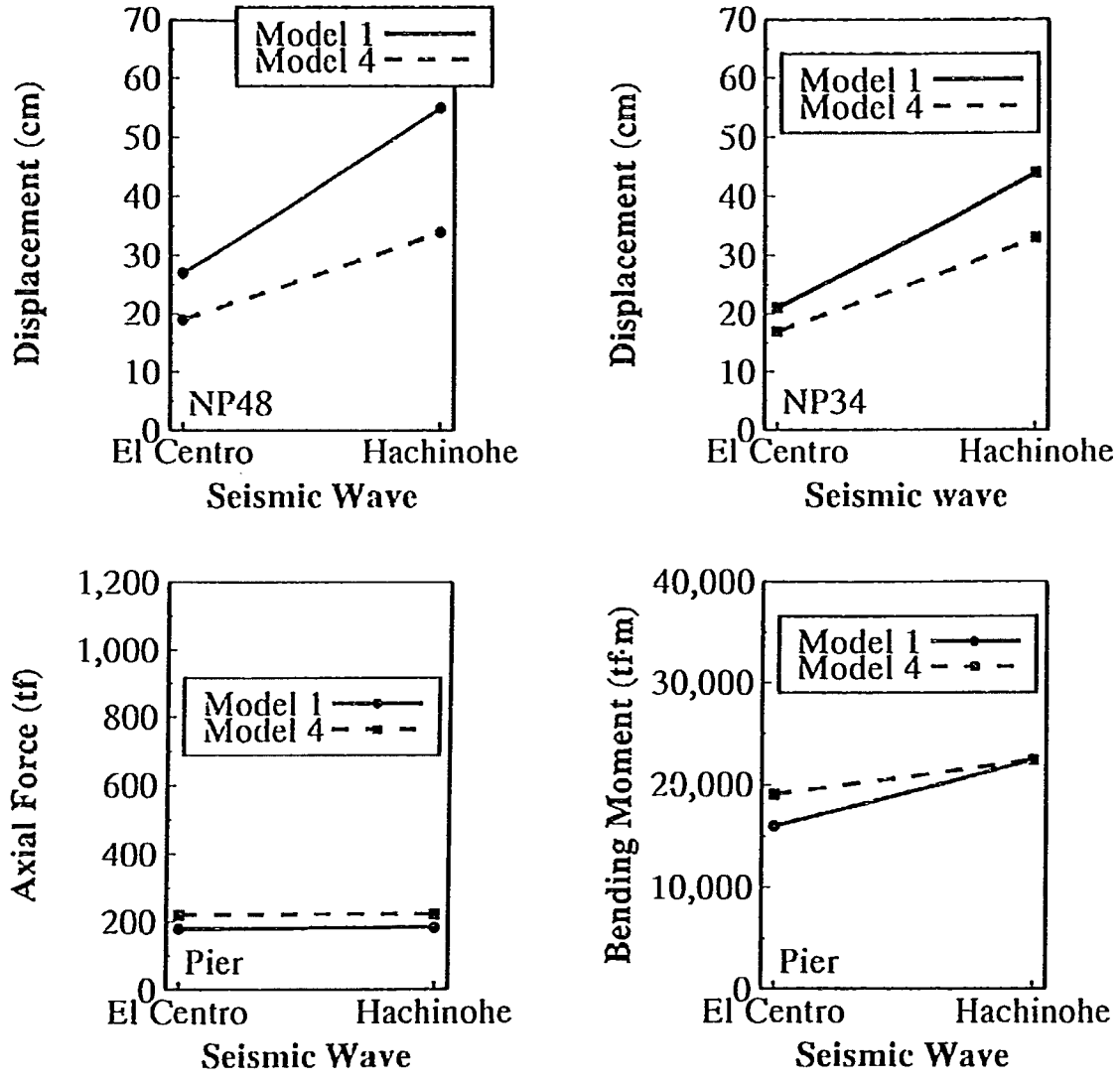


Figure 19 Difference of response between two seismic waves

The difference of displacements and bending moments due to two seismic waves in model 1 are larger than in model 4. To put it more precisely, response ratio of two waves in model 1 is about 2, but in model 4 the ratio becomes about 1.5. Therefore, here, we notice that cable–stay bridges with shear bearings is less sensitive for difference of seismic waves than bridges without shear bearings.

Crack of concrete and yielding of reinforcement

Crack distribution of members in model 1 and 4 for two seismic waves with peak acceleration of 500 cm/s^2 are shown in **Figure 21**. When the same seismic motion hits the different models, there is not big difference in the order of crack occurrence. But different seismic motions hit the same model, the order, locations, and range of crack occurrence are different. The order of crack occurrence subjected to Hachinohe and El Centro wave are as follows:

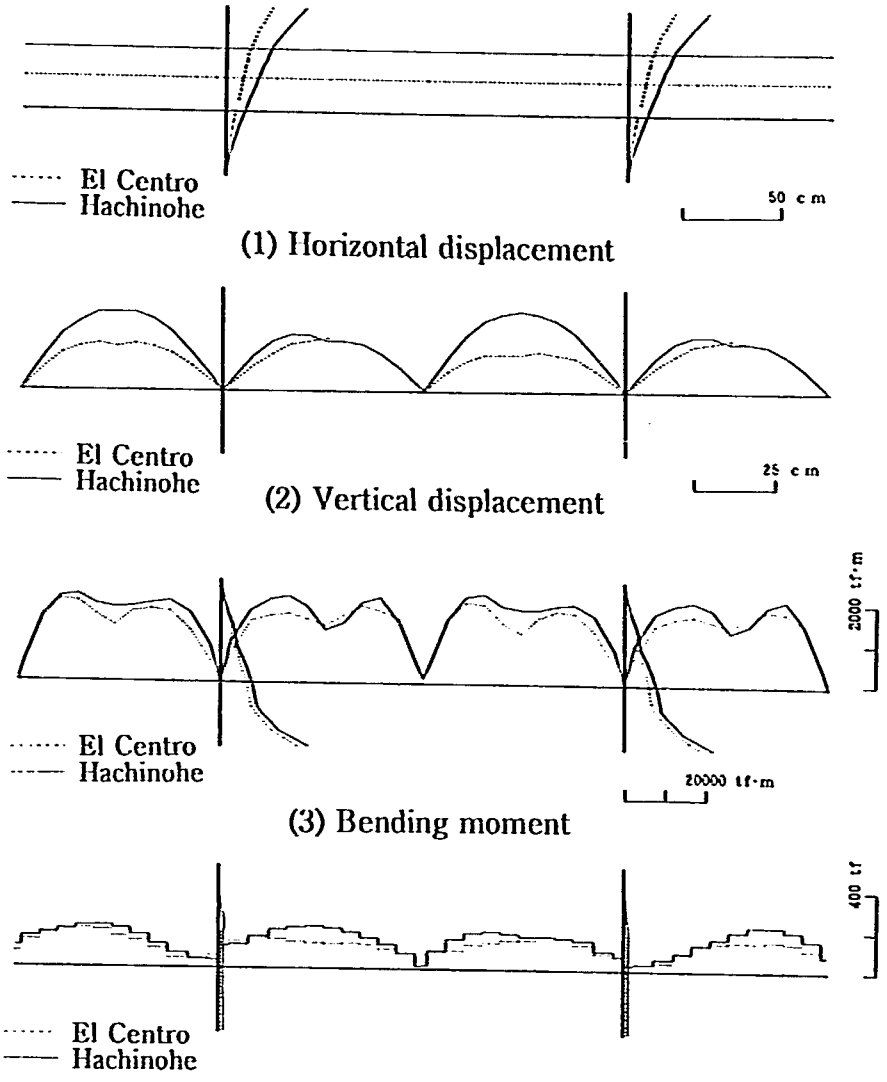


Figure 20 Comparison between El Centro and Hachinohe wave (Model 4, Elasto–plastic analysis)

Hachinohe wave:

bottom of pier → bottom of tower → deck → mid part of tower

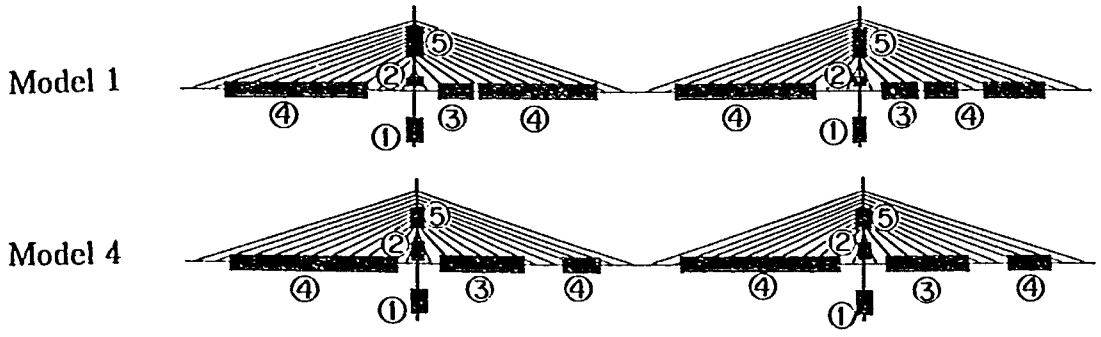
El Centro wave:

bottom of pier → deck → bottom of tower → deck → mid part of tower

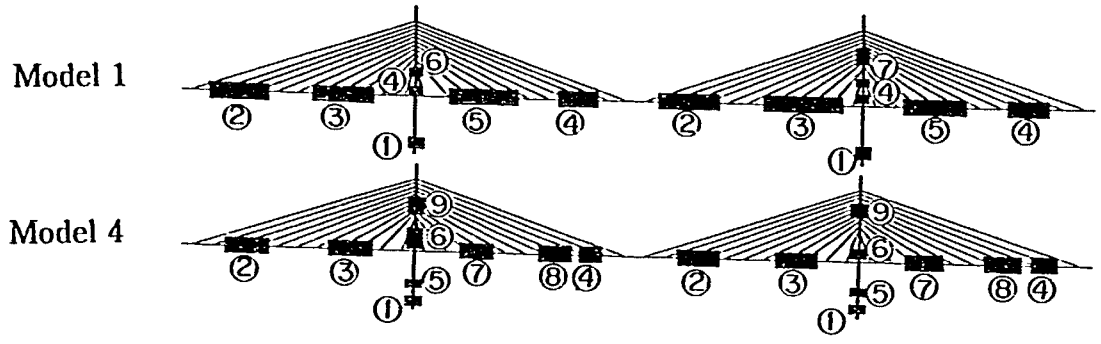
There was no members to reach yielding for peak acceleration of 500 cm/sec^2, hence the peak acceleration was increased until 800 cm/sec^2. The result is shown in **Figure 22.** In model 1 towers yield, but in model 4 towers does not yield. Therefore we may conclude that the cable–stayed bridges with shear bearing has advantage for big earthquake.
The following conclusion may be drawn by the numerical results presented in this paper.

CONCLUSION

(1) There is no remarkable difference of natural periods of vibration among four models except in horizontal vibration modes. Because shear bearing has certain effect only on horizontal vibration mode of bridge.



(a) Hachinohe wave



(b) El Centro wave

Figure 21 Crack distribution due to maximum acceleration 500 cm/sec^2

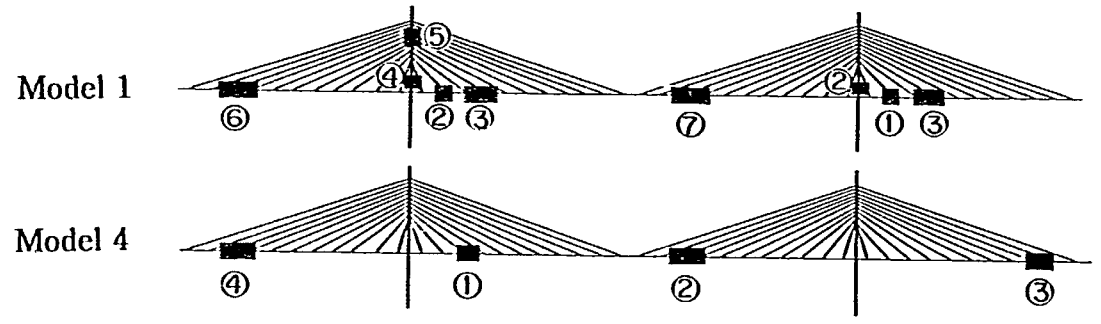


Figure 22 Crack distribution due to maximum acceleration 800 cm/sec^2 (Hachinohe wave)

(2) Conducting elasto–plastic analysis, amplitudes of response displacements in time histories decrease rapidly after the first period with shear bearing. Therefore it is clear the effectiveness of shear bearing as energy dissipation device.

(3) In model 1 towers yield due to the seismic wave with the peak acceleration 800 cm/sec^2, but in model 4 towers does not yield. Therefore the cable–stayed bridges with shear bearing has advantage for big earthquake.

(4) At least the object to decrease the horizontal displacement of deck and to delay yield occurrence of the tower would be accomplished by the shear bearing. Since the seismic induced response varies according to the hysteretic property of shear bearing, parametric study is necessary to find optimum stiffness of shear bearing.

(5) Both displacements and forces due to Hachinohe wave is larger than those due to El Centro wave. It seems to come from that Hachinohe wave has larger peak velocity than El Centro wave.

SEISMIC DESIGN FOR MAKING CONTINUOUS THE MULTIPLE SPANS OF A VIADUCT ON THE HONSHU-SHIKOKU HIGHWAY

by

Shoichi SAEKI,*1 Kazuo TADA,*2 Kazuhiko YAMAGISHI*3

*1 Executive Director, Honshu-Shikoku Bridge Authority
*2 Director, Design Department, Honshu-Shikoku Bridge Authority, 5-1-5 Toranomon, Minato-ku, Tokyo 105, Japan
*3 Manager, Design Division, Construction Affairs Department, First Construction Bureau, Honshu-Shikoku Bridge Authority, 5-1-14 Hamabe-dori, Chuo-ku, Kobe 651, Japan

ABSTRACT

In examining the making continuous of the multiple spans of a viaduct when, for example, the lengths of the piers are very different, the soil layers conditions are extremely varied, or bridges with different structural properties are to be integrated, the development of a seismic design is problematic because vibration behavior during earthquakes is extremely complex since the piers supporting inertia forces do not have uniform dynamic responses. This paper looks at some distinctive examples of the making continuous of the multiple spans of a viaduct and discusses how to disperse inertia forces, which increase during an earthquake, and ideas on rigidity, ultimate strength, and the deformation properties of each member.

INTRODUCTION

It goes without saying that the drivability of viaducts with continuous spans is high. However, ideal sites for the construction of continuous viaducts—flat terrain and uniform supporting soil layers for foundations—are quite rare. Therefore, even when a section to be bridged is long, it is common to build a series of different kinds of bridges.

In recent years, however, it has become desirable make continuous the multiple spans of viaducts in order to reduce the number of expansion joints and bearings, both of which lack durability and are thus expensive to maintain. Further, expansion joints generate noise, which disturbs people living nearby, and the maintenance costs of measures to minimize this disturbance can be high. And from the perspective of earthquake resistance as well, continuous-span viaducts are advantageous in that even when they are subjected to inertia forces from an earthquake that are greater than those assumed in calculations and the foundation ground deforms, the worst case scenario of bridge collapse can be avoided.

One example of the making continuous of the multiple spans of a viaduct is the use of the multi-dispersion elastic bearing method on a prestressed concrete bridge. This method, which employs laminated steel and rubber bearings to withstand the inertia forces generated by earthquakes, has been used on this type of bridge for many years. In recent years, the multiple spans of viaducts have been made continuous with base-isolated bearings, and viaducts in urban areas whose structures consisted of linked simple beams have been rebuilt into continuous girder-type bridges by the interconnection of girders.

In making continuous the multiple spans of a viaduct, it is important to examine the following problems created by the lengthening of girders: how to absorb the large displacement of girders generated in girder ends as a result of temperature changes; and how to distribute the increased inertia forces on girders during earthquakes through the use of piers with different dynamic responses. It is necessary to reduce the number of expansion joints and bearings, both of which lack durability, by making spans continuous, as well as to minimize the size of expansion joints by appropriately setting design displacement. It is also important to rationally design the substructure because the structural measurements of most piers and foundations are determined during checks for earthquake forces.

The following section introduces studies of examples of the making continuous of the multiple spans of viaducts on the Honshu-Shikoku Highway. The main topics of the studies are: the making continuous of the multiple spans of viaducts with piers of different lengths; the making continuous of the multiple spans of viaducts when soil layer conditions of sections are extremely varied; and the making continuous of different types of bridges. With each of these topics, seismic design problems accompanying the process of making spans continuous are examined.

DESIGN EXAMPLES

Table 1 shows how the multiple spans of bridges on the Kobe-Naruto section of the Honshu-Shikoku Highway were made continuous.

The following sections of the Honshu-Shikoku Highway provide distinctive examples of the making continuous of multiple spans: the Oda Viaduct, the second steel girder bridge; the Nuya Viaduct, the sixth prestressed concrete box girder bridge; and the Tateishigawa Bridge, the seventh bridge, which has a reinforced concrete arch and a viaduct with hollow slabs.

Table 1 Examples of the Making Continuous of the Multiple Spans of a Viaduct (Kobe-Naruto section of the Honshu-Shikoku Highway)

No.	Bridge name		Bridge type
1	Ogawa Viaduct 274 m	Before rebuild	(Superstructure and substructure) Steel plate girder: 4 + 4 continuous spans
		After rebuild	(Superstructure and substructure) Steel plate girder: 8 continuous spans
2	Oda Viaduct 223 + 181 m	Before rebuild	(Superstructure and substructure) Non-composite steel plate girder: 3 + 3 + 6 continuous spans
		After rebuild	(Superstructure and substructure) Non-composite steel plate girder: 6 + 6 continuous spans
3	Shakadogawa Bridge 328 m	Before rebuild	(Substructure) Non-composite steel plate girder: 4 + 5 continuous spans
		After rebuild	(Substructure) Non-composite steel plate girder: 9 continuous spans
4	Nuyabashiminami Viaduct 292 m	Before rebuild	(Substructure) Non-composite steel plate girder: 3 + 4 continuous spans
		After rebuild	(Substructure) Non-composite steel plate girder: 7 continuous spans
5	Tosatomariura Viaduct 586 m	Before rebuild	(Substructure) Non-composite steel plate girder: 3 + 4 continuous spans (two bridges) + 3 continuous spans (two bridges)
		After rebuild	(Substructure) Non-composite steel plate girder: 17 continuous spans
6	Nuya Viaduct 339 + 555 + 386 m	After rebuild	(Superstructure) Prestressed concrete box girder: 4 + 5 continuous spans (five bridges) + 6 continuous spans (one bridge)
		After rebuild	(Superstructure) Prestressed concrete box girder: 9 + 15 + 11 continuous spans
7	Tateishigawa Bridge 158 m	Before rebuild	(Superstructure and substructure) Reinforced concrete arch and a continuous 4-span reinforced concrete viaduct with hollow slabs
		After rebuild	(Superstructure and substructure) Reinforced concrete fixed arch (9 continuous spans of reinforced concrete cavity floors)

2.1 Making Continuous the Multiple Spans of a Viaduct with Piers of Different Lengths—the Oda Viaduct

As Figure 1 shows, the Oda Viaduct was originally planned as two non-composite steel plate girder bridges of three continuous spans and one non-composite steel plate girder bridge with six continuous spans. The supporting soil layers for the foundations were favorable and the foundations were all direct foundations. However, the second bridge crosses a deep valley so it was economical to use tall piers and long spans.

Therefore, the first and second bridges, which have different structural properties, were planned as separate bridges. But with an increase in the need for continuity, the issue of making the first and second bridges one continuous 6-span non-composite steel plate girder bridge was studied. The study looked at employing the following three methods to do this:

(1) The multi-dispersion elastic bearing method, which uses the rigidity of rubber bearings to disperse inertia forces from the superstructure into more than one substructure;

(2) The multiple-fixed point method, which uses hinged bearing plates; and

(3) The two-fixed point method, which uses hinged bearing plates only in the short piers P1 and P2.

The original plans for the construction of the two bridges and the above three methods for making the bridges continuous were analyzed. Figure 2 shows the results of an analysis done with the seismic coefficient method [1] of the dispersal ratios of inertia forces longitudinal to the bridge axis and sectional forces generated by an earthquake. The seismic coefficient method is a seismic calculation method in which inertia forces are determined by the product of the weight of the object and the design horizontal seismic coefficient, which acts statically in the acting direction (longitudinal to the bridge axis in this case). The design horizontal seismic coefficient is obtained with the following procedure: the static displacement is obtained when a force corresponding to the weight of the superstructure and substructure acts in the acting direction; the obtained static displacement is assumed to be a good estimate for the response of the first vibration mode; the natural period T is calculated using Rayleigh's energy method and the design horizontal seismic coefficient is obtained by modifying the standard design horizontal coefficient, which is 0.2, by region, ground, importance, and fundamental natural period T.

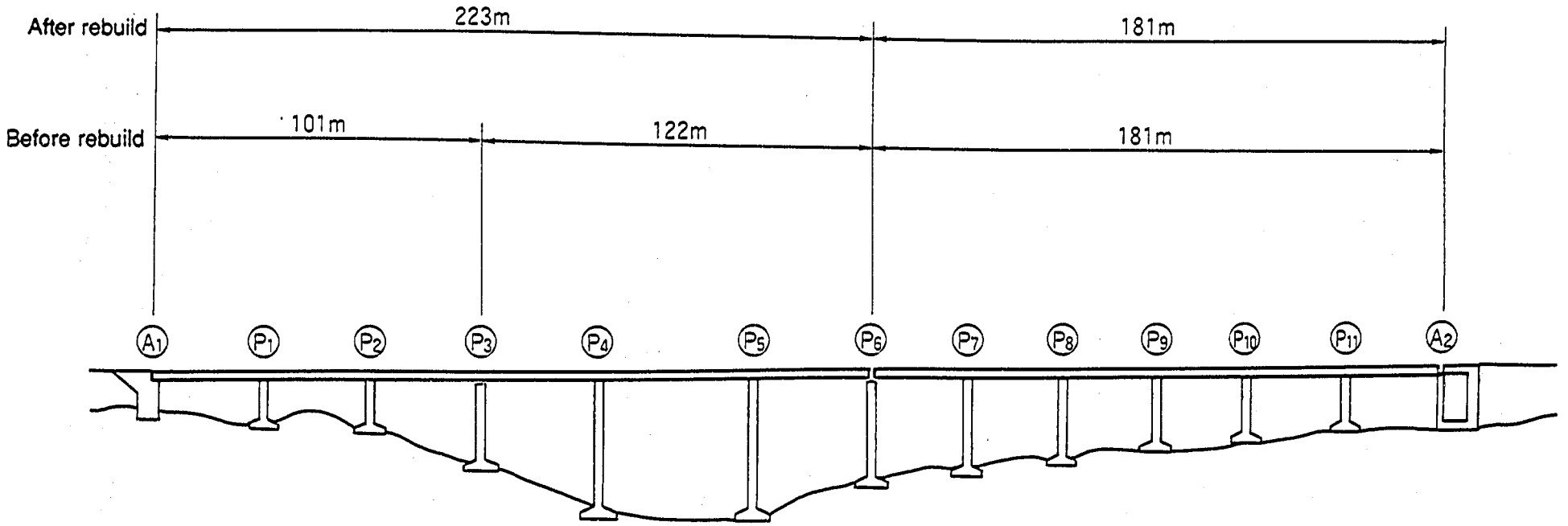
Figure 2 shows the three methods outlined below.

① Case 1: Multi-dispersion elastic bearings

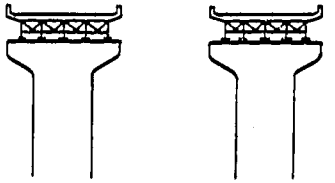
Rubber bearings with small spring constants were installed on piers to absorb the effects of responses generated by differences in pier rigidity. However, even when spring constants were adjusted to reduce the burden on the tall piers and horizontal inertia forces were reduced to one-half that of the short piers, the bending moment values on the bottom ends of the piers were still high, so the rubber bearings were ineffective.

② Case 2: All bearings hinged

The acting directions of the inertia forces of the superstructure of the two tall piers were reversed. This was because the tall piers did not resist the inertia forces of the superstructure and were supported by the girders because their own inertia forces were large. As a result, the acts of the inertia forces of the superstructure and the inertia forces of the two tall piers were concentrated on the short piers on the left side. However, since these piers are short, a seismic design for this sectional force can be developed. Compared with the increase in construction costs for short piers, construction costs for tall piers can be reduced because of the fewer number of sections. Case 3 is thus more economical.



a. Side elevation



b. Front view

Figure 1 Overall Perspective of the Oda Viaduct

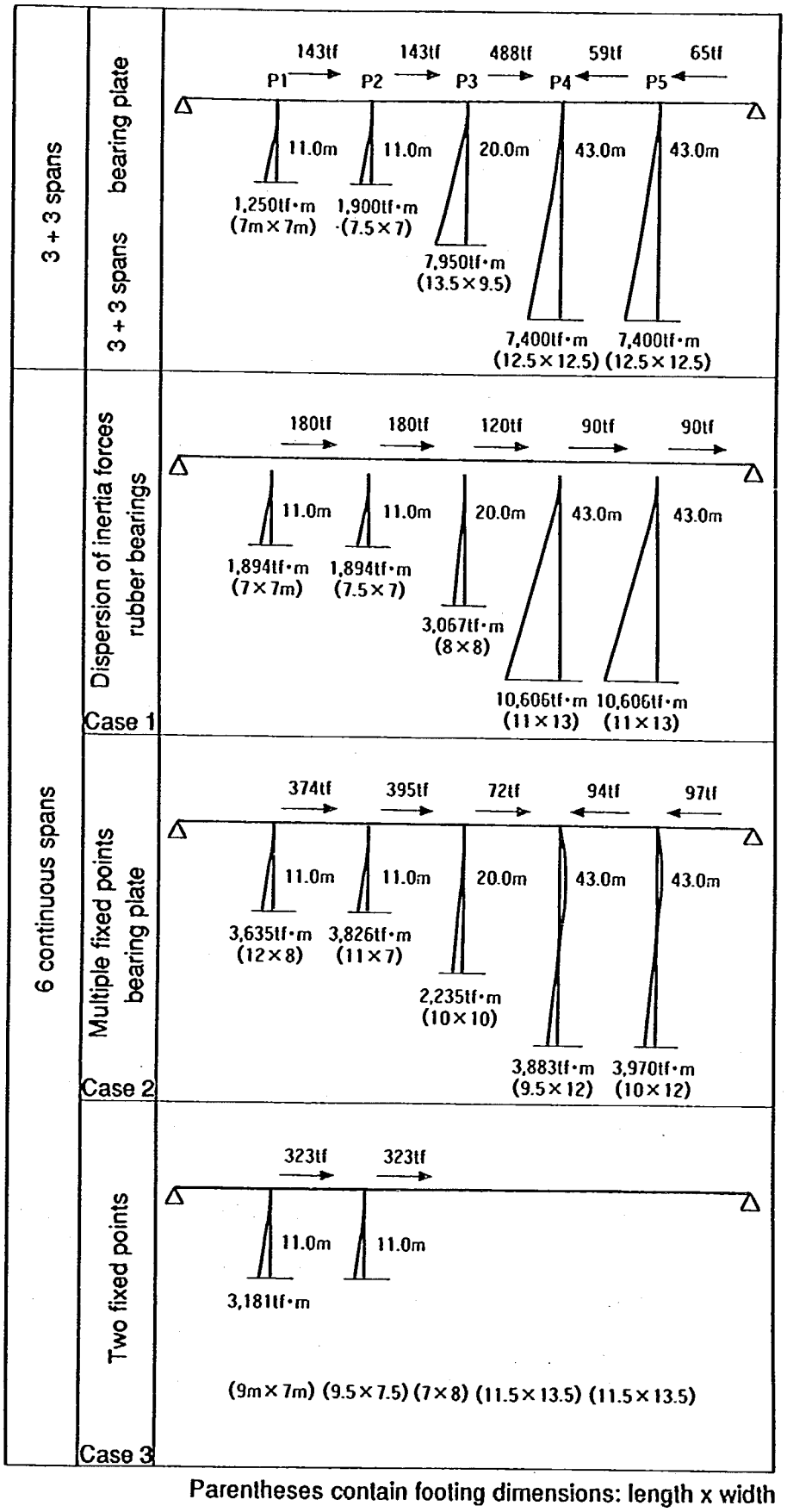


Figure 2 Inertia forces and moment of superstructure in an earthquake (seismic coefficient method, longitudinal to the bridge axis)

③ Case 3: Providing support with two short piers

This case appears to be the best because the inertia forces of the superstructure and the bending moments of the foundations were less than in Case 2. However, as shown in the column "Two fixed points" in Figure 3, specification 1) specifies that the tall piers must be checked by acting the force Rd • u (u: 0.15—friction of the coefficient of the movable bearings) horizontally on the top ends of the piers. This check indicated that the bending moment generated in the tall piers was greater than in Case 2, which is shown in Figure 2. Therefore, when both tall and short piers are used on a bridge, the bending moment of the tall piers becomes less when the bearing conditions are fixed as they were in Case 2, which is economically efficient. Also, hinged bearings are less expensive and more durable than movable bearings. With Case 3 structures, the degree of redundancy increases, which makes them desirable in terms of earthquake resistance.

From the analysis above it is evident that the use of all bearings hinged, such as in Case 2, is the best in terms of structural properties and economic efficiency. As mentioned before, the seismic coefficient method is a simplified method of analysis in which the vibration mode is approximated with static elastic displacement. We used dynamic analysis (the response spectrum method and time-history response analysis) to check the effects of high-order modes on responses because the structures we studied demonstrated complicated responses.

Figure 4b shows the results of analysis with the response spectrum method, and Figure 4c shows the results of time-history response analysis. Sectional forces, which show the results of the response spectrum method, are the values for the first mode. Since the vibration mode is a mode in which entire girders perform horizontal rigid body movements, it has the same configuration as static elastic displacement in the seismic coefficient method in which dead load is acted horizontally. Therefore, the sectional force results are considered to be almost the same. Sectional forces are evaluated with the square root of the square sum of the sectional forces of each mode based on the effects of the high-order modes. The first mode is the dominant factor in determining sectional force size, which differs little from the single first-mode value.

The results of time-history response analysis show each sectional force when the bending moments of the foundations of the tall piers are greatest. No large sectional forces were generated at other times, thus it can be concluded that the results match those obtained with the seismic coefficient method and the response spectrum method. For earthquake input in the time-history analysis, wave forms, which were seismic wave forms at the Kaihoku Bridge that were amplitude adjusted to match the response spectrum specified in specifications), were used.

The effects of the high-order modes on the bridge system, which were determined by the seismic coefficient method described above, were examined with dynamic analysis. Both dynamic analysis results were only slightly different from those of the seismic coefficient method, which confirmed that the seismic coefficient method can be used for bridges with a combination of tall and short piers.

Specification 1) states that the top ends of independent piers which must have at least a certain level of rigidity must be checked by acting horizontal loads Rd • Kh on them. When this is applied to bridges with tall and short piers, sections of the tall piers can be determined by this specification (as Case 2 in Figure 3 shows), sectional forces become great, and many reinforcing bars are required. However, as long as the fixing of the top ends of piers with girders is maintained throughout the bridge system, as shown in Case 2 in Figures 2 and 4, such large sectional forces will not be generated, which makes the application of this specification uneconomical.

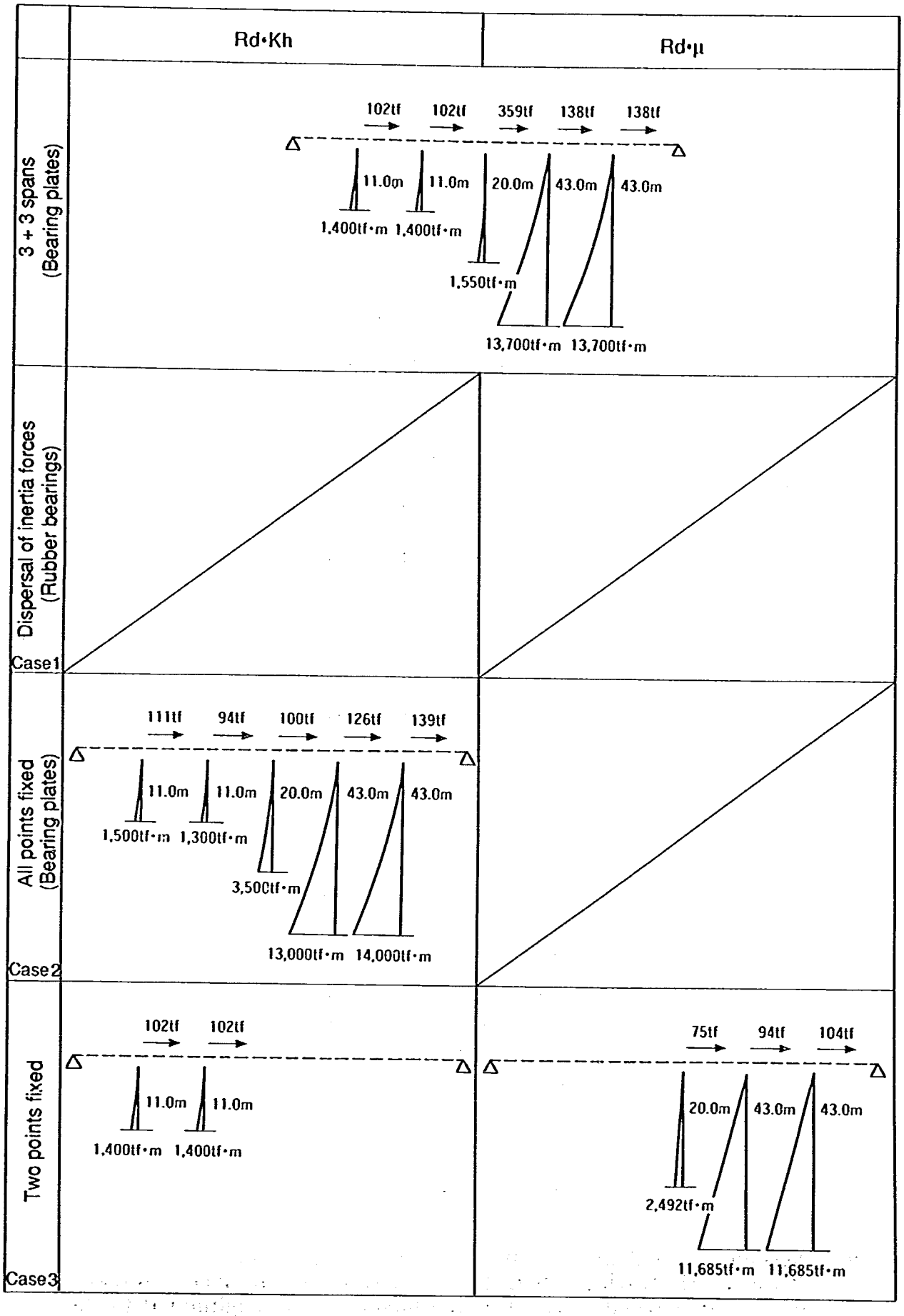
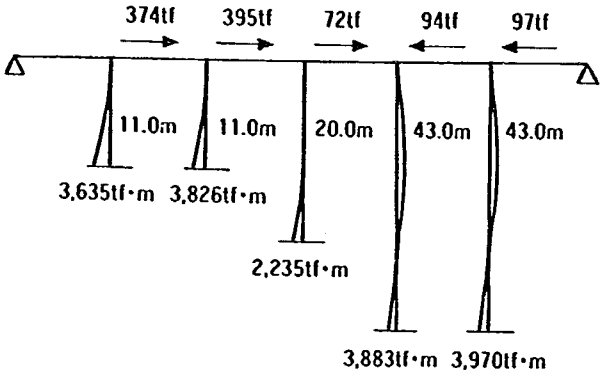
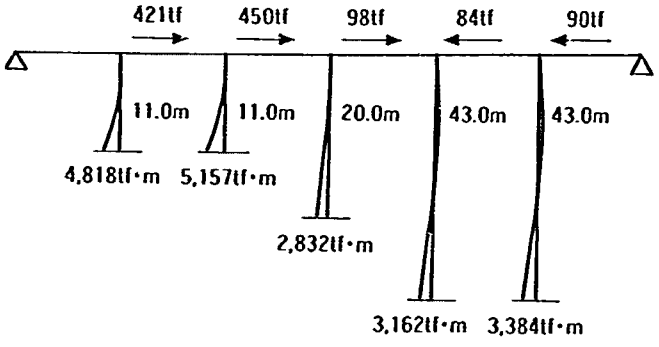


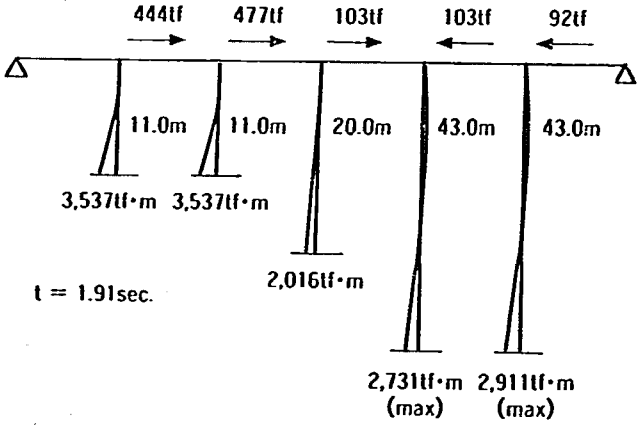
Figure 3 Check Using Rd • Kh and Rd •u



A. Seismic coefficient method



B. Response spectrum (first mode)



Time-history response analysis

Figure 4 Seismic Coefficient and Dynamic Analysis Methods (Case 2: All bearings hinged: In an earthquake the inertia forces of the superstructure and bending moments are longitudinal to the bridge axis.)

In terms of the ultimate strength and deformation properties of piers, the ultimate strength of tall piers is low, but their deformation properties are high. The ultimate strength of the whole bridge system is determined by the ultimate strength of its low piers, which have great ultimate strength and low deformation properties. Therefore, as long as the top ends of piers and girders are strongly connected, tall piers, whose deformation accounts for much of the deformation of the whole system, are strong enough and do not negatively effect the system. As a result, the rigidity and ultimate strength of tall piers do not need to be increased beyond what is necessary. Rather, total safety for the design horizontal forces of bearings and anchor bolts, in which inertia forces are concentrated, must be assured to restrict relative displacement between the superstructure and the substructure.

To determine the ultimate strength of the whole structure, the design ultimate horizontal strengths in an earthquakes of important short piers were checked. The tall piers did not resist the inertia forces on the superstructure. On the contrary, their own inertia forces acted on the girders, creating compressive forces on them. This point was checked but it was found that reinforcement of plate girders was not necessary.

As a result of design work, it was determined that making multiple spans continuous would have no significant effect on the economic efficiency of the superstructure, but would improve the economic efficiency of the substructure, particularly the tall piers. It was concluded, therefore, that there would be an overall economic advantage to carrying out the process.

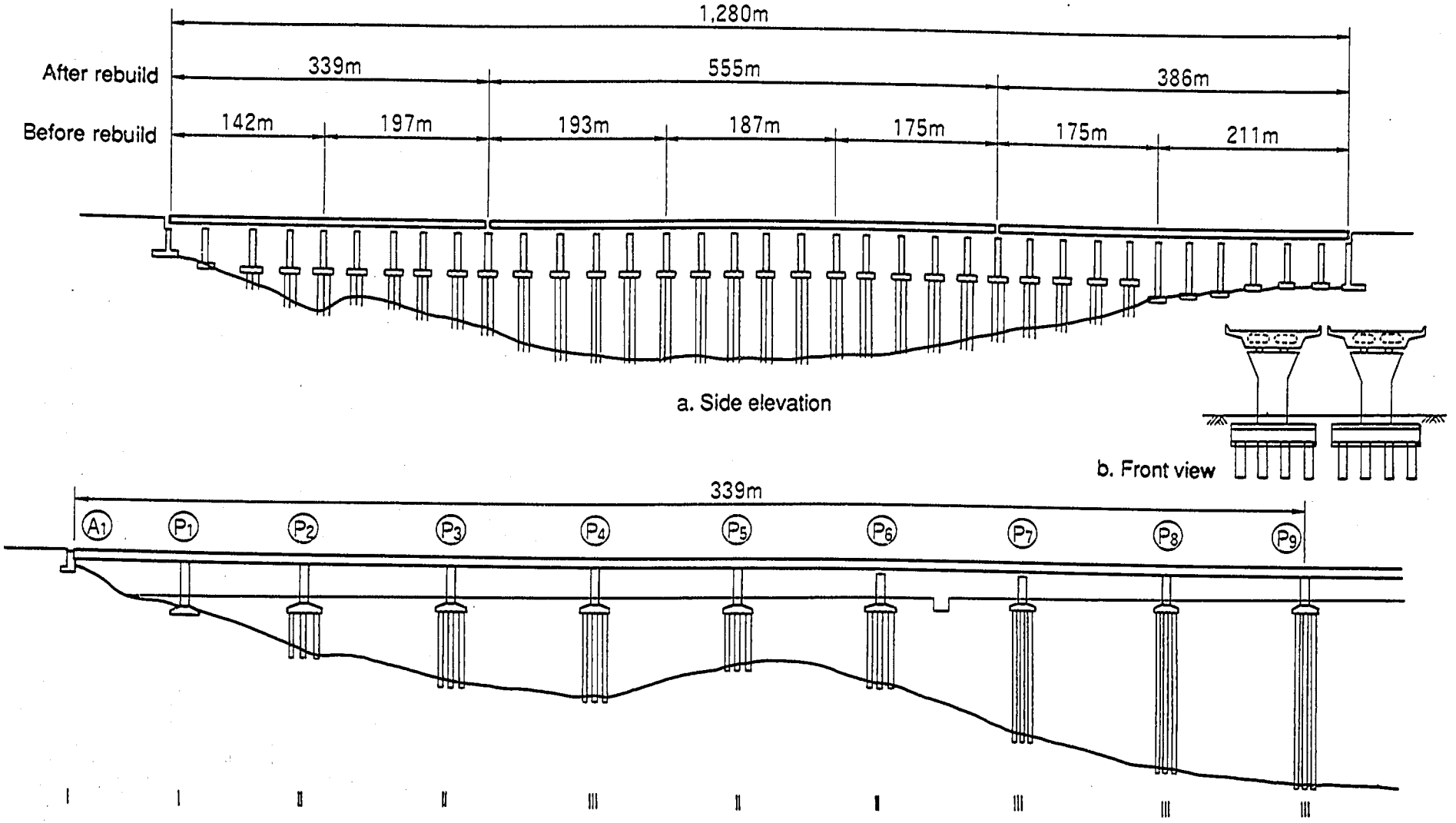
2.2 Making Continuous the Multiple Spans of a Viaduct with Variable Soil Layer Conditions—the Nuya Viaduct

The lanes of the Nuya Viaduct heading to Shikoku (total length of 1,294 m), which have been in use since May 1987, were constructed on a temporary basis. This viaduct consists of one continuous 4-span prestressed concrete box girder bridge, five continuous 5-span prestressed concrete box girder bridges, and one continuous 6-span prestressed concrete box girder bridge. At this time, plans have been developed to rebuild the lanes of the viaduct heading to Honshu. It is predicted that there will be an increase in large-vehicle traffic and traffic speed along the route; if use of the existing structure is continued, the problems of noise generated by the expansion joints and excessive maintenance will intensify, thus the plan is to increase the continuity of viaduct spans.

In developing plans to make the multiple spans continuous, much effort was put into minimizing environmental impact by making each span the same length as existing spans. The method adopted to maintain the bridge on its axis in an earthquake was the multi-dispersion elastic bearing method, which uses rubber bearings. This method was also used on the existing bridges.

The load combination in earthquake checks used to be earthquake plus temperature. However, as a result of studies, it has been judged that this type of combination is rare. Specifications [1] were revised and now only earthquakes are used for checking. Studies also showed that multiple spans can be made continuous, and that inertia forces on a superstructure are distributed equally to its substructure because the multi-dispersion elastic bearing method, which uses rubber bearings, is used and inertia forces in an earthquake have little influence on the substructure. Therefore, as Figures 5a and 5b show, the plan is to make the Nuya Viaduct a three-bridge viaduct consisting of one continuous 9-span prestressed concrete box girder bridge, one continuous 15-span prestressed concrete box girder bridge, and one continuous 11-span prestressed concrete box girder bridge.

As Figure 5c shows, changes in the ground conditions of spans A1 to P9 are particularly large. The ground surface in the design of abutment A1, a direct foundation, is shallow. The ground surface in the design becomes deeper and deeper in the direction of P9, though there are some irregularities. The foundation is converted to a pile foundation, and pile length increases in the direction of P9. Dynamic analysis was thus carried out to examine the response qualities of the viaduct where the design indicates variations in the ground surface.



c. Supporting soil layers for foundations in the designs of A1~P9

Figure 5 Nuya Viaduct

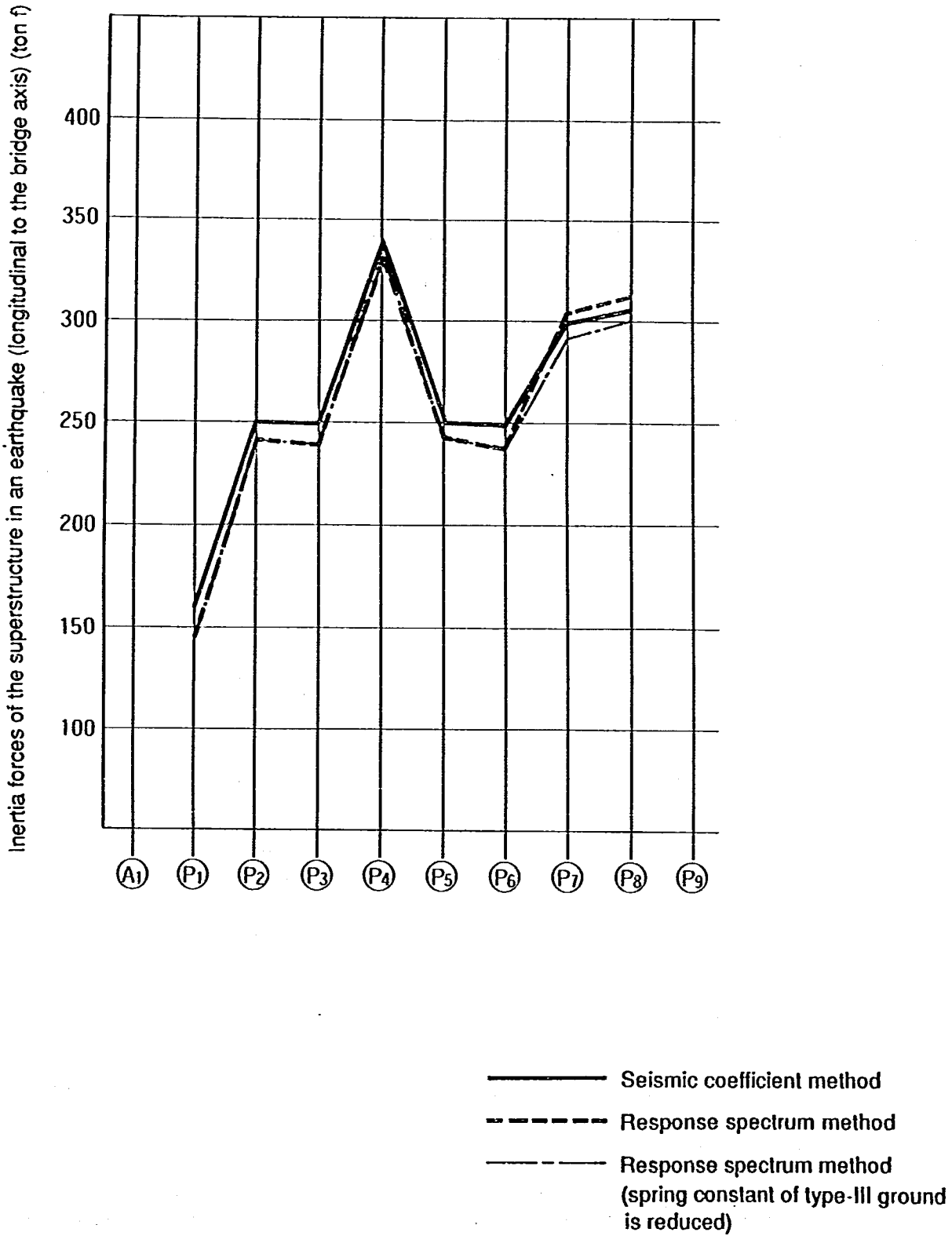


Figure 6 Inertia forces of the superstructure in an earthquake (longitudinal to the bridge axis)

In dynamic analysis, changes in soil layers are to be considered in the form of foundation ground springs. Therefore, spring values, which are softer than the assumed spring values of foundation ground springs of piers in type-III ground, are set to examine the effect of the viaduct on vibration behavior when the differences between with the spring values of piers in type-III ground get larger than those of type-I ground, which in the design has a shallow ground surface. Conceptually, type-I ground is base rock ground, type-II ground is a diluvial or alluvial layer, which in the design is a relatively good ground surface, and type-III ground is a weak alluvial layer.

To reduce the ground spring constant in type-III ground, the method for reducing the soil constant was based on the results of liquefaction tests at the location. The ground's spring coefficient in the horizontal direction of the set piles was reduced by two-thirds and the results of earthquake responses were compared.

In comparative analysis, earthquake motion in type-III ground was examined and dynamic analysis using the seismic coefficient method and the response spectrum method was performed. In dynamic analysis, the foundation springs of type-III ground were added to the set foundation springs for comparative purposes.

Figure 6 compares these results and shows the horizontal inertia forces in the direction of the bridge axis of the superstructure of the top ends of each pier. The results of the seismic coefficient method and the response spectrum method, both of which use the same soil coefficient, match well. When the soil coefficient of type-III ground is reduced, the results of analysis with the response spectrum method show that horizontal inertia forces are a little small, but the difference is minor. This is thought to be due to the low shearing rigidity of the rubber bearings, which limits the effect of the ground spring constant on the horizontal inertia forces in the direction of the axis of the superstructure.

In this way, even if the set ground spring constant is different from the actual spring to some degree, the ground spring constant is absorbed by the rubber bearings with low shearing rigidity.

2.3 Making Bridges of Different Types Continuous—Tateishigawa Bridge

The Tateishigawa Bridge has a 79-m reinforced concrete arch and a 68-m hollow slab bridge. From the perspective of seismic design, when bridges with different types are made continuous, there are considerable differences in the rigidity of the bridges along their axis. Since the arch is much more rigid than the hollow slab bridge, the vibration behavior of the whole system is determined by the rigidity of the arch, and the ultimate strength of the whole system is determined by the ultimate strength of the arch. The relationship between a highly rigid arch and a viaduct with low rigidity is similar to the relationship between short piers (high rigidity) and tall piers (low rigidity) described in Section 2.1. Therefore, the rigidity and ultimate strength of the piers of a viaduct can be low and there is no need to apply Rd • Kh to ensure minimum rigidity and to check the design ultimate horizontal strength in an earthquake of individual piers.

To confirm this, the rigidity of the piers of the viaduct were changed and the effect of this on the ultimate strength of the whole system was examined.

The deformation properties M-Ø of each acting state of axial force were set for members to be checked and elastic-plastic analysis, in which the load D + 2.0 • EQ was statically acted, was done. Figure 7 shows the analytical model and the members checked.

Viaduct piers with thicknesses of 1.25 m (Case 1) and 1.0 m (Case 2) were analyzed. Figure 7 also shows how plastic hinges were generated when the earthquake load was increased to D + 2.0 • EQ. The figure indicates that plastic hinges were generated in the following order:

① Right springing when earthquake loads were D + 1.67 • EQ
② Bottom of pier P1 when earthquake loads were D + 1.73 • EQ
③ Left side of the crown when earthquake loads were D + 1.90 • EQ

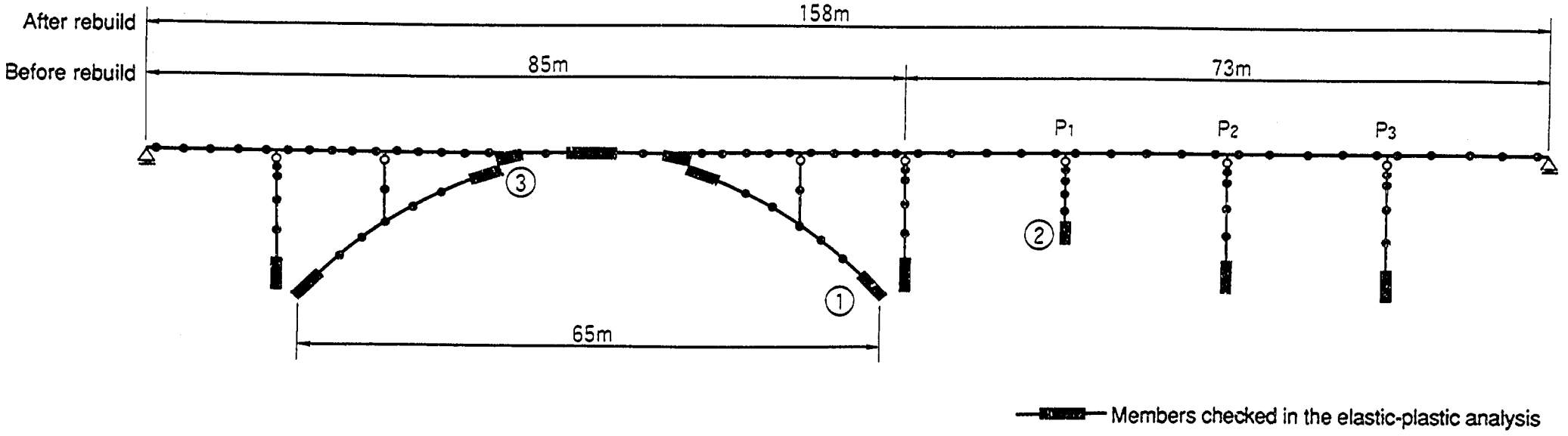


Figure 7 Static Elastic-Plastic Analytical Model of the Tateishigawa Bridge

There were only two plastic hinges generated in the arch and the stability of this section even when acted on by double the seismic force was confirmed.

Figure 8 compares the deformation states in Case 1 and Case 2 when earthquake loads were D + 2.0 • EQ using the deformation property M-Ø.

According to Figure 8, in Case 1 plastic hinges were generated at the left side of the crown and at the right springing. In Case 2, however, plastic hinges were generated at the left side of the crown, the right springing, and the bottom of pier P1. In terms of the advancement of the generation of plastic hinges, thick piers (Case 1) are advantageous. However, Case 2 also demonstrated stability when seismic forces were doubled, thus it was concluded that Case 2 had sufficient ultimate strength. As for the effects of piers on arch ribs, the M-Ø relationship of the left side of the crown of the arch in Case 1 and Case 2 did not differ. Thus, it can be concluded that pier thickness has virtually no effect on arch ribs. The curvature at the right springing in Case 1 was greater than in Case 2.

As a result, even when the thickness of the viaduct piers has the minimum rigidity determined with the seismic coefficient method, the whole system has the ultimate strength. The ultimate strength of the whole system is determined by the ultimate strength of the arch ribs, but the rigidity of the viaduct piers hardly affects ultimate strength.

As a result of the studies, means of improving the economic efficiency of viaduct piers and foundations were determined.

CONCLUSIONS

The results of the studies on the making continuous of the multiple spans of a viaduct, which is an improvement in terms of maintenance, noise, drivability, and earthquake resistance, are outlined below.

(1) Making continuous the multiple spans of a viaduct with piers of varying heights

① The response spectrum method was used and time-history response analysis was performed. It was confirmed that the first mode is dominant even when vibration behavior is complicated because the viaduct has both tall and short piers. Therefore, high-order modes do not affect responses and designs can be developed with the seismic coefficient method.

② To determine the ultimate strength of the whole structure, the design ultimate horizontal strength during an earthquake was checked for the primary short piers. Since the deformation properties of the tall piers are greater than those of the whole system, the tall piers have sufficient toughness until the whole system loses bearing force, therefore, there is no need to increase rigidity and ultimate strength beyond what is necessary.

③ The relative deformation between the superstructure and the substructure can be restrained and the whole bridge system can be maintained in the ultimate state by ensuring that the design horizontal forces of the bearings and anchor bolts, where inertia forces are concentrated, are limited.

④ As a result of design work, it was determined that making multiple spans continuous would have no significant effect on the economic efficiency of the superstructure, but would improve the economic efficiency of the substructure, particularly of the tall piers. It was concluded, therefore, that there would be an overall economic advantage to carrying out the process.

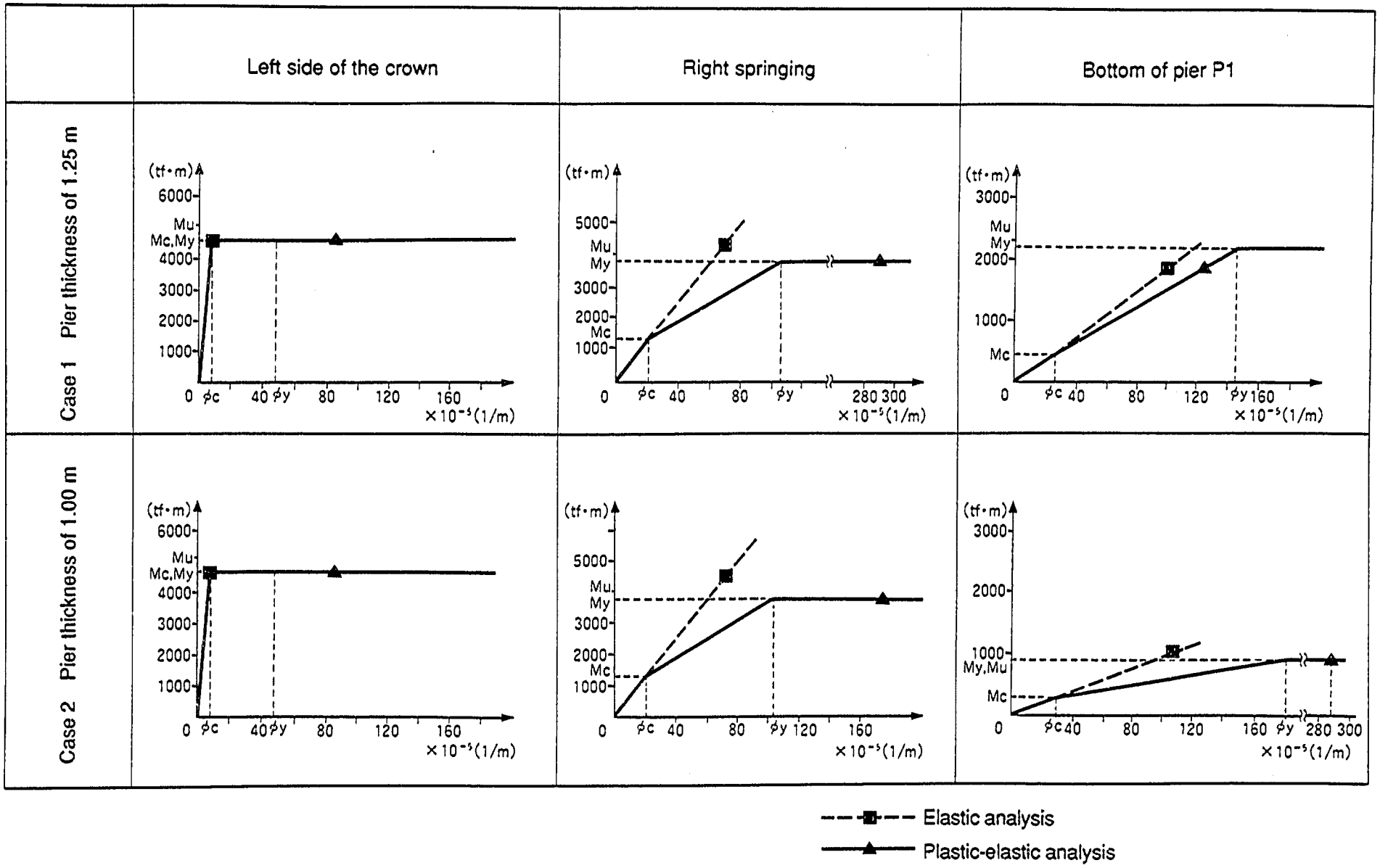


Figure 8 Comparison of the M-Ø Relationship

(2) Making continuous the multiple spans of a viaduct with variable soil layer conditions

① The multiple spans of the viaduct were made continuous using the rubber bearings. In this case, it was assumed that the set ground springs were different from the actual springs, and analysis was done with the response spectrum method by reducing only the soil constant. The results were compared with cases in which the soil constant was not reduced. By doing this it was confirmed that there were hardly any effects from reduction of the soil constant and on responses even with changes in the ground springs. This was thought to be due to the small shearing rigidity of the rubber bearings and the fact that the ground spring constant longitudinal to the axis of the whole bridge system is determined by the spring of the rubber bearings.

② Even when the ground is complicated, it is advantageous to make continuous the multiple spans of viaducts because even when they are subjected to inertia forces from an earthquake that are greater than those assumed in calculations and the foundation ground deforms, the worst case scenario of bridge collapse can be avoided. This is very significant. Moreover, drivability is enhanced and the number of expansion joints and bearings, both of which generate considerable noise, can be reduced from eight to four.

(3) Making bridges of different types continuous

① Static elastic-plastic analysis showed that the ultimate strength of the whole bridge system is determined by the ultimate strength of the arch ribs, and that the rigidity and ultimate strength of the tall piers hardly affects the ultimate strength of the whole bridge system.

② Therefore, even when the rigidity of the tall piers of a viaduct is minimized with the seismic coefficient method, the ultimate strength of whole bridge system is not affected.

③ As a result of these studies, it was confirmed that the economic efficiency of the tall piers and foundations could be improved.

ACKNOWLEDGMENTS

The above studies are about the design work done to make continuous the multiple spans of a viaduct that is presently under construction. We have used the results of design work done by sections of our organization involved in the process, consultants, and contractors. Mr. Kawashima, Head of the Earthquake Engineering Division of the Public Works Research Institute of the Ministry of Construction, provided us with invaluable guidance on the seismic design for making the multiple spans continuous, and for this we are extremely grateful.

REFERENCES

1) Specifications for Highway Bridges Part V: Seismic Design, Feb. 1990

Earthquake Response of Base-Isolated Multi-Span Continuous Bridge

by

Yozo GOTO

General Manager, Civil Engineering Department,
Technical Research Institute, Obayashi Corporation, Kiyose-si, Tokyo 204, Japan

ABSTRACT

The introduction and the first chapter of this paper present the concept of a very long multi-span continuous bridge and the application of the seismic isolation design on it. The second chapter introduces earthquake response characteristics of seismic isolated one-kilometer multi-span continuous bridges. The third chapter discusses optimum values of the period of fundamental natural vibration which seismic isolated multi-span continuous bridges should have. The fourth chapter presents a technique to adjust the isolators during the service stage.

INTRODUCTION

The expansion joints built into decks of highway bridges not only adversely affect the driving comfort of automobiles, but also harm the surrounding environment by causing noise and vibration. Moreover, their frequent breakage requires continual repair work, and this repair work causes severe traffic jams because of stopped traffic. These problems lead to a need in highway technology of Japan for a method that reduces the number of expansion joints from bridges. In order to make girders without expansion joints in multi-span continuous bridges, a structure is necessary that supports the girder while it expands or shrinks in the direction of the girder axis as a result of temperature changes as well as concrete shrinkage and creep. Previously, multi-span continuous bridges with support structures such as slip bearings, roller bearings with viscous dampers, and elastomeric bearings as well as flexible columns have been constructed in Japan. The longest continuous girder attained to date is an extension of 600 meters. The next goal is an extension of one-kilometer.

On the other hand, supporting the girder with a bearing with a small amount of stiffness in lateral directions to achieve the seismic isolation design enables the passing on of the expansion and shrinkage of the girder resulting from temperature changes and other factors. So the adoption of the seismic isolation design enables multi-span continuation as well.

Based on this concept, the Public Works Research Institute of the Ministry of Construction and twenty-eight private firms in Japan adopted the development of seismic-isolated one-kilometer multi-span continuous girder bridges as one of the objectives of their joint research, that is named "Joint Research on Menshin System for Highway Bridge" conducted from 1990 to 1992. One of the subjects of the development was to study the adjustability of the seismic isolation design to the jointless design of long bridges. Another subject was to clarify the response characteristics of an extremely long continuous girder supported by isolation bearings and how it responds during an earthquake. The author was in charge of the joint research as one of the members from private firms. The first and the second chapters of this paper are the accomplishments of the joint research (Refs. 6, 7). While the third and fourth chapter come from the development that the author has done focusing practical subjects after

the completion of the joint research (Refs. 8, 9).

1. Seismic Isolation Design of Multi-span Continuous Bridges

Model bridges

A feasibility survey was performed on a steel-girder bridge and a prestressed concrete-girder bridge (Refs. 2, 7). Figure 1 and 2 are drawings of the two bridges. The bridges were assumed to have one-kilometer continuous girder with sixteen spans for the steel bridge and twenty-six spans for the prestressed concrete bridge. Design requirements and specifications met the Japanese "Design Specifications for Highway Bridges (Ref. 1)" as follows:

Bridge grade : First class (TL-20, TT-43)
Seismic zoning : A (highest seismicity)
Rank of importance: First class
Design temperature change : ±20℃ for a prestressed concrete girder
±30℃ for a steel girder
Ground conditions : Group 2 (stiff soil site)

The plane alignment of the bridge was assumed to be straight to simplify the study.

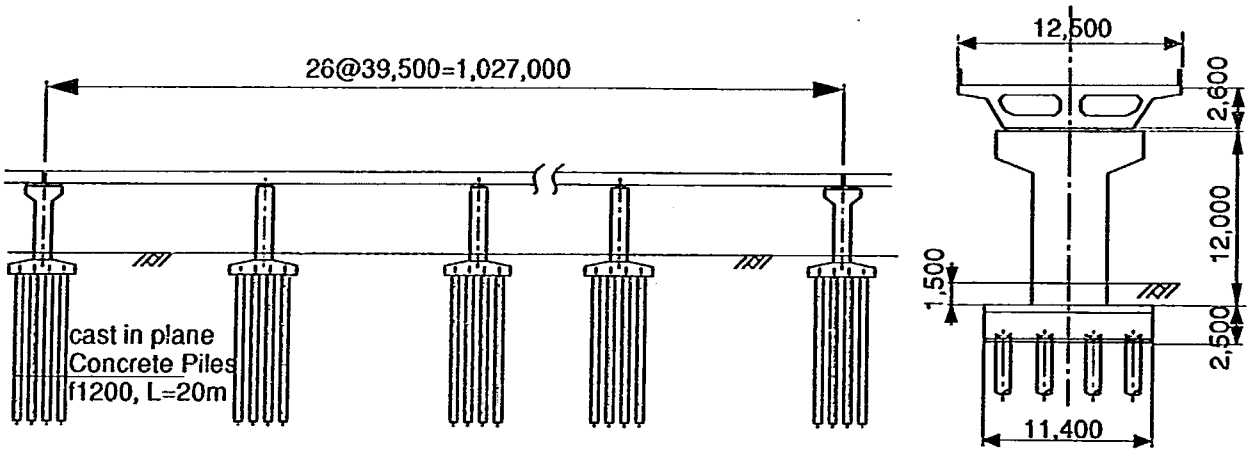


Fig. 1 Multi-Span Bridge with 1 kilometer continuous Prestressed Concrete Girder

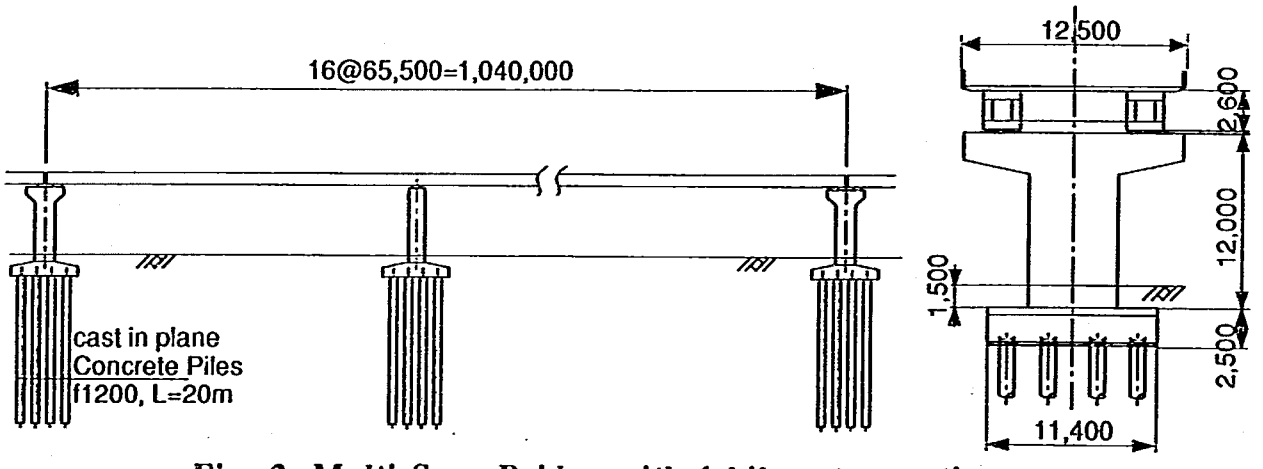


Fig. 2 Multi-Span Bridge with 1 kilometer continuous Steel Girder

Design principle

The procedure of the seismic isolation design followed the "Manual of Menshin Design for Highway Bridges (Draft)(Refs. 4, 5)". Lead rubber bearings (LRBs) were chosen as isolation bearings because of their low lateral stiffness at a slow rate of deformation resulting from temperature change and creep. This low stiffness comes from the creep characteristics of the lead core and sufficient stiffness manifests itself at a quick rate of deformation resulting from earthquakes.

Table 1 gives the design dimensions of the LRBs, which differed depending on their location along the girder. The static stiffness of the bearings at the end parts of the girder was designed to be lower than that of the central part, in order to decrease thermal stress efficiently. The dynamic stiffness of the bearings at the end parts was designed to be higher than that of the central part, in order to decrease the seismic deformations at the girder ends.

In the case of the prestressed concrete girder, construction work was assumed to start from the center of the bridge at two points, moving toward the ends separately at a speed of twenty days per one span. Fifty percent of the bearing deformation due to creep and shrinkage of the concrete girder was assumed to be canceled through the adjusting works on isolators at the construction site.

Table 1 Dimension of Menshin Bearing (LRB)

	P. C. Girder Bridge		
Pier No.	P1, P27	P2~P7, P21~P26	P8~P20
Dead load(tf/bearing)	220.	585.	525.
Plane Dimension (cm)	78×78	108×108	108×108
Total Thickness of Rubber (cm)	11× 2.5=27.5	10 ×2.5=25.0	9× 2.5=22.5
Dimension of Lead (cm)	φ10× 4	φ15× 4	φ15× 4
*Effective Stiffness (tf/m)	595.	1410.	160.
*Effective Damping Ratio (%)	29.	28.	27.

* Effective for input level of the Seismic Coefficient Method

Results of design calculation

Table 2 presents periods of natural vibrations, damping, and design seismic coefficients of the prestressed concrete girder bridge. Seismic load reduction as a result of the seismic isolation design came mainly from increased damping. Table 3 lists bending moments at the lower end of the columns and lateral deformation of bearings at representative piers. The bending moment due to temperature change is about sixty percent of that due to seismic load. Regarding lateral deformation of the bearings at the ends of the girder, the deformation due to seismic load is less than that due to temperature change. The size of the

Table 2 Design Seismic Coefficient

		P.C.Girder Bridge	
Direction		Axial	Lateral
Natural Period T (sec)		1.31	1.27
Damping of Bridge h (%)		22.3	22.3
Notification Factor	c_z	1.0	1.0
	c_G	1.0	1.0
	c_I	1.0	1.0
	c_T	1.25	1.25
	c_E	0.9	0.9
Design Seismic Coefficient		0.23	0.23

steel bars in the column was lowered and the number of piles in the foundation was decreased owing to the seismic isolation design.

Table 3 Bending Moment in Lower End of Column (tf·m) and Relative Displacement in Isolator (cm)

	Pier No.	Bending Moment		Relative Displacement	
		P1	P2	P1	P2
Axial Direction	Temperature	-	2,125	10.	9.0
	Seismic Coefficient Method	3,239	3,532	9.9	9.9
Lateral Direction	Seismic Coefficient Method	3,096	3,741	8.0	10.

2. Earthquake Response of Seismic-isolated Multi-span Continuous Bridges

Response analysis using a step-by-step integration procedure was performed on a steel-girder bridge and a prestressed concrete-girder bridge which were configured using the seismic isolation design described above. In the analysis, pier-to-pier differences among seismic waves were considered to account for the scattering of seismic waves along the bridge axis. Additionally, earthquake responses of a bridge having a S-curved alignment and that of a bridge extending on two different kinds of ground were studied (Ref. 2, 6).

2.1 Earthquake Response of a Multi-span Continuous Bridge with Phase Delayed Seismic Input

Input seismic wave

Seismic calculations for common bridges have generally been performed under the assumption that unified seismic waves are input simultaneously to their substructures. But it cannot be applied to our research in which structures with an extension in excess of one-kilometer are studied. As is well known, there is seismic wave scattering from irregular lineaments and local nonhomogeneity of soil, differences in propagation routes, and surface wave propagations. However, the correlation and disparity of point-to-point earthquake motion is still a topic of research, and its evaluation method for design has yet to be established. Therefore, an expedient method was used in this analysis based on engineering judgment. Namely, the point-to-point difference among seismic waves was assumed to come from only the ideal occurrence of a wave propagation. It was assumed that the unified seismic wave was input to each bridge pier with a constant phase delay.

There are three kinds of phase delay in the seismic wave considered in this analysis: 0.002 sec/m, 0.001sec/m, and no phase delay. As the phase delay increases, the propagation velocity slows down, and the strain occurring in the horizontal direction of the ground becomes larger. Even during a strong earthquake, when the ground is not very soft and is not liquefied, the horizontal strain along the surface of the ground is supposed to be on the order of 10^{-4}. Then, the maximum horizontal strain values of the ground due to wave propagation are set to be 3.6×10^{-4} (0.001 sec/m) and 1.8×10^{-4} (0.001 sec/m), respectively.

The wave form are shown in Figure 3a. The response spectrum of the wave at 5 percent damping was designed to fit the standard response spectrum for dynamic analysis for Group 2 of the Ground Condition (Figure 3b) as outlined in the "Design Specifications for Highway Bridges (Ref. 1)".

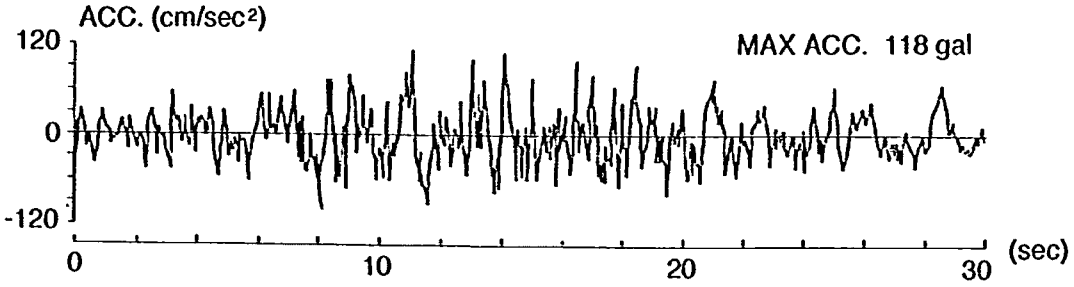


Fig. 3a Input seismic wave

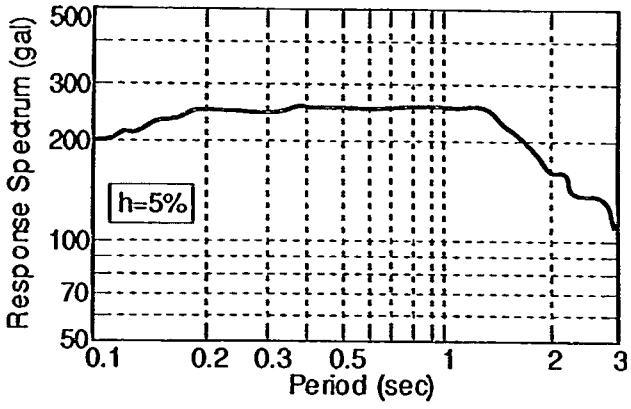


Fig. 3b Response Spectrum of the Wave

Modeling for Response Analysis

As Figure 4 shows, all bridge spans were modeled into the continuous spring-mass system establishing two kinds of two-dimensional models consisting of an in-plane response model and an out-of-plane response model. When the seismic force acts in the direction of the bridge axis, the in-plane response model is used, and when it acts in a direction lateral to the bridge axis, the out of-plane model is used. In addition, details of modeling the bridge pier components are shown in Figure 5. The isolation bearing was converted into a model using a visco-elastic spring equivalent to the hysteresis characteristic. The effect of interaction between the ground and bridge pier foundation was taken into account in a model by attaching an equivalent visco-elastic spring to the footing. Since damping is different in each structural component, it is expressed as viscous damping of each component.

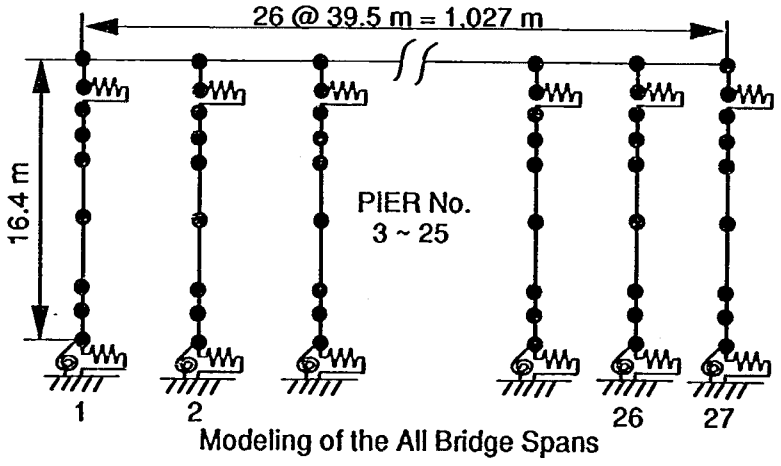


Fig. 4 Concept of Total Spring-Mass System

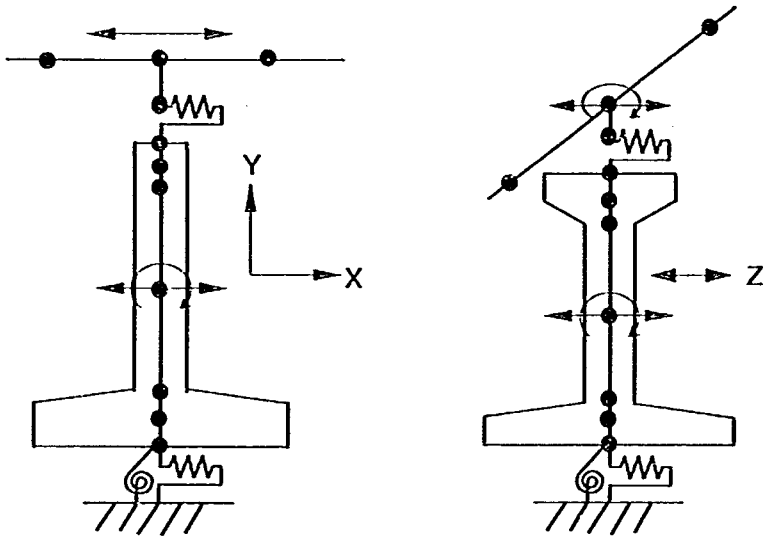


Fig. 5 Concept of Modeling the Pier Components

Natural periods and vibration modes

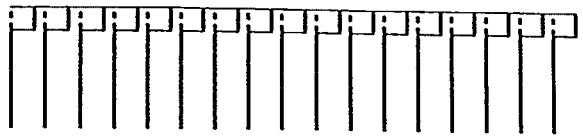
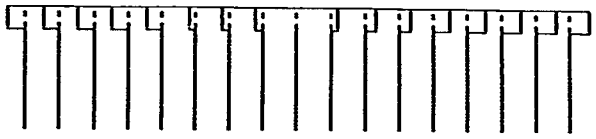
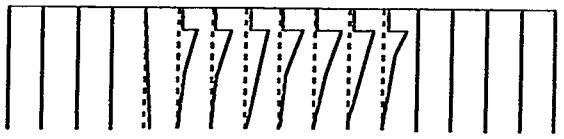
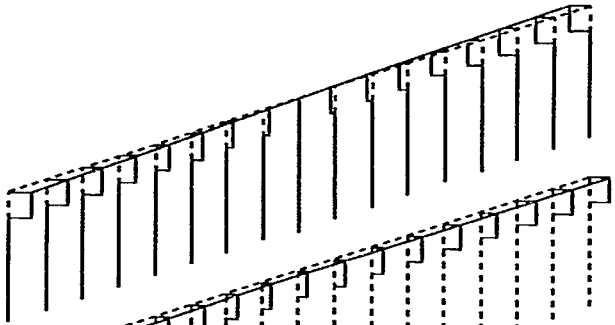
Table 4 gives typical vibration modes and natural periods of the steel girder bridge. The results of the concrete bridge lead to the same conclusion. From the vibration isolating effect of the isolation bearings, a clear division appears between the modes in which the girder shakes more than the pier and the modes in which the pier shakes more than the girder. In each case of in-plane and out-of-plane analyses in Table 4, there is a primary mode in which the sway of the girder predominates with a natural period of approximately 1.4 seconds and several post-secondary modes in which girder expansion or bending predominantly occur. On the other hand, modes in which the piers shake violently come out as high-order modes with natural periods of approximately 0.2 seconds or less.

Earthquake response

Figures 6 depicts time histories of response acceleration of a pier top and girder at representative piers and Figure 7 shows the distribution of maximum values for them. These figures are for the steel-girder bridge. The wave form at the pier top is only slightly amplified, which is almost the same as the input seismic wave form. Owing to the action of the isolation bearing, the shorter period component is absorbed from the girder response. When there is no phase delay in the input seismic wave, the response wave forms in directions both along and lateral to the bridge axis are almost the same, but when the phase delay is present, different response tendencies appear depending on the direction.

When there is a phase delay, the response acceleration in the direction of the bridge axis decreases both uniformly and abruptly. This is because the girder responds like a stiff body with a single degree of freedom even when the bridge girder is one-kilometer long. The stiffness of girder in this direction is
relatively high and it is supported on the isolation bearing, so the input seismic forces from each bridge pier cancel out each other due to the phase delay.

Table 4 Typical Vibration Models and Their Natural Periods (Steel Girder)

	Mode No.	Period (sec)	Mode shape	Comment
In Plane analysis	1	1.377		Sway of girder
	2	0.617		Tension & Compression of girder
	12	0.217		Bending of pier
Out of Plane analysis	1	1.372		Yawing of girder
	2	1.3716		Sway & Bending of girder
	28	0.186		Bending of pier

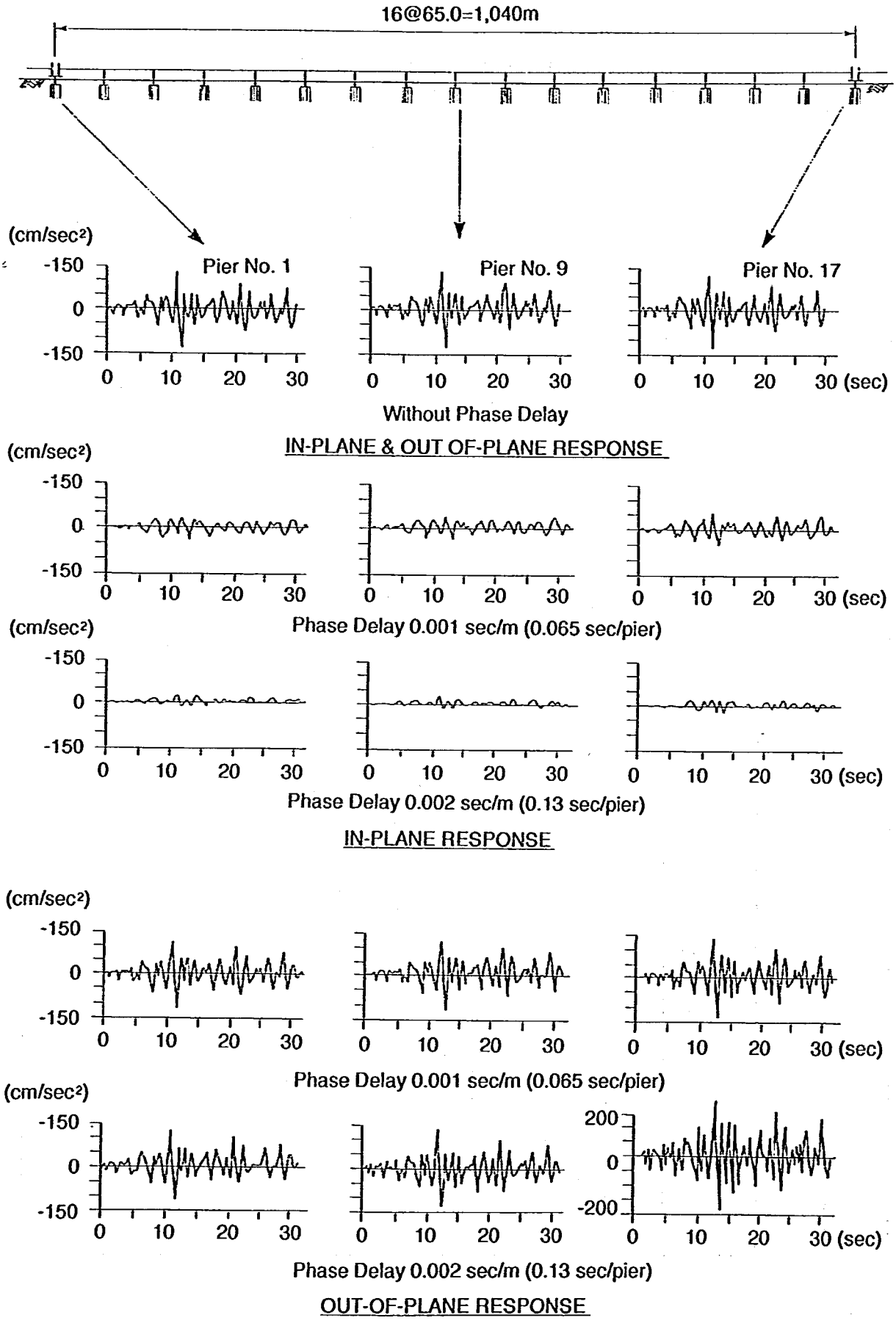
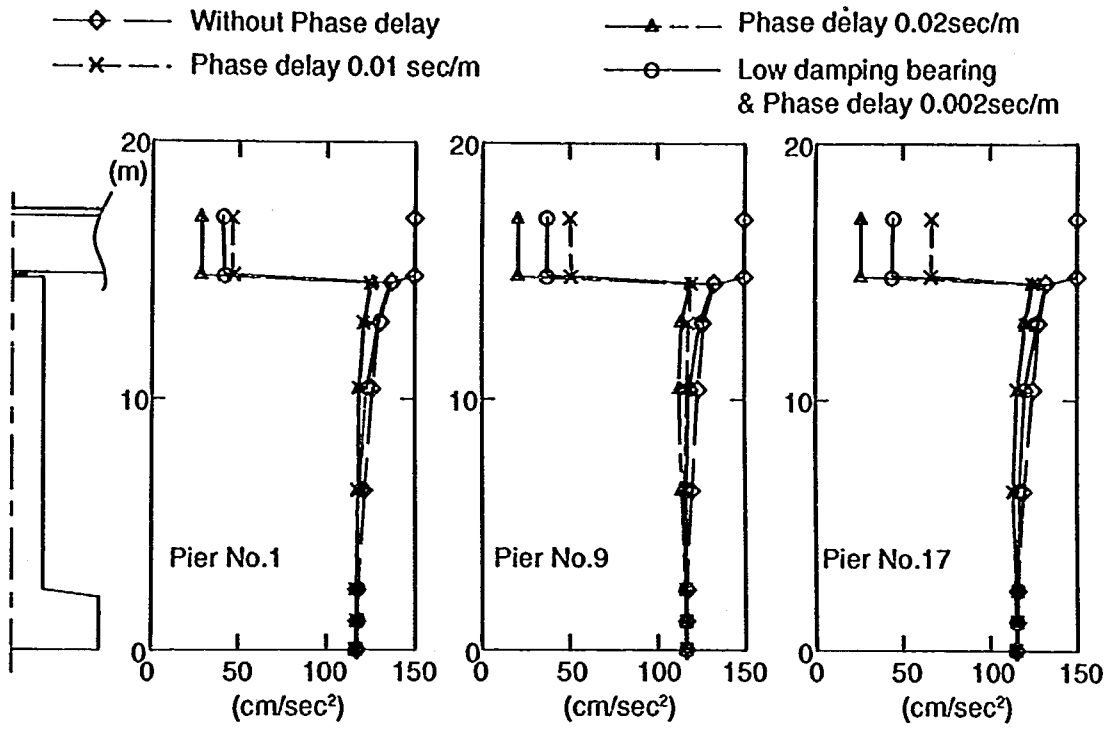
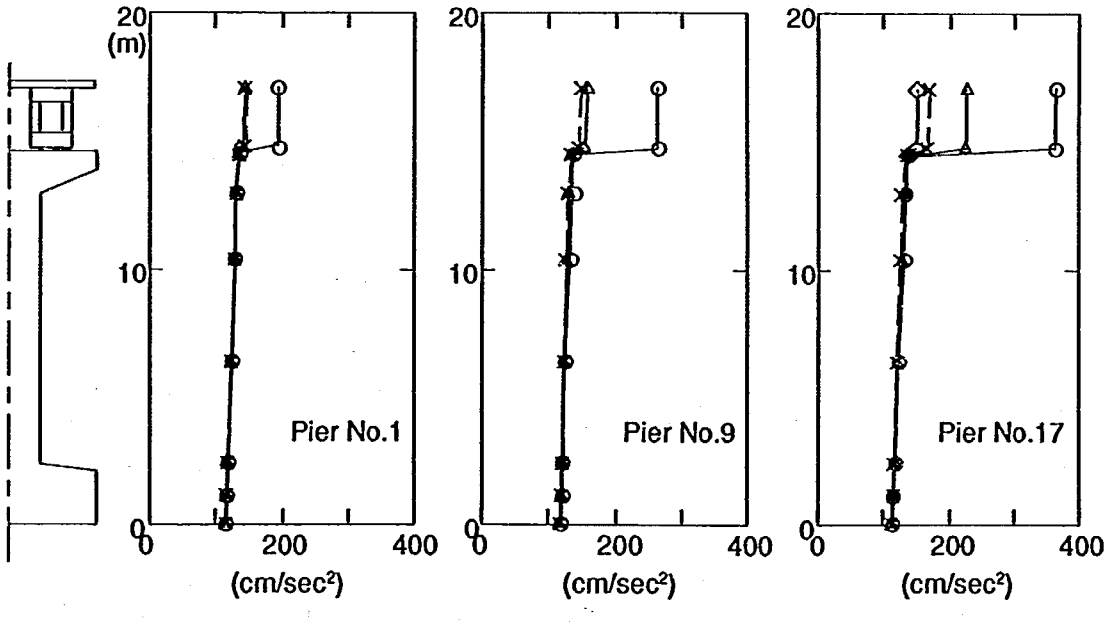


Fig. 6 Response Acceleration Wave Forms (In Plane Response and out of Plane Response)



Max acceleration in axial direction
(In plane analysis)



Max acceleration in the perpendicular direction
(Out of plane analysis)

Fig. 7 Distributions of Max. Response Acceleration

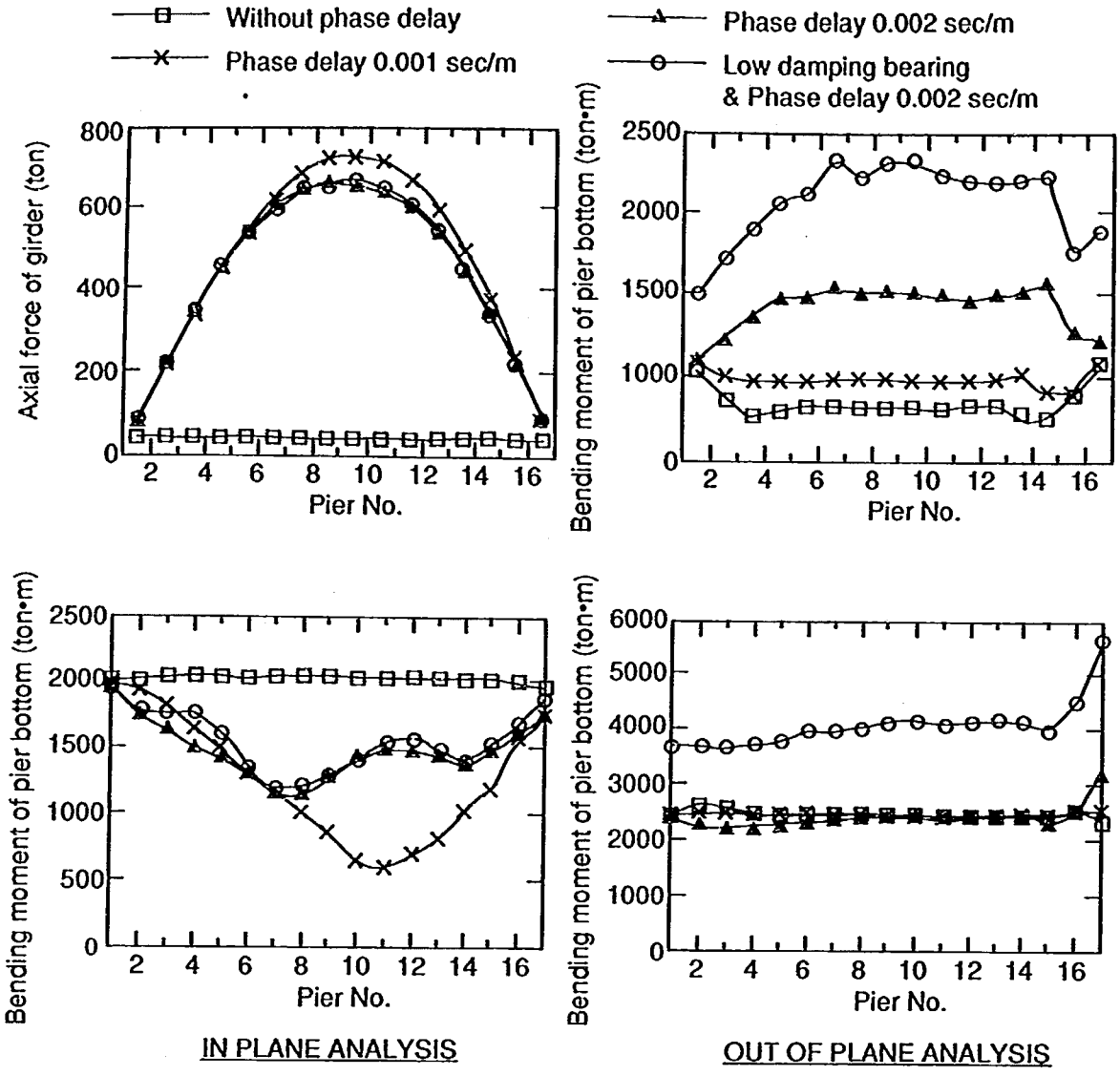


Fig. 8 Max. Response Values along Bridge Axis (Steel Girder)

On the other hand, in a direction lateral to the bridge axis, there is less stiffness since the girder is deformed by bending, and the girder on each bridge pier responds like a whip. For that reason, a decrease in the response acceleration does not occur. Conversely, when the phase delay is large, the large amplitude of response of a pier (No. 17) at one end is remarked. This is due to the occurrence of the so-called "whipping vibration." Namely, a bending mode wave propagates in the girder due to seismic wave action with a phase delay along the bridge axis and the wave energy propagated at the far end of the girder becomes concentrated there, causing a large response.

Figure 8 shows the moment and the axial force acts on the girders, and the moment the pier bases being taken from bridge piers on the horizontal axis. The axial force and the bending moment exhibit greater responses when there is a phase delay than when there is not. However, stress arising from these forces is limited to 10 percent of the allowable stress for girder material.

The results concerning the prestressed concrete-girder bridge are almost the same, both qualitatively and quantitatively. The weight of prestressed concrete girders is greater than that of steel-girders, but its span is shorter and the number of piers is greater, so that the

superstructure dead load corresponding to one isolation bearing and one pier becomes almost the same. Hence, bridge vibration characteristics are also the same.

2.2 Earthquake Response of a Curved Multi-span Continuous Bridge

Multi-span continuous bridges extending to a one-kilometer order do not always have straight alignment because of the configuration of the ground, the unwillful purchasing of the site, and so on. Thus, the effect of curved alignment on the earthquake response of a seismic-isolated multi-span continuous bridge has to be analyzed.

Analytical model and input seismic wave

The dimension of the model bridge is the same as that of the steel-girder bridge introduced in the former section. The girder is curved like an S-letter with a minimum radius of 300 meters and is supported by horizontally bi-directional isolation bearings on each pier top. Figure 9 shows a bird's eye view of the three dimensional analytical model. The input seismic wave form was the same as the wave form introduced in the former section. But, as the bridge alignment is curved here, the direction of vibration of the input seismic wave will affect the response of the bridge. So a series of response analyses was made taking the direction of vibration at 30 degrees pitch and overall maximum values of maximum responses were detected. The phase delay of the input seismic waves was not taken into account to simplify the results.

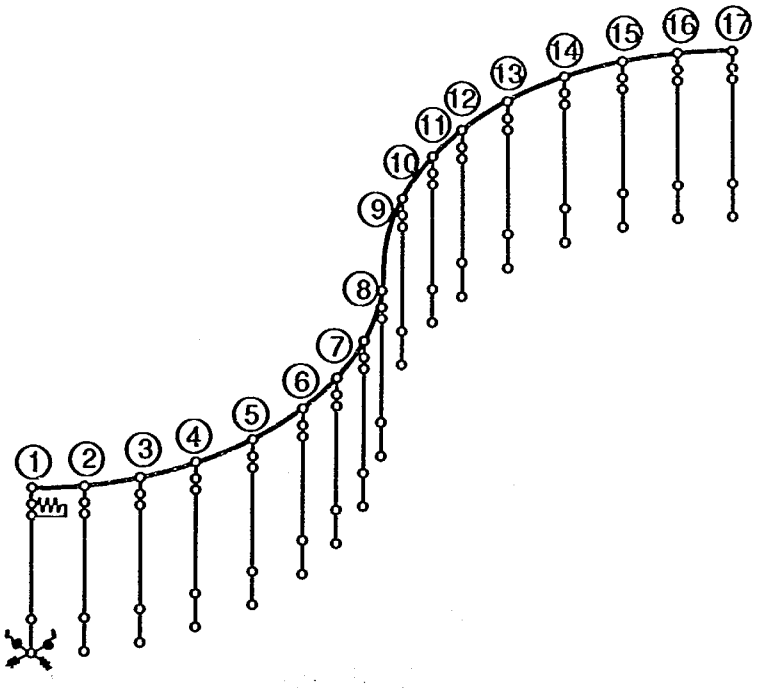


Fig. 9 Three Dimensional Model of S-Curved Multi-Span Continuous Bridge (Steel Girder)

Results of response analysis

Table 5 shows the maximum values obtained from a step-by-step response analysis. By comparing these results to those of the straight alignment bridge without a phase delay which are shown in Figure 8, you can find the relative displacement of the bearing and the bending

moment of the pier bottom which is nearly equal to those of the straight bridge. This means that the vibration of the curved girder and that of the skewed pier are well separated by the isolation bearing and do not affect each other. Thus, the curved girder responds like a rigid body, and this feature can simplify the design procedure and should be considered one of the advantages of the seismic isolation design.

Table 5 Maximum Relative Displacement of Isolation Bearing and Maximum Moment in the Lower End of Column

Pier No.	Maximum Relative Disp.		Maximum Moment	
	Axial (cm)	Lateral (cm)	Axial (tf•m)	Lateral (tf•m)
P1	5.7	5.8	1,037	1,268
P3	5.5	5.1	2,099	2,439
P5	5.4	5.4	2,097	2,579
P7	5.3	5.2	1,880	2,220
P9	5.4	5.0	1,871	2,109

2.3 Earthquake Response of a Multi-span Continuous Bridge under Different Ground Conditions

Multi-span continuous bridges of a one-kilometer order are not always found under uniform ground conditions. It is supposed that local ground conditions will affect seismic wave form and bridges extending over different kinds of ground will suffer from complex seismic input. Thus, the efficiency of a seismic isolation design against this kind of complex seismic input should also be analyzed. In this section, an earthquake response analysis of a seismic isolated bridge extending over two different kinds of ground conditions is introduced. Figure 10 shows a conceptual cross section of the bridge concerned. The dimension of the bridge is the same as the bridge introduced in section 2.2 except that the alignment is straight.

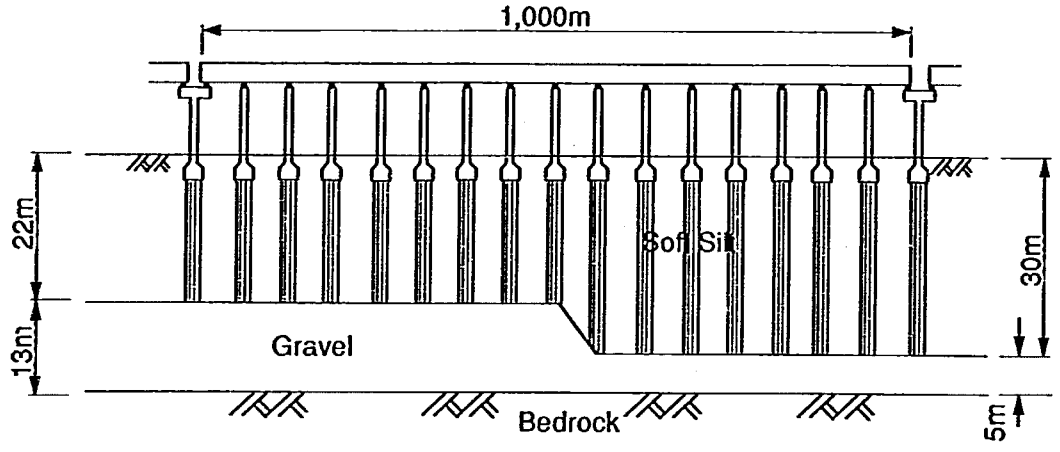


Fig. 10 Multi-Span Continuous Bridge Extending on Different Ground Conditions

Method of analysis

The ground response should be analyzed in order to take into account the effect of the change of ground conditions along the bridge axis. The ground model consisting of surface soil and bedrock only was formulated using FEM, and response acceleration waves along the bridge axis were evaluated using the usual step-by-step response analysis. The response of a multi-

span continuous bridge was then analyzed using step-by-step and multi-input response analysis and using the above mentioned waves as inputs.

Results of response analysis

Figure 11 shows distributions of, the maximum moment and the maximum axial force acting on the girders. Comparing this figure to Figure 8 in section 2. 1, it is seen that the effect of the change of ground conditions along the bridge axis is not as large as the effect of the phase delay in input seismic waves. Even considering the fact that the change of ground conditions in this study are not very abrupt, the effect of the change seems to be moderated by the effect of isolation bearings and is, therefore, not critical to the seismic safety of the bridge.

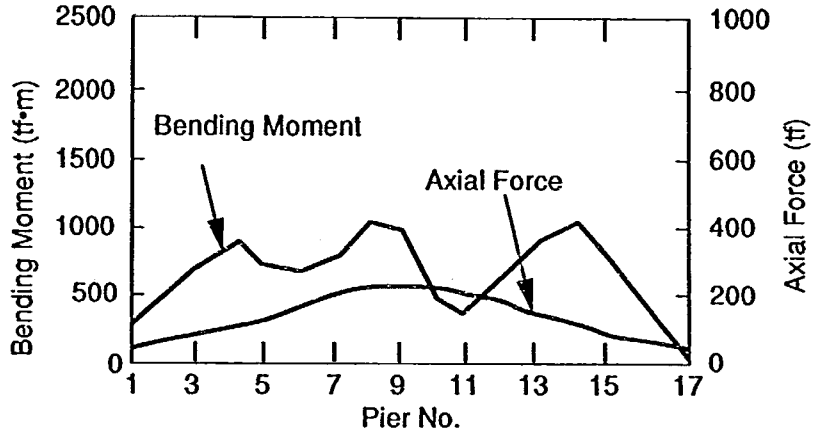


Fig. 11 Max Axial Force and Bending Moment of Girder (Steel Girder)

3. Optimum Natural Period of Seismic-Isolated Multi-span Continuous Bridges

As was discussed in the introduction, isolation bearings used for seismic-isolated bridges can not only isolate the seismic vibration but can also release statically indeterminate stress caused by expansion or shrinkage of the continuous girder. This feature of the seismic isolation design should be efficiently utilized to design very long multi-span continuous bridges. However, reduction of the lateral stiffness of the isolation bearing earthquake response displacement of the girder, which requires larger isolators and larger expansion joints to be set at the end of the girder. In this section, the optimum natural period is discussed in relation to the length of a continuous girder (Ref. 8).

Model bridge

A multi-span continuous bridge having a prestress concrete girder with straight alignment and constant cross section is considered. It is premised on that the stiffness of the piers is far greater than the lateral stiffness of the isolation bearings so that lateral displacement of the girder comes only from the deformation of the bearings.

Natural period to optimize displacement balance

As the expansion or shrinkage of a long continuous girder caused by temperature change and creep is large, the gap at the end of girder and the size of the expansion joint inevitably become large. Then, if the earthquake response displacement of the girder of the seismic-isolated bridge is smaller than the displacement caused by temperature change and creep, the

earthquake load does not push up the cost of the expansion joint. This condition can be simply stated as follows:

$$u_d \leq u_t \qquad \cdots\cdots(1)$$

where u_d : axial displacement of the girder caused by an earthquake (m)
u_t : axial displacement at the end of girder caused by temperature change (m)

In equation (1), piling up of thermal displacement on creep and earthquake response displacement is ignored to simplify matters. Evaluating the thermal expansion rate as 1.0×10^{-5} and temperature change as $\pm 20℃$, and ignoring the displacement caused by the lateral reaction of isolation bearings, u_t can be roughly expressed as follows:

$$u_t \fallingdotseq L\times 10^{-4} \qquad \cdots\cdots(2)$$

where L : length of a continuous girder (m)

On the other hand, as the girder may be assumed to be one lumped mass supported by one sum spring of isolation bearings in the axial direction, u_d can be denoted as follows:

$$u_d = \frac{W_u k_h}{K_D} \qquad \cdots\cdots(3)$$

where W_u : dead load of the superstructure (ton)
k_h : design seismic coefficient
K_D : equivalent linear spring constant of the isolation bearing for dynamic load (tf/m)

Further, the fundamental natural period of the bridge can be expressed by the following well-known formula for a one lumped mass system :

$$T = 2\pi\sqrt{\frac{W_u}{K_D g}} \fallingdotseq 2\sqrt{\frac{W_u}{K_D}} \qquad \cdots\cdots(4)$$

where T : fundamental natural period (sec)
g : acceleration of gravity (m/sec^2)

The following formula is obtained by substituting equations (1), (2) and (4) in equation (1) :

$$T \leq \frac{1}{50}\sqrt{\frac{L}{k_h}} \qquad \cdots\cdots(5)$$

Natural period to optimize lateral force balance

Dimensions of the foundation and pier are usually determined using the lateral seismic load. If the lateral force due to temperature change in the girder affects the dimensions, it will push up the cost of the bridge. Thus, the following norm is introduced to keep the configuration of the foundation and pier well balanced.

$$\alpha H_t \leq H_d \qquad \cdots\cdots\cdots\cdots\cdots\cdots\cdots\cdots\cdots\cdots(6)$$

where H_t : lateral force acting on top of the pier caused by temperature change
H_d : lateral force acting on top of the pier caused by earthquake
α : ratio of the allowable stress for dynamic load to that of static load

Ignoring the displacement of the pier and the inertia force of the pier itself, H_t and H_d at the end of the continuous girder are expressed as follows :

$$H_t = \beta K_D u_t \qquad \cdots\cdots\cdots\cdots\cdots\cdots\cdots\cdots\cdots\cdots(7)$$
$$H_d = W_u k_h \qquad \cdots\cdots\cdots\cdots\cdots\cdots\cdots\cdots\cdots\cdots(8)$$

where β : ratio of the static spring constant of the isolation bearing to the dynamic constant

Substituting equations (4), (7) and (8) for equation (6), the following formula is obtained :

$$T \geq \frac{1}{50}\sqrt{\frac{\alpha\beta L}{k_h}} \qquad \cdots\cdots\cdots\cdots\cdots\cdots\cdots\cdots\cdots\cdots(9)$$

β is evaluated to be 0.6 when usual Lead Rubber Bearing and High Damping Rubber Bearing are concerned. As a is usually 1.5, equation (9) can be re-written as :

$$T \geq \frac{1}{50}\sqrt{\frac{0.9L}{k_h}} \qquad \cdots\cdots\cdots\cdots\cdots\cdots\cdots\cdots\cdots\cdots(10)$$

Natural period to optimize thermal stress in girder

Statically indeterminate stress caused by temperature change occurs in the girder of multi-span continuous bridges. Thermal stress reaches its maximum at the middle of the girder and it is denoted as the following equation by replacing the lateral reaction forces in isolation bearings with a distributed lateral load along the bridge axis :

$$\sigma = \frac{\int_0^{L/2} \beta K_D U_t(x)dx}{A} = \frac{\frac{1}{4}\beta K_D u_t}{\frac{W_u}{\gamma_c L}} \qquad \cdots(11)$$

where σ : maximum thermal stress in the girder (tf/m^2)
$U_t(x)$: thermal expansion of the girder at location x (m)
γ_c : unit weight of reinforced concrete (ton/m^3)

Substituting equation (2) and (4) for equation (11) and evaluating γ_c as 2.4, the following equation is obtained :

$$T = 1.2\sigma^{-\frac{1}{2}} L \times 10^{-2} \qquad \cdots\cdots\cdots\cdots\cdots\cdots\cdots(12)$$

As the large value of tensile thermal stress demands additional prestressing to the girder and pushes up the cost of the bridge, σ should be designed to be less than 100 tf/m^2. Thus, equation (12) is re-written as follows :

$$T \geq 1.2L \times 10^{-3} \quad \cdots\cdots\cdots\cdots\cdots\cdots\cdots\cdots (13)$$

Optimum natural period

Optimum value of fundamental natural period should satisfy equations (5), (10) and (13). The design seismic coefficient k_h in equations (5) and (10) can be evaluated using the "Manual for Menshin-designed Highway Bridge (Draft) (Refs. 2, 4, 5)" as follows :

$$k_h = c_Z \cdot c_G \cdot c_I \cdot c_T \cdot c_E \cdot k_{h0} \quad \cdots\cdots\cdots\cdots (14)$$

Where k_{h0} : standard design seismic coefficient
c_z : seismic zoning factor
c_G : ground condition factor
c_I : importance factor
c_T : natural period factor
c_E : damping factor

Figure 12 shows the value of $c_G \cdot c_T \cdot k_{h0}$. Assuming c_Z and c_I are 1.0 and c_E is 0.9, k_h is evaluated and substituted in equations (5) and (10). Two relationships between T and L are drawn in Figure 13 together with the relationship defined by equation (14). The painted out strips in the figure are the optimum zones. Although the Menshin design is feasible outside the painted out strips, it will be trapped by one of the cost factors. For example, it can be easily recognized that thermal stress in the girder will be a cost factor in the case of the length of a continuous girder in a one-kilometer or more with poor ground conditions.

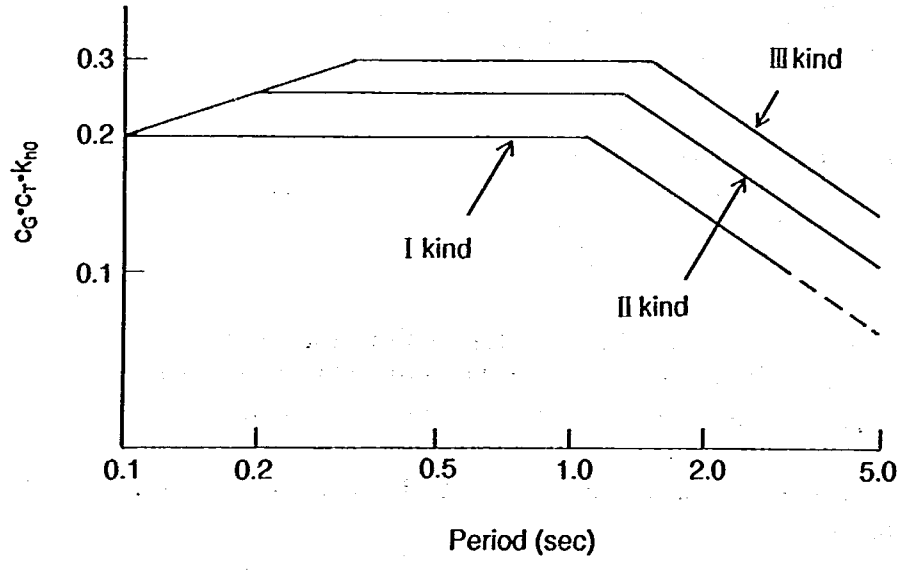


Fig. 12 Design Seismic Coefficients

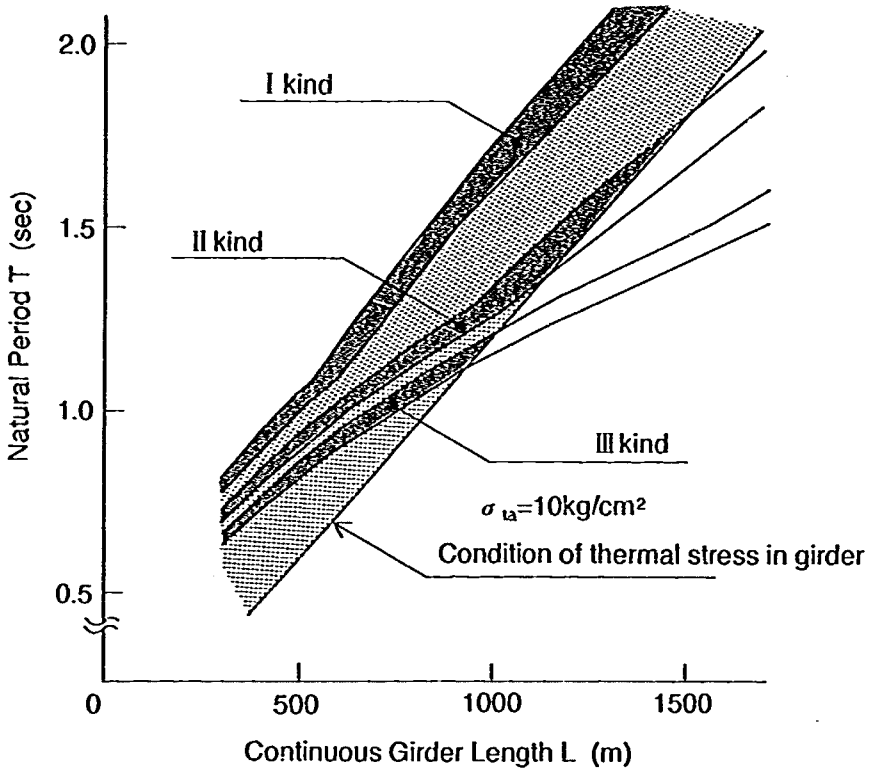


Fig. 13 Optimum Relation between Natural Period T and Girder Length L

4. Adjustment Method of Strained Isolators Supporting Multi-span Continuous Bridge

Prestressed concrete girders shrink in the direction of the girder axis as the result of concrete dry-shrinkage and creep during and after the construction. It becomes such amount of displacement as several ten centimeters at the end of the one-kilometer continuous girder. Consequently, the seismic isolation bearings that had to be placed to support the girder at the early stage of its construction are considerably strained and need adjustment. The adjusting work may have to be executed after the completion of the construction. Then, the development of a technique to adjust the strained isolators keeping the bridge in service becomes one of the key technologies for one-kilometer continuous prestressed concrete girder bridge.

Adjustment Method

Several methods have been proposed in Japan and two of them are schematically introduced in Figure 14. Their common concept is to slide the base plate of isolator by pulling or pushing it. The base plate is re-rocked after the completion of slide adjustment by welding or screw clamps.

Results of Slide Test

As we had a little experience of actual adjustment works, an indoor slide test was done to measure the friction and to know the workability of the method. Figure 15 shows a specimen in the loading system. The result of the test implies that a lubrication treatment on the surface of the base plate or a partially jacking the girder up will be necessary for efficient adjustment.

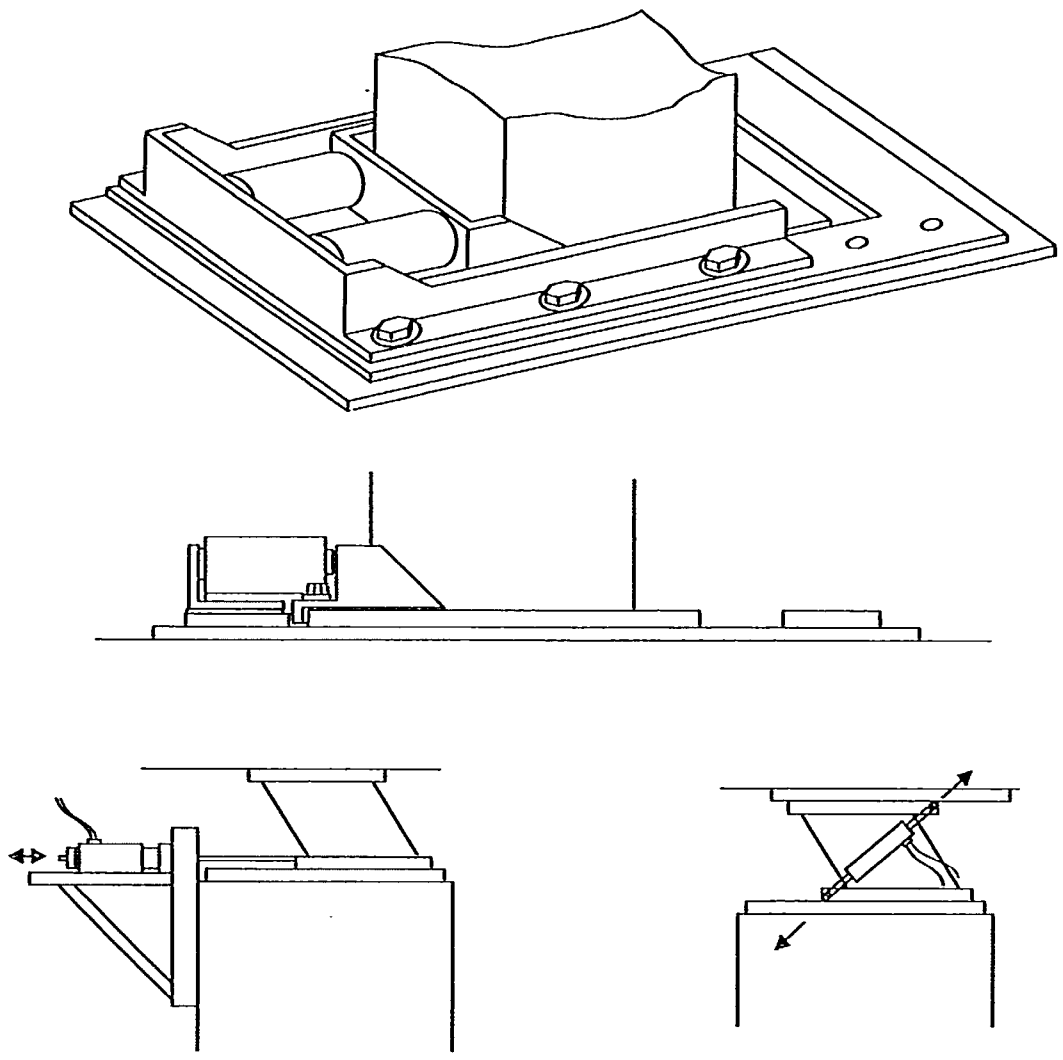


Fig. 14 Sketch of Adjusting Works

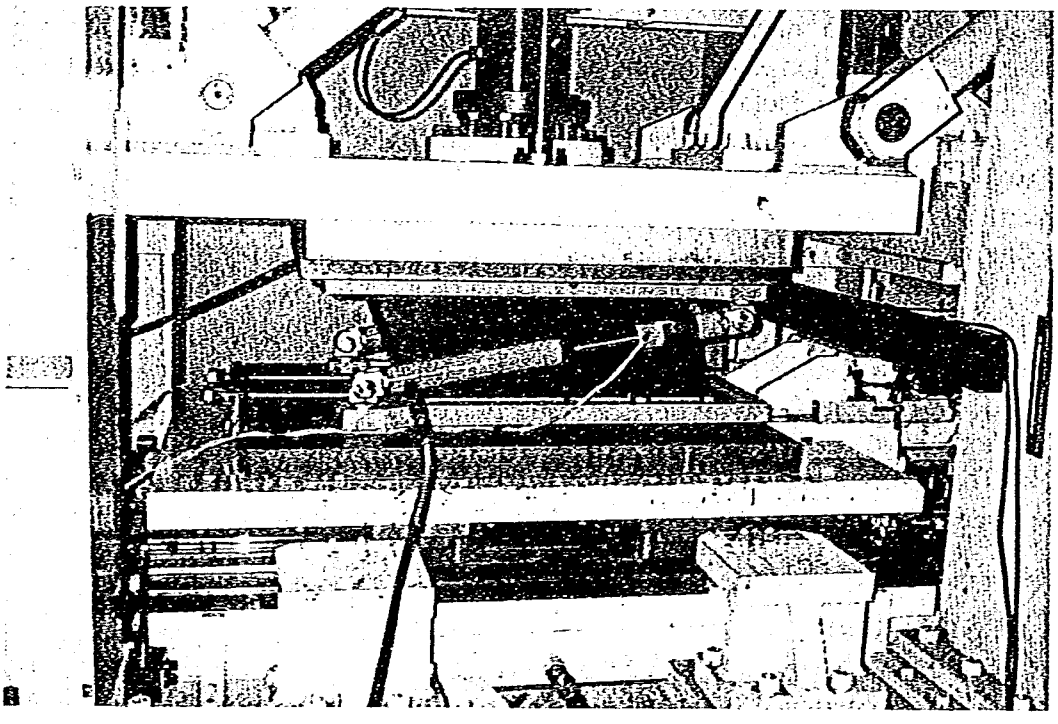


Fig. 15 In-door Test of Adjusting Work

CONCLUSIONS

(1) Multi-span continuous girder bridges with a one-kilometer long jointless deck become feasible with the application of the seismic isolation design.

(2) The effect of the phase delay input is noticeable in response acceleration and displacement in the axial direction and that these values decrease substantially. This means that the seismic isolation design can be applied effectively in this direction in multi-span continuous bridges with long girder since the effective input of the earthquake motion on the girders decreases as a result of the phase delay effect.

(3) On the other hand, the section force arising in the girders increases as a result of this delay input. However, the increase is only 10 percent of allowable stress.

(4) There is a tendency for the response of girders in the lateral direction to the bridge axis to increase at the end section of one-kilometer continuous girders. This is thought to arise from the response amplification caused by the bending mode wave propagation arising in the girder that is propagated in the direction of the girder axis and is reflected at the girder end. This response represents an increase of about 30 percent on most components.

(5) The curved alignment effect on the earthquake response of seismic isolated multi-span continuous bridges is moderated by the vibration separation effect of the isolation bearings. The curved girder on the bearings responds like a rigid body and the skewed piers respond in their own vibration axis.

(6) The change of ground conditions along the bridge axis does not have much effect on the earthquake response of seismic isolated multi-span continuous bridges.

(7) There is an optimum period of fundamental natural vibration which will ensure good balance in the seismic isolation design of multi-span continuous girder bridges. The optimum period is related to the continuous length of the girder and is reasonable up to a length of more than one-kilometer continuous girder.

(8) Adjustment of strained isolator by sliding is exactable when some assistant methods such as lubrication of base plate or partial lift up are accompanied even though the isolator supports the load of girder.

ACKNOWLEDGMENTS

The first and the second chapters of this paper come from the reports of the joint research between the Public Works Research Institute and 28 private firms in Japan on the Menshin System for Highway Bridges (Ref. 3). The author expresses his sincere thanks for Dr. Kazuhiko Kawashima who chaired the joint research and all other participants who involved the research works.

REFERENCES

1. Japan Road Association, Part · Seismic Design of the Specifications of the Design of Highway Bridges, (1990)(in Japanese)

2. Public Works Research Institute and 28 Private Firms, "Manual for Menshin Design of Highway Bridges (Draft)", Joint Research Report, Public Works Research Institute, (1992)(in Japanese)

3. Public Works Research Institute and 28 Private Firms, "Report of the Joint Research on Menshin System for Highway Bridges, No.1,(1990), No.2,(1991), No.3,(1992)", Joint Research Report, No.44, No.60 and No.75, Public Works Research Institute, (in Japanese)

4. Kawashima, K., "Manual for Menshin Design of Highway Bridges", Proc. of the Second U.S-Japan Workshop on Earthquake Protective Systems for Bridges, Tsukuba, Japan, pp.185 - 194, (1992)

5. Sugita, H. and Mahin S.A., "Manual for Menshin Design of Highway Bridges : Ministry of Construction, Japan", EERC Report No. UCB/EERC-94/10 August 1994

6. Goto, Y., Tokunaga, M., Yoshimura, T.and Shintaku, M., "Seismic Response of Multi-span Continuous Bridge with Deck Length of 1km", Proc. of the First U.S-Japan Workshop on Earthquake Protective Systems for Bridges, Buffalo, N.Y., U.S.A, (1991)

7. Mashiko, H., Arai, H. and Fujiwara, Y., "Application of Menshin Design to Bridges with Deck Length of 1,000m", Proc. of the First U.S-Japan Workshop on Earthquake Protective Systems for Bridges, Buffalo, N.Y., U.S.A, (1991)

8. Goto, Y., Kikuchi, T. and Ina, Y., "Consideration on Optimum Period of Menshin-Designed Multi-span Continuous Bridge with Very Long Jointless Deck", Proc. of the 22th Earthquake Engineering Workshop of JSCE, Kyoto, Japan, pp.811 - 814, (1993)(in Japanese)

SEISMIC CHARACTERISTICS AND VIBRATION CONTROL OF PC CABLE-STAYED BRIDGE UNDER CONSTRUCTION

by

Meguru TSUNOMOTO [1], Shunichi HIGUCHI [2] and Yozo GOTO [3]

1. Research Engineer for Research & Development Division,
   Oriental Construction Co., 2-1-1, Hirakawa-cho, Chiyoda-ku, Tokyo 102, Japan
2. Research Engineer for Civil Engineering Department, Technical Research Institute,
   Obayashi Co., 4-640, Shimokiyoto, Kiyose-shi, Tokyo 204, Japan
3. Section Chief, Ditto

ABSTRACT

This paper presents the seismic characteristics of long-span PC cable-stayed bridges under construction by the cantilever erection method, as well as the applicability of various vibration control systems during the construction phase.

INTRODUCTION

Long-span PC cable-stayed bridges are generally constructed using the cantilever erection method. Because of effectively utilizing the structural features, this construction method is best suited to the construction of long-span PC cable-stayed bridges. In addition, this method does not restrict the conditions of under the girder during the election. With this method, however, the bridge is supported only by a pier during election of the girder. This leads to poor stability . Therefore, countermeasures may be required to stabilize the bridge against external excitations, for example, earthquake and wind.

During construction, half of the after-completion value is usually adopted as the disign earthquake force. With this assumption, magnotude of the section force at the pier base becomes as large as the magnitude of after-completion. For bridges whose seismic response will be reduced after completion by use of the damper or other structural control system, certain sections become more critical during construction than after completion. Because some movable sections are temporarily fixed during construction, some vibration control systems or seismic protective systems that will be adopted after completion are not applicable. It is necessary, therefore, to develop the vibration control systems tailored to the construction period.

This paper investigates the seismic characteristics of PC cable-stayed bridges under construction, as well as vibration control systems applicable during the construction period. This study is intended to explore one of the themes of a joint research program on "Development of earthquake protective technologies for long-span bridges with high-damping systems".

BRIDGE MODEL AND SEISMIC FORCE

Bridge model summary

As the Bridge model for this study, a continuous three-span PC cable-stayed bridge with a central span length of 400 m is adopted. Considering its large scale, a floating type girder support system and a two-plane cable arrangement with fan shape is assumed. Fig. 1 shows a general view of the model bridge. Fig. 2 outlines the cantilever election method. For the weight of election machines, analysis for under construction phase assumed 140 tf of a Traveler at each end of main girder and 80 tf of a crane at the top of the tower. We use a damping ratio of 1.0% before and after construction without applying a vibration control or seismic protective systems.

Seismic force

Numerical simulations were performed to investigate the seismic performance and applicability of vibration control systems. The response-spectrum metod and time-history response analysis are mainly used for computation. The joint research adopts the ground motion for the type 1 ground. This record is based on strong-motion record of the Miyagi off-shore earthquake, and adjusting its amplitude to correspond to the response spectrum, shown in Fig. 3. Fig. 4 shows the input accelelation record for calculation. In the analyses, both before and after bridge completion periods, we used this same response-spectrum and seismic ground motion as the input seismic force.

SEISMIC CHARACTERISTICS OF BRIDGE UNDER CONSTRUCTION

To obtain basic data for the system and level of vibration control, we investigated the natural vibration characteristics and seismic performance of the model bridge before and after the completion of construction.

Natural vibration and seismic characteristics after completion

Fig. 5 shows the dominant natural vibration mode in an earthquake in the longitudinal direction. Table 1 shows the result from the response analysis. In this Table, the RMS value is the root mean square value in mode responses up to the natural period of 0.1 second. Case A is a bridge with a normal floating support system. In case B, the support at main pier is

elastically fixed in the longitudinal direction by elastic cables (EA = 2.14 x 10^5 tf). In case A, the 1st vibration mode with a natural period of about 8 second was most dominant. In case B, the 1st natural period comes to 1/3. The 2nd vibration mode comes to the dominant vibration mode, instead. The elastic suspension reduces the section force by about 40% at the tower bottom, however, it increases the magnitude at the pier base by about 25%.

Natural vibration and seismic characteristics under construction

We analyzed the natural vibration and seismic characteristics of bridge under construction at cantilever ratios of 25 to 100%, while assuming that the pier and the girder are temporarily fixed. (The tower is assumed to complete until the cantilever ratio comes to 25%.)

Fig. 6 shows the dominant natural modes at cantilever ratios of 50 and 100% during an earthquake along the longitudinal direction. Fig. 7 shows changes in the natural period of each mode. Fig. 8 shows the change in the effective mass ratio while the cantilever ratio increases. As the cantilever ratio increases, the natural period extends logarithmically, while its increase ratio is smaller in higher modes of vibration. Based on a comparison of cantilever ratios of 25% and 100%, the increase ratio at 100% is about 3 times larger than at 25% in antisymmetric 1st mode and about 1.5 times larger in antisymmetric 3rd mode. As the cantilever construction progresses, the dominant vibration mode of the effective mass ratio shifted from the antisymmetric 1st and 3rd modes at the cantilever ratio of about 25% to the antisymmetric 2nd mode at about 50%. When the cantilever ratio comes to 75%, the dominant mode changes to the antisymmetric 3rd mode.

To define changes in sectional force as construction progresses, Figs. 9 and 10 shows the changes in the maximum bending moment at the tower bottom and the pier base. The RMS value is the root mean square value in all mode responses up to a natural period of 0.1 second. The maximum bending moment at the tower bottom was dominant in antisymmetric 1st mode. Response value decreases as cantilever construction progresses, presumably due to the longer periods in the 1st mode. Maximum bending moment at the pier base tends to increase as cantilever construction progresses. The mode which the response value is dominant depends on the cantilever ratio, and coincides with the mode which the effective mass ratio is dominant (Fig. 8). In terms of the magnitude of maximum bending moment, the pre-completion value at the pier base is 1.5 to 2 times as large as the post-completion value.

To define changes in response displacement as construction progresses, Fig. 11 shows maximum longitudinal displacement at the tower top; Fig. 12, maximum vertical displacement at the end of the girder. Longitudinal displacement at the tower top tends to become larger than vertical displacement at the end of the girder when the cantilever ratio is 50% or less. On the other hand, when the cantilever ratio exceeded 50%, longitudinal displacement at the

tower top becomes smaller than the vertical one at the end of the girder. This suggests that tuned mass type vibration control devices are more effective when they are installed at the end of girder to work for the vertical direction than on the tower top for the longitudinal direction.

VARIOUS VIBRATION CONTROL SYSTEMS

In the section below, we discussed the effects of various vibration control systems applicable during bridge construction at an cantilever ratio of 100%.

Seismic protective cable

During construction, back stay cables are sometimes used to cope with weight imbalances. We also studied the effect of back stay cables as a means of vibration control. Fig. 13 is a sketch of a system of seismic protective cable. To minimize interference with construction, we assume that the seismic protective cable were installed between the tower top and the end-pier. We assumed a section of seismic protective cable was equivalent to that of two uppermost stay-cables.

Table 2 compares the seismic characteristics of bridges, one with seismic protective cable and one without, whichever having same damping ratio. Although the seismic protective cables reduce sectional force in the antisymmetric 1st mode, they display no seismic effects in other modes. Since the antisymmetric 1st mode contributes less to the seismic effect as the cantilever ratio increases, it seems that seismic protective cable are not effective during the construction period.

Variable stiffness control

During the construction period by the cantilever method, the girder is temporarily fixed to the main-tower pier to simplify construction works. This will significantly increase the bending moment at the pier base during earthquake. Concerning the applicability of a variable stiffness control system as illustrated in Fig. 14, seismic performance of the model bridge in terms of the rigidity of the girder is discussed in this section.

The eigenvalue analysis and the response analysis using the direct integration method are performed in this study. The rigidity of the girder is evaluated as a modules of the spring, which elastically links between the girder and the main-tower pier top in the bridge axial direction.

Fig. 15(a) gives the result of real eigenvalue analysis in terms of spring modules k which represent the rigidity of the girder. As k becomes larger, natural period of each mode comes smaller. Though the period of the 1st and the 2nd modes come to 1/4 of free case when k comes to larger than 10^5, the 3rd mode doesn't change as such. When rigidity of the girder is

small(i.e., k is small), the 1st mode's vibration is dominant, while the second mode's vibration is dominant in case of high rigidity (i.e., k is large). Fig. 15(b) shows the relation between the rigidity of the girder and maximum bending moment at the tower bottom and the pier base, result from response analysis. As the rigidity increased, bending moment of pier base tends to increase, however, bending moment of tower bottom decreases. This is because the pier mainly shares the inertia force of the girder during earthquake. In addition, isolation effect of the girder becomes small when the rigidity is large.

Variable damping control

To improve the damping performance of a bridge after the completion, installation of dampers between the girder and pier (Fig. 16) is proposed. In this section, effectiveness of this method for improvement of damping characteristics of a PC cable-stayed bridge under construction is discussed.

In case if the cantilever ratio of 100% model bridge, complex eigenvalue analysis is performed to evaluate damping performance of model bridge. The analysis is implemented with viscous damping coefficient as a parameter of the damper which was installed on the main tower's pier along the bridge axial direction.

Fig. 17(a) shows the relation between the viscous damping coefficient of the damper and the modal damping of the bridge. This figure confirms that a damper with damping coefficient of 1,000 tf*m/sec produces a modal damping of 80% for the 1st mode. In addition, about 8% of modal damping is obtained for the 2nd mode. In terms of the natural period of the bridge, however, this method extend the 1st natural period as shown in Fig. 17(b). This brings about instability againt wind excitation.

Tuned mass damper

In this section, we investigate the effects of Tuned Mass Dampers (hereafter, TMD) which are assumed to install at the ends of the girder and the tower top (Fig. 18). TMDs at the ends of the girder have weight of 20 tf each, and a weight of 40 tf TMD is located at the tower top. TMD is tuned to vibrate with antisymmetric 3rd mode, which contributes the most to sectional force at the pier base. TMD's mass ratio is totaled 0.0030 for the girder ends, and the mass ratio is 0.0004 for the tower top TMD. The TMD's optimal frequency ratio and damping ratio depends on the kind of excitation. In this calculation, we adopt the frequency ratio and the damping ratio as optimal values for harmonic external dynamic excitation.

Fig. 19 illustrates the response bending moment at the pier bottom when the TMDs were installed at the ends of the girder or the tower top. The broken line in the Figure represents the response value when TMDs were not used. When the TMDs were installed at the girder ends,

the vibration control effect emerged 5 seconds after the start of ground motion and reduced the response value of the maximum bending moment by about 10%. However, from 12 to 20 seconds after the start of the motion, response value is increased over without TMDs. When the TMD was installed at the tower top, the vibration control effect was insignificant, with maximum moment reduced by only about 2%.

Fig. 20 gives the response displacement of mass of the TMD. Comparing the girder ends value with the tower top value, the maximum response displacement is 50% larger than that of the girder end. TMD at the girder ends, a phase of response displacement was changed at 13 seconds after the start of input motion. This seems the reasons for response bending moment increase compared with without TMD. In this analysis, we reviewed the effectiveness of TMDs with limited parameter. It seems that effectiveness of TMD are influenced by the characteristics of excitations. This is partly due to the insensible characteristics of TMD's operation, and under certain circumstances, TMD increases the response of the main structure.

Active mass damper system

Recently, various active control system was applied to bridge during construction. These systems, however, aimed to control the response caused by wind excitation. In this section, effectiveness and applicability of the Active Mass Damper system (hereafter, AMD system) to the bridge during earthquake is examined.

Effectiveness of the AMD system is examined by the response analysis with direct integration method in terms of the response values and the section forces of the model. AMD systems are installed on the top of the tower in the bridge axial direction (Case 1) and installed on both girder edges in vertical direction (Case 2). AMD is controlled by the direct velocity feedback method with unlimited control force. The girder is temporarily fixed to the pier in this calculation.

(1) AMD at the top of the tower

Figs. 21(a) to (d) show the vertical displacement at the end of the girder, bending moments of at the tower bottom and pier base, and the AMD's control force. In the figures, dotted lined represent the response values of which no vibration measure were installed. Owing to the AMD system, the maximum vertical displacement can be reduced by 15% and quickly converged after the earthquake. The maximum bending moment at the tower bottom is also reduced by 15%, however, the maximum bending moment at the pier bottom is only 3% smaller than uncontrolled result. The maximum control force of AMD is 159 tf in this calculation.

(2) AMD at the ends of both girders

Figs. 22(a) to (d) similarly show the vertical displacement at the end of the girder, bending moments of at the tower bottom and pier base, and the AMD's control force. The maximum vertical displacement can be reduced to less than 30% of uncontrolled result and little oscillation is observed after the earthquake. The maximum bending moment at the tower bottom is also reduced by 30%, however, the maximum bending moment at the pier bottom is 3% larger than uncontrolled result. The maximum control force of AMD is 160 tf in this calculation.

CONCLUSIONS

For long-span PC cable-stayed bridges, seismic characteristics and various vibration control systems for under construction are investigated. The results are as follows.

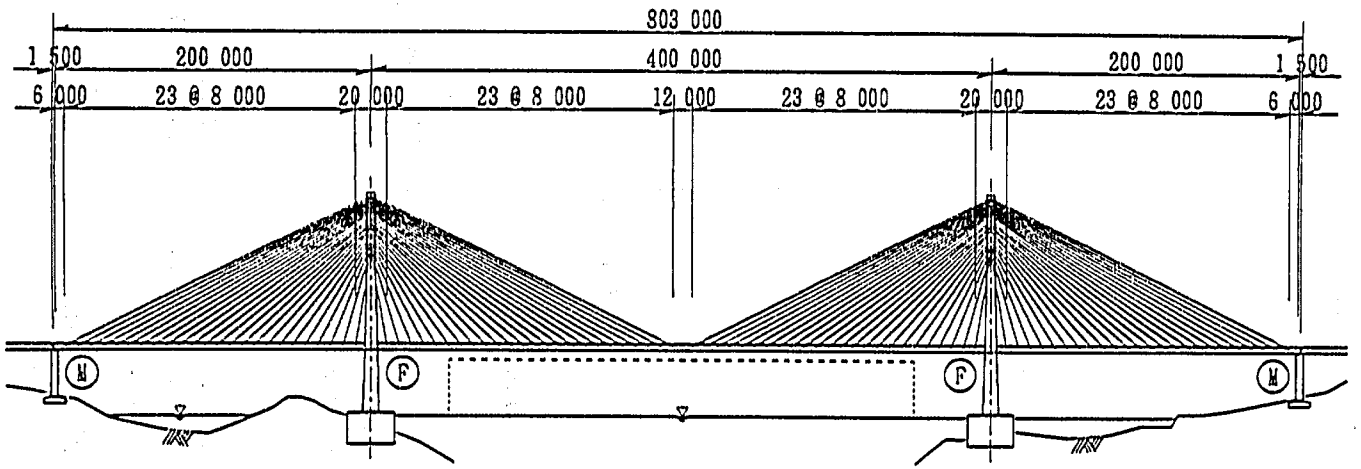
(1) As the cantilever construction prigresses, the dominant natural mode of the effective mass ratio shifts from the 1st mode to the 3rd mode.
(2) The maximum bending moment at the tower bottom is dominant in the response of the 1st mode. The value of that moment decreases as the cantilever construction progresses.
(3) The maximum bending moment at the pier base is dominant in the response of the mode of which the effective mass ratio is dominant. The value of that moment increases as the cantilever construction progresses.
(4) Since the 1st mode becomes less contribute to the seismic effect as the cantilever ratio increases, it seems that the seismic protective cables are not effective during the construction period.
(5) It is shown that the stiffness control is effective measure to reduce the bending moment of pier base. As the rifidity of the girder becomes small, the bending moment of pier base also becomes small. On the other hand, the bending moment of tower bottom becomes large at that time.
(6) Relatively larde modal damping can be added by the damping device installed between the girder and top of the peir. Large damping, however, extends the natural period of the 1st mode and brings about instability against wind excitation.
(7) TMDs show certain effectiveness in terms of the section force of the structure, however, the effectiveness is influenced by characteristics of excitations.
(8) AMD system can reduce response displacement and section force of the tower. In spite of relative large control force is added to the bridge, little effectiveness is observed in terms of the section force of the pier. This is partly due to the control algorism of the AMD system.

ACKNOWLEDGMENT

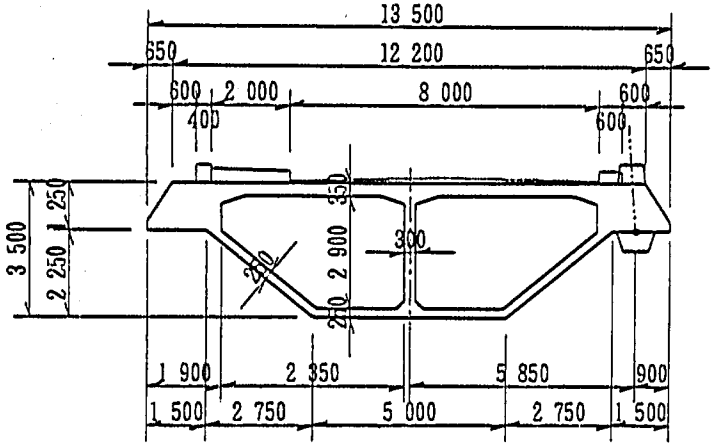
This study is intended to explore one of the themes of a joint research program on "Development of earthquake protective technologies for long-span bridges with high-damping systems" by the Public Works Research Institute, Ministry of Construction, and the Public Works Research Center. This joint research began in 1993 under a three-year plan and is being supported by researchers from 19 private groups. The authors would like to thank those participating in the joint research for their valuable advice and cooperation in this study.

REFERENCES

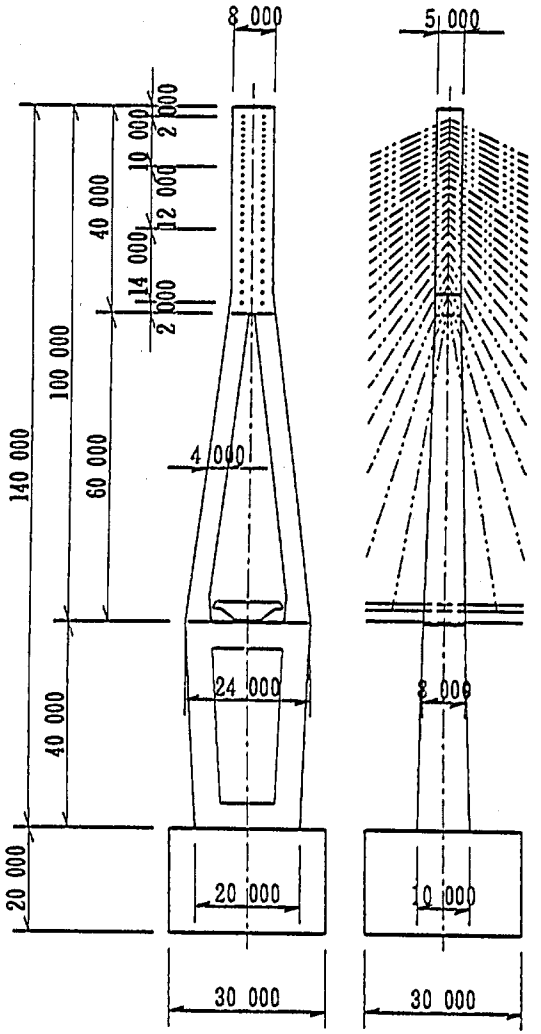
1. Subcommittee on Vibration Control : Proceedings of Colloquium on Control of Structures Part A, JSCE, July, 1991 (in Japanese).
2. Subcommittee on Vibration Control : Proceedings of 2nd Colloquium on Vibration Control of Structures Part A, JSCE, August, 1993 (in Japanese).
3. Subcommittee on Vibration Control : Proceedings of Colloquium on Control of Structures Part.B, JSCE, July, 1991 (in Japanese).
4. Subcommittee on Vibration Control : Proceedings of 2nd Colloquium on Vibration Control of Structures Part B, JSCE, August, 1993 (in Japanese).
5. Public Works Research Institute : Report of Joint Research Program on Development of Earthquake Protective Technologies for Long-Span Bridges with High-Damping Systems Part 1, March, 1994 (in Japanese).
6. Yoshimura, M., Ueki, Y. and Imai, Y. : Design and Construction of Prestressed Concrete Cable-Stayed Bridge "Tsukuhara Ohashi", Journal of Prestressed Concrete, Japan, January, 1987 (in Japanese).



(a) Side View



(b) Cross Section of Girder



(c) Towe and Pier

Fig. 1 General View of PC Cable - Stayed Bridge

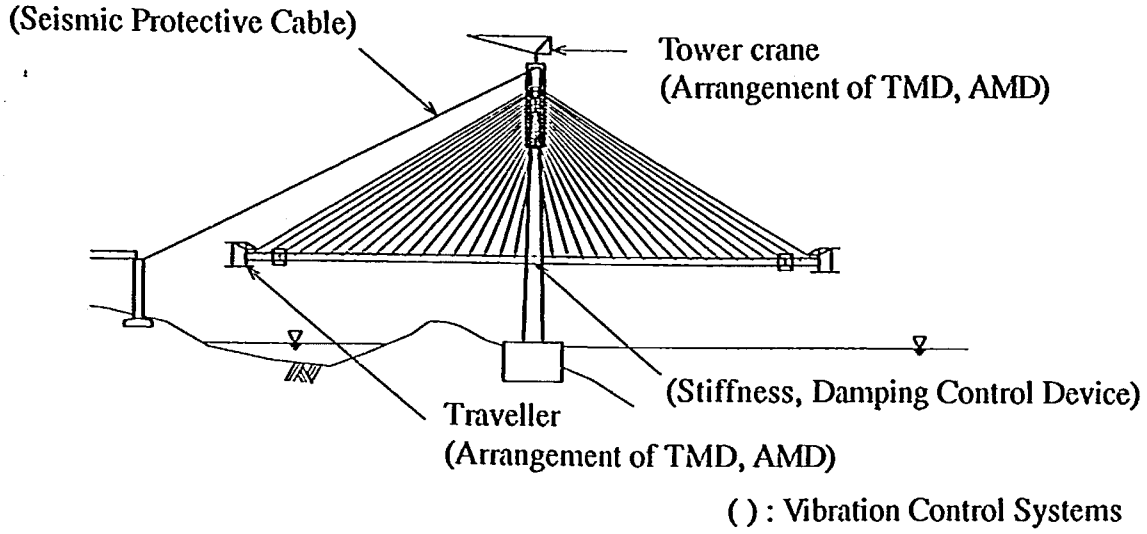


Fig. 2 Construction by Cantilever erection

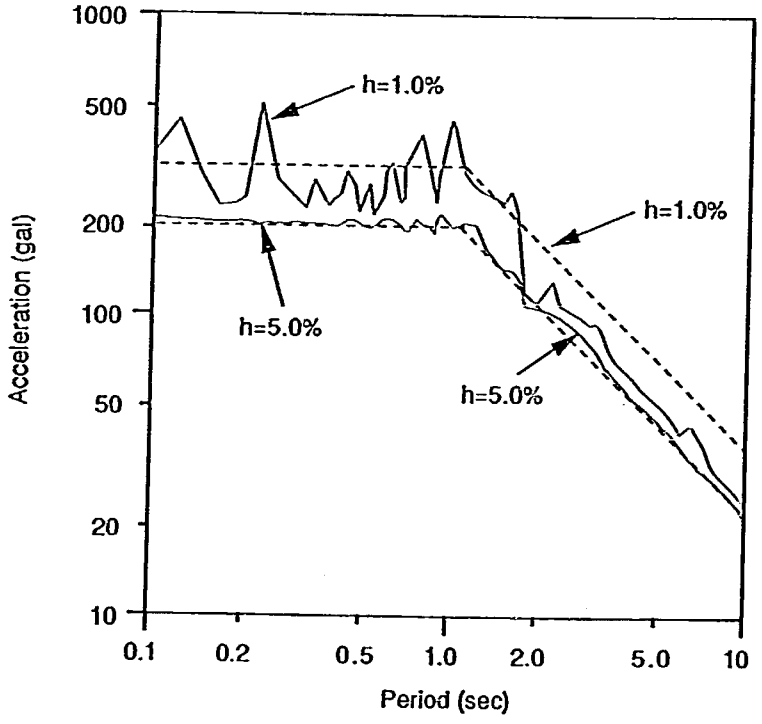


Fig. 3 Response Spectra

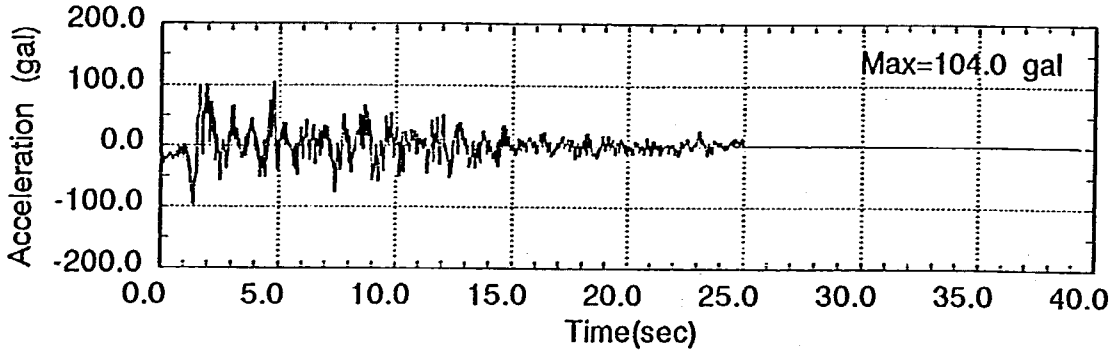
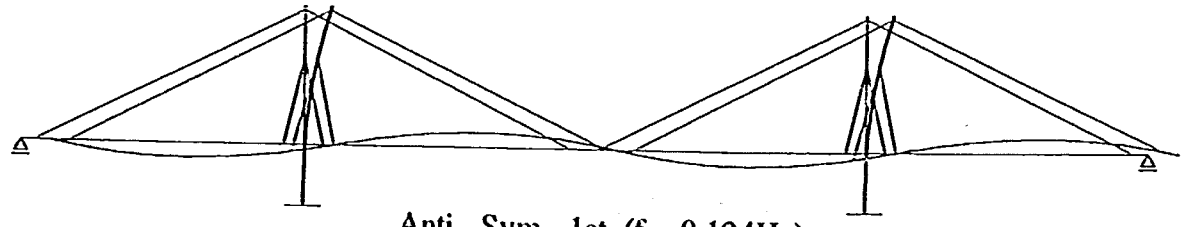
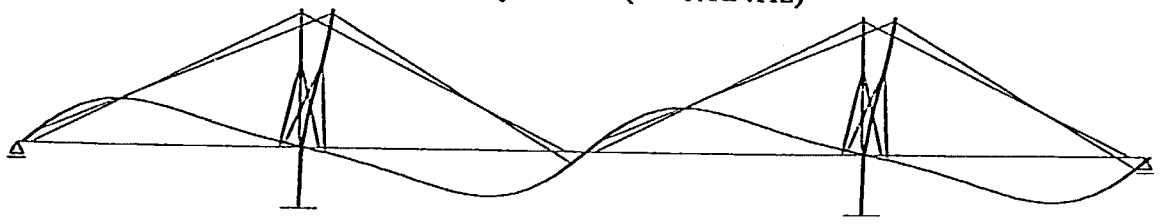


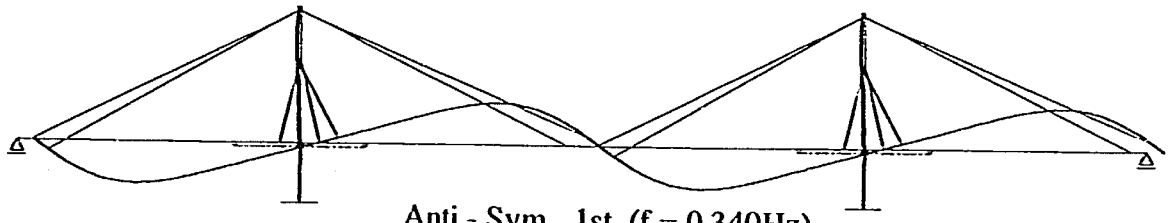
Fig. 4 Input Ground Motion



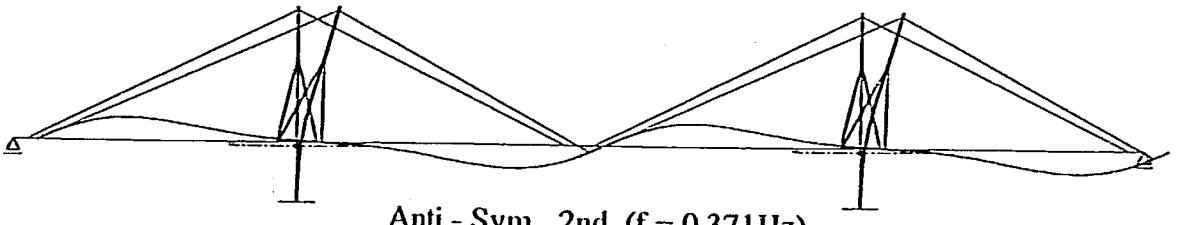
Anti - Sym. 1st (f = 0.124Hz)



Anti - Sym. 2nd (f = 0.355Hz)
Case A



Anti - Sym. 1st (f = 0.340Hz)



Anti - Sym. 2nd (f = 0.371Hz)
Case B

Fig. 5 Natural Mode after Completion

Table. 1 Response Bending Moment after Completion

Case	Mode No.	Natural Period (sec)	Effective Mass Ratio (%)	Bending Moment (tf·m)	
				Tower Bottom	Pier Bottom
A	1st	8.088	49.11	69557	100116
	2nd	2.818	9.17	19682	35948
	3rd	1.067	3.24	5904	20138
	R.M.S	~0.100	89.73	73342	122160
B	1st	2.944	10.23	8825	10576
	2nd	2.698	52.27	43708	145419
	3rd	1.063	2.10	4764	13877
	R.M.S	~0.100	89.73	45957	153396

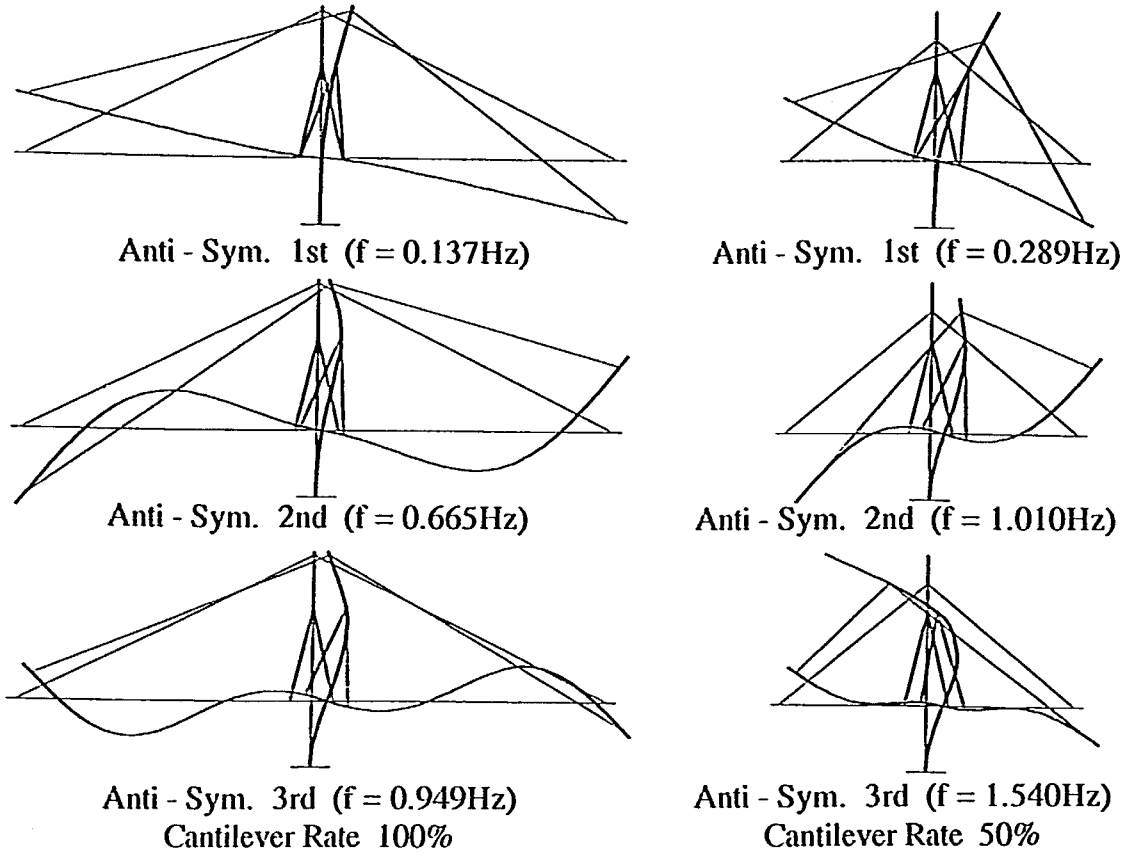


Fig. 6 Natural Mode under Construction

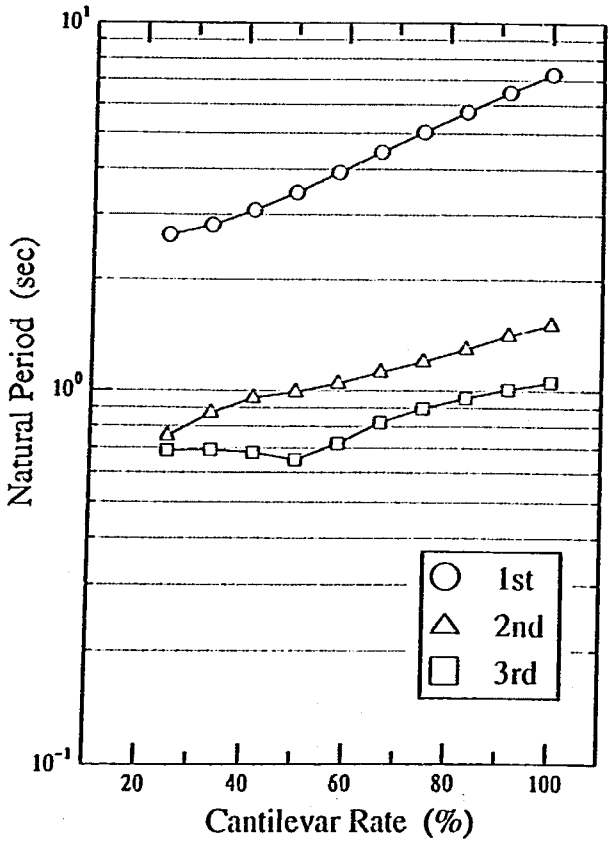


Fig. 7 Variation of Natural Period under Construction

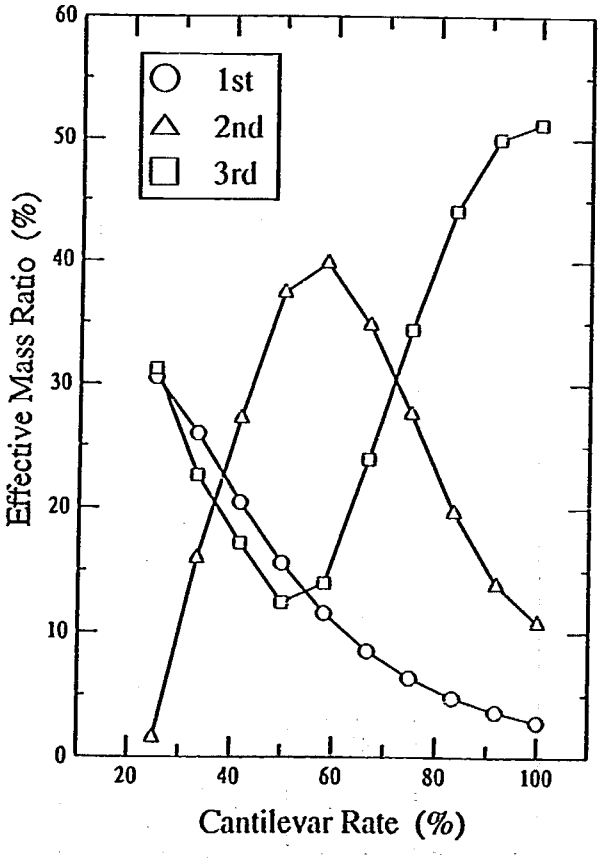


Fig. 8 Variation of Effective Mass Ratio under Construction

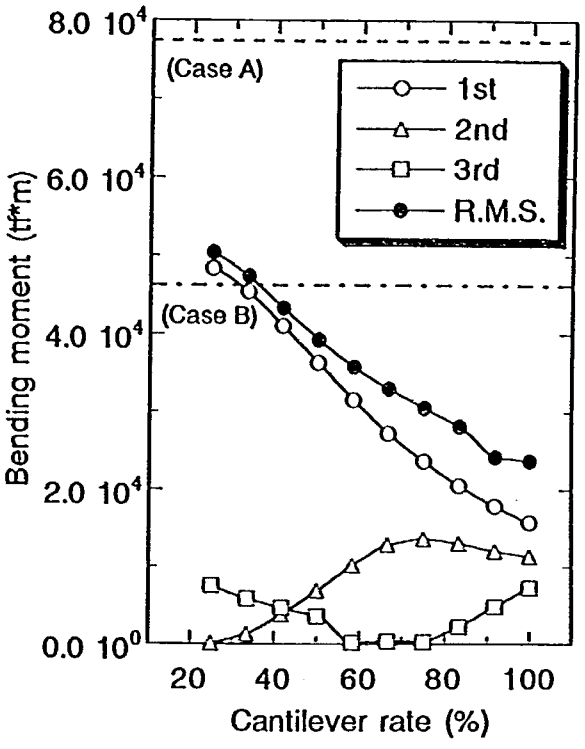


Fig. 9 Bending Moment at Tower Bottom under Construction

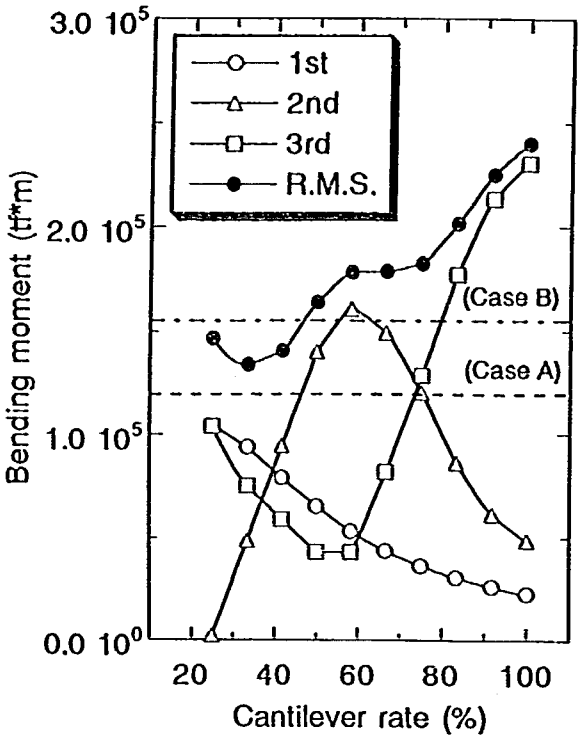


Fig.10 Bending Moment at Pier Base under Construction

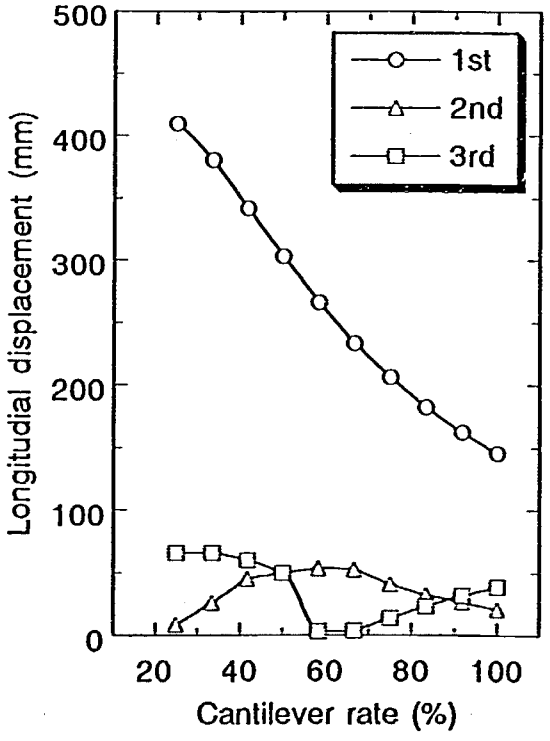


Fig.11 Displacement at Tower Top under Construction

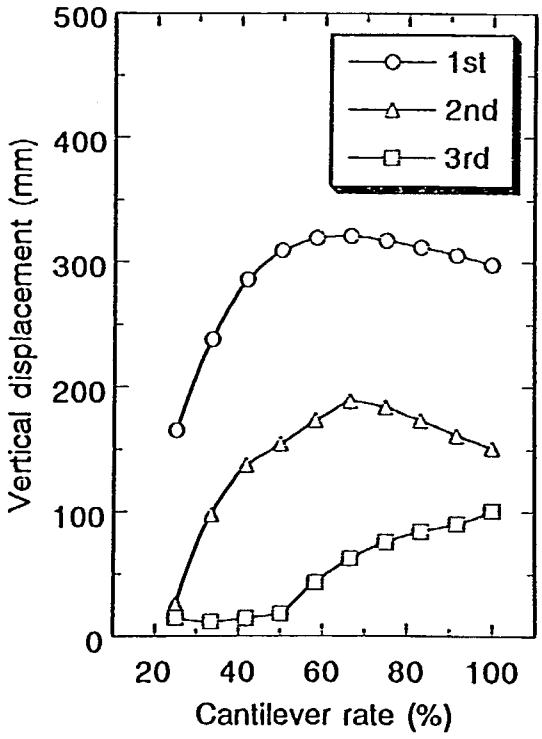


Fig.12 Displacement at Girder Edge under Construction

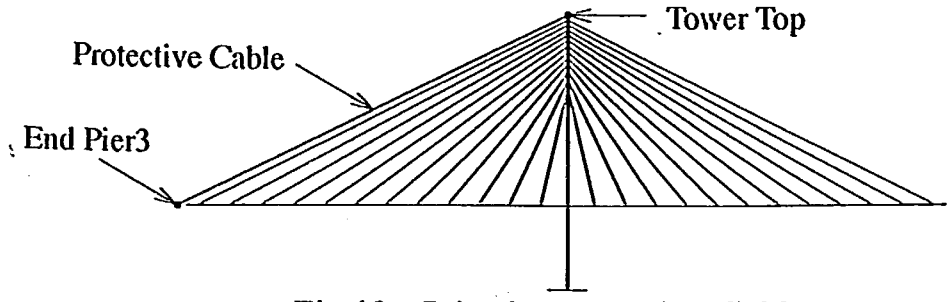


Fig.13 Seismic Protective Cable

Table. 2 Effect of Protective Cable

Mode No.	Natural Period (sec)		Bending Moment (tf·m)			
			Tower Bottom		Pier Bottom	
	Nothing	Exist	Nothing	Exist	Nothing	Exist
1st	7.283	5.490	15764	11692	22576	12754
2nd	1.503	1.500	11404	11552	48738	47594
3rd	1.054	1.052	7316	7876	230544	230750
R.M.S	~0.100	~0.100	23769	21736	240132	239442

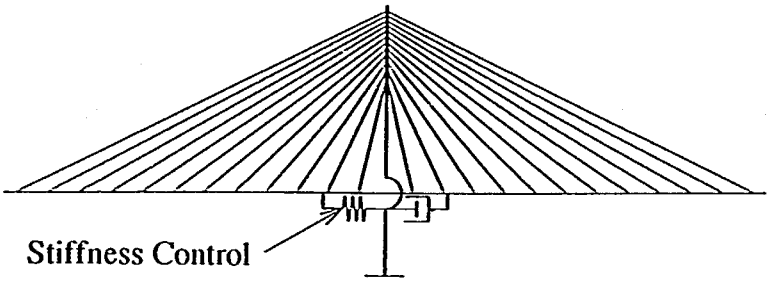


Fig.14 Stiffness Control Device

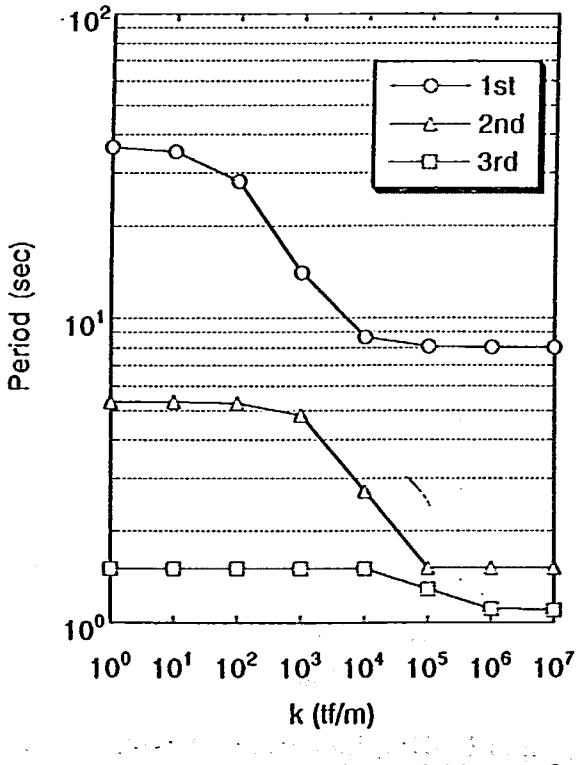


Fig.15(a) Variation of Natural Period and Rigidity k

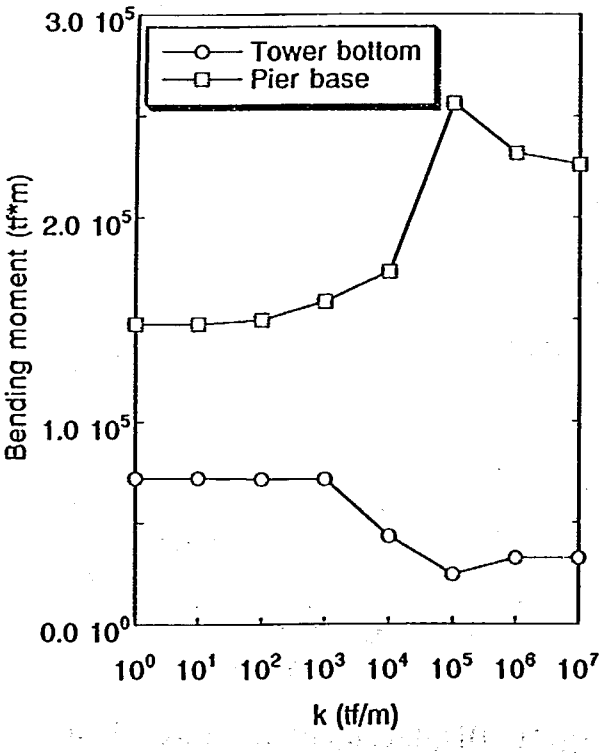


Fig.15(b) Variation of Bending Moments and Rigidity k

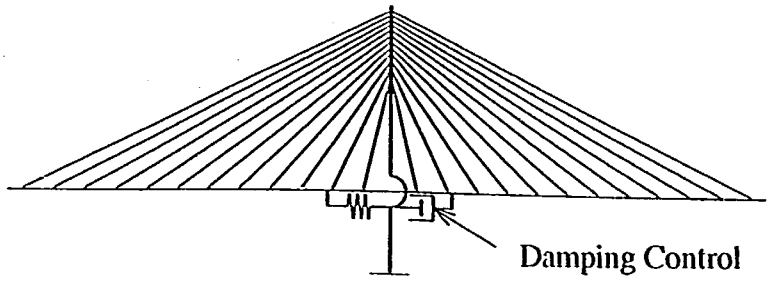


Fig.16 Damping Control Device

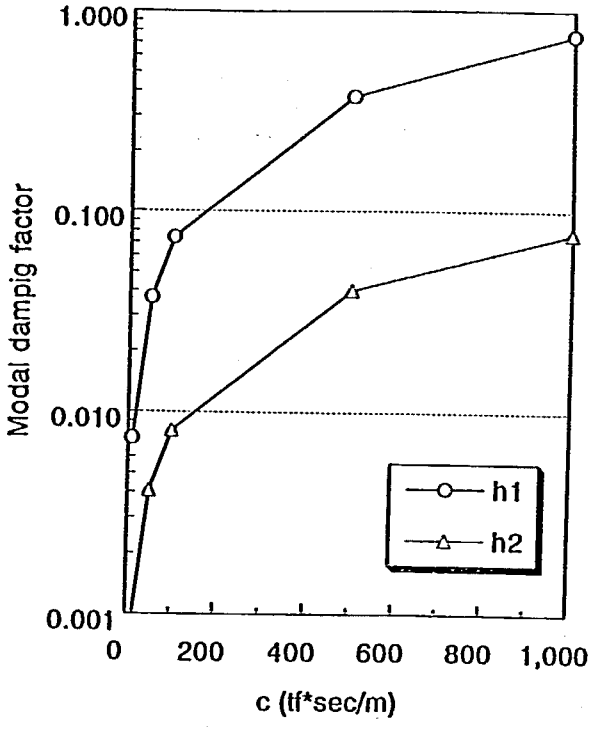


Fig.17(a) Variation of Modal Damping and Damping Coefficient c

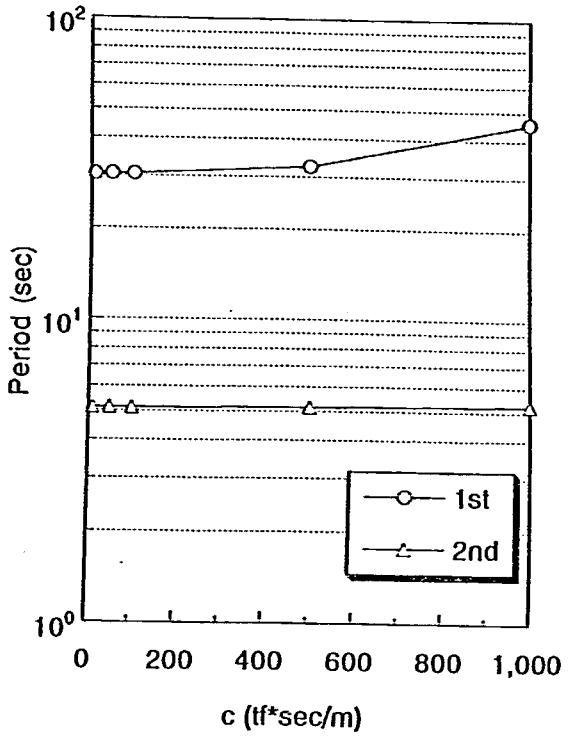


Fig.17(b) Variation of Natural Period and Damping Coefficient c

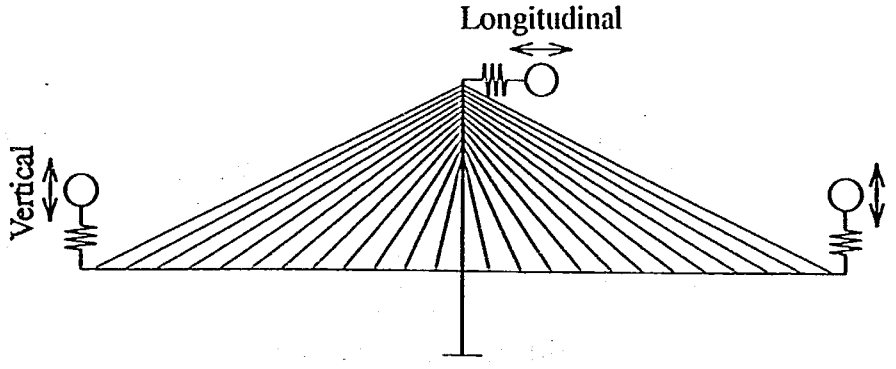
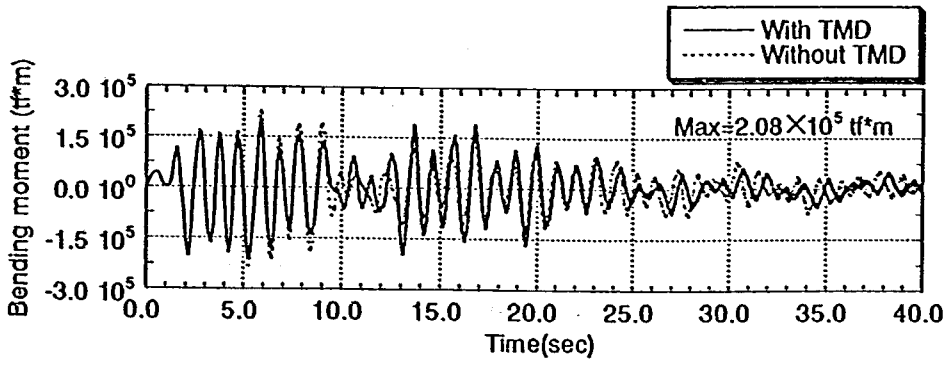
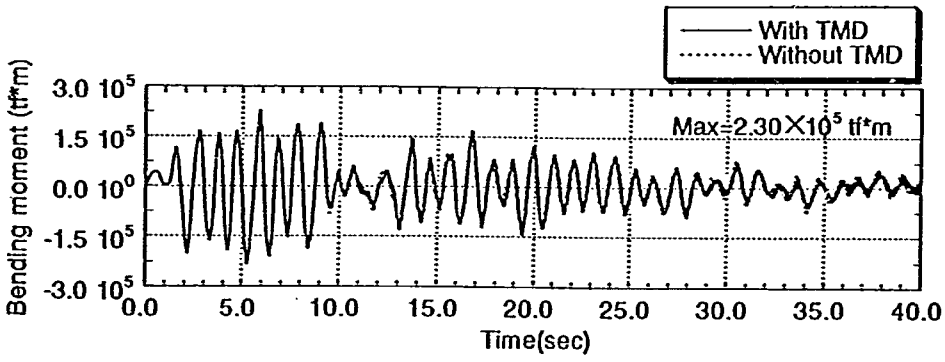


Fig.18 Arrangement of TMD, AMD

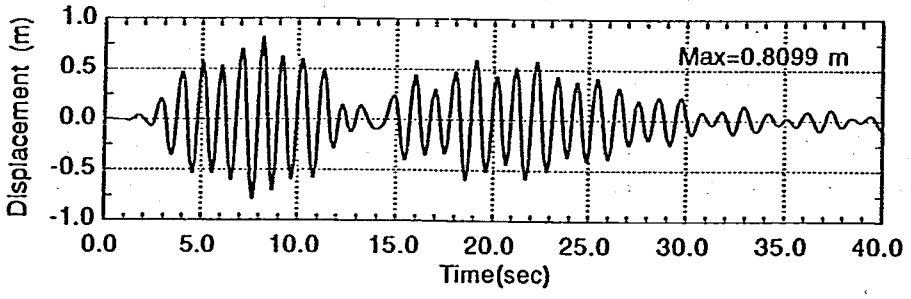


(a) TMD at Girder Edge

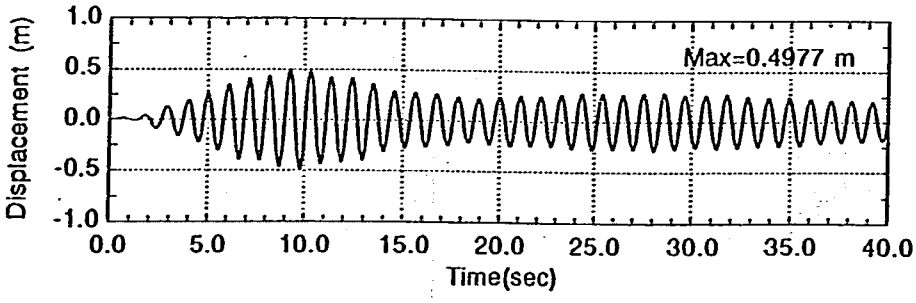


(b) TMD at Tower Top

Fig.19 Bending Moment at Pier Base

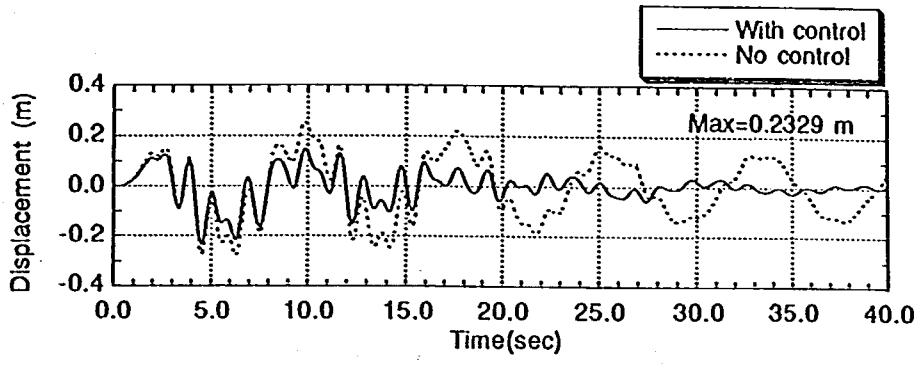


(a) TMD at Girder Edge

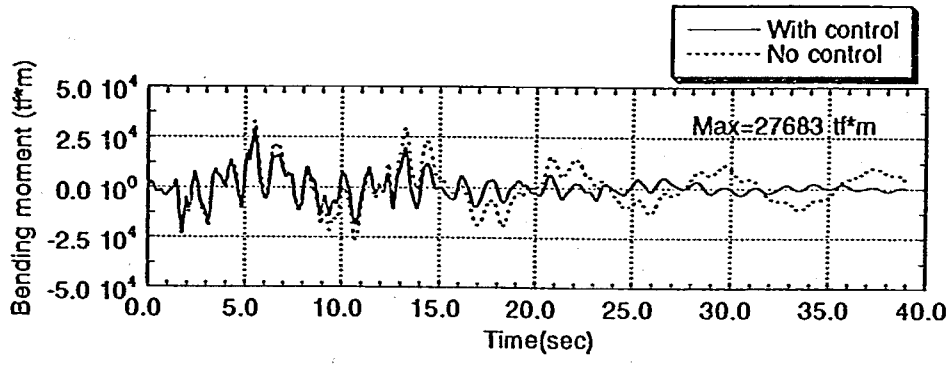


(b) TMD at Tower Top

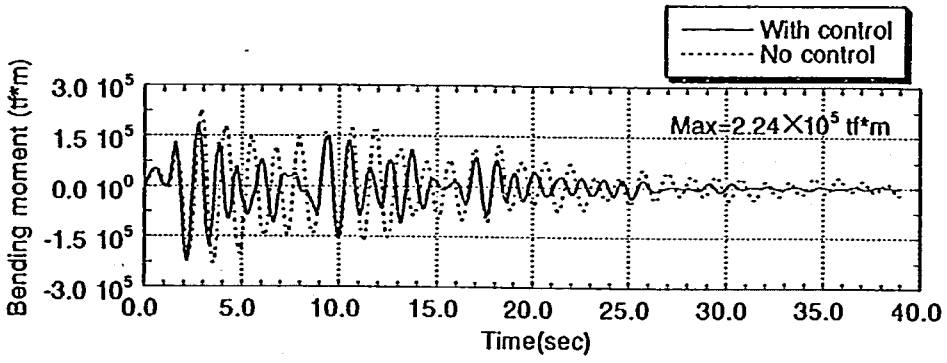
Fig.20 Relative Displacement of TMD



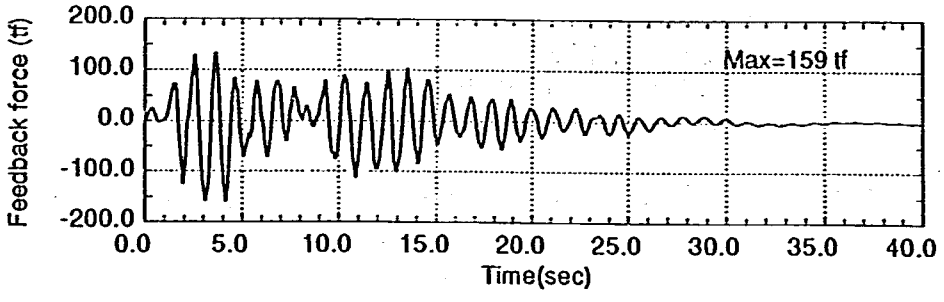
(a) Vertical Displacement of Girder Edge



(b) Bending Moment at Tower Bottom

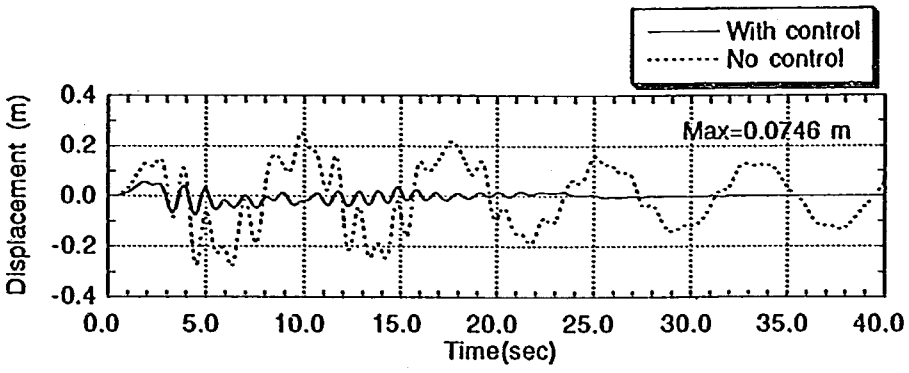


(c) Bending Moment at Pier Base

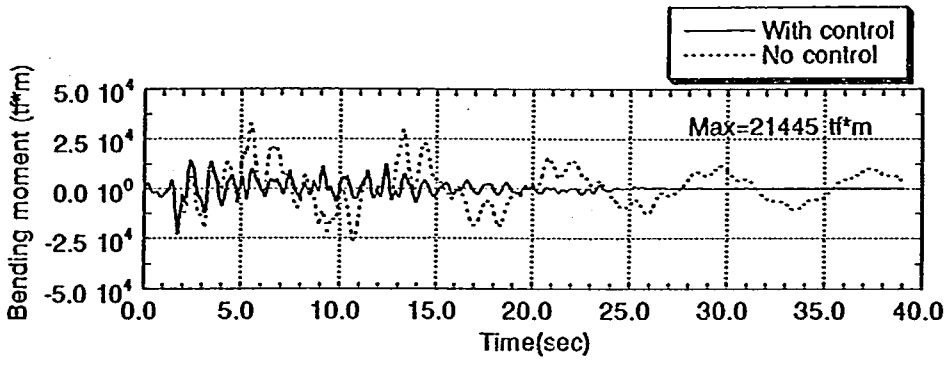


(d) AMD Force

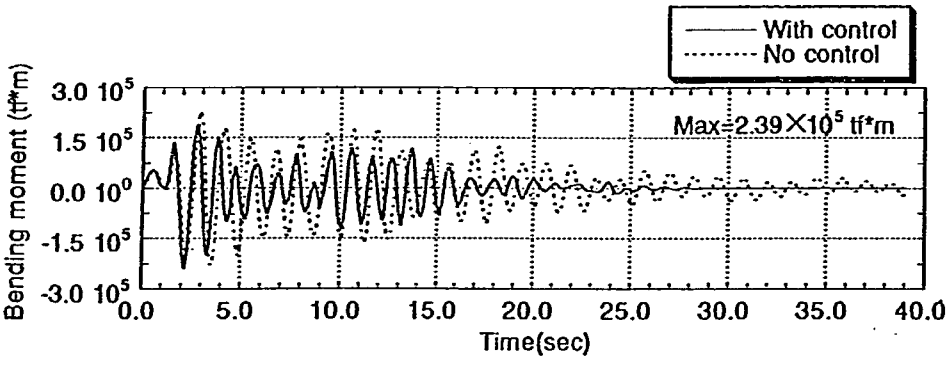
Fig.21 Results of Case 1 (AMD : Tower Top)



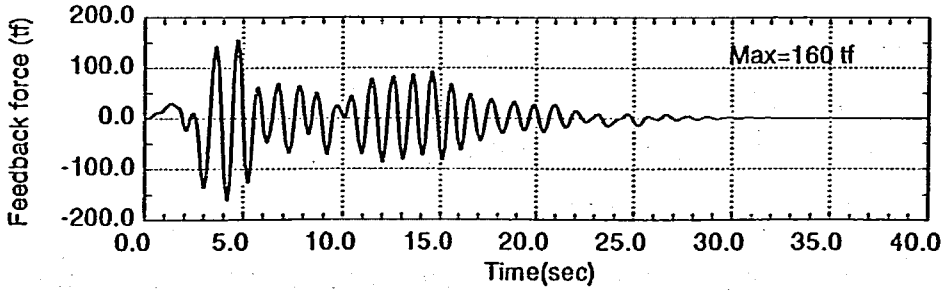
(a) Vertical Displacement of Girder Edge



(b) Bending Moment at Tower Bottom



(c) Bending Moment at Pier Base



(d) AMD Force

Fig.22 Results of Case 2 (AMD : Girder Edge)

RESOLUTION

RESOLUTION

APPENDICES

1. Schedule of the Workshop

March 12 (Sun) :	European and U.S. Members arrive in Japan	
		(Tsuchiura)
13 (Mon) :	Opening Ceremony	
	Session 1, 2 – European Side –	
	Session 3 – U. S. Side –	
	Visit to PWRI Laboratories	
	Dinner hosted by Director-General of PWRI	
		(Tsuchiura)
14 (Tue) :	Session 4 – Japan Side –	
	Closing Ceremony	
	Leave PWRI to Osaka	
		(Osaka)
15 (Wed) :	Study Tour	
	Visit to Hanshi Expressway	
		(Osaka)
16 (Thu) :	Study Tour	
	Visit to Japan Highway and Japan Railway	
		(Osaka)
17 (Fri) :	Leave Japan	

2. Opening Ceremony

1. Date and Time : Monday, March 13, 1995 (9:20–9:40)

2. Place : 8th Floor Conference Room, Public Works Research Institute, Ministry of Construction

3. Program : Call to order by Mr. Toshinori MIZUTANI, Director of Planning and Research Administration Department, Public Works Research Institute, Ministry of Construction

Address by Dr. Takashi IIJIMA, Director–General, Public Works Research Institute, Ministry of Construction

Address by Prof. Ing. Paolo E. Pinto, Department of Structural and Geotechnical Engineering, University of Rome "La Sapienza"

Address by Dr. H. S. Lew, Chief, Structures Division, Building and Fire Research Laboratory, National Institute of Standards and Technology, U.S. Department of Commerce

Introduction of Participants

Closure by Mr. Toshinori MIZUTANI

3. Session Program of the Workshop

Monday March 13 — 8F Conference Room

9:00 ~ 9:20 Registration

9:20 ~ 9:40 **Opening Ceremony**

9:40 ~ 9:50 Break

9:50 ~ 11:50 **Session 1 – European Side : Seismic Design Methods –**

(Chaiman : Dr. Y. Koga, Prof. I. G. Buckle)

9:50 ~ 10:10 Eurocode 8 Part.2 : Earthquake Resistant Design of Bridges
P. E. Pinto

10:10 ~ 10:30 Project Description and Seismic Design Criteria for the 2km Rion–Antirion Crossing in Southern Greece
M. N. Fardis

10:30 ~ 10:50 Displacement Based Seismic Design of Multi–degree–of–freedom Bridge Structures
G. M. Calvi

10:50 ~ 11:10 Shear, Normal Force, Bending Moment Interaction in Bridges Piers
G. Mancini

11:10 ~ 11:30 A Fiber Model Elements under Cyclic Bending and Shear
M. Petrangeli

11:30 ~ 11:30 Discussions

12:00 ~ 12:15 **Group Photograph** In Front of Main Building of PWRI

12:15 ~ 13:00 Lunch (1F Meeting Room)

13:00 ~ 14:10 **Session 2 – European Side**
: Experimenatal Study and Design Application –

(Chaiman : Dr. S. Unjoh, Dr. R. Imbsen)

13:00 ~ 13:20 Large–scale Pseudo–dynamic Tests on Highly Irregular Bridges
P. Negro

13:20 ~ 13:40 Inelastic Response of Conventional and Isolated Bridges under Non–synchronous Seismic Input
C. Nuti

13:40 ~ 14:00 Seismic Retrofitting of Two Large Span Bridges
M. Petrangeli

14:00 ~ 14:10 Discussions

14:10 ~ 14:30 Break

14:30 ~ 16:20 **Session 3 – U.S. Side –**

(Chaiman : Dr. H. Otsuka, Prof. G. M. Calvi)

14:30 ~ 14:45 Performance of Highway Bridges during the Northridge Earthquake
H. S. Lew

14:45 ~ 15:05 Influence of Recent Damaging Earthquake in California on Bridge Design in the U.S.
I. G. Buckle

15:05 ~ 15:20 Seismic Retrofitting Guidelines for Highway Bridges
P. Yen

15:20 ~ 15:40 Research Applied to Assessment and Retofit of Existing Bridges
S. Mahin

15:40 ~ 16:00
Seismic Performance & Design Considerations of Major Long Span Bridges
R. Imbsen

16:00 ~ 16:20 Discussions

16:20 ~ 17:40 **Visit to PWRI Laboratories**

16:20 ~ 16:40 Earthquake Engineering Laboratory

16:40 ~ 17:00 Vibration Laboratory

17:00 ~ 17:20 Structural Engineering Laboratory

17:20 ~ 17:40 Wind Tunnel Laboratory

18:00 ~ 18:30 Leave PWRI to Sansui-tei, by Bus

18:30 ~ 20:30 Dinner hosted by Dr. Takashi IIJIMA, Director-General, Public Works Research Institute, Ministry of Construction
(Sansui-tei, Tel:0298-52-1151)

Stay at Hotel Marroad Tsukuba
(Tel:0298-56-2211/Fax:0298-56-2679)

Tuesday March 14 — 8F Conference Room

9:00 ~ 12:30 **Session 4 – Japan Side : Hanshin–Awaji Earthquake –**
(Chairman : Prof. P. E. Pinto, Prof. S. Mahin)

9:00 ~ 9:20 Damage Characteristics of Bridges
H. IEMURA

9:20 ~ 9:40 Earthquake Ground Motion Characteristics
R. HAGIWARA

9:40 ~ 10:00 Analysis of a Damaged Bridge
S. UNJOH

10:00 ~ 10:20 Damage to Steel Bridges
K. NISHIKAWA

10:20 ~ 10:40 Damage to a Bridge by the Effect of Soil Liqeufaction
T. IWASAKI

10:40 ~ 11:00 Effect of the Hanashin–Aaji Earthquake on Bridge Seismic Design in Japan
K. KAWASHIMA

11:00 ~ 13:00 Discussions

13:00 ~ 14:00 Lunch (1F Meeting Room)

14:00 ~ 14:30 **Closing Session**
(Chaired by Dr. K. Kawashima and Prof. P. E. Pinto)

14:30 ~ 14:45 **Closing Ceremony**

15:00 Lv. PWRI to Tsuchiura St. by Bus

16:15 Lv. Tsuchiura St. by JR Express Hitachi #120

17:04 Ar. Ueno St.

17:56 Lv. Tokyo St. by JR Nozomi Super–Express #25

20:26 Ar. Shin–Osaka St.

Ar. Hotel by Taxi

Stay at Hotel KKR Osaka (Tel:0298–56–2211/Fax:0298–56–2679)

4. Closing Ceremony

1. Date and Time : Tuesday, March 14, 1995 (14:30 – 14:45)

2. Place : 8th Floor Conference Room, Public Works Research Institute

3. Program : Call to order by Mr. Hachiro TAKATA, Director of General Affairs Departmnet, Public Works Research Institue, Ministry of Construction

Address By Prof. Ing. Paolo E. Pinto, Department of Structural and Geotechnical Engineering, University of Rome "La Sapienza"

Address by Dr. H. S. Lew, Chief, Structures Division, Building and Fire Research Laboratory, National Institute of Standards and Technology, U.S. Department of Commerce

Address by Dr. Takashi IIJIMA, Director–General, Public Works Research Institute, Ministry of Construction

Closure by Mr. Hachiro TAKADA

5. Technical Study Tour

Wednesday March 15

Lv. Hotel KKR Osaka
Visit to Hanshin Expressway Public Corporation
Visit to Bridge Sites by Bus
Hanshin Expressway Route No.5 (Bay Route)
Hanshin Expressway Route No.3 (Kobe Route)
Walk around Sannomiya Area

Stay at Hotel KKR Osaka (Tel:0298-56-2211/Fax:0298-56-2679)

Thursday March 16

Lv. Hotel KKR Osaka
Visit to Bridge Sites by Bus
JH Meishin Expressway
JR Sanyo Express Railway
JH Chugoku Expressway

Stay at Hotel KKR Osaka (Tel:0298-56-2211/Fax:0298-56-2679)

6. List of Participants

OVERSEAS PARTICIPANTS

ITALY

Prof. Ing. G. Michele CALVI
Department of Structural Mechanics, University of Pavia

Prof. Ing. Giuseppe MANCINI
Department of Structural Engineering, University of Torino

Dott. Ing. Paolo NEGRO
Joint Research Centre, Ispra Establishment

Prof. Ing. Camillo NUTI
Department of Science and History of Architecture, University "G. D.'Annunzio" of Pescara

Prof. Ing. Mario P. PETRANGELI
Department of Structural and Geotechnical Engineering, University of Rome – La Sapienza

Prof. Ing. Paolo Emilio PINTO
Department of Structural and Geotechnical Engineering, University of Rome – La Sapienza

PORTUGAL

Dr. Eduardo C. CARVALHO
Principal Research Officer, Laboratorio Nacional de Engenharia Civil

GREECE

Prof. Ing. Michael N. FARDIS
Department of Civil Engineering, School of Engineers, University of Patras

UNITED STATES

Prof. Ian G. BUCKLE
Deputy Director, National Center for Earthquake Engineering Research, State University of New York at Buffalo

Dr. Roy A. IMBSEN
President, Imbsen & Associates, Inc.

Dr. H. S. LEW
Chief, Structures Division, Building and Fire Research Laboratory, National Institute of Standards and Technology, U.S. Department of Commerce

Prof. Stephen MAHIN
Byron L. and Elvira Nishkian Professor of Structural Engineering, Earthquake Engineering Research Center, Department of Civil Engineering, University of California at Berkeley

Dr. Phillip YEN
Structures Division, Turner–Fairbank Highway Research Center, Federal Highway Administration, U.S. Department of Transportation

JAPAN

Dr. Yoshitake EGAWA
Geotechnical Counseller, PWRI

Mr. Tadahiko FUJISAWA
Research Coordinator for Advanced Technology, PWRI

Mr. Ryoji HAGIWARA
Head, Ground Vibration Division, Earthquake Disaster Prevention Department, PWRI

Mr. Riki HONDA
Research Engineer, Ground Vibration Division, PWRI

Mr. Jun-ichi HOSHIKUMA
Research Engineer, Earthquake Engineering Division, PWRI

Prof. Hirokazu IEMURA
Department of Civil Engineering, Kyoto University

Dr. Takashi IIJIMA
Director-General, PWRI

Mr. Hideaki IWASAKI
Research Engineer, Ground Vibration Division, PWRI

Dr. Toshio IWASAKI
The Chairman of the Board of Directors, Civil-Works Research Laboratory

Mr. Masayuki KANDA
Senior Reaserch Enigneer, Bridge Engineering Division, PWRI

Mr. Masahiro KANEKO
Senior Research Engineer, Ground Vibration Division, PWRI

Mr. Hirotaka KAWANO
Head, Concrete Division, Material and Construction Method Department, PWRI

Dr. Kazuhiko KAWASHIMA
Research Coordinator for Geospace Use, PWRI

Mr. Yohshitomi KIMURA
Senior Research Engineer, Foundation Engineering Division, PWRI

Dr. Yasuyuki KOGA
Director, Earthquake Disaster Prevention Department, PWRI

Mr. Kiyokazu KUBOTA
Design and Research Division, Engineering Department, Metropolitan Expressway Public Corporation

Mr. Osamu MATSUO
Head, Soil Dynamics Division, Earthquake Disaster Prevention Department, PWRI

Mr. Toshinori MIZUTANI
Director, Planning and Research Administration Department, PWRI

Mr. Masanori NAKANO
Head, Foundation Engineering Division, Structure and Bridge Department, PWRI

Mr. Tomonobu NAKAOKA
Assistant Director-General, PWRI

Mr. Yoshio NINOMIYA
Senior Research Engineer, Ground Vibration Division, PWRI

Mr. Kazuhiro NISHIKAWA
Head, Bridge Engineering Division, Structure and Bridge Department, PWRI

Mr. Tomofumi NOZAKI
Research Engineer, Earthquake Engineering Division, PWRI

Mr. Tatsuo OGATA

Structural Engineering Division, Engineering Department, Japan Highway Public Corporation

Mr. Ryutaro OISHI
Research Coordinator on International Cooperation, PWRI

Dr. Hisanori OTSUKA
Head, Earthquake Engineering Division, Earthquake Disaster Prevention Department, PWRI

Mr. Shoichi SAEKI
Director, Honshu–Shikoku Bridge Authority

Mr. Kazuya SASAKI
Design and Research Division, Engineering Department, Metropolitan Expressway Public Corporation

Dr. Motoyuki SUZUKI
Senior Research Engineer, Earthquake Engineering Division, PWRI

Mr. Shigeru TAKAGI
Research Engineer, Foundation Engineering Division, PWRI

Mr. Hachiro TAKATA
Director, General Affairs Department, PWRI

Mr. Masahide TAMURA
Deputy Director–General, PWRI

Mr. Nobuhiko TANIGUCHI
Bridge Instructor, PWRI

Mr. Yuji TARUMI
Structural Engineering Division, Engineering Department, Japan Highway Public Corporation

Dr. Shigeki UNJOH
Senior Research Engineer, Earthquake Engineering Division, PWRI

Mr. Harutoshi YAMADA
Head, Advanced Transportation Division, Road Department, PWRI

Mr. Satoshi YAMAMOTO
Research Enigneer, Bridge Engineering Division, PWRI

Dr. Koichi YOKOYAMA
Director, Structure and Bridge Department, PWRI

PROCEEDINGS OF THE FIRST JAPAN-ITALY WORKSHOP ON SEISMIC DESIGN OF BRIDGES

ISSN 0386-5878
Technical Memorandum of PWRI No. 3369
March, 1995

This proceedings document the results of the First Japan-Italy Workshop on Seismic Design of Bridges. The Workshop was held at the Public Works Research Institute in Tsukuba Science City, Japan, on March 13 and 14, 1995.

Key words: Bridge, Seismic Design, Retrofitting, Design Code, Member Modeling

郵 便 は が き

Postage stamp

3 0 5 - □ □

建設省土木研究所地震防災部耐震研究室
〒305 茨城県つくば市大字旭1番地

Earthquake Engineering Division,
Public Works Research Institute
Tsukuba Science City
Japan 305

No.

No.

配布先氏名

配布先住所

Receipt of

Technical Memorandum of PWRI No. 3369

Name _____

Address _____

_____

_____